THE PHOTOCHEMISTRY OF AZAFERROCENE AND ITS DERIVATIVES

THIS THESIS IS PRESENTED FOR THE DEGREE OF

DOCTOR OF PHILOSOPHY

BY

Davnat Heenan B.Sc.

UNDER THE SUPERVISION OF DR. MARY PRYCE AND PROF. CONOR LONG

AT
DUBLIN CITY UNIVERSITY
SCHOOL OF CHEMICAL SCIENCES

SEPTEMBER-2002

DECLARATION

I hereby certify that this thesis, which I now submit for assessment on the programme of study leading to the award of Doctor of Philosophy is entirely my own work and has not been taken from the work of others save and to the extent that such work has been cited and acknowledged within the text of my work.

SIGNED: _____ SEPTEMBER 2002

STUDENT ID No. 97970654

TABLE OF CONTENTS

DEADICATION

To my parents and Christopher
And the memory of Patrick and Keara

ACKNOWLEDGEMENTS

I would like to sincerely thank my supervisors, Dr. Mary Pryce and Prof. Conor Long, for the opportunity to carry out this research. I am truly grateful for all your help, advise, patience and encouragement, not to mention your hospital visits.

I wish to thank Prof. Robin Perutz and Dr. Virginia Montiel-Palma of the University of York for the use of the matrix isolation equipment and for all their help during my visits to York.

Special thanks to all the technical staff. Life in a DCU lab without you would have been impossible. Particular appreciation is owed to Mick and Maurice who were always on hand to sort out the problems and offer excellent ideas on improvisation, and to Ambrose, you're the star who kept the supplies coming and the argon flowing!

My years as a postgraduate have been numerous to say the least, but those spent with Ollie, Ben, Colm, Brónagh, Peter, Siobhán, Mairéad, Kieran and Ger in AG07 deserve special mention. I can safely say, (although it wasn't always safe there), that there was never a dull moment and that they were the most enjoyable days I ever spent in a lab. Cheers for the constant entertainment and great memories.

The new lab brought new faces, for the fellow members of the CLRG research group, my thanks to Karl, Jonathan, Jennifer, Kevin K., Kevin M. and Claire - best of luck with it all. To those on the 'Other Side' in the HVRG research group, who adopted me when times got tough. Thanks to Marco (although I still can not dance despite all your efforts), and Scott (otherwise known as Scott-knowaloticous) for all the hugs, Anthea, Adrian, Dec, Fiona F., Fiona L., and Holger, the 'lonely child'. Thanks also to the non-alchemists across the hall, especially Cathal Ger and Rachel, and to all the other folk old and new I'm sure I've forgotten to mention.

A huge thank you to the Girls –Helen, Carol, Mairéad, Edel and Jenni for all the girlie chats and ongoing friendship. As Tigger still says – 'You're the Best!' What more can I say? To Chris, the Davster really appreciates you always being there, even when you are away in spite the fact that I was always causing lots of bother. It won't be long now till I ketch-up, so you better be ready!

Most importantly, thank you to my wonderful parents, for always understanding why this meant so much to me, for your love, encouragement and support (especially financial!) for all of my 28 years. Thanks to my sisters, Órla (and CAMIDA for printing services), Bróna, Antoinette and Rachel for setting such impossibly high standards! I'm sure I'll never attain them but I'll have fun trying.

ABSTRACT

Chapter one contains a literature survey of the relevant organometallic chemistry and the current understanding of the bonding in these systems, along with a theoretical description of the electronic structure of ferrocene. A brief outline of the techniques used to characterise the photochemical intermediates in this research is presented. The main part of the chapter consists of a literature review of the photo and thermal chemistry of half sandwich complexes, such as the η^6-arene-chromium tricarbonyl system.

Chapter two opens with a review of the photochemistry of ferrocene, $(\eta^5\text{-}C_5H_5)_2Fe$ and goes on to detail the results of the investigation into the photochemistry of azaferrocene, $(\eta^5\text{-}C_5H_5)(\eta^5\text{-}C_4H_4N)Fe$. The photochemistry of azaferrocene is then described in alkane solvents at room temperature using both steady-state photolysis and laser flash photolysis. The matrix photochemistry monitored by ultraviolet-visible (UV-vis) and Fourier transform infrared (FT-IR) spectroscopy is also presented. Room temperature photolysis using broad band irradiation ($\lambda_{exc.} > 500$ nm) in carbon monoxide saturated cyclohexane produced cyclopentadienyliron dicarbonyl η^1-pyrrolyl, while monochromatic irradiation ($\lambda_{exc.} = 532$ nm) also produced an allyl monocarbonyl complex, *exo*-$(\eta^5\text{-}C_5H_5)Fe(CO)(\eta^3\text{-}C\text{-}C_4H_4N)$, as identified by FT-IR. In carbon monoxide doped argon matrixes at 12 K, both $(\eta^5\text{-}C_5H_5)Fe(CO)_2(\eta^1\text{-}N\text{-}C_4H_4N)$, and $(\eta^5\text{-}C_5H_5)Fe(CO)(\eta^1\text{-}N\text{-}C_4H_4N)$ were observed following broad band irradiation ($\lambda_{exc.} > 495$ nm) of azaferrocene in a ratio dependent on the concentration of carbon monoxide in the matrix. Initial photolysis with monochromatic irradiation ($\lambda_{exc.} = 538$ nm) followed by broad band irradiation ($\lambda_{exc.} > 495$ nm) in carbon monoxide doped matrixes formed an additional monocarbonyl complex, assigned to an azaallyl complex, $(\eta^5\text{-}C_5H_5)Fe(CO)(\eta^3\text{-}N\text{-}C_4H_4N)$.

Chapter three reviews the photochemistry of $(\eta^5\text{-}C_5H_5)Fe(CO)_2X$, (X = Cl, Br, I or CH_3, C_3H_5, C_6H_5 etc.). In addition, photochemical studies of $(\eta^5\text{-}C_5H_5)Fe(CO)_2(\eta^1\text{-}N\text{-}C_4H_4N)$

and (η^5-C_5H_5)Fe(CO)$_2$(η^1-*N*-C_8H_6N) are detailed. Steady-state photolysis, laser flash photolysis and in the case of (η^5-C_5H_5)Fe(CO)$_2$(η^1-*N*-C_4H_4N), matrix isolation techniques were employed to detect and identify the photochemical intermediates. These results suggest that carbon monoxide loss is the dominant photoprocess. The activation parameters were also measured for the reaction of the monocarbonyl, (η^5-C_5H_5)Fe(CO)(η^1-*N*-C_4H_4N) with carbon monoxide to regenerate (η^5-C_5H_5)Fe(CO)$_2$(η^1-*N*-C_4H_4N) in carbon monoxide saturated cyclohexane at $\lambda_{exc.}$ = 355 nm. No significant variation in the rate constant was observed for the reaction of (η^5-C_5H_5)Fe(CO)(η^1-*N*-C_4H_4N) with carbon monoxide to reform -(η^5-C_5H_5)Fe(CO)$_2$(η^1-*N*-C_4H_4N), irrespective of the solvent used.

The results of an investigation into the photochemistry of 2,5-dimethylazaferrocene, (η^5-C_5H_5)(η^5-2,5-$C_4(CH_3)_2H_2N$)Fe are presented in chapter four. High energy photolysis ($\lambda_{exc.}$ > 410 or = 355 nm) of 2,5-dimethylazaferrocene in carbon monoxide saturated solutions leads to predominantly to the formation of the (η^5-C_5H_5)Fe(CO)$_2$(η^1-*N*-2,5-$C_4(CH_3)_2H_2N$) and the iron dimer [(η^5-C_5H_5)Fe(CO)$_2$]$_2$. Low energy photolysis ($\lambda_{exc.}$ > 500 or = 532 nm) on the other hand, leads to the formation of two more carbonyl containing complexes in addition to the dicarbonyl complex and the dimer described above. Matrix isolation studies in carbon monoxide doped argon matrixes revealed evidence of intramolecular C-H activation occurring.

The final chapter contains the experimental details of the complexes synthesised, the method used for sample preparation for the flash photolysis experiments. Details of the equipment used for the laser flash photolysis and matrix isolation experiments is also outlined.

Chapter One

1 Introduction

This introduction attempts to provide a framework of the relevant chemistry and experimental techniques, which were explored in this thesis. An extensive review of the appropriate literature is provided at the beginning of each chapter.

1.1 A brief history of organometallic chemistry

Organometallic chemistry may be viewed as lying at the interface between classical organic and inorganic chemistry, for it views the interaction between inorganic metal ions and the organic molecules. However, it is with transition metals that the full diversity of organometallic chemistry becomes apparent.

The classical period of organometallic chemistry began with the synthesis of metal derivatives in which an unsaturated organic compound (specially an olefin) was bonded to a transition metal. Thus the preparation of the platinum complex, $K^+[C_2H_4PtCl_3]^-$ by the Danish pharmacist Zeise[1] in 1827 marked the birth of transition metal organometallic chemistry. However it was centuries later, when the structure was adequately explained, and the importance of these compounds was recognised.

The first application of organometallic chemistry from an industrial standpoint was Langer and Mond's[2] discovery of nickel-tetracarbonyl in 1890. Its application was understood much more rapidly and crude nickel has been refined by the Mond carbonylation – decarbonylation process for many decades, Scheme 1-1.

$$Ni + 4CO \rightarrow [Ni(CO)_4] \rightarrow Ni + 4CO$$

Scheme 1-1

The second metal carbonyl, $Fe(CO)_5$ followed in 1891 independently by Mond[3] in England and Berthelot[4] in France. Subsequently the carbonyl complexes of cobalt

(1910), molybdenum (1910), chromium (1926), tungsten (1928), ruthenium (1936) and iridium (1940) were prepared. This work laid the foundation for further developments. Hein[5] isolated the first molecular arene-metal complexes in 1919, which he named polyphenyl chromium, but definitive composition and structural characterisation of these complexes was not achieved until the mid 1950's.

The commercial importance of the catalytic properties of transition metal organometallic complexes began to emerge with the heterogeneous catalysed Fischer-Tropsch process[6] in 1925. It allows the conversion of synthesis gas (CO/H_2) into a mixture of hydrocarbons and was used in Germany for converting coal into petrol during the last world war. The discovery of a remarkable inert complex between the normally reactive 1,3-butadiene and iron carbonyl was described by Reilen[7] in 1930. This was followed by Roelen's [8] discovery of the homogeneous, cobalt-catalysed 'oxo' process / hydroformylation in 1938 for transforming olefins into aldehydes through the addition of CO and H_2 to the double bond. This was the first truly viable commercial process, which is catalysed by soluble transition metal compounds. German chemists up to the Second World War dominated transition metal molecular chemistry.

The Second World War saw a decline in research into organometallic chemistry, but the first post-war break-through occurred in 1951 when dicyclopentadienyliron was discovered by two groups of chemists independently. Kealy and Pauson[9] in 1951, when a reaction was carried out on cyclopentadienyl magnesium bromide with anhydrous iron (III) chloride in ether in an attempt to synthesise fulvalene via oxidation of the cyclopentadienyl Grignard reagent. Meanwhile, Miller, Tebboth and Tremaine[10] reported in 1952 the formation of the orange crystals $C_{10}H_{10}Fe$ by direct reaction of cyclopentadiene with iron in the presence of aluminium, potassium or molybdenum oxides at 300° C, when they were investigating the preparation of amines. Both groups erroneously proposed a σ complex, however the correct formulation as a π complex was established a year later by Wilkinson, Woodward[11] and Fischer.[12] With the discovery of ferrocene, the recognition of a new type of bonding between metal and organic unsaturated molecules prompted an enormous interest in these compounds and the classical period of organometallic chemistry drew to a close and the modern era began.

The application of organometallic chemistry was for a long time confined to laboratory use, however commercial importance of catalytic properties of transition metal organometallic complexes is now firmly established. Processes such as the 'oxo' process, which produces aldehydes and aldehyde derivatives is the most important industrial synthesis where a metal carbonyl complex is used as a catalyst.[13]. Monsanto developed the use of Ziegler-Natta catalysts (organo-aluminium-titanium compounds) for the polymerisation of olefins, and also by the production of acetic acid from the reaction between methanol and carbon monoxide in 1971.[14] In all such processes the active site is an unsaturated metal centre.

The modern era of organometallic chemistry has been sustained by the physical methods of investigation such as infrared, nuclear magnetic resonance, single crystal X-ray diffraction and mass spectrometry. These methods have provided detailed information about the structure and bonding in these compounds and make it possible to understand their behaviour to a greater extent than ever before. Computer modelling of transition metal systems is now booming with much of the activity directed at the application of quantum chemistry, notably Density Functional Theory (DFT).[15] Quantum chemistry will bring a much deeper insight into the nature of the transition metal-ligand interaction and more refined models of bonding for transition metal compounds will be developed. Such developments will no doubt improve the selectivity of organometallic compounds in future catalytic systems.

1.2 Definition of an organometallic complex

Organometallic chemistry by definition is the discipline dealing with compounds containing at least one direct metal-carbon bond. Therefore the nature and stability of this bond determines the stability of organometallic compounds. The metal ions in organometallic complexes are in low–positive, zero or negative formal oxidation states with a partially filled d-shell. It is a characteristic of the ligands that they can stabilise low oxidation states. This property is associated with the fact that, in addition to lone

pairs, the unsaturated organic molecule possesses vacant π^* orbitals. These vacant orbitals accept electron density back from filled metal d-orbitals to form π-backbonding that supplements the σ bonding arising from the lone pair donation. High electron density on the metal, which is of necessity in low oxidation states, can thus be de-localised onto the ligands. Therefore bonds between transition metal atoms and the unsaturated organic molecules are formed by electron donation in two opposite directions: from the ligand to the metal (direct donation) and from the metal to the ligand (back donation). There have been significant advances in computational chemistry in the last two decades. As a result there are a large number of theoretical papers concerning the electronic and bonding properties of saturated transition metal complexes. [15(e),16]

1.3 Organometallic bonds encountered in this study

In order to discuss the photochemical properties of specific organometallic compounds in detail, it is necessary to develop an appreciation of the bonding and the electronic structure of organometallic complexes. Three types of bonding will be considered here:

- Bonding in metal-carbonyl complexes
- Bonding in metal-cyclopentadienyl complexes
- Bonding in metal-allyl complexes

1.3.1 Bonding in metal-carbonyl complexes

The transition metal carbonyl bond arises from two mutually enhancing sources. The dominant model as described in a recent review by Frenking *et al.*[15(e)] considers the metal-carbon monoxide bond in terms of donor-acceptor interactions.

(a) CO → M σ donation arises from donation from the slightly anti-bonding 5σ 'lone pair' function on carbon monoxide into an empty transition metal atomic orbital (AO) of σ symmetry (usually d_z^2 orbital). This electron donation makes the metal more electron rich, and in order to compensate for this increased electron density

the second component of this bonding takes place, as described in part (b). Analysis of this component of the bonding in metal-carbonyl complexes indicates[17] that it ranges from a true carbon monoxide → metal donation to a situation where the carbon monoxide 5σ-orbitals polarise toward the metal and is stabilised by the positive charge on the metal. (i.e. a situation of carbon monoxide polarisation rather than true carbon monoxide donation to the metal).

(b) M → CO π type back-donation results form overlap of occupied or partially occupied π-type d orbitals of appropriate symmetry on the transition metal with the low lying strongly anti-bonding degenerate $2\pi^*$ molecular orbital (MO) of carbon monoxide. This decreases the internal bonding in the carbon monoxide ligand and acts to lower the carbon monoxide stretching frequencies in the infrared. This is reflected in a shift of carbonyl frequency in the infrared spectrum to lower frequency on complexation; free carbon monoxide exhibits a ν_{CO} = 2149 cm^{-1}, while $Cr(CO)_6$ has a ν_{CO} = ~1985 cm^{-1}. The π-back bonding is also shown schematically in Figure 1-1.

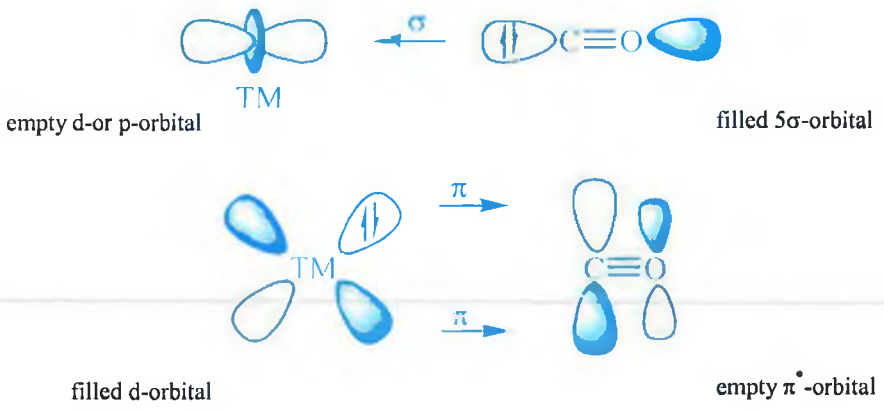

Figure 1-1 Schematic representation of the synergistic carbon monoxide → transition metal σ-donation and transition metal → carbon monoxide π-back-donation.

The two components of this bonding are synergistic. The more σ-donation by the carbonyl (or other σ-donors on the metal), the stronger the π-back-bonding donation.

Although this involves the occupation of a π^* orbital on the CO, it is still a bonding interaction as far as the metal is concerned, refer to Figure 1-2.

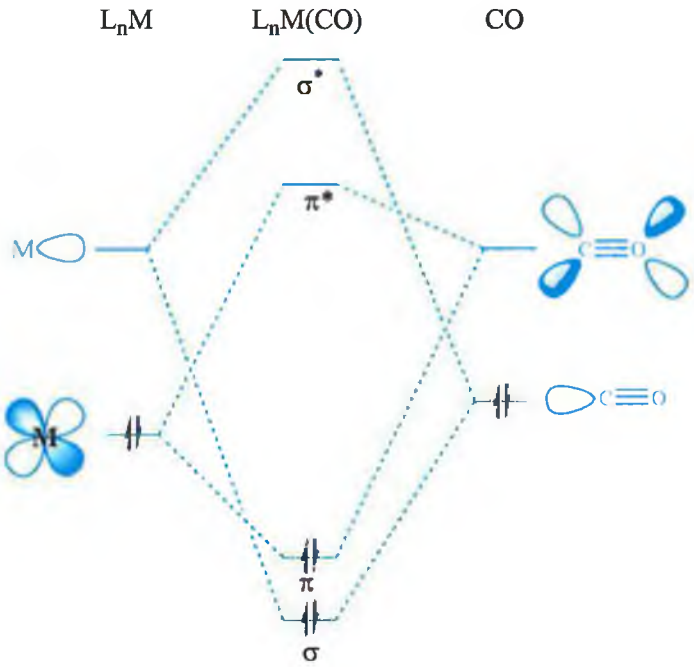

Figure 1-2 Molecular orbital diagram for $L_nM(CO)$.

Many theoretical studies using *ab initio* methods appeared in the 1980's and 1990's evaluating the relative contribution of σ-donation and π-back-donation to the M-CO interactions. Using different partitioning techniques all studies agree that for transition metal–carbon monoxide bond energy, π-back-donation is more important than σ-donation.[18]

1.3.2 Bonding in metal-cyclopentadienyl complexes

The cyclopentadienyl ligand, (η^5-C_5H_5) is considered a monoanionic ligand, because its co-ordination requires the formal transfer of one electron from the metal into its π system. The cyclopentadienyl ligand has strong aromatic character, reminiscent of the isoelectronic benzene ligand. The first characterised example of a cyclopentadienyl complex was ferrocene, $(\eta^5\text{-}C_5H_5)_2Fe$, which can be described as an iron atom 'sandwiched' between two planar cyclopentadienyl rings, while complexes with only

one cyclopentadienyl ligand are described as having 'half sandwich' geometries. The normal bonding mode for the cyclopentadienyl ligand is η^5-(penta-hapto), for which several different resonance structures can be drawn for the bonding of an η^5-cyclopentadienyl ligand to a transition metal complex, as presented in Figure 1-3.

Figure 1-3 The different resonance forms of the cyclopentadienyl ligand.

Most cyclopentadienyl complexes display completely de-localised bonding with equivalent C-C bond length in the C_5 ring, with all five carbons roughly equidistant from the metal. The cyclopentadienyl group is perhaps the most important of all the polyenyls because is generally inert to both nucleophilic and electrophilic reagents. Cyclopentadienyl complexes are generally electron rich, and the presence of the cyclopentadienyl ligand encourages back donation from the metal to the other ligands present.

1.3.2.1 Bonding in ferrocene

There are eighteen valence electrons to be accommodated in ferrocene, five π-electrons from each of the C_5H_5 rings, therefore ten electrons and eight valence electrons from the iron atom. Although the cyclopentadienyl ligands in the gas phase are eclipsed, the orbital interactions are usually discussed using D_{5d} symmetry (staggered ligands) rather than using D_{5h} symmetry (eclipsed ligands).[19, 20, 21]

The bonding is best explained using molecular orbital (MO) theory. The five p-orbitals on the planar C_5H_5 group can combine to produce five molecular orbitals. Of these five molecular orbitals produced, one is strongly bonding (a), which is a node-less 'doughnut' of electron density above and below the plane of the ring. At slightly higher energy there is a doubly degenerate set of orbitals, weakly bonding (e_1), each of which has one nodal plane containing the principle axis. At yet higher energy lies another set

of doubly degenerate orbitals that are markedly anti-bonding (e_2), with two nodal planes, as shown in Figure 1-4.

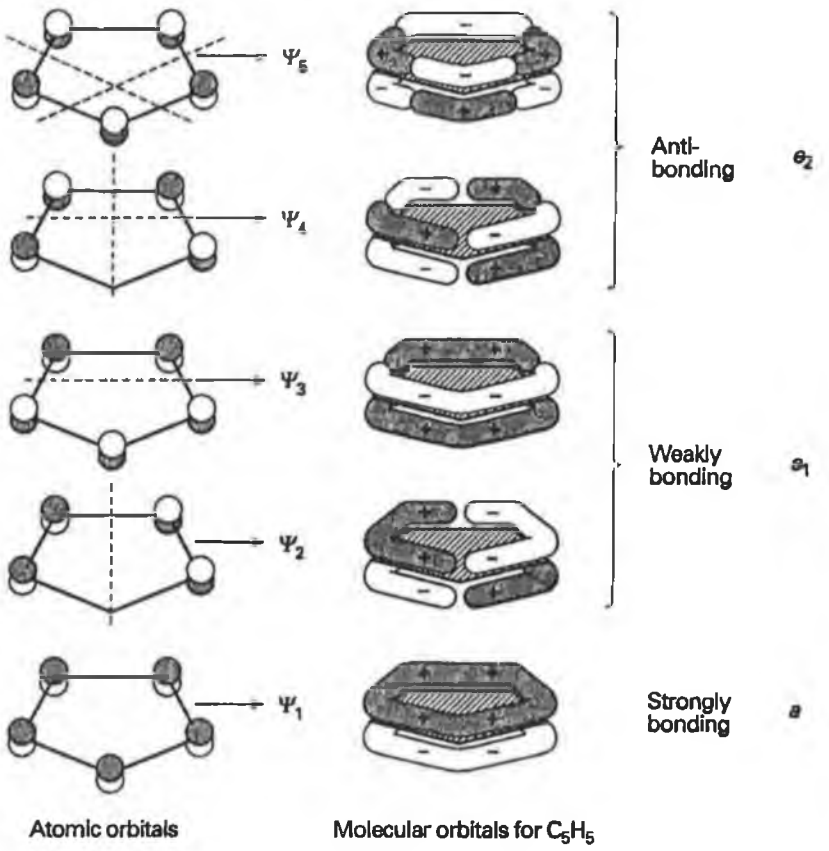

Figure 1-4 The π molecular orbitals formed from the set of p_π orbitals of a C_5H_5 ring.[21]

In discussing the bonding in ferrocene, a pair of rings must be taken together, so the sum and the difference of each molecular orbital must be considered, thereby forming the ligand group orbitals (LGOs). This gives rise to three sets of π orbitals; a low lying set of a_{1g} and a_{1u} symmetry, a filled set of e_{1g} and e_{1u} symmetry; and an unfilled set of anti-bonding orbitals of e_{2g} and e_{2u} symmetry at higher energy, refer to Figure 1-5.

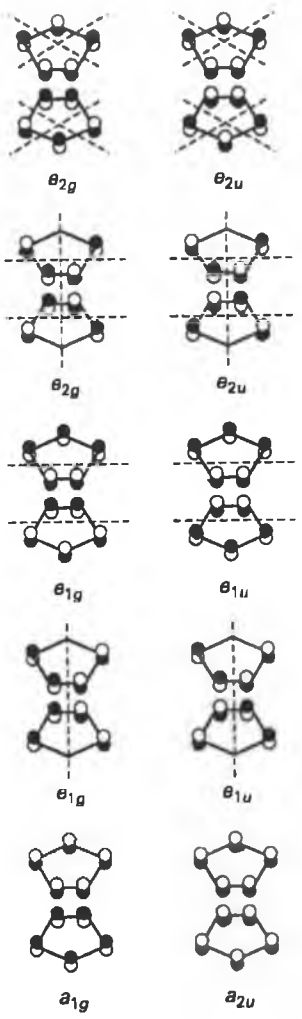

Figure 1-5 Examples of the overlap of the sum and difference ligand orbital-metal combinations.[21]

These three sets of ligand group orbitals can then be combined with atomic orbitals of matching symmetry on iron to form the molecular orbitals of ferrocene. The molecular orbitals of ferrocene may be constructed by considering the extent to which the ligand orbitals overlap with the metal orbitals of appropriate symmetry. Assuming that the energy levels are not very different, each of the combinations (ligand orbital + metal orbital) leads on principle to a bonding molecular orbital of the molecule, refer to Figure 1-6.

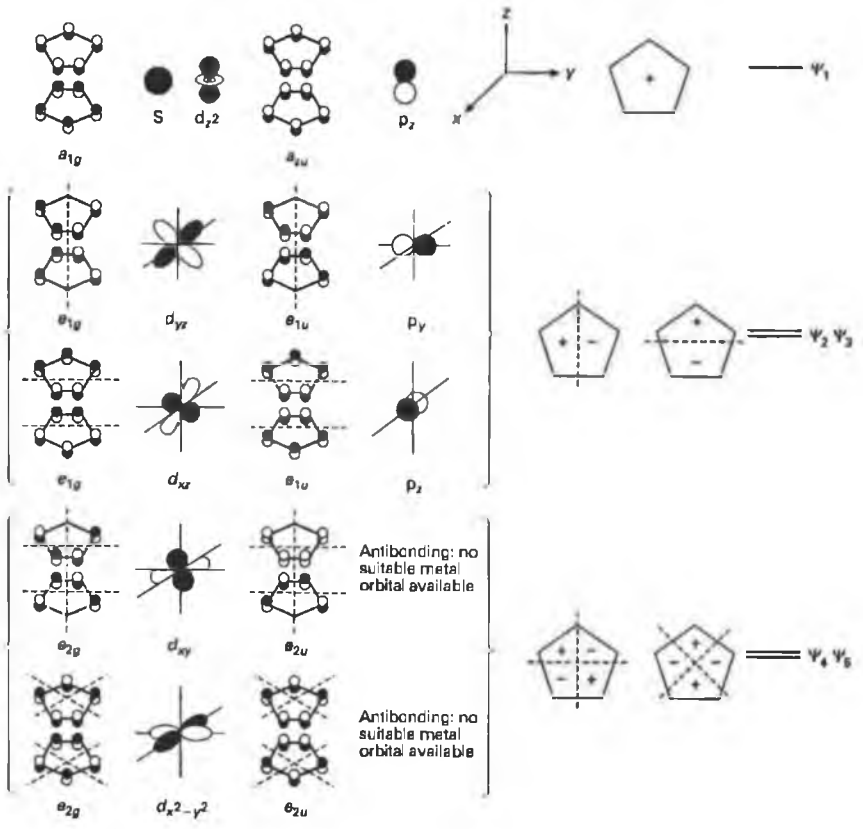

Figure 1-6 Symmetry matching of the ligand molecular orbitals with those of the metal atomic orbitals.[21]

A qualitative molecular orbital diagram for ferrocene in its staggered conformation (D_{5d}) is shown in Figure 1-7. The a_{1g} (σ-completely cylindrical symmetry - no nodes) bonding molecular orbital is mainly ligand-based, as it is so stable relative to the metal orbitals (4s and $3d_z^2$) that they interact very little, (i.e. ligand is a poor σ-donor). The $4p_z$ orbital on the iron atom is at high energy, and although it formally has the correct symmetry to combine with the a_{2u} level there is virtually no interaction with it. Most of the strength of the ferrocene molecule is created by two strong π-bonds formed by the overlap of the best-matched orbitals of the cyclopentadienyl ligand, the e_{1g} orbitals and the iron $3d_{xz}$ and $3d_{yz}$ orbitals. The corresponding anti-bonding e^*_{1g} set are unoccupied in the ground state. The e_{1u} bonding molecular orbitals are mainly ligand based with some contribution from the iron 4p orbitals, and are at high energy, (the e_{1u} set do not contribute much to the bonding). The remaining three d-orbitals of the metal, the a'_{1g} (dz^2) and the e_{2g} ($d_{x^2-y^2}$, d_{xy}) remain essentially non-bonding. This is because for the former, the ligand π orbitals of a'_{1g} symmetry point towards the nodal cone of the metal

$3d_z^2$ orbital, whilst for the latter the δ-type overlap (two nodes) with the ligand e_{2g} set is poor.

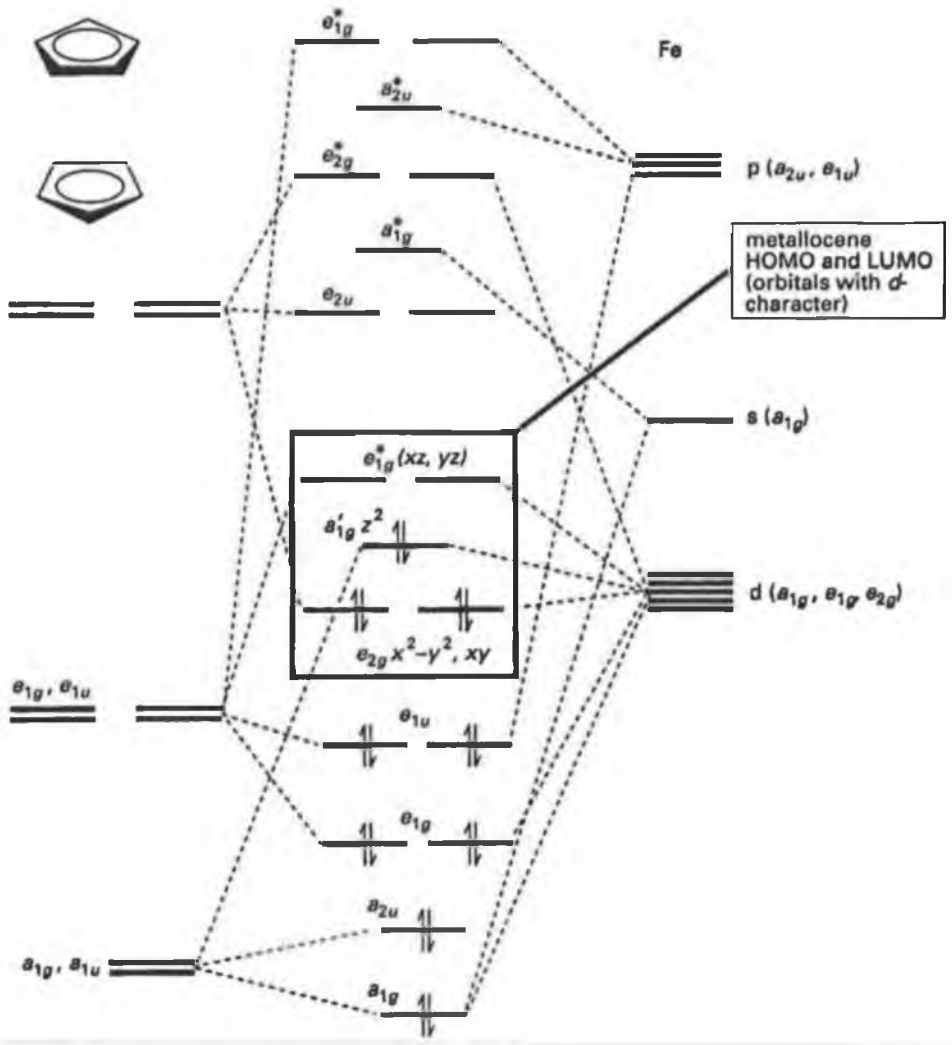

Figure 1-7 A qualitative molecular orbital diagram for ferrocene.

1.3.3 Bonding in metal-allyl complexes

The allyl group, CH_2=CH-CH_2 may bind in a monohapto form, primarily σ-bonded to a transition metal, as shown below in Figure 1-8(a). It may also function as a trihapto

ligand, using the remaining double bonds delocalised π orbitals to π-bond with the transition metal, as shown in Figure 1-8(b). If such a π-bond is formed in addition to the σ-bond, the resultant π-allyl bond can be expressed in resonance forms as in Figure 1-8(b). Also it may be expressed in molecular orbital terms as in Figure 1-8(c) as the interaction between the transition metal orbitals and the orbitals of the planar allyl group, where the electrons are delocalised over three carbon atoms.

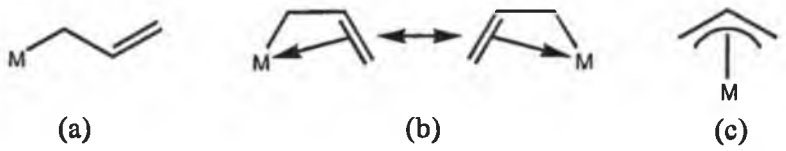

Figure 1-8 The monohapto and different resonance forms of the trihapto unsubstituted allyl ligand.

Bonding in the allylic groups and the metal is illustrated in Figure 1-9. The three-pπ orbitals of the allyl group combine to form three molecular orbitals, ψ_1 (bonding), ψ_2 (non-bonding), ψ_3 (anti-bonding). Also depicted in Figure 1-9, are the metal orbitals, which can overlap with these ligand orbitals. The ψ_1 (bonding) orbital overlaps with the metal s, d_z^2, and p_z orbitals or hybrid orbitals constructed from them. The ψ_2 (nonbonding) orbital is suitable for overlap with the metal p_y, d_{yz} orbitals or hybrid orbitals, whereas the ψ_3 (anti-bonding) has the correct symmetry to overlap with the metal p_x and d_{xz} orbitals or hybrids there of, to form metal-to-ligand backbonding.

In the trihapto form, the C-C distance is about 1.35-1.4 Å (comparable to ferrocene) and the bond angle C-C-C is about 120°. The plane of the allyl ligand is typically tilted away from the perpendicular to maximise orbital overlap.

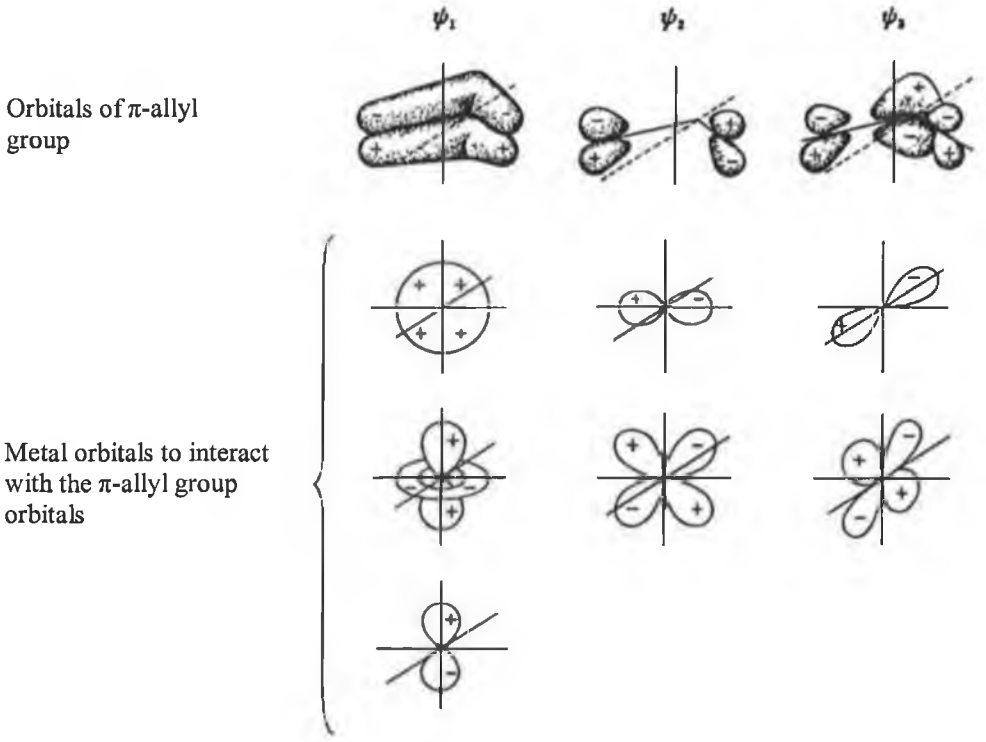

Figure 1-9 π-Allyl group orbitals ψ_1, ψ_2, and ψ_3 and the corresponding metal orbitals, which overlap most effectively with ligand group orbitals. The metal lies below the allyl group along the vertical axis.

1.4 The measurement of photochemical reactions

A study of photochemical kinetics is the most important method in the elucidation of the reaction mechanism and the determination of the roles played by the electronically excited molecules and the free radicals formed in photo-dissociation. Knowledge of the properties of the transient species is an integral feature in understanding the rate and mechanism of reactions. The technique used to examine their properties depends on their reactivity. The lifetime of transient species is controlled by self-reaction, reaction with solvent, buffer etc. The rate of photochemical reaction is generally dependent upon the initial component concentration and the magnitude of the total flux that is absorbed by the reaction system.

The direct result of a kinetic study can at best be a rate law, that is an equation showing how the velocity of a reaction at a given temperature and pressure and in a given medium varies as a function of the concentration of the reactant. The ultimate purpose of a rate and mechanism study is usually to interpret the rate law correctly so as to determine the correct mechanism for the reaction.

It is the half-life of a reaction that will govern the choice of the initiation method and it is the character of the reaction that will dictate the monitoring procedure.

- Static methods: ($t_{½} \geq$ 1min) – steady state photolysis
- Relaxation methods: ($t_{½} \leq$1 sec) – flash photolysis

1.4.1 Static methods

Static methods are the classical ones in which a complex is placed in a vessel and the progress of the reaction is followed by the observation of the time variation of some physical or chemical observable change (e.g. light absorption, gas evolution, pH, isotopic exchange etc.). In this study of organometallics complexes, the static method employed was that of continuous photolysis. The basic idea is to irradiate the sample in a non-polar solvent with a xenon arc lamp, whereby the energy absorbed by the sample from the incoming light is controlled by means of cut-off filters placed in front of the sample. Although the concentration of reactant decreases with time and those of the product increase, it is quite common in this type of experiment for the concentration of the intermediates to remain roughly the same, i.e. steady-state concentration for a substantial part of the time of the experiment.

The energy absorbed by the sample may be sufficient to produce excited states in the molecule and initiate a photochemical reaction. The product is formed in real time ($t_{½} \geq$ 1 minute) and is stable enough for infrared and UV-vis analysis to be carried out. However the product detected by spectroscopy in this manner may be the secondary photochemical product. Therefore static methods possibly do not provide any

information on the kinetics of the reaction or identify the primary photoproduct, which may have been intermediary on the way to the stable photochemical product.

1.4.2 Relaxation methods

Relaxation methods depend on creating a single disturbance in a state of equilibrium in a very short period of time and following the process of relaxation to an equilibrium state by a combination of spectrophotometric and fast electronic recording devices.

Initial studies on the transient photochemical intermediates involved in a photochemical reaction, were identified by stabilising them in low temperature matrices. Here the life times of the reactive intermediates, which exist only transiently under standard conditions are greatly extended and can be studied using a range of conventional spectroscopic techniques. Unfortunately kinetic studies are impossible using this technique. Nevertheless the development of pulsed laser flash photolysis made it possible to study the photochemistry of transient intermediates under ambient conditions. The limitation of UV-vis monitored flash photolysis technique is that structural information about the intermediate is unavailable, however its strength is that it enables useful kinetic data about the photochemical process to be obtained.

1.5 Properties of electronically excited states

The photochemical investigations of organometallic complexes have been fewer than those of classical inorganic co-ordination complexes. However this situation has been changing rapidly in the last three decades. In part this is due to the demonstrated importance of this chemistry, since organometallic complexes have proven to be extremely useful reagents for catalysing or assisting a large number of organic transformations. Also there have been significant advances in the field of electronic spectroscopy and hence organometallic reaction mechanisms. The dynamics and the reactivity of different excited electronic states of organometallic complexes are now

routinely monitored with numerous sophisticated experimental techniques, as discussed in Section 1.7. The photochemistry of most organometallic complexes differs from that of inorganic co-ordination complexes because in general the quantum yields for dissociation of organometallic species are high while those of co-ordination complexes are low. A considerable amount of information is available about organometallic intermediates but little is known about the electronically excited states from which the intermediates are formed.

Organometallic complexes in the excited states undergo a number of different chemical reactions. These are sometimes the counterpart of the thermal reactions, but in many cases the photochemical pathway is anti-thermal. The behaviour of an electronically excited molecule with an extremely short lifetime has a number of features that diverge from those of ordinary chemical species. In part, this is because only very fast reactions can participate. Such molecules, by virtue of their electronic excitation have an excess of free energy about the equilibrium, they often have a different structure, at least with respect to small changes in bond lengths and angles. Most importantly, specific bond weakening in an excited state may cause greatly enhanced chemical activity. Knowledge of excited states is important for an understanding of why particular intermediates are generated and of the wavelength dependence of photochemical pathways.

1.6 Classification of the excited states encountered in this study

It is convenient to describe the electronic transitions of organometallic complexes in three categories.

1 Those primarily centred on the metal orbital (MC or Ligand field, LF: $d \rightarrow d$)

2 Charge transfer (CT) types involving the electrons on the central metal and the ligands. The charge transfer process can be further subdivided into charge transfer from the metal-to-ligand (MLCT: $d \rightarrow \pi^*$), ligand to metal (LMCT: σ_L or $\pi_L \rightarrow d^*$) and metal-to-solvent charge transfer (MSCT).

3 Those primarily centred in the ligand orbitals (LC: $\pi \rightarrow \pi^*$)

Problems begin with unequivocal assignment of the excitation since differentiation between metal centred (d → d) and charge transfer (CT) transitions find only limited application to organo-transition metal complexes.

1.6.1 Metal centred / Ligand field transitions

Covalent bonding dominates the bonding found in organometallic complexes. As previously discussed in Section 1.3, the d-orbitals are significantly involved in the metal-ligand bond. Therefore electronic transitions originating and/or terminating in the d-orbitals in organometallic complexes have a significant perturbation on the metal-ligand bond. Consequently it is known that excitation into ligand field states of an octahedral complex (e.g. $Cr(CO)_6$) often brings about efficient ligand dissociation particularly in complexes containing a carbonyl ligand. This may be explained by the fact that a d-d transition is from a filled t_{2g} orbitals of π bonding with respect metal-carbon monoxide bond, to the empty e_g orbitals of σ symmetry and strongly σ-anti-bonding with respect to the metal-carbon monoxide bond. The transition results in substantial labilisation of the metal-carbon monoxide bond, which is a result of both the depopulation of the π bonding levels and population of the σ-anti-bonding orbital, the latter appearing to be the most consequential. The covalency and hence the ligand character of these orbitals allows a relaxation of the selection rules. This results in relatively high molar absorptivities for ligand field transitions of organometallic complexes far exceeding those of metal ions.

1.6.2 Charge transfer transitions

1 Metal-to-ligand charge transfer

A metal-to-ligand charge transfer (MLCT) results from movement of a metal electron from a filled d-orbital on the metal to an empty π-orbital on the ligand. These transitions are commonly observed in organometallic complexes because of the low-valent nature of the metal centre and the low energy positions of the π-acceptors orbitals

in many ligands. The depopulation of a filled d-orbital on the metal and the population of the ligand localised orbital is believed to have little influence on the metal-to-ligand bond, explaining why MLCT transitions are not followed by dissociative photochemistry. In addition, on transferring an electron from the metal to the ligand, the metal becomes cationic and the ligand anionic, generating an electrostatic attraction between them, which may make the bond more inert. Such transitions may be valuable as the introduction of a similar ligand with lower-lying acceptor to a complex will interfere with the ligand field transition, creating an inert complex with respect to photo-substitution or vice verse, thereby enabling the 'tuning' of the photochemical behaviour for particular applications.

2 Ligand-to-metal charge transfer

Such excited states have relatively little importance to organometallic chemistry, as it requires the complex to have low-lying unoccupied metal acceptor orbitals and an easily oxidised ligand. Unfilled d-orbitals are placed at high energy due to the high ligand field strengths associated with organometallic complexes. The number of unequivocally LMCT assignments is relatively few and there seem to be few claims that such organometallic excited states are photo-reactive.

3 Metal-to-solvent charge transfer

Metal-to-solvent charge transfer, (MSCT) originates from the electronic transitions from metal-centred orbitals and terminates in solvent localised orbitals. This tends to result in oxidation of the metal complex and reduction of the solvent. The energy positions of these states are governed by the ease of reduction of the solvent and the ease of ionisation of the metal complex. Only a few MSCT states have been characterised for organometallic complexes and these have usually been in halocarbon solvents. Ferrocene is one example of a complex that exhibits such a transition. Irradiation into the MSCT absorption results in efficient photo-oxidation of the complex, while in poor acceptor solvents there is no reaction.

1.6.3 Ligand centred transitions

Intraligand (IL) or ligand centred (LC) photochemistry: organic ligands, which can be co-ordinated to metals, have their own set of excited states. Frequently, the $\pi \rightarrow \pi^*$ transitions of free ligands are only slightly perturbed by co-ordination of the ligand to transition metal.[22] As a consequence, organometallic complexes have ligand localised excited states which are not too dissimilar to those of the free ligand. Thus comparing the spectrum of the complex with the spectrum of the free ligand can usually identify the spectral bands associated with IL/LC transitions. However, when the intra-ligand transition arises from an orbital involved in the ligand bonding it is usually of very different character from the free ligand transition. For complexes having positively charged metal centres the spectrum of the protonated ligand may provide a better comparison.[23]

1.7 The study of short lived intermediates

Inherent in any photochemical process is the generation of molecules in the excited states and the formation of highly reactive short-lived intermediates. One of the major problems is how to study molecules in excited states and how to characterise the highly reactive intermediates generated photochemically, many of which have lifetimes of pico-seconds or less. A variety of techniques have been developed to elucidate the structures and kinetics of these short-lived intermediates.

1.7.1 Low Temperature Matrix Isolation

One method to record the spectra of short-lived transient species in reactions is to increase their lifetime by a method known as matrix isolation. The father of this technique was George Pimentel.[24] Basically, the technique involves the low temperature trapping of isolated guest molecules in a large excess of an inert rigid host material, the matrix. The reactive intermediate(s) is usually generated by photolysis of the sample *in situ*. Diffusion of the trapped species is prevented because of the low temperatures used and therefore the possibility of bimolecular reactions is avoided, except those with the host matrix, which may be a reactive gas. The probability of unimolecular decomposition is greatly reduced provided that the sample is in sufficiently high dilution (~1:1000) in the matrix gas(es) and that the temperature is kept low (12-20 K for most matrix host materials).

Once trapped within the matrix, the lifetime of the reactive intermediate, which exists only transiently under standard conditions, is greatly extended. These stabilised intermediates can examined by conventional spectroscopic methods such as UV-vis, Raman[25], photoelectron[26] (PES), or M¬ssbauer[27] spectroscopy during the reaction. However, infrared and UV-vis spectroscopy are the methods most commonly used. Typical host materials are frozen inert gases such as nitrogen, methane or noble gases, primarily argon, these requiring temperatures in the region of 10-20 K.[28] Nevertheless it is known that the photo-fragment may interact with the inert matrix material and

known examples include $Cr(CO)_5N_2$,[29] $Cr(CO)_5Ar$[29] and $Fe(CO)_4(CH_4)$.[30] Mixed matrix experiments and comparison with spectra of stable species revealed that the shifts in spectra are due to specific interactions between the photo-fragment and the matrix species occupying the co-ordination site. Kinetic information cannot be obtained from matrix isolation experiments due to the very restrictive temperature range and limited diffusion. Another restrictive aspect of matrix isolation is that the vapour pressure of the complex to be investigated must be sufficient to permit the complex to be transferred to the matrix in the vapour phase, with no decomposition of the vapour before condensation on the cold window. Also the solid matrix 'cage' ('cage effect')[31] can effectively block some pathways in photochemical reactions by preventing the reactant species escaping, thus promoting the recombination processes.

1.7.2 Low temperature solution and liquid noble gases

Another way to study photochemical reactions of carbonyls or other species without the necessity for such extreme low temperatures and high vacuum is the use of glassy media such as hydrocarbons[32] at liquid nitrogen temperature (77 K) and more recently the use of cast polymer films[33] and liquefied noble gases.[34] The advantage of these media is that the complexes to be investigated do not need to be volatile. The reaction in these media may be viewed as being slowed down rather than paused, as is the case with matrix isolation. However, these techniques do introduce some added limitations, as hydrocarbon solvents and polymer films have absorptions in the infrared, which may mask the bands of the species under investigation. Also the infrared bands tend to be broader, which reduces their value for structural characterisation since overlapping features may easily be missed. Furthermore, it has been shown that the polymer films are not quite inert, and can interact significantly with the unsaturated intermediates produced upon photolysis.[86] Low temperature solution studies in liquid noble gases have proved very valuable in this area of low temperature solution work, as they combine great chemical inertness with unrivalled spectroscopic transparency, which allows detection of weak absorptions. The low temperature solvent method thus permits the study of novel photogenerated species, however a limiting factor is that the species

have to be relatively stable, which therefore precludes the examination of highly reactive intermediates including co-ordinately unsaturated species. As the reactive species are being studied in a liquid environment, it is possible to monitor kinetics and by measuring kinetic changes with temperature, to extract thermodynamic information. However gaining kinetic information in this media is very limited due to the restrictive temperature range available and limited diffusion. Neither matrix isolation nor low temperature solution is easily applicable to charged species.[35]

1.7.3 Solution Phase Flash Photolysis

The basic principle of flash photolysis have not changed much since the original experiments by Nobel prize winners Norrish and Porter,[36] but the duration of the flash and the speed of apparatus for detection have changed greatly.[37]

In general, when a short duration pulse of high intensity light from an UV source (flash photolysis) is absorbed by a sample, a relatively high concentration of excited molecules and/or free radicals are formed. The concentration of the reactive intermediate is monitored by means of a second light source producing a longer less intense flash of light at a wavelength, which is absorbed by the species under investigation. The time resolution of the flash photolysis experiments is governed by the duration of the flash, which can be anything from microseconds with the use of plasma flash lamps to as short as pico-seconds or even femto-seconds with pulsed lasers. Figure 5-1 (chapter five) shows the outline of a flash photolysis set-up.

1.7.3.1 Detection by UV-vis spectroscopy

Using UV-vis detection an absorption spectrum over the complete wavelength range can be recorded at a particular time interval. Alternatively a single selected wavelength from the absorption spectrum can be recorded and kinetic data is obtained. Used in a point-by-point manner, at any selected time interval after the flash, the UV-vis spectrum of the transient species may be acquired. Kelly and Körner von Gustorf[38] were the

pioneers of using flash photolysis with UV-vis detection to monitor the photo-fragments of $Cr(CO)_6$ produced following irradiation. Metal carbonyl intermediates in solution are quite easily detected, quantum yields for their formation are high and their UV-vis absorptions are intense. Flash photolysis with UV-vis detection is effective in establishing the broad outline of the photochemistry of particular metal carbonyls through kinetic data. However it rarely provides any significant structural information because UV-vis spectroscopy has severe limitations when applied to organometallic species. These limits arise from the general broadness and lack of resolvable fine structure in the electronic absorptions of most organometallic species. Identification of the transient species has to rely mainly on kinetic consistency unless further evidence is available from complimentary spectroscopic data such as matrix isolation.

1.7.3.2 Detection by Time-Resolved Infra-Red (TR-IR) Spectroscopy

This method of detection coupled with flash photolysis was developed by Pimentel *et al.*[39] The conventional nano-second TR-IR system uses a flash photolysis pump-probe technique where transient species are generated by a laser pulse and the resulting solution is then probed by a continuous infrared probe source operating at a single (but tuneable) infrared frequency monitored by a fast-rise time diode detector. Therefore, the frequency must be re-tuned and the experiment repeated. By repeating the experiment numerous times, data are accumulated at frequencies across the region of interest (i.e. carbonyl region 2200-1750 cm^{-1}) in a point-by-point manner. Thus in the TR-IR spectrum, bands due to parent appear as negative absorption, bands due to products appear as positive absorption and static infrared absorption, due to solvent do not register, because their absorption does not vary. TR-IR detection allows structural information to be gathered without the loss of kinetic data, it also can be applied to both the solution and the gas phase. The UV-vis detection method nevertheless, remains superior over TR-IR for kinetic data at short time basis.

Two other methods of TR-IR exist, one utilises step scan FT-IR detection techniques, which allow much easier data collection over wide frequencies and the third type

involves an ultra-fast laser pump source with an infrared probe-pulse generated in conjunction with the excitation pulse. In this set-up, temporal responses are determined by differences between the pump and probe light beam path length. In contrast to UV-vis detection, light absorption by hydrocarbon solvents in the infrared must be taken into account as they are not negligible and this results in the optical path length being restricted to 1-2 mm.

1.7.4 Gas Phase flash photolysis

Time-resolved absorption spectroscopy has become a probe for co-ordinatively-unsaturated metal carbonyls in the gas phase due to the advances in light sources and detectors. Gas phase studies require very fast detection systems (sub-nanosecond spectroscopy to study primary photoproducts). This requirement arises because kinetic reactions in the gas phase are usually one to two orders of magnitude faster than the corresponding diffusion controlled reactions in solution (diffusion limit ~10^9-10^{10} $M^{-1}s^{-1}$ [40]). The gas phase allows the study of metal carbonyl photochemistry free of perturbing solvents or matrixes. Weitz, Seder and Ouderkirk[41] have described this as investigating the 'naked' unsaturated species. It has been proven that metal carbonyls in solution co-ordinate with the solvent on very short time scale and thus the structure of these species may distort the 'naked' co-ordinatively-unsaturated species. Comparison of gas phase studies to solution studies will help to determine whether or not it is possible to have a solvent that is truly non co-ordinating.

Gas phase allows for real-time kinetic information to be obtained on co-ordinatively unsaturated intermediates and also offers a far richer photochemistry than is solution.[42] In the gas phase there is a possibility for multiple carbon monoxide dissociation[43] from the metal carbonyl after the absorption of a single UV photon, as observed in the case of $Cr(CO)_6$, where $Cr(CO)_5$ were produced. The ejection of a second ligand with one photon is prevented in solution due to dissipation of the excess energy of the photon by the relaxation of the internal vibration-rotation energy through collisions with the solvent environment. In the gas phase collisions are the principal pathway for the loss

of excess energy. In the gas phase photolysis, the mean time between collisions is relatively long and the excess energy cannot be lost before the loss of further carbon monoxide ligands occurs.

1.8 Photochemical metal carbonyl substitution

The primary photo-induced photoreaction of metal carbonyls involves decarbonylation. UV or visible light accelerates substitution reactions of metal carbonyls. The rate constant for the dissociation $Cr(CO)_6 \rightarrow Cr(CO)_5 + CO$, which precedes the entrance of a new ligand L, is increased upon photochemical excitation $Cr(CO)_6 \rightarrow Cr(CO)_6^*$ by a factor of 10^{16}.[44]

The labilisation of carbon monoxide has been explained by referring to the molecular orbital diagram in Figure 1-2. The highest occupied orbital subset is the t_{2g} orbitals and the lowest unoccupied orbitals are the e_g. The ligand-field transition from a filled t_{2g} $(\pi) \rightarrow e_g(\sigma^*)$ which leads to the depopulation of an metal-carbon monoxide bonding and the population of an metal-carbon monoxide anti-bonding molecular orbitals. This transition results in substantial labilisation of the metal-carbon monoxide bond.

Current understanding of the photochemical reactions of organometallics has been based on molecular orbital diagrams coupled with the analysis in terms of the bonding and the anti-bonding character of the orbitals involved. Conceptually, this type of analysis is very appealing since it is very simple and certainly useful, but it suffers from some draw backs as outlined by Veillard,[45] one of these being that it does not easily explain the existence of concurrent photochemical reactions observed at a given wavelength. A number of reports in the literature reveal a photochemical reaction being observed upon excitation at different wavelengths. This seems difficult to interpret on the basis that the photo-cleavage of a bond result from exciting an electron from the bonding to the anti-bonding i.e. from excitation into a single electronic state.

However, recent publications by Rosa, Baerends *et al.*,[46] review the role of the ligand field excited states in the photochemical dissociation of metal-carbon monoxide bonds in metal carbonyl compounds, using density functional calculations performed on the excited states of $Cr(CO)_6$. The important implication, which is also relevant for other complexes, is that photochemical metal-carbon monoxide dissociation may take place regardless of the nature of the excited states into which the excitation takes places at equilibrium geometry. The orbital energies suggest that the ligand field states are not the lowest states in the excitation spectrum, that the lowest excitations are calculated to be sets of symmetry forbidden charge transfer (CT) excitations. Carbon monoxide dissociation occurs due to high-lying ligand field states descending rapidly upon metal-carbon monoxide bond lengthening, and crossing with non-dissociative lower states. Since this appears to be a general mechanism, carbon monoxide dissociation occurs generally, with little or no relation to the nature of the lowest excited state at ground state equilibrium. The accepted picture that metal-ligand dissociation occurs from a ligand field excited state, is based on an underlying assumption, namely that ligand field states are dissociative, is fully corroborated by Baerends' calculations. Even if they are too high to be populated directly by irradiation into the lowest absorption band, they are actually so strongly dissociative, that they cross so soon with the lowest excited states that the lowest excited state potential energy curve (PEC) becomes dissociative. They conclude that it is not necessary to excite to ligand field states in order to induce photo-dissociation of ligands, but that the dissociation may also occur from the CT states. The observed photo-activity may therefore not be used for assigning the low energy absorption to ligand field excitation.

1.9 Brief literature review of the photochemistry of (η^6-arene)$Cr(CO)_3$

The chemistry of chromium arene complexes had been studied in some considerable detail and has now become textbook material.[44] Two photosubstitution paths for (η^6 arene)$Cr(CO)_3$ complexes have been reported in the work by Strohmeier *et al.*[47] who claimed that both carbon monoxide loss and arene exchange[48] were the general photoreactions, these are outlined in Reaction 1-1 and Reaction 1-2.

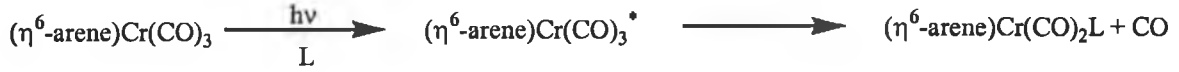

Reaction 1-1

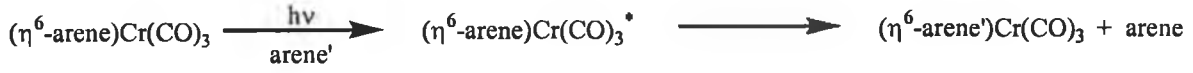

Reaction 1-2

As with other metal carbonyls, the co-ordinatively unsaturated intermediates generated by photolysis of (η^6-arene)$Cr(CO)_3$ can be involved as intermediates in redox reactions generally resulting in an oxidised central metal,[49] Reaction 1-3. Non-destructive oxidation addition to the (η^6-benzene)$Cr(CO)_2$ intermediate also appears to be possible,[50] Reaction 1-4.

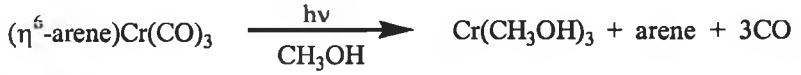

Reaction 1-3 Oxidation addition reaction.

Reaction 1-4 Non-destructive oxidation reaction.

The spectral changes which occur during continuous irradiation of (η^6-arene)$Cr(CO)_3$ in cyclohexane solution have been described by Yavourskii *et al.*[51] and Trembolver *et*

al.[52] Their conclusions were that the spectral data are compatible with formation of the uncomplexed arene and $Cr(CO)_6$ during the reaction. Quantum yield determinations by Trembolver *et al.*[52] as a function of light intensity led to the proposal of the simultaneous occurrence of three photo-decay processes with different dependencies on light intensity. However, no conclusions about the detailed photolytic reactions were reached.

The product yield for the carbon monoxide substitution reaction, Reaction 1-1, is very high. Nasielski and Denisoff[53] undertook the task of determining the quantum yield for the substitution of carbon monoxide by *N*-n-doecylmaleimide, upon photolysis of (η^6-mesitylene)$Cr(CO)_3$ in benzene. The quantum yield was high, $\phi = 0.9 \pm 0.09$ at $\lambda_{exc.} = 313$ nm. No detectable mesitylene–benzene exchange was observed. The examination by Wrighton and Haverty[54] of the photosubstitution of (η^6-arene)$Cr(CO)_3$ according to Reaction 1-1, in which the arene is benzene or mesitylene and the ligand, L is pyridine found that the quantum yield for the formation (η^6-arene)$Cr(CO)_2$(pyridine) was 0.72 ± 0.07. The data from these experiments show that the quantum yield efficiency is independent of the wavelength ($\lambda_{exc.} = 313$, 366 or 436 nm), arene, entering group and entering group concentration. The high overall product yields for Reaction 1-1 led to questions about the importance of Reaction 1-2.

Photoinduced carbon monoxide substitution of (η^6-benzene)$Cr(CO)_3$ was also studied by Gilbert *et al.*,[55] who confirmed the quantum yield values of Wrighton and Haverty[54] in addition to reporting that the quantum efficiency of arene exchange, Reaction 1-2 is approximately a sixth of the value for the quantum yield of carbon monoxide substitution (i.e. $\phi = 0.12$). Gilbert *et al.'s*[55] flash photolysis of (η^6-benzene)$Cr(CO)_3$ in cyclohexane solution revealed a weakly absorbing species immediately after the flash, which reacted further within the first millisecond to form a second transient species, which absorbed throughout the visible spectrum ($\lambda_{max.}$ ~500 nm). The presence of 1.1×10^{-1} M benzene in the solution did not alter the concentration or the rate of reaction of either species. However, the formation of both species is strongly suppressed if the

solution is saturated with carbon monoxide. These observations led Gilbert *et al.*[55] to propose that the first species observed is (η^6-benzene)$Cr(CO)_2$ and that exchange with benzene involves this intermediate and does not occur through a one step dissociation of the excited state molecule to give $Cr(CO)_3$ and benzene. Results obtained by Gilbert *et al.*[55] conflicted with the original proposals of Strohmeier and von Hobe.[48] The nature of the second transient species formed during flash photolysis was not discussed by Gilbert *et al.*[55]

A subsequent investigation of the photochemistry of (η^6-benzene)$Cr(CO)_3$ and (η^6-toluene)$Cr(CO)_3$ by Bamford *et al.*[56] concurred with the proposal by Gilbert *et al.*[55] of arene exchange occurring *via* the (η^6-benzene)$Cr(CO)_2$ intermediate. However, because the evolution of arene from (η^6-arene)$Cr(CO)_2$ is not a simple dissociation Bamford *et al.*[56] proposed a possible explanation involving a more complex route as outlined in Scheme 1-2. The formation of complex (I) formed by the reaction outlined in Scheme 1-2, was suggested to account for the second transient species observed by Gilbert *et al.*[55] in their flash photolysis study, since secondary photo-decomposition of complex (I) could lead to $Cr(CO)_6$, which is the reported end product.

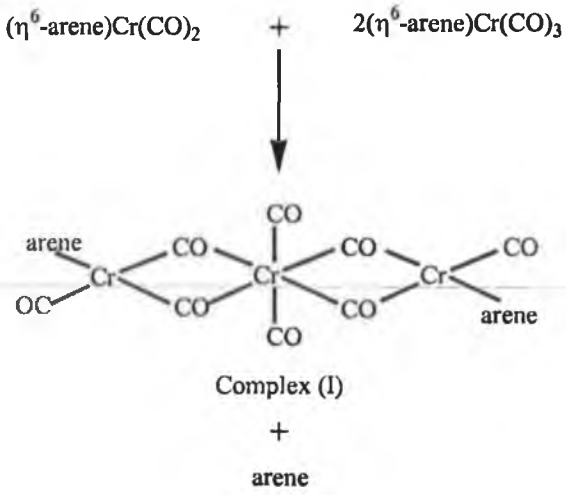

Scheme 1-2 Formation of complex (I) as proposed by Bamford.[56]

The first matrix isolation experiments on (η^6-arene)$Cr(CO)_3$ in argon, methane and dinitrogen gas matrices at 12 K were carried out by Rest *et al.*[57] The changes induced by photolysis were monitored by means of infrared spectroscopy. New bands in the carbonyl region of the infrared spectrum at 1938 and 1885, 1925 and 1870, and 1940 and 1896 cm^{-1} in argon, methane and dinitrogen matrices respectively were attributed to the formation of the dicarbonyl intermediate (η^6-benzene)$Cr(CO)_2$. In the case of photolysis of (η^6-benzene)$Cr(CO)_3$ in the dinitrogen matrix, there was also evidence of interaction of the matrix with the dicarbonyl fragment, leading to the formation of (η^6-benzene)$Cr(CO)_2(N_2)$ (ν_{NN} stretch at 1896 cm^{-1}). No evidence was obtained in these experiments for the ejection of the arene ligand, to give the $M(CO)_3$ fragment and the primary photolysis step was readily reversed by visible light.

Bitterwolf and co-workers[58] experiments involved the use of glassy hydrocarbons or nujol mulls at 77 K. They reported that photolysis of (η^6-benzene)$Cr(CO)_3$ yielded the carbon monoxide loss fragment, (η^6-benzene)$Cr(CO)_2$. Annealing the matrix and long wavelength irradiation reversed carbon monoxide loss to yield the original complex. Dinuclear complexes were also formed upon initial photolysis or annealing. These dinuclear products are believed to be due to the reaction of the dicarbonyl products with the unphotolysed parent material as outlined in Reaction 1-5.

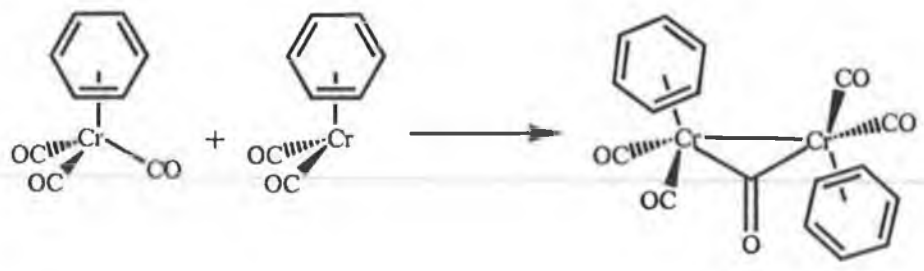

Reaction 1-5 Reaction of the dicarbonyl photoproduct with the unphotolysed parent material in hydrocarbon glasses at 77 K.

In the gas phase,[59] photolysis of (η^6-arene)$Cr(CO)_3$ at $\lambda_{exc.}$ = 355 nm, induced the formation of the dicarbonyl species (η^6-arene)$Cr(CO)_2$, identified by time-resolved infrared spectroscopy. However, shorter wavelength photolysis at $\lambda_{exc.}$ = 266 nm leds to

the formation of mono-and-dicarbonyl species (η^6-arene)Cr(CO) and (η^6-arene)$Cr(CO)_2$ in a ratio 5:2. The reactivity of co-ordinatively unsaturated species is demonstrated by Zheng *et al.*[60], who observed the addition of N_2 and H_2 to the dicarbonyl fragment, (η^6-arene)$Cr(CO)_2$, forming (η^6-arene)$Cr(CO)_2(H_2)$ and (η^6-arene)$Cr(CO)_2(N_2)$ respectively. The position of the carbon monoxide absorption bands in the infrared spectra of the dihydrogen and the dinitrogen complexes are very close to those found in the condensed phase, thereby indicating that the interaction of H_2 and N_2 to the metal centres in both phases is similar.

The primary photoproduct of the photolysis of (η^6-arene)$Cr(CO)_3$ following flash photolysis was identified as (η^6-arene)$Cr(CO)_2$(S) (S = alkane solvent).[55] The reactivity of this primary photoproduct was shown to be affected by the nature of the solvent.[61] The solvated dicarbonyl reacts with carbon monoxide to yield the parent tricarbonyl more than twice as fast in heptane as it does in cyclohexane. Furthermore, the number and the size of the alkyl substituent on the arene ligand can introduce a greater degree of steric control over the sixteen-electron intermediate.[62] This work also demonstrated[62] that in determining the second order rate constant for the reaction of the sixteen electron species with carbon monoxide, the entropy term ($\Delta S^{\ddagger}$) is more diagnostic of reactivity, as no variation in the enthalpy ($\Delta H^{\ddagger}$) of activation was observed, irrespective of the substituent on the ring.

Strohmeier and von Hobe[48] observed photochemically induced arene exchange, and the quantum yield was determined by Gilbert *et al.*[55] as previously discussed, but there had been suggestions[63,64] that this may have been due to a possible decrease of hapticity of the benzene ligand on irradiation. However no success in confirming this photoinduced haptotropic shift was observed until Long *et al.*[65] resorted to molecules for which an intramolecular trapping of the primary product is possible. Instead of using η^6-arenes, they focused on complexes with an η^6-co-ordinated pyridine ligand (η^6-$X_2C_5H_3N$)$Cr(CO)_3$ (X = H, CH_3, or $(CH_3)_3Si$). This ligand contains a built in donor functionality, the nitrogen atom, which can easily co-ordinate to the metal as soon as ring slippage occurs. Experiments showed that two parallel photo-process occurred

upon the irradiation of $(\eta^6\text{-}X_2C_5H_3N)Cr(CO)_3$ as outlined in Reaction 1-6 and Reaction 1-7 shown below.

$$(\eta^6\text{-}X_2C_5H_3N)Cr(CO)_3 \underset{}{\overset{h\nu}{\rightleftharpoons}} (\eta^1\text{-}2,6\text{-}X_2C_5H_3N)Cr(CO)_3 \quad (a)$$

$$(\eta^1\text{-}2,6\text{-}X_2C_5H_3N)Cr(CO)_3 + 2CO \longrightarrow (\eta^1\text{-}2,6\text{-}X_2C_5H_3N)Cr(CO)_5 \quad (b)$$

Reaction 1-6 Low energy photolysis ($\lambda_{exc.}$ = 460 nm) in low temperature matrixes induced a hapticity shift from $\eta^6 \rightarrow \eta^1$ co-ordination.

$$(\eta^6\text{-}X_2C_5H_3N)Cr(CO)_3 \underset{S}{\overset{h\nu}{\rightleftharpoons}} (\eta^6\text{-}X_2C_5H_3N)Cr(CO)_2(S) + CO$$

Reaction 1-7 High-energy photolysis ($\lambda_{exc.}$ = 308 nm) in a low temperature matrix induced the carbon monoxide dissociation product as well as the ring-slipped product predominant at low energy photolysis, Reaction 1-6(a).

The photochemistry of these systems displayed a wavelength dependency. The hapticity change was dominant following low energy photolysis with visible light. However high energy photolysis with UV light induced both a hapticity change and carbon monoxide dissociation, Reaction 1-7.

1.10 Brief literature review of the thermal chemistry of $(\eta^6\text{-arene})Cr(CO)_3$

The dominant photochemical process for $(\eta^6\text{-arene})Cr(CO)_3$ results in the formation of a solvated dicarbonyl species. In contrast to it's photochemical behaviour, $(\eta^6\text{-arene})Cr(CO)_3$ is found to yield an arene exchange product upon heating. The replacement of one arene by another can be attributed to the greater stability of one over the other due to increased electron donating capability of the ligand. This situation is reflected in the greater ease of displacement with increasing alkyl substitution on the incoming arene.

The initial kinetic studies of arene exchange in hydrocarbon solvents were the ^{14}C-labelled exchange results of Strohmeier *et al.*[66] The exchange reaction took place between ^{14}C–labelled benzene, toluene and chlorobenzene (arene*) with their correspondingly unlabelled (η^6-arene)$Cr(CO)_3$ complexes, as outlined in Reaction 1-8.

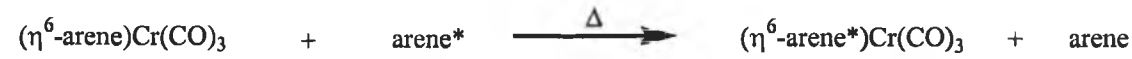

Reaction 1-8

The rate was found to be second order in (η^6-arene)$Cr(CO)_3$ and approximately one third order in benzene. This result was interpreted in terms of two rate determining steps refer to Scheme 1-3; a fast step that is second order in (η^6-arene)$Cr(CO)_3$ and a slow step that is first order in both (η^6-arene)$Cr(CO)_3$ and arene. [66] On the basis of their initial rate measurements Strohmeier *et al.* obtained the rate law outlined Equation 1-1.

$$-d[(arene^*)Cr(CO)_3]/dt = k_2[(arene)Cr(CO)_3]^2 + k_2'[(arene)Cr(CO)_3][(arene^*)]$$

Equation 1-1 Rate law as outlined by Strohmeier *et al.*,[66] where arene* denotes the ^{14}C-labelled arene.

However Scheme 1-3 was criticised on a number of counts, as it failed to account for the acceleration of the reaction rates in the presence of a co-ordinating ligand as observed by Mahaffy and Pauson's[67] and Willeford and co-workers.[68] Furthermore Scheme 1-3 is not compatible with the observation of Jackson *et al.*[69] that cis-trans complexes of 1, or 2-methylindane failed to isomerise on heating in the absence of free arene.

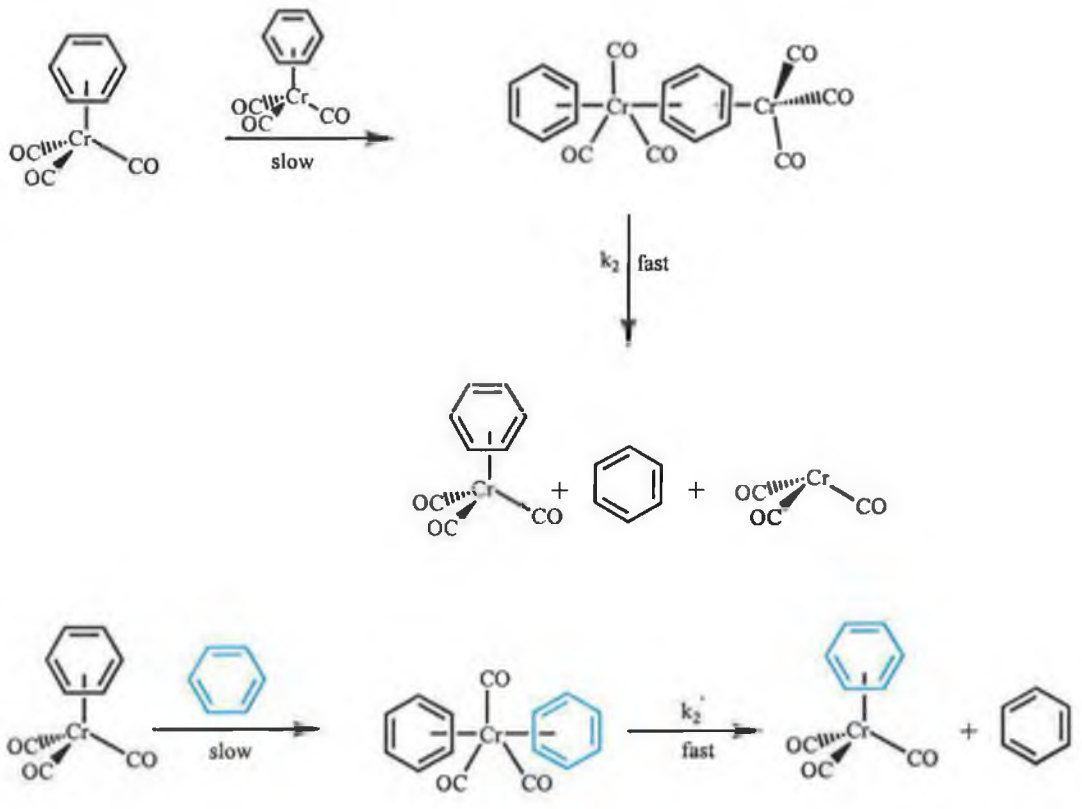

Scheme 1-3 Mechanism proposed by Strohmeier *et al.*[66]

Mahaffy and Pauson[67] postulated an alternative mechanism for arene exchange, refer to Scheme 1-4, where partial displacement of the arene ($\eta^6 \rightarrow \eta^4$) from the metal was initiated by the co-ordinating solvent. In the absence of a co-ordinating solvent Traylor and Stewart[70] have proposed that a second molecule of the (η^6-arene)$Cr(CO)_3$ complex could catalyse the reaction by co-ordination through the oxygen of a carbonyl group.

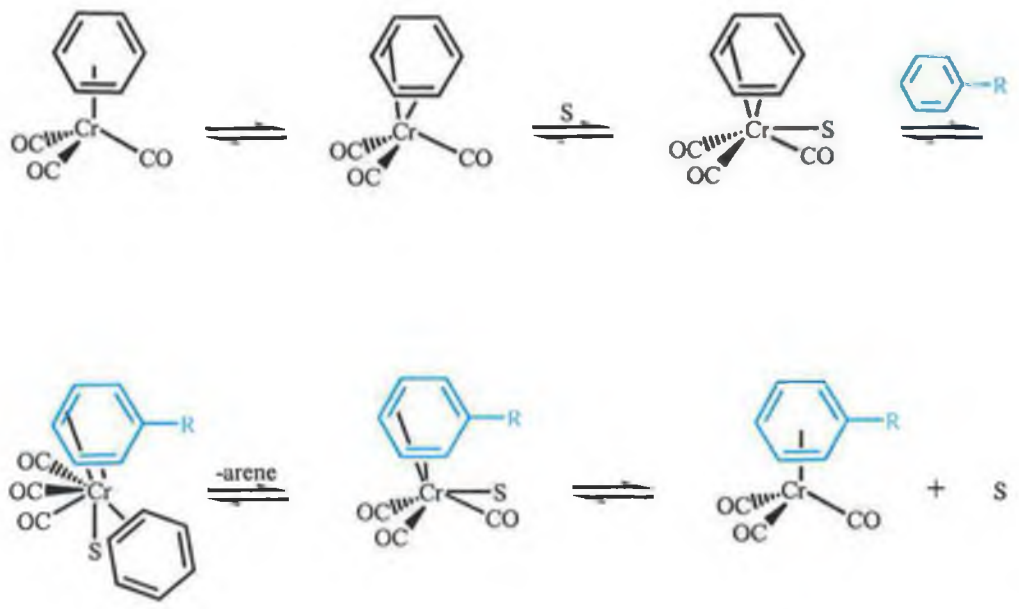

Scheme 1-4 Solvent initiated arene exchange mechanism proposed by Mahaffy and Pauson.[67]

Mahaffy and Pauson[67] reported that resistance to arene exchange of (η^6-arene)-tricarbonyl complexes of chromium decrease in the order hexamethylbenzene > mesitylene > *N*,*N*-dimethylaniline ≥xylene > toluene = benzene > chlorobenzene >> naphthalene. This order of reactivity clearly displays that electronic factors govern the reactivity of these types of complexes, such that more electron-rich arenes give more unreactive complexes, and thermal stability shows similar trends.

On account of the importance of formation and displacement of transition metal π bond display in catalysis, there has been a significant interest in the study of this type of complex. Traylor and his research group[70,71] carried out extensive investigation into the thermal arene exchange reaction during the 1980s, and have clarified aspects of the rate laws and the arene exchange process involving monocyclic substrates. The nature of the second order dependence of Equation 1-1 was queried. When an inert Cr complex is added a first order dependence on the added complex is observed.[70] It appears now that the true second order term should be, $k_2[(arene)Cr(CO)_3][\{(arene)Cr(CO)_3\}\{(arene^*)Cr(CO)_3)]$. Therefore, in the absence of

a co-ordinating solvent, the reaction is likely to be self-catalysed, (i.e. the carbon monoxide group operates as a nucleophilic catalyst). The intermediate is postulated to be dimeric,[71(c)] possibly bridging in nature, because of the capability of carbon monoxide to act as a bridging ligand.

Arene exchange on poly-cyclic chromium tricarbonyls was established as being much more facile[72] than in monocyclic complexes due to the relative favourable energies of ring-slippage to generate an η^4-arene intermediate, which results in the retention of the aromaticity in the uncomplexed ring. Kinetic results on the un-catalysed arene exchange of poly-cyclic and heterocyclic substrates were published by Howell, Albright and co-workers,[73] wherein they introduce the results of molecular orbital calculations at the extended Hückel level in order to discriminate between a variety of mechanistic choices. Potential energy surfaces were constructed for ring-slippage in benzene, naphthalene, and pyrene chromium tricarbonyl complexes. There is lower potential energy required for slipping the $Cr(CO)_3$ along an $\eta^6 \rightarrow \eta^1$ path in the case of pyrene, whereas it requires less energy to attain an $\eta^6 \rightarrow \eta^4$ path in the naphthalene system. The predicted arene lability was calculated to be in the order benzene << naphthalene << pyrene.

1.11 Brief literature review of photochemistry of (η^5-cyclopentadienyl)$Mn(CO)_3$

Cyclopentadienyl manganese tricarbonyl is isoelectric with the previously discussed (η^6-arene)$Cr(CO)_3$ system and substitution of carbon monoxide ligands by a variety of reagents can be achieved almost exclusively through the photochemical process.[74] The thermal dissociation of (η^5-C_5H_5)$Mn(CO)_3$ into (η^5-C_5H_5)$Mn(CO)_2$ occurs at such high temperatures that most of the substituted complexes thus formed decompose readily.[75] Consequently the majority of synthesis of the substitution products (η^5-C_5H_5)$Mn(CO)_2L$ have been carried out using photochemical procedures.[76] A common technique is to carry out the photolysis in tetrahydrofuran (THF), which yields the labile complex (η^5-C_5H_5)$Mn(CO)_2$(THF). Subsequently, the solvent can be displaced by the addition

of the appropriate ligand, L, without further irradiation.[77] Alternatively direct irradiation of $(\eta^5\text{-}C_5H_5)Mn(CO)_3$ in the presence of a photostable ligand may be performed in hydrocarbon solvents, but this method is prone to side reactions and decomposition during photolysis.[76,78] The co-ordinatively unsaturated intermediate $(\eta^5\text{-}C_5H_5)Mn(CO)_2$ is susceptible to oxidation addition,[50] like the $(\eta^6\text{-arene})Cr(CO)_2$ analogue.

Rest *et al.*[57] provided infrared spectroscopic evidence for the formation of the co-ordinatively unsaturated species $(\eta^5\text{-}C_5H_5)Mn(CO)_2$ upon the UV photolysis of $(\eta^5\text{-}C_5H_5)Mn(CO)_3$ in argon, (ν_{CO} = 1972 and 1903 cm^{-1}) methane (ν_{CO} = 1961 and 1893 cm^{-1}) and dinitrogen, $(\eta^5\text{-}C_5H_5)Mn(CO)(N_2)$ (ν_{CO} = 1979 and 1927 cm^{-1}, ν_{NN} = 2173 cm^{-1}) low temperature matrices at 12 K. Long wavelength irradiation following the initial photolysis did not reverse the primary photo-reaction, which is in contrast to the results of $(\eta^6\text{-arene})Cr(CO)_3$ under similar conditions. The infrared band positions for the $(\eta^5\text{-}C_5H_5)Mn(CO)_2$ in argon and methane matrices agree well with those of the previously published by Braterman and Black[79] for $(\eta^5\text{-}C_5H_5)Mn(CO)_3$ in a methylcyclohexane nujol glasses at 77 K. No evidence was obtained for the ejection of the cyclopentadienyl ligand from $(\eta^5\text{-}C_5H_5)Mn(CO)_3$ complexes not even on prolonged photolysis in reactive carbon monoxide matrices.[80]

Further low temperature work carried out by Bitterwolf *et al.*[58] in nujol solution at 77 K, displayed new infrared bands in the carbonyl region at 2132, 1957, 1888 cm^{-1} following photolysis $\lambda_{exc.} < 390$ nm. The carbonyl band stretch (ν_{CO}) at 2132 cm^{-1} was attributed to free carbon monoxide, with the remaining bands assigned to the carbonyl loss fragment $(\eta^5\text{-}C_5H_5)Mn(CO)_2$, as described in previous investigations. However, annealing the solution for 75 minutes, followed by re-freezing to 77 K, revealed the presence of a new species with bands at 1991, 1955, 1908 and 1170 cm^{-1}, which they suggested was a dinuclear species, as outlined below in Scheme 1-5.

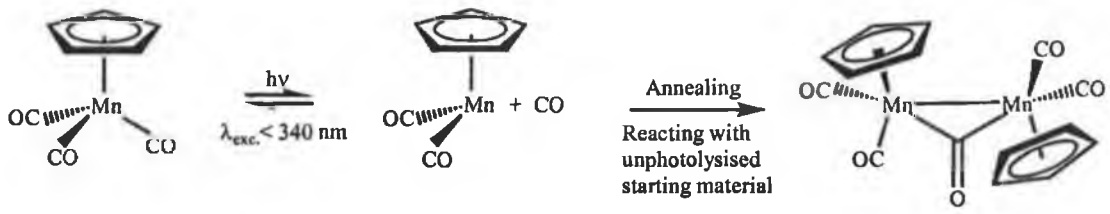

Scheme 1-5 Reaction of the dicarbonyl photoproduct with un-photolysised starting material to yield the dinuclear species.

More recently flash photolysis[81] and time resolved-infrared (TR-IR) spectroscopy have been used to show that on photolysis of $(\eta^5\text{-}C_5H_5)Mn(CO)_3$ in room temperature alkane solution two transient species are formed. One of the species was identified as the primary photoproduct $(\eta^5\text{-}C_5H_5)Mn(CO)_2$. The reaction of the primary photoproduct $(\eta^5\text{-}C_5H_5)Mn(CO)_2(S)$ is affected by the nature of the alkane solvent, with reactions in linear alkanes being approximately twice as fast as those in cyclic-alkanes.[81] The second transient species is attributed to the dinuclear $[(\eta^5\text{-}C_5H_5)Mn]_2(CO)_5$ formed from the reaction of $(\eta^5\text{-}C_5H_5)Mn(CO)_3$ (in the absence of added reagent) with un-photolysed $(\eta^5\text{-}C_5H_5)Mn(CO)_3$, as outlined previously in Scheme 1-5. The experimental data is consistent with a dinuclear species with a single bridging carbon monoxide group and a metal-metal bond.

The most recent investigations into the photo-chemistry of $(\eta^5\text{-}C_5H_5)Mn(CO)_3$ has taken advantage of super critical fluid (SCF) technology. Poliakoff *et al.*[82] reported almost complete conversion of $(\eta^5\text{-}C_5H_5)Mn(CO)_3$ to $(\eta^5\text{-}C_5H_5)Mn(CO)_2(\eta^2\text{-}H_2)$ in SCF H_2/CO_2 upon photolysis monitored by infrared spectroscopy. Although the first observation of $(\eta^5\text{-}C_5H_5)Mn(CO)_2(\eta^2\text{-}H_2)$ was in THF solution,[83] the isolation of such a complex from conventional solvents is difficult because the labile $\eta^2\text{-}H_2$ ligand is lost together with the evaporating solvent. Linehan and co-workers[84] investigated the stability and reactivity of $(\eta^5\text{-}C_5H_5)Mn(CO)_3$ and $(\eta^5\text{-}(CH_3)C_5H_4)Mn(CO)_3$ in SCF under extreme conditions. This offered the first demonstration of photolysis in high pressure SCF, with *in situ* nuclear magnetic resonance (NMR) detection of the substitution reactions of $(\eta^5\text{-}C_5H_5)Mn(CO)_3$ and $(\eta^5\text{-}(CH_3)C_5H_4)Mn(CO)_3$ by ethylene and hydrogen. However, Linehan *et al.*[84] reported a much lower photochemical

conversion of $(\eta^5\text{-}C_5H_5)Mn(CO)_3$ to $(\eta^5\text{-}C_5H_5)Mn(CO)_2(\eta^2\text{-}H_2)$. In a subsequent publication by Poliakoff *et al.*[85] the lower conversion in Linehan's experiments was attributed to the use of monochromatic light in the NMR experiment as opposed to the broad band irradiation used in the preparative method. Moreover a higher concentration of $(\eta^5\text{-}C_5H_5)Mn(CO)_3$ and lower concentration of H_2 appeared to have been used in the NMR experiments.

It has been shown[86] that UV photolysis of an impregnated polyethylene (PE) film at 21 K leads to the formation of the co-ordinatively unsaturated intermediate $(\eta^5\text{-}C_5H_5)Mn(CO)_2$, with ν_{CO} bands similar to those observed in frozen hydrocarbon glasses[79] and solid methane.[57] Repeating the experiment at room temperature however leads to the formation of a stable species containing the $(\eta^5\text{-}C_5H_5)Mn(CO)_2$ moiety bound to a vinyl, pendant or interval C=C bond in the polyethylene chain. In the presence of other gases, H_2 or N_2, there is a competitive formation of $(\eta^5\text{-}C_5H_5)Mn(CO)_2(\eta^2\text{-}C{=}C)$ and $(\eta^5\text{-}C_5H_5)Mn(CO)_2X$ (X = H_2 or N_2). The $(\eta^5\text{-}C_5H_5)Mn(CO)_2(\eta^2\text{-}C{=}C)$ product is difficult to extract by either super critical carbon dioxide or n-heptane, indicating that the $(\eta^5\text{-}C_5H_5)Mn(CO)_2$ moiety is bound to the polyethylene rather than just impregnating it as was the case before photolysis. The ν_{CO} bands of $(\eta^5\text{-}C_5H_5)Mn(CO)_2(\eta^2\text{-}C{=}C)$ provide a convenient diagnostic tool for establishing the degree of un-saturation of different polyethylene polymers, Figure 1-10. However it is also clear from this investigation that although polyethylene holds considerable promise as a matrix for low temperature experiments, the presence of olefinic C=C groups in a particular sample of polyethylene could render it unsuitable due to unwanted side reactions. Therefore the polyethylene film for low temperature matrix work should be chosen with care.

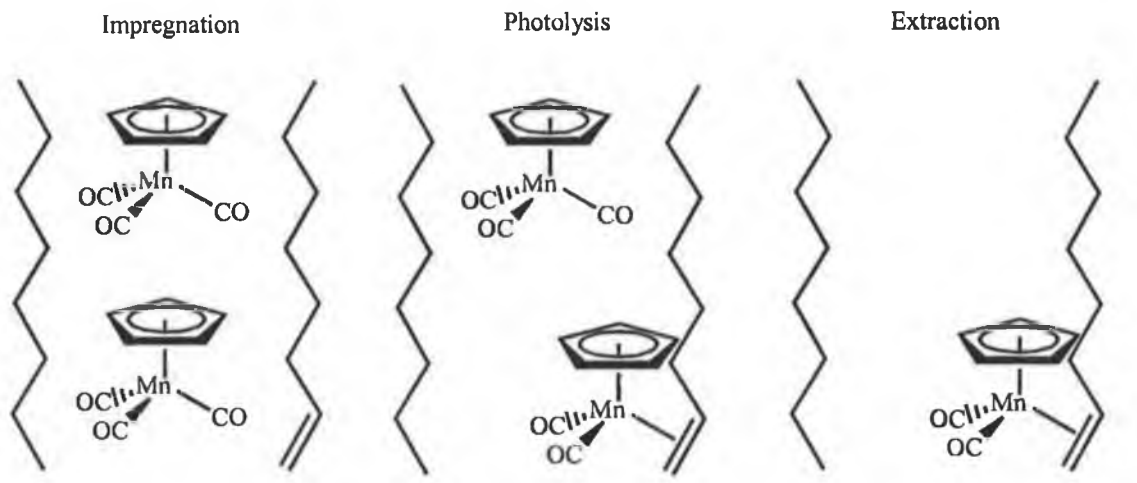

Figure 1-10 Summary of the three stages of the experiment. In each stage, the zig-zag lines are a symbolic representation of the polyethylene chains, they are not intended to imply any particular structure of conformation of the polyethylene chains in actual samples.

When $(\eta^5\text{-}C_5H_5)Mn(CO)_3$ carries a side-chain on the cyclopentadienyl ring with co-ordinating groups, there is a possibility for the side-chain to develop into a self-chelating species following photo-dissociation of carbon monoxide. Pang, Burkey and Johnston[87] have achieved this by using complexes of the type $(\eta^5\text{-}C_5H_4R)Mn(CO)_3$, where R = $COCH_2SCH_3$, $(CH_2)_2COCH_3$. They proposed that these compounds possess a unity quantum yield for carbon monoxide loss, due to the fact that the ring substituent traps the metal centre before carbon monoxide can recombine with the metal. Casey, Czerwinski and Fraley[88] achieved a similar result in terms of self-chelating species through the use of alkyl halide side-chains attached to the cyclopentadienyl ligand such as $(\eta^5\text{-}C_5H_4CH_2CH_2Br)Mn(CO)_3$ and $(\eta^5\text{-}C_5H_4CH_2CH_2I)Mn(CO)_3$. Photolysis in a hydrocarbon solvent resulted in carbon monoxide dissociation and intramolecular co-ordination of the alkyl halide to manganese producing $(\eta^5{:}\eta^1\text{-}C_5H_4CH_2CH_2Br)Mn(CO)_2$ and $(\eta^5{:}\eta^1\text{-}C_5H_4CH_2CH_2I)Mn(CO)_2$ as shown in Reaction 1-9.

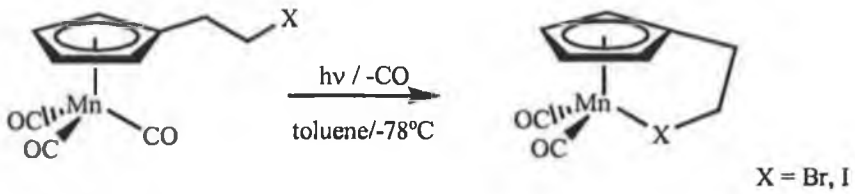

Reaction 1-9 Photolysis of $(\eta^5\text{-}C_5H_4CH_2CH_2X)Mn(CO)_3$(X=Br,I) to form chelated alkyl halide manganese complexes.

An investigation into the photochemistry of $(\eta^5\text{-}C_5H_5)Mn(CO)_3$ in toluene solution[89], provides infrared spectroscopic evidence for the formation of $(\eta^5\text{-}C_5H_5)Mn(CO)_2$(toluene) at low temperature in which the toluene ligand is probably bound in an η^2 fashion. This study found that unlike other solvated organometallics complexes like $(\eta^6\text{-arene})Cr(CO)_2(S)$[62] and $M(CO)_5(S)$[90] (M = Cr, Mo, W), which react primarily through a interchange or associative process with donor solvents, displacement of toluene from the manganese centre by THF was through a dissociative pathway. An estimation of the $(\eta^5\text{-}C_5H_5)Mn(CO)_2$-(toluene) bond strength (from analysis of the activation parameters) was determined to be 14.2 ± 0.8 kcal mol^{-1}. Combining these results with the previously measured $(\eta^5\text{-}C_5H_5)Mn(CO)_2$-(THF)[91] bond energy, suggests that the toluene complex is approximately 10 kcal mol^{-1} less stable than the $(\eta^5\text{-}C_5H_5)Mn(CO)_2$(THF) complex. Therefore unlike $(\eta^5\text{-}C_5H_5)Mn(CO)_2$(THF), $(\eta^5\text{-}C_5H_5)Mn(CO)_2(\eta^2$-toluene) would be difficult to isolate at room temperature.

A novel route to substituted cyclopentadienes has recently been reported,[92] this occurs by de-complexation of substituted cyclopentadienyl-manganese tricarbonyls following photolysis in the presence of a proton source. It is proposed that upon photolytic loss of a carbon monoxide ligand, co-ordination of methanol or water facilitate an intramolecular proton transfer to the cyclopentadienyl ring, to form the η^4-cyclopentadiene and finally liberation of the diene, as outlined in Scheme 1-6. Finally no one to date has claimed that the substitution of the η^5-cyclopetadienyl ring is a primary photo-process.

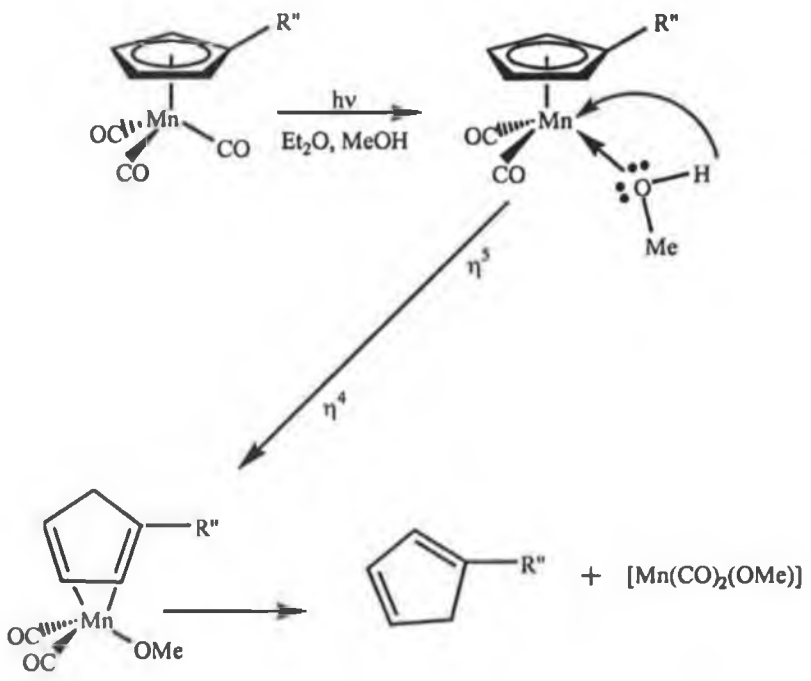

Scheme 1-6 Photolytic elimination of CO, co-ordination of the ROH ligand, intramolecular proton transfer to form the η^4-cyclopentadiene, and ultimately the liberation of the diene.

1.12 Brief literature review of thermal chemistry of $(\eta^5$-pyrrolyl$)Mn(CO)_3$

In contrast to the thermal stability of the carbon monoxide ligands in $(\eta^5\text{-}C_5H_5)Mn(CO)_3$, Basolo, Kershner *et al.*[93] reported a kinetic study of carbon monoxide substitution of the isoelectric pyrrolyl compound $(\eta^5\text{-}C_4H_4N)Mn(CO)_3$, which is estimated to react approximately 10^8 times faster than the analogous cyclopentadienyl complex, $(\eta^5\text{-}C_5H_5)Mn(CO)_3$. The rate enhancement was attributed to nitrogen being more electronegative that carbon, resulting in a greater tendency for electron withdrawal from the metal by the *N*-heterocycle relative to the carbocycle. Another factor considered was that the azaallyl might be more stable than the allyl type species as shown in Figure 1-11.

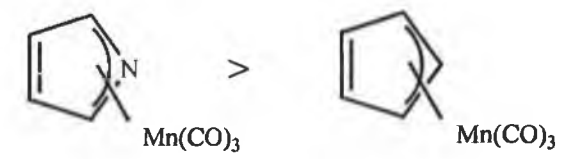

(η^3-azaallyl) (η^3-allyl)

Figure 1-11 The η^3-azaallyl type species and the η^3-allyl type species.

There is nuclear quadrupole resonance evidence that the parent complex $(\eta^5\text{-}C_4H_4N)Mn(CO)_3$ should be view as an azaallyl-olefinic system similar to Figure 1-11. However more recent ^{13}C NMR studies raise doubts over such a bonding mode.[94]

When the rates of reaction of three η^5-heterocyclic-$Mn(CO)_3$ complexes; $(\eta^5\text{-}C_4H_4N)Mn(CO)_3$, $(\eta^5\text{-}3,4\text{-}(CH_3)_2C_4H_2N)Mn(CO)_3$, and $(\eta^5\text{-}2,5\text{-}(CH_3)_2C_4H_2N)Mn(CO)_3$ were compared, another interesting observation was made by Kershner, Basolo *et al.*[95] The addition of two methyl substituents, which are electron donating to the pyrrolyl ligand are expected to decrease the rate of carbon monoxide substitution by an associative $\eta^5 \rightarrow \eta^3 \rightarrow \eta^5$ mechanism by making the ring more electron rich, thus less likely to accept an electron pair from the metal. While it was shown that the rates of reaction of the dimethyl derivatives are less than the parent, it was not anticipated that the position of the methyl groups on the pyrrolyl ligand would have such a large effect. It was observed that the 3,4-dimethylpyrrolyl complex reacts 10^2 times faster than does the 2,5-dimethylpyrrolyl complex. These researchers suggested that the preferred ring-slippage be towards the formation of an η^3-azaallyl bonding mode of the metal moiety to the pyrrolyl ligand in the transition state. Thus ring-slippage towards nitrogen results in a much more crowded transition state for the 2,5-dimethylpyrrolyl complex than for the corresponding 3,4-dimethylpyrrolyl complex and thus the greater retardation on the rate of carbon monoxide substitution. Analysis of these results suggested that a low energy associative reaction pathway involving an eighteen-electron active intermediate is most likely,[96] refer to Scheme 1-7. This mechanism was suggested only on the bases of kinetic data, no spectroscopic data was provided to substantiate it. Further support for ring-slip toward nitrogen is provided by

the X-ray structure of $(\eta^5\text{-}3,4\text{-}(CH_3)_2C_4H_2N)Mn(CO)_3$,[95] which shows a slippage even in the ground state.

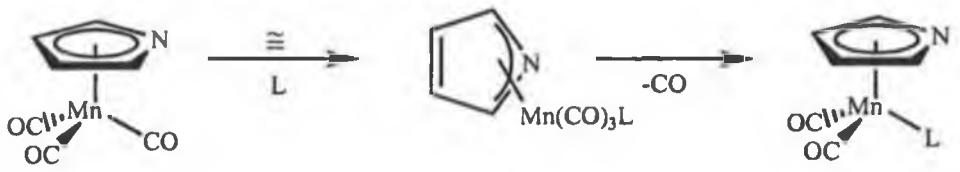

Scheme 1-7 The low energy associative reaction pathway, involving an electron active intermediate proposed by Kersher, Basolo *et al.*[95]

It has been demonstrated that the half sandwich complex, $(\eta^5\text{-}C_5H_5)Mn(CO)_3$ is almost inert to thermal substitution of a carbon monoxide ligand and that carbon monoxide substitution is best achieved by photochemical means. The carbon monoxide substitution of $(\eta^5\text{-}C_4H_4N)Mn(CO)_3$ on the other hand may be achieved thermally as just described. In addition to this, the carbon monoxide ligand is found to be photochemically labile. The second order rate constant obtained for the reaction of the solvated dicarbonyl with carbon monoxide in order to regenerate $(\eta^5\text{-}C_4H_4N)Mn(CO)_3$ was found to be 3×10^6 M^{-1} s^{-1}, an increase of one order of magnitude over the $(\eta^5\text{-}C_5H_5)Mn(CO)_3$ analogue (3×10^5 M^{-1} s^{-1}).[97] This rate enhancement although not as dramatic as that found in the case of thermal substitution was also attributed to the formation of a ring-slip $\eta^5 \rightarrow \eta^3$ intermediate as outlined by Basolo *et al.*[95,96]

However a very recent publication by Veiros,[98] studied the electronic structure and bonding of a series of tricarbonyl-manganese complexes. Using molecular orbital calculations, haptotropic shifts in organometallic complexes with η^5 co-ordinated π ligands were investigated. All the hydrocarbon polyenic complexes studied presented $\eta^5 \rightarrow \eta^3$ ring-slippage, after two electron reduction. However no local minimum was found for a slipped or folded η^3 co-ordination of heterocyclic ligands, pyrrolyl and thiophene. Both reduced complexes presented σ bonded ligands, consistent with a $\eta^5 \rightarrow \eta^1$ ring-slippage, the η^1-metal bond being achieved through the heteroatom lone pair pointing towards the metal. In light of these results, perhaps it best to consider the rate enhancement as being due to N being more electronegative that C, resulting in

a greater tendency for electron withdrawal form the metal by the nitrogen-heterocycle relative to the carbocycle.

1.13 References

1 W. C. Zeise, *Pogg. Ann. Phy. Chem.*, **1827, 9,** 623.

2 L. Mond, C. Langer, F. Quincke, *J. Am. Chem. Soc.*, **1890,** 749.

3 L.Mond, C.Langer, *J. Chem. Soc.*, **1891,** 1090.

4 M. Berthelot, *Acad. Sci. Paris*, **1891,** 1343.

5 F. Hein, *Chem. Ber.*,**1919,** 52, 195.

6 F. Fischer, H. Tropsch, German patents, **1925,** 411416, **1922,** 484337.

7 H. Reihlen, A. Gruhl, G. von Hessling, O. Pfrengle, *Liebigs. Ann. Chem.*, **1930,** 482, 161.

8 O. Roelen, German patent, **1938,** 849548.

9 T. P Kealy, P. L Pauson, *Natur*, **1951,** 168, 1039.

10 S. A. Miller, J. A. Tebboth,, J. F. Tremaine, *J. Chem. Soc.*, **1952,** 632.

11 G. Wilkinson, M. Rosenblum, M. C. Whiting, R. B. Woodward, *J. Am. Chem. Soc.*, **1952,** 74, 2125.

12 E. O. Fischer, W. Pfab, *Z. Naturforsch.*, **1952,** 67 B, 543.

13 M. Orchin, *Acc. Chem. Res.*, **1981,** 14, 259.

14 R. Roth, J. H. Craddock, A. Hershman,, F. E. Paulik, *Chem. Tech.*, **1971,** 1, 600.

15 (a) M. R. Bray, R. J. Deeth, V. J. Paget, *Prog. React. Kinetics*, **1996,** 21, 169.
(b) R. J. Deeth, *Struct. Bonding*, **1995,** 82, 1.
(c) R. J. Deeth, *Coord. Chem. Rev.*, **2001,** 212, 11.
(d) S. Niu, M. B. Hall, *Chem. Rev.*, **2000,** 100, 353.
(e) G. Frenking, N. Fröhlich,; *Chem. Rev.*, **2000,** 100, 717.

16 A. Diefenbach, F. M. Bickelhaupt, G. Frenking, *J. Am. Chem. Soc.*, **2000,** 122, 6449.

17 (a) C. W. Blauschlicher Jr., P. S. Bagus, C. J. Nelin, B. O. Roos, *J. Chem. Phys.*, **1986,** 85, 354.
(b) C. W. Blauschlicher Jr, *J. Chem. Phys.*, **1986,** 84, 260.

18 Ref. 15(e), and references 132-156 therein.

19 F. A. Cotton, G. Wilkinson, C. A. Murillo, M. Bochmann, *Advanced Inorganic Chemistry*, 6th Ed., Wiley, New York, **1999.**

20 J. E. Huheey, E. A. Keiter, R. L. Keiter, *Inorganic Chemistry: Principles of Structure and Reactivity*, 4th Ed., Benjamin/Cummings, New York, **1993.**

21 N. L. Long, *Metallocenes: An introduction to sandwich complexes*, Blackwell Science Ltd. Oxford, **1988.**

22 K. Kalyanasundraram, *Photochemistry and Photophysics of Polypyridine and Porphyrin Complexes*, Academic Press, London, **1992.**

23 (a) M. S. Wrighton, D. L. Morse, L. Pdungsap, *J. Am. Chem. Soc.*, **1975,** 97, 2073.
(b) P. D. Fleischauer, P. Fleischauer, *Chem. Rev.*, **1970,** 70, 199.

24 (a) E. Whittle, D. A. Dows, G. C. Pimentel, *J. Chem. Phys.*, **1954**, 22, 1943.
(b) J. D. Baldeschwieler, G. C. Pimentel; *J. Chem. Phys.*, **1960**, 33, 1008.

25 J. K. Burdett, A. J. Downs, G.P. Gaskill, M. A. Graham, J. J. Turner, R. F. Turner, *Inorg. Chem.*,**1978**, 17, 523.

26 R. N. Perutz, *Roy. Soc. Chem. Ann. Rep. Prog. Chem.*, **1985**, 157, C85.

27 C. H. F. Peden, S. F. Parker, P. H. Barrett, R. G. Pearson, *J. Phys. Chem.*, **1983**, 87, 2329.

28 R. L. Sweaney, *Inorg. Chem.*, **1984**, 19, 351.

29 R. N. Perutz, J. J. Turner, *J. Am. Chem. Soc.*,**1975**, 97, 4791.

30 M. Poliakoff, J. J. Turner, *J. Chem. Soc., Dalton Trans.*, **1974**, 2276.

31 (a) R. B. Hitman, M. H. Mahmoud, A. J. Rest, *Co-ord. Chem. Rev.* **1984**, 55, 1.
(b) R. N. Perutz, *Chem. Rev.*, **1985**, 85, 77.

32 A. F. Hepp, J. P. Blatha, C. Lewis, M. S. Wrighton, *Organometallics*, **1984**, 3, 174.

33 R. J. Hooker, K. A. Mahmoud, A. J. Rest, *J. Chem. Soc., Chem. Comm.*; **1983**, 1022.

34 J. J. Turner, M. A. Healy, M. Poliakoff, 'Infrared spectroscopy of organometallic intermediates' in ' *High Energy Process in Organometallic Chemistry*', K. S. Suslick, Ed., ACS Symposium Series, **1987**, 333, 110.

35 P. A. Breeze, J. K. Burdett, J. J. Turner; *Inorg. Chem.*, **1981**, 20, 3369.

36 R. G. W. Norrish; *Nature*, (London), **1949**, 164, 658.

37 M. Poliakoff, E. Weitz; *Adv. Organomet. Chem.*, **1986**, 25, 277.

38 J. M. Kelly, H. Hermann, E. Koerner von Gustorf, *J. Chem. Soc., Chem. Comm.*, **1973**, 103.

39 (a) A. S. Lepfohn, G. C. Pimentel, *J. Phys. Chem.*, **1971**, 55, 1213.
(b) L. Y. Tan, A. M. Winter, G. C. Pimentel, *J. Phys. Chem.*, **1972**, 57, 4028.

40 R. D. Levine, R. B. Bergstein, *Molecular Reaction Dynamics and Chemical Reactivity*, Oxford University Press, Oxford, **1987**.

41 T. A. Seder, A. J. Ouderkirk, E. Weitz, *J. Chem. Phys.*, **1986**, 85, 1977.

42 E. Weitz, *J. Phys. Chem.*, **1987**, 91, 3945.

43 Y. Ishikawa, C. E. Brown, P. A. Hackett, D. M. Raynor, *J. Phys. Chem.*, **1990**, 94, 2404.

44 C. Elschenbroich, A. Salzer, *Organometallics: A Concise Introduction*, 2nd Ed., Verlagsgesellschaft, GmbH, Weinheim, **1992**.

45 A. Veillard in *Photoprocess in Transition Metal Complexes, Biosystems and Other Molecules. Experiment and Theory*, pg 173-216, E. Kochanski (Ed.), Kluwer Academic Publishers, Dorttrecht, **1992**.

46 (a) C. Pollak, A. Rosa, E. J. Baerends, *J. Am. Chem. Soc.*, **1997**, 119, 7324.
(b) E. J. Baerends, A. Rosa, *Coord. Chem. Rev.*, **1998**, 177, 97.

47 (a) W. Strohmeier, H. Hellman, *Z. Naturforsch.*, **1963**, 18B, 769.
(b) W. Strohmeier, H. Hellman, *Chem. Ber.*, **1963**, 96, 2859.
(c) W. Strohmeier, H. Hellman, *Chem. Ber.*, **1964**, 97, 1877.
(d) W. Strohmeier, H. Hellman, *Chem. Ber.*, **1965**, 98, 1598.
(e) W. Strohmeier, G. Popp, J. F. Guttenberg, *Chem. Ber.*, **1966**, 99, 165.
(f) W. Strohmeier, J. F. Guttenberger, F. J. Müller, *Z. Naturforsch.*, **1963**, 22B, 1091.
(g) J. F. Guttenberger, W. Strohmeier, *Chem. Ber.*, **1967**, 100, 2807.

48 W. Strohmeier, D. von Hobe, *Z. Naturforsch.*, **1963**, 18B, 981.

49 D. A. Brown, D. Cunningham, W. K. Glass, *J. Chem. Soc., Chem. Commun.*, **1966**, 306.

50 W. Jetz, W. A. G. Graham, *Inorg. Chem.*, **1971**, 10, 4.

51 (a) B. M. Yavourskii, N. K. Baranetskaya, V. N. Trembolver, V. N. Sektina , *Doklady Akad. Nauk. SSS R.*, **1972**, 207, 1147.
(b) B. M. Yavourskii, V. N. Trembolver, V.N. Sektina, N. K. Baranetskaya, G. B. Zaslavskaya, M. G. Evookimora, *Russ. J. Phys. Chem.*, **1974**, 3, 1231.
(c) B. M. Yavourskii, V. N. Trembolver, V.N. Sektina, N. K. Baranetskaya, G. B. Zaslavskaya, *Doklady Akad. Nauk. SSSR.*, **1974**, 218, 1153.

52 N. K. Trembolver, N. K. Baranetskaya, N. V. Fok, G. B. Zaslavskaya, B. M. Yavourskii, V. N. Setkina, *J. Organomet. Chem.*, **1976**, 117, 339.

53 J. Naisielski, O. Denisoff, *J. Organomet. Chem.*, **1975**, 102, 65.

54 M. S. Wrighton, J. L. Haverty, *Z. Naturforsch.*, **1975**, 30B, 245.

55 A. Gilbert, J. M. Kelly, M. Budazwait, E. Körner von Gustorf, *Z. Naturforsch.*, **1976**, 316, 1091.

56 C. H. Bamford, K. G. Al-Lamee, C. J. Konstantantinov, *J. Chem. Soc., Faraday Trans. 1*, **1977**, 73, 1406.

57 A. J. Rest, J. R. Sodeau, D. J. Taylor, *J. Chem. Soc. Dalton Trans.*, **1978**, 651.

58 T. E. Bitterwolf, K. A. Lott, A. J. Rest, J. Mascetti, *J. Organomet. Chem.*, **1991**, 419, 113.

59 W. Wang, Y. Sin, Y. S. Liu, K.–J. Fu, *J. Phys. Ch*em., **1992**, 96, 1278.

60 Y. Zheng, W. Wang, J. Liu, Y. She, K.-J. Fu, *J. Phys. Chem.*, **1992**, 96, 9821.

61 M. T. Pryce, Ph.D. Thesis, Dublin City University, **1994**.

62 B. S. Creaven, M. George, A. G. Ginzbug, C. Huhges, J. M. Kelly, C. Long, I. M. McGrath, M. T. Pryce, *Organometallics*, **1993**, 12, 3127.

63 G. L. Geoffroy, M. S. Wrighton, *Organometallic Photochemistry*, Academic Press, New York, **1979**.

64 D. M. Roundhill, *Photochemistry and Photophysics of Metal Complexes*, Plenum Press, New York, **1994**.

65 C. J. Breheny, S. M. Draper, F.-W. Grevels, W. E. Klotzbücher, C. Long, M. T. Pryce, G. Russell, *Organometallics*, **1996**, 15, 3679.

66 (a)W. Strohmeier, H. Mittnacht, *Chem. Ber.*, **1960**, 93, 2085.
(b) W. Strohmeier, H. Mittnacht, *Z. Phys. Chem.,(Frankfurt am Main)*, **1961**, 29, 339.
(c) W. Strohmeier, E. H. Staricco, *Z. Phys. Chem.(Frankfurt am Main)*, **1963**, 38, 315.
(d) W. Strohmeier, R. Müller, *Z. Phys. Chem., (Frankfurt am Main)*, **1964**, 40, 85.
67 (a) C. A. L. Mahaffy, P. L. Pauson, *J. Chem. Res.(synop.)*, **1979**, 126.
(b) C. A. L. Mahaffy, P. L. Pauson, *J. Chem. Res.(miniprint)*, **1979**, 1752.
68 (a) C. L. Zimmerman, S. L. Shaner, S. A. Roth, B. R. Willeford, *J. Chem. Res.,(synop.)*, **1980**, 108.
(b) C. L. Zimmerman, S. L. Shaner, S. A. Roth, B. R. Willeford, *J. Chem. Res.,(miniprint)*, **1979**, 1289.
69 D. E. F. Gracey, W. R. Jackson, C. H. McMullen, N. Thompson, *J. Chem. Soc.*, (B), **1969**, 1197.
70 T. G. Traylor, K. J. Stewart, *Organometallics*, **1984**, 3, 325.
71 (a) T. G. Traylor, K. J. Stewart, M. J. Goldberg, *J. Am. Chem. Soc.*, **1984**, 106, 4445.
(b) T. G. Traylor, K. J. Stewart, M. J. Goldberg, *Organometallics*, **1986**, 5, 2062.
(c) T. G. Traylor, K. J. Stewart, M. J. Goldberg, *J. Am. Chem. Soc.*, **1986**, 108, 6977
72 E. L. Muetterties, J. R. Bleeke, E. J. Wucherer, T. A. Albright, *Chem. Rev.*, **1982**, 82, 499.
73 J. A. S. Howell, N. F. Ashford, D. T. Dixon, J. Kola, T. A. Albright, S. K. Kang, *Organometallics*, **1991**, 10, 1852-1864.
74 K. G. Caulton, *Coord. Chem. Rev.*, **1981**, 38, 1.
75 R. S. Nyholm, S. S. Sandhu, M. H. B. Stiddard, *J. Chem. Soc.*, **1963**, 5916.
76 W. Strohmeier, *Angew. Chem. Int. Ed. Engl.*, **1964**, 3, 730.
77 W. Strohmeier, R. Müller, *Chem. Ber.*, **1969**, 102, 3608.
78 N. G. Connelly, M. Kitchen, *J. Chem. Soc.,Dalton Trans.*, **1977**, 931.
79 P. S. Braterman, J. D. Black, *J. Organomet. Chem.*, **1972**, 39, C3.
80 M. Herberhold, W, Kremnitz, H. Trampisch, R. B. Hitman, A. J. Rest, D. J Taylor, *J. Chem. Soc.*, **1982**, 1261.
81 B. S. Creaven, A. J. Dixon, J. M. Kelly, C.Long, M. Poliakoff, *Organometallics*, **1987**, 6, 2600.
82 J. A. Banister, P. D. Lee, M. Poliakoff, *Organometallics*, **1995**, 14, 3876.
83 V. S. Leong, N. J. Cooper, *Organometallics*, **1988**, 7, 2080.
84 J. C Linehan, S. L. Wallen, C. R. Yonker, T. E. Bitterwolf, J. T. Bays, *J. Am. Chem. Soc.*, **1997**, 119, 10170.
85 P. D. Lee, J. L. King, S. Seebald, M. Poliakoff, *Organometallics*, **1998**, 17, 524.
86 M. J. Clarke, S. M. Howdle, M. Jobling, M. Poliakoff, *J. Am. Chem. Soc.*, **1994**, 116, 8621.
87 Z. Pang, T. J. Burkey, R. F. Johnston, *Organometallics*, **1997**, 16, 120.
88 C. P. Casey, C. J. Czerwinski, M. E. Fraley, *Inorg. Chim. Acta.*, **1998**, 280, 316.
89 A. A. Bengali, *Organometallics*, **2000**, 19, 4000.
90 S. Wieland, R. van Eldik, *Organometallics*, **1991**, 10, 3110.

91 J. E. Coleman, K. E. Dunlaney, A. A. Bengali, *J. Organomet. Chem.*, **1999**, 572, 65.

92 S. Top, E. B. Kaloun, S. Toppi, A. Herrbach, M. J. McGlinchey, G. Jaouen, *Organometallics*, **2001**, 4554.

93 J.-N. Liang, D. L. Kershner, F. Basolo, *J. Orgnomet. Chem.*, **1985**, 296, 83.

94 A. Efraty, N. Jubran, A. Goldman, *Inorg. Chem.*, **1982**, **21**, 868.

95 D. L. Kershner, A. L. Rheingold, F. Basolo, *Organometallics*, **1987**, 6, 196.

96 F. Basolo, *Inorg. Chim. Acta*, **1985**, 100, 33.

97 P. Brennan, PhD Thesis, Dublin City University, not yet submitted.

98 L. F. Veiros, *J. Organomet. Chem.*, **1999**, 587, 221.

Chapter Two

2 The photochemistry of azaferrocene

2.1 Literature Survey of the photochemistry of ferrocene

Despite the extensive investigations into the chemical and spectroscopic properties of ferrocene, the photochemistry of ferrocene has not been the subject of much research.

The earliest report appeared in 1956[1], it examined the photochemistry of ferrocene by flash photolysis in the gas phase. In this work, irradiation of ferrocene led to the formation of cyclopentadienyl radicals. Following investigations by Tarr and Wiles,[2] solutions of ferrocene in decalin, acetone, methanol, propan-1-ol and propan-2-ol were found to be completely photoinert. However irradiation of ferrocene under similar conditions in carbon tetrachloride caused extensive decomposition. In addition Tarr and Wiles showed that substituted ferrocenes display a markedly increased photosensitivity.[2] 1,1-Dibenzolferrocene shows colour a change followed by decomposion upon photolysis in alcohols, ethers, esters, acetone, acetonitrile, pyridine, or dimethylsulphoxide (DMSO), although Tarr and Wiles made no further investigation of the photoreaction products.

In contrast to ferrocene's inertness in non-polar/non-halogenated solvents, Brand and Snedden[3] demonstrated that the UV-vis spectrum of ferrocene in halogen-containing solvents displayed an additional intense band in the range 300-400 nm. The new band was attributed to a solvent charge transfer transition. They observed that irradiation into the metal-to-solvent charge transfer band, resulted in the decomposition of ferrocene via a primary photo-oxidation process. Körner von Gustorf and Grevels[4] later confirmed this observation in their studies on the photo-oxidation of ferrocene in various organic halide solvents. Invariably a solid product was obtained, which was formulated as ferricenium-tetrahalo-ferrate $[(\eta^5\text{-}C_5H_5)_2Fe]^+[FeX_4]^-$.

No distinction was made between primary photochemical, secondary thermal or secondary photochemical processes in these early studies, which were predominately of

a qualitative nature. Traverso and Scandola[5] addressed this oversight in their investigation into the photochemistry of ferrocene in carbon-tetrachloride/ethanol and chloroform/ethanol mixtures, where the solubility of the cationic product was increased. When the binary solvent contained more than ~ 40% ethanol, the kinetics of the photochemical formation of ferricenium cation could be followed. These results showed that irradiation of the ferrocene to halocarbon solvent charge transfer band caused the oxidation of ferrocene to the ferricenium cation, while intra-molecular excitation of ferrocene failed to result in any photochemistry.

The overall photo-oxidation reaction was found to involve a primary photochemical process and a secondary thermal reaction, both producing the ferricenium cation. The primary photochemical process is the dissociation of the charge-transfer-to-solvent excited state into a ferricenium cation, a chloride ion and an organic radical, refer to Reaction 2-1.

$$(\eta^5\text{-}C_5H_5)_2Fe \xrightarrow[\text{halogenated solvent}]{h\nu} (\eta^5\text{-}C_5H_5)_2Fe^+ + X^- + R^\bullet$$

Reaction 2-1 Primary photoprocess proposed by Traverso and Scandola.[5]

In both carbon tetrachloride and chloroform, the primary photoprocess occurrs with unit quantum efficiency. The secondary thermal oxidation of ferrocene was initiated by the radical species produced in the primary photoprocess, refer to Reaction 2-2.

$$(\eta^5\text{-}C_5H_5)_2Fe + R^\bullet \longrightarrow (\eta^5\text{-}C_5H_5)_2Fe^+ + R^-$$

Reaction 2-2 Secondary thermal reaction proposed by Traverso and Scandola.[5]

The efficiency of the secondary oxidation depends on the concentration of ferrocene, dissolved oxygen, and the radical scavengers (i.e. the presence of acrylamide, which detected and trapped any radicals). It should be noted that Traverso and Scandola relied on UV-vis spectroscopy for confirmation of the formation of $[(\eta^5\text{-}C_5H_5)_2Fe]^+Cl^-$.

Traverso and Scandola's[5] qualitative work was confirmed by results obtained by Hoshi *et al.*[6] and Akiyama *et al.*[7], however in these experiments the photoproducts were isolated and characterised. Hoshi, Akiyama and co-workers[6,7] demonstrated that photolysis of ferrocene in halocarbon ethanol solvent mixtures gave not only formation of $[(\eta^5\text{-}C_5H_5)_2Fe]^+Cl^-$ but also products derived by substitution of one of the cyclopentadienyl rings, Reaction 2-3

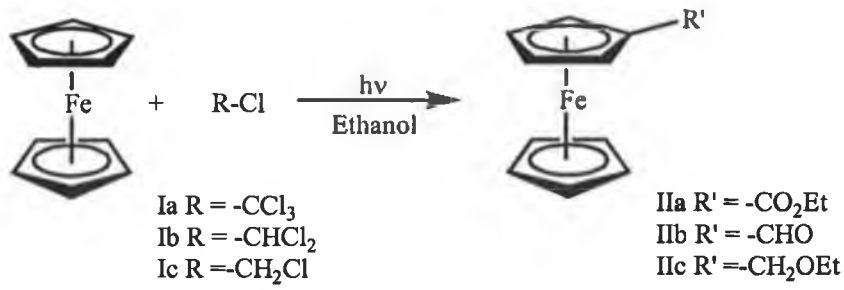

Reaction 2-3 Ultraviolet irradiation of ferrocene in haloalkane–ethanol solvents leads to mono-substitution of ferrocene

A subsequent publication by Akiyama *et al.*[8] set out to outline the mechanism of photosubstitution of ferrocene in haloalkane-ethanol solution. In order to elucidate the mechanism, several chemical methods and flash photolysis were applied to the ferrocene-chloroform system containing ethanol and other bases. The various substitution products apparently arise through the ethanolysis of a halocarbon-substituted ferrocene, as outlined in Scheme 2-1.

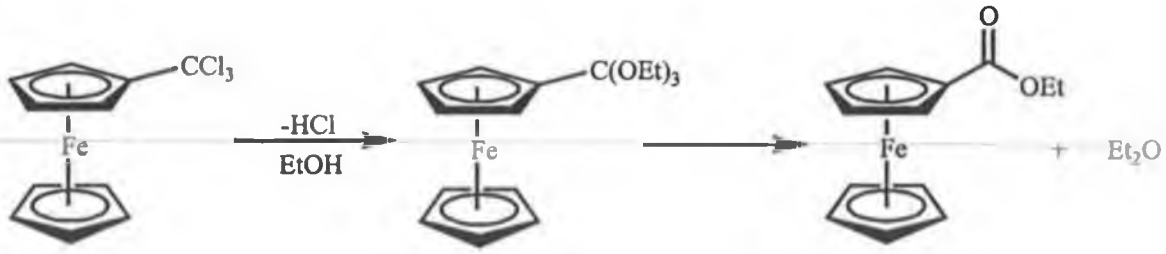

Scheme 2-1 Ethanolysis of a halocarbon substituted ferrocene.

The results of Akiyama *et al.*[7,8] and Traverso and Scandola[5] would seem initially to be contradictory, however their experimental observations taken together may be summarised as in Scheme 2-2. The primary step in the photo-process is dissociation of

the metal-to-solvent-charge-transfer state to give $[(\eta^5\text{-}C_5H_5)_2Fe]^+Cl^-$ and $\bullet CCl_3$. In the absence of either ethanol or acrylamide, photolysis proceeds through reactions (2), (4) and (5) in Scheme 2-2 to give $[(\eta^5\text{-}C_5H_5)_2Fe][FeCl_4]$ as originally observed by Brand and Snedden.[3] In the presence of acrylamide, as a radical scavenger, the $\bullet CCl_3$ radicals are efficiently trapped, (6), therefore reaction (2) does not proceed and conversion to $[(\eta^5\text{-}C_5H_5)_2Fe]Cl$ occurs. In the absence of acrylamide, but in the presence of ethanol, substitution of ferrocene occurs by the sequence of reactions (1), (2) and (3).

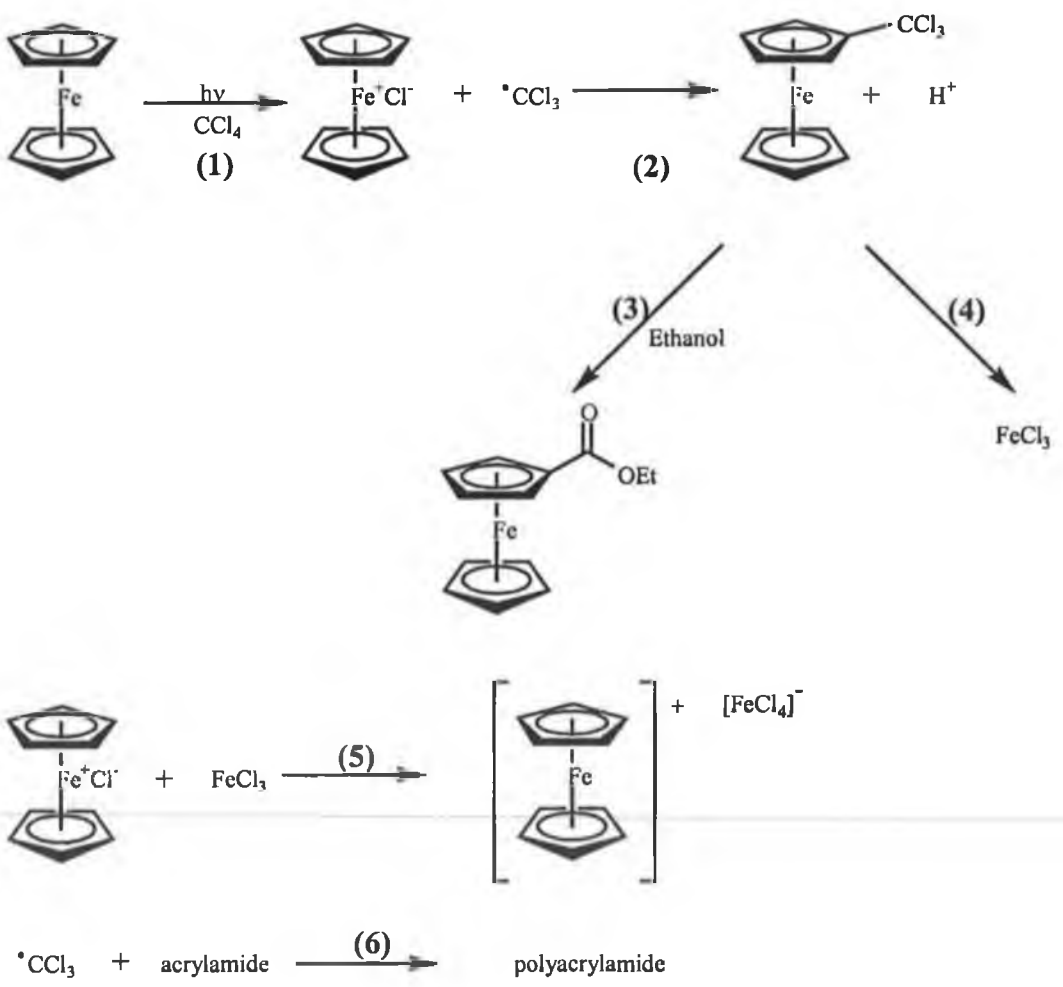

Scheme 2-2 Summary of the proposed mechanism of ferrocene photoreaction.

Substitution of the ferrocene molecule by photoactive functional groups, such as that of an aromatic carbonyl compound (i.e. ketone or acid) can impart a remarkable change in the level and direction of photoactivity.[9] Ali, Cox and Kemp[10] reported the rapid

photoreaction of benzoylferrocene and related compounds of the general formula ferrocenyl-COX (where X = C_6H_5, CH_3, H, OH, OR, or NH_2) in dimethyl-sulphoxide (DMSO), dimethylformamide (DMF) and pyridine. Their results indicate that the photoreaction does not involve radicals derived from ferrocene. But rather a photo-aquation involving solvent impurities by followed both ring-metal and ring-carbonyl cleavage in the case of the ketones, and ring-metal cleavage in the case of ferrocenyl-CO_2H followed by a decarboxylation to give a second carboxylate from which starting material could be recovered. In every case the photoproducts are complex and in most cases the photochemistry is that of the organic functional group.

A more recent investigation by Davis, Vaughan and Cardosi[11] attempted to determine the factors responsible for the photosensitivity by investigating the photo-reactivity and electrochemical properties of nine monosubstituted ferrocene derivatives of varying functionality in aqueous pH 7.4 buffer. The reaction mechanism involved in the decomposition process is not fully understood, with the nature of the resulting products dependent on the ferrocene derivative used. It would appear rupture of the ring system occurs, resulting in the loss of the ferrocene component and formation of inorganic iron compounds and organic debris. Analysis of the organic products was attempted using ^{1}H NMR spectroscopy, however the spectra were extremely complex. In addition to this, UV-vis analysis during photo-decomposition displayed no isosbestic points. Both the ^{1}H NMR and UV-vis spectroscopy indicate that the route to photo-decomposition is not well understood, and a variety of products result. Davis, Vaughan and Cardosi[11] suggested trace amounts of water in solvents might be a contributing factor to the decomposition process observed.

Einaga, Yamada and Tominaga studied the photochemistry of ferrocene in a low temperature nitrogen matrix[12] in order to investigate the mechanism of its photochemical reaction in an isolated system and to characterise unstable products obtained at low temperature. Irradiation of ferrocene in a dinitrogen matrix without co-condensed carbon tetrachloride failed to produce a photochemical change as monitored by ^{57}Fe Mössbauer spectroscopy. Photochemical products were found after irradiation when CCl_4, $CHBr_3$, or C_6H_{12} were co-condensed with ferrocene. The

explanation provided for this observation was, that the ferrous ion in ferrocene is oxidised to form the ferric ion in the low temperature dinitrogen matrix because of a charge transfer formed between ferrocene and carbon tetrachloride similar to the metal-to-solvent charge-transfer reaction in alkyl halide solutions. Both $[(\eta^5\text{-}C_5H_5)_2Fe]^+$ and $[(\eta^5\text{-}C_5H_5)_2Fe]$ (high spin) were produced by irradiation of ferrocene co-condensed with CCl_4, $CHBr_3$, or C_6H_{12} in a dinitrogen matrix. The photoproducts are unstable and disappear on annealing the matrix to reform ferrocene. It was shown that $[(\eta^5\text{-}C_5H_5)_2Fe]$ (high spin) was produced by prolonged irradiation of the ferricenium cation, $[(\eta^5\text{-}C_5H_5)_2Fe]^+$. Following short irradiation times (i.e. less than 2 hours), the only photoproduct was the ferricenium cation, $[(\eta^5\text{-}C_5H_5)_2Fe]^+$, with no high spin species being observed. On prolonged irradiation, yields of the ferricenium cation, $[(\eta^5\text{-}C_5H_5)_2Fe]^+$ increased for up to two hours, and then remained constant during further irradiation, while the high spin species appeared following two hours of irradiation and then continued to increase at the expense of ferrocene, as outlined in Scheme 2-3 below.

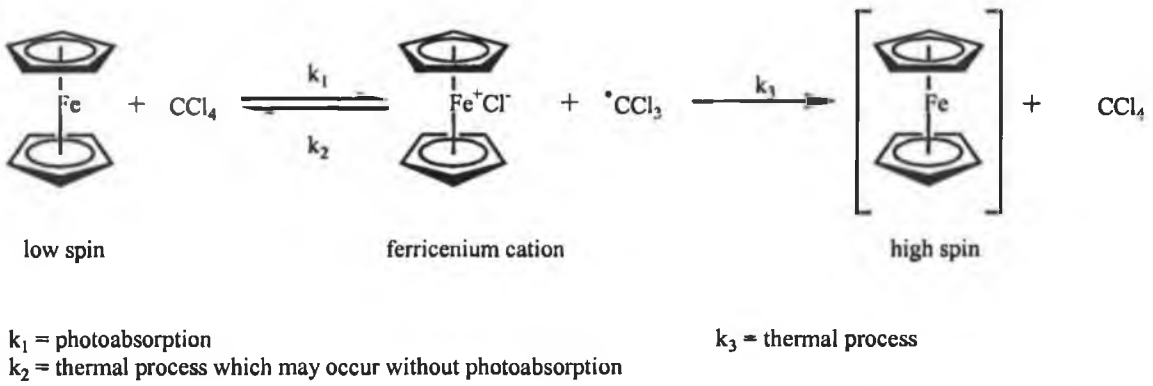

Scheme 2-3 Reaction scheme for ferrocene following photolysis in a dinitrogen low temperature matrix.

2.2 Literature survey of the photochemistry of mixed metallocenes

It was foreseen that considerable synthetic utility could have been gained if a ring interchange reaction as outlined in Reaction 2-4 and/or ring replacement reaction as in Reaction 2-5 could have been achieved photochemically.

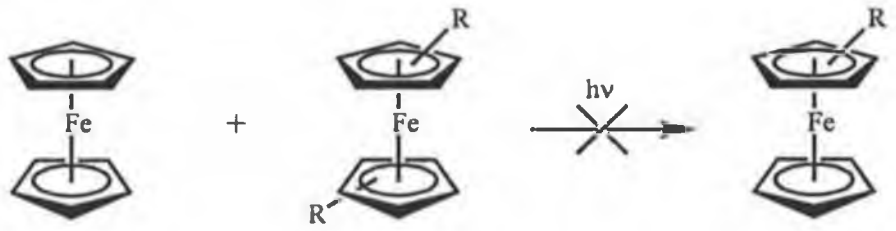

Reaction 2-4 Ring interchange reaction.

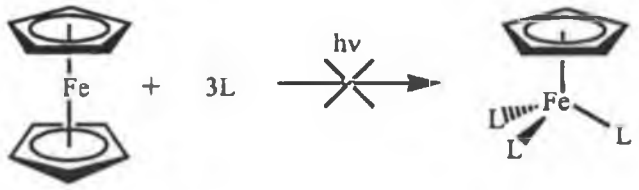

Reaction 2-5 Ring replacement reaction.

In the majority of transition metal systems studied, the ligand field excitation is thought responsible for the M-L bond scission. However this type of reaction could not be induced photochemically as already outlined in Section 2-1, on the photochemistry of ferrocene.

The bonding found in mixed metallocene complexes such as $[(\eta^5\text{-}C_5H_5)Fe(\eta^6\text{-arene})]^+$, is essentially similar to that already postulated for ferrocene, refer to section 1.3.2.1 in chapter one. Although mixed metallocenes of the type, $[(\eta^5\text{-}C_5H_5)Fe(\eta^6\text{-arene})]^+$ no longer have the high symmetry of ferrocene (D_{5d} or D_{5h}). Nevertheless, mixed metallocene, $[(\eta^5\text{-}C_5H_5)Fe(\eta^6\text{-arene})]^+$ may still be treated as having pseudo-axial symmetry so long as it is recognised that there is no natural centre of inversion (no u or g distinction).

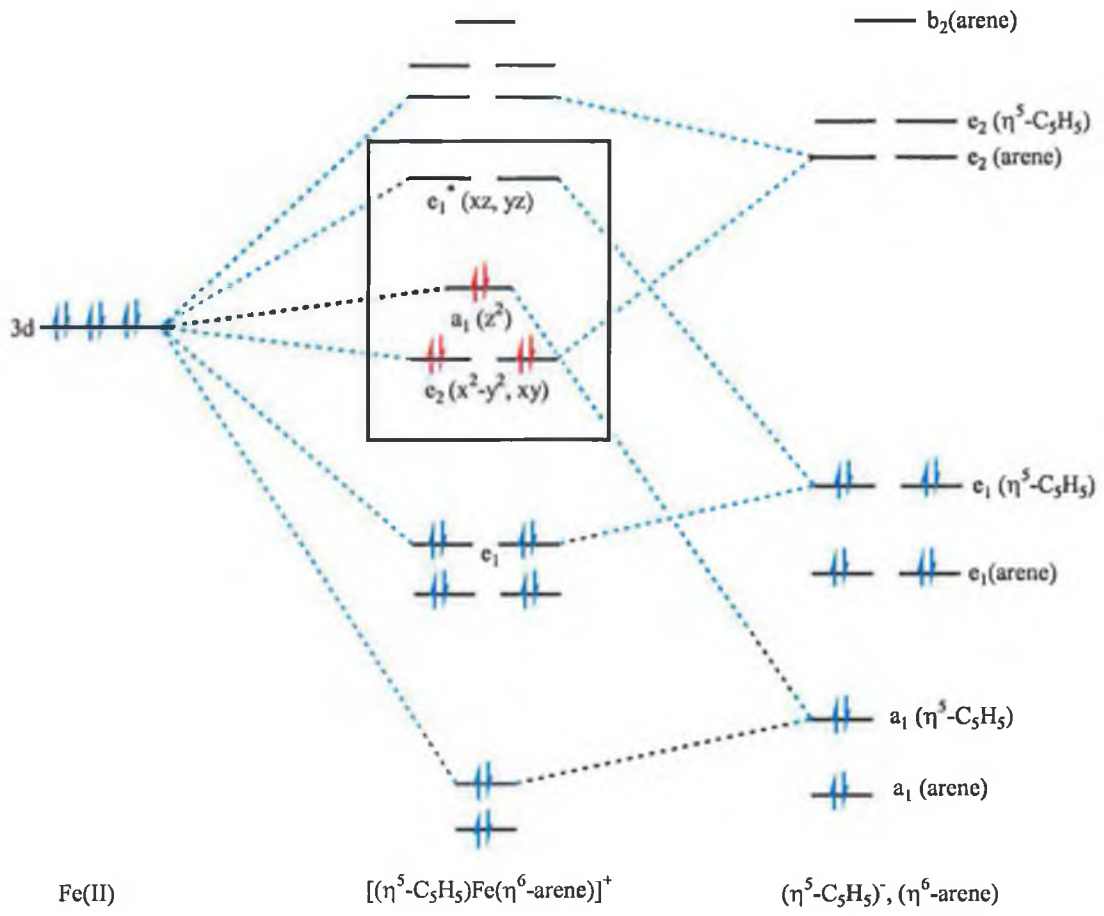

Figure 2-1 Qualitative molecular orbital diagram for $[(\eta^5\text{-Cp})Fe(\eta^6\text{-benzene})]^+$cation. The box depicts the molecular orbitals that contain appreciable metal d-character.

In idealised cases, the six pπ-orbitals of the benzene ring and the five pπ-orbitals of the cyclopentadienyl ring adapt combinations a_1, e_1, e_2, b_2 and a_1, e_1, e_2 respectively. The molecular orbital characteristics of the complex are generated by the interaction of these ligand orbitals with the metal 3d valence orbitals of appropriate symmetry. The strongest interaction occurs between $3d_{xz}$, $3d_{yz}$ of the metal valence orbitals and the energetically closer cyclopentadienyl e_1 orbitals rather than the more distant benzene ligand e_1 orbitals, refer to Figure 2-1. The resulting e_1 molecular orbitals have appreciable metal $3d_{xz}$, $3d_{yz}$ involvement but are mainly ligand in character. These are filled with two pairs of electrons and are strongly bonding. This contrasts with the e_1^* anti-bonding orbitals, which are mostly metal in character and unoccupied, these

anti-bonding orbitals are the lowest unoccupied molecular orbitals (LUMO) in the complex.[13]

As a result of weak bonding interaction between the $3d_{x^2-y^2}$, $3d_{xy}$ valence orbitals of the metal and the energetically closer benzene e_2 orbitals, the filled e_2 molecular orbitals retain a large degree of metal character (~73%).[13] The a_1 molecular orbital is non-bonding and overwhelmingly metal in character (~94%)[13] due to the negligible interaction between the $3d_{z^2}$ valence orbital of the metal and the a_1 orbital of cyclopentadienyl ligand orbital. This orbital contains two electrons and is the highest occupied molecular orbital (HOMO) in the complex.

However in contrast to the inability of irradiation to lead to cleavage of the cyclopentadienyl ligand in ferrocene, the use of photons to cleave the arene moiety from mixed sandwich complexes has now become routine. The first report of arene cleavage was by Nesmeyanov and co-workers,[14] who demonstrated that photolysis of $[(\eta^5\text{-}C_5H_5)Fe(\eta^6\text{-benzene})]^+X^-$ salts in the absence of suitable ligands and in aprotic solvents lead to the release of benzene, formation of ferrocene and iron(II) salts, refer to Reaction 2-6.

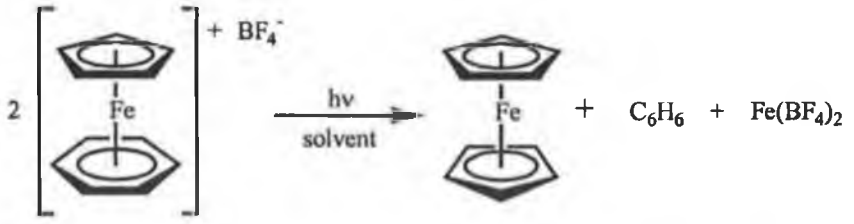

Reaction 2-6 Photolysis of mixed sandwich complex in the absence of suitable ligands.

Gill and Mann[15] exploited synthetic applications of this reaction. They revealed that photolysis of the eighteen-electron $[(\eta^5\text{-}C_5H_5)Fe(\eta^6\text{-arene})]^+X^-$ complexes lead to formation of $CpFeL_3$ in the presence of suitable two electron ligands, L, (where L = CO, C_6H_5CN, $P(OMe)_3$), refer to Scheme 2-4(a) and the replacement of arene in the presence of a six electron donor ligand, L_3, (where $L_3 = C_6Me_6$, C_7H_8), refer to Scheme 2-4(b).

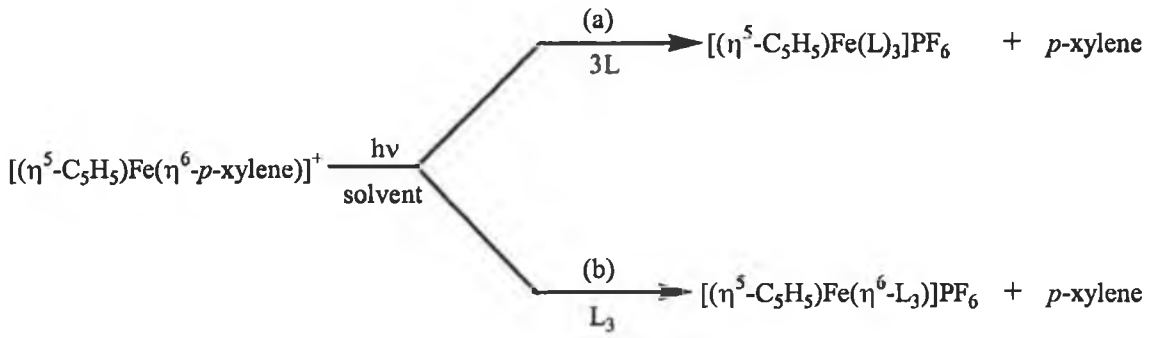

Scheme 2-4 Photolysis of mixed sandwich complex in the presence of suitable ligands.

Some insight into the nature of the reaction intermediates was provided initially by static techniques such as ^{1}H NMR and UV-vis spectroscopy as well as chemical reaction studies.[16] Subsequently Gill and Mann proposed that $(\eta^5\text{-}C_5H_5)Fe(CH_3CN)_3^+$ was an intermediate species produced upon the photolysis of $(\eta^5\text{-}C_5H_5)Fe(p\text{-xylene})^+$ in acetonitrile solution at low temperature (-40° C), which yielded ferrocene according to Scheme 2-5.

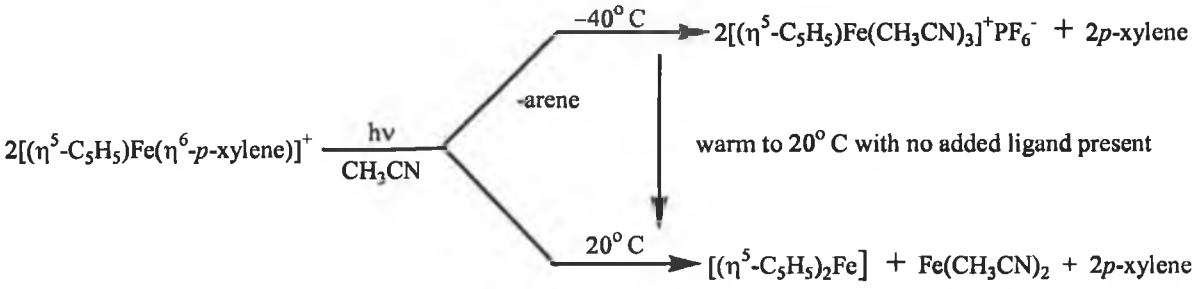

Scheme 2-5 Photolysis of mixed sandwich complex in acetonitrile at low temperature.

This photochemical method of arene liberation has significant synthetic utility because the arene liberated may be thermally labile or may contain functional groups, which are readily reduced. These features are all in addition to the high yield of the reaction and the ease at which the arene can be isolated from the side products (i.e. ferrocene and iron(II) salts) via column chromatography or extraction.

Several workers[17-20] have investigated the mechanism of photochemical arene release from mixed metallocenes complexes, $[(\eta^5\text{-}C_5H_5)Fe(\eta^6\text{-arene})]^+$, where the excitation wavelength = 436 nm. These studies have revealed that the quantum yields of arene loss is dependent on a number of factors. Namely; the substitution groups on the cyclopentadienyl ligand;[17] the nature of the arene ligand;[18] the polarity of the solvent and in the absence of a nucleophilic solvent, the quantum yield was also affected by the counter anion.[19]

Permethylation of the cyclopentadienyl ligand decreases the arene release quantum yield as compared to those of the analogous cyclopentadienyl complexes.[17] These decreases are factors of 113 and 20,500 where the arene is toluene and hexamethylbenzene respectively. It was shown that the decrease in the quantum yield for arene replacement that occurs on permethylation of the cyclopentadienyl ligand in an iron complex such as $[(\eta^5\text{-}C_5(CH_3)_5)Fe(\eta^6\text{-arene})]^+$, results from a steric effect.

The nature of the arene in the $[(\eta^5\text{-}C_5H_5)Fe(\eta^6\text{-arene})]^+$ complex also affects arene release quantum yields through electronic and steric inhibition of the arene.[18] The steric effect results from a high degree of arene methylation (i.e. five or six groups) or from very bulky substituents (ethyl or *tetra*-butyl), arene substituents that protect the excited metal centre from nucleophilic attack.

Nucleophilic solvents increase the arene release quantum yield, suggesting that they may co-ordinate with the metal to form intermediate complexes.[19] In the absence of a nucleophilic solvent, the counter anion will affect the quantum yield, indicating that anions present in solution may also weakly co-ordinate to the metal centre. Thus for solvents the quantum yield increases in the order $CH_2Cl_2 < CH_2CN < CH_3OH < H_2O <$ propylene carbonate, while the order of counter-ions is SF_6^- *ca.* AsF_6^- *ca.* $PF_6^- < ClO_4^-$ *ca.* $Br^- < BF_4^- < CF_3SO_3^-$.

Furthermore, it has been observed that quantitative triplet sensitisation initiated the arene substitution as did direct irradiation at longer excitation wavelength into the presumed singlet-triplet absorption band of the complex.[15(c),16-20] These studies stated

that the quantum efficiency for inter system crossing is unity and that the reactivity occurs exclusively from a lowest energy ligand field triplet state (a^3E_1).

Schuster *et al.*[21] carried out a time-resolved spectroscopic investigation of the photochemistry of the cationic iron complex, $[(\eta^5\text{-}C_5H_5)Fe(\eta^6\text{-arene})]^+$. They provided a model to explain the solvent dependency of the reaction in terms of reactions involving ion-paired and freely solvated species, as outlined in Scheme 2-6.

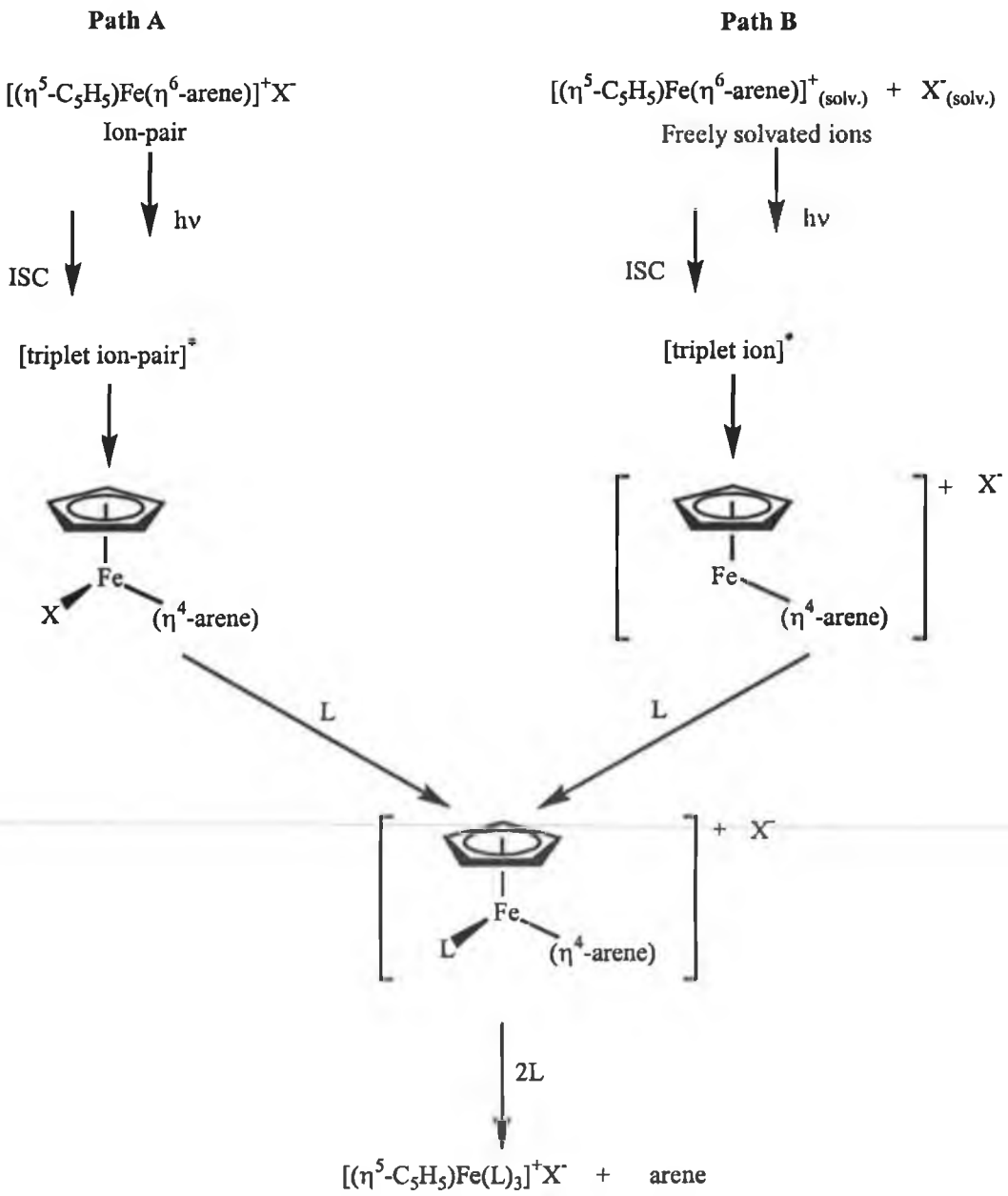

Scheme 2-6 Reaction Scheme proposed by Schuster *et al.*[21]

Irradiation of either freely solvated (i.e. $[(\eta^5\text{-}C_5H_5)Fe(\eta^6\text{-arene})]^+_{(solv.)} + X^-_{(solv.)}$, in solvents with a high dielectric constant) or ion-paired (i.e. $[(\eta^5\text{-}C_5H_5)Fe(\eta^6\text{-arene})]^+X^-$, in solvents with a low dielectric constant) complexes initiates the same first step: the excited singlet state, which crosses to the triplet state by intersystem crossing and a labilised arene ligand slips from $\eta^6 \rightarrow \eta^4$ hapticity, thus opening a co-ordination site on the iron. In the case of the ion-paired moiety, path A, Scheme 2-6, $[(\eta^5\text{-}C_5H_5)Fe(\eta^6\text{-arene})]^+X^-$ forms a neutral ring-slipped η^4-arene intermediate containing a co-ordinated counter-ion, $[(\eta^5\text{-}C_5H_5)Fe(\eta^4\text{-arene})]X$, subsequently a molecule L (i.e. two electron donor ligand) replaces the counter-ion X in the η^4-arene intermediate via a much slower thermal step to yield $[(\eta^5\text{-}C_5H_5)Fe(\eta^4\text{-arene})L]^+X^-$. Meanwhile, in the case of the freely solvated ions, path B, Scheme 2-6, the cationic co-ordinately unsaturated ring-slipped η^4-arene intermediate formed, reacts rapidly and thermally with a molecule of L to produce $[(\eta^5\text{-}C_5H_5)Fe(\eta^4\text{-arene})L]^+X^-$. Both routes converge at the $[(\eta^5\text{-}C_5H_5)Fe(\eta^4\text{-arene})L]^+X^-$ intermediate and the relatively rapid displacement of the arene by two more molecules of L (incoming nucleophiles) in two subsequent thermal steps yielding the ligand exchange product.

Triplet sensitisation experiments that bypass the singlet states or irradiation into the lowest-lying singlet of either the ion-pair or the freely solvated ion with excitation wavelength = 532 nm resulted in the same reaction intermediates. These observations may be seen as verification of the existence of efficient inter system crossing from the singlet to the corresponding lower-energy triplet excited states and confirmation of the reactive role of the triplet manifold.

Investigations by Román *et al.*[22] into the luminescence from mixed metallocene complexes revealed visible fluorescence at 520 nm following excitation at 430 nm for several complexes of the type $[(\eta^5\text{-}C_5H_5)Fe(\eta^6\text{-arene})]^+X^-$ in dichloromethane solution at room temperature. Their results indicate that emission yields increase as the electron density of the arene ring increases. The quantum efficiency for fluorescence of $[(\eta^5\text{-}C_5H_5)Fe(\eta^6\text{-}p\text{-xylene})]^+X^-$ was observed to increase with the presence of added hexamethylbenzene (HMB), Reaction 2-7. At higher concentrations of HMB the fluorescence quantum yield approaches that for direct irradiation of

$[(\eta^5\text{-}C_5H_5)Fe(\eta^6\text{-HMB})]^+X^-$. These findings were attributed to ligand exchange on the excited singlet state surface without significant deactivation of the excited mixed metallocene complex.

$$[(\eta^5\text{-}C_5H_5)Fe(\eta^6\text{-arene})]^{+*} + \text{HMB} \longrightarrow [(\eta^5\text{-}C_5H_5)Fe(\eta^6\text{-HMB})]^+ + \text{arene}$$

Reaction 2-7

Mixed metallocene photochemistry has taken on special significance since the mid 1980's, when Meier and Zweifel[23(a)] reported that these type of complexes are highly efficient visible-light photo-initiators for the cationic polymerisation of epoxides.[23] As few compounds are known to have properties satisfactory for application in this area, it is important to gain good mechanistic detail about the photo-dearylation process, in order to aid the design of future cationic polymerisation initiators.

Jabúbek and Lees[24] investigated the mechanistic detail of the photoinduced arene release in mixed metallocenes further. Previous investigations into the system were hampered by inner filtering effects because of light absorption by the entering ligand taking place at high energy and the fact that mixed metallocene complexes have low absorptivity at low energy. As a consequence, the photochemistry was limited to wavelengths of excitation equal to 436 nm to avoid the aforementioned interference. However this restriction in wavelength excitation was overcome by the development of a photo-kinetic procedures, which enabled wavelength dependency of photo-reactive systems to be investigated where inner filter absorbency problems exist.[25]

Jabúbek and Lees[24] found that irrespective of the wavelength of excitation, the overall photochemical quantum efficiencies of arene displacement from the mixed metallocene, $[(\eta^5\text{-}C_5H_5)Fe(\eta^6\text{-isopropylbenzene})]PF_6$ are controlled by the branching ratio of the initial $\eta^6 \rightarrow \eta^4$ dissociation pathway to the non-radiative pathways to the ground state. The photochemical quantum efficiencies are further diminished by any thermal processes that return the molecule to the initial parent complex, such as a reverse arene-slippage ($\eta^4 \rightarrow \eta^6$) of the sixteen electron $[(\eta^5\text{-}C_5H_5)Fe(\eta^4\text{-isopropylbenzene})]^+$ complex, and other back reactions including counter-ion and/or solvent rearrangement,

or substitution. In the case $[(\eta^5\text{-}C_5H_5)Fe(\eta^6\text{-isopropylbenzene})]PF_6$ complex, the lowest lying singlet (a^1E_1) and triplet (a^3E_1) ligand field states have distinctive photo-reactive pathways. The initial reaction mechanism for the arene dissociation reaction in the mixed metallocene $[(\eta^5\text{-}C_5H_5)Fe(\eta^6\text{-isopropylbenzene})]PF_6$ complex is summarised in Scheme 2-7.

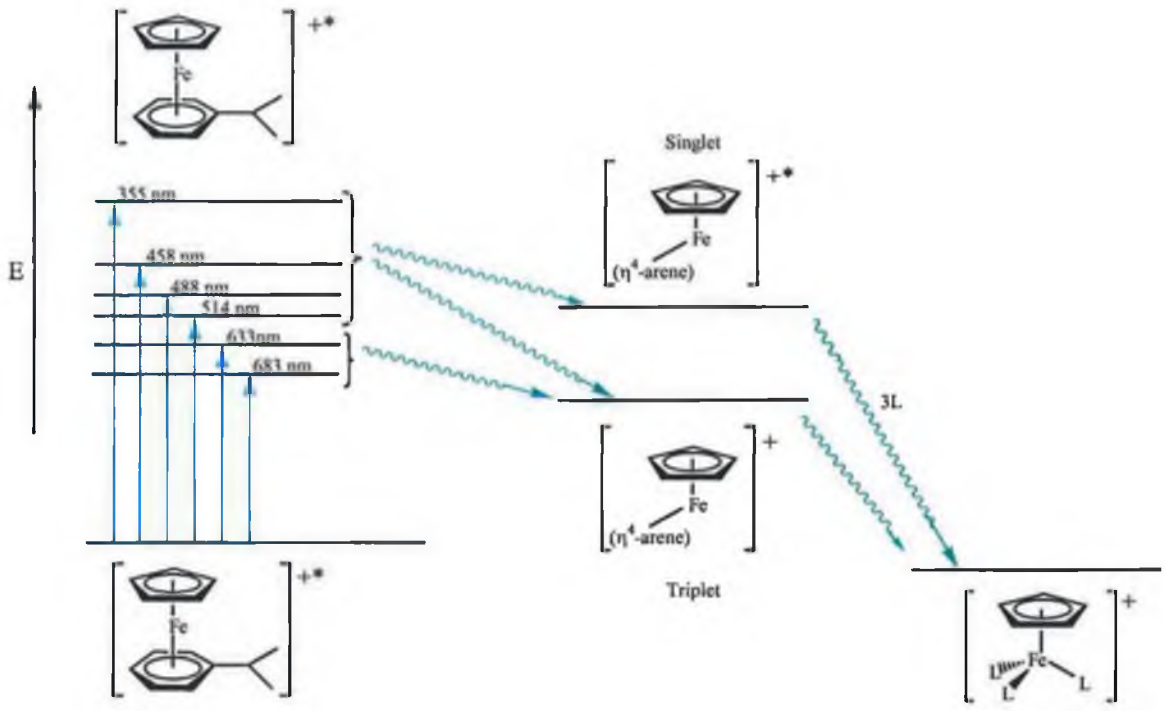

Scheme 2-7 The initial reaction mechanism for arene dissociation from the mixed metallocene, $[(\eta^5\text{-}C_5H_5)Fe(\eta^6\text{-isopropylbenzene})]PF_6$.[24] For purposes of clarity, radiative and non-radiative decay from the excited states and return pathways of reaction intermediates to the parent complex are omitted.

The photochemical reaction was found to be extremely efficient throughout the entire UV and visible region, and it is evident form this that the photochemical reaction can be efficiently carried out throughout the whole visible spectrum. Irradiation with low energy light at 683 nm lead to the population of the triplet state directly. The wavelength dependency of the photochemistry reveals that the reactivity does not solely derive from the lowest triplet ligand field state as previously assumed and that the corresponding singlet state also participates directly in the reactivity.

2.3 Why investigate the photochemistry of azaferrocene?

It has been demonstrated in the introduction that half sandwich complexes of the type (η^6-arene)$Cr(CO)_3$ display different photochemical and thermal chemistries.[26] Benzene chromium tricarbonyl undergoes thermally induced arene exchange, [27] while carbon monoxide loss is the dominant photochemical process.[28] The arene exchange proceeds[27] *via* a haptotropic shift of the arene ligand, however the only report of a photoinduced haptotropic shift[29] of (η^6-arene)$Cr(CO)_3$ comes from the investigation of the photochemistry of π co-ordinated pyridine complexes, which demonstrated that such process may be induced, particularly following low energy photolysis.

The investigation of half sandwich complexes, has now been extended to full-sandwich complexes, in order to investigate the possibility that the introduction of a hetero-aromatic ligand may lead to a change in the photochemistry observed for this class of complex. As already shown, ferrocene itself is remarkably photostable in hydrocarbon solvents. However to date there have been no reports about the photochemistry of azaferrocene, the closest and most accessible heterocyclic analogue of ferrocene. Therefore, azaferrocene was chosen as the starting point in the investigation of sandwich complexes, as the relationship between ferrocene and azaferrocene is similar to that between (η^6-benzene)$Cr(CO)_3$ and (η^6-pyridine)$Cr(CO)_3$.

2.3.1 Some theoretical aspects of chemistry of the η^5-pyrrolyl ligand and azaferrocene

A large array of η^5-cyclopentadienyl transition metal complexes is known, and it should be possible to synthesise the η^5-pyrrolyl analogue of all these complexes. Although there are such examples in the literature, the number of complexes is small. This situation arises because unlike cyclopentadienyl complexes, the pyrrolyl ligand can form stable η^1-complexes due to the presence of a lone pair of electrons on the nitrogen atom. The replacement of one methine unit in cyclopentadienyl ligand with a nitrogen atom to form the pyrrolyl ligand has several consequences. Firstly, pyrrolyl with its

nitrogen lone pair can σ and/or π co-ordinate to transition metals as already mentioned. Secondly, replacing the methine group by an iso-electronic, albeit electro-negative, nitrogen atom results in an electronic perturbation that removes the degeneracy of the e_1 and e_2 levels (symmetry lowering from D_{5h} to C_{2v}). The orbitals with a coefficient on the replaced carbon atom decrease in energy, while the others remain unaffected. Thus χ_1, χ_2, and χ_4 are the orbitals lowered in energy. The resulting order of energies of the pyrrolyl orbitals is depicted in Figure 2-2, where the molecular orbitals of the pyrrolyl ligand are compared to those of the cyclopentadienyl ligand.

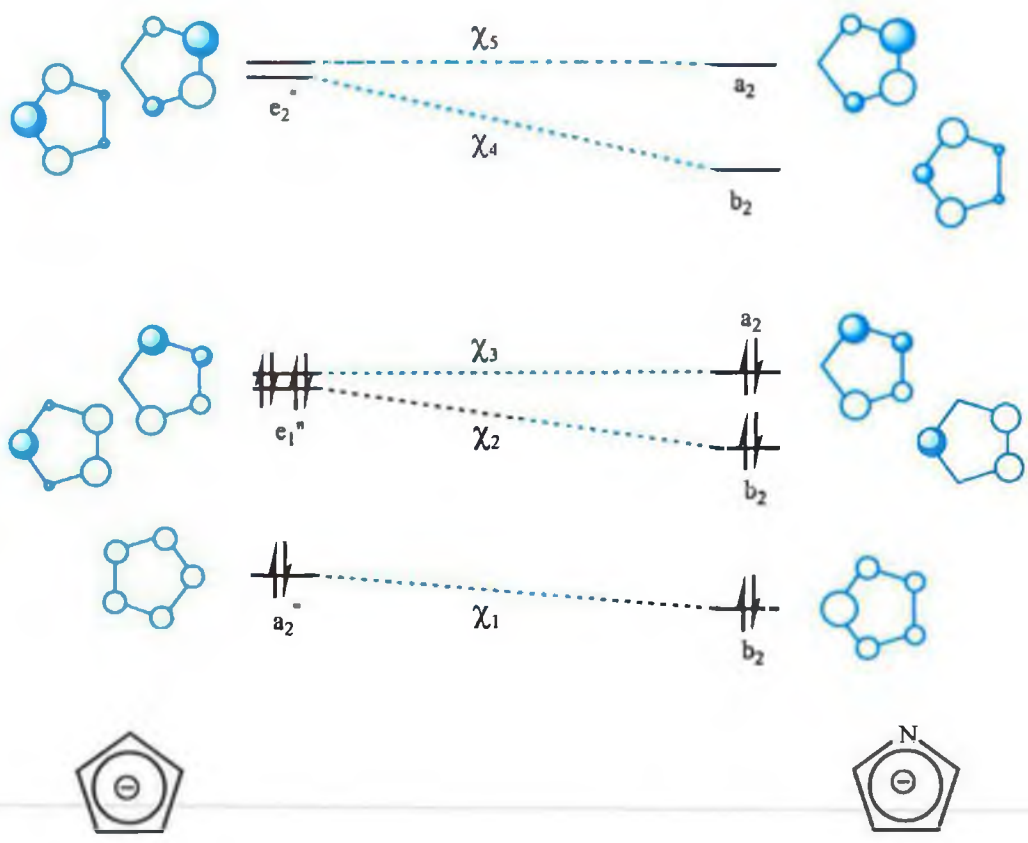

Figure 2-2 A comparison of the π-orbitals of the cyclopentadienyl ligand with the π-orbitals of the pyrrolyl ligand.[30]

The molecular structure of azaferrocene has been reported by Joshi, Pauson, Qazi and Stubbs[31] and is isomorphous with ferrocene.

Although distinctly less stable and possessing lower melting points, the physical properties of η^5-bound pyrrolyl complexes are generally very similar to those of their η^5-cyclopentadienyl counterparts.[32] A comparison of the infrared spectrum of azaferrocene with ferrocene in the range 400-300 cm^{-1} by Catalliotti, Foffani and Pignataro[33] shows that azaferrocene has many more bands than ferrocene. Furthermore many of the azaferrocene bands arise at the same frequency as the corresponding ones of ferrocene. However the influence of the hetero-atom is sufficient to make several Raman or inactive modes of ferrocene infrared active (i.e. substitution of the carbon atom by nitrogen causes a lowering of the D_{5h} symmetry of the ferrocene molecule, acting almost as an isotopic substitution of the carbon atom). Table 1 outlines the infrared bands of azaferrocene compared to ferrocene as reported with their assignments. A similar case was reported[34] for the half-sandwich complexes $(\eta^5\text{-}C_5H_5)Mn(CO)_3$ and $(\eta^5\text{-}C_4H_4N)Mn(CO)_3$. Here again the replacement of carbon by nitrogen in the ring scarcely affected the mechanical properties of the ring. Splitting of the degenerate modes was not observed in spite of lowering of local symmetry of the five-membered ring from C_{5v} to C_s. However as above in the case of the sandwich complexes, modes that were only Raman active for the cyclopentadienyl ring, became infrared active in the infrared spectrum of $(\eta^5\text{-}C_4H_4N)Mn(CO)_3$.

Azaferrocene			Ferrocene[35]	
ν_1	3106	A_{1g}(Raman)	ν_1	3110
ν_2	806		ν_2	1105 (804)
ν_3	1104		ν_3	1390, 1105
ν_4	308		ν_4	306
ν_5	1266	A_{1u}(Inactive)	ν_5	(1253)
ν_6	------		ν_6	------
ν_7	1257		ν_7	1249
ν_8	3080	A_{2u}(Infrared)	ν_8	3086
ν_9	815		ν_9	1104, 811
ν_{10}	1107		ν_{10}	1408, 1108
ν_{11}	472		ν_{11}	478
ν_{12}	3090	E_{1g}(Raman)	ν_{12}	3089
ν_{13}	995		ν_{13}	998
ν_{14}	806		ν_{14}	818
ν_{15}	1404		ν_{15}	1412
ν_{16}	385		ν_{16}	390
ν_{17}	3080	E_{1u}(Infrared)	ν_{17}	3086
ν_{18}	1003		ν_{18}	1004
ν_{19}	815		ν_{19}	814
ν_{20}	1408		ν_{20}	1408
ν_{21}	492		ν_{21}	190
ν_{22}	-----		ν_{22}	(107)
ν_{23}	3048	E_{2g}(Raman)	ν_{23}	3045
ν_{24}	1382		ν_{24}	1361
ν_{25}	1184		ν_{25}	1184
ν_{26}	1530		ν_{26}	1527
ν_{27}	1054		ν_{27}	1054
ν_{28}	601		ν_{28}	591
ν_{29}	------		ν_{29}	(3035)
ν_{30}	1351	E_{2u}(Inactive)	ν_{30}	(1351)
ν_{31}	1189		ν_{31}	(1188)
ν_{32}	------		ν_{32}	------
ν_{33}	1054		ν_{33}	1054
ν_{34}	628		ν_{34}	567

Table 2-1 Comparison of the infrared spectrum of azaferrocene with ferrocene, taken from reference 33.

Some of the early ^{57}Fe Mössbauer data on azaferrocene available in the literature is contradictory,[36,37] this discrepancy being possibly because of the instability of the early Mössbauer spectrometers. However better consistency has been obtained between a more recent publication[37] and the latest publication,[38] which re-examined azaferrocene and the 2,5-dimethylazaferrocene complex. In these papers the quadrupole splitting (Q.S.) parameter for iron complexes is reported. This parameter depends on the relative populations of the e_2 ($d_{x^2-y^2}$, d_{xy}) and e_1 (d_{xz}, d_{yz}) orbitals. The d_{z^2} orbital appears to be

fully occupied in all iron sandwich complexes and is therefore discounted when comparing quadrupole-splitting values. The e_2 orbitals contributes twice as strongly to the electron field gradient as the e_1 orbitals, leading to the relationship, quadrupole splitting $\propto 2p_1-p_2$, where p_1 and p_2 are the electronic populations of the e_2 and e_1 molecular orbital sets respectively. The ferrocene quadrupole splitting value (2.37 mm s^{-1}) is lower than that of azaferrocene (2.51 mm s^{-1}), showing that the pyrrolyl rings are more electro-negative than the cyclopentadienyl rings in terms of the bonding orbitals to the iron. So the pyrrolyl ring requires less backbonding from the e_2 iron based orbitals, as the e_1 molecular orbital from the pyrrolyl ring is more electron donating. This causes enhanced quadrupole splitting relative to ferrocene. The ferrocene value is considered to be high and derived from filled and largely unperturbed e_2 levels, resulting in a large imbalance of the e_2 and e_1 populations. Although the symmetry is reduced from D_{5h} in ferrocene to C_{2h} in azaferrocene, this imbalance of the e_2 and e_1 populations must also exist in azaferrocene, (i.e. little mixing of the iron d-orbitals). Therefore the introduction of the heteroatom into the cyclic ligand causes only minor changes in the electron density and the electric field gradient at the metal atom.

2.3.2 Some synthetic aspects of chemistry of the η^5-pyrrolyl ligand and azaferrocene

It has been shown that the pyrrolyl ligand reacts with metal carbonyl halides to form a η^1-complex,[31] which then may be converted via loss of two carbon monoxide ligands (thermally), into the corresponding η^5 complexes, Scheme 2-8. The η^1-bound intermediates vary in stability and ability to transform into η^5-complexes, as a function of the substituent on the pyrrolyl ligand. While $(\eta^5\text{-}C_5H_5)Fe(CO)_2(\eta^1\text{-}C_4H_4N)$ rearranges to azaferrocene under mild conditions (40°C), 2-acetylpyrrolyl, indolyl and carbazole all exhibit greater thermodynamic stability in the form of the corresponding η^1-bound complexes.[39]

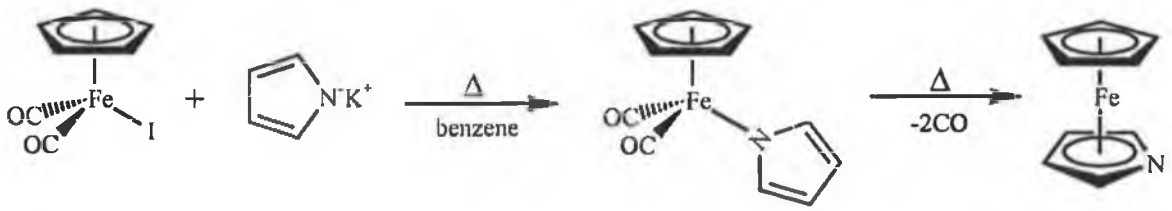

Scheme 2-8 Reaction of pyrrolyl ligand with metal carbonyl halide to form the η^1-complex and further reaction to form the η^5-complex.

Efraty and Jubran[40] compared the chemistry of the η^5-pyrrolyl ligand with the η^5-cyclopentadienyl ligand. They showed the facile $\pi \rightarrow \sigma$ rearrangement of the pyrrolyl in azaferrocene is effected by a variety of π-acidic ligands (L) including CO, PF_3, R_2NPF_2 (R = CH_3, C_2H_5), $CH_3N(PF_2)_2$, C_6H_5NC, t-C_4H_9NC, $CH_3(CH_2)_2NC$ and $(CH_3)N(CH_2)_3NC$, as outlined in Reaction 2-8.

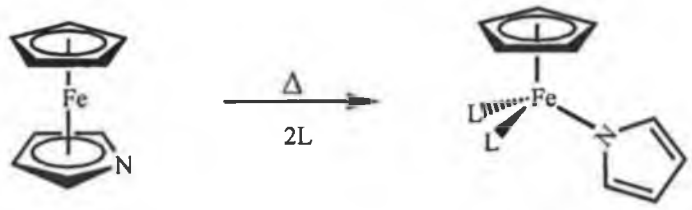

Reaction 2-8 The thermal reaction of azaferrocene with π-acidic ligands, where L = π-acidic ligands.

By contrast, the thermal reactions of azaferrocene with σ-donor ligands (L) of the type EPh_3 (E = P, As, or Sb) have been observed to accelerate the decomposition of azaferrocene because of the formation of labile intermediates of the type $(\eta^5\text{-}C_5H_5)Fe(L)_2(\eta^1\text{-}C_4H_4N)$, which degrade further to 'bare' iron and ferrocene, refer to Scheme 2-9. The amount of ferrocene formed was less than under thermal conditions (e.g. boiling toluene for two hours) in the absence of additional ligands, refer to Scheme 2-10.

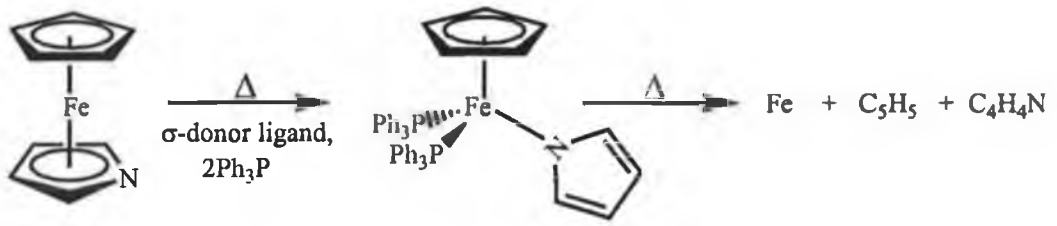

Scheme 2-9 The thermal reaction of azaferrocene with σ-donor ligands, leading to bare iron and ferrocene.

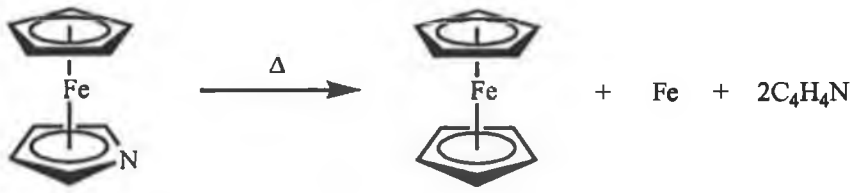

Scheme 2-10 The thermal reaction of azaferrocene in the absence of additional ligands.

However Efraty, Jubran and Goldman[40(b)] proposed that the decomposition of azaferrocene in the presence of σ-donor ligands does not necessarily proceed by the same mechanism as thermal degradation. It is possible that a bimolecular mechanism due to the presence of the nitrogen atom in azaferrocene, involving intermediates of the types, I ,II and III is responsible for the auto-decomposition observed in the absence of donor ligands, refer to Scheme 2-11. The σ-co-ordination bond is thought to facilitate the C_5H_5 ligand transfer[41] by the enhancement of the nucleophilicity of the cyclopentadienyl ligand, and the electrophilicity of the iron atom. Initiation of the ligand transfer by the creation of carbon-iron bond as in II, followed by stepwise transfer process would explain the formation of ferrocene in 50% yield or less. The formation of 'bare' iron metal in this reaction may be account for, by homolytic cleavage of III.

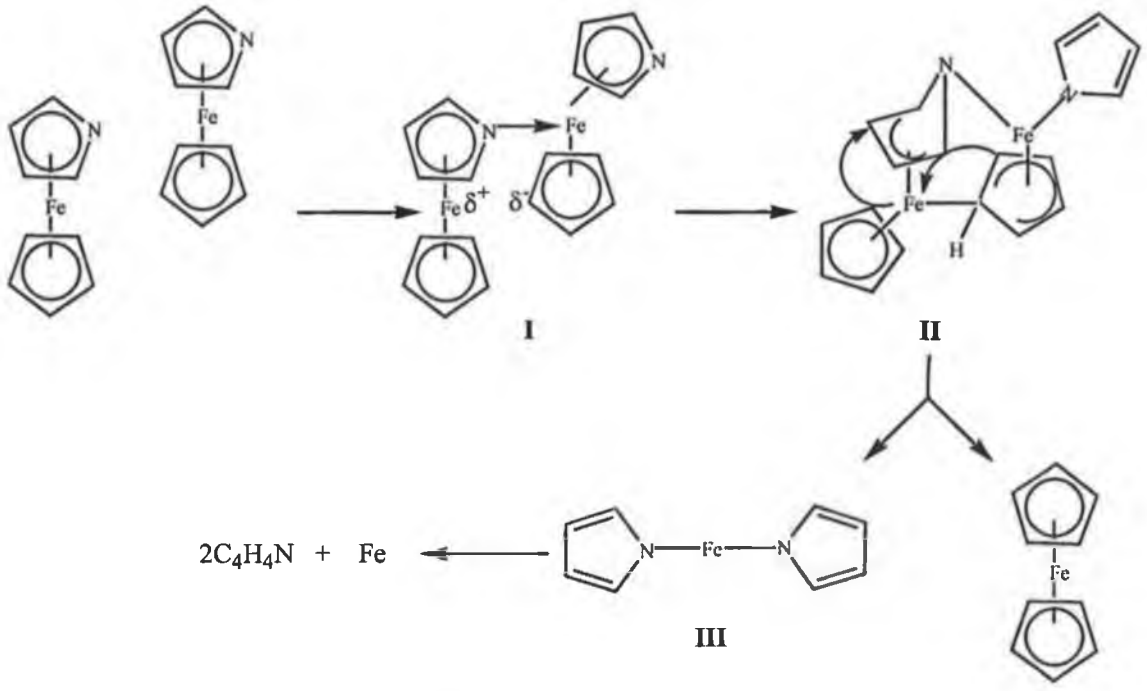

Scheme 2-11 Mechanism proposed by Efraty, Jurban and Goldman[40(b)] for the formation of iron metal and ferrocene in the thermal decomposition of azaferrocene in the absences of added ligands.

Azaferrocene was also reported to undergo carbonylation to $(\eta^5\text{-}C_5H_5)Fe(CO)_2(\eta^1\text{-}C_4H_4N)$ in benzene at 50° C under a carbon monoxide pressure of 2.5 atm., Reaction 2-9. The reaction, which was 50% complete after two hours, involves a $\pi \rightarrow \sigma$ rearrangement of the pyrrolyl ligand. This reaction however was carried out in a glass reactor, and consequently the possibility that the reaction is photochemically in nature cannot be discounted.

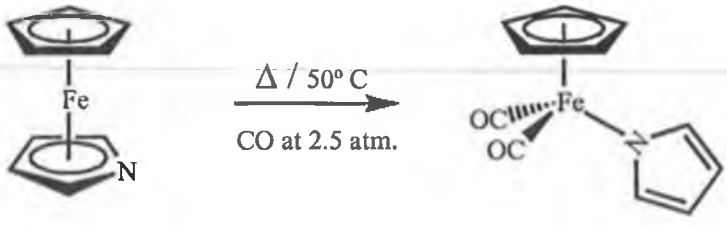

Reaction 2-9 Reaction of azaferrocene with carbon monoxide under high pressure and elevated temperature.

Frequently, permethylation of the cyclopentadienyl ligand is known to stabilise the ligand to metal bond.[42] Pentamethylpyrrole reacts with the sulphane complex $(\eta^5\text{-}C_5H_5)Fe(SMe_2)_3$[43] to give cationic $[(\eta^5\text{-}C_5H_5)Fe(\eta^5\text{-}C_4(CH_3)_5N)]^+$, which is stable in

solution and in the solid phase. Spectroscopic structural analysis (X-ray and ^{13}C NMR) confirms the metallocene character of the complex.[44] The photochemistry observed for $[(\eta^5\text{-}C_5H_5)Fe(\eta^5\text{-}C_4(CH_3)_5N)]^+$ cation correlates with that observed for $[(\eta^5\text{-}C_5H_5)Fe(\eta^6\text{-arene})]^+$ cations previously discussed, as this complex also undergoes substitution reactions with other neutral ligands (e.g. CO, $P(OMe)_3$) following irradiation, refer to Reaction 2-10.

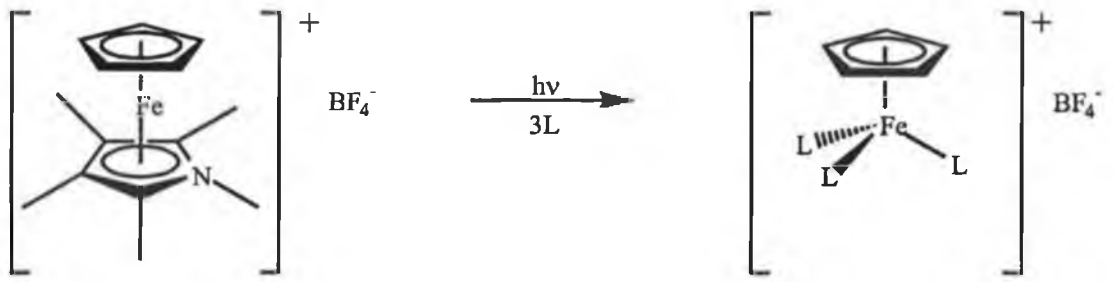

Reaction 2-10 The photochemical reaction of $[(\eta^5\text{-}C_5H_5)Fe(\eta^5\text{-}$pentamethylpyrrolyl) with neutral ligands.

The original attempts to synthesise derivatives of ferrocene with a methine group substituted by a nitrogen atom in both η^5-rings were unsuccessful.[45] The reason for this is the tendency of the nitrogen atom to act as a two electron donor ligand and the fact that the pyrrolyl group is a weaker π-donor and/or stronger π-acceptor than the cyclopentadienyl ligand. Stabilisation of 1,1-diazaferrocene was eventually achieved through blocking of the non-bonding electron pair on the nitrogen atom,[44] or through steric crowding of the 2,5-positions on the pyrrolyl ligand with bulky substituents.[46]

2.4 Results and discussion of the photochemistry of azaferrocene

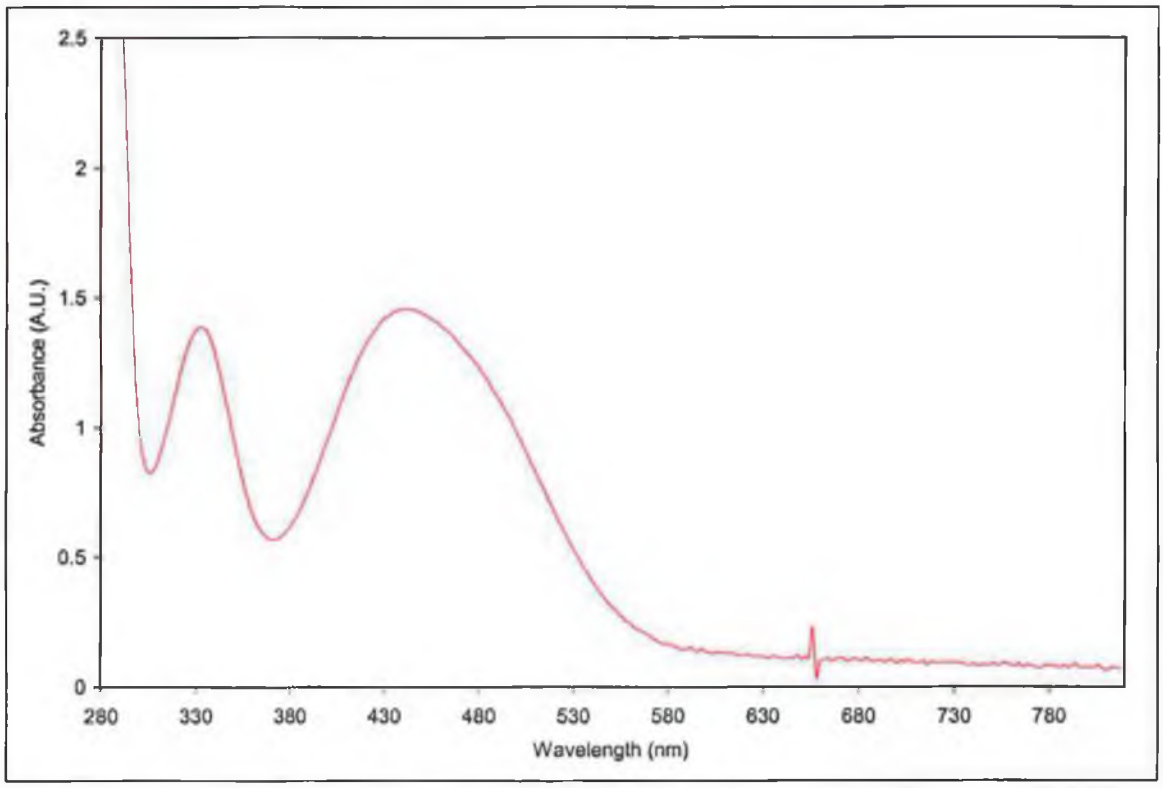

Figure 2-3 UV-vis spectrum of azaferrocene, (η^5-C_5H_5)Fe(η^5-C_4H_4N) (~2.8 × 10^{-2} M) in cyclohexane.

The UV-vis spectrum of azaferrocene, (η^5-C_5H_5)Fe(η^5-C_4H_4N) in cyclohexane as shown in Figure 2-1 displays weak absorptions centred at λ = 336 nm and λ = 446 nm, it also exhibits an absorption tail right into the visible region of the spectrum (λ > 550 nm).

2.4.1 Broad band steady state photolysis of azaferrocene monitored by UV-vis spectroscopy

Photolysis of azaferrocene, $\lambda_{exc.}$ > 500 nm under an inert argon atmosphere produced the spectral changes presented in Figure 2-4. Initially photolysis for fifteen-second intervals within the first minute of photolysis and subsequent irradiation times were increased to thirty seconds, giving a total photolysis time of three minutes. An increase in absorption was observed across the entire spectral region. An increase in the

turbidity followed photolysis. In addition no isosbestic points were obtained in these spectral changes. None of the components in this reaction has intense diagnostic absorptions in the infrared region. However the solvent was removed following the photolysis experiments under inert conditions and in the absence of light. The residue was dissolved in $CDCl_3$ and a ^1H NMR spectrum was obtained, Figure 2-5. The ^1H NMR spectrum displays peaks at 5.41, 4.58, 4.29 ppm, which may be attributed to the 2H, α-pyrrolyl, 2H, β-pyrrolyl and the 5H of the cyclopentadienyl ring of azaferrocene respectively. An additional peak at 4.13 ppm was assigned to ferrocene by comparison with an authentic sample of ferrocene.

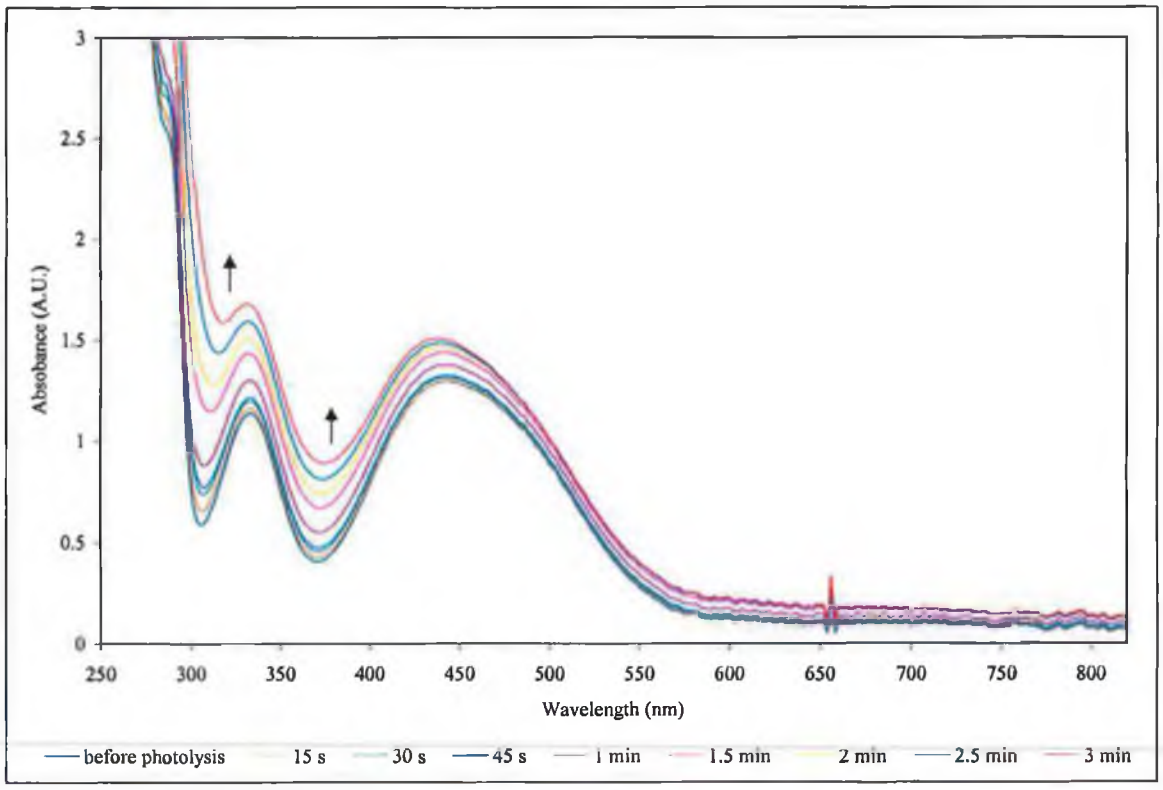

Figure 2-4 Changes observed in the UV-vis spectrum of azaferrocene (~2.3 × 10^{-2} M) in cyclohexane following photolysis at $\lambda_{exc.} > 500$ nm under an atmosphere of argon.

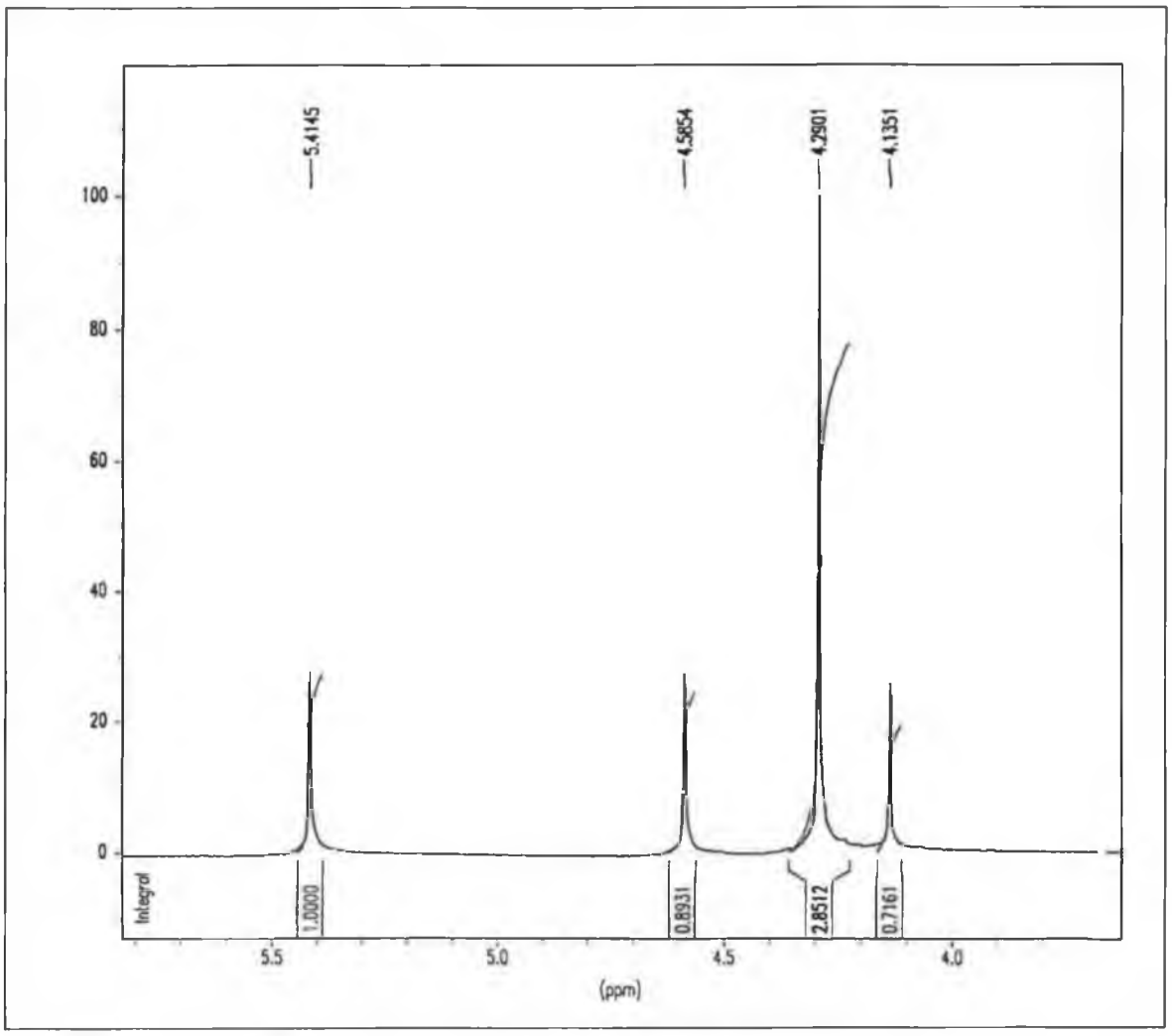

Figure 2-5 ^{1}H NMR of azaferrocene following photolysis at $\lambda_{exc.}$ > 500 nm under an atmosphere of argon.

Photolysis of azaferrocene, $\lambda_{exc.}$ > 500 nm in carbon monoxide saturated cyclohexane solutions resulted in comparable changes in the UV-vis spectrum, Figure 2-6, as to those observed in the absence of added carbon monoxide, except that the solution remained clear throughout the photolysis.

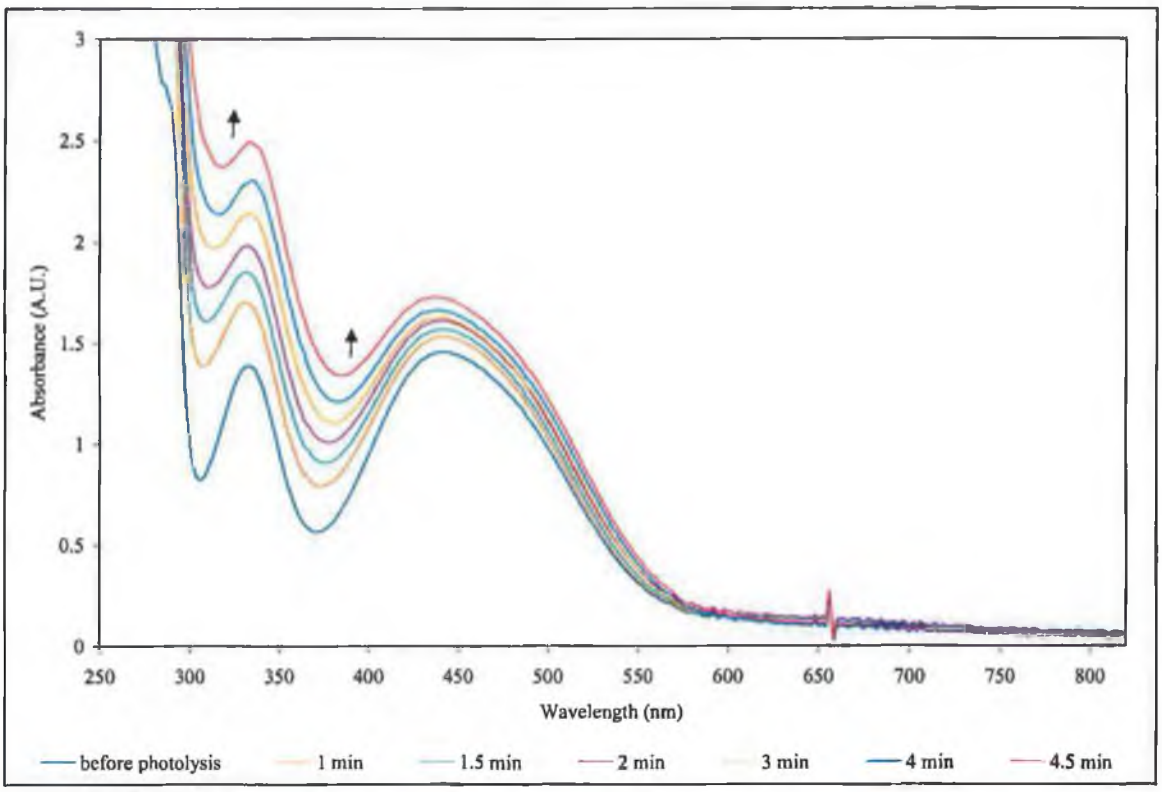

Figure 2-6 Changes observed in the UV-vis spectrum of azaferrocene (~2.8 × 10^{-2} M) following photolysis at $\lambda_{exc.} > 500$ nm, in carbon monoxide saturated cyclohexane.

Following photolysis the solution volume was reduced under reduced pressure and an infrared spectrum of the solution was obtained. The spectrum contains two bands in the carbonyl region at 2048 and 2002 cm^{-1}, Figure 2-7. These bands have been assigned to the (η^5-C_5H_5)Fe(CO)$_2$(η^1-pyrrolyl) species by comparison with an authentic sample of (η^5-C_5H_5)Fe(CO)$_2$(η^1-pyrrolyl) prepared by an independent method.[47] It is noteworthy that the values for the ν_{CO} bands for (η^5-C_5H_5)Fe(CO)$_2$(η^1-pyrrolyl) presented in the literature are incorrect. The values reported in this thesis have been confirmed by correlating our infrared spectral data obtained from a single sample of the compound with the results of high-resolution mass spectrometry and single X-ray diffraction techniques.

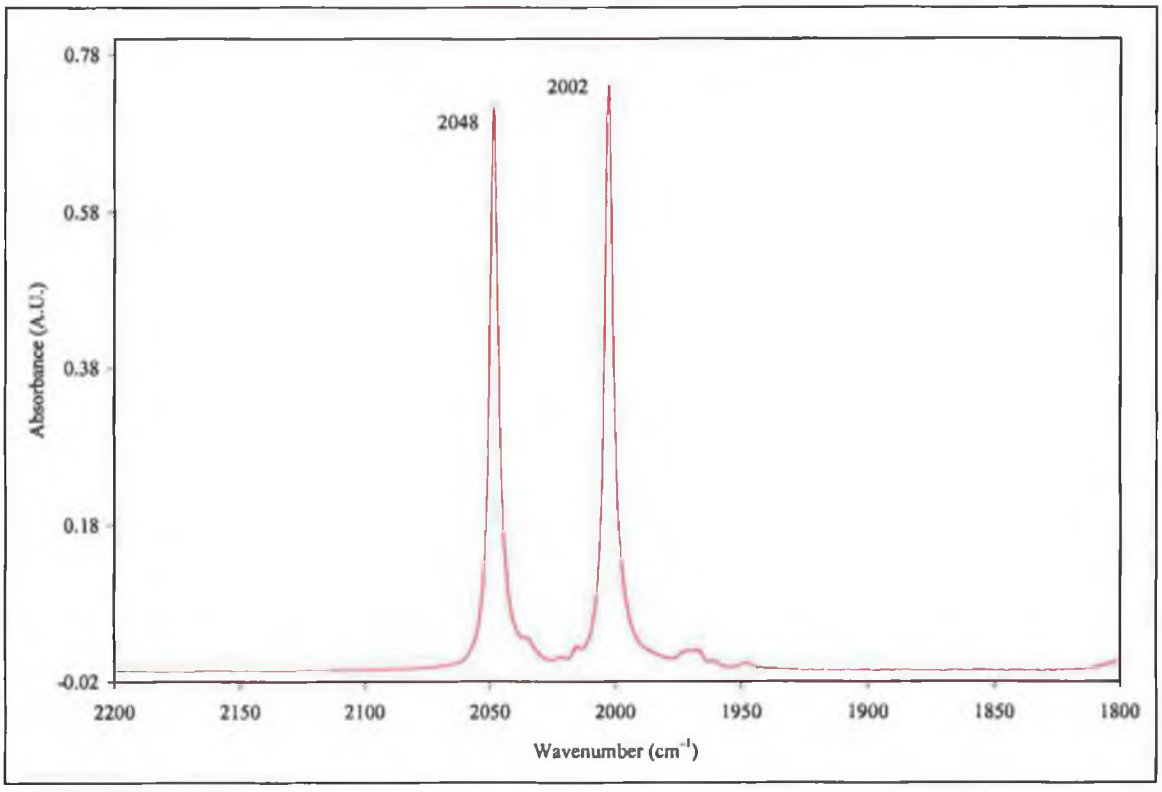

Figure 2-7 Infrared spectrum recorded of azaferrocene following photolysis at $\lambda_{exc.} > 500$ nm, in carbon monoxide saturated cyclohexane.

Experiments using higher energy photolysis ($\lambda_{exc.} > 400$nm) also produced the dicarbonyl species, $(\eta^5\text{-}C_5H_5)Fe(CO)_2(\eta^1\text{-}C_4H_4N)$ as the major photoproduct, however it also lead to the production of small amounts of iron dimer species $[(\eta^5\text{-}C_5H_5)Fe(CO)_2]_2$, ($\nu_{CO}$ = 2002, 1961, 1793 cm^{-1} in cyclohexane; the high energy band is obscured by the low energy absorption of the dicarbonyl complex $(\eta^5\text{-}C_5H_5)Fe(CO)_2(\eta^1\text{-}C_4H_4N)$, Figure 2-8. The yield of the dimer species appears to be low (based on band intensities), although it was greatest in experiments where the solution was simply flushed with carbon monoxide rather than rigorously degassed by freeze-pump-thaw procedures, followed by admission of carbon monoxide. The formation of the dimer species is not without precedence, it was also produced following photolysis of $(\eta^5\text{-}C_5H_5)Fe(CO)_2I$ in pyridine and dimethylsulphoxide.[48]

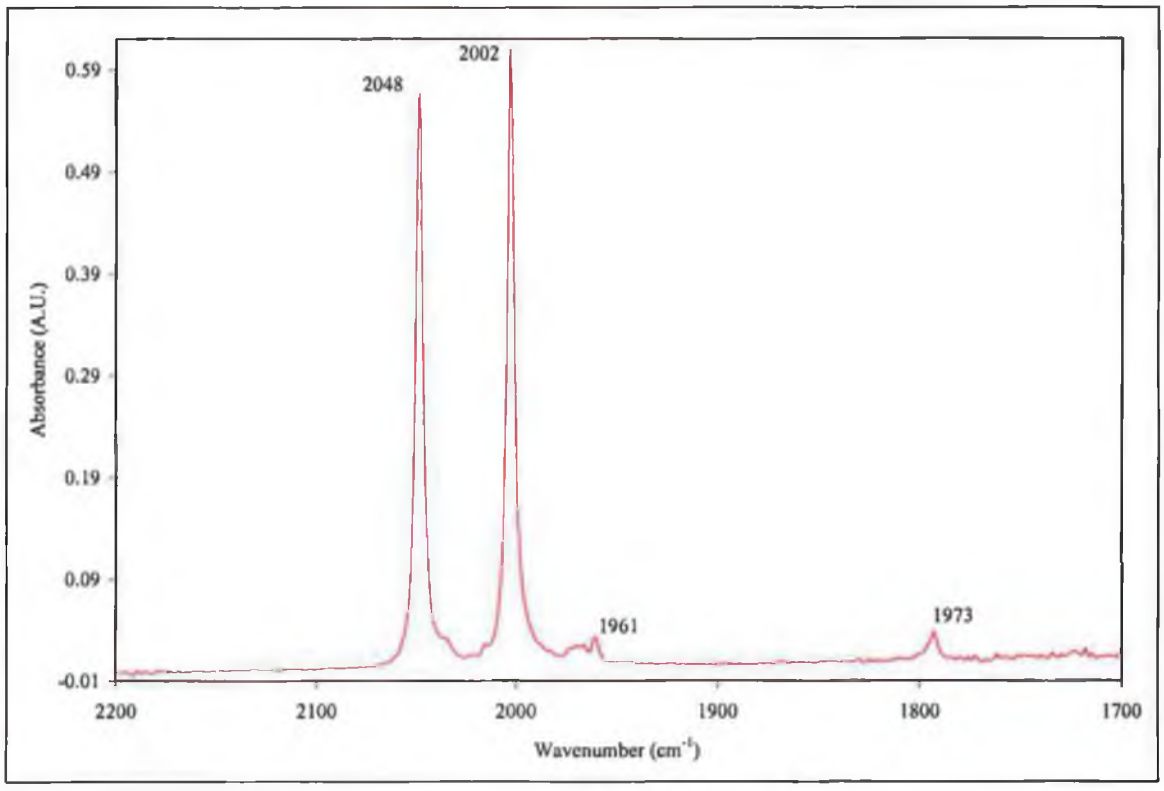

Figure 2-8 Infrared spectrum of azaferrocene following photolysis at $\lambda_{exc.} > 400$ nm, in carbon monoxide saturated cyclohexane.

Azaferrocene was also photolysised in cyclohexane under an inert atmosphere in the presence of other ligands, L = bi-pyridyl, 2,5-nornbornadiene, *cis*-cyclooctadiene and tetracyanoethylene. The UV-vis spectral changes in these experiments were identical to those observed following the photolysis of azaferrocene under an atmosphere of argon. Although the efficiency at which the changes occurred in the case of the added ligands was much more rapid than in the case of irradiation of azaferrocene under an inert atmosphere. In addition, these experiments always resulted in increased turbidity in the solution, mirroring the results of photolysis under inert conditions in the absence of added ligands rather than photolysis in the presence of added ligand carbon monoxide. Again in the case of bi-pyridyl, 2,5-nornbornadiene, *cis*-cyclooctadiene, there was no significant spectroscopic infrared absorptions, so the solvent was removed following photolysis and the ^{1}H NMR of the residue obtained in $CDCl_3$. The ^{1}H NMR spectra reveal peaks for azaferrocene at 5.41, 4.58, 4.29 ppm, a peak at 4.13 ppm attributed to ferrocene as already mentioned following photolysis under inert conditions. It is clear

from these findings, that the added ligands are not co-ordinating to the ligand to form an η^1-pyrrolyl type complex.

The photolysis of azaferrocene in the presence of tetracyanoethylene could potentially have significant infrared absorptions, however no bands were observed in the nitrile region of the infrared spectrum that would indicate that the cyano ligand was co-ordinating to the iron to form an η^1-pyrrolyl type complex. The indications are that the only ligand capable of co-ordinating and forming stable products under photochemical conditions is carbon monoxide, despite several attempts with various other ligands.

UV-vis photolysis of azaferrocene was also undertaken in co-ordinating solvents such as acetonitrile and toluene. In the case of toluene, photolysis of azaferrocene under 1 atm of argon, $\lambda_{exc.}$ >500 nm, induced a decrease in the UV-vis absorption across the entire region. A precipitate was produced during photolysis. Photolysis of azaferrocene in acetonitrile, under 1 atm argon, $\lambda_{exc.}$ >500 nm, displayed an increase in absorption across the entire spectral region. The sample was photolysed for ten minutes in total, after which time an orange crystalline precipitate was produced. After removing the solvents following photolysis under reduced pressure, attempts were made to obtain ^{1}H NMR spectra of these precipitates in $CDCl_3$. However the attempts failed, as the precipitates decomposed on exposure to air.

Azaferrocene absorbs substantially in the high-energy region of the spectrum, in order to ensure that no spectroscopic detail was being missed in the upper region of the spectrum, experiments under atmospheres of argon were conducted at low concentration. The results were no different to those at higher concentrations. The absorbance increased over the whole region, and no isosbestic point was observed, even in the high-energy region of the spectrum, Figure 2-9.

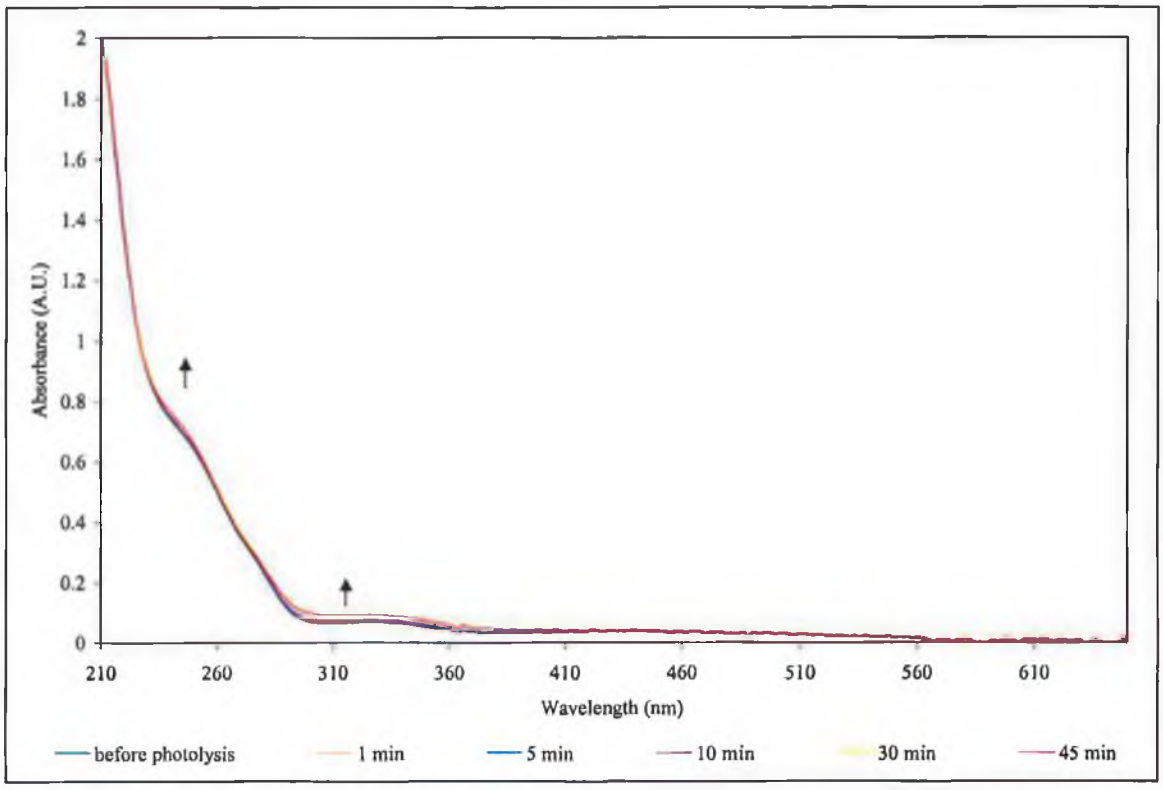

Figure 2-9 Changes observed in the UV-vis spectrum of azaferrocene at very low concentration (~1.48 × 10^{-3} M) in cyclohexane following photolysis at $\lambda_{exc.} > 500$ nm under an inert atmosphere of argon.

Finally, azaferrocene was photolysed with broad band irradiation at $\lambda_{exc.} > 500$ nm under vacuum. A solution of azaferrocene in cyclohexane was degassed by three cycles of freeze-pump-thaw, followed by 50% removal of the solvent. Broad band irradiation, $\lambda_{exc.} > 500$ nm, of the sample was carried out without the admission of any gas, and the photolysis was monitored by UV-vis spectroscopy. The changes in the UV-vis spectrum were consistent with the previous observations (i.e. increase in absorption across the entire region). However turbidity in the sample was also observed, along with the deepening in the colour of the solution from orange to red. Eventually a precipitate was produced. Following irradiation the solution was kept in darkness, 1 atm of carbon monoxide was then added to the solution cell. Infrared spectra were recorded at various time intervals, meanwhile the precipitate slowly disappeared and the solution clarified. The initial spectrum at time zero, just after addition of carbon monoxide reveals no bands in the ν_{CO} region, however subsequent spectra at time intervals of 10-30 minutes exhibit bands at 2048 and 2002 cm^{-1}, assigned to

(η^5-C_5H_5)Fe(CO)$_2$(η^1-pyrrolyl), Figure 2-10. The intensity of these ν_{CO} bands continued to increase over several hours. Although attempts to isolate and characterise the precipitate have failed to date, it is possible that it is a dimeric species, as shown in Figure 2-11.

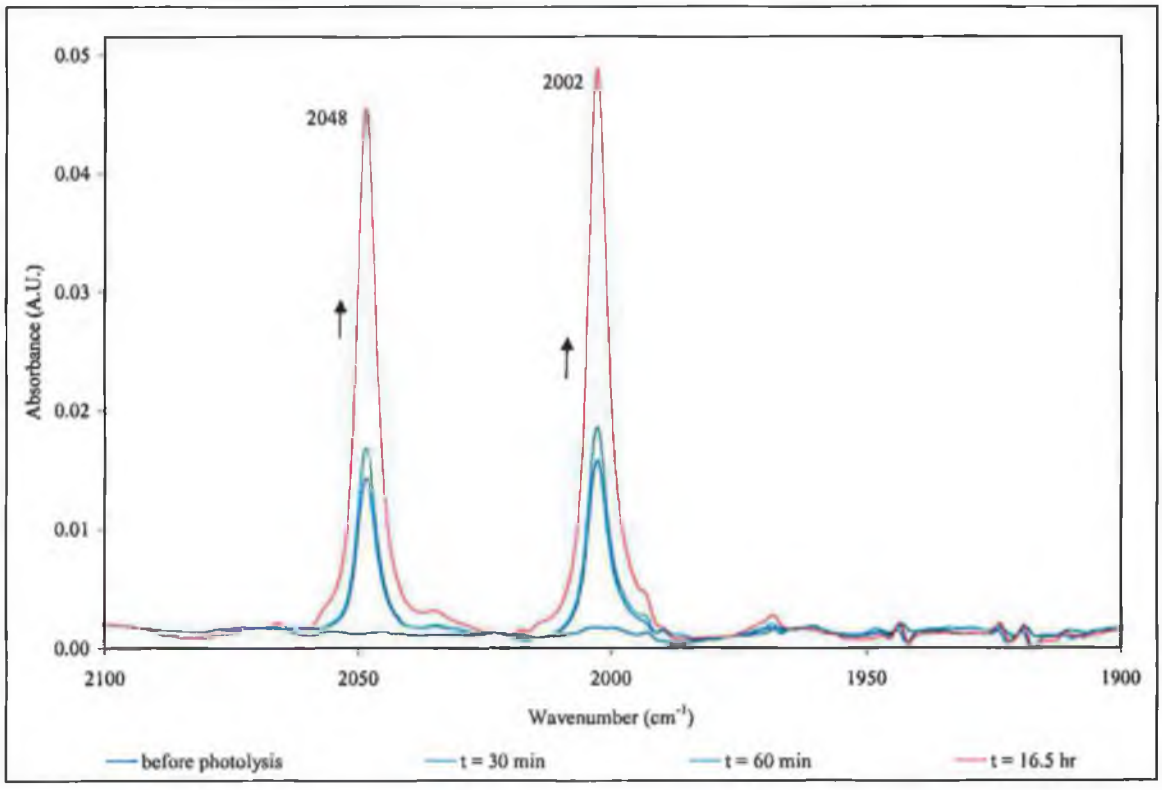

Figure 2-10 Azaferrocene photolysed under vacuum ($\lambda_{exc.}$ > 500 nm), followed by addition of 1 atm CO. Infrared spectra recorded after addition of CO while sample remained in the dark.

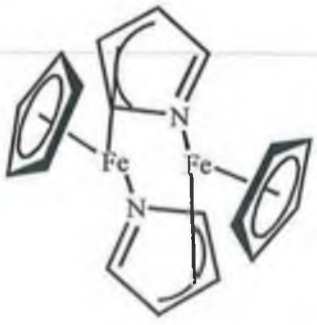

Figure 2-11 Dimeric species bonded through the lone pair on the nitrogen and through an η^3-allyl bond.

2.4.2 *Broad band ($\lambda_{exc.}$ > 500 nm) and monochromatic irradiation of azaferrocene monitored by both infrared and UV-vis spectroscopy*

A solution of azaferrocene in cyclohexane was fully degassed by the freeze-pump-thaw technique and as before, an atmosphere of carbon monoxide added to the photolysis cell. Broad band photolysis ($\lambda_{exc.}$ > 500 nm) of azaferrocene in the carbon monoxide saturated cyclohexane solution resulted in the spectral changes presented in Figure 2-12. Two new bands grew in the ν_{CO} region of the infrared spectrum at 2048 and 2002 cm^{-1}. These bands were assigned to the photoproduct (η^5-C_5H_5)Fe(CO)$_2$(η^1-pyrrolyl) as in the UV-vis monitored experiments outlined in Section 2.4.2. These results demonstrate that the pyrrolyl ligand has undergone a haptotropic shift from $\eta^5 \rightarrow \eta^1$ upon photolysis as depicted in Reaction 2-11.

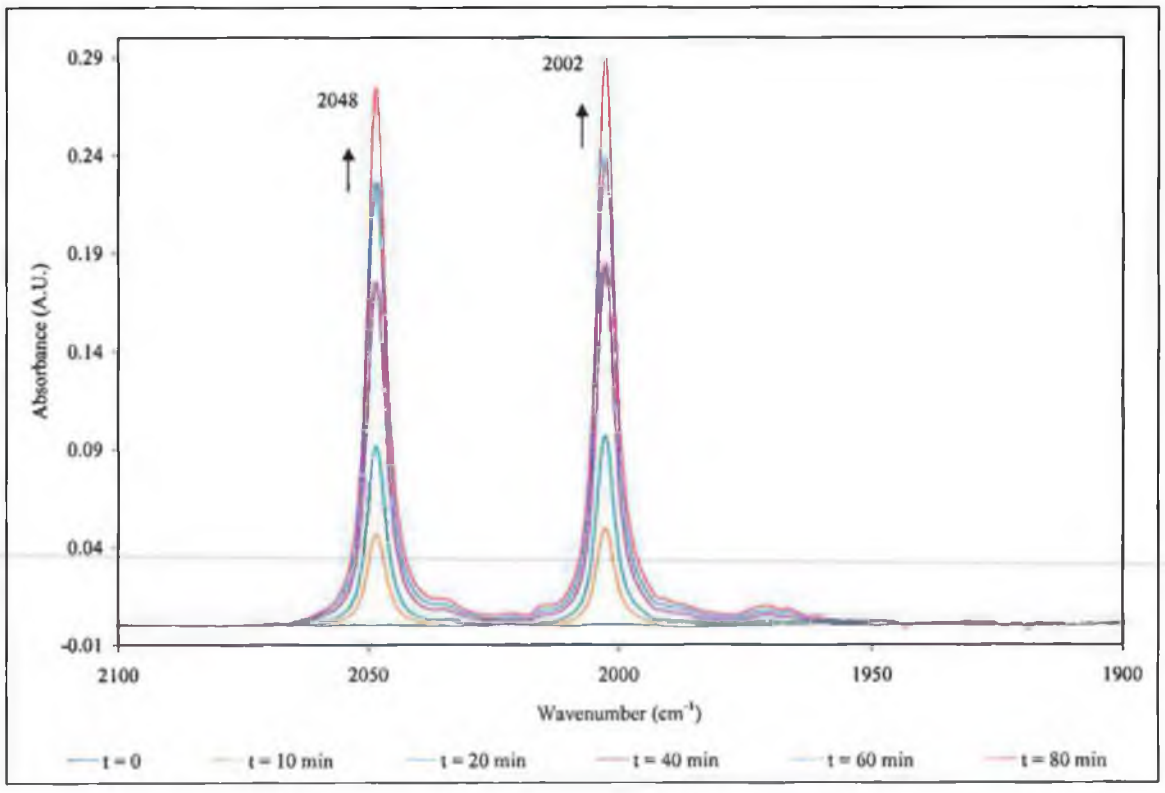

Figure 2-12 The ν_{CO} region spectral changes upon the broad band photolysis ($\lambda_{exc.}$ > 500 nm) of azaferrocene in CO saturated solution.

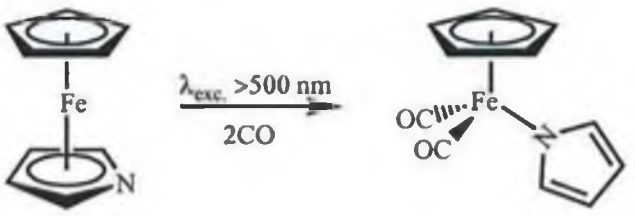

Reaction 2-11

Broad band irradiation was replaced by monochromatic light, and both UV-vis and infrared spectroscopy were employed to monitor changes in the photolysis solution. High energy monochromatic pulsed photolysis ($\lambda_{exc.}$ = 355 nm) of azaferrocene in carbon monoxide saturated cyclohexane solution at room temperature produced an increase across the whole range in the UV-vis spectrum, Figure 2-13. The infrared spectrum of the solution following photolysis displays two carbonyl stretches at 2048 and 2002 cm^{-1}. This indicates that (η^5-C_5H_5)Fe(CO)$_2$(η^1-pyrrolyl) is the sole observable carbonyl containing product formed, Figure 2-14

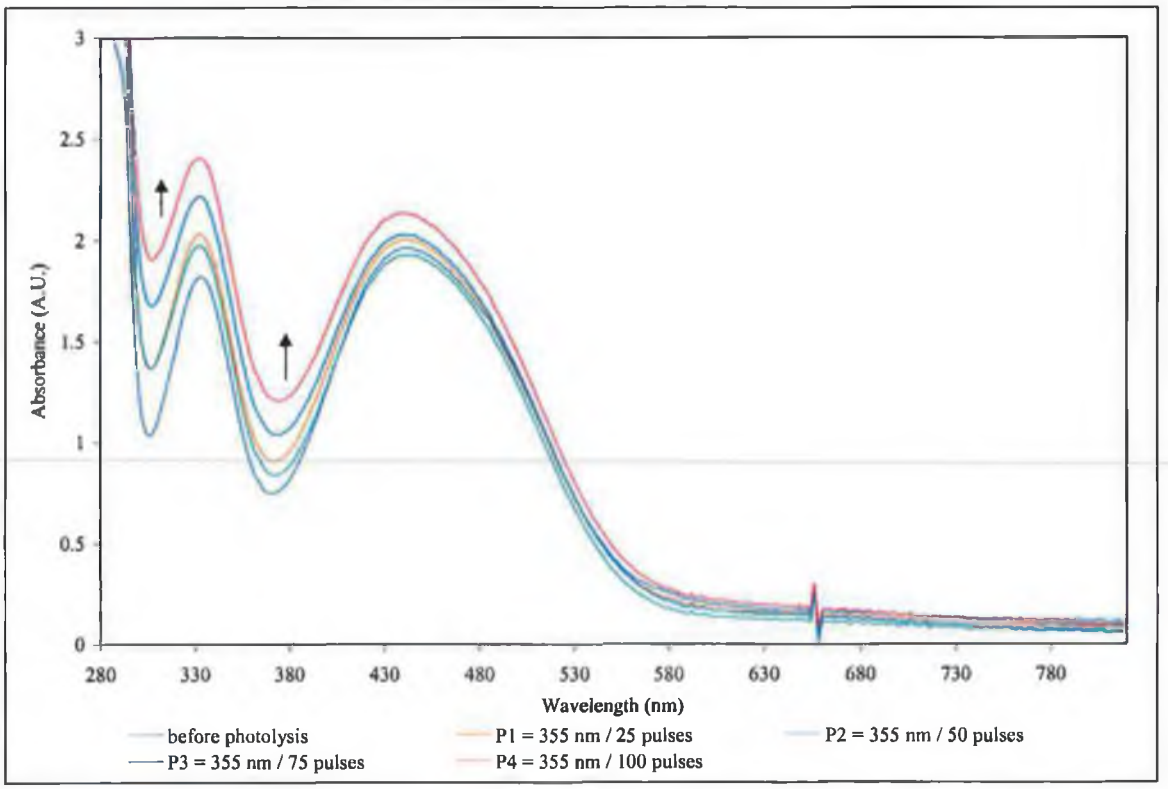

Figure 2-13 The UV-vis spectral changes following monochromatic photolysis ($\lambda_{exc.}$ = 355 nm) of azaferrocene (~3.7 × 10^{-2} M) in carbon monoxide saturated cyclohexane solution.

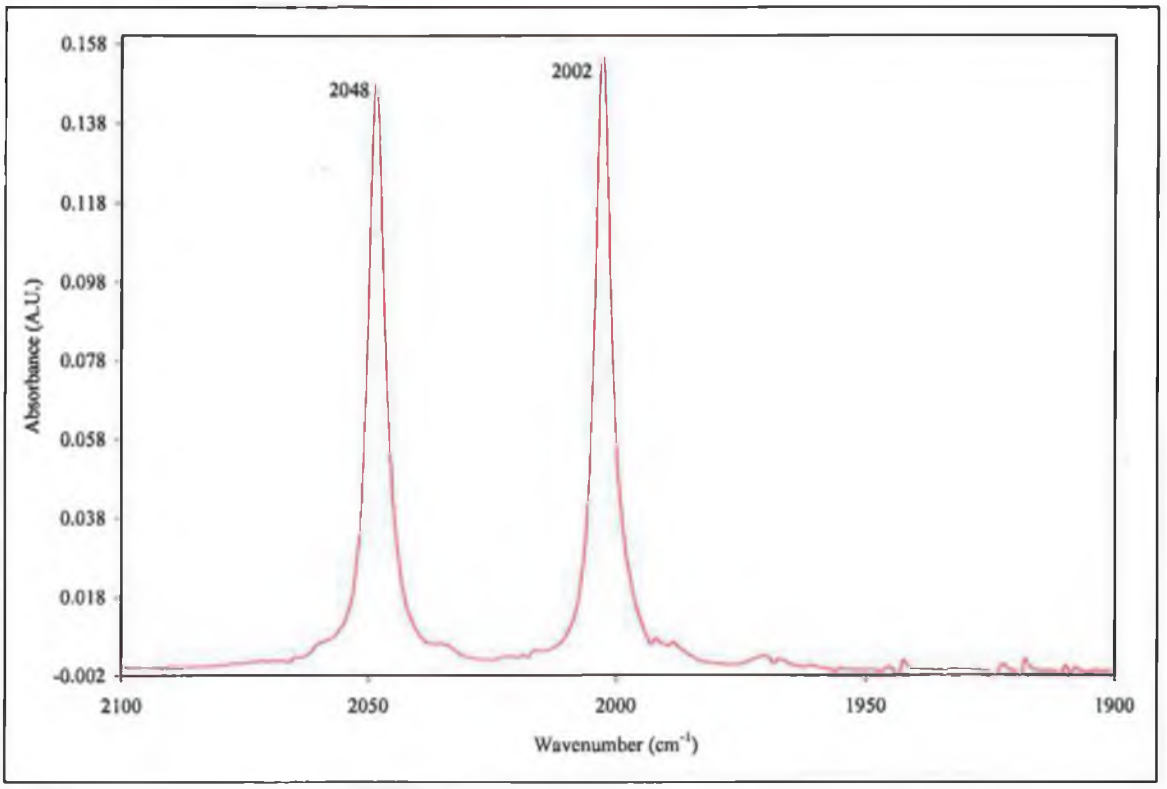

Figure 2-14 The ν_{CO} infrared spectral changes following monochromatic photolysis ($\lambda_{exc.}$ = 355 nm) of azaferrocene under 1 atm CO.

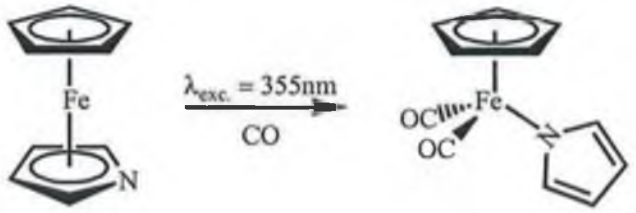

Reaction 2-12 High-energy monochromatic photolysis ($\lambda_{exc.}$ = 355 nm) of azaferrocene, leads to one identifiable photoproduct at room temperature, a dicarbonyl species.

Monochromatic pulsed photolysis of azaferrocene in carbon monoxide saturated cyclohexane at room temperature with lower energy photons at $\lambda_{exc.}$ = 532 nm, led to the growth of a new band in the UV-vis spectrum (λ_{max} ≈640 nm), as shown in Figure 2-15.

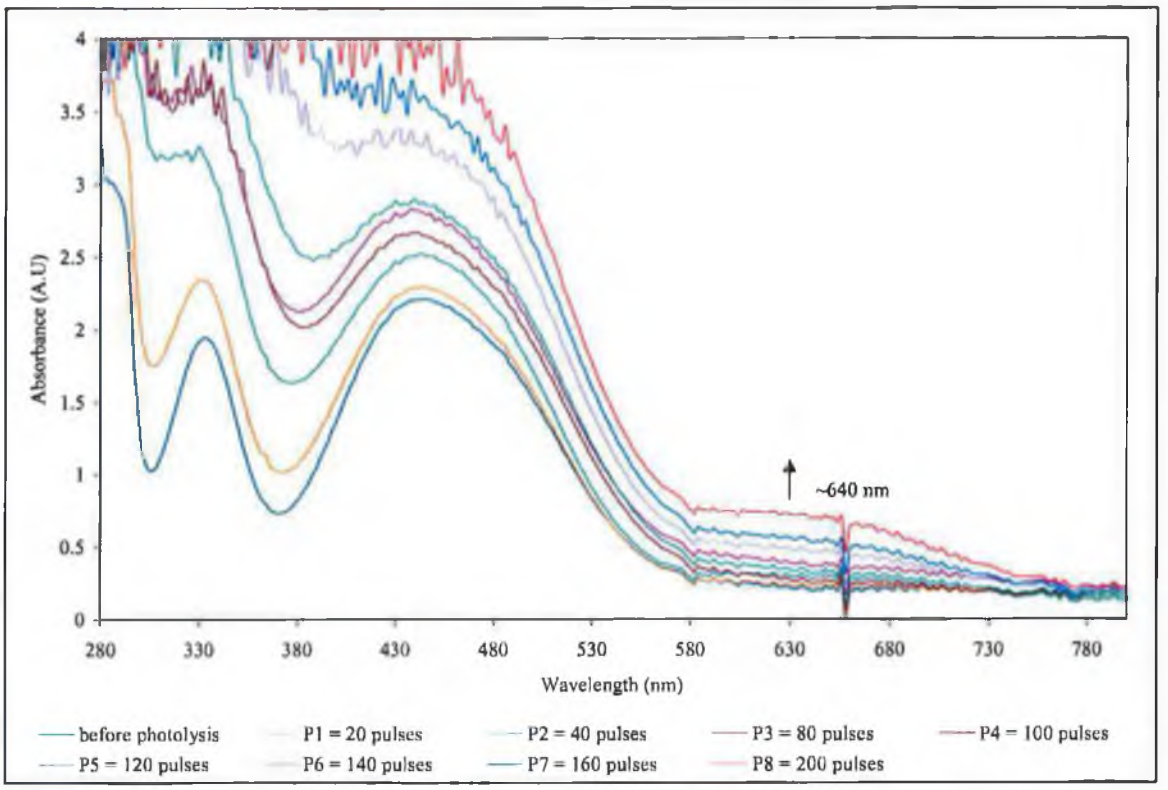

Figure 2-15 The UV-vis spectral changes following monochromatic photolysis ($\lambda_{exc.}$ = 532 nm) of azaferrocene (~4.0×10^{-2} M) in carbon monoxide saturated cyclohexane.

A similarly prepared sample monitored by infrared spectroscopy shows the formation of the dicarbonyl species $(\eta^5\text{-}C_5H_5)Fe(CO)_2(\eta^1\text{-}C_4H_4N)$ with bands at 2048 and 2002 cm^{-1}, as seen in the case of higher energy photolysis at $\lambda_{exc.}$ = 355 nm. Furthermore, an additional carbonyl containing species is produced upon monochromatic photolysis at $\lambda_{exc.}$ = 532 nm, which displays a ν_{CO} at 1948 cm^{-1}, Figure 2-16. This band has been assigned to $(\eta^5\text{-}C_5H_5)Fe(CO)(\eta^3\text{-}C\text{-}C_4H_4N)$, Figure 2-16 as it is close to the ν_{CO} bands observed for $(\eta^5\text{-}C_5H_5)Fe(CO)(\eta^3\text{-}C_3H_5)$ or $(\eta^5\text{-}C_5H_5)Fe(CO)(\eta^3\text{-}C_4H_7)$ (ν_{CO} = 1950 cm^{-1} and 1948 cm^{-1} respectively) in carbon tetrachloride or as a thin film.[49]

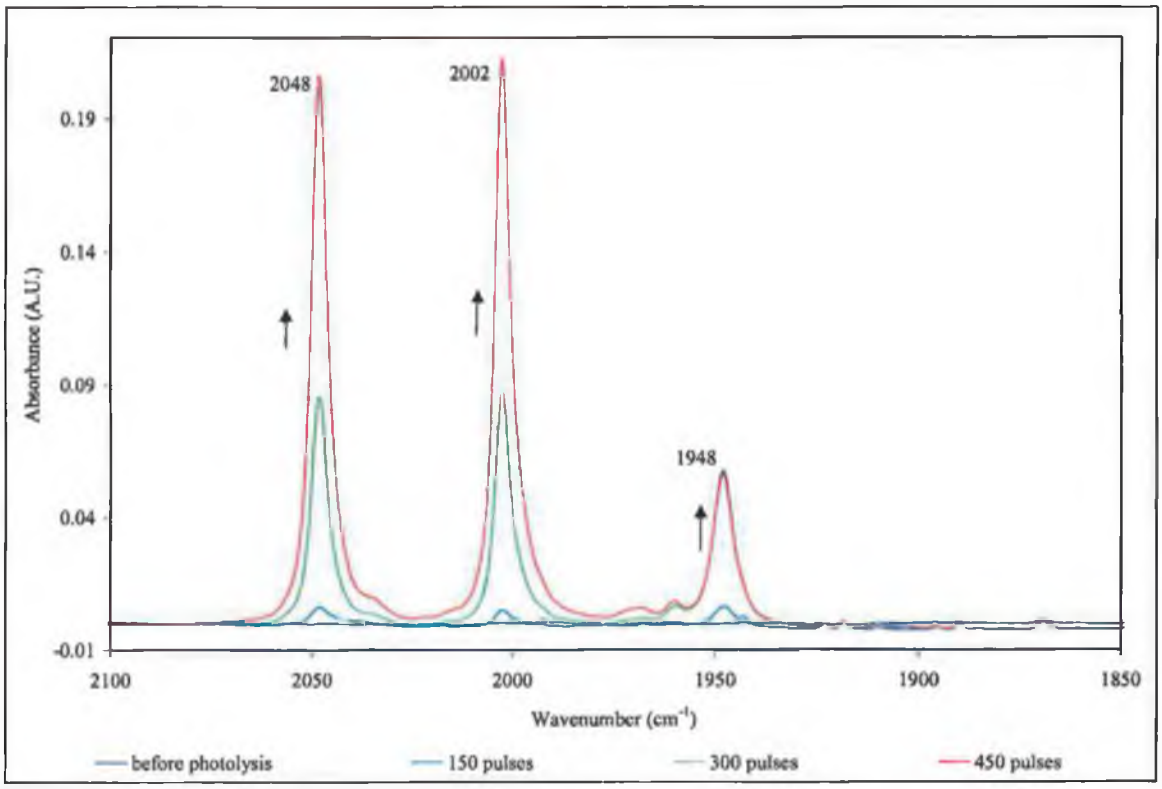

Figure 2-16 The ν_{CO} infrared spectral changes following monochromatic photolysis ($\lambda_{exc.}$ = 532 nm) of azaferrocene carbon monoxide saturated cyclohexane.

Reaction 2-13 Low energy monochromatic photolysis ($\lambda_{exc.}$ = 532 nm) of azaferrocene, lead to two identifiable photoproducts at room temperature, a monocarbonyl and a dicarbonyl species.

Subsequent steady state photolysis of the solution with broad band irradiation ($\lambda_{exc.}$ > 500 nm) results in the decrease in the intensity of the band at 1948 cm^{-1}, assigned to the monocarbonyl $(\eta^5\text{-}C_5H_5)Fe(CO)(\eta^3\text{-}C\text{-}C_4H_4N)$ and an increase in the intensity of the dicarbonyl bands for $(\eta^5\text{-}C_5H_5)Fe(CO)_2(\eta^1\text{-}C_4H_4N)$ at 2048 and 2002 cm^{-1}, refer to Figure 2-17. This indicates that the η^3-intermediate, $(\eta^5\text{-}C_5H_5)Fe(CO)(\eta^3\text{-}C\text{-}C_4H_4N)$ is also photo-active.

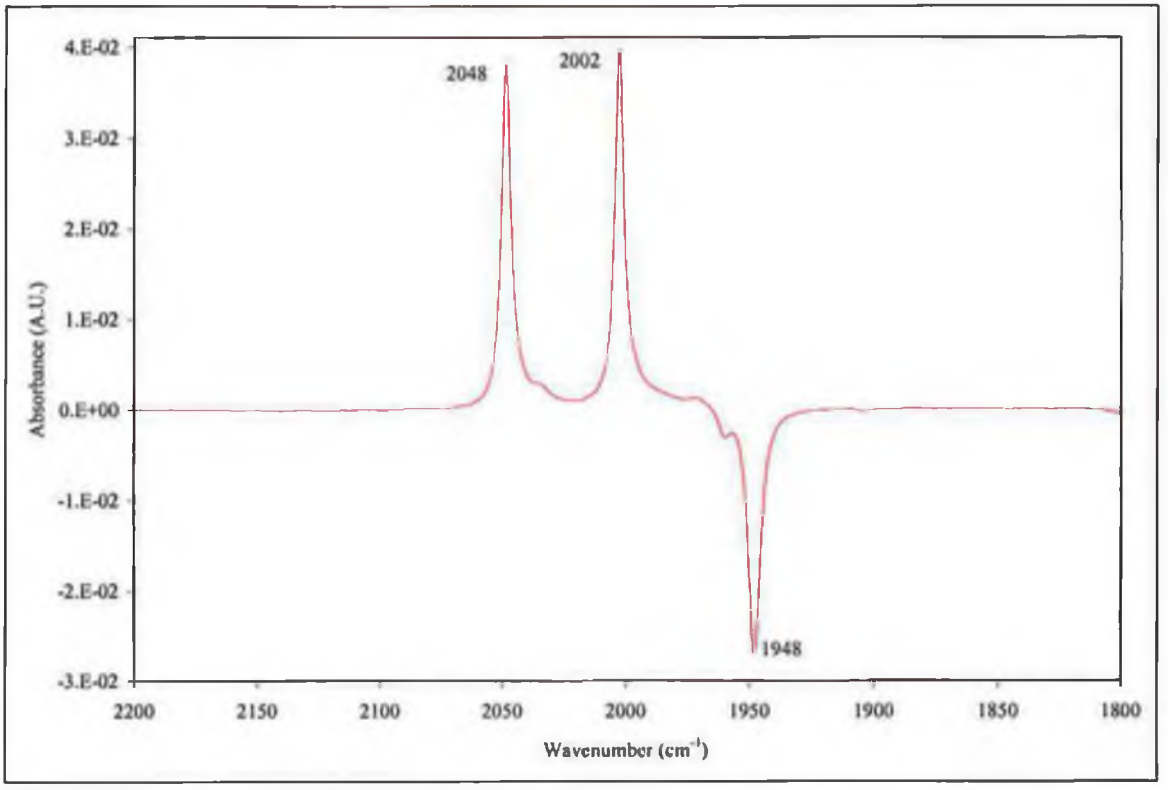

Figure 2-17 Infrared difference spectrum obtained when a carbon monoxide saturated solution of azaferrocene previously subjected to monochromatic irradiation ($\lambda_{exc.}$ = 532 nm) was exposed to broad band irradiation ($\lambda_{exc.}$ > 500 nm).

2.4.3 Laser Flash photolysis of azaferrocene

Following flash photolysis of azaferrocene in cyclohexane under one atmosphere of carbon monoxide or argon at both $\lambda_{exc.} > 532$ nm and 355 nm, an absorption change was observed across the entire region of the spectrum investigated but was strongest at 375 nm. The transient species was formed within the duration of the flash (10 ns). A typical transient signal recorded at 375 nm is shown below in Figure 2-18. No decay of the absorption change was evident even at the longest time scale available on the system (10 ms), consequently its lifetime could not the measured, therefore no kinetic data could be collected from these experiments.

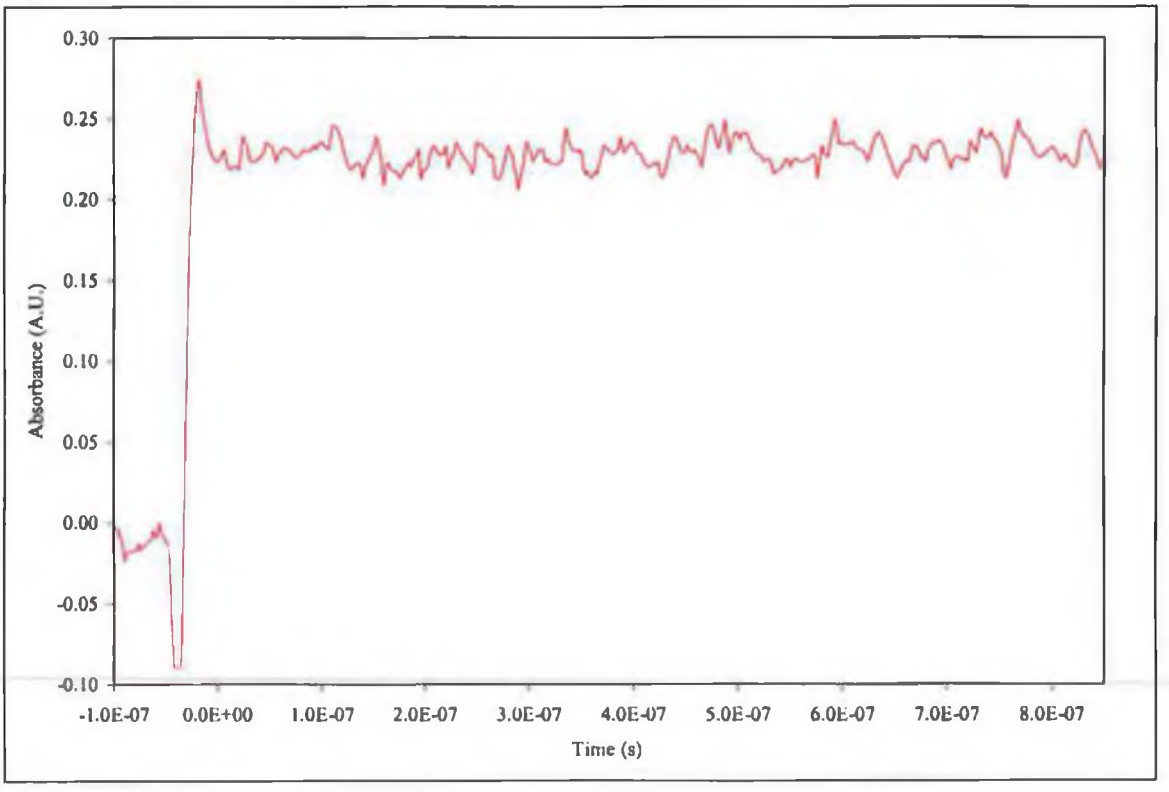

Figure 2-18 A typical absorption change observed for azaferrocene under 1 atm carbon monoxide or argon gas at 375 nm ,($\lambda_{exc.}$ = 532 nm), in cyclohexane.

The infrared spectra of the solution obtained following laser flash photolysis experiments (under one atmosphere of carbon monoxide) confirmed the formation of (η^5-C_5H_5)Fe(CO)$_2$(η^1-pyrrolyl) as the final carbonyl containing product. The turbidity produced upon photolysis in cyclohexane renders time resolved experiments on

azaferrocene both difficult and prone to artefacts from photoacoustic effects. The time resolved behaviour of the initial intermediate species indicates that the reaction with carbon monoxide is slow. It is tentatively proposed that the dimer species, Figure 2-11, is possibly the initial photoproduct, followed by a slow reaction with carbon monoxide, in the case of experiments performed under an atmosphere of carbon monoxide. Under an atmosphere of argon this dimeric species decomposes to form ferrocene.

The initial laser flash photolysis experiments on azaferrocene revealed that the primary photoproduct(s) was forming on a time-scale beyond the response time of the laser flash photolysis system. Thereby establishing the fact that this method of investigating the photochemistry was not appropriate for the azaferrocene system. However, as a consequence of the formation of a new band in the UV-vis spectrum of azaferrocene upon excitation with low-energy photons at 532 nm (refer to Figure 2-15). Due to formation of the $(\eta^5\text{–}C_5H_5)Fe(CO)(\eta^3\text{–}C\text{-}C_4H_4N)$, the laser flash photolysis of azaferrocene was reinvestigated, with particular attention being paid to the lower energy region of its UV-vis spectrum. A grow-in transient signal was detected at 640 nm, which is relatively weak, refer to Figure 2-19. On a longer time scale, this grow-in transient signal fails to return to the pre-irradiated baseline, and a new band is observed in the UV-Vis spectrum centred at 640 nm. Attempts to obtained stronger transient signals, by increasing the concentration of the solution unfortunately resulted in shock waves, which masked the true absorption changes so consequently the signals could not be analysed.

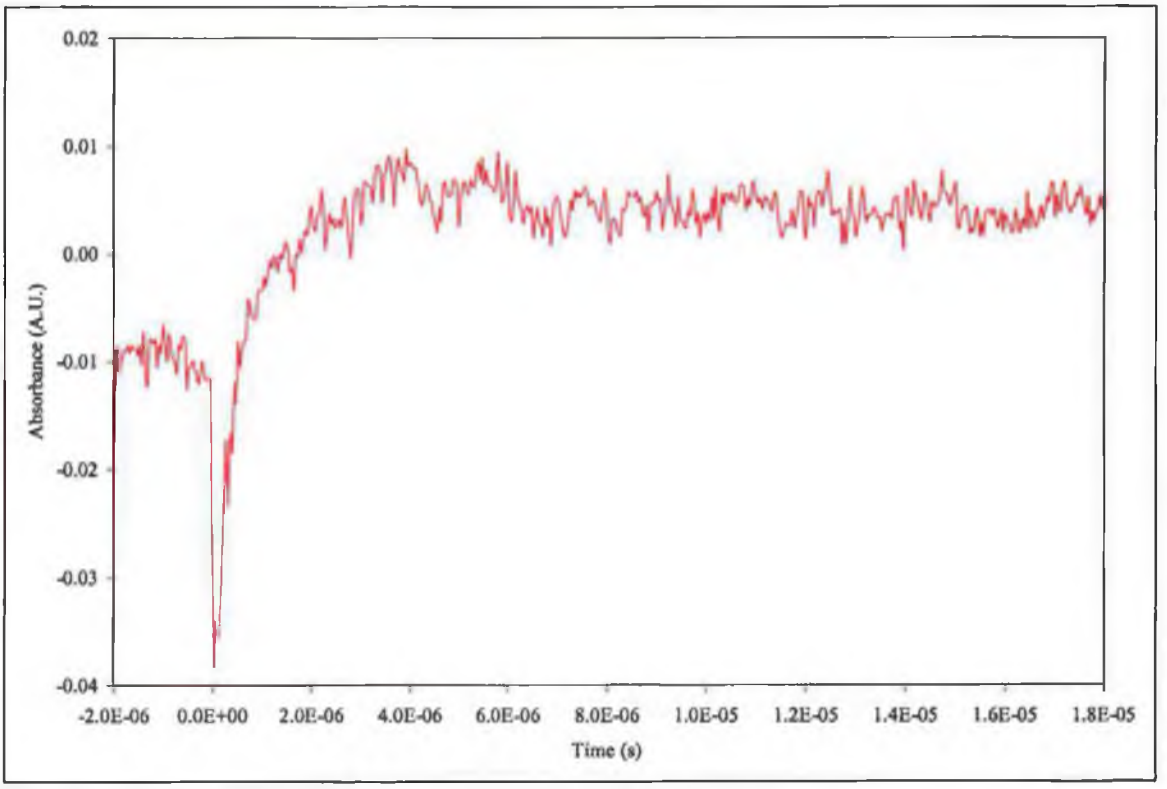

Figure 2-19 A weak grow-in transient signal for the formation of (η^5-C_5H_5)Fe(CO)(η^3-*C*-C_4H_4N) species at 640 nm, in carbon monoxide saturated cyclohexane following laser flash photolysis ($\lambda_{exc.}$ = 532 nm).

2.4.3.1 Discussion of room temperature solution photochemistry

The photo-activity for azaferrocene reported here is in contrast with the reported photochemical inertness of ferrocene. Broad band photolysis of azaferrocene at $\lambda_{exc.} >$ 500 nm in degassed cyclohexane at room temperature initially produced turbidity followed by a precipitation and a deepening of the solution colour. Subsequent addition of carbon monoxide to the photolysed solution yielded the dicarbonyl, $(\eta^5\text{-}C_5H_5)Fe(CO)_2(\eta^1\text{-}N\text{-}C_4H_4N)$ complex over several hours, presumably the result of a slow reaction of carbon monoxide with the precipitate. Attempts to isolate and characterise this precipitate failed.

Broad band photolysis ($\lambda_{exc.} >$ 500 nm) of a carbon monoxide saturated cyclohexane solution ([CO] = 9.0×10^{-3} M) of azaferrocene produced the dicarbonyl $(\eta^5\text{-}C_5H_5)Fe(CO)_2(\eta^1\text{-}N\text{-}C_4H_4N)$, confirming that the η^5-co-ordinated pyrrolyl ligand undergoes a photoinduced haptotropic shift. An additional carbonyl containing complex, observed only upon monochromatic irradiation at 532 nm, was identified as the *exo*-isomer of $(\eta^5\text{-}C_5H_5)Fe(CO)(\eta^3\text{-}C\text{-}C_4H_4N)$. This assignment was based on a comparison of its ν_{CO} band position (1948 cm^{-1}) with that of $(\eta^5\text{-}C_5H_5)Fe(CO)(\eta^3\text{-}C_3H_5)$ (1950 cm^{-1}).[49] The observation of what appears to be an intermediate η^3-species suggests that two photons are required for the overall $\eta^5 \rightarrow \eta^1$ transformation. Indeed, subsequent broad band visible irradiation of the η^3-intermediate indicates that it too is photosensitive, presumably yielding the η^1-species. It is not possible to be certain of this, as the additional dicarbonyl species produced could be the result of further photolysis of the parent species still in solution.

2.4.4 Matrix isolation experiments on azaferrocene

Photolysis of azaferrocene was undertaken in both reactive and inert matrix gases. In this work dinitrogen and methane did not react with any photoproduct of azaferrocene. Consequently both dinitrogen and methane can be considered inert for this system, although these matrix gases are known not to be completely inert in many cases.

The infrared spectroscopic changes observed following photolysis of azaferrocene, (η^5–C_5H_5)Fe(η^5–C_4H_4N) by broad band photolysis ($\lambda_{exc.}$ > 495 nm) and monochromatic photolysis ($\lambda_{exc.}$ = 538 nm) in pure argon matrices are presented in Figure 2-20. The changes are assigned to the depletion of (η^5–C_5H_5)Fe(η^5–C_4H_4N), and the formation of a ring-slip product. The co-ordination mode of the pyrrolyl ligand remains uncertain, however there are only subtle differences observed in the spectral changes, between those induced by broad band photolysis ($\lambda_{exc.}$ > 495 nm) and those induced by monochromatic photolysis ($\lambda_{exc.}$ = 538 nm). The ratio and intensity of the two bands between 780-770 cm^{-1}, is reversed on going from the monochromatic photolysis experiment to broad band photolysis. In the region from ~1200 to~1000 cm^{-1} a similar pattern exits. There is also a prevalence of shoulders on the bands in the broad band photolysis spectra.

However *ab initio* calculations[50] on (η^5–C_5H_5)(η^1–*N*-C_4H_4N)Fe were undertaken to calculate the infrared properties of this fourteen electron species. The starting geometry was based on the molecular structure published for (η^5–C_5H_5)Fe(CO)$_2$(η^1–*N*-C_4H_4N),[51] but with both carbon monoxide ligands removed from the atom list. A full geometry optimisation was undertaken at B3LYP/LANL2DZ model chemistry using the Gaussian-98 program suite. The Hessian matrix again calculated using the same model chemistry revealed only one trivial negative frequency (-55 cm^{-1}) associated with the rotation of the cyclopentadienyl ligand. The results of these calculations are presented in Table 2-2. On the basis of these results the spectral features observed in the matrix experiments can be assigned to the fourteen-electron (η^5-C_5H_5)(η^1-*N*-C_4H_4N)Fe.

Observed band position (cm^{-1})	Calculated band position (cm^{-1})
719	715
772	749
781	763
788	777
831	834
1034	1009
------	1012
------	1023
1080	1049
------	1055
1168	1142
------	1154
1465	1440

Table 2-2 Infrared bands observed (for photolysis product of azaferrocene in argon matrices) and calculated band positions for $(\eta^5\text{-}C_5H_5)(\eta^1\text{-}N\text{-}C_4H_4N)Fe$ based on an optimised geometry at B3LYP/LANL2DZ model chemistry.

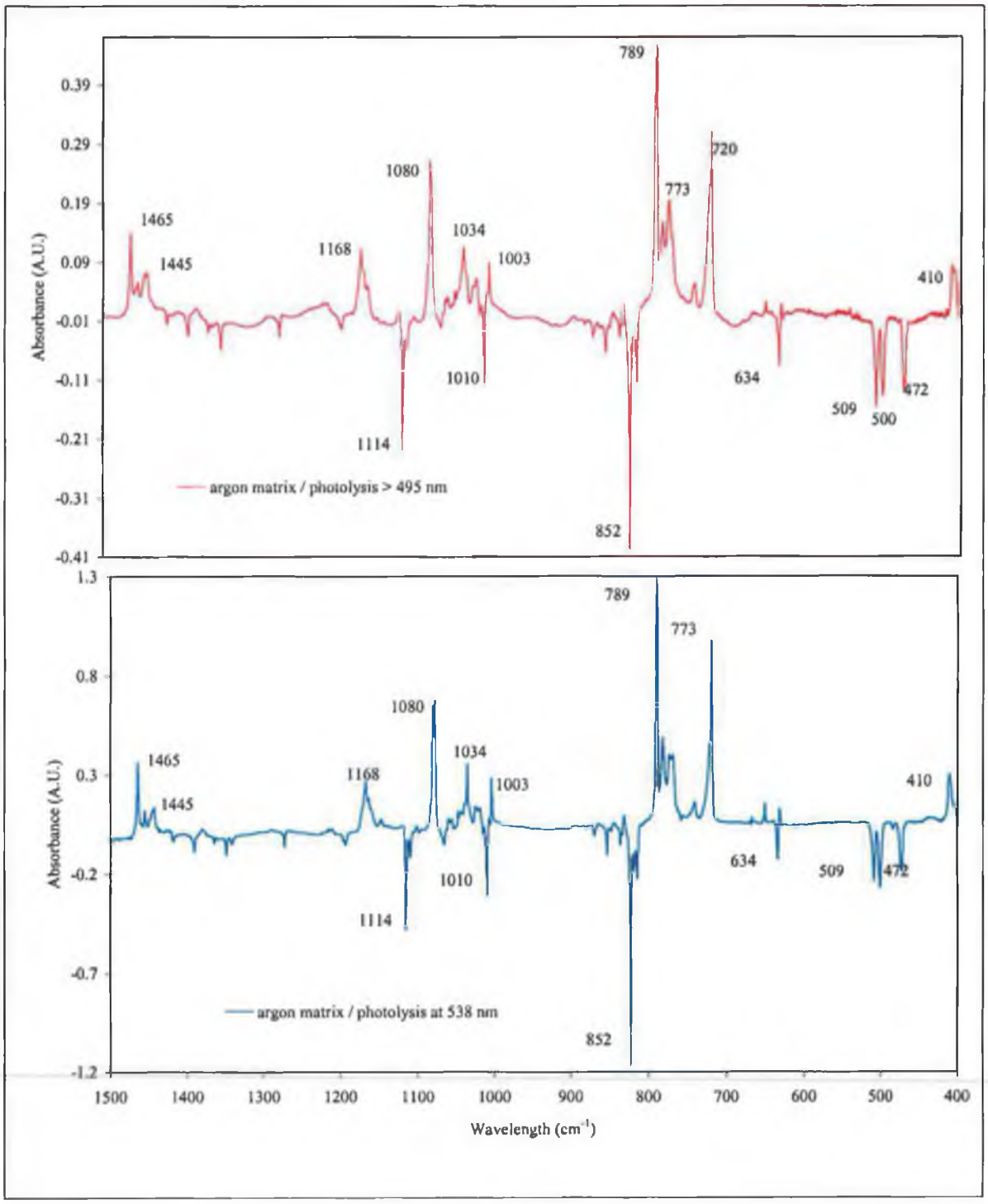

Figure 2-20 The difference spectra obtained following photolysis of azaferrocene in pure argon matrices with broad band ($\lambda_{exc.}$ > 495 nm) and monochromatic ($\lambda_{exc.}$= 538 nm) irradiation respectively.

The UV-vis spectral changes accompanying photolysis with broad band irradiation ($\lambda_{exc.}$ > 495 nm) and monochromatic irradiation ($\lambda_{exc.}$ = 538 nm) respectively are shown in Figure 2-21 and Figure 2-22.

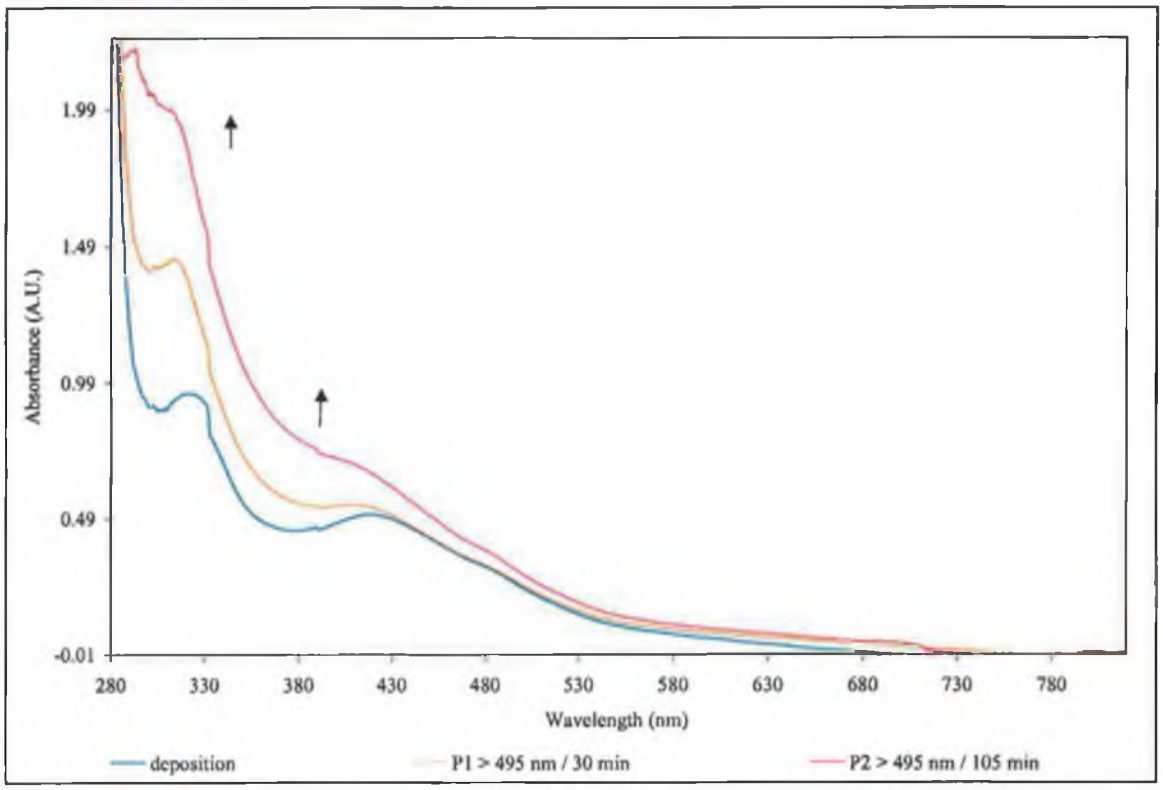

Figure 2-21 UV-vis spectral changes observed following monochromatic photolysis ($\lambda_{exc.}$ > 500 nm) of azaferrocene isolated in an argon matrix at 20 K.

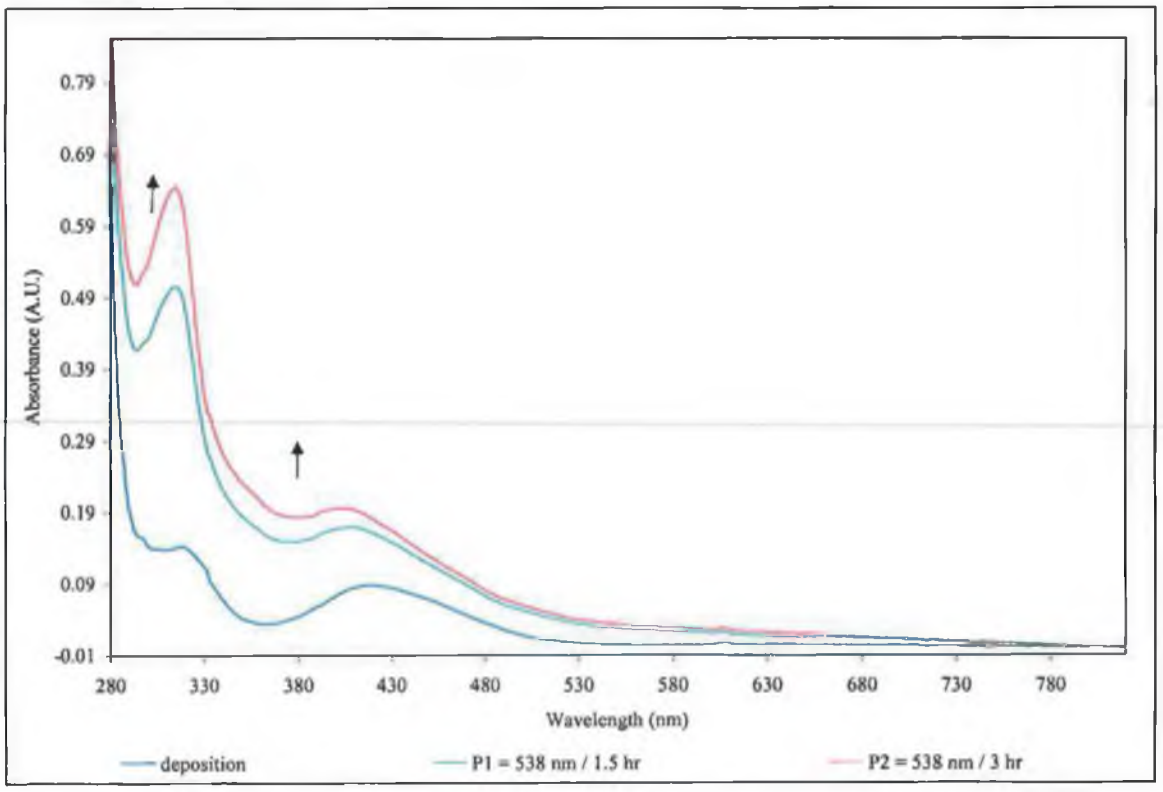

Figure 2-22 UV-vis spectral changes observed following monochromatic photolysis ($\lambda_{exc.}$ = 538 nm) of azaferrocene isolated in an argon matrix at 20 K.

The changes in the infrared spectrum upon broad band ($\lambda_{exc.}$ > 495 nm) photolysis of azaferrocene in dinitrogen matrices are identical to those observed in pure argon matrices. This indicates that a similar ring-slip photoproduct is occurring. There is no evidence of dinitrogen stretching bands or shifts in the wavenumbers of the carbonyl stretching bands, which would suggest that the photoproduct(s) is not interacting with the matrix to any significant extent.

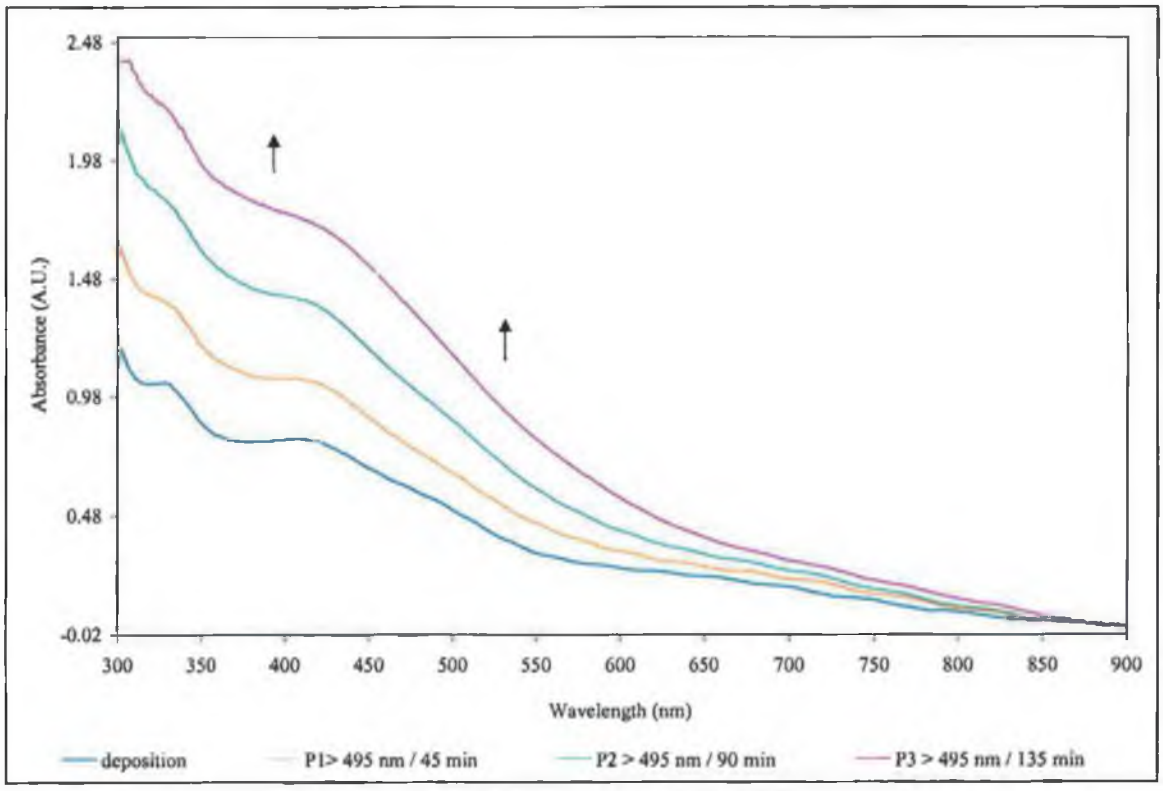

Figure 2-23 UV-vis spectral changes observed following broad band photolysis ($\lambda_{exc.}$ > 495 nm) of azaferrocene isolated in a dinitrogen matrix at 20 K.

The UV-vis of azaferrocene, $(\eta^5\text{-}C_5H_5)Fe(\eta^5\text{-}C_4H_4N)$, in a dinitrogen matrix displays maxima at 328 and 406 nm, with a absorption tail out into the visible ($\lambda \sim 740$ nm). The UV-vis spectrum of azaferrocene, photolysed in a dinitrogen matrix at 20 K, shows a similar pattern to the broad band photolysis spectrum taken in solutions, in that, it increases across the entire range as shown in Figure 2-23.

Photolysis of azaferrocene in a methane matrix at 12 K produced similar changes in the 1600-800 cm^{-1} region of the infrared spectrum, which suggest that like argon and dinitrogen matrixes, methane is not interacting with the photoproduct in any way.

Photolysis of azaferrocene was also conducted in reactive matrixes. The reactive matrix used in these experiments were pure argon matrices doped with varying percentages of carbon monoxide. Azaferrocene exhibits UV-vis bands at 325 and 424 nm in a carbon monoxide doped argon matrices. Irradiation of azaferrocene isolated in these reactive matrixes was with both broad band and monochromatic light.

Broad band photolysis ($\lambda_{exc.} > 495$ nm) of azaferrocene in a 2 % carbon monoxide doped argon matrix produced at least two carbonyl-containing species. One with two ν_{CO} bands of approximately equal intensity at 2054 and 2007 cm^{-1}, and the other with a single band at 1974 cm^{-1}. The band at 1974 cm^{-1} is asymmetric, with shoulders on the low energy side, possibly indicating the formation of further carbonyl containing species, Figure 2-24. The ratio of the intensities of these product bands varied depending on the concentration of carbon monoxide in the matrix. In the case of the 2% carbon monoxide doped argon matrix, the ratio of the band at 1974 cm^{-1} was twice those of the photoproduct at 2054 and 2007 cm^{-1}. Comparison of the ν_{CO} bands with the infrared spectrum of $(\eta^5\text{-}C_5H_5)Fe(CO)_2(\eta^1\text{-}C_4H_4N)$ in an argon matrix, confirmed that the complex is $(\eta^5\text{-}C_5H_5)Fe(CO)_2(\eta^1\text{-}C_4H_4N)$. The band at 1974 cm^{-1} is assigned to the sixteen-electron monocarbonyl species, $(\eta^5\text{-}C_5H_5)Fe(CO)(\eta^1\text{-}C_4H_4N)$. Support for this assignment came from matrix isolation experiments carried out on $(\eta^5\text{-}C_5H_5)Fe(CO)_2(\eta^1\text{-}C_4H_4N)$, which produced $(\eta^5\text{-}C_5H_5)Fe(CO)(\eta^1\text{-}C_4H_4N)$ and free carbon monoxide, as discussed in chapter three of this thesis.

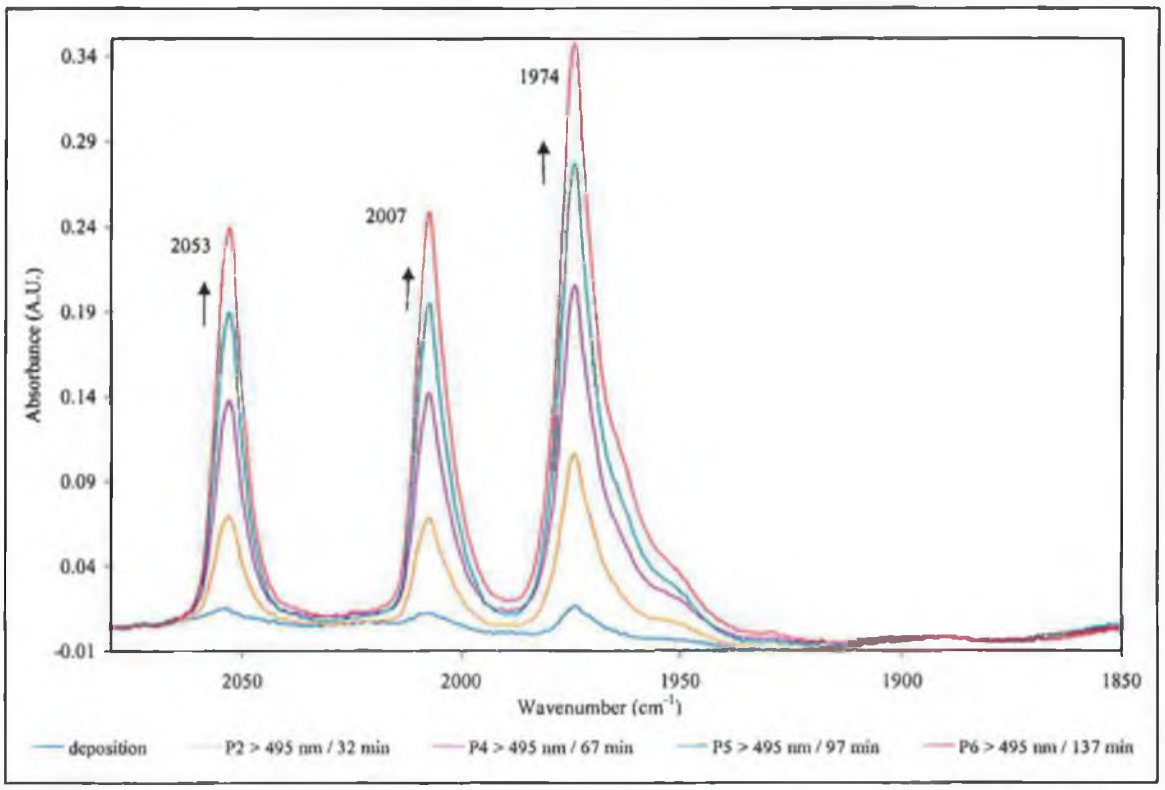

Figure 2-24 Infrared spectral changes observed following broad band irradiation ($\lambda_{exc.}$ > 495 nm) of azaferrocene in a 2% carbon monoxide doped argon matrix at 12 K.

Broad band photolysis ($\lambda_{exc.}$ > 495 nm) of azaferrocene in a 0.5% carbon monoxide doped argon matrix, produced results similar to those previously observed in experiments in a 2% carbon monoxide doped argon matrix, refer to Figure 2-25. Three ν_{CO} bands were observed at 2053, 2007 and 1974 cm^{-1} respectively. The assignment of these bands is to the dicarbonyl complex, $(\eta^5\text{-}C_5H_5)Fe(CO)_2(\eta^1\text{-}C_4H_4N)$ and monocarbonyl complex, $(\eta^5\text{-}C_5H_5)Fe(CO)(\eta^1\text{-}C_4H_4N)$, as in the previous experiments. Again the intensity of the bands at 2053 and 2007 cm^{-1} were approximately the same, yet the intensity of the band at 1975 cm^{-1} was four times that of the other two ν_{CO} bands. The change in relative intensity of the ν_{CO} bands on going from the 2% carbon monoxide doped argon matrix, Figure 2-24 to the 0.5% carbon monoxide doped argon matrix, Figure 2-25, indicates that the greater availability of carbon monoxide results in higher yields of the dicarbonyl photoproduct, $(\eta^5\text{-}C_5H_5)Fe(CO)_2(\eta^1\text{-}C_4H_4N)$. This suggests that the sixteen-electron monocarbonyl, $(\eta^5\text{-}C_5H_5)Fe(CO)(\eta^1\text{-}C_4H_4N)$ is an intermediate in the formation of the dicarbonyl, $(\eta^5\text{-}C_5H_5)Fe(CO)_2(\eta^1\text{-}C_4H_4N)$.

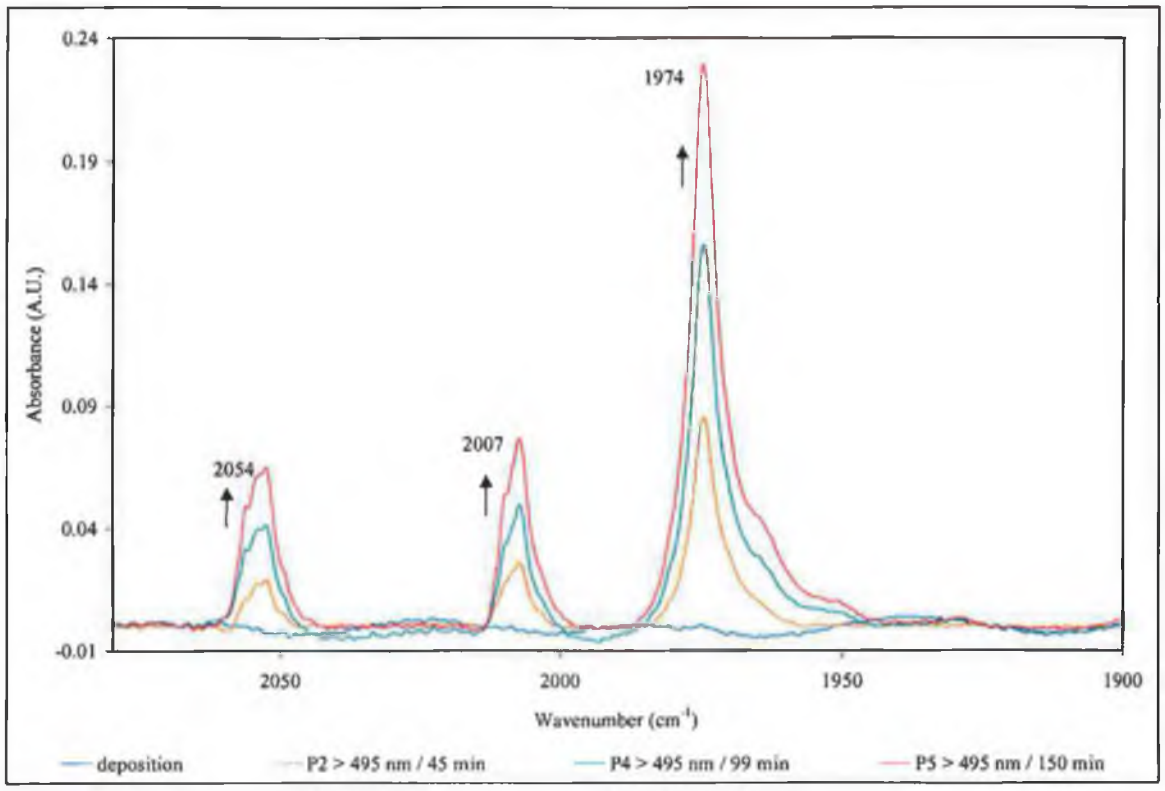

Figure 2-25 Infrared spectral changes observed following broad band irradiation ($\lambda_{exc.}$ > 495 nm) of azaferrocene in a 0.5% carbon monoxide doped argon matrix at 12 K.

Upon photolysis of azaferrocene in either a 0.5% or 2% carbon monoxide doped argon matrix with broad band irradiation of $\lambda_{exc.}$ > 495 nm, the ratio of the ν_{CO} bands for the monocarbonyl species relative to the dicarbonyl remains constant throughout the experiment. However, upon photolysis at shorter wavelength (initially $\lambda_{exc.}$ > 325 nm and subsequently $\lambda_{exc.}$ > 295 nm in the case of the 0.5% carbon monoxide doped argon matrix), the intensity for the monocarbonyl product (η^5-C_5H_5)Fe(CO)(η^1-C_4H_4N), increased more rapidly than those assigned to the dicarbonyl product, (refer to Figure 2-26 and Figure 2-27 for the subsequent changes observed following $\lambda_{exc.}$ > 325 nm 2% and 0.5% carbon monoxide doped argon matrixes respectively). In addition the shoulders on the low-energy side of the monocarbonyl band at 1974 cm^{-1} become more pronounced. In fact the band at 1962 cm^{-1} almost becomes completely resolved from the band at 1974 cm^{-1} and the lower-energy shoulder at 1950 cm^{-1} becomes more apparent, refer to Figure 2-26 and Figure 2-27. This is in contrast to broad band photolysis at longer wavelength (i.e. $\lambda_{exc.}$ > 495 nm), and suggested that the dicarbonyl,

$(\eta^5\text{-}C_5H_5)Fe(CO)_2(\eta^1\text{-}C_4H_4N)$, is undergoing photo-induced carbon monoxide loss upon higher energy irradiation. Indeed, this was confirmed during matrix isolation experiments and time resolved experiments carried out on an authentic sample of $(\eta^5\text{-}C_5H_5)Fe(CO)_2(\eta^1\text{-}C_4H_4N)$.

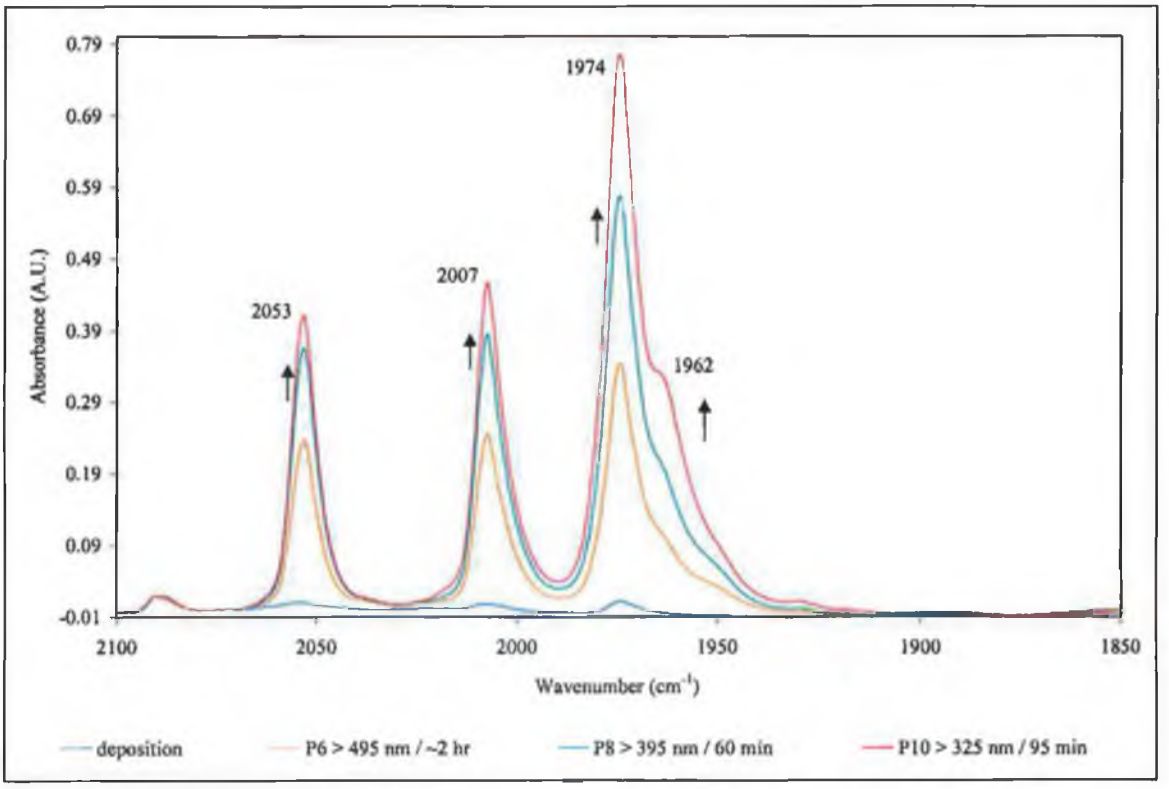

Figure 2-26 Azaferrocene in a 2% carbon monoxide doped argon matrix following broad band photolysis initially with $\lambda_{exc.} > 495$ nm, followed by $\lambda_{exc.} > 395$ nm and finally $\lambda_{exc.} > 325$ nm.

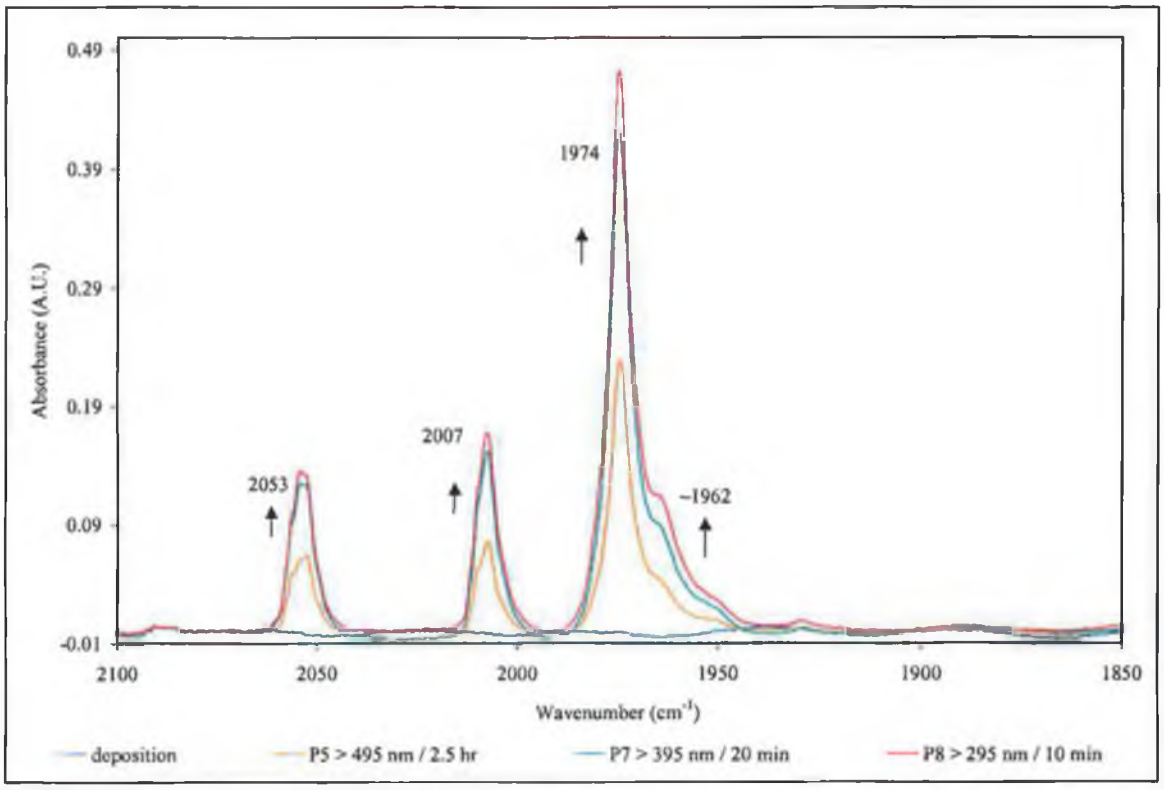

Figure 2-27 Azaferrocene in a 0.5% carbon monoxide doped argon matrix following broad band photolysis initially with $\lambda_{exc.} > 495$ nm, followed by $\lambda_{exc.} > 395$ nm and finally $\lambda_{exc.} > 295$ nm.

Low energy monochromatic photolysis ($\lambda_{exc.} = 538$ nm) of azaferrocene in a 2% carbon monoxide doped argon matrix produced possibly four carbonyl containing species. As observed upon broad band photolysis, two ν_{CO} bands of approximately equal intensity were produced at 2053 and 2007 cm^{-1}, the relative intensity of these bands remained constant, despite variations in the photolysis conditions confirming that they result from a single complex. These have been assigned to the dicarbonyl, $(\eta^5\text{-}C_5H_5)Fe(CO)_2(\eta^1\text{-}C_4H_4N)$. The three remaining bands occur at 1974, 1962 and 1950 cm^{-1}. The band at 1974 cm^{-1} has been assigned to $(\eta^5\text{-}C_5H_5)Fe(CO)(\eta^1\text{-}C_4H_4N)$ as before, based on a comparison with results obtained from the matrix photochemistry results of the dicarbonyl, $(\eta^5\text{-}C_5H_5)Fe(CO)_2(\eta^1\text{-}C_4H_4N)$ discussed in chapter three. The lower energy band (i.e. 1962 cm^{-1}) is asymmetrical, with a shoulder to the lower energy side at approximately 1950cm^{-1}. The terminal ν_{CO} band at 1962 cm^{-1} is assigned to a ring-slip product, $(\eta^5\text{-}C_5H_5)Fe(CO)(\eta^3\text{-}N\text{-}C_4H_4N)$ and the addition shoulder on this band at lower energy (~1950cm^{-1}) is assigned to the ring-slip product,

$(\eta^5\text{-}C_5H_5)Fe(CO)(\eta^3\text{-}C\text{-}C_4H_4N)$. Further discussion of these assignments will follow in the discussion of the matrix results. The ratio of all the bands varied according to the subsequent photolysis conditions.

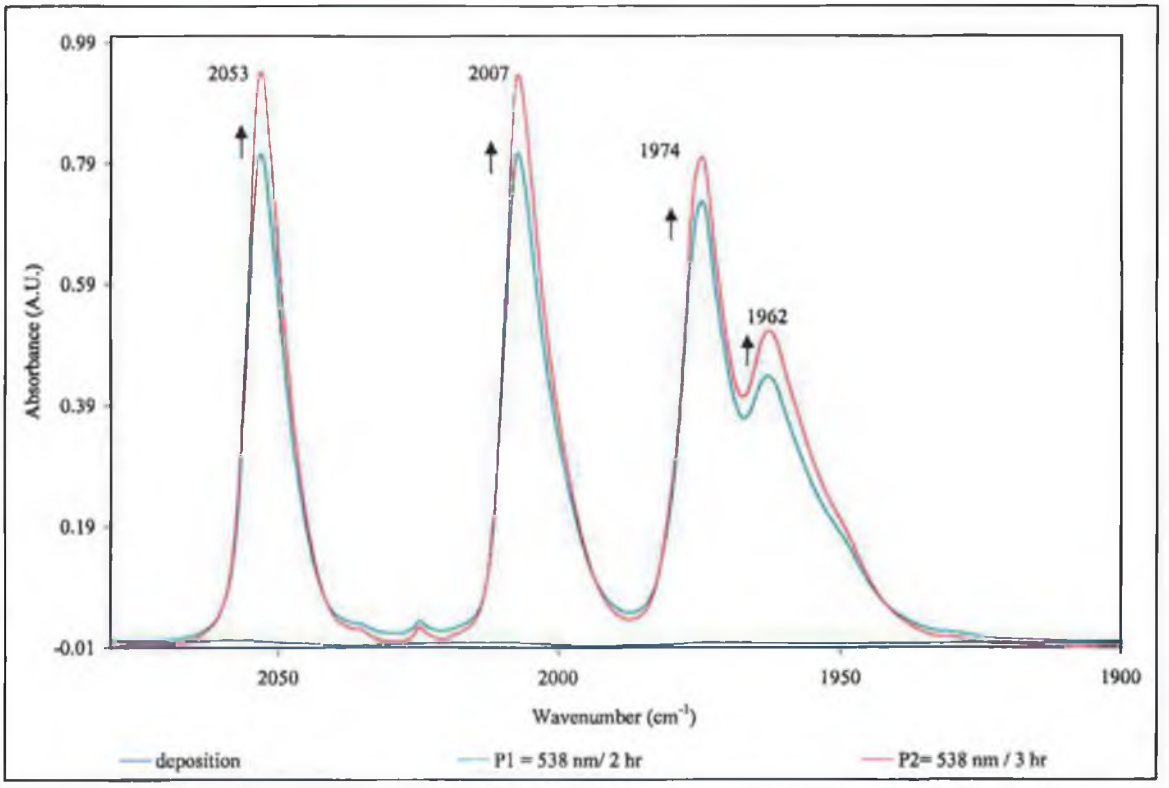

Figure 2-28 Infrared spectral changes following monochromatic irradiation ($\lambda_{exc.}$ = 538 nm) of azaferrocene in a 2% carbon monoxide doped argon matrix at 20 K.

The accompanying UV-vis spectral changes that occurred upon low energy monochromatic photolysis ($\lambda_{exc.}$ = 538 nm) are displayed in Figure 2-29. Photolysis induces the growth of a new band at 730 nm, this band was not observed in the pure argon matrices (for comparison see Figure 2-22).

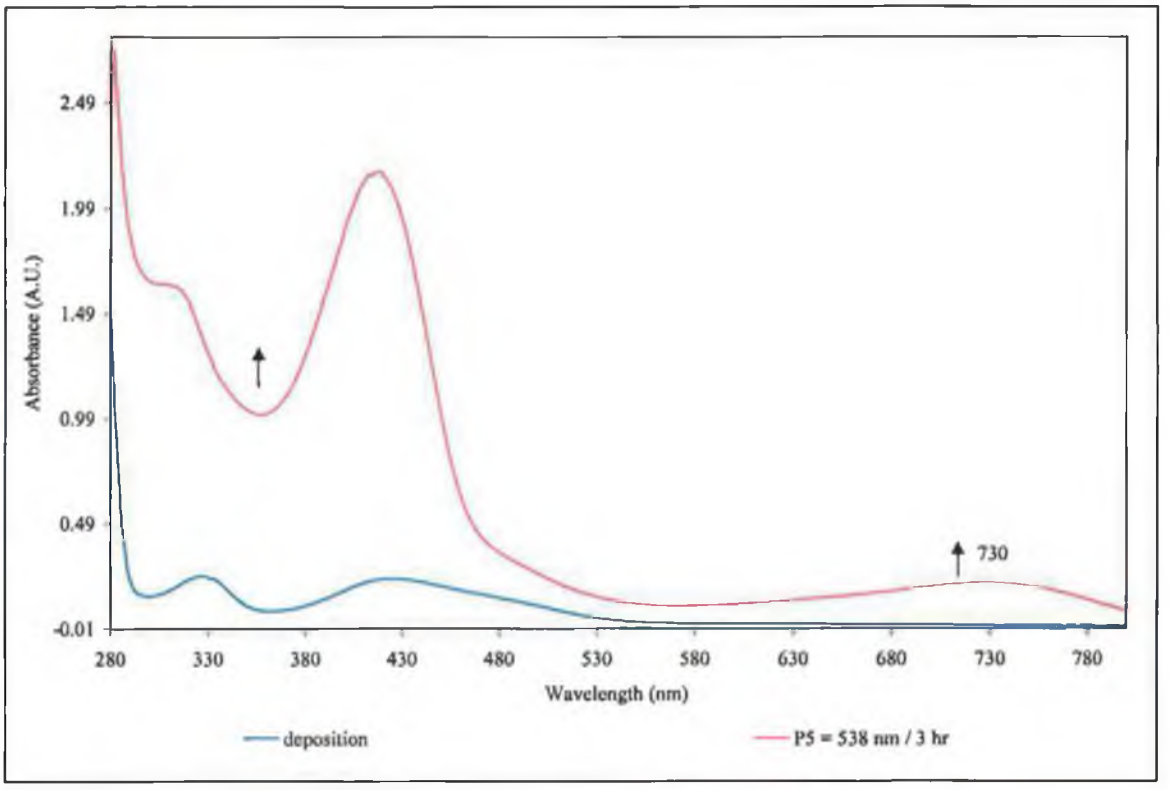

Figure 2-29 UV-vis spectral changes following monochromatic irradiation of azaferrocene in a 2% carbon monoxide doped argon matrix ($\lambda_{exc.}$ = 538 nm) at 20 K.

Subsequent irradiation of this matrix with broad band irradiation ($\lambda_{exc.}$ > 495 nm), induced a substantial increase of the ν_{CO} bands at 2053, 2007 cm^{-1} (i.e. the dicarbonyl complex, $(\eta^5\text{-}C_5H_5)Fe(CO)_2(\eta^1\text{-}C_4H_4N)$) and the band at 1962 cm^{-1} (i.e. the η^3-azaallyl monocarbonyl, $(\eta^5\text{-}C_5H_5)Fe(CO)(\eta^3\text{-}N\text{-}C_4H_4N)$), while the intensity of the band at 1974 cm^{-1} assigned to $(\eta^5\text{-}C_5H_5)Fe(CO)(\eta^1\text{-}C_4H_4N)$ decreases slightly, refer to Figure 2-30. Broad band photolysis ($\lambda_{exc.}$ > 495 nm) also induced spectral changes in the UV-vis spectrum, the low energy band continued to grow, however the $\lambda_{max.}$ shifted to higher energy from $\lambda_{max.}$ ~730 nm to $\lambda_{max.}$ ~ 705 nm, Figure 2-31. The inset in Figure 2-31, shows a UV-vis difference spectrum (i.e UV-vis spectrum following $\lambda_{exc.}$ > 495 minus the UV-vis spectrum following $\lambda_{exc.}$ = 538 nm). It displays a feature at 660 nm, which is associated with the species absorbing at 1962 and ~1950 cm^{-1} in the infrared spectrum.

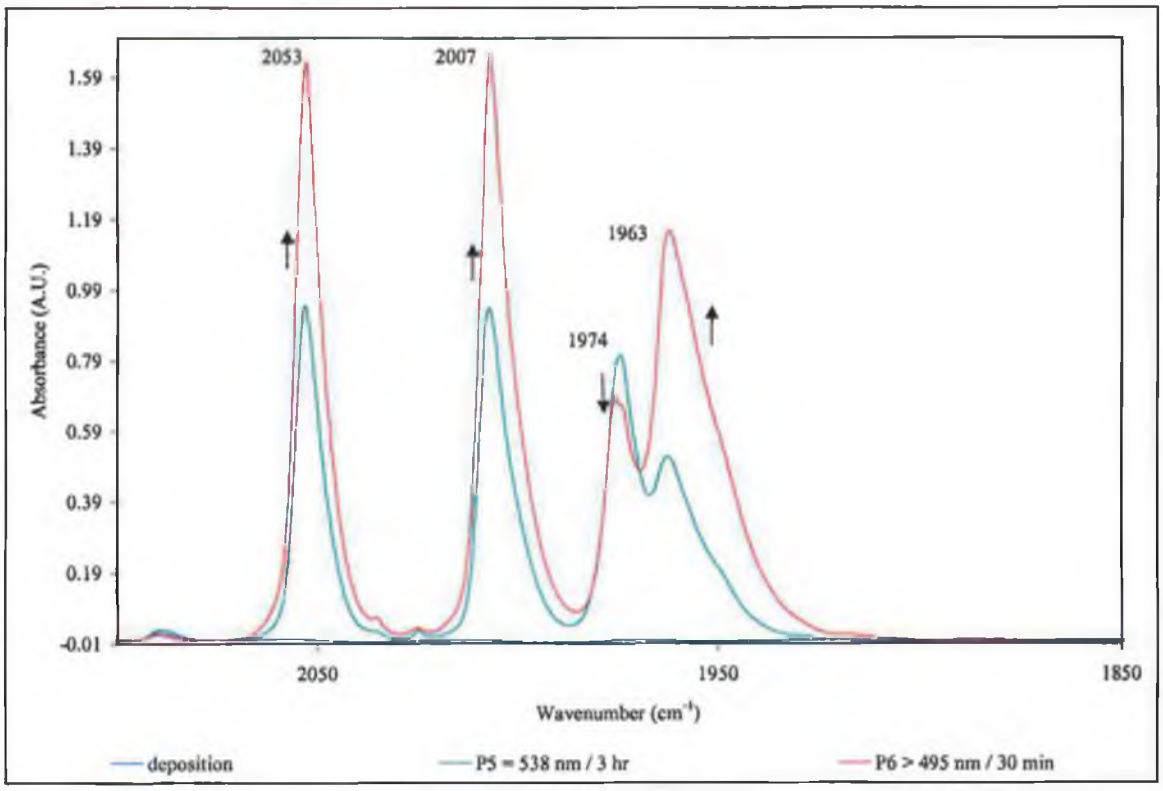

Figure 2-30 The infrared spectral changes observed following monochromatic irradiation of azaferrocene in a 2% CO doped argon matrix at 20 K ($\lambda_{exc.}$ = 538 nm), which was subsequently followed by broad band irradiation ($\lambda_{exc.}$ > 495 nm).

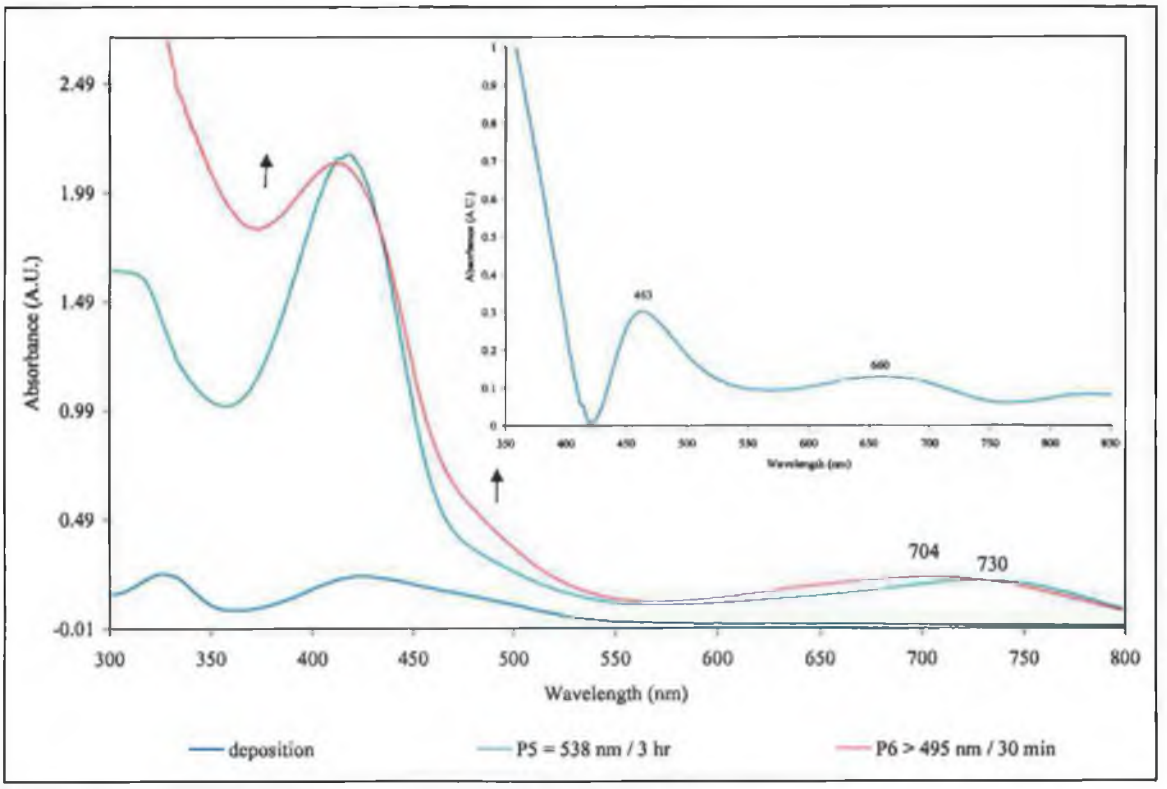

Figure 2-31 The UV-vis spectral changes observed following monochromatic irradiation ($\lambda_{exc.}$ = 538 nm) of azaferrocene in a 2% carbon monoxide doped argon matrix at 20 K. Initial irradiation at $\lambda_{exc.}$ = 538 nm was then followed by broad band irradiation ($\lambda_{exc.}$ > 495 nm). Inset shows the difference spectrum $\lambda_{exc.}$ > 495 nm - $\lambda_{exc.}$ = 538 nm.

The experiment was repeated, this time the monochromatic irradiation, $\lambda_{exc.}$ = 538 nm was followed by broadband irradiation at $\lambda_{exc.}$ > 695 nm. The consequences of which was depletion in both the 1975 and 1962 cm^{-1} bands, but the extent of the depletion of the 1975 cm^{-1} was greater, refer to Figure 2-32. A decrease of the bands of the dicarbonyl, $(\eta^5\text{–}C_5H_5)Fe(CO)_2(\eta^1\text{–}C_4H_4N)$ at 2053 and 2007 cm^{-1} was also observed. It would appear that the bands of the complexes at 1975 and 1962 cm^{-1}, in addition to the low-energy shoulder at 1950 cm^{-1} are generated by photolysis at $\lambda_{exc.}$ = 538 nm.

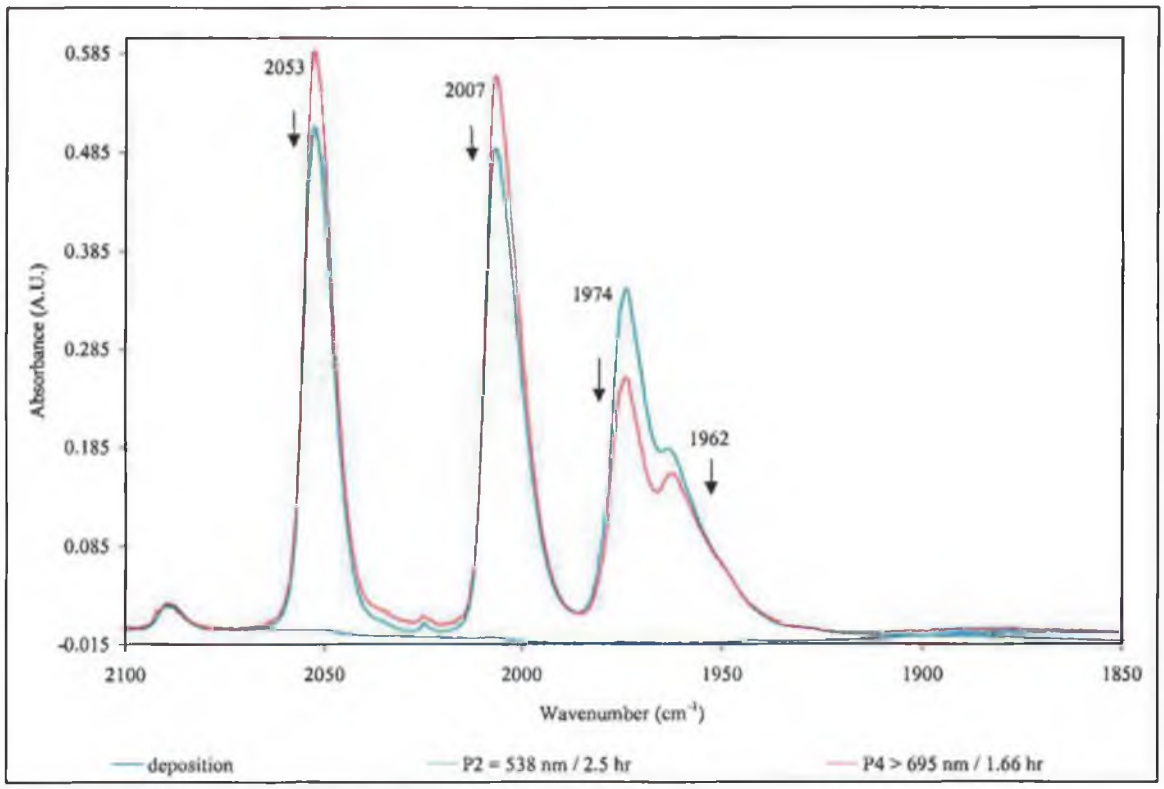

Figure 2-32 The infrared spectral changes observed following initial monochromatic irradiation ($\lambda_{exc.}$ = 538 nm), and subsequently broad band irradiation ($\lambda_{exc.}$ > 695 nm) of azaferrocene in a 2% carbon monoxide doped argon matrix at 20 K.

The UV-vis spectral changes upon monochromatic irradiation, $\lambda_{exc.}$ = 538 nm, are as described before, with the growth of the new band at $\lambda_{max.}$ ~ 730 nm concomitant with an increase in absorption across the entire spectrum, Figure 2-29. Upon photolysis at $\lambda_{exc.}$ = 695 nm, the band at $\lambda_{max.}$ ~ 730 nm continued to increase. However, the increase at the low-energy band is very slight with respect to the changes observed in the rest of the spectrum. Exchanging the broad band photolysis ($\lambda_{exc.}$ > 695 nm) with higher energy monochromatic photolysis ($\lambda_{exc.}$ = 434 nm) regenerates the dicarbonyl, (η^5-C_5H_5)Fe(CO)$_2$(η^1-C_4H_4N); (ν_{CO} ~ 2053 and 2007 cm^{-1}), the monocarbonyl, (η^5-C_5H_5)Fe(CO)(η^1-C_4H_4N); (ν_{CO} ~ 1974 cm^{-1}) and the ν_{CO} band at ~1962 cm^{-1}, assigned to the ring slip product, (η^5-C_5H_5)Fe(CO)(η^3-*N*-C_4H_4N). The UV-vis spectral changes that accompany these infrared changes, are increases across the entire spectrum as would be expected for the regeneration of the dicarbonyl and monocarbonyl.

Photolysis of azaferrocene with high-energy monochromatic light ($\lambda_{exc.}$ = 434 nm) in 2% carbon monoxide doped argon matrixes resulted in five bands in the carbonyl region of the infrared spectrum at 2053, 2007, 1974, 1962, and ~ 1950 cm^{-1}, Figure 2-32. The high energy bands at 2053, 2007 cm^{-1} are attributed to the dicarbonyl (η^5–C_5H_5)Fe(CO)$_2$(η^1–C_4H_4N) and the band at 1974 cm^{-1} to the monocarbonyl, (η^5–C_5H_5)Fe(CO)(η^1–C_4H_4N) as before. Photolysis at $\lambda_{exc.}$ = 434 nm provides the best resolution of the ν_{CO} bands of the ring-slip photoproducts, at 1962 and 1950 cm^{-1}. These are assigned to η^3-type monocarbonyl species, (η^5-C_5H_5)Fe(CO)(η^3-*N*-C_4H_4N) and (η^5-C_5H_5)Fe(CO)(η^3-*C*-C_4H_4N) respectively. The consequence of introducing further photolysis with broad band irradiation ($\lambda_{exc.}$ > 495 nm), was a considerable increase in the intensity of the dicarbonyl species bands at 2053 and 2007 cm^{-1}, while the other three bands remained extensively unchanged.

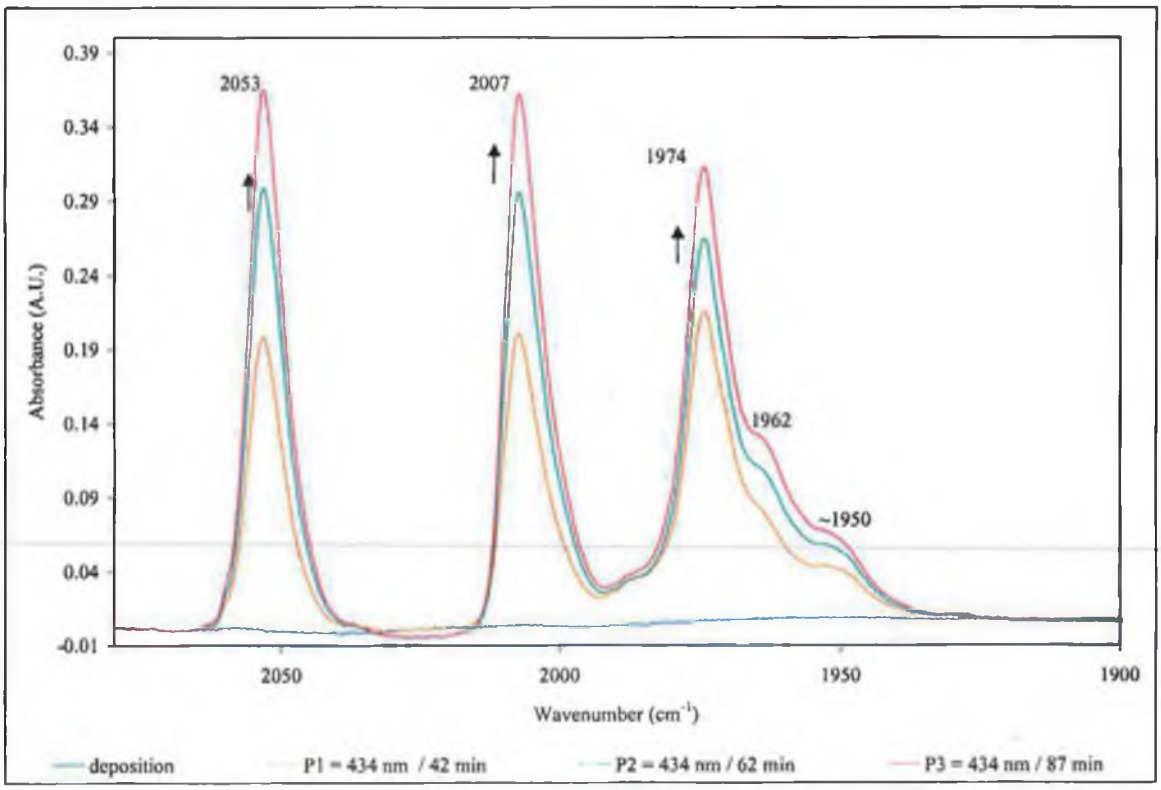

Figure 2-33 Infrared spectral changes observed following monochromatic irradiation ($\lambda_{exc.}$ = 434 nm) of azaferrocene in a 2% carbon monoxide doped argon matrix at 20 K.

The UV-vis spectral changes monitored during the experiment, display an increase across the entire spectrum upon monochromatic irradiation ($\lambda_{exc.}$ = 434 nm), including the growth of a new band at 730 nm, which was also observed following monochromatic irradiation at $\lambda_{exc.}$ = 538 nm. The broad band photolysis ($\lambda_{exc.}$ > 495 nm), which followed the monochromatic photolysis ($\lambda_{exc.}$ = 434 nm) resulted in a decrease in the band at 410 nm and no change in the band at 730 nm, Figure 2-34.

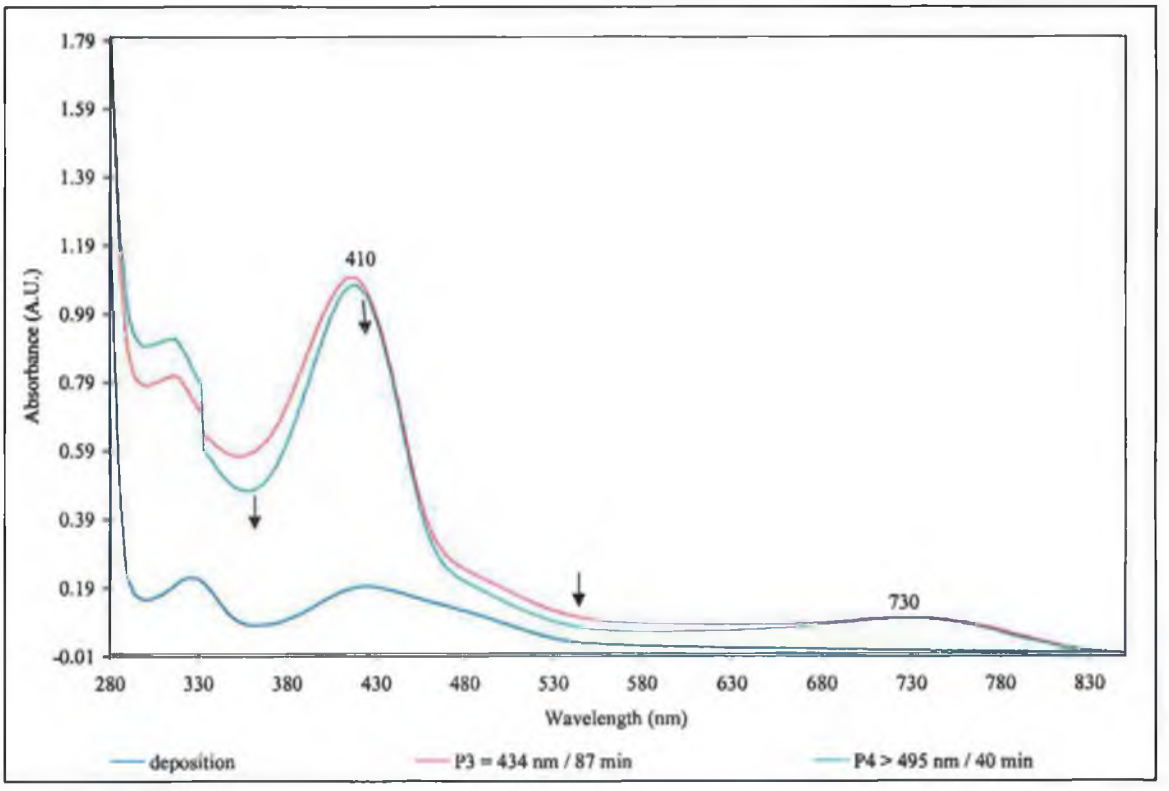

Figure 2-34 UV-vis spectral changes of azaferrocene in a 2% carbon monoxide doped argon matrix. Initial monochromatic photolysis $\lambda_{exc.}$ = 434 nm, followed by broad band $\lambda_{exc.}$ > 495 nm. The arrows indicate the changes following broad band photolysis.

2.4.4.1 Discussion of the results obtained in matrix isolation experiments.

The matrix experiments used to identify the nature of the ring-slip intermediates may be divided into two groups; those in which the isolating matrix is inert and those in which the matrix material reacts with the photo-fragments produced upon photolysis. Experiments carried out in dinitrogen and methane matrixes showed that they were inert to the photo-fragments produced. Therefore, the active matrix in this thesis consisted of various concentrations (expressed as %) of carbon monoxide in argon matrixes. It was through an examination of the ν_{CO} absorption bands, that the co-ordination of carbon monoxide to the photo-fragments was unambiguously established.

Broadband ($\lambda_{exc.} > 495$ nm) photolysis and monochromatic ($\lambda_{exc.} = 538$ nm) photolysis of $(\eta^5\text{-}C_5H_5)Fe(\eta^5\text{-}C_4H_4N)$ in argon matrices resulted in the depletion of the infrared bands in the fingerprint region, and the formation of new bands. An infrared spectrum of a likely product was calculated by Density Functional theory (DFT) methods. The band positions calculated for $(\eta^5\text{-}C_5H_5)(\eta^1\text{-}C_4H_4N)Fe$ provide the best match to those observed in the inert matrix experiments. The changes observed in the dinitrogen and methane matrices were essentially identical to those observed in the argon matrices. This lead to the conclusion that the photoproduct(s) did not react with the matrix, as there was no evidence in the infrared spectrum of $\nu_{N\text{-}N}$ bands in a dinitrogen matrix or C-H activation in a methane matrix. The observation is consistent with the previous observation by Rest and co-workers[52] who also failed to detect any interaction between the sixteen-electron species $(\eta^5\text{-}C_5H_5)Fe(CO)(Cl)$ and a dinitrogen matrix.

Experiments in the reactive carbon monoxide doped argon matrices provide considerably more information on the nature of the photoproducts. Following low-energy broadband photolysis of azaferrocene in both 0.5 % and 2 % CO doped argon matrixes at 12 K, the monocarbonyl, $(\eta^5\text{-}C_5H_5)Fe(CO)(\eta^1\text{-}C_4H_4N)$ and the dicarbonyl, $(\eta^5\text{-}C_5H_5)Fe(CO)_2(\eta^1\text{-}C_4H_4N)$ were identified as the major photoproducts. Assignment of the ν_{CO} bands to these complexes, was based on the isolation of an authentic sample of $(\eta^5\text{-}C_5H_5)Fe(CO)_2(\eta^1\text{-}C_4H_4N)$ in a similar matrix, and also by the

subsequent loss of carbon monoxide from $(\eta^5\text{-}C_5H_5)Fe(CO)_2(\eta^1\text{-}C_4H_4N)$ to yield $(\eta^5\text{-}C_5H_5)Fe(CO)(\eta^1\text{-}C_4H_4N)$ upon photolysis. In addition, the ν_{CO} band for the monocarbonyl photoproduct is very similar to the spectroscopic properties of $(\eta^5\text{-}C_5H_5)Fe(CO)Cl$ as measured by Rest and co-workers.[52] Experimental data in the literature[53] confirms that a η^1-*N*-co-ordinated pyrrolyl ligand has similar electronic properties to those of the halogens resulting in similar ν_{CO} frequencies.

The monocarbonyl and dicarbonyl species were formed concomitantly, and in the same ratio throughout the photolysis at $\lambda_{exc.} > 495$ nm. A feature, which suggests that they were both formed by the reaction of the single photoproduct with carbon monoxide (i.e. a fourteen electron species). A further observation that the ratio of the mono- to-the-dicarbonyl products were strongly dependent on the concentration of carbon monoxide further supported this conclusion. The relative yield of the dicarbonyl species is greatest in matrixes containing a greater concentration of carbon monoxide.

The ν_{CO} band of the monocarbonyl photoproduct $(\eta^5\text{-}C_5H_5)Fe(CO)_2(\eta^1\text{-}C_4H_4N)$ at 1974 cm^{-1} was asymmetric. This asymmetry occurred whether the monocarbonyl species was formed by photolysis of azaferrocene in a carbon monoxide doped matrix or from the photolysis of $(\eta^5\text{-}C_5H_5)Fe(CO)_2(\eta^1\text{-}C_4H_4N)$ in a pure argon matrix. The presence of the shoulder on the low-energy side of the ν_{CO} band at 1974 cm^{-1} is indicative of a further carbonyl containing species rather than matrix splitting effect, as only this band exhibited the asymmetry. The ν_{CO} band at 1950 cm^{-1} could be assigned to *exo*-isomer $(\eta^5\text{-}C_5H_5)Fe(CO)(\eta^3\text{-}C\text{-}C_4H_4N)$ based on the observation of a similar band in the room temperature photolysis of azaferrocene in carbon monoxide saturated cyclohexane following monochromatic irradiation $\lambda_{exc.} = 532$ nm.

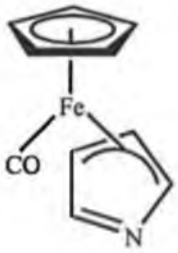

exo-allyl isomer

Species 2-1

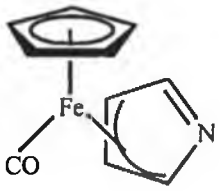

endo-allyl isomer

Species 2-2

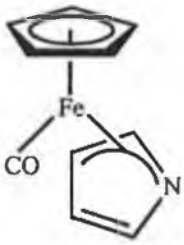

exo-aza-allyl

Species 2-3

The assignment of the species absorbing at 1962 cm^{-1} is more difficult. One possible assignment is the *exo*-aza-allyl isomer $(\eta^5\text{-}C_5H_5)Fe(CO)(\eta^3\text{-}N\text{-}C_4H_4N)$, Species 2-3 or alternatively the *endo*-isomer of $(\eta^5\text{-}C_5H_5)Fe(CO)(\eta^3\text{-}C\text{-}C_4H_4N)$, Species 2-2. Generally it is accepted that the *endo*-isomers of allyl complexes are less stable than the *exo*-isomers, and that the carbonyl stretching absorptions of the *endo*-isomer occur at lower energy than those of the *exo*-isomer. Consequently, an assignment of the 1962 cm^{-1} band to Species 2-2 is not consistent with the previously published assignments for related systems.[54] Therefore the assignment of the 1962 cm^{-1} band to the *exo*-azaallyl isomer, Species 2-3 is favoured.

The yield of the species absorbing at 1962 cm^{-1} was significantly increased by monochromatic irradiation ($\lambda_{exc.}$ = 538 nm) initially, followed by broadband photolysis ($\lambda_{exc.}$ > 495 nm). This suggests that photolysis of azaferrocene produced a precursor species, presumably containing an η^3-co-ordinated pyrrolyl ligand, which then reacted with carbon monoxide producing the observed species. The yield of a particular carbonyl species is dependent on the initial photolysis wavelength as all precursor species, were themselves photosensitive.

2.5 Conclusions

The investigation of the photochemistry of azaferrocene, $(\eta^5\text{-}C_5H_5)(\eta^5\text{-}C_4H_4N)Fe$ demonstrates that it displays an extensive photochemistry, which is dominated by haptotropic shifts of the co-ordinated pyrrolyl ligand. A photoinduced stepwise shift from η^5-co-ordination through η^3-co-ordination, ultimately yields an η^1-co-ordinated species. The relative importance of the various intermediates shows a strong dependence on the photolysis conditions employed. This reflects the photosensitive nature of many of the intermediates formed. The co-ordinatively-unsaturated intermediates also appear to be discriminating with what they will react with, a feature also observed with other iron systems.

The ability of the pyrrolyl ligand to adopt a variety of co-ordination modes highlights its importance in elucidating the mechanistic details of the photoinduced haptotropic shift reactions.

2.6 References

1 B. A. Thrush, *Nature*, **1956**, 178, 155.

2 A. M. Tarr, D. M. Wiles, *Can. J. Chem.*, **1968**, 46, 2745.

3 J. C. D. Brand, W. Snedden, *Trans. Faraday Soc.*, **1957**, 53, 894.

4 E. Körner von Gustorf, F.-W. Grevels, *Fortschr. Chem. Forsch.*, **1969**, 13, 366.

5 O. Traverso, F. Scandola, *Inorg. Chim Acta*, **1970**, 4, 493.

6 Y. Hoshi, T. Akiyama, A. Sugimori, *Tetrahedron Lett.*, **1970**, 1485.

7 T. Akiyama, Y. Hoshi, S. Goto, A. Sugimori, *Bull. Chem. Soc. Jpn.*, **1973**, 46, 1851.

8 T. Akiyama, A. Sugimori, H. Hermann, *Bull. Chem. Soc. Jpn.*, **1973**, 46, 1855.

9 R. E. Bozak, *Adv. Photochem.*, **1971**, 8, 227.

10 L. H. Ali, A. Cox, T. J. Kemp, *J. Chem. Soc., Dalton Trans.*, **1973**, 1428.

11 J. Davis, D. H. Vaughan, M. F. Cardosi, *Electroanalysis*, **1997**, 9, 650.

12 Y. Einaga, Y. Yamada, T. Tominaga, *J. Radioanalytical and Nuclear Chem.*, **1997**, 218, 97.

13 (a) K. D. Warren, *Struct. Bonding (Berlin)*, **1976**, 27, 45.

(b) D. W. Clarke, K. D. Warren,, *Struct. Bonding (Berlin)*, **1980**, 39, 1.

14 A. N. Nesmeyanov, N. A. Vol'kenau, L. S. Shilovtesa, *Dokl. Akad. Nauk. SSSR*, **1970**, 190, 857.

15 (a) T. P. Gill, K. R. Mann, *Inorg. Chem.*, **1980**, 19, 3007.

(b) T. P. Gill, K. R. Mann, *J. Organomet. Chem.*, **1981**, 216, 65.

(c) T. P. Gill, K. R. Mann, *Organometallics*, **1982**, 1, 485.

16 T. P. Gill, K. R. Mann, *Inorg. Chem.*, **1983**, 22, 1986.

17 J. L. Schrenk, A. McNair, F. B. McCormick, K. R. Mann, *Inorg. Chem.*, **1986**, 25, 3501.

18 A. M. McNair, J. L. Schrenk, K. R .Mann, *Inorg. Chem.*, **1984**, 23, 2633.

19 J. L Schrenk, M. C. Palazzotto, K. R. Mann, *Inorg. Chem.* **1983**, 22, 4047.

20 J. L. Schrenk, K. R. Mann, *Inorg. Chem.*, **1986**, 25, 1906.

21 D. R. Chrisope, K. M. Park, G. B. Schuster, *J. Am. Chem. Soc.*, **1989**, 111, 6195.

22 E. Román, M. Barrera, S. Hernández, E. Lissi, *J. Chem. Soc. Perkin Trans. 2*, **1988**, 939.

23 (a) K. Meier, H. Zweifel, *J. Imaging Sci.*, **1986**, 30, 174.

(b) A. Roloff, K. Meier, M. Riediker, *Pure Appl. Chem.*, **1986**, 9, 1267.

(c) B. Klingert, M. Riediker, A. Roloff, *Comments Inorg. Chem.*, **1988**, 7, 109.

24 V. Jakubek, A.J. Lees, *Inorg. Chem.*, **2000**, 39, 5779.

25 A. J. Lees, *J. Anal. Chem.*, **1996**, 68, 226.

26 F. Basolo, *New J. Chem.*, **1994**, 18, 19.

27 (a) J. M. O'Connor, C. D. Casey, *Chem. Rev.*, **1987**, 87, 307.
(b) T. G. Traylor, K. J. Stewart, M. L. Goldberg, *Organometallics*, **1986**, 5, 2062.
(c) T. G. Traylor, K. J. Stewart, *J. Am. Chem. Soc.*, **1986**, 108, 6977.
(d) T. G. Traylor, M. L. Goldberg, *Organometallics*, **1987**, 6, 2413.
(e) T. G. Traylor, M. L. Goldberg, *Organometallics*, **1987**, 6, 2531.

28 (a) W. Strohmeier, D. von Hobe, *Z. Naturforsch.*, **1963**, 18B, 981.
(b) M. S. Wrighton, J. L. Haverty, *Z. Naturforsch.*, **1975**, 30B, 245.
(c) J. Nasielski, O. Denishoff, *J. Organomet. Chem.*, **1975**, 102, 65.
(d) A. Gilbert, J. M. Kelly, M. Budzwait, E. Koerner von Gustorf, *Z. Naturforsch.*, **1976**, 31B, 1091.
(e) A. J. Rest, J. R. Sodeau, D. J. Taylor, *J. Chem. Soc., Dalton Trans.*, **1978**, 651.

29 C. J. Breheny, S. M .Draper, F.-W. Grevels, W. E. Klotzbücher, C. Long, M. T. Pryce, G. Russell, *Organometallics*, **1996**, 15, 3679.

30 N. Kuhn, G. Henkel, J. Kreutzberg, S. Stubenrauch, *J. Organomet. Chem.*, **1993**, 456, 97.

31 K.K. Joshi, P. L. Pauson, A. R. Qazi, W. H. Stubbs, *J. Organomet. Chem.*, **1964**, 1, 471.

32 K. H. Pannell, B. L. Kalsotra, C. Pàrkànyi, *J. Heterocyclic. Chem.*, **1978**, 15, 1057.

33 R. Cataliotti, A, Foffani, S. Pignataro, *Inorg. Chem.*, **1970**, 9, 2594.

34 B. V. Lokshin, E. B. Rusach, V. N. Sektina, N. I. Pyshnograeva, *J. Organomet. Chem.*, **1974**, 77, 69.

35 H. P. Fritz, *Adv. Organometal. Chem.*, **1964**, 1, 239.

36 R. B. King, L. M. Epstein, E. W. Gowling, *J. Inorg. Nucle. Chem.*, **1970**, 32, 441.

37 R. D. Ernst, D. R. Wilson, R. H. Herber, *J. Am. Chem. Soc.*, **1984**, 106, 1646.

38 A. Houlton, R. M. G. Roberts, J. Sliver, J. Zakrzewski, *J. Organomet. Chem.*, **1993**, 456, 107.

39 P. L. Pauson, A. R. Qazi, *J. Organomet. Chem.*, **1967**, 7, 321.

40 (a) A. Efraty, N. Jurban, *Inorg. Chim. Acta*, **1980**, 44, L191.
(b) A. Efraty, N. Jurban, A. Goldman, *Inorg. Chem.*, **1982**, 21, 868.

41 A. Efraty, *J. Organomet. Chem.*, **1973**, 57, 1.

42 (a) R. B. King, *Co-ord. Chem. Rev.*, **1976**, 20, 155.
(b) P. T. Wolczanski, T. E. Bercaw, *Acc. Chem. Res.*, **1980**, 13, 121.

43 N. Kuhn, H. Schumann, M. Winter, E. Zauder, *Chem. Ber.*, **1988**, 121, 111.

44 N. Kuhn, E.-M. Horn, E. Zauder, D. Bläser, R. Böse, *Angew. Chem. Int. Ed. Engl.*, **1988**, 27, 579.

45 F. Seel, V. Sperber, *J. Organomet. Chem.*, **1968**, 14, 405.

46 N. Kuhn, R. Jendal, R. Böse, D. Bläser, *Chem. Ber.*, **1991**, 124, 89.

47 J. Zakrewski, *J. Organomet. Chem.*, **1987**, 327, C41.

48 X. Pan, C. E. Philbin, M .P. Castellani, D. R. Tyler, *Inorg. Chem.*, **1988**, 27, 671.

49 M. H. L. Green, P. L. I. Nagy, *J. Chem. Soc.*, **1963**, 189.

50 D. P. Heenan, C. Long, V. Montiel-Palma, R. Perutz, M. T. Pryce, *Organometallics*, **2000**, 19. 3867.

51 M. A. Powell, R. D. Bailey, C. T. Eagle, G. L. Schimel, T. W. Hanks, W. T. Pennington, *Acta Crystallogr.*, **1997**, C53, 1611.

52 R. H. Hooker, K. A. Mahmoud, A. J. Rest, *J. Chem. Soc., Dalton Trans.*, **1990**, 1231.

53 D. G. Alway, K. W. Barnett, *Inorg. Chem.*, **1978**, 17, 2826.

54 (a) J. A. Belmont, M. S. Wrighton, *Organometallics*, **1986**, 5, 1421.

(b) R. W. Fish, W. P. Giering, D. Marten, M. Rosenblum, *J. Organomet. Chem.*, **1976**, 105, 101.

Chapter Three

3 The photochemistry of cyclopentadienyl-iron dicarbonyl η^1-pyrrolyl and cyclopentadienyl-iron dicarbonyl η^1-indolyl

3.1 Literature survey of the photochemistry of cyclopentadienyl-iron dicarbonyl halide complexes

A great deal of insight about the variety of photochemical deactivation pathways exhibited by cyclopentadienyl metal carbonyl complexes containing one electron halide ligands has been acquired in the last four decades. This is especially the case for complexes where the metal in question is iron, (i.e. complexes of the type $(\eta^5\text{-}C_5H_5)Fe(CO)_2X$, where X = Cl, I, or Br). It has been established that three major deactivation processes are possible following one electron excitation; these are heterolytic metal-halogen bond cleavage, reaction (1), Figure 3-1; homolytic metal-halide bond cleavage, reaction (2), Figure 3-1; or dissociation of a carbon monoxide ligand, reaction (3), Figure 3-1.

$$(\eta^5\text{-}C_5H_5)Fe(CO)_2X \xrightarrow{h\nu} (\eta^5\text{-}C_5H_5)Fe(CO)_2^{+} + X^{-} \quad (1)$$

$$(\eta^5\text{-}C_5H_5)Fe(CO)_2X \xrightarrow{h\nu} (\eta^5\text{-}C_5H_5)Fe(CO)_2^{\bullet} + X^{\bullet} \quad (2)$$

$$(\eta^5\text{-}C_5H_5)Fe(CO)_2X \xrightarrow{h\nu} (\eta^5\text{-}C_5H_5)Fe(CO)X + CO \quad (3)$$

Figure 3-1 Outline of the major photo-deactivation processes possible for complexes of the type $CpFe(CO)_2X$, X = Cl, Br or I.

The electronic spectra of $(\eta^5\text{-}C_5H_5)Fe(CO)_2X$ complexes, where X = Cl, I, or Br, are dominated by an intense absorption near 350 nm, which tails into the visible region. Weaker absorptions in the visible region and shoulders on the more intense band are also observed in some instances. The low energy bands are believed to be ligand field in character, while the higher energy band in the near UV is assigned to a M → CO (π^*) charge transition.[1] Because of the fact that no photochemically active bands have been

attributed to X (π^*) → M (π^*) or X (σ^*)→ M (σ^*) transitions, efficient homolysis of the M-X bond is not expected to be a primary photochemical deactivation process, as M-X homolysis would generally require these types of transition.[2] Lichtenberger and Fenske[3] presented a series of He(I) photoelectron spectra of (η^5-C_5H_5)$Fe(CO)_2X$ complexes and undertook *ab initio* calculations on the same type of complexes, where X is Cl, I, or Br in both instances. They showed that the highest occupied molecular orbitals (HOMO) are a doubly degenerate set of iron-halogen π-antibonding orbitals. The consequence of a one-electron excitation from this level, regardless of which orbital is populated due to the excitation, is a net increase in the metal-halogen bond order, and so heterolytic cleavage is not an expected outcome of photolysis based on these calculations.

Theoretical calculations therefore indicate that heterolysis or homolysis of the iron-halogen bond is unlikely upon photolysis of $CpFe(CO)_2X$ complexes. It is clear that carbon monoxide dissociation should be the prevailing photochemical deactivation process, which in actual fact it is, as will be discussed in due course. However, in contrast to the prevailing carbon monoxide dissociation photochemistry observed for these types of complexes, which is similar to the photochemistry already outlined for (η^6-arene)$Cr(CO)_3$ and (η^5-C_5H_5)$Mn(CO)_3$ in chapter one, an early study by Ali, Cox and Kemp[4] identified the formation of the iron dimer [(η^5-C_5H_5)$Fe(CO)_2$]$_2$ following the photo-decomposition ($\lambda_{exc.}$ > 400 nm) of (η^5-C_5H_5)$Fe(CO)_2Cl$ in dimethyl sulphoxide (DMSO) or pyridine. A disproportionation pathway based on the stoichiometric analysis of the products as outlined in Scheme 3-1 was proposed. No reaction was observed in non-polar solvents.

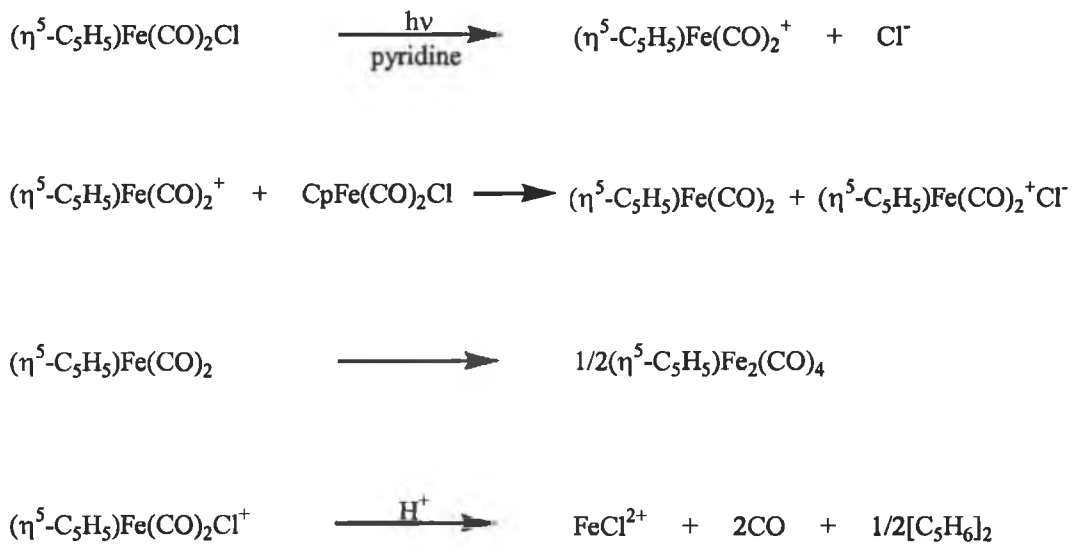

Scheme 3-1 Disproportionation pathway proposed by Ali, Cox and Kemp.[4]

A more recent investigation into the formation of ionic products following photolysis of $(\eta^5\text{-}C_5H_5)Fe(CO)_2I$ in pyridine, revealed that although carbon monoxide loss is the dominant photochemical reaction, small amounts of dimer were formed by a mechanism similar to that outlined in Scheme 3-1. Initially Fe-I bond homolysis was suspected, however irradiation of $(\eta^5\text{-}C_5H_5)Fe(CO)_2I$ in neat tetrachloride solution failed to yield $(\eta^5\text{-}C_5H_5)Fe(CO)_2Cl$, nor was there dimer formation following photolysis in a non-polar solvent (benzene or hexane). Therefore the initial step it would seem is heterolysis of the Fe-I bond, a step, which is proposed to be pyridine assisted.[1]

This base assisted heterolysis of the Fe-I bond was exploited by Zakrzewski *et al.*[5] to provide a new method for the synthesis of $(\eta^5\text{-}C_5H_5)Fe(CO)_2(\eta^1\text{-pyrrolyl})$. Synthesis is achieved by long wavelength photolysis of $(\eta^5\text{-}C_5H_5)Fe(CO)_2I$ in the presence of pyrrole and a scavenging base, diisopropylamine, which leads to the effective replacement of the iodide ligand by η^1-pyrrolyl. Later Borja, Jakúbek and Lees[6] reported the optimum excitation wavelength conditions and the photo-efficiencies for the heterolytic Fe-I dissociation reaction of $(\eta^5\text{-}C_5H_5)Fe(CO)_2I$ in solution. This work demonstrated the effective heterolytic cleavage of the Fe-I bond upon long-wavelength photolysis of $(\eta^5\text{-}C_5H_5)Fe(CO)_2I$. The most effective photo-conversions of $(\eta^5\text{-}C_5H_5)Fe(CO)_2I$ (in the presence of excess pyrrole and diisopropylamine) to form $(\eta^5\text{-}C_5H_5)Fe(CO)_2(\eta^1\text{-pyrrolyl})$

were found to take place with excitation at long wavelength (580–647 nm) into weak low-energy absorption bands. The quantum efficiency for the substitution of the iodide ligand by the pyrrolyl ligand in toluene at room temperature is ϕ = 0.38 (± 0.02) upon photolysis at $\lambda_{exc.}$ = 647 nm. In addition, it was also found to be independent of solution temperature in the 283-323 K range. This is a relatively efficient photo process and provides a very accessible route to new types of $(\eta^5\text{-}C_5H_5)Fe(CO)_2L$ complexes, where L = η^1-pyrrolyl, which are valuable precursors to azaferrocene.

These results are in accordance with the most recent valence energy photoelectron spectroscopy and molecular orbital calculations on $(\eta^5\text{-}C_5H_5)Fe(CO)_2I$. Hu *et al.*[7] postulated that the HOMO orbitals of $(\eta^5\text{-}C_5H_5)Fe(CO)_2I$ posses a greater degree of *d*-orbital character than either $(\eta^5\text{-}C_5H_5)Fe(CO)_2Cl$ or $(\eta^5\text{-}C_5H_5)Fe(CO)_2Br$, and so a one-electron excitation is therefore predicted to decrease the Fe-I bond order, promoting heterolytic cleavage of the bond. This is in contrast to $(\eta^5\text{-}C_5H_5)Fe(CO)_2Cl$ previously discussed,[3] where the HOMO orbitals are considered to be a doubly degenerate set of iron-halide π-antibonding-orbitals. Thus excitation of $(\eta^5\text{-}C_5H_5)Fe(CO)_2Cl$ increases the bond order of Fe-Cl, thereby hindering heterolytic cleavage.

Gianotti and Merle[8] reported that photolysis ($\lambda_{exc.}$ 300-700 nm) of $(\eta^5\text{-}C_5H_5)Fe(CO)_2X$, where X = Cl or Br, in chloroform or benzene, resulted in the formation of ferrocene, Fe^{2+} and X^-. It has been suggest in later publications that these results are perhaps because of thermal chemistry from the use of a high intensity light source in conjunction with insufficient temperature control.

Consequently, the predominant photochemistry observed for complexes of the type $(\eta^5\text{-}C_5H_5)Fe(CO)_2X$ is the dissociative loss or exchange of one carbon monoxide ligand.[10] The irradiation of $(\eta^5\text{-}C_5H_5)Fe(CO)_2X$ complexes for synthetic purposes had been exploited for quite awhile[9] prior to details of the mechanistic aspects of the reaction being investigated by Alway and Barnett.[10] They reported that the primary photochemical process for $(\eta^5\text{-}C_5H_5)Fe(CO)_2Br$ and $(\eta^5\text{-}C_5H_5)Fe(CO)_2I$ following excitation at 366 or 436 nm was dissociative loss of carbon monoxide. Photolysis of $(\eta^5\text{-}C_5H_5)Fe(CO)_2X$, where X = Cl, I or Br, in benzene solutions saturated with ^{13}CO yielded $(\eta^5\text{-}C_5H_5)Fe(CO)(^{13}CO)X$. Irradiation of the bromo-or iodo-derivatives of $(\eta^5\text{-}C_5H_5)Fe(CO)_2X$, in the presence of

triphenylphosphine (PPh_3) lead to the formation of the covalent complex (η^5-C_5H_5)Fe(CO)(PPh_3)X, where X = I or Br. Irradiation of (η^5-C_5H_5)Fe$(CO)_2$Cl was precluded from this part of the study as it was observed that (η^5-C_5H_5)Fe$(CO)_2$Cl reacts rapidly with triphenylphosphine in the dark at room temperature producing a mixture of covalent (η^5-C_5H_5)Fe(CO)(PPh_3)Cl and ionic (η^5-C_5H_5)Fe$(CO)_2(PPh_3)^+Cl^-$ derivatives.[10(a)] The high quantum yield for the substitution of a carbon monoxide ligand in (η^5-C_5H_5)Fe$(CO)_2$X, X = Br or I, by triphenylphosphine was independent of the irradiation wavelength but increased with increasing triphenylphosphine concentration, reaching limits of $\phi = 0.96$ and $\phi = 0.95$ for the bromide and iodide complexes respectively. Furthermore, the quantum yields for substitution were not affected to any significant extent by changing the solvent from benzene to the more polar solvents, acetonitrile or nitromethane. This behaviour is expected for dissociative processes in which the incoming nucleophile must react with a co-ordinatively-unsaturated intermediate present in low concentrations. Photolysis of (η^5-C_5H_5)Fe$(CO)_2$X, where X = Cl, I or Br, at $\lambda_{exc.} = 366$ or 436 nm were also reported by Alway and Barnett[10] in benzene, acetonitrile, nitromethane and tetrahydrofuran (THF) in the absence of added nucleophiles. Under these conditions there was no detectable photochemical reaction, suggesting that the earlier reports[8] of ferrocene formation in conjunction with Fe^+ and Cl^- ions may not be reliable.

Photolysis of (η^5-C_5H_5)Fe$(CO)_2$Cl at low temperature (*ca.* 12 K) in methane, dinitrogen, carbon monoxide and carbon monoxide doped methane matrices was carried out by Hooker, Mahmoud and Rest.[11] UV excitation of (η^5-C_5H_5)Fe$(CO)_2$Cl, ($290 < \lambda_{exc.} < 370$ nm) in low temperature matrixes lead to the production of the monocarbonyl, (η^5-C_5H_5)Fe(CO)X and free carbon monoxide. This indicated that dissociation of the carbon monoxide ligand rather cleavage than metal-chlorine bond as the principal photochemical reaction pathway. Irradiation of (η^5-C_5H_5)Fe$(CO)_2$Cl in reactive dinitrogen matrices also produced the sixteen-electron species, [(η^5-C_5H_5)Fe(CO)Cl], with no evidence for the formation of (η^5-C_5H_5)Fe(CO)(N_2)Cl. This may be because the dinitrogen ligand competes less effectively for the [(η^5-C_5H_5)Fe(CO)Cl] fragment than does carbon monoxide.[12]

Hooker, Mahmoud and Rest[11] also conducted similar experiments in poly-vinyl chloride (PVC) films, where the range of temperatures available for investigation is much broader. The primary photoreaction of carbon monoxide dissociation is thermally reversible (*ca.* 60

K) in the polymer film. Alternatively, the sixteen-electron species [(η^5-C_5H_5)Fe(CO)Cl)] reacts with tetrahydrofuran (THF) in films cast from THF solution to give (η^5-C_5H_5)Fe(CO)(THF)Cl. No evidence for the formation of iron dimer,[(η^5-C_5H_5)$Fe(CO)_2$]$_2$ was obtained in these experiments, which was expected given the high dilution of (η^5-C_5H_5)Fe(CO)X complex in the polymer film.

3.2 Literature survey of the photochemistry of cyclopentadienyl-iron dicarbonyl alkyl complexes

The photochemistry of (η^5-C_5H_5)$Fe(CO)_2$R complexes, where R = alkyl, allyl, aryl, silyl or similar organic functional group have been researched extensively. As a result, various researchers have identified four different processes as the primary photochemical step, depending on the experimental conditions used. These four processes are outlined (1)-(4) in Figure 3-2. The photochemical processes are carbon monoxide dissociation, reaction (1); η^5 → η^3 ring-slip of the cyclopentadienyl ring, reaction (2); carbon monoxide insertion into the metal-alkyl bond, reaction (3); and finally metal-alkyl bond cleavage, reaction (4). The photochemistry is dominated by dissociation of a carbon monoxide ligand, reaction (1), Figure 3-2, under most experimental conditions[13] and the remaining photoreactions (2)-(4), Figure 3-2 are only a minor component of the photochemistry observed for these types of complexes, as will be discussed in the following section.

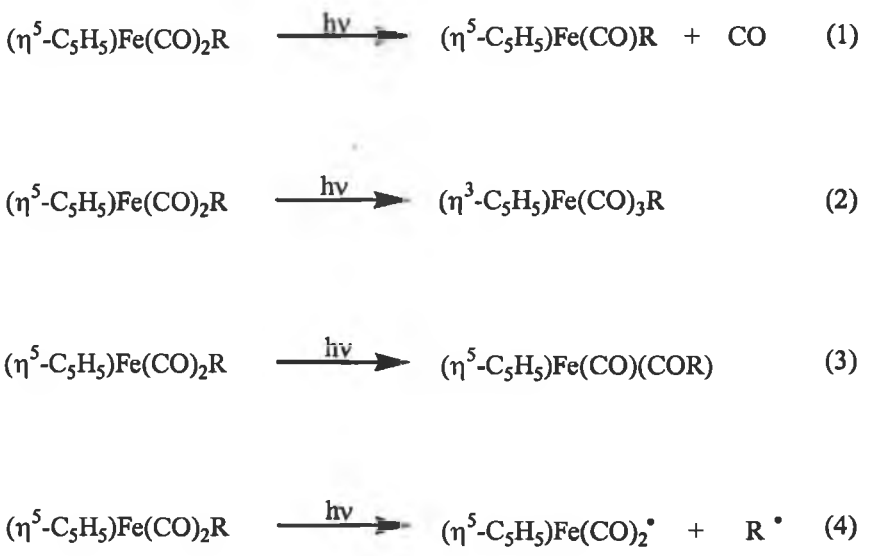

Figure 3-2 Outline of the four different photochemical pathways observed for $(\eta^5\text{-}C_5H_5)Fe(CO)_2R$ complexes.

Irradiation of $(\eta^5\text{-}C_5H_5)Fe(CO)_2R$, where R = CH_3, in the presence of triphenylphosphine (PPh_3) resulted in a high yield of the alkyl complex $(\eta^5\text{-}C_5H_5)Fe(CO)(PPh_3)CH_3$, with no evidence for the formation of an acyl intermediate complex, $(\eta^5\text{-}C_5H_5)Fe(CO)(COCH_3)(PPh_3)$.[14] However, if the reaction temperature is increased during the photolysis the outcome is the formation of significant quantities of the acyl derivative formed *via* a competing thermal process,[15] as outlined in Scheme 3-2.

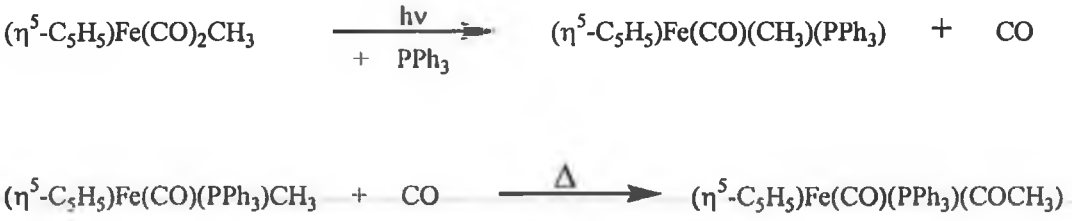

Scheme 3-2

Subsequently, Folkes and Rest[16] investigated this system quantitatively using NMR spectroscopy. They reported that the sole product formed following photolysis ($\lambda_{exc.}$ > 300 nm) at or above 300 K was $(\eta^5\text{-}C_5H_5)Fe(CO)(PPh_3)(CH_3)$, with no evidence for formation of the acyl complex. Nevertheless, it was noted by these researchers that formation of the acyl complex, $(\eta^5\text{-}C_5H_5)Fe(CO)(COCH_3)(PPh_3)$ did occur when photolysis was carried out at lower temperatures (293 K), and when the concentration of the incoming ligand (L =

$As(Ph_3)$ or $Sb(Ph_3)$) was low. These results led Folkes and Rest to propose that acyl complex formation is a competing photochemical process rather than a thermal process as had been previously been claimed.[14,15]

Photolysis of $(\eta^5\text{-}C_5H_5)Fe(CO)_2CH_3$ in methane, argon and dinitrogen matrixes at 12 K by Rest *et al.*[17] using progressively higher energy failed to induce the formation of the monocarbonyl, $(\eta^5\text{-}C_5H_5)Fe(CO)CH_3$. This result was confirmed by Gerhertz *et al.*[18] in argon matrixes at 10 K. Although no sixteen-electron monocarbonyl species was observed in the gas matrixes, $^{12}CO/^{13}CO$ exchange was shown to be induced photochemically when the matrix is doped with ^{13}CO.[17,18] Attempts to generate $CpFe(CO)CH_3$ in solid paraffin matrixes (40-70 K) were also unsuccessful. Although this monocarbonyl species proved elusive in the above matrixes, it is reported as being detected in polyvinyl chloride (PVC) films at 12 K.[19] The difference in behaviour between the matrixes was attributed to the rapid cage recombination in the more closely confined gas matrix environment as opposed to the more cavernous polymer film medium.[20] Although it is probable that the PVC film is interacting with the monocarbonyl fragment, $(\eta^5\text{-}C_5H_5)Fe(CO)(CH_3)$ in a similar manner as shown in Section 1.11 of the introduction chapter for $(\eta^5\text{-}C_5H_5)Mn(CO)_3$.

Kazlauskas and Wrighton[21] investigated a range of $(\eta^5\text{-}C_5H_5)Fe(CO)_2R$ type complexes, where R is CH_3, C_2H_5, or $n\text{-}C_5H_{11}$, in room temperature alkane solution and in low temperature alkane solutions at 77 K. Carbon monoxide dissociation was established as the primary photoprocess following near-UV excitation and the quantum yield ($\phi = 0.70 \pm 0.03$) for substitution of $(\eta^5\text{-}C_5H_5)Fe(CO)_2CH_3$ is independent of the incoming ligand or its concentration (above 10^{-3} M). By contrast, direct evidence for the formation of a sixteen-electron monocarbonyl species is provided when $(\eta^5\text{-}C_5H_5)Ru(CO)_2CH_3$ is irradiated in an alkane matrix at 77 K.[21] The infrared spectral changes observed are consistent with the formation of $(\eta^5\text{-}C_5H_5)Ru(CO)CH_3$.

Irradiation of $(\eta^5\text{-}C_5H_5)Fe(CO)_2CH_3$ ($\lambda_{exc.} < 370$ and > 550 nm) at high dilution in a pure carbon monoxide matrix at 12 K[17] gave rise to three new bands in the terminal ν_{CO} stretching region of the infrared spectra. Rest *et al.*[17] attributed these bands to the formation of the ring-slipped product $(\eta^3\text{-}C_5H_5)Fe(CO)_3CH_3$, based on the assumption that Fe-R bond homolysis is an inefficient process and that the excess carbon monoxide in these matrix experiments causes efficient recombination with the sixteen-electron photo-generated

(η^5-C_5H_5)Fe(CO)(CH_3) complex, to suppress this pathway and allow the observation of the ring-slip reaction.

The most recent investigation of the (η^5-C_5H_5)Fe(CO)$_2CH_3$ system employed Fourier transform infrared spectroscopy, (FT-IR), and time resolved infrared, (TR-IR), spectroscopy to elucidate information about the transient species formed during the flash photolysis of (η^5-C_5H_5)Fe(CO)$_2CH_3$ in glassy methylcyclohexane at 77 K and ambient temperature, respectively.[22] The FT-IR spectrum recorded after flash photolysis in methylcyclohexane at 77 K, displayed a single new band in the ν_{CO} terminal stretching region expected for a monocarbonyl complex. Warming to ambient temperature induced the regeneration of the initial FT-IR spectrum, which is consistent with reversible labilisation of a carbon monoxide ligand from (η^5-C_5H_5)Fe(CO)$_2CH_3$ as the principle reaction pathway. There was no indication for the formation of the dimer, [(η^5-C_5H_5)Fe(CO)$_2$]$_2$ which rules out the homolytic fragmentation of the Fe-CH_3 bond.

The TR-IR spectra of the transient species at room temperature also displays a single ν_{CO} absorption band, which forms within < 100 ns after the flash photolysis. The reaction of this monocarbonyl species with carbon monoxide occurs with second order kinetics and displays a solvent dependency, where the value of k_2 is 6.8 (± 0.2) × 10^6 M^{-1} s^{-1} and 3.4 (± 0.4) × 10^6 M^{-1} s^{-1} in cyclohexane and THF respectively. Based on these results the transient species is identified as being the solvento complex, (η^5-C_5H_5)Fe(CO)(solvent)CH_3.

In cases where the complex (η^5-C_5H_5)Fe(CO)$_2$R contains an alkyl ligand with a β-hydrogen, e.g. C_2H_5, good yields of the monosubstituted derivatives according to reaction (1), Figure 3-2, may also be obtained provided that the irradiation times are short.[14,21,23] At low concentrations of entering ligand however, the products (η^5-C_5H_5)Fe(CO)$_2$H and dimer, [(η^5-C_5H_5)Fe(CO)$_2$]$_2$ are formed. Photochemical formation of the hydride upon photolysis of (η^5-C_5H_5)Fe(CO)$_2C_2H_5$ occurs at 77 K in alkane matrixes, with no infrared detectable intermediates following a 5% conversion.[21] Competitive β-hydrogen elimination is proposed to occur from a photo-generated sixteen-electron species (η^5-C_5H_5)Fe(CO)C_2H_5 intermediate as high concentration of added triphenylphosphine suppresses the formation of the iron-hydride. Further investigations of (η^5-C_5H_5)Fe(CO)$_2C_2H_5$ by Rest *et al.*[24] in solution at 243 K and frozen gas matrices at 12 K provided similar results. Furthermore, no

evidence of the sixteen-electron species $(\eta^5\text{-}C_5H_5)Fe(CO)C_2H_5$ was found in either the gas matrices or the low temperature solutions.

Irradiation of $(\eta^5\text{-}C_5H_5)Ru(CO)_2C_2H_5$ in an alkane matrix at 77 K[21] on the other hand, initially gave rise to infrared spectral changes consistent with the formation of $(\eta^5\text{-}C_5H_5)Ru(CO)(C_2H_4)(H)$, although the hydride-olefin intermediate was only observed spectroscopically at low temperature, as it could not be isolated due to its thermal and photochemical instability. Further irradiation of $(\eta^5\text{-}C_5H_5)Ru(CO)(C_2H_4)(H)$ resulted in the formation of $(\eta^5\text{-}C_5H_5)Ru(CO)_2(H)$, which decomposed to the dimer, $[(\eta^5\text{-}C_5H_5)Ru(CO)_2]_2$ upon prolonged photolysis.

It is clear from reviewing the literature that photoinduced metal-alkyl bond cleavage, reaction (4), Figure 3-2, does not readily occur in $(\eta^5\text{-}C_5H_5)Fe(CO)_2R$ complexes, where R = CH_3, C_2H_5 or C_2H_4R. An electron spin resonance (ESR) study[25] of $(\eta^5\text{-}C_5H_5)Fe(CO)_2CH_3$ following photolysis at 243 K provides the only direct evidence for the formation of free radicals, $CH_3^{\bullet}$ and $[CpFe(CO)]^{\bullet}$, although the signals were reported as being quite weak. It is on this evidence that a pathway involving radicals has been forwarded as the reason for the photochemical formation of the iron dimer, $[CpFe(CO)_2]_2$, which is found to form in the absence of incoming nucleophiles.

Although previous research established that dissociative loss of carbon monoxide dominates the photochemistry of $CpFe(CO)_2R$, there are three reports[26] of light induced loss of R, when R = $CH_2C_6H_5$ according to Reaction 3-1 below.

$$(\eta^5\text{-}C_5R_5)Fe(CO)_2(\eta^1\text{-}CH_2C_6H_5) \xrightarrow{h\nu} [(\eta^5\text{-}C_5R_5)Fe(CO)_2]_2 + \text{bibenzyl}$$

Reaction 3-1

This stimulated an investigation by Blaha and Wrighton[27] into the photochemistry of $(\eta^5\text{-}C_5R_5)Fe(CO)_2(\eta^1\text{-}CH_2C_6H_5)$. Irradiation of $(\eta^5\text{-}C_5R_5)Fe(CO)_2(\eta^1\text{-}CH_2C_6H_5)$, where R = H or CH_3, yielded both loss of the $CH_2C_6H_5$ radical and carbon monoxide as the primary photoprocesses. In rigid alkane matrices at 77 K the only detectable photoreaction is loss of carbon monoxide to form $(\eta^5\text{-}C_5R_5)Fe(CO)(\eta^3\text{-}CH_2C_6H_5)$, whereas in alkane solution at room temperature formation of the dimer $[(\eta^5\text{-}C_5R_5)Fe(CO)_2]_2$ dominates, unless the

reaction is actively purged with a stream of inert gas such as argon or nitrogen. In such cases (i.e. when solutions are purged with argon during photolysis), there are two main photoproducts, (η^5-C_5R_5)Fe(CO)(η^3-$CH_2C_6H_5$) (90-95 %) and [(η^5-C_5R_5)Fe(CO)$_2$]$_2$ (5-10 %). The quantum efficiency ($\lambda_{exc.}$ = 366 nm) for carbon monoxide loss is, ~0.5, whereas that for $CH_2C_6H_5$ loss is ~0.05.

Blaha and Wrighton[27] demonstrated that irradiation of (η^5-C_5R_5)Fe(CO)$_2$(η^1-$CH_2C_6H_5$), R = H or CH_3, under 2 atm of carbon monoxide in alkane solution at room temperature led to the formation of (η^4-$C_5R_5(CH_2C_6H_5)$)Fe(CO)$_3$ in good yield (> 50 %). The ν_{CO} bands for this species were found to be almost identical to those reported by Rest *et al.*[17] for the ring-slipped product, (η^3-C_5H_5)Fe(CO)$_3CH_3$. The formation of (η^4-$C_5R_5(CH_2C_6H_5)$)Fe(CO)$_3$ occurs *via* light induced loss of $CH_2C_6H_5$ radical from (η^5-C_5R_5)Fe(CO)$_2$(η^1-$CH_2C_6H_5$), followed by reaction of (η^5-C_5R_5)Fe(CO)$_2$ with carbon monoxide to form (η^5-C_5R_5)Fe(CO)$_3$, which then couples with a $CH_2C_6H_5$ radical to give an *exo*-isomer of (η^4-$C_5R_5(CH_2C_6H_5)$)Fe(CO)$_3$. Since the structure of (η^4-$C_5R_5(CH_2C_6H_5)$)Fe(CO)$_3$ was established by X-ray crystallography for R = CH_3, it seems that (η^4-$C_5R_5(CH_2C_6H_5)$)Fe(CO)$_3$ must be considered as the alternative to ring-slip product, (η^3-C_5H_5)Fe(CO)$_3CH_3$ proposes by Rest *et al.*[17] Scheme 3-3 outlines the photochemistry proposed by Blaha and Wrighton[27] for the (η^5-C_5R_5)Fe(CO)$_2$(η^1-$CH_2C_6H_5$) complex, R = H or CH_3.

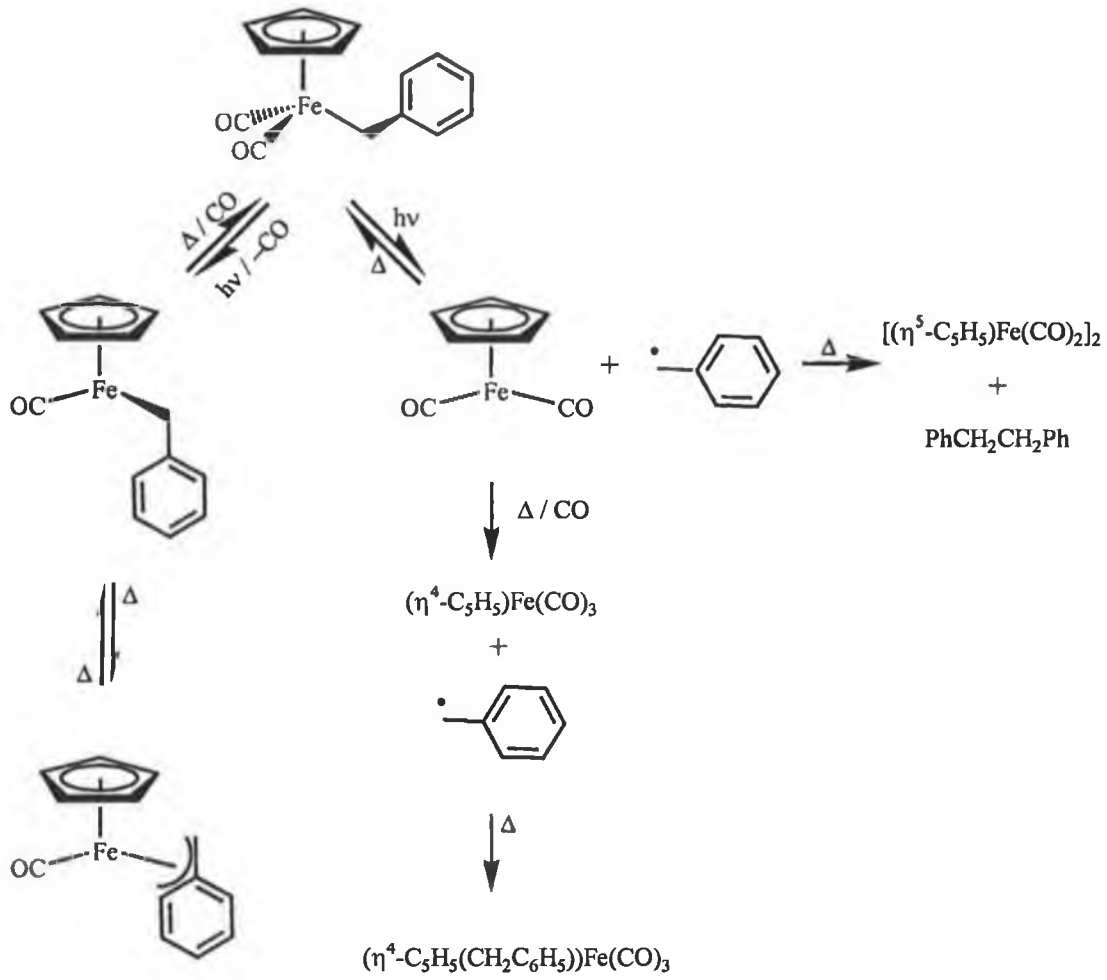

Scheme 3-3 Summary of the photochemistry of $(\eta^5\text{-}C_5R_5)Fe(CO)_2(\eta^1\text{-}CH_2C_6H_5)$ as proposed by Blaha and Wrighton.[27]

An interesting consequence of photo-induced carbon-monoxide dissociation from $(\eta^5\text{-}C_5H_5)Fe(CO)_2(\eta^1\text{-allyl})$ complexes is the intra-molecular rearrangement, as shown in Scheme 3-4.

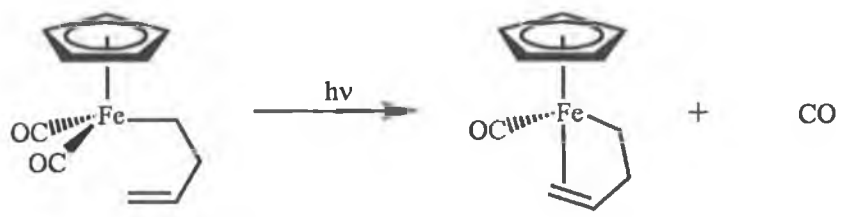

Scheme 3-4 Intra-molecular re-arrangement.

Green and Nagy[28] reported the preparation of monocarbonyl $(\eta^5\text{-}C_5H_5)Fe(CO)(\eta^3\text{-allyl})$ complexes, by the photochemical displacement of carbon monoxide from the metal centre of the corresponding dicarbonyl complex, $(\eta^5\text{-}C_5H_5)Fe(CO)_2(\eta^1\text{-allyl})$, Scheme 3-5.

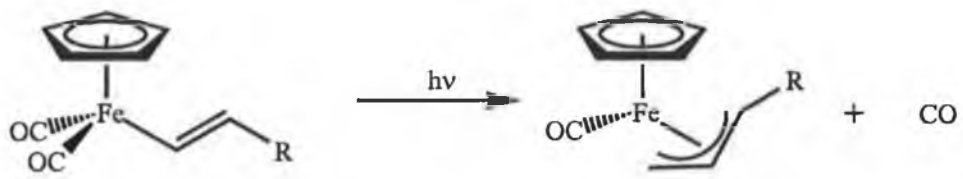

Scheme 3-5 Formation of an η^3-allyl complex.

Later a report by King and Ishaq[29] on the photochemistry of the corresponding ruthenium-(η^1-allyl) complexes, $(\eta^5\text{-}C_5H_5)Ru(CO)_2(\eta^1\text{-allyl})$, provided spectroscopic evidence for the formation of two stereoisomers. This was followed by a study by Faller, Johnson and Dyrja[30] who reported only one stereoisomeric form of the η^3-allyl-iron and ruthenium complexes, which they assigned to the *exo*-isomer based on NMR spectroscopic properties. It was however considered by this group that two isomers were formed and that the purification methods could have lead to the decomposition or inter-conversion of one of the isomers during isolation. Indeed this was to prove to be the reason for their failure to observe two stereoisomeric forms of the η^3-allyl-iron complex. Further study[31] of the system following irradiation of $(\eta^5\text{-}C_5H_5)Fe(CO)_2(\eta^1\text{-}C_3H_5)$ at lower temperature (283 K), resulted in the observation of the two stereoisomers. The less stable *endo*-isomer thermally isomerises to the more stable *exo*-isomer with a moderate rate at room temperature, refer to Scheme 3-6.

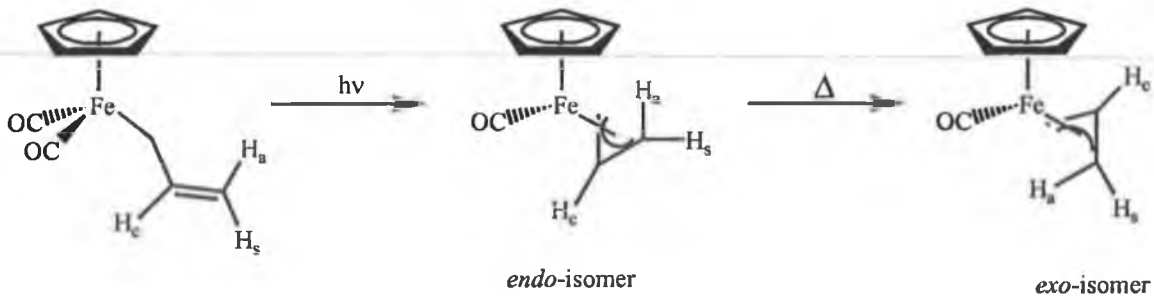

Scheme 3-6 The two isomers formed following the photolysis of $(\eta^5\text{-}C_5H_5)Fe(CO)_2(\eta^1\text{-allyl})$, the *endo*-isomer thermally isomerises to the more stable *exo*-isomer at room temperature.

This hapticity change in co-ordination mode of the η^1-ally ligands or η^1-$CH_2C_6H_5$[27] from η^1 → η^3 upon the photoinduced loss of carbon monoxide has particular relevance to further work carried out by Belmont and Wrighton[32] on (η^5-C_5H_5)Fe(CO)$_2$(η^1-C_5H_5), (η^5-C_5H_5)Fe(CO)$_2$(η^1-indenyl) and (η^5-indenyl)Fe(CO)$_2$(η^1-indenyl). Irradiation of these complexes in low temperature alkane solutions at 77 K allowed the detection of the monocarbonyl products because the rapid η^1 → η^3 conversion of the η^1-C_5H_5 and η^1-indenyl bound ligand can trap the sixteen-electron fragment and saturate the metal centre once more to yield monocarbonyl products of the type, (η^5-C_5H_5)Fe(CO)(η^3-C_5H_5), (η^5-C_5H_5)Fe(CO)(η^3-indenyl) and (η^5-indenyl)Fe(CO)(η^3-indenyl). These monocarbonyl complexes are thermally labile and annealing of the matrix lead to the formation of metallocenes (i.e. η^3 → η^5 conversion) concomitant with the loss of carbon monoxide, Scheme 3-7. The infrared spectral studies showed that the chemistry was complicated by the fact that the starting dicarbonyl complexes and the monocarbonyl complexes can exist as two isomers, which is in good agreement with previously characterised complexes of η^3-allyl ligands.[31] The less thermodynamically stable of the monocarbonyl isomer, the *endo*-isomer, thermally isomerises to the more stable *exo*-form.

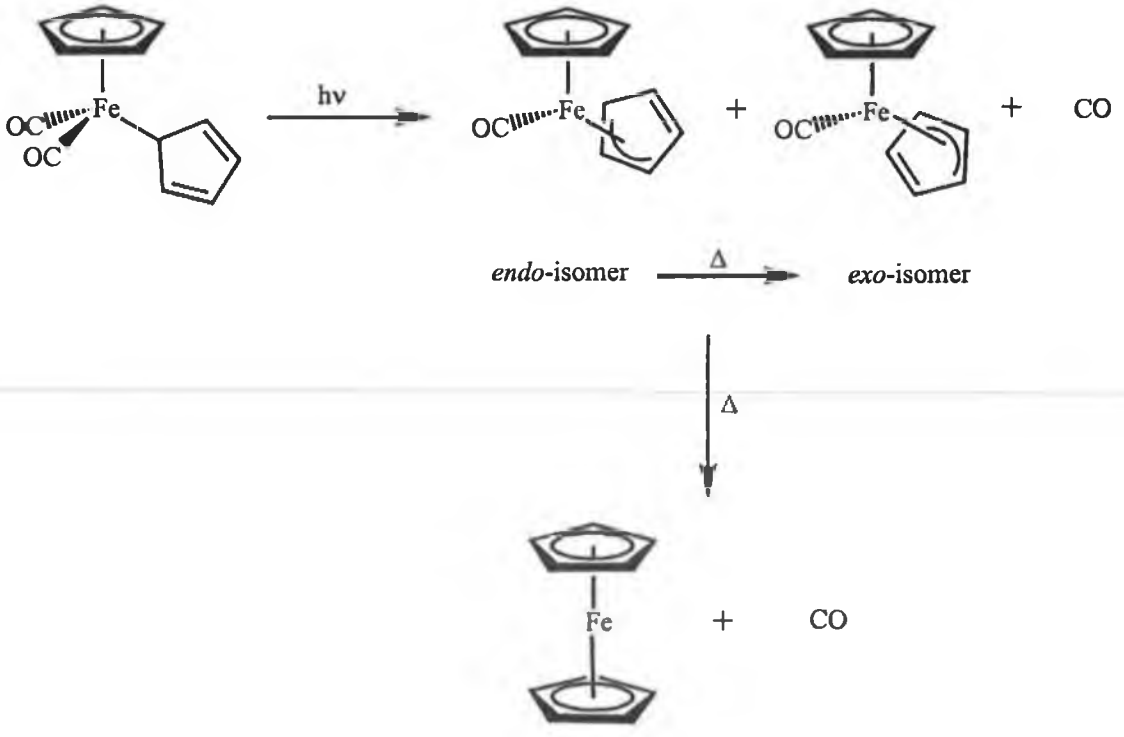

Scheme 3-7 Outline of the photochemistry of (η^5-C_5H_5)Fe(CO)$_2$(η^1-C_5H_5).

On the basis of the well established photosubstitution reactions (η^5-C_5H_5)$Fe(CO)_2R$ with triphenylphosphine (PPh_3), Carpenter *et al.*[33] expected to produce (η^5-C_5H_5)$Fe(CO)[CHPh(OSiMe_3)](PPh_3)$ upon photolysis of (η^5-C_5H_5)$Fe(CO)_2[CHPh(OSiMe_3)]$. However, formation of η^4-{*exo*-(η^5-C_5H_5)$[CHPh(OSiMe_3)]$}$Fe(CO)_2PPh_3$ was reported as the actual product. Although ligand substitution is the dominant pathway in photoreactions of (η^5-C_5H_5)$M(CO)_2R$ complexes, iron-to-cyclopentadienyl ligand migration of alkyl groups has also been observed.[27] The quantum yield for substitution of the carbon monoxide ligand has been found to be much higher than that for metal-carbon bond homolysis, but migration to form (η^4-cyclopentadienyl)$Fe(CO)_3$ complexes can become significant under high carbon monoxide pressure, since the net carbon monoxide substitution is suppressed. Carpenter *et al.*'s[33] results, in which alkyl migration greatly predominates over substitution even under inert conditions, is extraordinary when contrasted with the exclusive photosubstitution observed for the electronically similar (η^5-C_5H_5)$Fe(CO)_2R$, R = CH_2OCH_3. The *exo* relationship of the migrated alkyl group relative to iron strongly suggested a dissociative migration pathway.

3.3 The results and discussion of the photochemistry of cyclopentadienyliron-dicarbonyl-η^1-pyrrolyl. $(\eta^5\text{-}C_5H_5)Fe(CO)_2(\eta^1\text{-}C_4H_4N)$

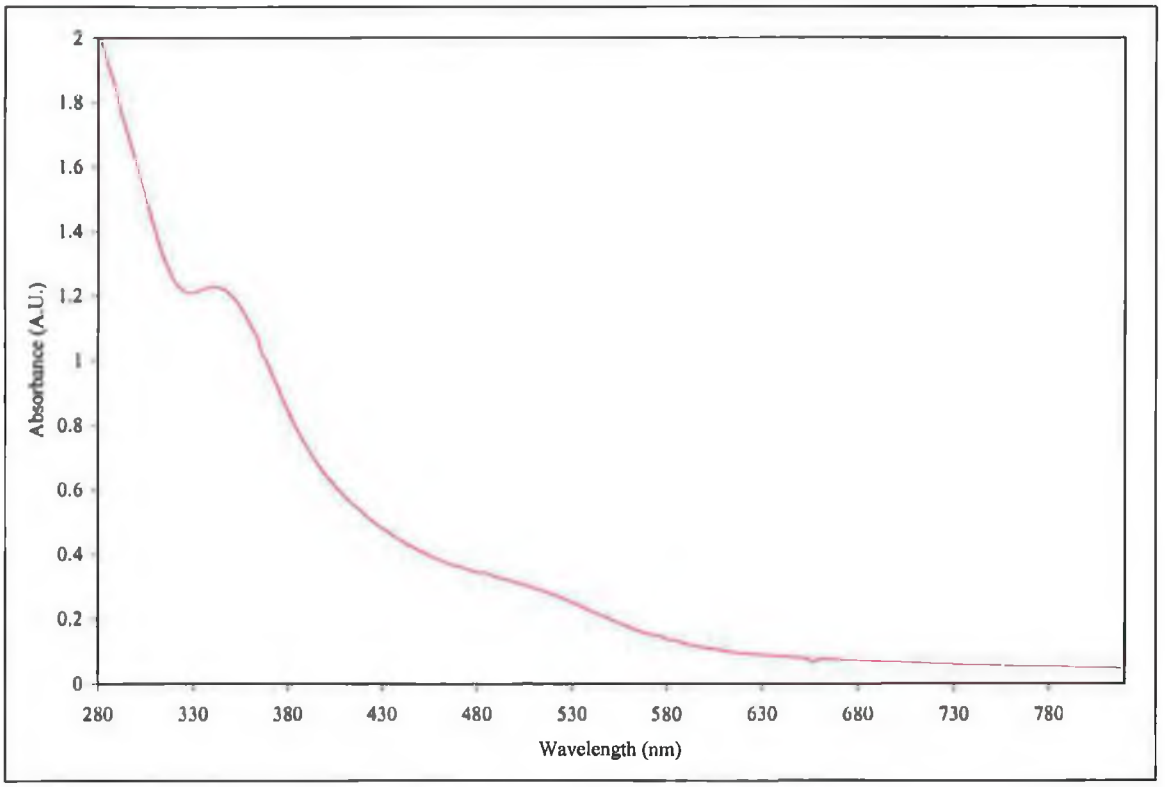

Figure 3-3 UV-vis spectrum of cyclopentadienyliron dicarbonyl-η^1-pyrrolyl. $(\eta^5\text{-}C_5H_5)Fe(CO)_2(\eta^1\text{-}C_4H_4N)$ (1.18×10^{-3} M) in cyclohexane.

The UV-vis spectrum of $(\eta^5\text{-}C_5H_5)Fe(CO)_2(\eta^1\text{-}C_4H_4N)$ in cyclohexane as shown in Figure 3-3. This complex displays weak absorptions centred at 340 nm ($\varepsilon = 1.47 \times 10^3$ L mol^{-1} cm^{-1}) and 484 nm ($\varepsilon = 3.63 \times 10^2$ L mol^{-1} cm^{-1}), and also exhibits an absorption tail into the visible region of the spectrum (> 580 nm). Although these low-energy bands have not been previously assigned, they are believed to be ligand field transitions for the following reasons. The molar absorptivities of these absorptions bands are fairly low, consistent with orbitally forbidden transitions in organometallic complexes. In addition, the energy position of the bands have been determined to be not particularly solvent dependent, which is typical behaviour of the behaviour of d-d transitions. Finally, earlier photochemical studies have shown that similar complexes, $(\eta^5\text{-}C_5H_5)Fe(CO)_2X$, where X is a halide undergo highly efficient carbon monoxide dissociation following excitation at 366 and 436

nm.[1] However this final reason deserves a note of caution when assigning these bands to ligand field transitions, as a recent publication by Rosa and Baerends *et al.*[34] reviewed the role of ligand field excited states in the photochemical dissociation of the metal-carbon monoxide bond. Based on density functional calculations on the excited states of $Cr(CO)_6$, it was shown that the lowest lying states are a set of symmetry forbidden charge transfer excitations, and photo-activity may not be used for the assigning of low energy absorption to ligand field excitation. These finding have been discussed previously in chapter one, Section 1.8.

3.3.1 Broad band steady-state photolysis ($\lambda_{exc.} > 400$ nm) of $(\eta^5\text{-}C_5H_5)Fe(CO)_2(\eta^1\text{-}C_4H_4N)$ monitored by UV-vis spectroscopy

Irradiation of $(\eta^5\text{-}C_5H_5)Fe(CO)_2(\eta^1\text{-}C_4H_4N)$ in cyclohexane under inert conditions (1 atm argon) at room temperature, results in a decrease in absorption across the whole UV-vis spectrum. An infrared spectrum of the photolysis solution contained four bands in the ν_{CO} stretching region of the infrared spectrum. The ν_{CO} bands at 2048 and 2002 cm^{-1} are those of the parent complex, $(\eta^5\text{-}C_5H_5)Fe(CO)_2(\eta^1\text{-}C_4H_4N)$. The two bands at 1961 and 1793 cm^{-1} are assigned to the dimer complex, $[(\eta^5\text{-}C_5H_5)Fe(CO)_2]_2$ by comparison with an authentic sample. The high-energy band of the dimer species at 2004 cm^{-1} has been hidden by the lower energy band of the parent complex, $(\eta^5\text{-}C_5H_5)Fe(CO)_2(\eta^1\text{-}C_4H_4N)$. The photoinduced dissociation of the carbon monoxide ligand and the generation of a sixteen-electron species is assumed to be the first step in the reaction. Support for this assumption comes from the fact that two-electron ligands are able to stabilise the $(\eta^5\text{-}C_5H_5)Fe(CO)_2(\eta^1\text{-}C_4H_4N)$ fragment.

The formation of the dimer is consistent with the results of the first reported photolysis reactions of $(\eta^5\text{-}C_5H_5)Fe(CO)_2R$ complexes,[13] (R = CH_3, C_2H_5, or C_6H_5) in the absence of potential ligands. In pentane or other non co-ordinating solvents, photolysis of $(\eta^5\text{-}C_5H_5)Fe(CO)_2R$ yielded $[(\eta^5\text{-}C_5H_5)Fe(CO)_2]_2$ as the sole metal containing product. Irradiation of $(\eta^5\text{-}C_5H_5)Fe(CO)_2(\eta^1\text{-}CH_2C_6H_5)$ and $(\eta^5\text{-}C_5(CH_3)_5)Fe(CO)_2(\eta^1\text{-}CH_2C_6H_5)$ in the absence of potential ligands in methylcyclohexane at room temperature also produced the iron dimer complexes, $[(\eta^5\text{-}C_5H_5)Fe(CO)_2]_2$ and $[(\eta^5\text{-}C_5(CH_3)_5)Fe(CO)_2]_2$ respectively.[27] Steady state photolysis ($\lambda_{exc.} > 400$ nm) of $(\eta^5\text{-}C_5H_5)Fe(CO)_2(\eta^1\text{-}C_4H_4N)$ in a carbon

monoxide saturated cyclohexane resulted in the spectral changes displayed in, Figure 3-4. A decrease in absorption occurs over the whole UV-vis range.

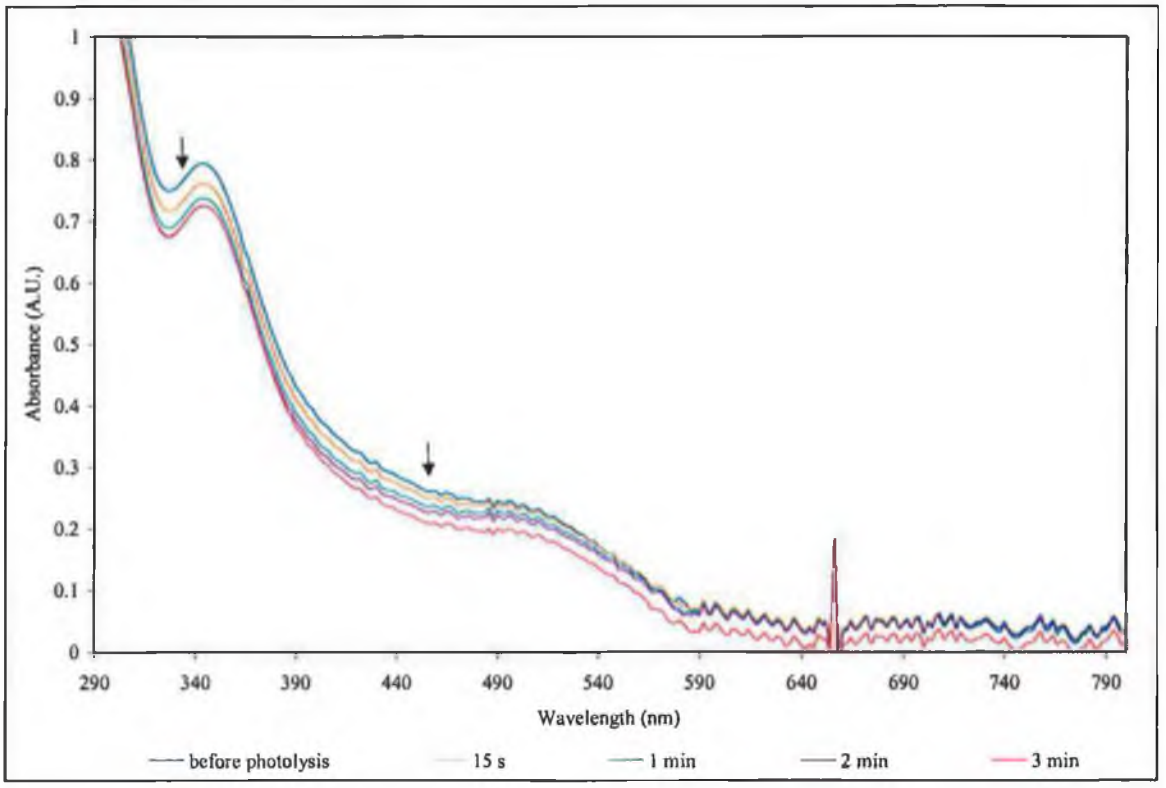

Figure 3-4 Changes observed in the UV-vis spectrum of $(\eta^5\text{-}C_5H_5)Fe(CO)_2(\eta^1\text{-}C_4H_4N)$ (~5.4 × 10^{-4} M) following photolysis (λ_{exc} > 400 nm) in carbon monoxide saturated cyclohexane.

An infrared spectrum of the solution following photolysis contained four bands in the ν_{CO} stretching region as observed under inert conditions, refer to Figure 3-5. The assignment of the bands is as in the case of photolysis of $(\eta^5\text{-}C_5H_5)Fe(CO)_2(\eta^1\text{-}C_4H_4N)$ under inert conditions. However, it is important to note that the extent of iron dimer formation is reduced, based on the ratio of intensities of the parent bands at 2048 and 2002 cm^{-1} to those of the dimer species at 1961 and 1793 cm^{-1}. This observation supports the assumption that carbon monoxide loss is the first step in the formation of the dimeric species, $[(\eta^5\text{-}C_5H_5)Fe(CO)_2]_2$, as under an atmosphere of carbon monoxide, dissociation of a carbon monoxide ligand is reversed, and so the formation of the dimer should also be reduced.

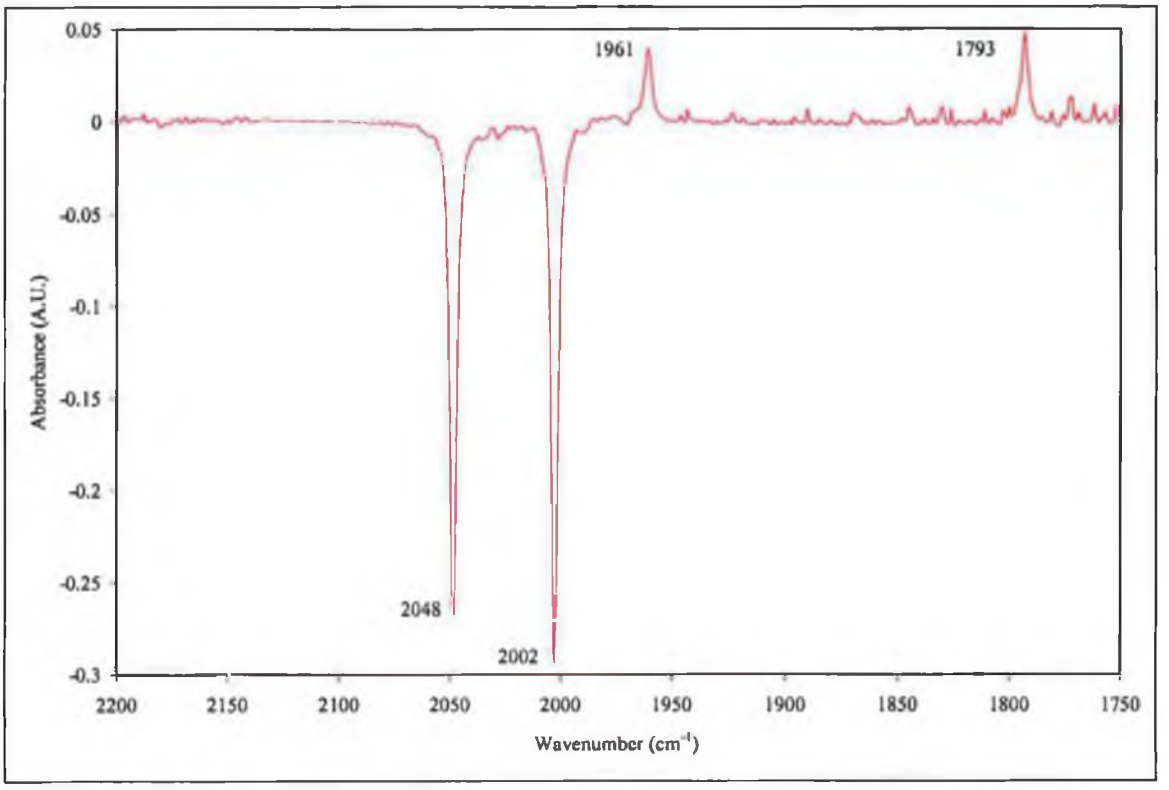

Figure 3-5 Infrared difference spectrum of $(\eta^5\text{-}C_5H_5)Fe(CO)_2(\eta^1\text{-}C_4H_4N)$ following photolysis (λ_{exc} > 400 nm) in carbon monoxide saturated cyclohexane.

Irradiation of $(\eta^5\text{-}C_5H_5)Fe(CO)_2(\eta^1\text{-}C_4H_4N)$ in degassed cyclohexane solution containing an excess of triphenylphosphine (PPh_3) resulted in the spectroscopic changes presented in Figure 3-6. Spectral sequences recorded during photolysis reveal that the photoreaction involves a clean and complete conversion to the corresponding photoproduct. Unfortunately quantum yields for the substitution process could not be obtained, owing to a substantial increase in light absorption over the entire 320-600 nm range following photolysis.

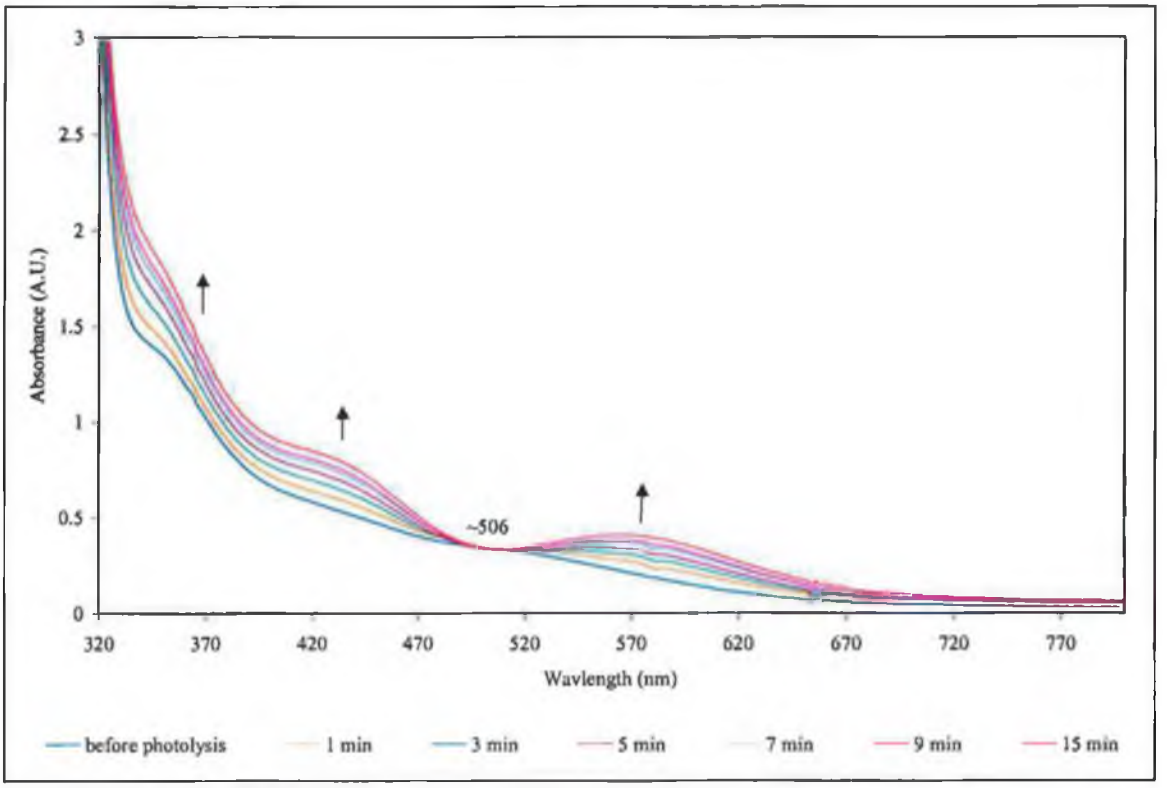

Figure 3-6 UV-vis spectral changes observed upon the photolysis of $(\eta^5\text{-}C_5H_5)Fe(CO)_2(\eta^1\text{-}C_4H_4N)$ (~1.0×10^{-3} M) in cyclohexane with PPh_3 ligand added in excess.

3.3.2 Broad band steady state photolysis ($\lambda_{exc.} > 400$ nm) of $(\eta^5\text{-}C_5H_5)Fe(CO)_2(\eta^1\text{-}C_4H_4N)$ monitored by infrared spectroscopy

A degassed cyclohexane solution of $(\eta^5\text{-}C_5H_5)Fe(CO)_2(\eta^1\text{-}C_4H_4N)$ with triphenylphosphine added in excess was irradiated in the infrared solution cell at $\lambda_{exc.} > 400$ nm. Infrared spectra were recorded at various time intervals during photolysis, (total photolysis time ~ 50 seconds) and the resulting changes in the ν_{CO} region of the spectra are given in Figure 3-7.

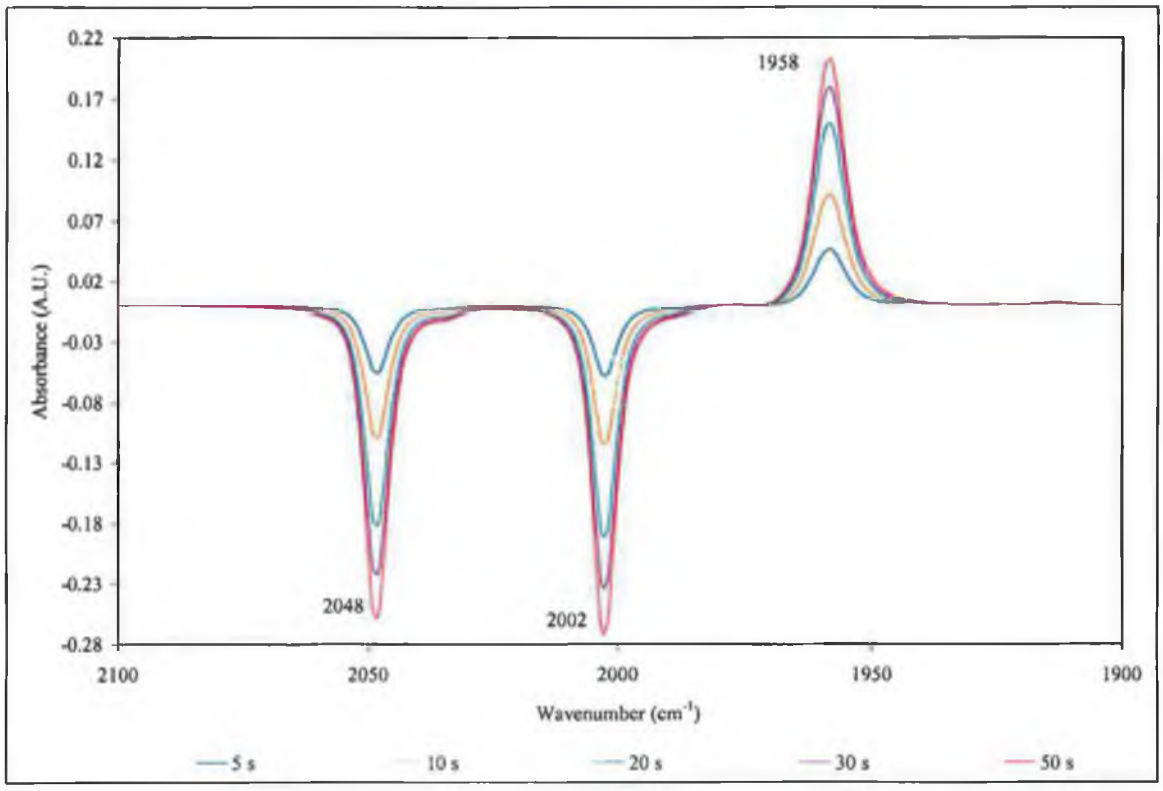

Figure 3-7 Infrared spectral changes observed upon the photolysis (λ_{exc} > 400nm) of $(\eta^5\text{-}C_5H_5)Fe(CO)_2(\eta^1\text{-}C_4H_4N)$ in cyclohexane with PPh_3 ligand added in excess.

As the reaction proceeded an isosbestic point in the infrared spectrum was apparent at 1976 cm^{-1}, which is consistent with the smooth transformation of the parent complex, $(\eta^5\text{-}C_5H_5)Fe(CO)_2(\eta^1\text{-}C_4H_4N)$ to a single photoproduct. The intensity of the two ν_{CO} stretching frequencies at 2048 and 2002 cm^{-1}, corresponding to the two terminal carbonyls of the starting complex, $(\eta^5\text{-}C_5H_5)Fe(CO)_2(\eta^1\text{-}C_4H_4N)$ decrease and simultaneously there is the appearance of a single ν_{CO} stretch at 1958 cm^{-1}. This new band at 1958 cm^{-1} is assigned to the monosubstituted photoproduct $CpFe(CO)(PPh_3)(\eta^1\text{-pyrrolyl})$. Substitution of the carbon monoxide ligand in $(\eta^5\text{-}C_5H_5)Fe(CO)_2R$[15] (where R is alkyl or allyl) and $(\eta^5\text{-}C_5H_5)Fe(CO)_2X$[10] (where X is a halide) is well known to dominate the photochemical reaction of these type of complexes. For example irradiation of $(\eta^5\text{-}C_5H_5)Fe(CO)_2Cl$ in the presence of PPh_3, gave rise to $(\eta^5\text{-}C_5H_5)Fe(CO)(PPh_3)Cl$, which displays a monocarbonyl ν_{CO} stretch at 1960 cm^{-1}, other examples of photoinduced mono-substitution of these types of complexes are outlined in Table 3-1. Therefore findings of this work for $(\eta^5\text{-}C_5H_5)Fe(CO)_2(\eta^1\text{-}C_4H_4N)$ are in agreement with previous studies on similar complexes.

Complex	ν_{CO} / cm^{-1}	Medium	Temperature / K
$(\eta^5\text{-}C_5H_5)Fe(CO)(PPh_3)(C_2H_5)$[21]	1906	toluene	298
$(\eta^5\text{-}C_5H_5)Fe(CO)(PPh_3)(\eta^1\text{-}C_6H_5)$[27]	1909	isooctane	298
$(\eta^5\text{-}C_5H_5)Fe(CO)(PPh_3)(CH_3)$[21]	1921	isooctane	195
$(\eta^5\text{-}C_5H_5)Fe(CO)(PPh_3)I$[15]	1938	chloroform	298
$(\eta^5\text{-}C_5H_5)Fe(CO)(pyridine)(Cl)$[10]	1957	hexane	183
$(\eta^5\text{-}C_5H_5)Fe(CO)(1\text{-pentene})(CH_3)$[21]	1957	isooctane	183
$(\eta^5\text{-}C_5H_5)Fe(CO)(C_2H_4)(CH_3)$[24]	1960	pentane	243
$(\eta^5\text{-}C_5H_5)Fe(CO)(PPh_3)Cl$[15]	1960	Nujol mull	298
$(\eta^5\text{-}C_5H_5)Fe(CO)(PPh_3)Br$[15]	1965	chloroform	298

Table 3-1 The ν_{CO} stretching frequencies of similar monocarbonyl type complexes.

3.3.3 Laser Flash Photolysis Experiments

The photochemistry of $(\eta^5\text{-}C_5H_5)Fe(CO)_2(\eta^1\text{-}C_4H_4N)$ was investigated with irradiation at $\lambda_{exc.}$ = 355 and 532 nm, under both atmospheres of argon and carbon monoxide.

Following flash photolysis, $\lambda_{exc.}$ = 355 nm of $(\eta^5\text{-}C_5H_5)Fe(CO)_2(\eta^1\text{-}C_4H_4N)$ in carbon monoxide-saturated cyclohexane a transient species was observed. The difference spectra obtained one microsecond and two microseconds after the laser pulse are given in Figure 3-8. It can be seen that the only region of the spectrum where the photoproduct absorbs significantly is at 430 nm. This transient species is assigned to the formation and subsequent decay of the sixteen-electron species $(\eta^5\text{-}C_5H_5)Fe(CO)(\eta^1\text{-}C_4H_4N)$. The parent complex $(\eta^5\text{-}C_5H_5)Fe(CO)_2(\eta^1\text{-}C_4H_4N)$ also absorbs in this region of the spectrum, see Figure 3-3.

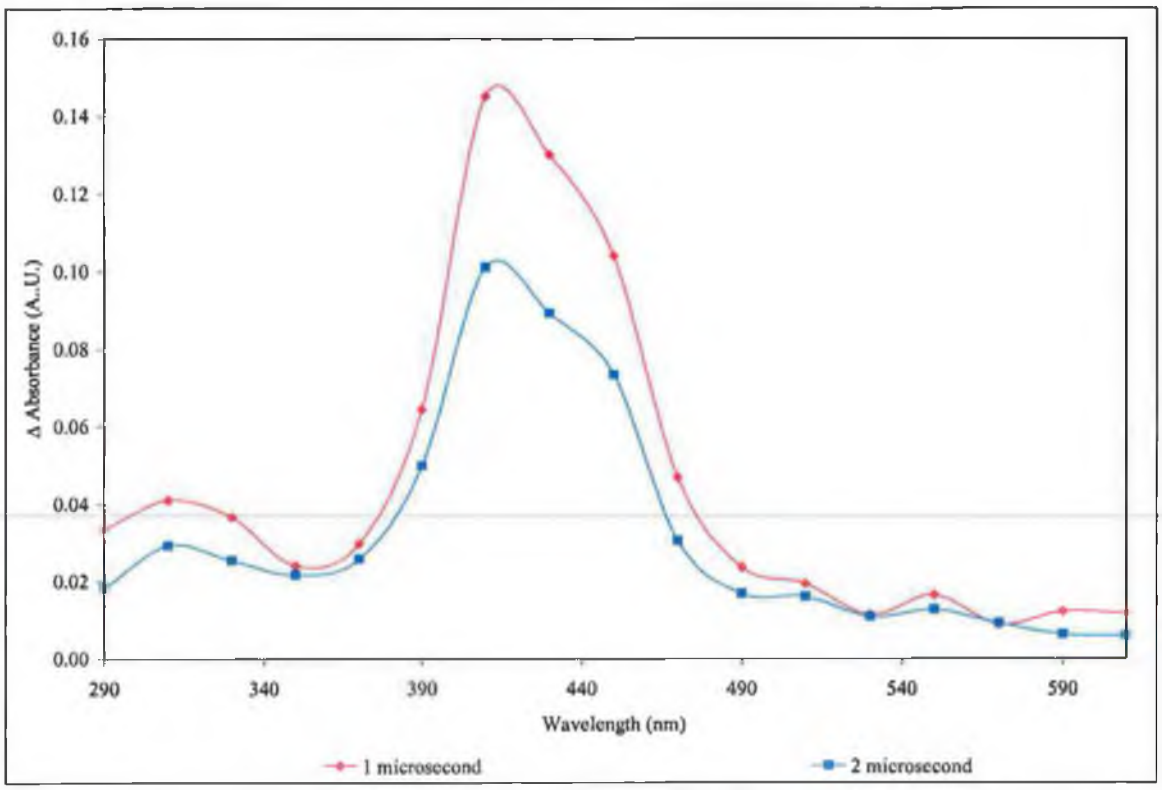

Figure 3-8 UV-vis difference spectra after 1 μs and 2 μs following irradiation of $(\eta^5\text{-}C_5H_5)Fe(CO)_2(\eta^1\text{-}C_4H_4N)$ in carbon monoxide saturated cyclohexane.

Analysis of the decay kinetics associated with the transient absorption at 410 nm yielded the rate constant for the reaction of the monocarbonyl, $(\eta^5\text{-}C_5H_5)Fe(CO)(\eta^1\text{-}C_4H_4N)$ with carbon monoxide. A typical transient signal (average of 5 shots) at 410 nm obtained following laser flash photolysis of $(\eta^5\text{-}C_5H_5)Fe(CO)_2(\eta^1\text{-}C_4H_4N)$ in carbon monoxide saturated cyclohexane (i.e. CO concentration is 9×10^{-3} M) is presented in Figure 3-9.

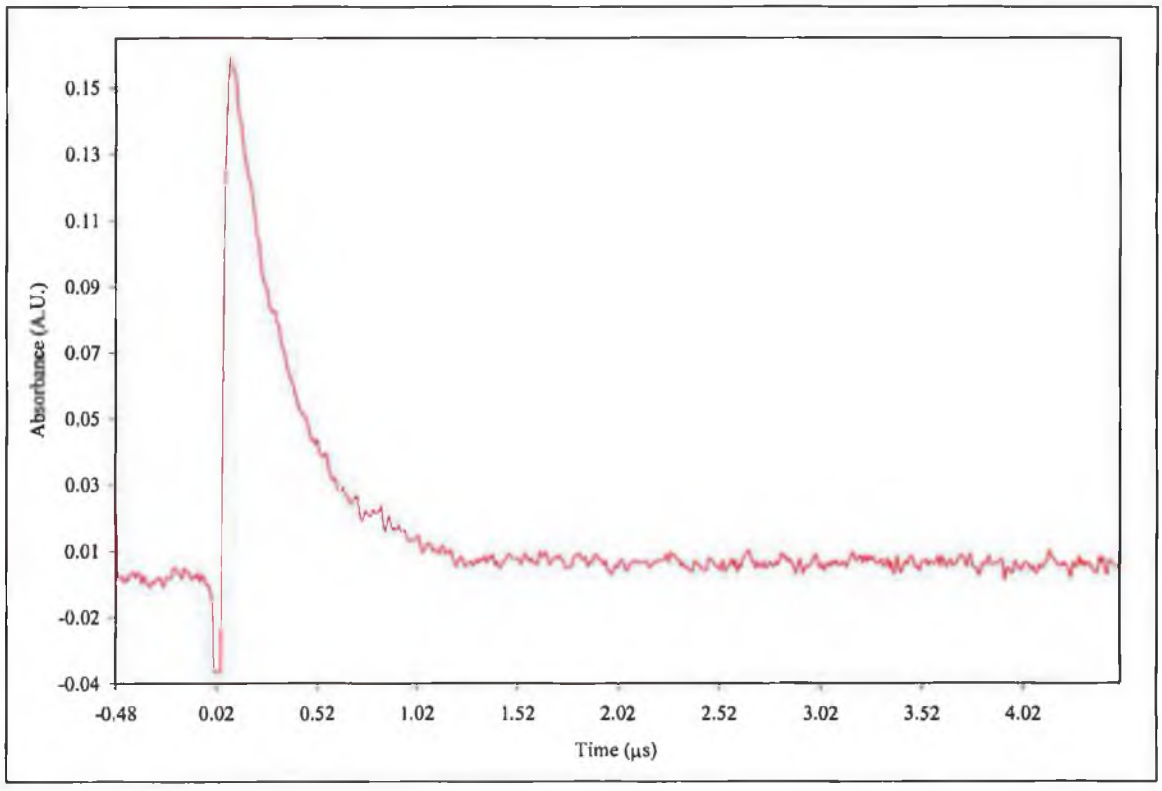

Figure 3-9 A typical transient signal obtained for the decay of $(\eta^5\text{-}C_5H_5)Fe(CO)(\eta^1\text{-}C_4H_4N)$, ($6.7 \times 10^{-4}$ M), monitored at 410 nm in carbon monoxide saturated cyclohexane.

Under these conditions, this transient signal decays to the pre-irradiated baseline in less than 2 μs, refer to Figure 3-9, indicating the reversible nature of the process. The steady-state UV-vis spectrum of the flash photolysis solution was monitored throughout the experiment, and showed that no significant absorption change occurred, confirming that the overall process is reversible. The lifetime of the transient species is dependent on the concentration of carbon monoxide, as the concentration of carbon monoxide is increased from 2.25×10^{-3} M to 9.0×10^{-3} M, the lifetime of the transient species at 410 nm decreased. The observed rate constant data (k_{obs}) accumulated under different concentrations of carbon monoxide

provide the second order rate constant (k_2) for the reaction of $(\eta^5\text{-}C_5H_5)Fe(CO)(\eta^1\text{-}C_4H_4N)$ with carbon monoxide as outlined in Reaction 3-2.

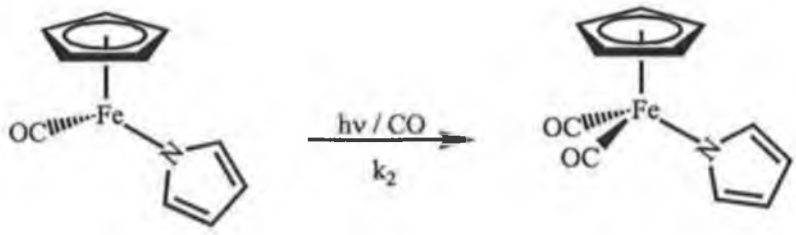

Reaction 3-2

The plot of the observed rate constant versus the concentration of carbon monoxide, Figure 3-10, is linear with negligible intercept, which indicates that under these conditions no other reaction(s) contribute significantly to the decay of the monocarbonyl species. The slope of the line represents the second order rate constant, for the reaction of $(\eta^5\text{-}C_5H_5)Fe(CO)(\eta^1\text{-}C_4H_4N)$ with carbon monoxide to regenerate the parent complex $(\eta^5\text{-}C_5H_5)Fe(CO)_2(\eta^1\text{-}C_4H_4N)$, i.e. $k_2 = 3.0\ (\pm\ 0.3) \times 10^8\ M^{-1}s^{-1}$ at 298 K in cyclohexane.

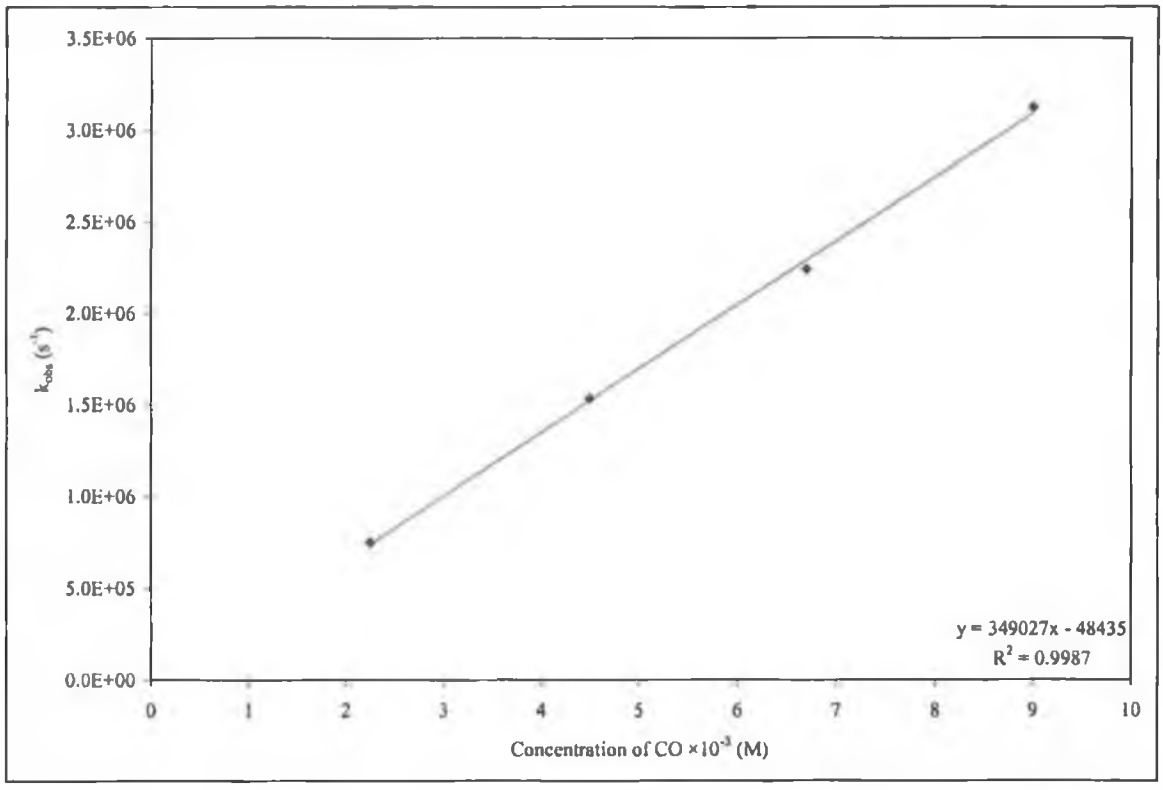

Figure 3-10 Plot of k_{obs} - vs - concentration of carbon monoxide for the decay of $(\eta^5\text{-}C_5H_5)Fe(CO)(\eta^1\text{-}C_4H_4N)$ in cyclohexane to regenerate the parent complex $(\eta^5\text{-}C_5H_5)Fe(CO)_2(\eta^1\text{-}C_4H_4N)$.

Previous results on the flash photolysis of $(\eta^6\text{-arene})Cr(CO)_3$[35] showed that the primary photoproduct upon carbon monoxide loss is the solvated species $(\eta^6\text{-arene})Cr(CO)_2(S)$, where the solvent (S) is considered a 'token' ligand for the intermediate species before it decays in the presence of carbon monoxide to regenerate $(\eta^6\text{-arene})Cr(CO)_3$. If the 'token' ligand is a good co-ordinating solvent, it is more difficult for it to be displaced by the carbon monoxide moiety. This leads to a slower rate of reaction for the reaction of carbon monoxide with the solvated dicarbonyl species, $(\eta^6\text{-arene})Cr(CO)_2(S)$. Hence it is possible to determine whether an intermediate species is solvated or not by varying the solvents according to their co-ordinating abilities, and thereby investigating the consequences this variation in solvent has on the second order rate constants for the reaction.

Consequently, the photochemistry of $(\eta^5\text{-}C_5H_5)Fe(CO)_2(\eta^1\text{-}C_4H_4N)$ was investigated in a better co-ordinating solvent, toluene. A similar decay signal indicative of a reversible process was observed, refer to Figure 3-11.

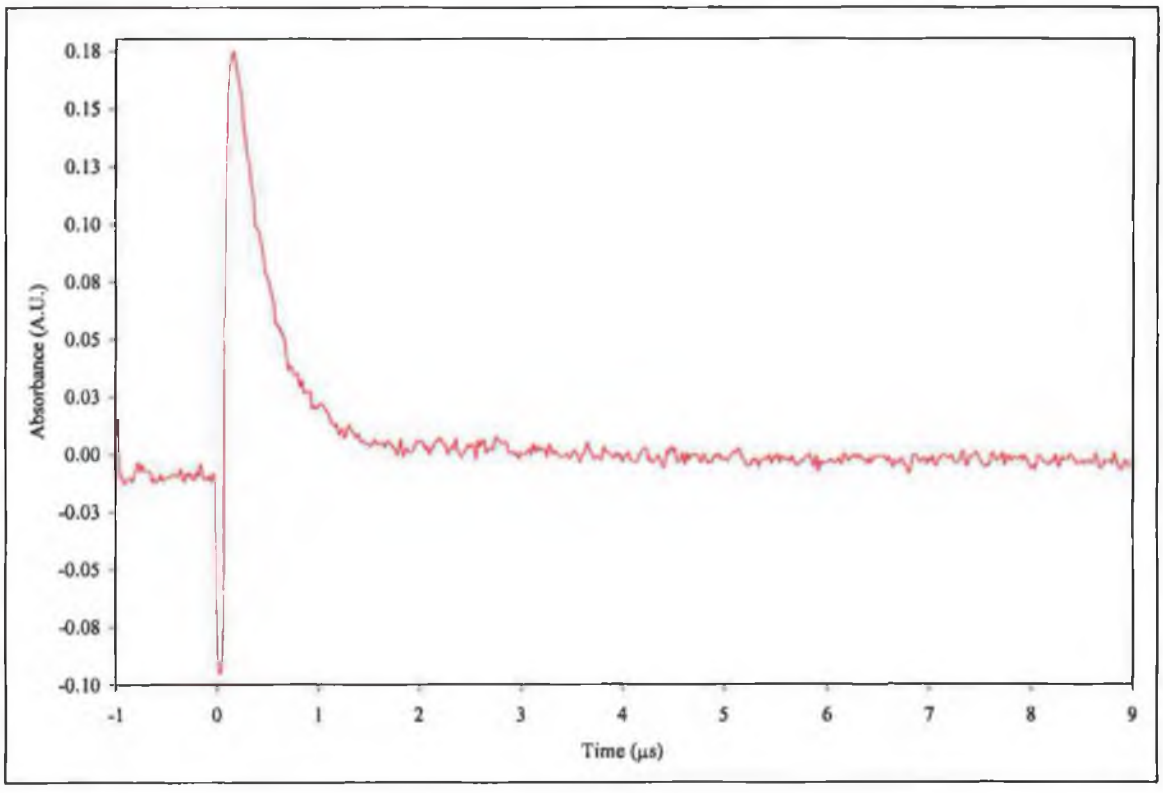

Figure 3-11 A typical transient signal obtained for the decay of (η^5-C_5H_5)Fe(CO)(η^1-C_4H_4N) monitored at 410 nm in carbon monoxide saturated toluene.

The lifetime of the transient species (η^5-C_5H_5)Fe(CO)(η^1-C_4H_4N), was found to decrease upon an increase in the concentration of carbon monoxide as observed in cyclohexane solution. The second order rate constant in toluene was calculated as before from the slope of a plot of the rate constant observed (k_{obs}) for the reaction versus the concentration of carbon monoxide, and was found to be 3.3 ($\pm$ 0.3)$\times$ 10^8 M^{-1} s^{-1}, Figure 3-12.

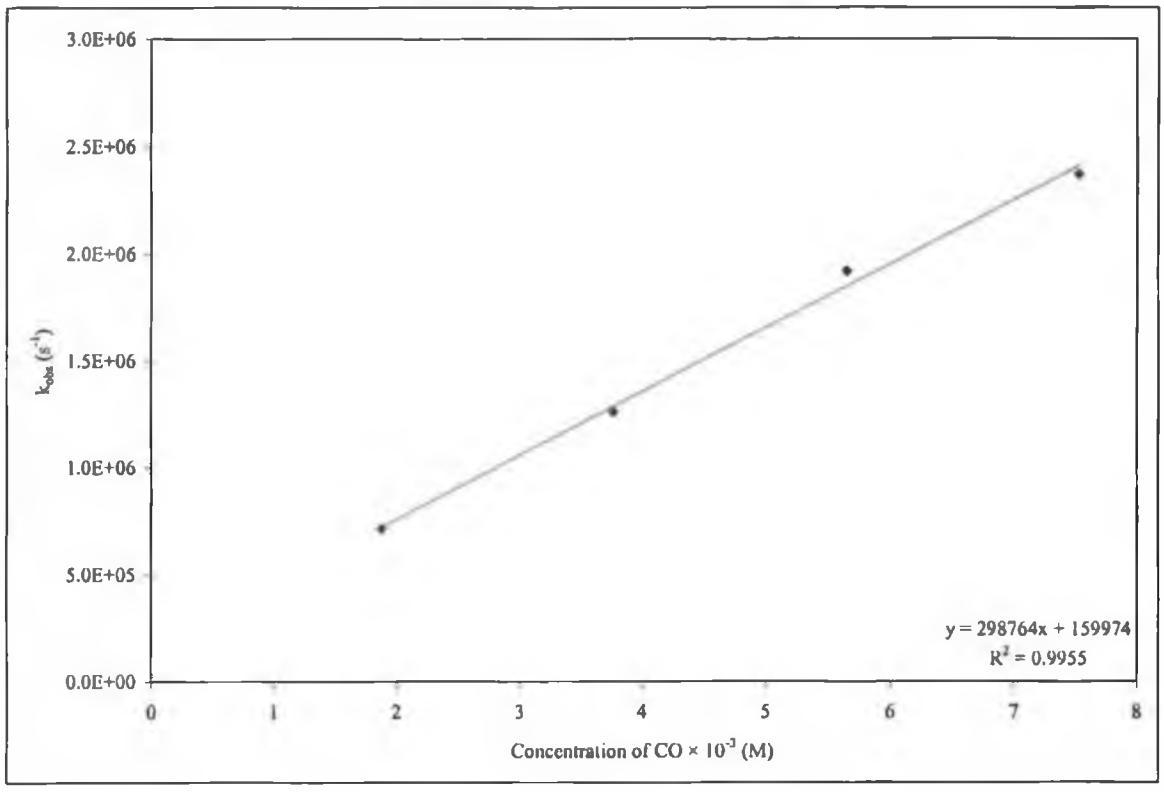

Figure 3-12 Plot of k_{obs} - vs - concentration of carbon monoxide for the decay of $(\eta^5\text{-}C_5H_5)Fe(CO)(\eta^1\text{-}C_4H_4N)$ in toluene to regenerate the parent complex $(\eta^5\text{-}C_5H_5)Fe(CO)_2(\eta^1\text{-}C_4H_4N)$.

This demonstrates that there is almost no change in the rate of the reaction in going from the poorly co-ordinating solvent, cyclohexane to toluene. These results would seem to indicate that neither the alkane nor the aromatic solvent interact to any significant extent with the sixteen-electron species, $(\eta^5\text{-}C_5H_5)Fe(CO)(\eta^1\text{-}C_4H_4N)$. The magnitude of the second order rate constant would also indicate that this sixteen-electron carbon monoxide-loss intermediate does not interact with the solvent. This is in contrast to sixteen-electron transient species of group six metals. For example, the rate of the displacement of solvent by carbon monoxide in $(\eta^6\text{-}C_6H_6)Cr(CO)_2$(toluene) is an order of magnitude slower than that for $(\eta^6\text{-}C_6H_6)Cr(CO)_2$(cyclohexane).[36]

In alkane solution it is difficult to use simple rate comparisons or effects on the terminal ν_{CO} stretching frequencies positions alone to differentiate between the possibility that intermediate(s) is solvated or non-solvated. It has been proposed in this study that the intermediate formed upon carbon monoxide loss due to photolysis may not be a solvated species due to the magnitude of the second order rate constant ($k_2 = 3\ (\pm\ 0.3) \times 10^8\ M^{-1}\ s^{-1}$),

which is close to the diffusion controlled rate limit.* Although this second order rate constant appears very fast, it is consistent with the second order rate constant determined for the recombination of the monocarbonyl intermediate, $(\eta^5\text{-}C_5H_5)Fe(CO)CH_3$ with carbon monoxide following flash photolysis of $(\eta^5\text{-}C_5H_5)Fe(CO)_2CH_3$ with TR-IR detection, i.e. $k_2 = 6.3\ (\pm\ 0.2) \times 10^8\ M^{-1}\ s^{-1}$ in cyclohexane.[22] In addition the ν_{CO} attributed to the intermediate in Ford's study proved to be solvent sensitive, with ν_{CO} values of 1938 and 1914 cm^{-1} in cyclohexane and THF respectively. Thus, this coupled with second order rate constants of $k_2 = 6.3\ (\pm\ 0.2) \times 10^8\ M^{-1}\ s^{-1}$ in cyclohexane and $k_2 = 3.4\ (\pm\ 0.2) \times 10^6\ M^{-1}\ s^{-1}$ in THF respectively lead these researchers to propose that the monocarbonyl species formed was the solvated species, $(\eta^5\text{-}C_5H_5)Fe(CO)(S)CH_3$.

Therefore identifying the sixteen-electron intermediate as a non-solvated species would be very unusual, because it is generally well established that in the condensed phase, a solvent molecule often occupies the vacant site.[37] Laser flash photolysis with UV-vis detection on a picosecond time scale has found that $Cr(CO)_5$(cyclohexane) formed within the experimental rise time (0.8 pico-seconds) of the apparatus following flash photolysis of $Cr(CO)_6$ in cyclohexane.[38] Subsequent experiments showed that the solvation occurs within 0.5 pico-seconds.[39] However, since the method of detection of the intermediate species in this study was UV-vis and not infrared spectroscopy, there was no way to provide direct information on the structure of the intermediate formed upon flash photolysis. In order to gain more insight into the reaction mechanism for $CpFe(CO)_2(\eta^1\text{-pyrrolyl})$ following UV-vis flash photolysis, the activation parameters for the reaction of $CpFe(CO)(\eta^1\text{-pyrrolyl})$ with carbon monoxide were determined,[40] refer to Section 3.3.4.

Laser excitation of $(\eta^5\text{-}C_5H_5)Fe(CO)_2(\eta^1\text{-}C_4H_4N)$, $\lambda_{exc.} = 355$ nm under an atmosphere of argon yielded similar decay transients as those under an atmosphere of carbon monoxide, Figure 3-13.

* The diffusion control limit in cyclohexane was calculated by P.C. Ford *et al.* to be 7.3×10^9, see reference 36 for details.

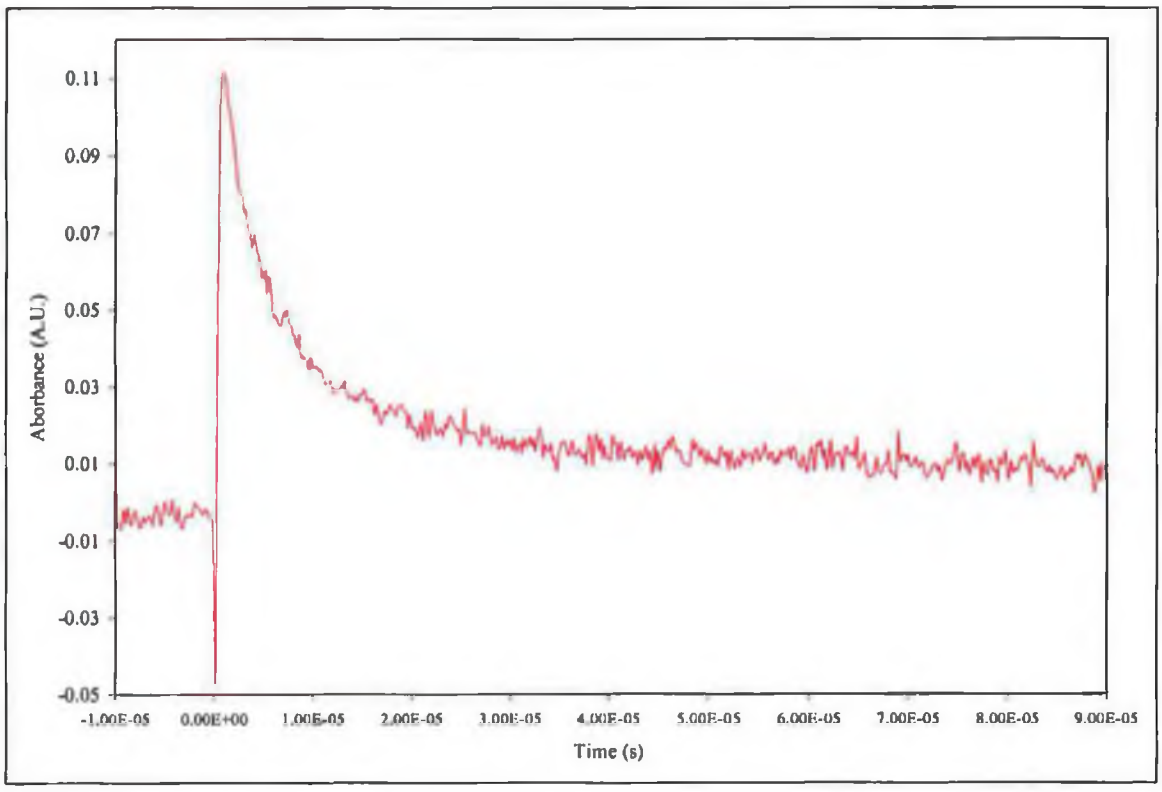

Figure 3-13 A typical transient signal obtained for the decay of $(\eta^5\text{-}C_5H_5)Fe(CO)_2(\eta^1\text{-}C_4H_4N)$ monitored at 410 nm in cyclohexane under argon, showing a residual baseline following the flash photolysis.

The value of k_{obs} in cyclohexane under one atmosphere of carbon monoxide is 3.1×10^6 s^{-1}. Under an atmosphere of argon, the k_{obs} value is one order of magnitude smaller at 2.52×10^5 s^{-1}. This is expected given that the observed rate of decay of the monocarbonyl species is directly proportional to the concentration of carbon monoxide as shown in Figure 3-10. Under an inert atmosphere, the transient at 410 nm, Figure 3-13, represents a decay of the monocarbonyl species to regenerate the parent dicarbonyl complex. However the decay transient does not return to the pre-irradiated baseline (i.e. there is a residual baseline), indicating that the process is not fully reversible. This is expected given that the concentration of carbon monoxide is very low. A difference spectrum for the formation of the transient induced following irradiation under one atmosphere of argon is shown in Figure 3-14. As under an atmosphere of carbon monoxide, the transient produced has a $\lambda_{max.} = 430$ nm, is assigned to the monocarbonyl intermediate.

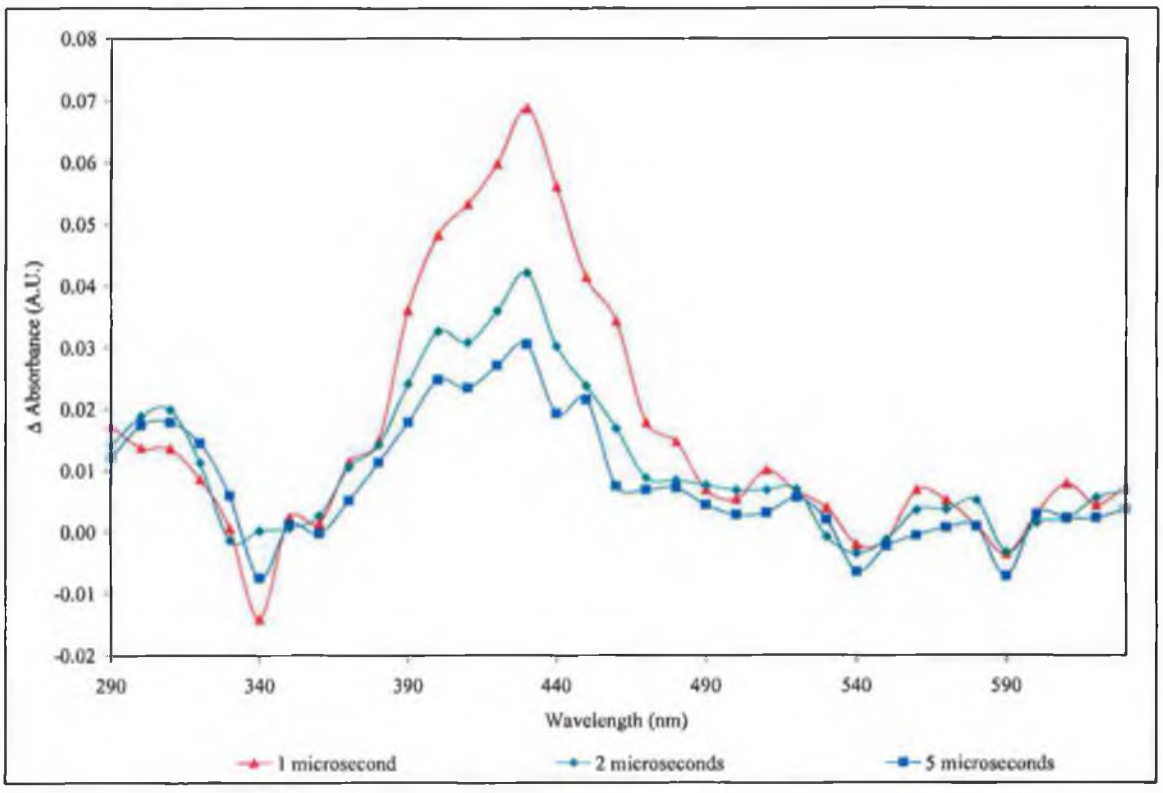

Figure 3-14 UV-vis difference spectrum after 1μs, 2 μs and 5μs following laser flash photolysis ($\lambda_{exc.}$ = 355 nm) of $(\eta^5\text{-}C_5H_5)Fe(CO)_2(\eta^1\text{-}C_4H_4N)$ in cyclohexane under inert conditions.

Laser flash photolysis of $(\eta^5\text{-}C_5H_5)Fe(CO)_2(\eta^1\text{-}C_4H_4N)$, was also carried out at 532 nm excitation, however these experiments were only conducted in toluene solution, as the solubility of $(\eta^5\text{-}C_5H_5)Fe(CO)_2(\eta^1\text{-}C_4H_4N)$ was too poor in cyclohexane to achieve a sufficient absorbance at 532 nm to conduct laser flash photolysis experiments. In these experiments, which were conducted under both inert atmospheres of argon and reactive atmospheres of carbon monoxide, the photochemistry observed was similar to that observed following flash photolysis at excitation $\lambda_{exc.}$ = 355 nm. The transient signal observed is a decay transient, which under an atmosphere of carbon monoxide is reversible. The second order rate constant for the decay of the transient is essentially that observed following flash photolysis at $\lambda_{exc.}$ = 355 nm. Under an inert atmosphere the decay does not return to the pre-irradiated baseline, again similar to the results following flash photolysis at $\lambda_{exc.}$ = 355 nm. These results are taken to indicate that the transient species produced following long wavelength photolysis ($\lambda_{exc.}$ = 532 nm) is the monocarbonyl, $(\eta^5\text{-}C_5H_5)Fe(CO)(\eta^1\text{-}C_4H_4N)$, which reacts with carbon monoxide to reform the dicarbonyl, $(\eta^5\text{-}C_5H_5)Fe(CO)_2(\eta^1\text{-}C_4H_4N)$.

3.3.3.1 *Possible mechanisms for the displacement of the solvent molecule from the co-ordination sphere of the metal complex*

Three possible mechanisms exist by which $(\eta^5\text{-}C_5H_5)Fe(CO)(S)(\eta^1\text{-}C_4H_4N)$ reacts with incoming ligands, these are dissociative, associative and interchange as outlined in Figure 3-15.

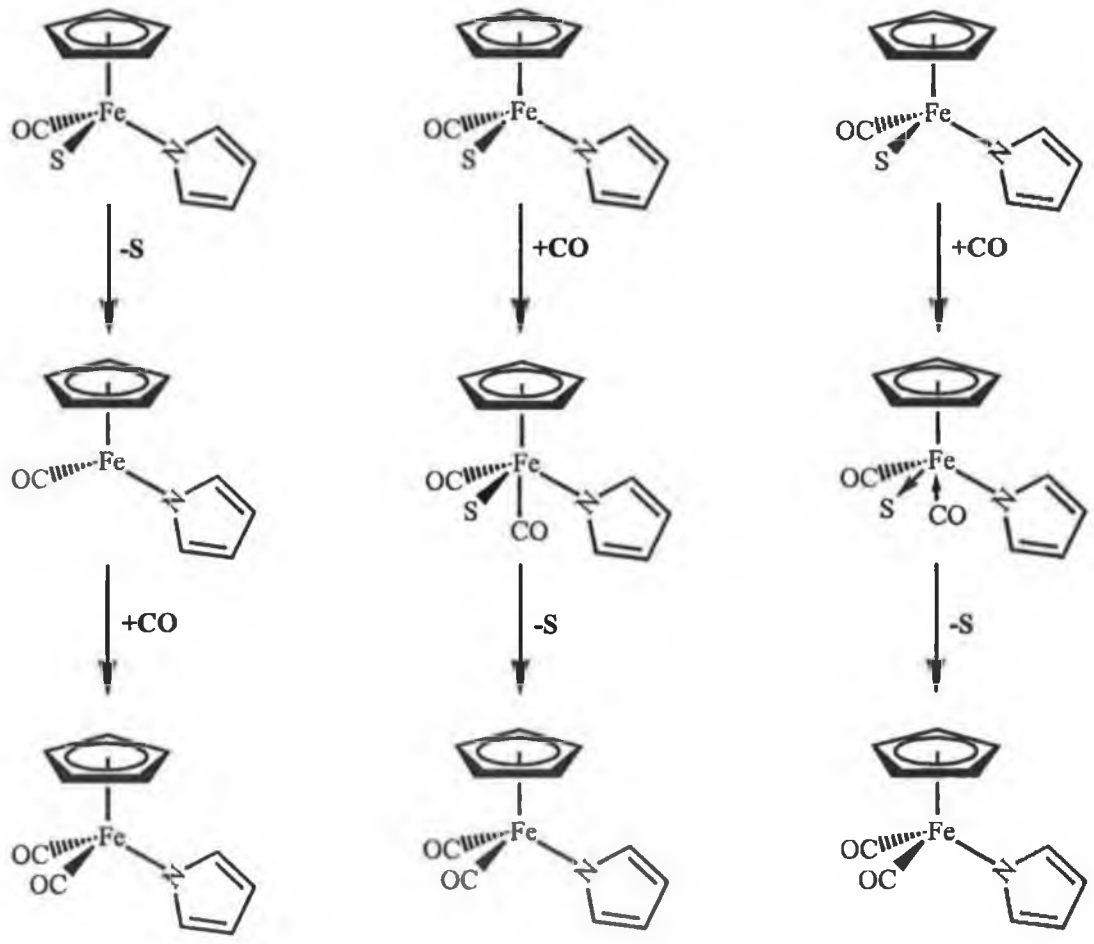

Figure 3-15 Possible mechanisms for solvent displacement.

A dissociative mechanism requires the dissociation of the solvent to form an intermediate of lower co-ordination number than in the reactant, which with subsequent co-ordination of the carbon monoxide leads to reformation of $(\eta^5\text{-}C_5H_5)Fe(CO)_2(\eta^1\text{-}C_4H_4N)$. The metal-solvent bond strength is close to the activation enthalpy ($\Delta H^{\neq}$) required in dissociation reactions

because the bond is broken in going to the transition state. A moderately positive entropy ($\Delta S^{\neq}$), is consistent with dissociation of the solvent ligand from the metal centre and reflects the increased disorder of the transition state.

The second possible mechanism is associative, in which carbon monoxide enters the reaction sphere before the solvent is dissociated and forms an intermediate of higher co-ordination number than the reactant, before the ejection of the solvent. An associative reaction would have low enthalpy ($\Delta H^{\neq}$) values. Negative entropy ($\Delta S^{\neq}$) values (~ 100 J K^{-1} mol^{-1}) are expected to result from the more ordered transition state.

The third possibility is an interchange mechanism in which the partial dissociation of the solvent and partial association of carbon monoxide is concerted. The entropy values in such reactions are expected to lie between the other two possibilities.

3.3.4 Determination of the activation parameters for (η^5-C_5H_5)Fe(CO)(S)(η^1-C_4H_4N) with carbon monoxide

The kinetic information was obtained from the decay of the (η^5-C_5H_5)Fe(CO)(η^1-C_4H_4N) transient species at 410 nm, as this is in the region where the transient species absorbs strongly. Pseudo first order conditions were maintained as the concentration of carbon monoxide greatly exceeds that of (η^5-C_5H_5)Fe(CO)(η^1-C_4H_4N). The k_{obs} for the reaction were obtained from the slope of plots of $\ln(A_\infty - A_0)/(A_\infty - A_t)$-versus-time as previously described,[41] A_t and A_∞ are absorbances at time t and at infinite time respectively. In order to determine the activation parameters for the reaction of the intermediate with carbon monoxide, the second order rate constant, k_2 was recorded at different temperatures in the range 283-313 K, enabling Arrhenius and Eyring plots to be constructed, Figure 3-16. These plots provided the enthalpy, $\Delta H^{\neq}$and entropy, $\Delta S^{\neq}$terms for Scheme 3-8.

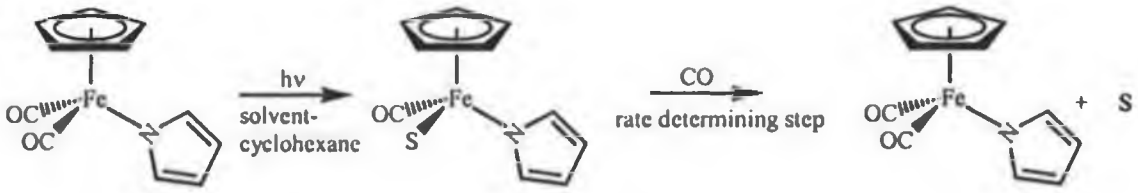

Scheme 3-8 Reaction scheme proposed for $(\eta^5\text{-}C_5H_5)Fe(CO)_2(\eta^1\text{-}C_4H_4N)$ in carbon monoxide saturated cyclohexane.

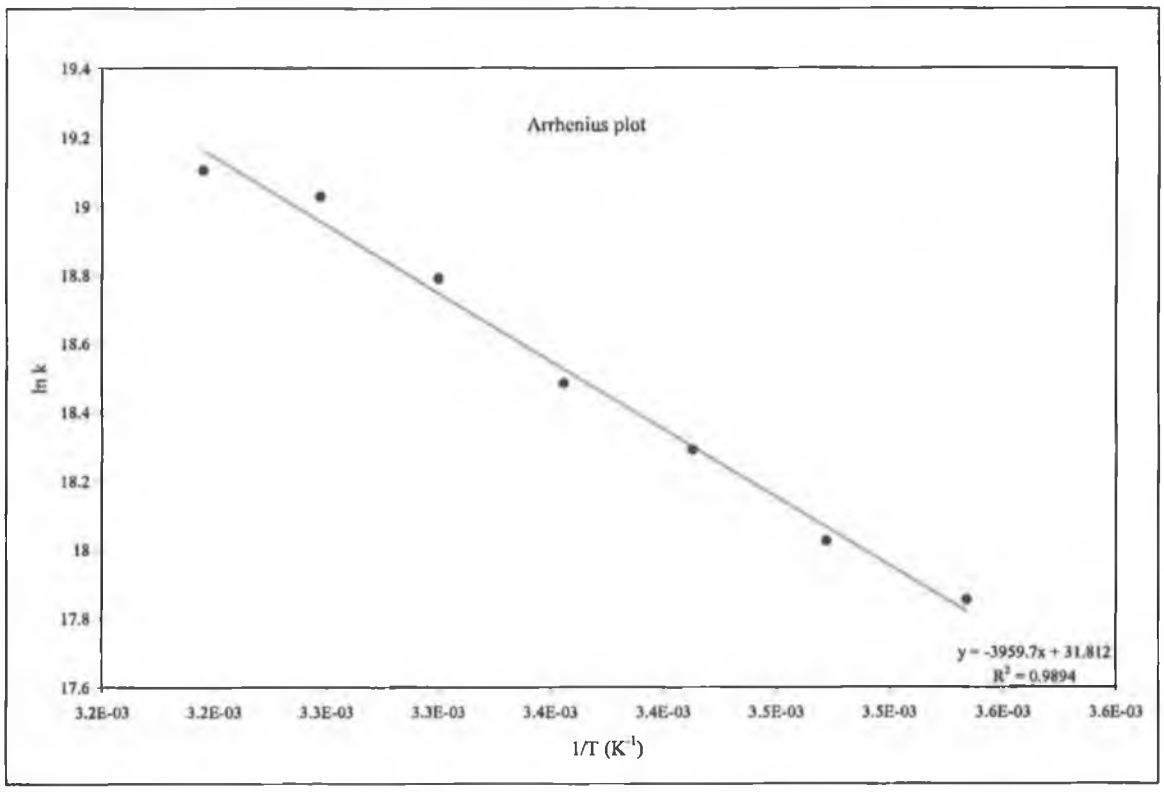

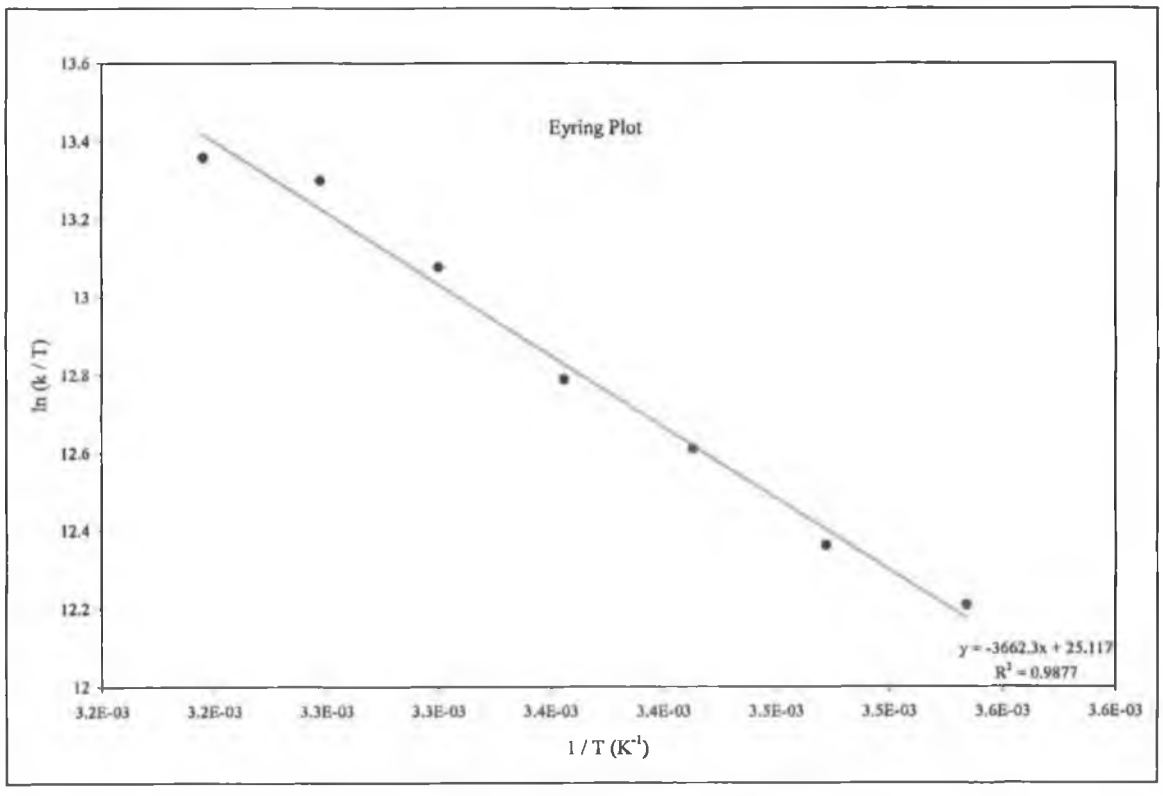

Figure 3-16 Arrhenius and Eyring plots for the reaction of (η^5-C_5H_5)Fe(CO)(η^1-C_4H_4N) with CO.

The activation energy for the carbon monoxide recombination with $(\eta^5\text{-}C_5H_5)Fe(CO)(\eta^1\text{-}C_4H_4N)$ in the case of $(\eta^5\text{-}C_5H_5)Fe(CO)_2(\eta^1\text{-}C_4H_4N)$ is E_a = 33 kJ mol^{-1}. The enthalpy of activation, $\Delta H^{\neq}$= 30 (± 2) kJ mol^{-1} and the entropy, $\Delta S^{\neq}$= 11 (± 5) J mol^{-1} K^{-1}. Previous estimates in the literature for the reaction of carbon monoxide-loss intermediates with carbon monoxide, for $Cr(CO)_5(S)$[36] and $(\eta^6\text{-benzene})Cr(CO)_2(S)$[41] which yielded an enthalpy value, $\Delta H^{\neq}$= 22 (± 2) kJ mol^{-1} for both complexes in cyclohexane. The binding energy for Cr-cyclohexane obtained from photoacoustic calorimetry (PAC) measurements was 52 kJ mol^{-1}.[42] A dissociative mechanism for the reaction of $Cr(CO)_5(S)$ and $(\eta^6\text{-benzene})Cr(CO)_2(S)$ with carbon monoxide would require a enthalpy value approximating the interaction energy obtained in the PAC measurements. As the enthalpy values obtained following the kinetic investigations[36,41] were half the interaction energy determined by PAC, it was evident that a dissociative mechanism was precluded and that an interchange mechanism should be considered.

However, the photochemistry of iron-pentacarbonyl analogue, $Fe(CO)_5$ in solution is distinctly different from that of the other metal carbonyls mentioned.[43] Most notably two carbonyl ligands are substituted in a single-photon process[44] for some nucleophiles but not for others. In cases where the incoming ligand is a phosphine, the quantum yield varies with the structure of the phosphine ligand. Due to the complexity of the photochemistry of $Fe(CO)_5$, detailed photoacoustic calorimetric studies have been prohibited and there are no reports in the literature for the strength of the iron-solvent bond in $Fe(CO)_4(S)$. Burkey *et al.*[45] did employ photoacoustic calorimetry and laser flash photolysis to investigate the solution photochemistry of phosphine derivatives of $Fe(CO)_5$. The conclusion reached in this study was that the intermolecular iron-cyclohexane bonds were significantly weaker than observed in the group six metal hexacarbonyls.[44(b),46] The rate constants for phosphine addition for iron complexes are large, and within an order of magnitude of the diffusion controlled limit. In this study too, the rate constant for carbon monoxide recombination with $(\eta^5\text{-}C_5H_5)Fe(CO)(\eta^1\text{-}C_4H_4N)$ is close to the diffusion controlled limit (i.e. 3.0 (± 0.3) × 10^8 $M^{-1}s^{-1}$), thus co-ordination of the solvent to the iron metal centre must be a fairly weak interaction, as the rate of alkane displacement on $Cr(CO)_5$(alkane) is typically an order of magnitude slower than those of iron-complexes.

In light of the fact that iron-alkane bond strengths have not been determined by photoacoustic calorimetry, there are no values for the iron-alkane bond to compare with the values presented here, and so identifying the possible mechanism even after determination of the activation parameters is made more difficult. The entropy value $\Delta S^{\neq} = 11\ (\pm\ 5)$ J mol^{-1} K^{-1} is moderately positive, which would imply a dissociative mechanism as this suggests that there is increased disorder at the intermediate site, the enthalpy value however is a low positive value which indicates that an associative mechanism may be taking place. Thus it is evident that an interchange mechanism must be considered in the case of loss of solvent from $(\eta^5\text{-}C_5H_5)Fe(CO)(S)(\eta^1\text{-}C_4H_4N)$ given the conflicting results, where significant dissociation of the solvent occurs, before association of the carbon monoxide ligand.

The rate of the reaction of $(\eta^5\text{-}C_5H_5)Fe(CO)(toluene)(\eta^1\text{-}C_4H_4N)$ with carbon monoxide, generated by laser flash photolysis of $(\eta^5\text{-}C_5H_5)Fe(CO)_2(\eta^1\text{-}C_4H_4N)$ in toluene solution over the temperature range 283-313 K were also measured. The maximum absorption for the transient is at 430 nm, consistent with the previous observation for the $(\eta^5\text{-}C_5H_5)Fe(CO)(cyclohexane)(\eta^1\text{-}C_4H_4N)$. Over this temperature range it was evident that the second-order rate constant showed no significant temperature dependence. Therefore the reaction of $(\eta^5\text{-}C_5H_5)Fe(CO)_2(\eta^1\text{-}C_4H_4N)$ in carbon monoxide saturated toluene is as a result of a different mechanism than that of $(\eta^5\text{-}C_5H_5)Fe(CO)_2(\eta^1\text{-}C_4H_4N)$ in cyclohexane. In order to interpret these results, the reaction mechanism for carbon monoxide substitution needs to be identified. As indicated previously, the observed rate of this reaction showed a linear dependence on the concentration of carbon monoxide, Figure 3-12, which is consistent with both a dissociative and associative mechanism of toluene displacement from the iron centre. If the displacement of toluene by carbon monoxide proceeds by an associative mechanism (i.e. $k_1 = 0$) the observed rate constant (k_{obs}) would be a simple function of carbon monoxide concentration, $k_{obs} = k_3[CO]$, consistent with the data in Figure 3-12.

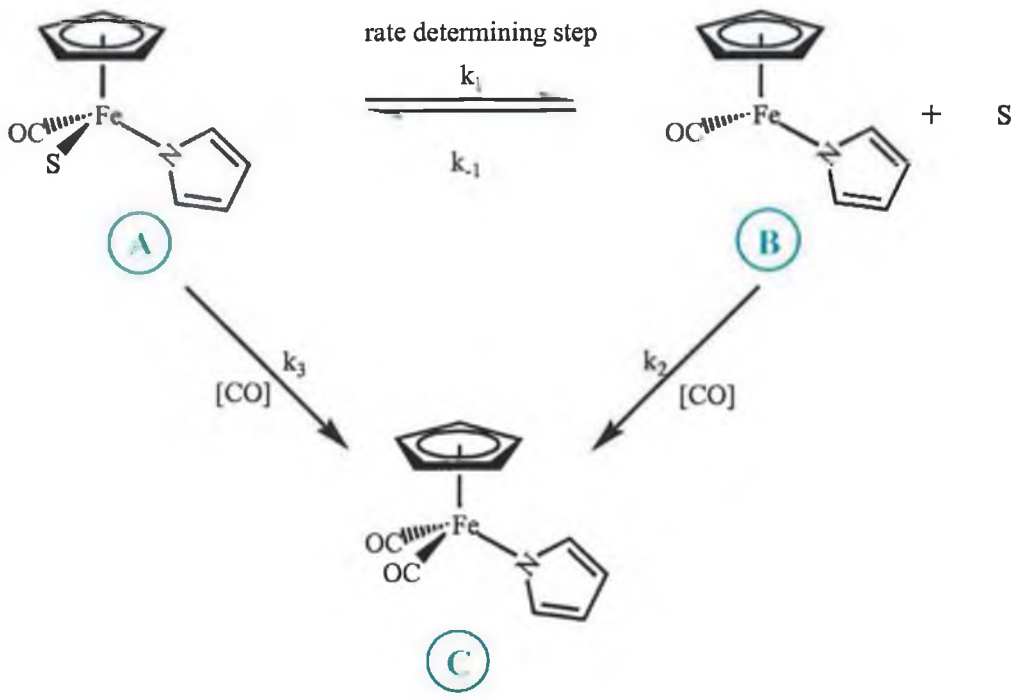

Scheme 3-9 Associative and dissociative reaction mechanism possible for reaction of $(\eta^5\text{-}C_5H_5)Fe(CO)_2(\eta^1\text{-}C_4H_4N)$ following photolysis.

The second order rate constant for the reaction of $(\eta^5\text{-}C_5H_5)Fe(CO)(toluene)(\eta^1\text{-}C_4H_4N)$ with carbon monoxide gives a non-zero intercept, which is inconsistent with a associative reaction mechanism. For a dissociative mechanism the dependence of $k_{obs.}$ on the concentration of carbon monoxide can be derived by assuming a steady-state concentration of $(\eta^5\text{-}C_5H_5)Fe(CO)(\eta^1\text{-}C_4H_4N)$, i.e.[B].

$$d[B]/dt = 0$$

$$d[B]/dt = k_1[A]-k_{-1}[B][S]-k_2[B][CO] = 0 \qquad [S] = 1$$

$$k_{-1}[B] + k_2[B][CO] = k_1[A]$$

$$[B](k_{-1} + k_2[CO]) = k_1[A]$$

$$[B] = k_1[A] / k_{-1} + k_2[CO]$$

Formation of $(\eta^5\text{-}C_5H_5)Fe(CO)_2(\eta^1\text{-}C_4H_4N)$, i.e. [C]

$$d[C]/dt = k_2[B][CO]$$

$$d[C]/dt = k_2 k_1[A][CO] / k_{-1} + k_2[CO]$$

$$k_{obs.} = k_1k_2[CO] / k_{-1}[toluene] + k_2[CO]$$

Because in the present work [toluene] >> [CO] and a plot of $k_{obs.}$ versus [CO] does not show any deviation from linearity, it is assumed that $k_{-1}[toluene] >> k_2[CO]$, thus the $k_{obs.}$ expression then reduces to,

$$k_{obs.} = k_1k_2[CO]/k_{-1}[toluene]$$

The rate of the decay of the monocarbonyl in toluene is the same as that observed in cyclohexane within experimental error, (i.e. 3.3 (± 0.3) × 10^8 M^{-1} s^{-1} in toluene as opposed to 3.0 (± 0.3) × 10^8 M^{-1} s^{-1} in cyclohexane). However the lack of activation parameters for the reaction of (η^5-C_5H_5)Fe(CO)(S)(η^1-C_4H_4N) with carbon monoxide in toluene would suggest that this is not the rate determining step, and that a pre-equilibrium has been established between the solvated species (η^5-C_5H_5)Fe(CO)(toluene)(η^1-C_4H_4N) and (η^5-C_5H_5)Fe(CO)(η^1-C_4H_4N) which is the rate determining step, Scheme 3-9. The displacement of a solvent molecule from (η^5-C_5H_5)$Mn(CO)_2$S, where S = THF[47] and toluene[48] has also been reported as occurring *via* a dissociative mechanism. The kinetic analysis yielded a value of 24 (±3) kcal mol^{-1} for the (η^5-C_5H_5)$Mn(CO)_2$-THF bond energy, and a value of 14.2 (±0.8) kcal mol^{-1} for the (η^5-C_5H_5)$Mn(CO)_2$-toluene bond energy respectively.

3.3.5 Matrix isolation experiments

Following deposition in inert matrixes of argon and dinitrogen, the photoreactivity of $(\eta^5\text{-}C_5H_5)Fe(CO)_2(\eta^1\text{-}C_4H_4N)$ was examined using both broad band and monochromatic irradiation. The spectrum of $(\eta^5\text{-}C_5H_5)Fe(CO)_2(\eta^1\text{-}C_4H_4N)$ isolated at high dilution in an argon matrix shows two terminal ν_{CO} stretching bands at 2053 and 2007 cm^{-1}. These bands correspond to the symmetric (A') and anti-symmetric (A'') modes expected for a molecule with C_s symmetry, together with two very weak bands (marked with an asterisk) arising from the ^{13}C present in natural abundance, Figure 3-17.

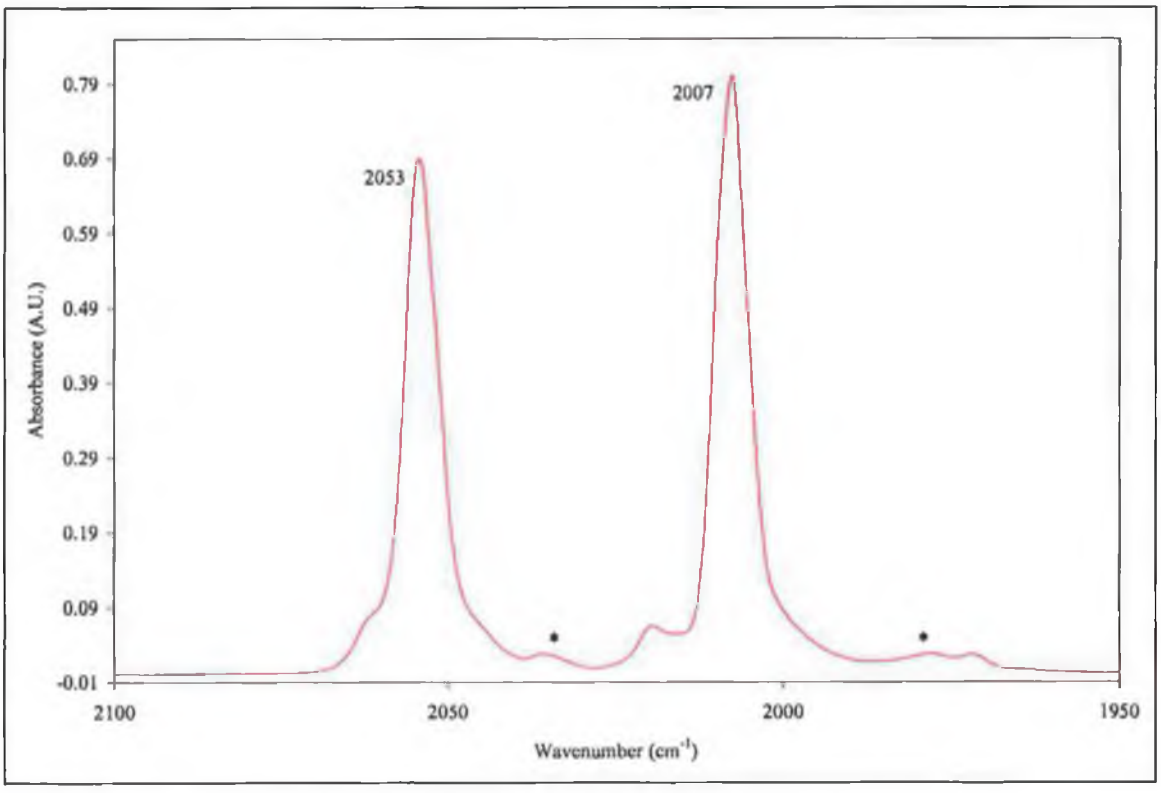

Figure 3-17 The infrared spectrum of the carbonyl region for $(\eta^5\text{-}C_5H_5)Fe(CO)_2(\eta^1\text{-}C_4H_4N)$ at high dilution in an argon matrix at 20 K.

Irradiation of $(\eta^5\text{-}C_5H_5)Fe(CO)_2(\eta^1\text{-}C_4H_4N)$ with $\lambda_{exc.} > 400$ nm, in an argon matrix at 12 K produced two new bands at 2138 and 1974 cm^{-1}, in tandem with the depletion of the parent bands at 2053 and 2007 cm^{-1}, Figure 3-1. The band at 2138 cm^{-1} corresponds to free carbon monoxide in the matrix. The band at 1974 cm^{-1} with further shoulders on the low energy

side, is assigned to the carbon monoxide loss monocarbonyl photoproduct, (η^5-C_5H_5)Fe(CO)(η^1-C_4H_4N).

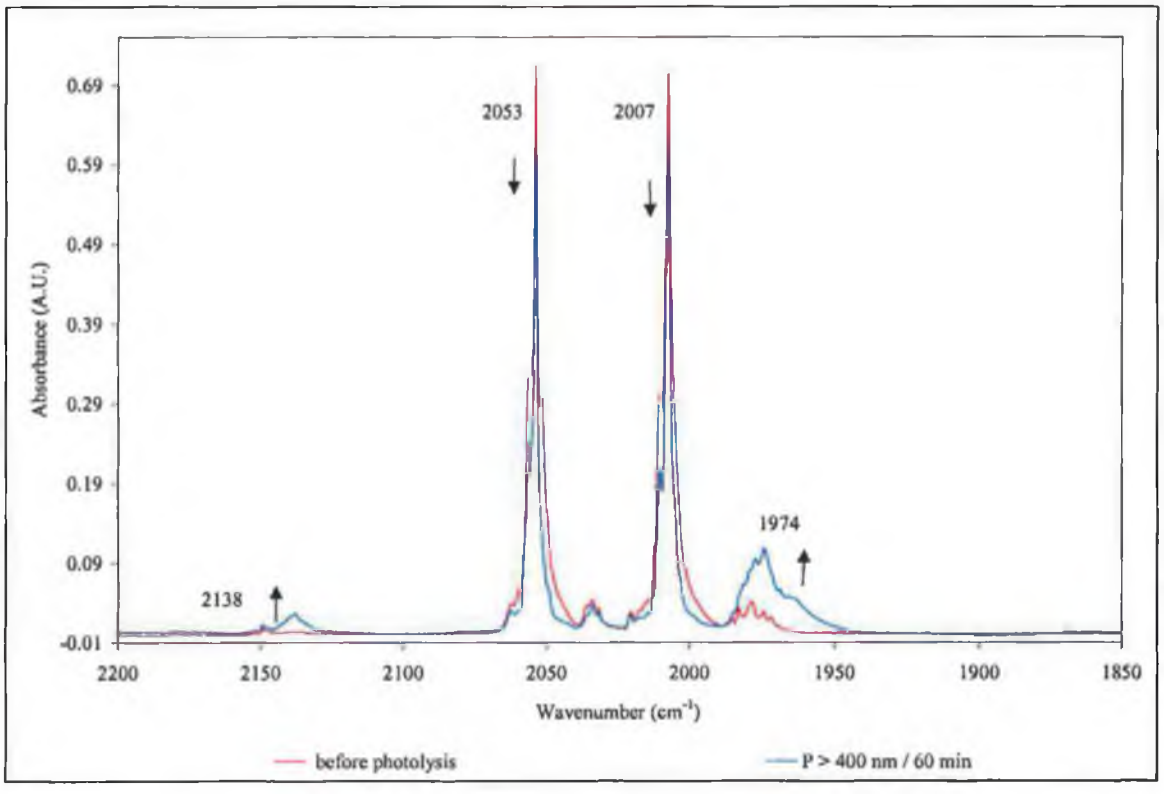

Figure 3-18 Infrared spectral changes observed following broad band photolysis (λ_{exc} > 400 nm) of (η^5-C_5H_5)Fe(CO)$_2$(η^1-C_4H_4N) in an argon matrix at 12 K.

Although there is quite significant matrix splitting in the spectra in Figure 3-18, the new ν_{CO} absorbance appears to be a single band as would be expected for a monocarbonyl complex formed by carbon monoxide photo-dissociation, rather than two or more independent bands. Nevertheless, the later alternative cannot be excluded given these data alone as subsequent results will show. The origin of this matrix splitting[49] is not entirely clear, but environment variations such as different orientations of the trapped species in the matrix cage, different cage structures and variations in the cage occupation are thought to be some of the options available to explain origins of the effect.

The matrix isolation experiments of (η^5-C_5H_5)Fe(CO)$_2$(η^1-C_4H_4N) were repeated in a dinitrogen matrix at 20 K. The spectral changes were essentially identical to those obtained in the argon matrix, Figure 3-19. The ν_{CO} stretch for the monocarbonyl species formed in

the dinitrogen matrix is at 1973 cm^{-1}. Therefore the monocarbonyl ν_{CO} stretch is essentially unshifted on changing from argon to a dinitrogen matrix, (i.e. 1974 cm^{-1} in an argon as opposed to1973 cm^{-1} in a dinitrogen). If the dinitrogen matrix was co-ordinating to the monocarbonyl intermediate, $(\eta^5\text{-}C_5H_5)Fe(CO)(\eta^1\text{-}C_4H_4N)$ a shift in the ν_{CO} stretch to higher wavenumber would have been expected, this was not observed however. Furthermore no bands, which could be attributed to $\nu_{N\text{-}N}$ stretches were observed (i.e. no new bands formed in the $\nu_{N\text{-}N}$ region, (2300-2100 cm^{-1}), of the infrared spectrum). This provides conclusive evidence that N_2 is not co-ordinating to the monocarbonyl species and that the dinitrogen matrix is effectively inert.

These results are in contrast to the observation of $(\eta^5\text{-}C_5H_5)Mn(CO)_2(N_2)$, ($\nu_{CO}$ = 1978, 1947 cm^{-1}, $\nu_{N\text{-}N}$ = 2175 cm^{-1}) following photoinduced carbon monoxide loss from $(\eta^5\text{-}C_5H_5)Mn(CO)_3$; $(\eta^6\text{-}C_6H_6)Cr(CO)_2(N_2)$, ($\nu_{CO}$ = 1940, 1896 cm^{-1}, $\nu_{N\text{-}N}$ = 2148 cm^{-1}) upon photolysis of $(\eta^6\text{-}C_6H_6)Cr(CO)_3$ and $(\eta^4\text{-}C_4H_4)Fe(CO)_2(N_2)$, ($\nu_{CO}$ = 2013, 1961 cm^{-1}, $\nu_{N\text{-}N}$ = 2207 cm^{-1}) upon photolysis of $(\eta^4\text{-}C_4H_4)Fe(CO)_3$, all in dinitrogen matrices.[50]

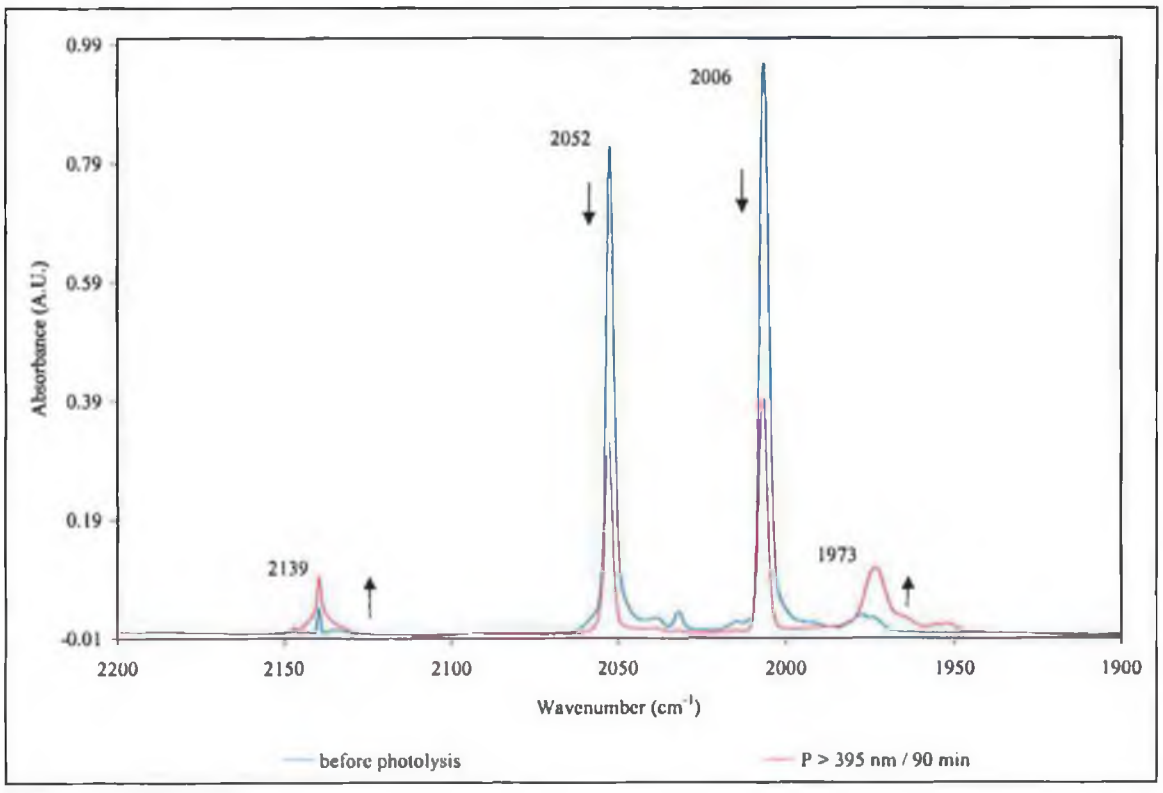

Figure 3-19 Infrared spectral changes observed following broad band photolysis (λ_{exc} > 395 nm) of $(\eta^5\text{-}C_5H_5)Fe(CO)_2(\eta^1\text{-}C_4H_4N)$ in a dinitrogen matrix at 20 K.

An investigation of the photochemistry of $(\eta^5\text{-}C_5H_5)Fe(CO)_2Cl$ by Rest and co-workers[11] in various matrices also identified carbon monoxide loss as the dominant photochemical process. However, photolysis in a dinitrogen matrix failed to lead to the formation of $(\eta^5\text{-}C_5H_5)Fe(CO)(N_2)Cl$. Instead, similar to the results presented in this work the dinitrogen matrix proved to be inert to the monocarbonyl species formed, and the ν_{CO} band positions for the monocarbonyl species were essentially unshifted, i.e. ν_{CO} = 1977 and 1979 cm^{-1} in methane and dinitrogen matrices respectively.

When the dinitrogen matrix in this study was annealed to 35 K and then cooled back to 20 K by means of the temperature controller, the intensity of the ν_{CO} band at 1974 cm^{-1} of the sixteen-electron monocarbonyl species, $(\eta^5\text{-}C_5H_5)Fe(CO)(\eta^1\text{-}C_4H_4N)$ decreased, while the intensity of the ν_{CO} bands of the parent complex recovered slightly, refer to Figure 3-20. Observation of reversibility of the photoinduced carbon monoxide loss on annealing lends further support to the assignment of the ν_{CO} band at 1974 cm^{-1} to the unsaturated monocarbonyl species, $(\eta^5\text{-}C_5H_5)Fe(CO)(\eta^1\text{-}C_4H_4N)$.

As a consequence of the flash photolysis results, the choice of excitation wavelength for the initial matrix isolation experiments was unfortunate as these results showed that the monocarbonyl intermediate formed upon photolysis has a maximum absorption at 430 nm. Therefore the irradiation of $(\eta^5\text{-}C_5H_5)Fe(CO)_2(\eta^1\text{-}C_4H_4N)$ in the matrixes with $\lambda_{exc.} > 400$ or 395 nm, may also have photoinduced recombination of the monocarbonyl species with carbon monoxide, (in addition to photoinduced carbon monoxide loss). This would explain why longer irradiation periods ($\lambda_{exc.} > 400$ or 395 nm), failed to lead to significant increases in the formation of the monocarbonyl species.

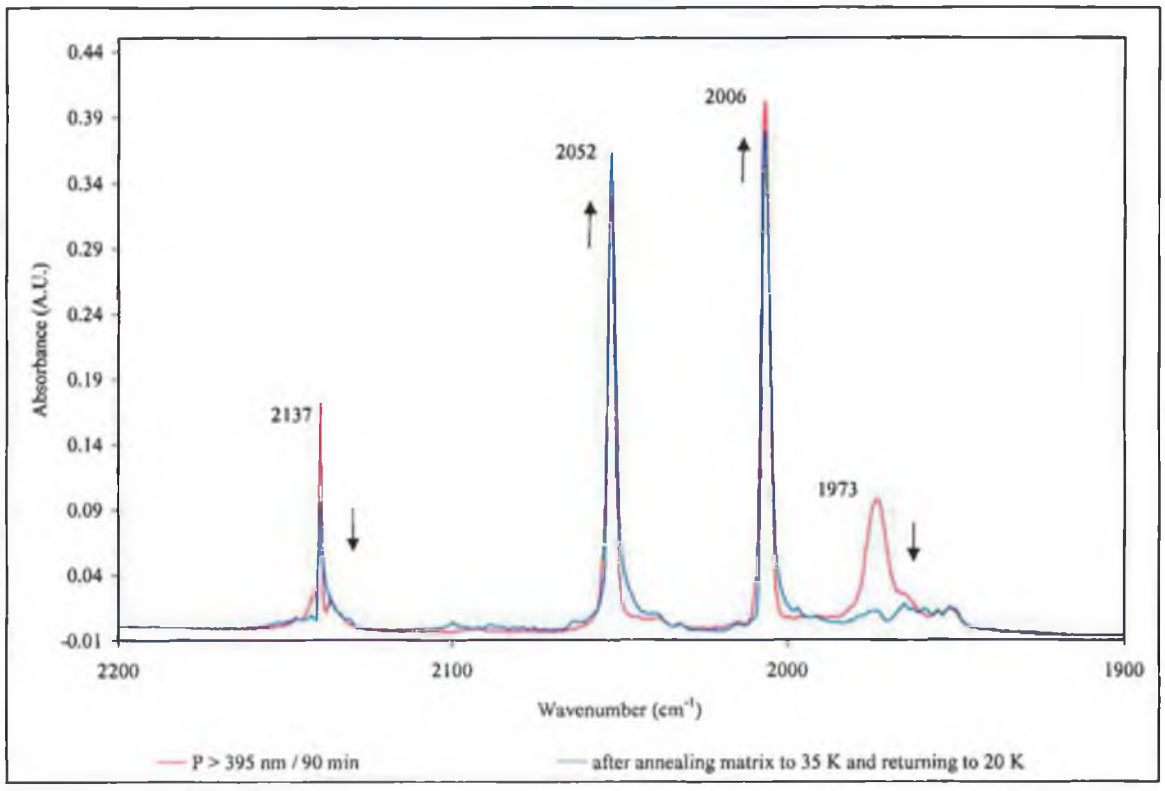

Figure 3-20 Infrared spectral changes observed following broad band photolysis ($\lambda_{exc.}$ > 395 nm) of (η^5-C_5H_5)Fe(CO)$_2$(η^1-C_4H_4N) in a dinitrogen matrix at 20 K, followed by annealing the matrix to 35 K before returning the matrix to 20 K.

Photolysis of (η^5-C_5H_5)Fe(CO)$_2$(η^1-C_4H_4N) in an argon matrix was repeated using $\lambda_{exc.}$ > 320-395 nm. The changes induced in the infrared spectra are essentially those previously discussed following irradiation at $\lambda_{exc.}$ > 400 nm, i.e. a decrease in the parent bands at 2053 and 2007 cm^{-1}, and an appearance of new bands at 2138 and 1974 cm^{-1} assigned to the free carbon monoxide and monocarbonyl, (η^5-C_5H_5)Fe(CO)(η^1-C_4H_4N) respectively. In addition however, there is a pronounced shoulder on the low energy side of the monocarbonyl band at 1974 cm^{-1} at approximately 1968 cm^{-1}, refer to Figure 3-21. It was shown in chapter two, that a similar low energy band was observed following the photolysis of azaferrocene following monochromatic irradiation ($\lambda_{exc.}$ = 538 nm) in a 2% carbon monoxide doped argon matrix. Threfore this band at ~ 1968 cm^{-1} was assigned to the *exo*-azaallyl species, (η^5-C_5H_5)Fe(CO)(η^3-*N*-C_4H_4N), as in the case of photolysis of azaferrocene in a 2% doped carbon monoxide matrix.

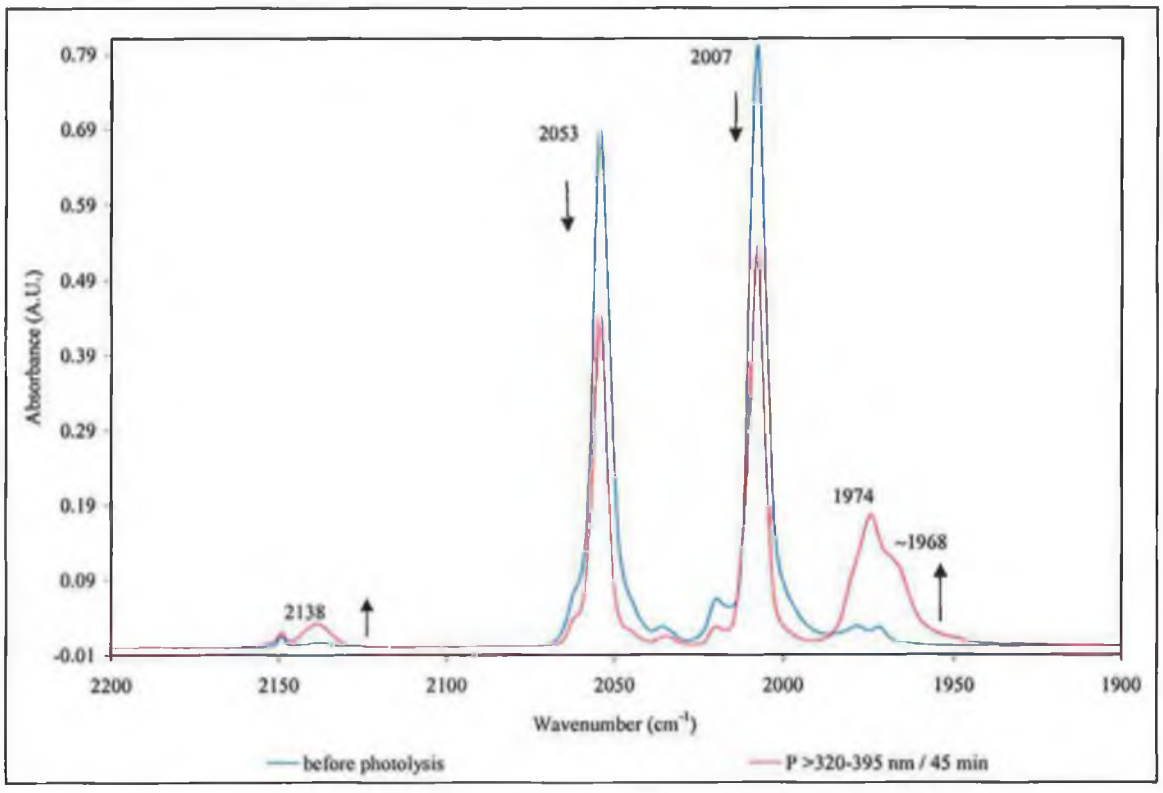

Figure 3-21 Infrared spectral changes observed following broad band photolysis (λ_{exc} > 320-395 nm) of (η^5-C_5H_5)Fe(CO)$_2$(η^1-C_4H_4N) in an argon matrix at 20 K.

Isolation of the parent complex, $(\eta^5\text{-}C_5H_5)Fe(CO)_2(\eta^1\text{-}C_4H_4N)$ was repeated again in an argon matrix and the photolysis was switched to monochromatic irradiation. Excitation at 577 nm lead to the formation of two photoproducts, both monocarbonyl, $(\eta^5\text{-}C_5H_5)Fe(CO)(\eta^1\text{-}C_4H_4N)$, ν_{CO} = 1974 cm^{-1} and the *exo*-azaallyl monocarbonyl species, $(\eta^5\text{-}C_5H_5)Fe(CO)(\eta^3\text{-}N\text{-}C_4H_4N)$, ν_{CO} = 1964 cm^{-1}. The intensity of both monocarbonyl product bands is almost equal, refer to the difference spectrum in Figure 3-22.

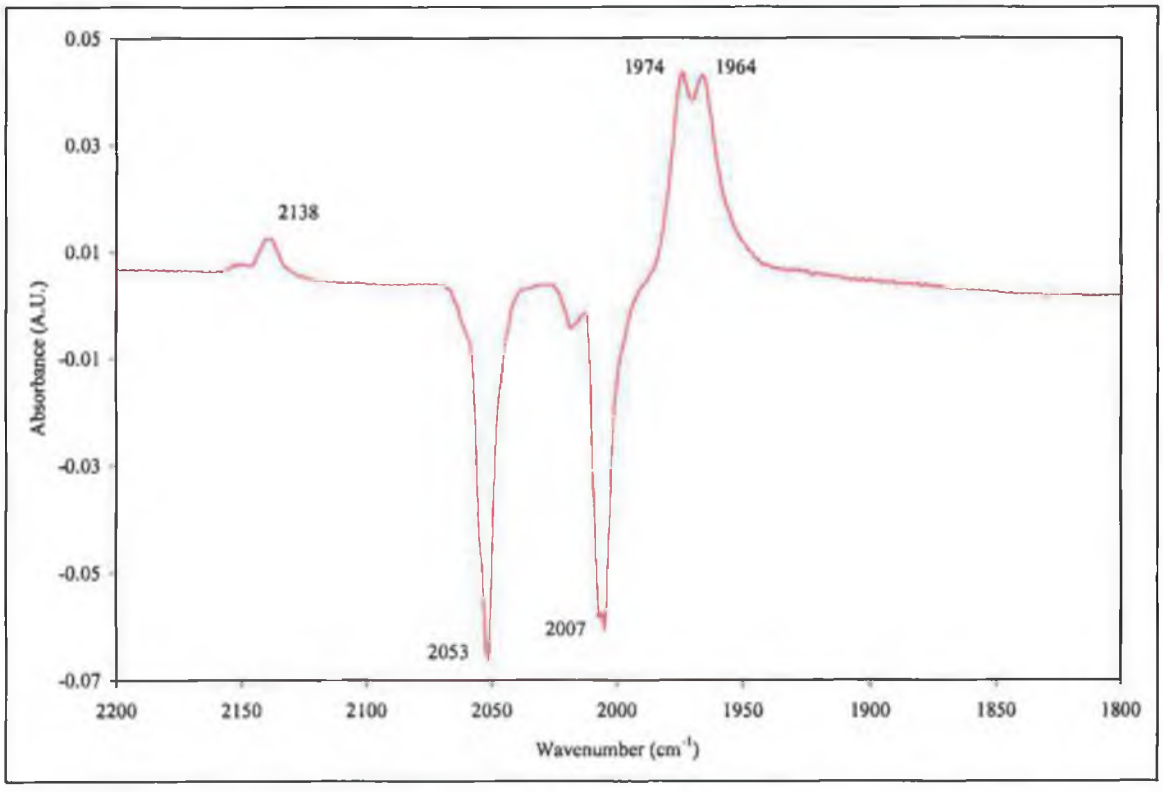

Figure 3-22 The infrared difference spectrum following monochromatic photolysis (λ_{exc} = 577 nm) of $(\eta^5\text{-}C_5H_5)Fe(CO)_2(\eta^1\text{-}C_4H_4N)$ for two hours in an argon matrix at 20 K.

Further photolysis of $(\eta^5\text{-}C_5H_5)Fe(CO)_2(\eta^1\text{-}C_4H_4N)$ in the argon matrix with higher-energy photolysis ($\lambda_{exc.}$ = 546 nm) induced the spectral changes presented in Figure 3-23. It is evident from this spectrum that the intensity of the $(\eta^5\text{-}C_5H_5)Fe(CO)(\eta^1\text{-}C_4H_4N)$ monocarbonyl band at 1974 cm^{-1} increases to a greater extent (~25 %) than that due to the *exo*-azaallyl species, $(\eta^5\text{-}C_5H_5)Fe(CO)(\eta^3\text{-}N\text{-}C_4H_4N)$ at 1964 cm^{-1}.

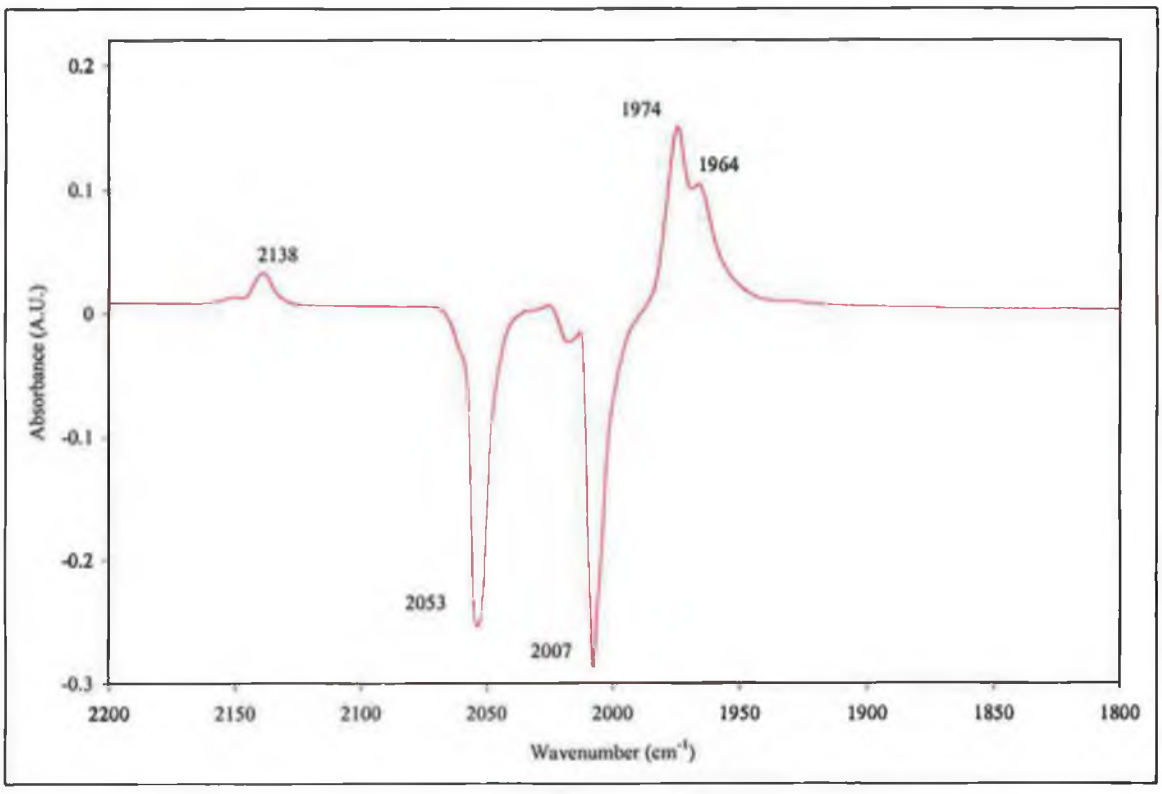

Figure 3-23 The infrared difference spectrum following further higher energy monochromatic photolysis ($\lambda_{exc.}$ = 546 nm) of $(\eta^5\text{-}C_5H_5)Fe(CO)_2(\eta^1\text{-}C_4H_4N)$ for two hours in an argon matrix at 20 K.

Following photolysis at 546 nm, the matrix was again irradiated with lower-energy light, $\lambda_{exc.}$ = 577 nm. This induced further formation of the *exo*-azaallyl species, $(\eta^5\text{-}C_5H_5)Fe(CO)(\eta^3\text{-}N\text{-}C_4H_4N)$, while there was very little evidence of further formation of $(\eta^5\text{-}C_5H_5)Fe(CO)(\eta^1\text{-}C_4H_4N)$, refer to Figure 3-24.

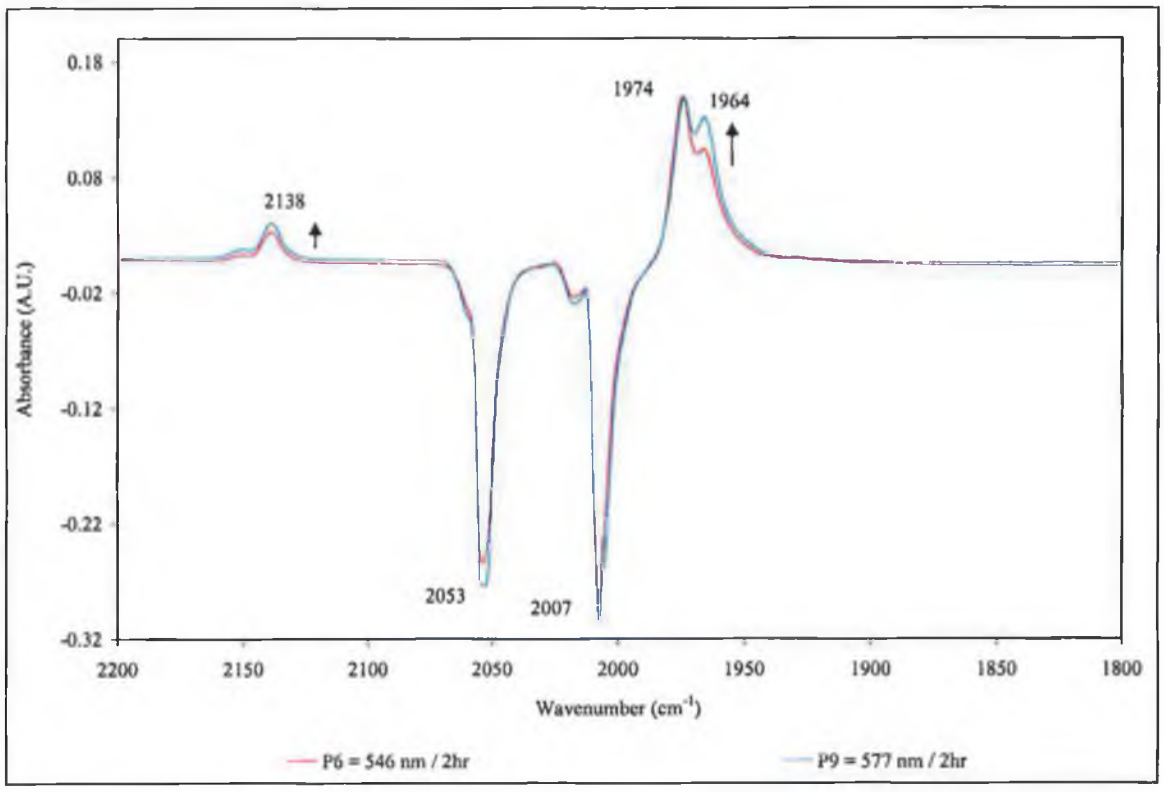

Figure 3-24 The infrared difference spectrum following further higher energy monochromatic photolysis (λ_{exc} = 546 nm) of (η^5-C_5H_5)Fe(CO)$_2$(η^1-C_4H_4N) for two hours, overlaid with the difference spectrum following subsequent photolysis at 577 nm in an argon matrix at 20 K.

Finally the matrix was subjected to broad band photolysis initially at $\lambda_{exc.} > 500$ nm, after which the energy of the light was increased to $\lambda_{exc.} > 400$ nm and ultimately to $\lambda_{exc.} > 300$ nm. Broad band photolysis at this point resulted in a decrease in the intensity of the band at 1964 cm^{-1} assigned to the *exo*-azaallyl species, (η^5-C_5H_5)Fe(CO)(η^3-N-C_4H_4N), and an increase in the free carbon monoxide in the matrix, Figure 3-25. There was no evidence to suggest regeneration of the parent complex, (η^5-C_5H_5)Fe(CO)$_2$(η^1-C_4H_4N).

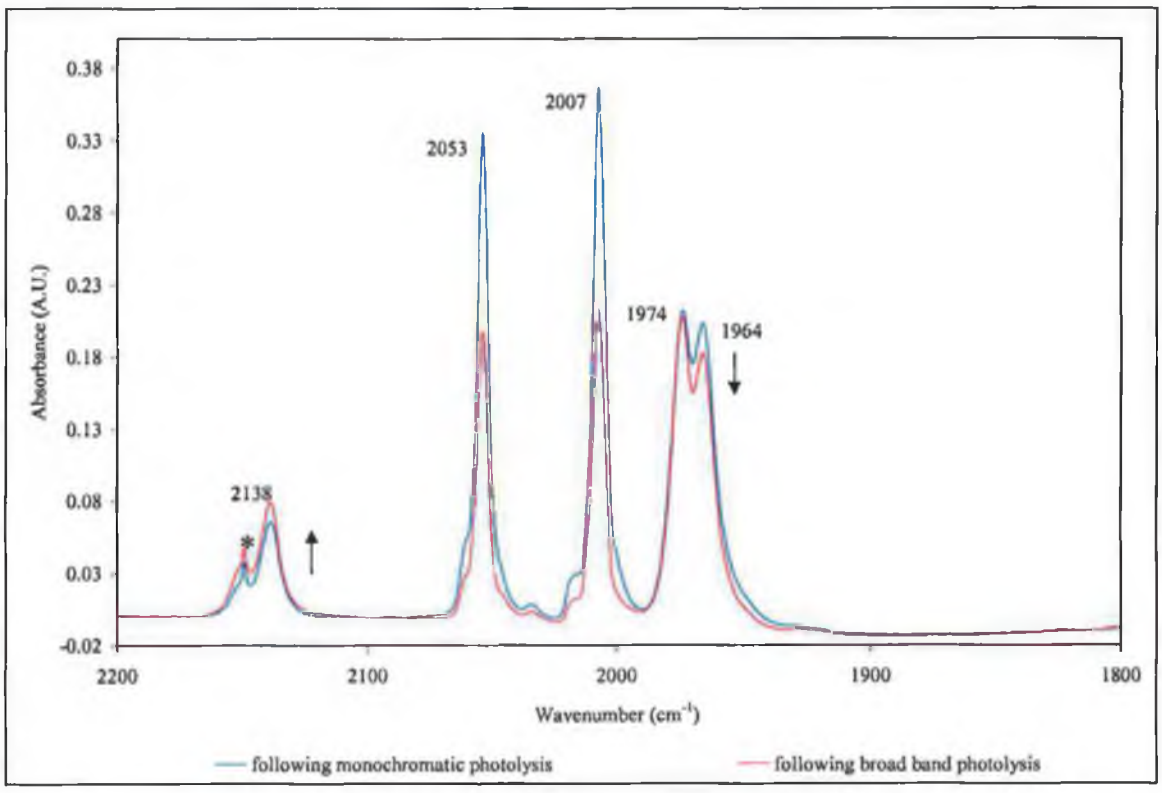

Figure 3-25 Infrared spectral changes induced when the irradiation source was changed from monochromatic photolysis to broad band photolysis during irradiation of $(\eta^5\text{-}C_5H_5)Fe(CO)_2(\eta^1\text{-}C_4H_4N)$ in an argon matrix at 20 K. (The band marked with an asterisk is due to the carbon monoxide band being perturbed by a adjacent water impurity molecule.)

3.4 The photochemistry of cyclopentadienyliron-dicarbonyl-η^1-indolyl, $(\eta^5\text{-}C_5H_5)Fe(CO)_2(\eta^1\text{-}C_8H_6N)$

Evidence of ring slippage following photolysis of azaferrocene and $(\eta^5\text{-}C_5H_5)Fe(CO)_2(\eta^1\text{-}C_4H_4N)$ in both the matrix isolation and solution phase studies, prompted this investigation of the photochemistry of $(\eta^5\text{-}C_5H_5)Fe(CO)_2(\eta^1\text{-}C_8H_6N)$. There was the possibility that the presence of the indolyl ligand attached to the metal centre may stabilise an η^3-azaallyl type species if formed upon photolysis through the increased aromaticity in the six membered-ring brought about by the slippage of the ring from η^1-co-ordination to η^3-co-ordination, something along the lines of the 'indenyl' effect.[51]

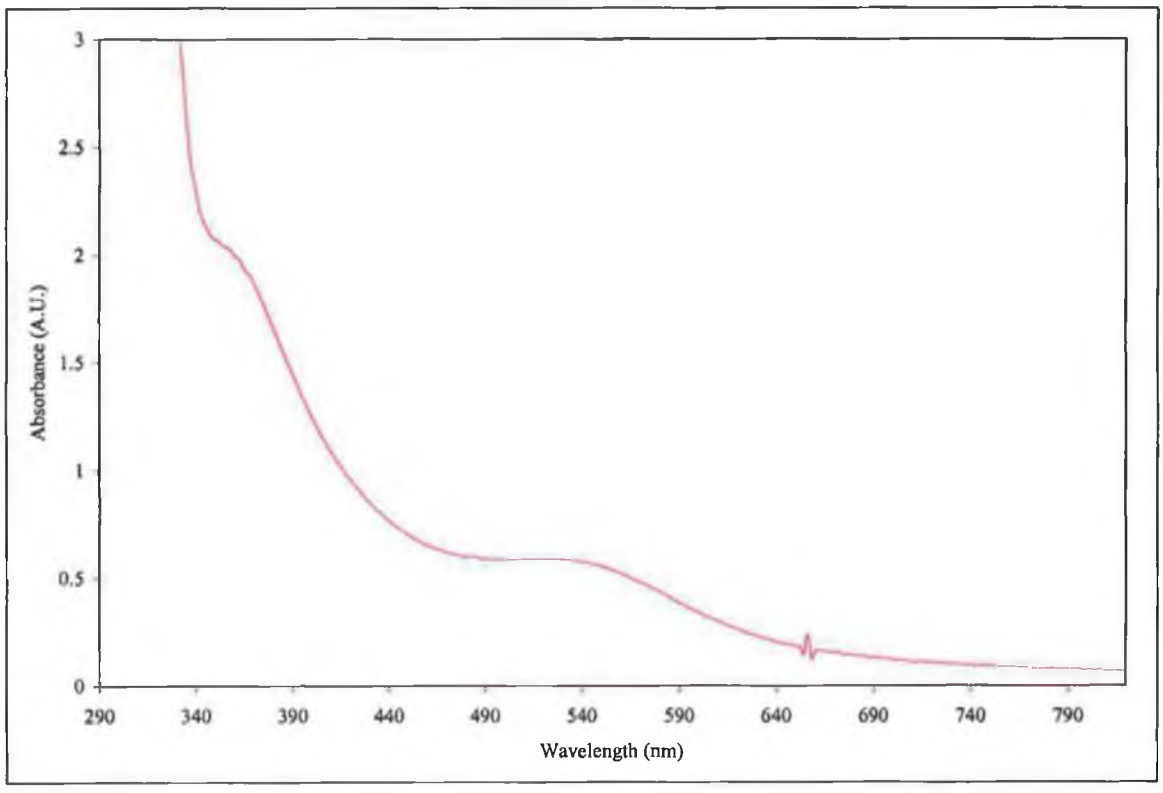

Figure 3-26 UV-vis spectrum of cyclopentadienyliron dicarbonyl-η^1-indolyl, $(\eta^5\text{-}C_5H_5)Fe(CO)_2(\eta^1\text{-}C_8H_6N)$ (1.19×10^{-3} M) in toluene.

The UV-vis spectrum of $(\eta^5\text{-}C_5H_5)Fe(CO)_2(\eta^1\text{-}C_8H_6N)$ in toluene as shown in Figure 3-26 displays weak absorptions centred at 358 nm ($\varepsilon = 1.7 \times 10^3$ L mol^{-1} cm^{-1}) and 518 nm ($\varepsilon =$

4.6×10^2 L mol^{-1} cm^{-1}), it also exhibits an absorption tail into the visible region of the spectrum ($\lambda > 620$ nm).

3.4.1 Broad band steady state photolysis ($\lambda_{exc.} > 520$ nm) of $(\eta^5\text{-}C_5H_5)Fe(CO)_2(\eta^1\text{-}C_8H_6N)$ monitored by UV-vis spectroscopy

Irradiation of $(\eta^5\text{-}C_5H_5)Fe(CO)_2(\eta^1\text{-}C_8H_6N)$ in toluene under an atmosphere of argon at room temperature was initially carried out at $\lambda_{exc.} > 520$ nm, which induced no change in the UV-vis spectrum, refer to Figure 3-27. Irradiation with increased energy, i.e. $\lambda_{exc.} > 410$ nm resulted in very small changes in the absorption spectrum. In the valley of the spectrum at ~ 480 nm the absorption increased slightly, while decreasing at the lower energy band at ~ 540 nm. Additionally there was a further increase in absorption at > 600 nm, because of an increased turbidity of the sample following photolysis. An infrared spectrum of the solution following photolysis, contained only the two bands in the ν_{CO} stretching region at 2044 and 1995 cm^{-1}, which are those of the parent complex $(\eta^5\text{-}C_5H_5)Fe(CO)_2(\eta^1\text{-}C_8H_6N)$. In contrast to the results following photolysis of $(\eta^5\text{-}C_5H_5)Fe(CO)_2(\eta^1\text{-}C_4H_4N)$ under similar conditions, there is no evidence to suggest the formation of a dimeric species.

Irradiation of $(\eta^5\text{-}C_5H_5)Fe(CO)_2(\eta^1\text{-}C_8H_6N)$ under an atmosphere of carbon monoxide produced similar results to those under argon with the exception that the solution did not become turbid upon photolysis. There was very little change in the UV-vis spectrum following photolysis. There was no formation of any new carbonyl containing photoproducts, i.e. infrared spectra obtained following photolysis revealed only the presence of the starting complex.

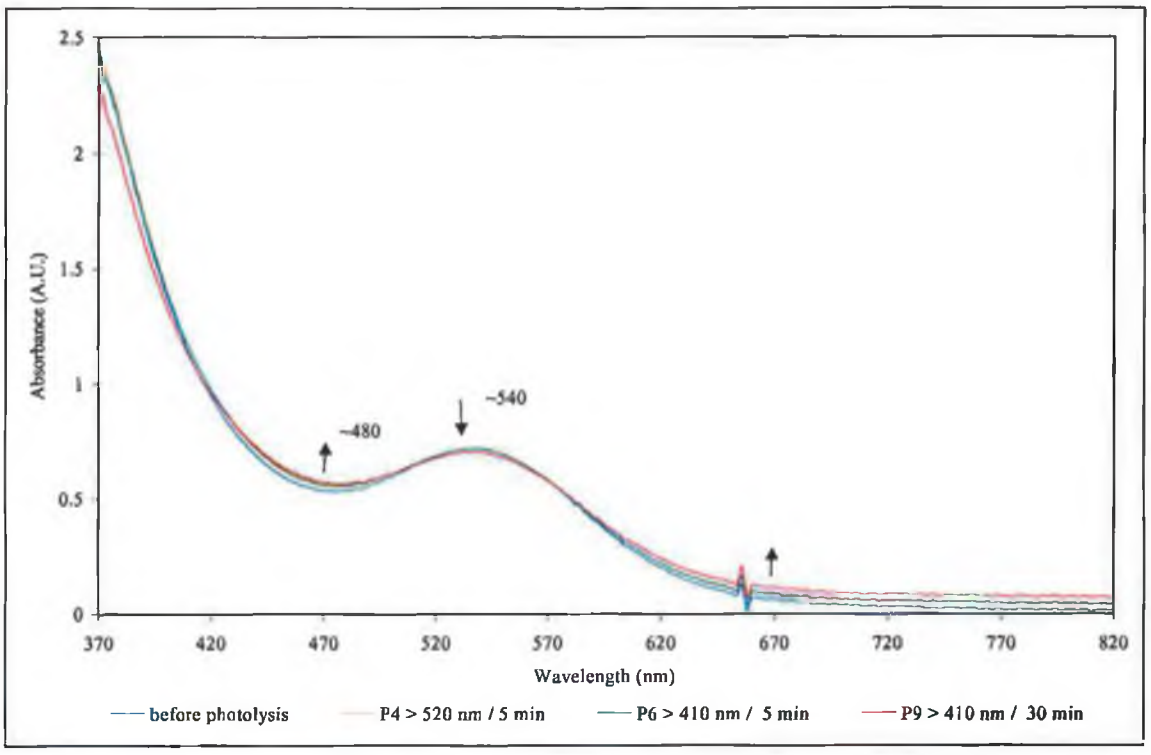

Figure 3-27 Changes observed in the UV-vis spectrum of $(\eta^5\text{-}C_5H_5)Fe(CO)_2(\eta^1\text{-}C_8H_6N)$ (~1.5 × 10^{-3} M) following initially photolysis at λ_{exc} > 520 nm, followed by λ_{exc} > 410 nm in toluene under argon.

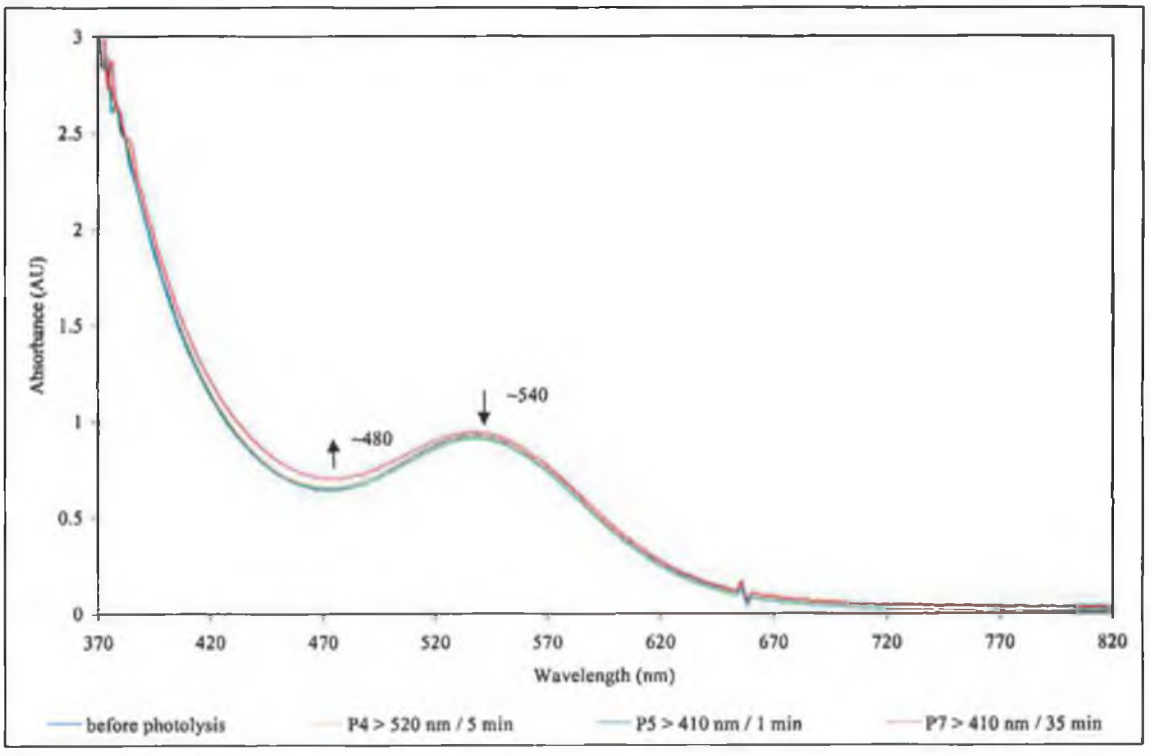

Figure 3-28 Changes observed in the UV-vis spectrum of $(\eta^5\text{-}C_5H_5)Fe(CO)_2(\eta^1\text{-}C_8H_6N)$ (~1.9 × 10^{-3} M) following initially photolysis at λ_{exc} > 520 nm, followed by λ_{exc} > 410 nm in carbon monoxide saturated toluene.

Broad band steady-state photolysis ($\lambda_{exc.} > 520$ nm) of $(\eta^5\text{-}C_5H_5)Fe(CO)_2(\eta^1\text{-}C_8H_6N)$ in degassed toluene solutions containing an excess of triphenylphosphine (PPh_3) resulted in the spectroscopic changes presented in Figure 3-29. The isosbestic points at 504 and 550 nm suggest a reaction uncomplicated by side or subsequent reactions.

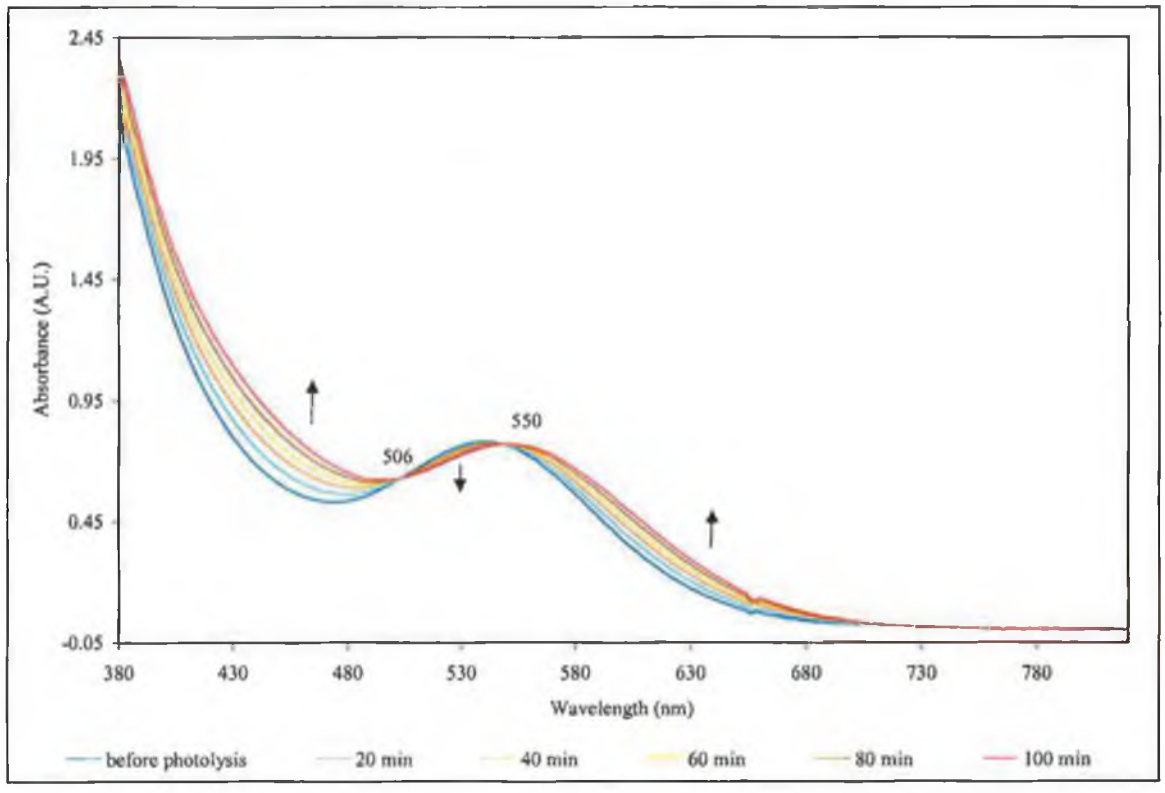

Figure 3-29 UV-vis spectral changes observed upon the photolysis ($\lambda_{exc.} > 520$ nm) of $(\eta^5\text{-}C_5H_5)Fe(CO)_2(\eta^1\text{-}C_8H_6N)$ (1.6×10^{-3} M) in toluene with excess PPh_3 ligand.

3.4.2 Broad band steady state photolysis ($\lambda_{exc.} > 520$ nm) of $(\eta^5\text{-}C_5H_5)Fe(CO)_2(\eta^1\text{-}C_8H_6N)$ monitored by infrared spectroscopy

A toluene solution of $(\eta^5\text{-}C_5H_5)Fe(CO)_2(\eta^1\text{-}C_8H_6N)$, degassed with argon, in the presence of excess triphenylphosphine was irradiated ($\lambda_{exc.} > 520$) in an infrared solution cell, (total photolysis time 10 minutes). The difference spectra displaying a new ν_{CO} absorption at 1948 cm^{-1} and the bleaching of the parent bands at 2044 and 1995 cm^{-1} are presented in Figure 3-30. As the reaction proceeded an isosbestic point at 1970 cm^{-1} in the infrared spectrum was apparent, which is consistent with the smooth transformation of the parent complex, $(\eta^5\text{-}C_5H_5)Fe(CO)_2(\eta^1\text{-}C_8H_6N)$ to a single photoproduct. There was no evidence of

any other carbonyl containing products. The new band at 1948 cm^{-1} is assigned to the monosubstituted photoproduct $(\eta^5\text{-}C_5H_5)Fe(CO)(PPh_3)(\eta^1\text{-}C_8H_6N)$.

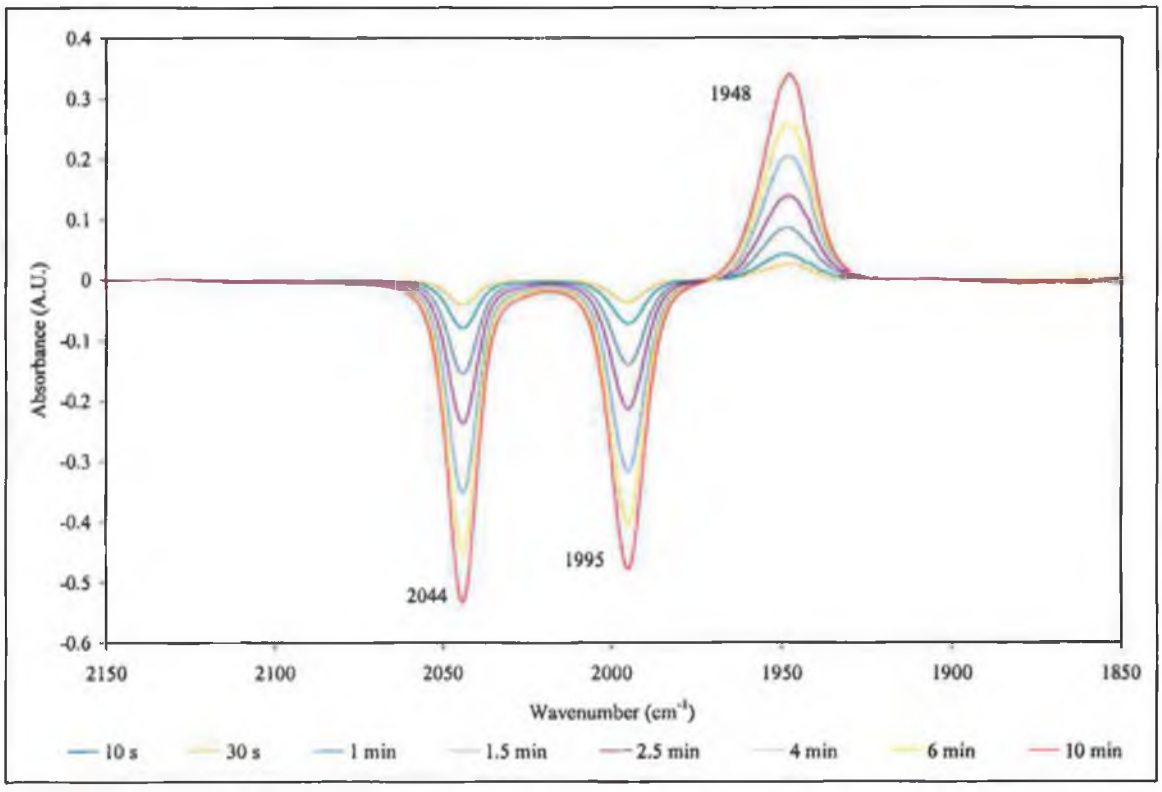

Figure 3-30 Infrared spectral changes observed upon the photolysis (λ_{exc} > >520 nm) of $(\eta^5\text{-}C_5H_5)Fe(CO)_2(\eta^1\text{-}C_8H_6N)$ in toluene with PPh_3 ligand added in excess

As mentioned before, substitution of the carbon monoxide ligand in $(\eta^5\text{-}C_5H_5)Fe(CO)_2R$[15] (where R is alkyl or allyl group) and $(\eta^5\text{-}C_5H_5)Fe(CO)_2X$[10] (where X = Cl, Br, or I) is well documented to be the dominant photochemical reaction of these type of complexes. The findings of this work for $(\eta^5\text{-}C_5H_5)Fe(CO)_2(\eta^1\text{-}C_8H_6N)$ are similar to those obtained previously previous for $(\eta^5\text{-}C_5H_5)Fe(CO)_2(\eta^1\text{-}C_4H_4N)$.

3.4.3 *Laser flash photolysis experiments on (η^5-C_5H_5)Fe(CO)$_2$(η^1-C_8H_6N)*

The photochemistry of (η^5-C_5H_5)Fe(CO)$_2$(η^1-C_8H_6N) was investigated by UV-vis flash photolysis with $\lambda_{exc.}$ = 355 nm and $\lambda_{exc.}$ = 532 nm in carbon monoxide saturated toluene and under inert conditions.

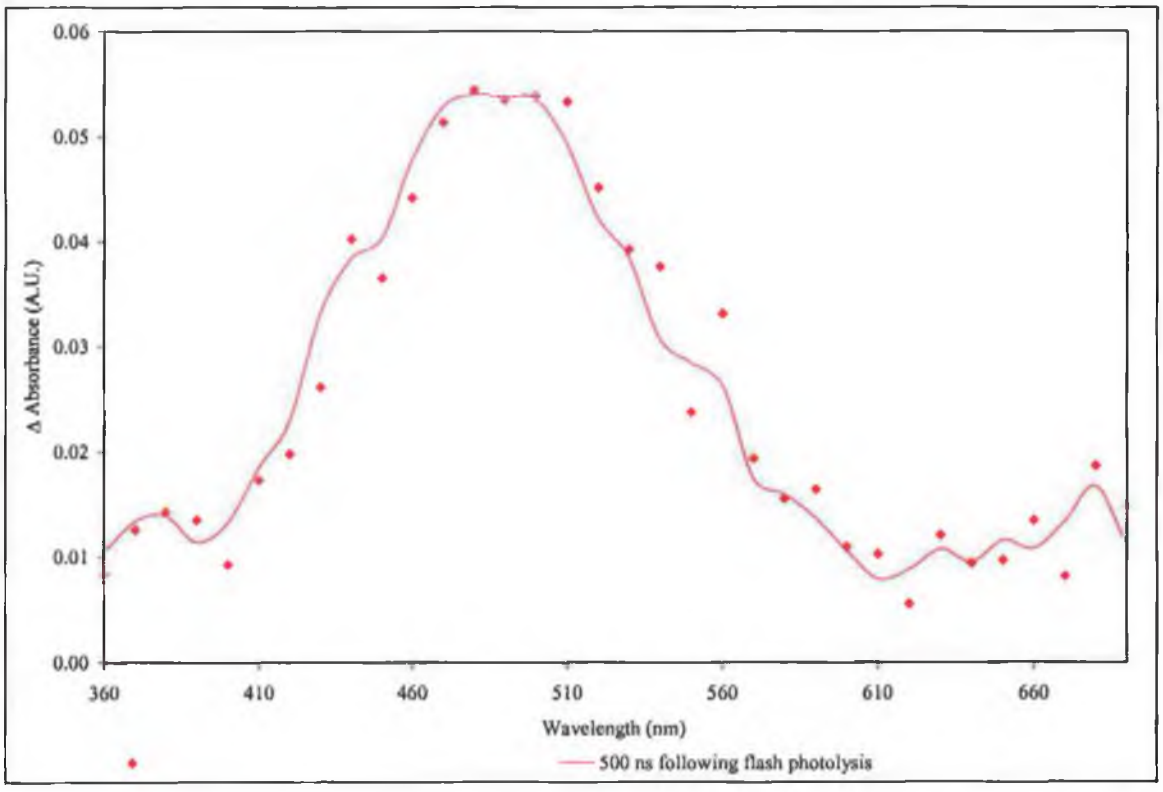

Figure 3-31 UV-vis difference spectrum obtained 500 ns after flash photolysis ($\lambda_{exc.}$ = 355 nm) of (η^5-C_5H_5)Fe(CO)$_2$(η^1-C_8H_6N) in carbon monoxide saturated toluene at room temperature.

The difference spectrum obtained five hundred nanoseconds after the laser pulse at 355 nm in carbon monoxide saturated toluene is given in Figure 3-31. The UV-vis spectrum of the transient species has a maximum absorption at 480 nm, in addition to a weak absorption > 600 nm. This transient species is the sixteen-electron species (η^5-C_5H_5)Fe(CO)(η^1-C_8H_6N). The photoproduct absorbs in the valley (480 nm) of the absorption spectrum of the parent species, refer to Figure 3-26. The transient decay signal of the monocarbonyl species under an atmosphere of carbon monoxide is presented in Figure 3-32. From this it can be seen that the monocarbonyl species responsible for the absorption decays fully to regenerate the parent complex within ~ 5 μs. The decay of the monocarbonyl and regeneration of the

parent under an atmosphere of carbon monoxide is typical of carbon monoxide dissociation. The steady-state UV-vis spectra of the flash photolysis solution obtained during the experiment showed that no significant absorption change had occurred, which is consistent with the reversibility observed for the transient species. Consequently, the infrared spectrum of the final flash photolysis solution displayed only the ν_{CO} stretches of the parent complex and no other photoproducts.

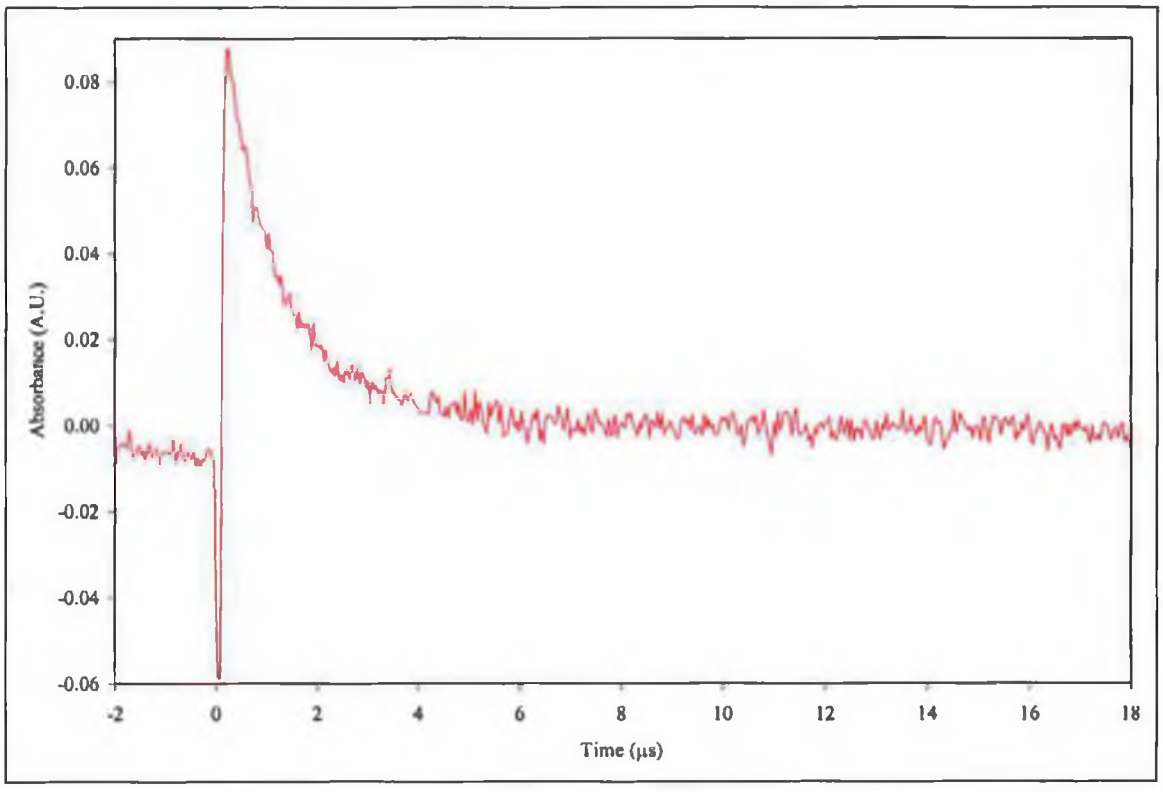

Figure 3-32 A typical transient signal obtained for the decay of $(\eta^5\text{-}C_5H_5)Fe(CO)(\eta^1\text{-}C_8H_6N)$ monitored at 480 nm in carbon monoxide saturated toluene.

The lifetime of the decay transient at 480 nm is dependent on the concentration, of carbon monoxide. Increasing concentrations of carbon monoxide result in a decreasing lifetime of the transient, Figure 3-33.

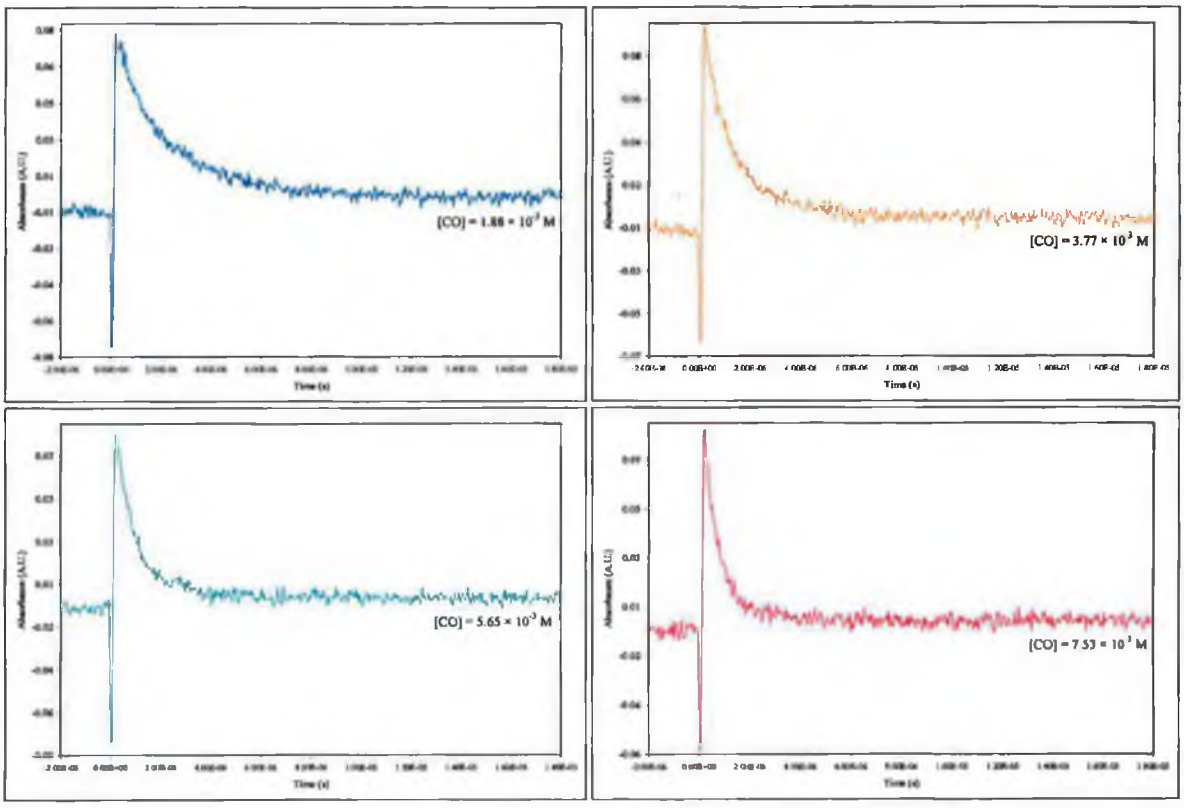

Figure 3-33 The decay transient monitored at 480 nm following laser flash photolysis ($\lambda_{exc.}$ = 355 nm) of $(\eta^5\text{-}C_5H_5)Fe(CO)_2(\eta^1\text{-}C_8H_6N)$ in varying concentrations of carbon monoxide in toluene solution.

A plot of the observed rate constant ($k_{obs.}$) for the decay of the monocarbonyl species, $(\eta^5\text{-}C_5H_5)Fe(CO)(\eta^1\text{-}C_8H_6N)$ versus the carbon monoxide concentration, Figure 3-34, is linear with negligible intercept, indicative of the fact that under these conditions no other reactions are contributing significantly to the decay of the monocarbonyl species. The slope of the plot provides the second order rate constant, $k_2 = 1.99\ (\pm 0.19) \times 10^8$ $M^{-1}\ s^{-1}$ for the reaction of $(\eta^5\text{-}C_5H_5)Fe(CO)(\eta^1\text{-}C_8H_6N)$ with carbon monoxide.

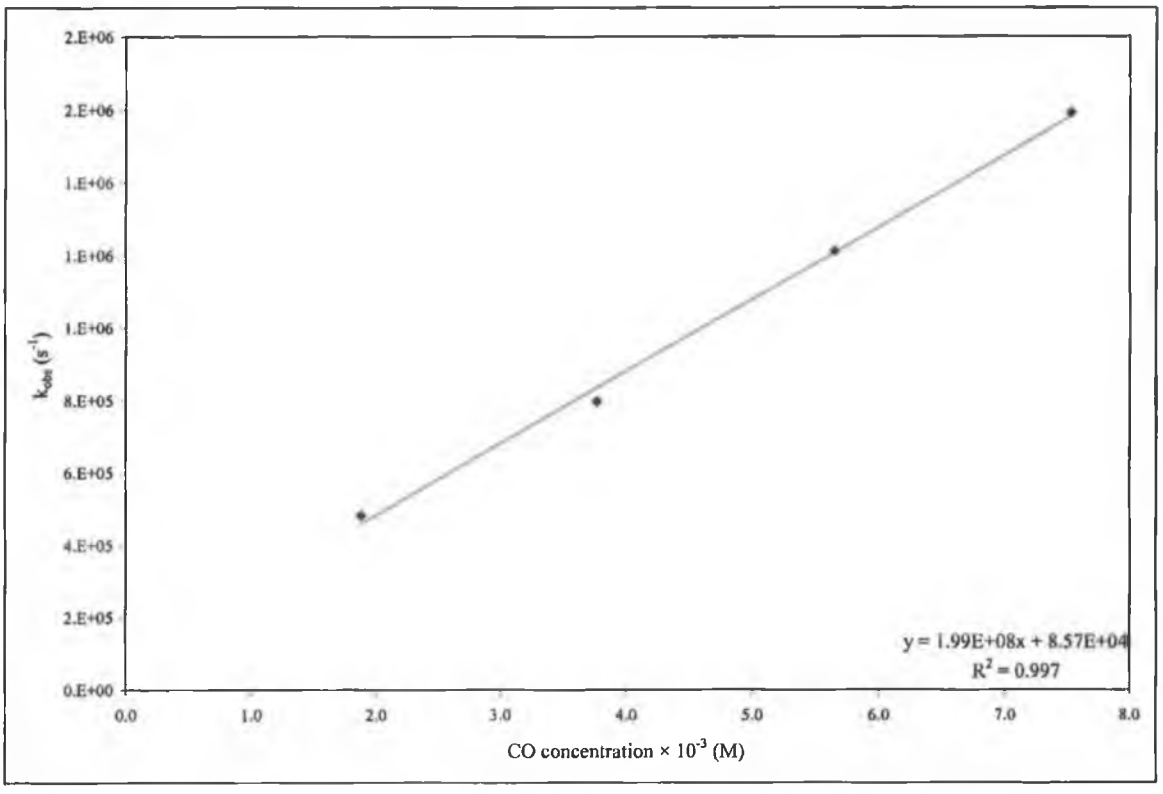

Figure 3-34 Plot of k_{obs} - vs - concentration of carbon monoxide for the decay of $(\eta^5\text{-}C_5H_5)Fe(CO)(\eta^1\text{-}C_8H_6N)$ in carbon monoxide saturated toluene to regenerate the parent complex $(\eta^5\text{-}C_5H_5)Fe(CO)_2(\eta^1\text{-}C_8H_6N)$, following irradiation at λ_{exc} = 355 nm.

An attempt to measure the activation parameters for the reaction of $(\eta^5\text{-}C_5H_5)Fe(CO)(S)(\eta^1\text{-}C_8H_6N)$ with carbon monoxide were unsuccessful as the observed rate constant did not vary significantly upon variation of the reaction temperature. This can be explained by proposing that a pre-equilibrium has been established between the solvated species $(\eta^5\text{-}C_5H_5)Fe(CO)(\text{toluene})(\eta^1\text{-}C_8H_6N)$ and $(\eta^5\text{-}C_5H_5)Fe(CO)(\eta^1\text{-}C_8H_6N)$, which is the rate determining step, Scheme 3-10, similar to that proposed previously for $(\eta^5\text{-}C_5H_5)Fe(CO)(\eta^1\text{-}C_4H_4N)$ in carbon monoxide saturated toluene.

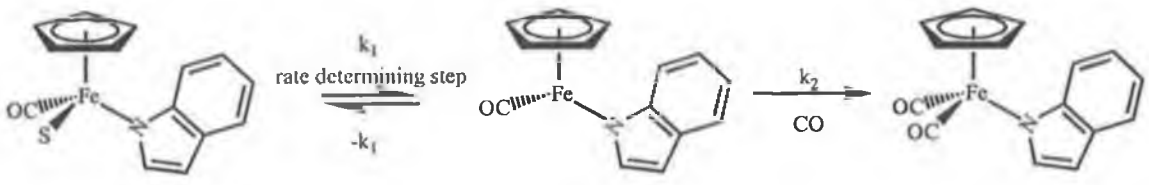

Where S = toluene

Scheme 3-10 Reaction scheme proposed for $(\eta^5\text{-}C_5H_5)Fe(CO)_2(\eta^1\text{-}C_8H_6N)$ in CO saturated toluene.

The photochemistry of $(\eta^5\text{-}C_5H_5)Fe(CO)_2(\eta^1\text{-}C_8H_6N)$ was also investigated by laser flash photolysis in carbon monoxide saturated toluene solution with lower energy photons at $\lambda_{exc.}$ = 532 nm. The difference spectra recorded at 500ns, 1, 2, and 3 μs following the laser pulse are given in Figure 3-35. It is clear from Figure 3-35 that the region of the spectrum where the photoproduct(s) absorb significantly is in the valley of the parent absorption spectrum at 480 nm, in addition a weak absorption features at > 600nm, which is more apparent 3 μs after the laser pulse. These results are the same as those observed following laser flash photolysis at $\lambda_{exc.}$ = 355 nm. Analysis of the decay kinetics associated with the transient absorption at 480 nm versus the concentration of carbon monoxide yields the rate of the reaction of the monocarbonyl with carbon monoxide, $k_2 = 1.23\ (\pm 0.23) \times 10^8\ M^{-1}\ s^{-1}$, Figure 3-36.

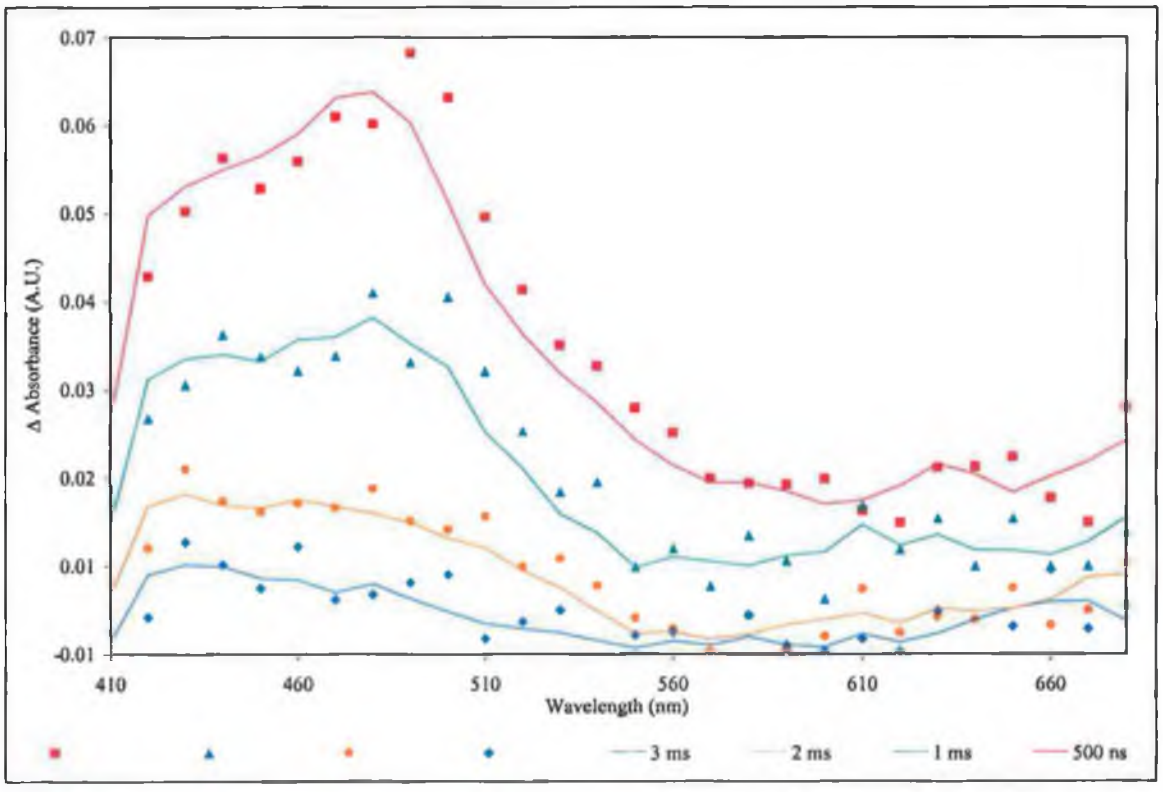

Figure 3-35 UV-vis difference spectrum obtained 500 ns, 1μs, 2μs and 3 μs after flash photolysis (λ_{exc} = 532 nm) of $(\eta^5\text{-}C_5H_5)Fe(CO)_2(\eta^1\text{-}C_8H_6N)$ in carbon monoxide saturated toluene solution.

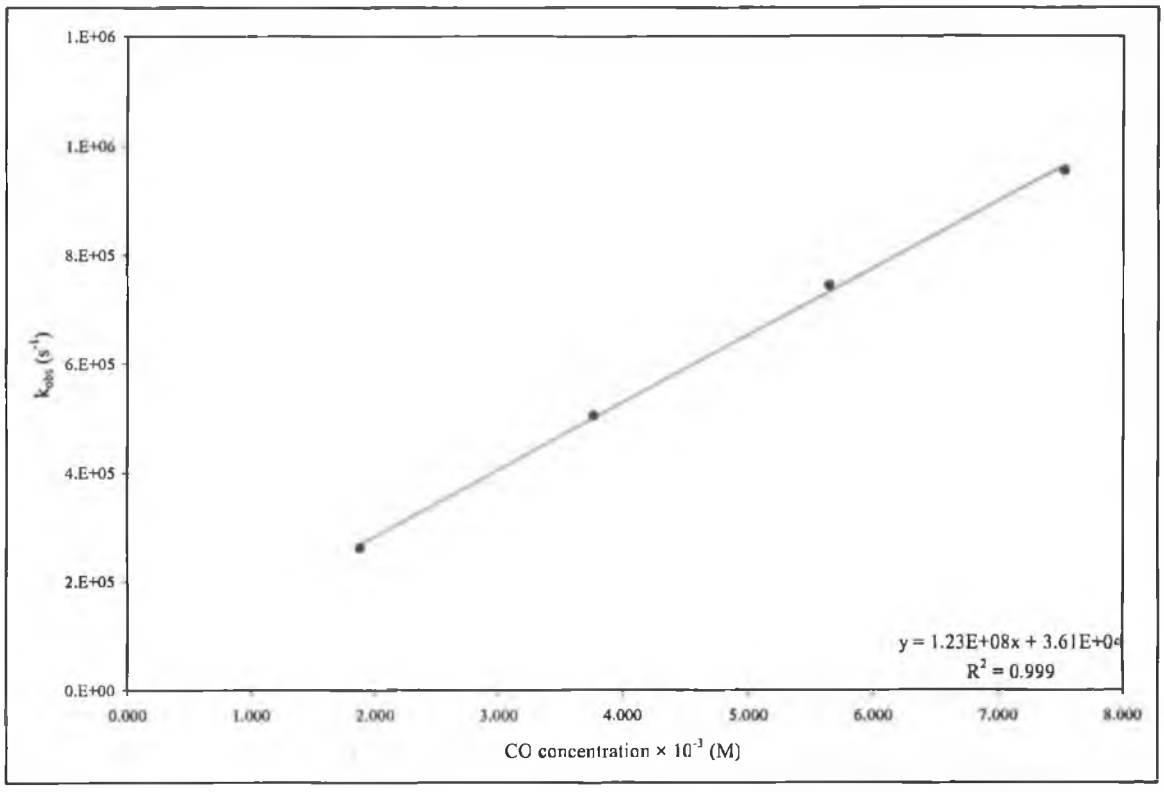

Figure 3-36 Plot of k_{obs} - vs - concentration of carbon monoxide for the decay of $(\eta^5\text{-}C_5H_5)Fe(CO)(\eta^1\text{-}C_8H_6N)$ in toluene to regenerate the parent complex $(\eta^5\text{-}C_5H_5)Fe(CO)_2(\eta^1\text{-}C_8H_6N)$, following irradiation at λ_{exc} = 532 nm.

Flash photolysis ($\lambda_{exc.}$ = 355 nm) of $(\eta^5\text{-}C_5H_5)Fe(CO)_2(\eta^1\text{-}C_8H_6N)$ under one atmosphere of argon in toluene revealed two distinct transient signals at 380 and 480 nm respectively. The transient observed at 480 nm for $(\eta^5\text{-}C_5H_5)Fe(CO)_2(\eta^1\text{-}C_8H_6N)$ does not return to the pre-irradiated baseline, Figure 3-37, indicating that under inert conditions the reaction is not fully reversible. However, it does decay to a post-irradiation baseline within 50 μs. Under inert conditions, $(\eta^5\text{-}C_5H_5)Fe(CO)_2(\eta^1\text{-}C_4H_4N)$ displayed a residual baseline also, refer to Figure 3-13, however in the case of $(\eta^5\text{-}C_5H_5)Fe(CO)_2(\eta^1\text{-}C_8H_6N)$ there is a significant difference between the pre-irradiated baseline and the post-irradiated baseline. This suggests that a second, longer-lived transient species may be absorbing underneath this transient signal. The observed rate constant (k_{obs}) for the decay of the monocarbonyl species to the post-irradiation baseline under argon (1.2×10^5 s^{-1}), is an order of magnitude slower than observed rate constant, (1.59×10^6 s^{-1}) in carbon monoxide saturated toluene. Further confirmation of the irreversibility of the system is evident from the steady state UV-vis monitoring of the laser flash solution during the experiment, which showed an

increase across the entire spectrum following photolysis refer to inset in Figure 3-37 for UV-vis steady-state monitoring during the flash photolysis experiments.

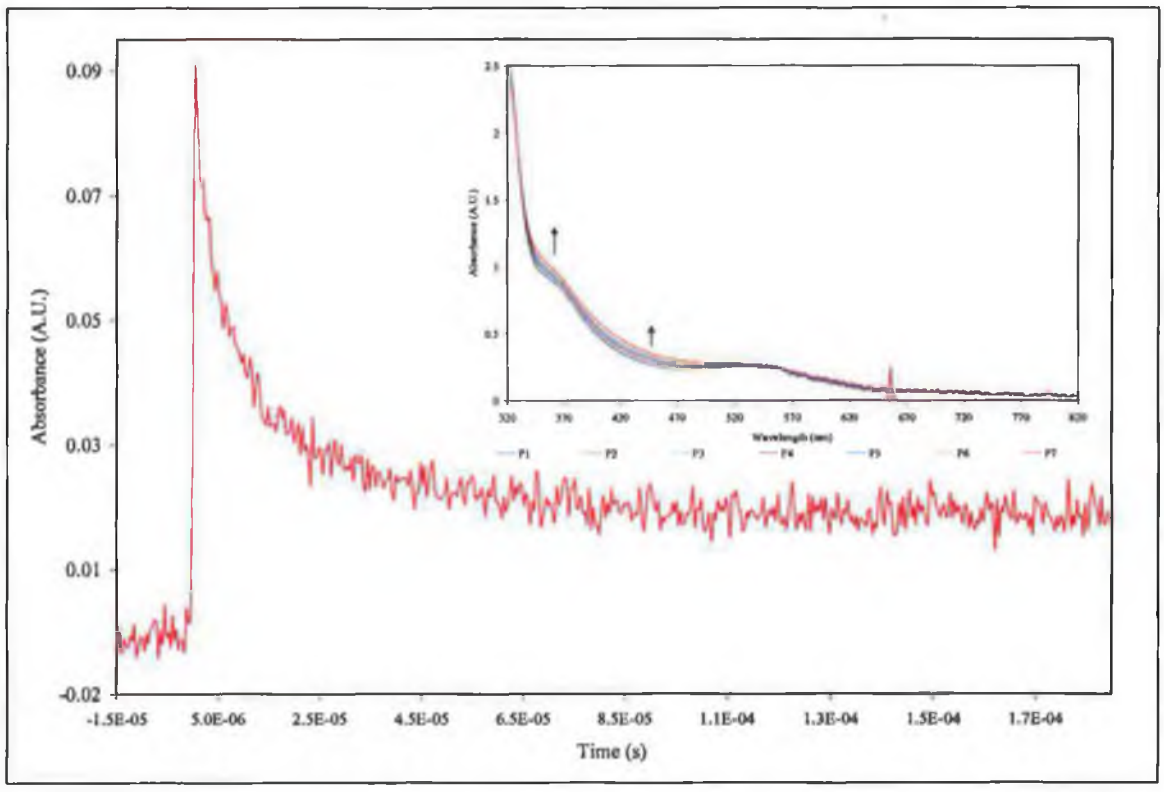

Figure 3-37 A typical transient signal obtained for the decay of $(\eta^5\text{-}C_5H_5)Fe(CO)(\eta^1\text{-}C_8H_6N)$ monitored at 480 nm in toluene under 1 atm of argon. Inset displays the UV-vis steady-state spectra recorded during the flash photolysis.

The second transient signal observed at 380 nm is presented in Figure 3-38. If this transient signal is examined on a longer time-base as shown in the inset in Figure 3-38, it is possible to see that there is some evidence of decay of the transient signal. This decay corresponds to the decay of the monocarbonyl species, $(\eta^5\text{-}C_5H_5)Fe(CO)(\eta^1\text{-}C_8H_6N)$ as seen for the transient signal at 480 nm, as it too decays to a post-irradiation baseline within 50 μs. The longer lived transient signal remains, even up to a millisecond following the flash photolysis. The transient signal at 380 nm is suppressed in the presence of carbon monoxide.

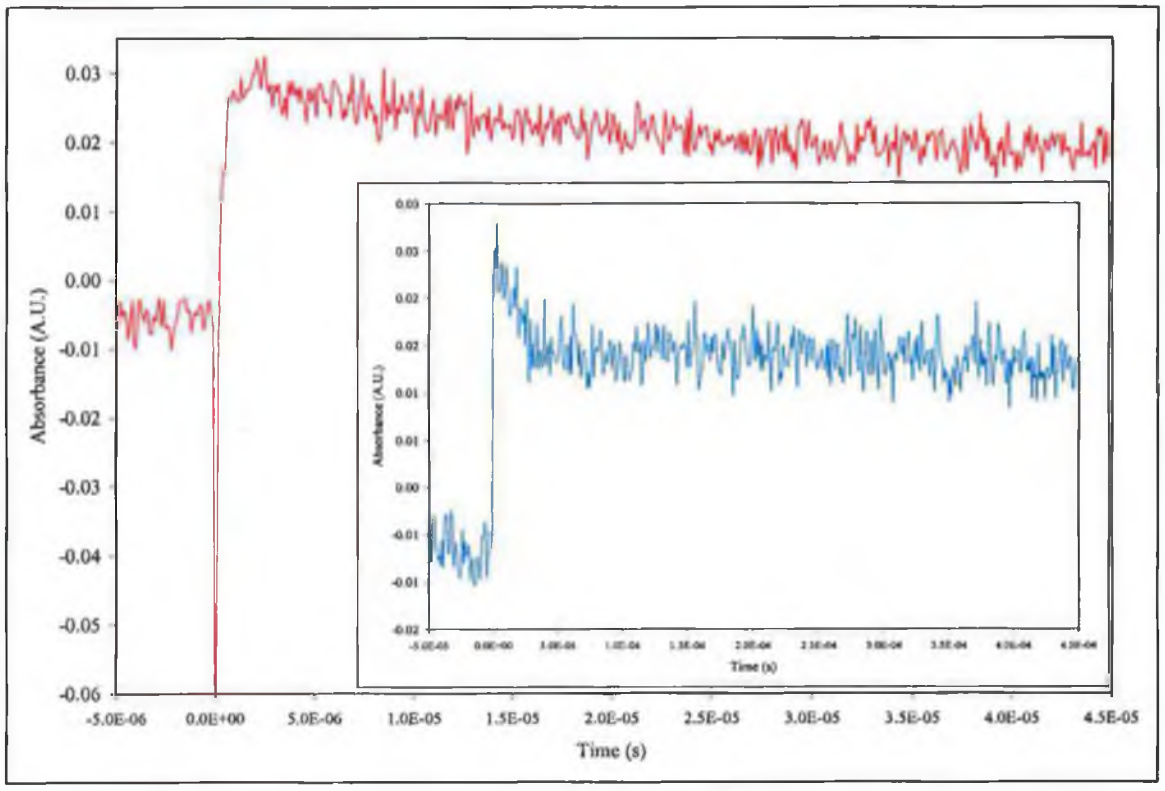

Figure 3-38 A typical transient signal observed upon the photolysis (λ_{exc} = 355 nm) of (η^5-C_5H_5)Fe(CO)(η^1-C_8H_6N) monitored at 380 nm in toluene under 1 atm of argon (time-base 5 μs). The inset shows that over a longer time-base (50 μs) this transient shows a slight decay, with evidence of a much longer lived transient species underneath.

UV-vis difference spectra obtained 1 μs following flash photolysis under argon reveals a λ_{max} = 480 nm for the transient species, this has been assigned to the absorption of the monocarbonyl transient species. It can be seen from Figure 3-39, this absorption at $\lambda_{max.}$ = 480 nm has almost disappeared by 10 μs following flash photolysis, indicating that the monocarbonyl species is almost completely consumed. However when the UV-vis difference spectrum was recorded at a longer time-base - 50 μs, it revealed a shift in the max absorption band to $\lambda_{max.}$ 380 nm, Figure 3-40, indicating that there is a second transient species, which has a longer lifetime.

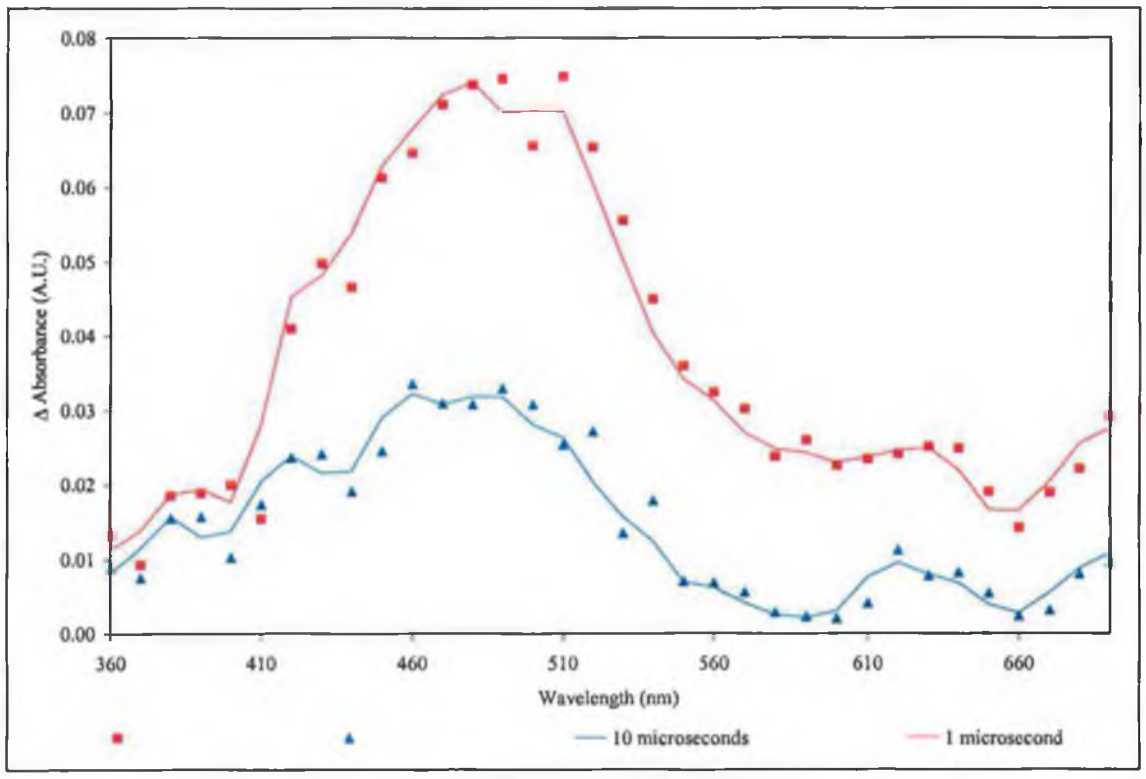

Figure 3-39 UV-vis difference spectrum obtained 1μs and 10 μs after flash photolysis (λ_{exc} = 355 nm) of $(\eta^5\text{-}C_5H_5)Fe(CO)_2(\eta^1\text{-}C_8H_6N)$ in toluene solution under an atmosphere of argon at room temperature.

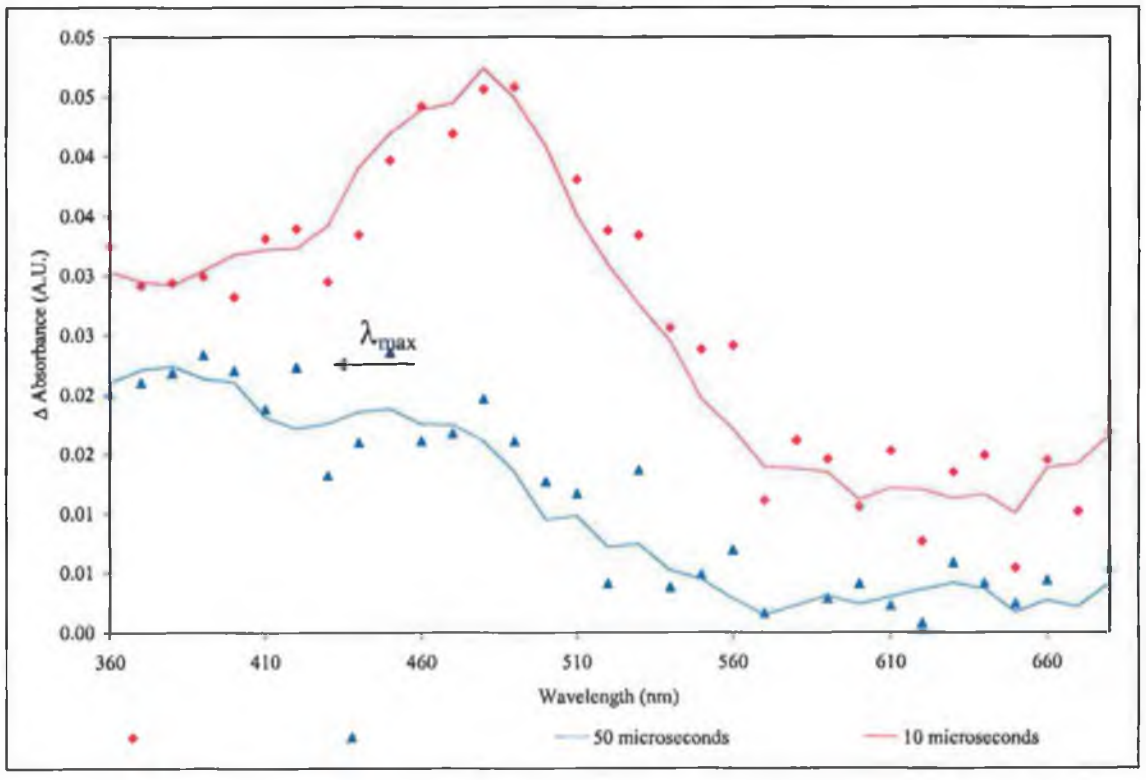

Figure 3-40 UV-vis difference spectrum obtained 10μs and 50 μs after flash photolysis (λ_{exc} = 355 nm) of $(\eta^5\text{-}C_5H_5)Fe(CO)_2(\eta^1\text{-}C_8H_6N)$ in toluene solution under an atmosphere of argon at room temperature.

Therefore it can be concluded that the longer lived transient species has a maximum absorption at 380 nm. It is proposed that the photochemistry of $(\eta^5\text{-}C_5H_5)Fe(CO)_2(\eta^1\text{-}C_8H_6N)$ under argon is best explained by the formation of an η^3-type monocarbonyl species, $(\eta^5\text{-}C_5H_5)Fe(CO)(\eta^3\text{-}C\text{-}C_8H_6N)$, as outlined in the reaction Scheme 3-11 shown below. The UV-vis steady-state monitoring of the flash photolysis solution also revealed an increase across the entire spectral region, consistent with the formation of a longer lived species.

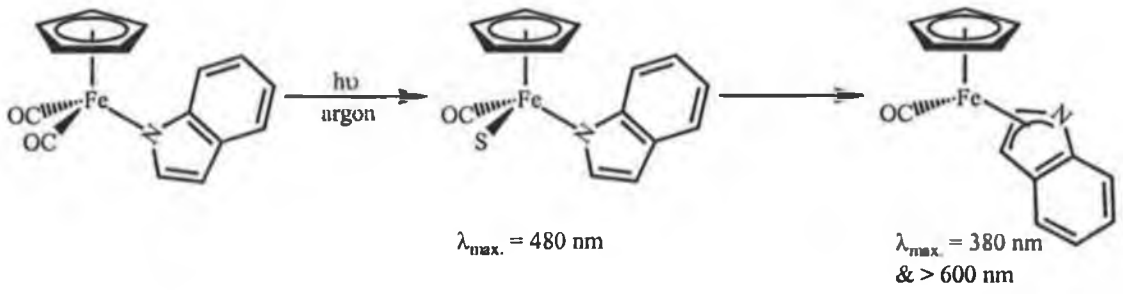

Scheme 3-11 Proposed reaction following laser flash photolysis of $(\eta^5\text{-}C_5H_5)Fe(CO)_2(\eta^1\text{-}C_8H_6N)$ in toluene solution under an atmosphere of argon.

UV-vis laser flash photolysis of $(\eta^5\text{-}C_5H_5)Fe(CO)_2(\eta^1\text{-}C_8H_6N)$ at $\lambda_{exc.}$ = 532 nm under argon produced analogous results. The transient signal, refer to inset in Figure 3-41, was observed across the entire UV-vis region (410-700 nm) investigated following flash photolysis. The maximum absorption for this transient species was at 480 nm, as deduced from the UV-vis difference spectrum, Figure 3-41. Unfortunately, because of the low extinction coefficient of $(\eta^5\text{-}C_5H_5)Fe(CO)_2(\eta^1\text{-}C_8H_6N)$ at $\lambda_{exc.}$ = 532 nm, higher solution concentrations were required for the laser flash photolysis work at $\lambda_{exc.}$ = 532 nm making it impossible to record the difference spectrum beyond 410 nm, as the absorbance of the solution in the higher energy region of the UV-vis spectrum was too large. This also inhibited an attempt to established whether or not the transient observed at 380 nm following excitation at $\lambda_{exc.}$ = 355 nm, is also present following excitation at $\lambda_{exc.}$ = 532 nm.

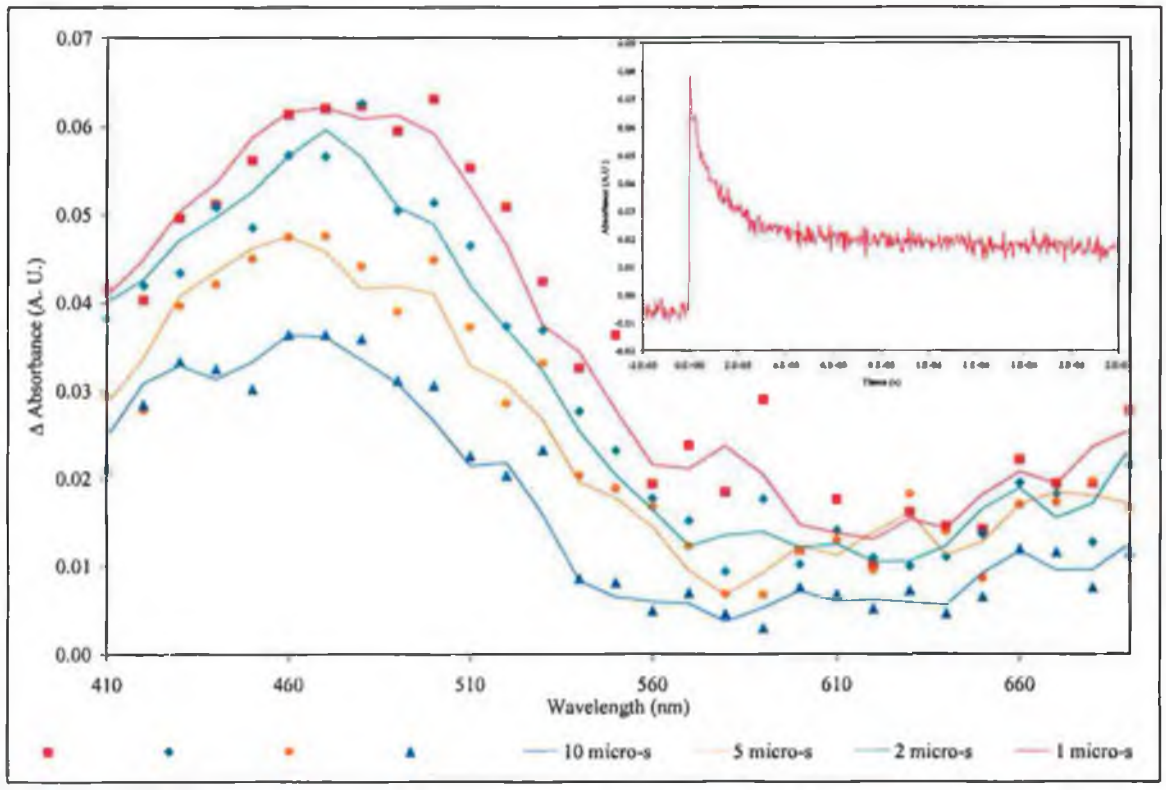

Figure 3-41 UV-vis difference spectrum obtained, 1, 2, 5 and 10 μs after flash photolysis (λ_{exc} = 532 nm) of (η^5-C_5H_5)Fe(CO)$_2$(η^1-C_8H_6N) in toluene under an inert atmosphere. Inset features a typical transient monitored at 480 nm following flash photolysis with λ_{exc} = 532 nm.

The transient at 480 nm is identical to that observed following excitation with 355 nm photons in toluene under an atmosphere of argon, and therefore has been assigned to the decay of the monocarbonyl, (η^5-C_5H_5)Fe(CO)(η^1-C_8H_6N) to generate the second longer lived transient species, (η^5-C_5H_5)Fe(CO)(η^3-C_8H_6N). Indications that the reaction is not fully reversible under inert conditions from the transient signals are confirmed by the fact that the steady state UV-vis monitoring of the laser flash photolysis solution during the experiment also revealed an increase across the entire spectrum. The greatest increase was in the valley of the parent complexes at 380-480 nm. Infrared spectra of the solutions following flash photolysis do not show any evidence of an η^3-type monocarbonyl species. The lifetime of the second transient species (η^5-C_5H_5)Fe(CO)(η^3-*C*-C_8H_6N) is too long to detect its decay on the laser flash photolysis system (i.e. lifetime > 10 ms).

3.4.3.1 Discussion of the laser flash photolysis of (η^5-C_5H_5)Fe(CO)$_2$(η^1-C_8H_6N) results

Laser flash photolysis of (η^5-C_5H_5)Fe(CO)$_2$(η^1-C_8H_6N) in carbon monoxide saturated toluene at both $\lambda_{exc.}$ = 355 and 532 nm leads to the formation of one transient species, which absorbs strongly at 480 nm. This is assigned to the monocarbonyl species (η^5-C_5H_5)Fe(CO)(η^1-C_8H_6N). The return of the transient absorption signal to the pre-irradiated baseline indicates the complete reversibility of the system. The second order rate constant for the reaction of (η^5-C_5H_5)Fe(CO)(η^1-C_8H_6N) with carbon monoxide was determined to be 1.99×10^8 $M^{-1}s^{-1}$, which is only slightly slower than that observed for the reaction of (η^5-C_5H_5)Fe(CO)(η^1-C_4H_4N) with carbon monoxide (3.0×10^8 $M^{-1}s^{-1}$). As with (η^5-C_5H_5)Fe(CO)$_2$(η^1-C_4H_4N) in toluene, there was no activation parameters for the reaction of the monocarbonyl with carbon monoxide, indicating that for both these complexes, that the rate determining step is a pre-equilibrium between the solvated species (η^5-C_5H_5)Fe(CO)(toluene)(η^1-R), R = C_4H_4N or C_8H_6N and (η^5-C_5H_5)Fe(CO)(η^1-R). The absorption maxima for the transient monocarbonyl species formed following flash photolysis of (η^5-C_5H_5)Fe(CO)$_2$(η^1-C_8H_6N) and (η^5-C_5H_5)Fe(CO)$_2$(η^1-C_4H_4N) are at 480 and 430 nm respectively.

In contrast to the photochemical similarity between (η^5-C_5H_5)Fe(CO)$_2$(η^1-C_8H_6N) and (η^5-C_5H_5)Fe(CO)$_2$(η^1-C_8H_6N) in toluene solution under an atmosphere of carbon monoxide, the photochemistry of these complexes is quite different from one another under an atmosphere of argon. In the case of (η^5-C_5H_5)Fe(CO)$_2$(η^1-C_4H_4N) in toluene solution under argon the transient assigned to the monocarbonyl species, $\lambda_{max.}$ = 430 nm returns to the pre-irradiated baseline, regenerating the parent complex. There is no evidence to suggest the presence of a second transient species. These results are in contrast to those observed for (η^5-C_5H_5)Fe(CO)$_2$(η^1-C_8H_6N) in which two transient species, assigned to the monocarbonyl species (η^5-C_5H_5)Fe(CO)(η^1-C_8H_6N) and (η^5-C_5H_5)Fe(CO)(η^3-*C*-C_8H_6N) are detected. The η^3-bound indolyl species is long-lived, and shows only a very slight decay on the maximum time-scale for monitoring transients available on the laser system (10 ms). It displays a maximum absorption at 380 nm. The formation of (η^5-C_5H_5)Fe(CO)(η^3-*C*-C_8H_6N) is suppressed under an atmosphere of carbon monoxide. Although UV-vis spectroscopy provides no structural evidence for this species, there is some justification for supposing that it is an η^3-bound species. Monochromatic

long-wavelength irradiation ($\lambda_{exc.}$ = 532 nm) of azaferrocene in cyclohexane solution under an atmosphere of carbon monoxide led to the formation of an η^3-pyrrolyl species, (η^5-C_5H_5)Fe(CO)(η^3-*C*-C_4H_4N) which was identified by infrared spectroscopy. This η^3-bound monocarbonyl complex also gave rise to absorption in the visible region of the spectrum at ~640 nm. Further confirmation for this assignment would be best obtained from laser flash photolysis with time resolved infrared spectroscopic monitoring, as this method could provide structural detail (through the detecting of the ν_{CO} stretch) about this longer-lived transient species.

3.5 Conclusions

The data presented in this study is consistent with carbon monoxide loss as a principle result of the excited state decay in solution for of $(\eta^5\text{-}C_5H_5)Fe(CO)_2(\eta^1\text{-}C_4H_4N)$ and $(\eta^5\text{-}C_5H_5)Fe(CO)_2(\eta^1\text{-}C_8H_6N)$. These observations are in keeping with previous investigations on complexes $(\eta^5\text{-}C_5H_5)Fe(CO)_2R$, where R = halide or alkyl group.

Laser flash photolysis experiment in carbon monoxide saturated cyclohexane and toluene revealed a decay transient signal, which has been assigned to the formation of a monocarbonyl species, $(\eta^5\text{-}C_5H_5)Fe(CO)R$, R = $(\eta^1\text{-}C_4H_4N)$ or $(\eta^1\text{-}C_8H_6N)$ within the duration of the flash. This species is solvated and subsequently reacts with the carbon monoxide dissolved in the solvent to regenerate the parent species. The $\lambda_{max.}$ absorption for this monocarbonyl species is 430 and 480 nm for $(\eta^5\text{-}C_5H_5)Fe(CO)_2(\eta^1\text{-}C_4H_4N)$ and $(\eta^5\text{-}C_5H_5)Fe(CO)_2(\eta^1\text{-}C_8H_6N)$ respectively. The rate of decay (k_2) for the monocarbonyl species in carbon monoxide saturated toluene is 3 (±0.3) × 10^8 $M^{-1}s^{-1}$ and 1.99 (±0.2) × 10^8 $M^{-1}s^{-1}$ for $(\eta^5\text{-}C_5H_5)Fe(CO)_2(\eta^1\text{-}C_4H_4N)$ and $(\eta^5\text{-}C_5H_5)Fe(CO)_2(\eta^1\text{-}C_8H_6N)$ respectively. These rates are close to the diffusion controlled rate, and reflect the fact that the bond between the metal and the solvent in the intermediate species, $(\eta^5\text{-}C_5H_5)Fe(CO)(S)R$, R = $(\eta^1\text{-}C_4H_4N)$ or $(\eta^1\text{-}C_8H_6N)$ is weaker than that observed for groups six metals. The rate of reaction for the η^1-indolyl complex, $(\eta^5\text{-}C_5H_5)Fe(CO)_2(\eta^1\text{-}C_8H_6N)$ is marginally slower that that of the η^1-pyrrolyl complex, $(\eta^5\text{-}C_5H_5)Fe(CO)_2(\eta^1\text{-}C_4H_4N)$. This data indicates that the steric bulk of the co-ordinated η^1-indolyl may affect the rate of carbon monoxide attack on the iron-centre, however since the rate difference is small, it is unlikely that a ring-slip intermediate is involved, as this should have induced greater discrepancy between the rate constants.

While the time-resolved spectral properties and the dynamics of the intermediates formed by flash photolysis of the η^1-indolyl complex, $(\eta^5\text{-}C_5H_5)Fe(CO)_2(\eta^1\text{-}C_8H_6N)$ are quite similar to those of the η^1-pyrrolyl complex analogue, $(\eta^5\text{-}C_5H_5)Fe(CO)_2(\eta^1\text{-}C_4H_4N)$ under an atmosphere of carbon monoxide, they are quite different under an atmosphere of argon. Laser flash photolysis of $(\eta^5\text{-}C_5H_5)Fe(CO)_2(\eta^1\text{-}C_8H_6N)$ under argon revealed a second longer live transient species. It is proposed that this is due to the formation of a ring-slipped intermediate, $(\eta^5\text{-}C_5H_5)Fe(CO)(\eta^3\text{-}C\text{-}C_8H_6N)$.

The photochemistry of $(\eta^5\text{-}C_5H_5)Fe(CO)_2(\eta^1\text{-}C_4H_4N)$ examined in matrix isolation experiments provide infrared spectroscopic for the formation of a sixteen-electron monocarbonyl intermediate, $(\eta^5\text{-}C_5H_5)Fe(CO)(\eta^1\text{-}C_4H_4N)$, variations in the photolysis conditions also revealed the presence of ring-slip intermediate, the *exo*-azaallyl species, $(\eta^5\text{-}C_5H_5)Fe(CO)(\eta^3\text{-}N\text{-}C_4H_4N)$. Unfortunately a similar examination of the photochemistry of $(\eta^5\text{-}C_5H_5)Fe(CO)_2(\eta^1\text{-}C_8H_6N)$ with matrix isolation experiments was prohibited as this complex is not sufficiently volatile to sublime without decomposition.

3.6 References

1 X. Pan, C. E. Philbin, M. P. Castellani, D. R. Tyler, *Inorg. Chem.*, **1988**, 27, 671.

2 J. F. Eddicott, in 'Concepts in Inorganic Chemistry', A. W. Adamson, P. D. Fleischauer, Eds., Wiley Interscience, Nwy York, **1975**.

3 D. L. Lichtenberger, R. F. Fenske, *J. Am. Chem. Soc.*, **1976**, 98, 50.

4 L. H. Ali, A. Cox, T. J. Kemp, *J. Chem. Soc., Dalton Trans.*, **1973**, 1475.

5 (a) J. Zakrzewski, *J. Organomet. Chem.*, **1987**, 327, C41.
(b) J. Zakrzewski, C, Gionotti, *J. Organomet. Chem.*, **1990**, 388, 175.

6 (a) C. E. Borja, V. Jakúbek, A. L. Lees, *Inorg. Chem.*, **1998**, 37, 2281.
(b) A. L. Lees, *Co-ord. Chem. Rev.*, **2001**, 211, 255.

7 Y.-F. Hu, G. M. Bancroft, K. H. Tan, J. S. Tse, D. S. Yang, *Can. J. Chem.*, **1996**, 74, 2240.

8 C. Gianotti, G. Merle, *J. Organomet. Chem.*, **1976**, 105, 97.

9 (a) M. Wrighton, *Chem. Rev.*, **1974**, 74, 401.
(b) P. M. Treichel, R. L. Shubkin, K. W. Barnett, D. Reichard, *Inorg. Chem.*, **1966**, 5, 1177.
(c) R. B. King, P. N. Kapoor, M. S. Saran, R. N. Kapoor, *Inorg. Chem.*, **1971**, 10, 1851.
(d) R. B. King, P. N. Kapoor, R. N. Kapoor, *Inorg. Chem.*, **1971**, 10, 1841.
(e) R. B. King, W. C. Zipperer, M. Ishaq, *Inorg. Chem.*, **1972**, 11, 1361.

10 (a) D. G. Alway, K. W. Barnett, *Inorg. Chem.*, **1978**, 17, 2826.
(b) D. G. Alway, K. W. Barnett, *Adv. Chem. Ser.*, **1978**, 168, 115.

11 R. H. Hooker, K. A. Mahmoud, A. J. Rest, *J. Chem., Soc., Dalton Trans.*, **1990**, 1231.

12 (a) J. L. Hughey IV, C. R. Bock, T. J. Meyer, *J. Am. Chem. Soc.*, **1975**, 97, 4440.
(b) A, Albini, H. Kisch, *J. Am. Chem. Soc.*, **1976**, 98, 3869.
(c) J. M. Kelly, D. V. Bent, H. Hermann, D. Schultefröhlinde, E. Körner von Gustorf, *J. Organomet. Chem.*, **1974**, 69, 259.

13 D. B. Pourreau, G. L. Geoffroy, *Adv. Organomet. Chem.*, **1985**, 24, 249.

14 S. R. Su, A. Wojcicki, *J. Organomet. Chem.*, **1971**, 27, 231.

15 P. M. Treichel, R. L. Shubkin, K. W. Barnett, D. Reichard, *Inorg. Chem.*, **1966**, 5, 1177.

16 C. R. Folkes, A. J. Rest, *J. Organomet. Chem.*, **1977**, 136, 355.

17 D. J. Fettes, R. Narayanaswamy, A. J. Rest, *J. Chem., Soc., Dalton Trans.*, **1981**, 2311.

18 W. Gerhartz, G. Elberhorst, P. Dahler, P. Eilbracht, *Liebigs Ann. Chem.*, **1980**, 1296.

19 R. H. Hooker, A. J. Rest, I. Whitwell, *J. Organomet. Chem.*, **1984**, 266, C27.

20 J. K. Burdett, *Co-ord. Chem. Rev.*, **1987**, 17, 1.

21 R. J. Kazlauskas, M. S. Wrighton, *Organometallics*, **1982**, 1, 602.

22 K. L. McFarlene, P. C. Ford, *Organometallics*, **1998**, 17, 1166.

23 H. G. Alt, M. E. Eichner, B. M. Jansen, U. Thewalt, *Z. Naturforsch.*, **1982**, 37B, 1109.

24 K. A. Mahmoud, A. J. Rest, H. G. Alt, *J. Chem. Soc., Dalton Trans.*, **1985**, 1365.

25 A. Hudson, M. F. Lappert, W. B. Lednor, J. J. MacQuitty, B. K. Nicholson, *J. Chem. Soc.,*

Dalton Trans., **1981**, 2159.

26 (a) G. O. Nelson, M. E. Wright, *J. Organomet. Chem.*, **1980**, 206, C21.

(b) G. O. Nelson, M. E. Wright, *J. Organomet. Chem.*, **1982**, 239, 353.

(c) A. V. Nesmeyanov, T. B. Chenskaya, G. N. Babakhina, I. I. Kritskaya, *Bull. Acad. Sci. USSR, Div. Chem. Sci., (Engl. Transl.)*, **1970**, 1129.

27 J. P. Blaha, M. S. Wrighton, *J. Am. Chem. Soc.*, **1985**, 107, 2694.

28 M. H. L. Green, P. L. I. Nagy, *J. Chem. Soc.*, **1963**, 189.

29 R. B. King, M. Ishaq, *Inorg. Chim. Acta*, **1970**, 4, 258.

30 J. W. Faller, B. V. Johnson, T. P. Dryja, *J. Organomet. Chem.*, **1974**, 105. 395.

31 R. W. Fish, W. P. Giering, D. Marten, M. Rosenblum, *J. Organomet. Chem.*, **1976**, 105, 101.

32 J. A. Belmont, M. S. Wrighton, *Organometallics*, **1986**, 5, 1481.

33 N. E. Carpenter, M. A. Khan, K. M. Nicholas, *Organometallics*, **1999**, 18, 1569.

34 (a) C. Pollak, A. Rosa, E. J. Baerends, *J. Am. Chem. Soc.*, **1997**, 119, 7324.

(b) E. J. Baerends, A. Rosa, *Coord. Chem. Rev.*, **1998**, 177, 97.

35 A. Gilbert, J. M. Kelly, M. Budazwait, E. Körner von Gustorf, *Z. Naturforsch.*, **1976**, 316, 1091.

36 C. J. Breheny, J. M. Kelly, C. Long, S. O'Keeffe, M. T. Pryce, G. Russell, M. M. Walsh, *Organometallics*, **1998**, 17, 3690.

37 C. Hall, R. N. Perutz, *Chem. Rev.* **1996**, 96, 3125.

38 J. D. Simon, X. L. Xie, *J. Phys. Chem.*, **1986**, 90, 6751.

39 X. L. Xie, J. D. Simon, *J. Am. Chem. Soc.*, **1990**, 112, 1130.

40 J. M. Kelly, H. Hermann, E. Körner von Gustorf, *J. Chem. Soc., Chem. Comm.*, **1973**, 105.

41 B. S. Creaven, M. W. George, A. G. Ginsburg, C. Hughes, J. M. Kelly, C. Long, I. McGrath, M. T. Pryce, *Organometallics*, **1993**, 12, 3127.

42 S. K. Nayak, T. J. Burkey, *Organometallics*, **1991**, 10, 3745.

43 (a) H. Angermund, A.K. Bandyopadhyay, F.-W. Grevels, F. Mark, *J. Am. Chem. Soc.*, **1989**, 111, 4656.

(b) M. A .Shröder, M. S. Wrighton, *J. Am. Chem. Soc.*, **1976**, 98, 551.

44 (a) S. P. Church, F.-W. Grevels, H. Hermann, J. Kelly, W. E. Klotzbücher, K. Schaffner, *J. Chem. Soc., Chem. Commun.* **1985**, 594.

(b) S. K. Nayak, T. J. Burkey, *Inorg. Chem.*, **1992**, 3, 1125.

45 S. N. Nayak, T. J. Burkey, *J. Am. Chem. Soc.*, **1993**, 115, 6391.

46 (a) T. J. Burkey in '*Energetics of organometallic species*', J. A. Martinoho Simoes Ed., NATO Series C no. 367, Kluwer, Dordrecht, **1992**, 75.

47 J. E. Coleman, K. E. Dulaney, A. A. Bengali, *J. Organomet. Chem.*, **1999**, 572, 65.

48 A. A. Bengali, *Organometallics*, **2000**, 19, 4000.

49 J. Down, S. C. Peake, *Specialist periodical Reports, Chemical Society*, London, **1973**, 1, 535.

J. J. Turner, in *Matrix Isolation Spectroscopy*, A. J. Barnes, W. Orville-Thomas Eds., Reidel Publishing Co., Boston, **1981**, 496.

50 A. J. Rest, J. R. Sodeau, D. J. Taylor, *J. Chem. Soc., Dalton Trans.*, **1978**, 651.

51 (a) A.J.Hart-Davis, R. J. Mawby, *J. Chem. Soc., A*, **1969**, 2403.

(b) A. J. Hart-Davis, C. White, R. J Mawby, *Inorg. Chem.*, **1970**, 4, 441.

(c) C. White, R. J. Mawby, *Inorg. Chim Acta*, **1970**,4, 261.

(d) D. J. Jones, R. J. Mawby, *Inorg, Chim Acta*, **1972**, 6, 157.

(f) M. E. Rerek, L.-N. Ji, F. Basolo, *J. Chem. Soc., Chem. Commun.*, **1983**, 1208.

(g) L.-N. Ji, M. E. Rerek, F. Basolo, *Organometallics*, **1984**, 3, 740.

Chapter Four

4 The photochemistry of 2,5-dimethylazaferrocene

4.1 Literature survey acyl iron complexes, (η^5-C_5H_5)Fe(CO)(L)(COR),(L = CO, phosphite or phosphate, R = alkyl groups)

In chapter one of this thesis, the photochemistry of the half-sandwich complexes of the type (η^6-2,6-$X_2C_5H_3N$)$Cr(CO)_3$ was discussed and it was shown that ring slippage of the η^6-co-ordinated aromatic ligand, leading to a *N*-co-ordinated pyridine was the dominant process upon irradiation with visible light. Carbon monoxide dissociation dominated under UV irradiation. Steric hindrance of the 2,6-positions on the pyridine ligand did not restrict the formation of (η^1-2,6-$X_2C_5H_3N$)$Cr(CO)_3$ primary photoproducts, but it did prevent the formation of stable hexa-co-ordinated products such as (η^1-2,6-$X_2C_5H_3N$)$Cr(CO)_3(N_2)_2$ or (η^1-2,6-$X_2C_5H_3N$)$Cr(CO)_5$.

In the case of azaferrocene, chapter two contains evidence that irradiation with visible light also leads to photoinduced ring-slip photoproducts, i.e. (η^5-C_5H_5)$Fe(CO)_2$(η^1-C_4H_4N) and (η^5-C_5H_5)$Fe(CO)_2$(η^3-C_4H_4N). The apparent yield of the η^1-type species formed following photolysis was greater than that of the η^3-type, based on the intensity of the infrared bands. In view of these observations, an investigation into the photochemistry of 2,5-dimethylazaferrocene was carried out. This was undertaken in order to establish whether the presence of bulky substituents α, α' to the nitrogen atom in the pyrrolyl ligand would hinder the formation of the η^1-type species and possibly stabilise an η^3-type species.

Although carbon monoxide insertion/alkyl migration was mentioned as one of four different photochemical processes which can occur upon irradiation of (η^5-C_5H_5)$Fe(CO)_2R$ complexes[1] (where R = alkyl or aryl ligand), such reactions were not explored to any great extent in chapter three because of the dominance of carbon monoxide dissociation following irradiation of (η^5-C_5H_5)$Fe(CO)_2R$ complexes. However, since the photolysis of 2,5-dimethylazaferrocene is complicated by the

formation of (η^5-C_5H_5)Fe(CO)$_2$(COR) species, a study of the formation of acyl species and their subsequent thermal and/or photochemistry is important.

The formation of acyl complexes of the type CpFe(CO)$_2$(COR) is usually achieved by the thermal reaction of the alkyl complex, CpFe(CO)$_2$R with a ligand, L, (L = CO, EPh$_3$, where E = P, As, or Sb).[2] Under mild thermal conditions the reaction yields CpFe(CO)(L)(COR) according to Reaction 4-1 below.

$$CpFe(CO)_2(R) + L \xrightarrow{\Delta} CpFe(CO)(L)(COR)$$

Reaction 4-1

However it should be noted that, forcing conditions (125°C and ~140 atm CO) are required to obtain the acyl complex, CpFe(CO)$_2$(COCH$_3$) when the incoming ligand is carbon monoxide.[3] The only report of photochemical formation of acyl complexes was by Gingell and Rest.[4] They reported that irradiation of CpFe(CO)$_2$CH$_3$ in the presence of EPh$_3$ in acetonitrile at 20°C yields the acetyl complex CpFe(CO)(EPh$_3$)(COCH$_3$), (where E = As or Sb). A subsequent ^{1}H NMR investigation of the photochemical reaction of CpFe(CO)$_2$CH$_3$ with ligands EPh$_3$ (E = P, As, or Sb) at 300 K by Folkes and Rest,[1(b)] reported that formation of the alkyl complex dominates, although at 293 K appreciable amounts of the acyl complex were formed. It was suggested that the extra energy available in these photolysis reactions at higher temperature was sufficient to eject the labilised carbon monoxide from the solvent cage[5] and so prevent the secondary formation of the acyl complex. These results are in contrast to those[1(a),,6] obtained for the photochemical reaction of CpFe(CO)$_2$R with phosphine donors, which yielded acyl complexes along with the expected photoproduct CpFe(CO)(L)(R). However in these instances, the solutions were also heated upon photolysis, and formation of the acyl product was suggested to be a competing thermal process.

Normally decarbonylation of transition metal acyl complexes can be achieved under more vigorous thermal conditions.[7] However, acyl complexes of the type CpFe(CO)$_2$(COR) have been shown to be inert to thermal decarbonylation[3,8] and that

decarbonylation is only achieved following photolysis.[2] Electron Spin Resonance (ESR) studies revealed[9] the presence of radicals following the photolysis of $CpFe(CO)_2(CH_3)$ in the absence of an incoming nucleophile, however similar studies on the acyl complex $CpFe(CO)_2(COCH_3)$ indicates that photolysis does not cause M-R homolysis because $CH_3CO^{\bullet}$ radicals were not detected. Studies[10] using a ^{13}C labelled acyl group have revealed that the photochemical decarbonylation reaction involves the terminal carbon monoxide ligand rather than the carbonyl group of the acyl because the ^{13}C label in the acyl group of $(\eta^5\text{-}C_5H_5)Fe(CO)_2(^{13}COCH_3)$ was fully retained in the alkyl product, $(\eta^5\text{-}C_5H_5)Fe(CO)(^{13}CO)CH_3$. $(\eta^5\text{-}C_5H_5)Fe(CO)(COCH_3)$ was proposed as the reactive intermediate in the photochemical decarbonylation. Alexander[10] demonstrated that $(\eta^5\text{-}C_5H_5)Fe(CO)(COCH_3)$ had a sufficient lifetime to be trapped by PPh_3 to give $(\eta^5\text{-}C_5H_5)Fe(CO)(^{13}COCH_3)(PPh_3)$ in competition with the methyl migration process.

Rest *et al.*[11] continued their investigation of the acyl complex, $(\eta^5\text{-}C_5H_5)Fe(CO)_2(COCH_3)$ in frozen gas matrixes at 12 K. Photolysis of $(\eta^5\text{-}C_5H_5)Fe(CO)_2(COCH_3)$ in methane, argon, dinitrogen and carbon monoxide matrixes produced $(\eta^5\text{-}C_5H_5)Fe(CO)_2CH_3$ *via* the co-ordinatively unsaturated intermediate $(\eta^5\text{-}C_5H_5)Fe(CO)(COCH_3)$. This intermediate was also observed following the photolysis in polyvinyl chloride (PVC) film matrices[12] at 12 K. As PVC films provide a larger working temperature range than frozen gas matrices, these experiments showed that the back reaction of $(\eta^5\text{-}C_5H_5)Fe(CO)(COCH_3)$ with carbon monoxide occurs upon warming the film to *ca.* 200 K regenerating the parent $(\eta^5\text{-}C_5H_5)Fe(CO)_2(COCH_3)$ and $(\eta^5\text{-}C_5H_5)Fe(CO)_2(CH_3)$.

In the last decade Ford *et al.*[13,14,15,16] have investigated the photochemistry of the acyl complex $(\eta^5\text{-}C_5H_5)Fe(CO)_2(COCH_3)$ with time-resolved infrared (TR-IR) and low temperature FT-IR. These studies showed that UV photolysis generates a reactive intermediate $(\eta^5\text{-}C_5H_5)Fe(CO)(COCH_3)$ by dissociation of a terminal carbonyl group, the intermediate then underwent rearrangement to yield the methyl complex, $(\eta^5\text{-}C_5H_5)Fe(CO)_2CH_3$ with high quantum efficiency (Φ = 0.62 in organic solvents). For pressures of carbon monoxide up to one atmosphere, this quantum yield remains constant, indicating that the back-reaction of the intermediate (I), Scheme 4-1 with

carbon monoxide is not competitive with methyl migration, k_m, at concentrations of carbon monoxide ≤0.001 M. However, photolysis in the presence of trapping ligands (L) such as PPh_3 and $P(OCH_3)_3$ ([L]> 0.001 M), k_l, gives rise to the substituted acyl product $CpFe(CO)(L)(COCH_3)$.

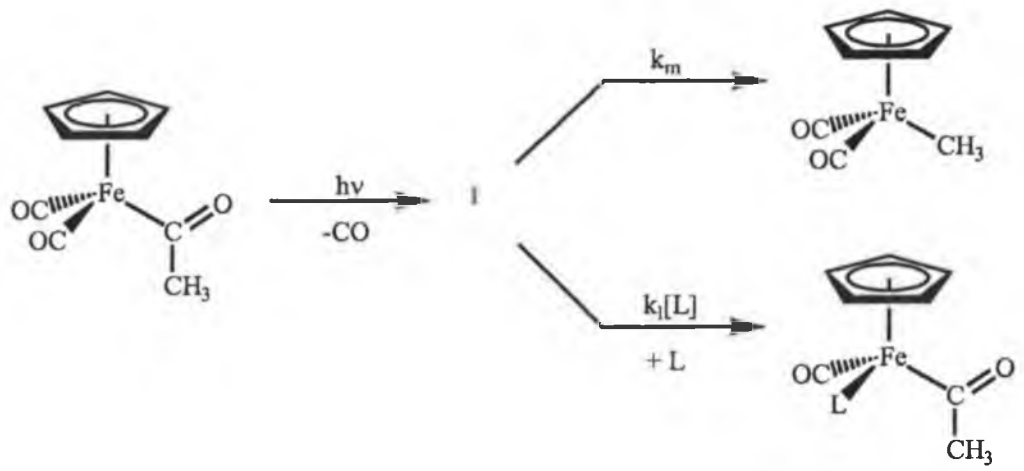

Scheme 4-1

4.2 Carbon-hydrogen bond activation

There are many examples of transition metal complexes capable of activating carbon-hydrogen bonds.[17] In the case of oxidative addition two processes occur, intermolecular activation, refer to general reaction, Reaction 4-2 or intramolecular activation, refer to general reaction, Reaction 4-3.

Reaction 4-2 Intermolecular carbon-hydrogen activation.

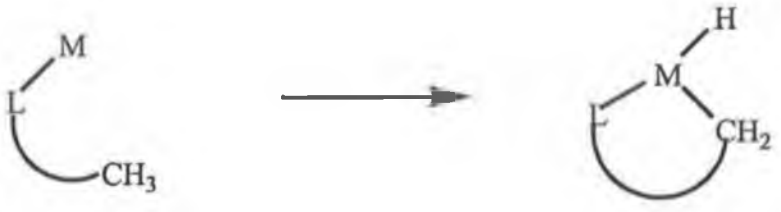

Reaction 4-3 Intramolecular carbon-hydrogen activation.

The insertion of the metal into the C-H bond of a ligand already attached to the metal, as outlined in Reaction 4-3 is a ubiquitous process when aromatic or otherwise activated C-H bonds are involved. Chatt and Davidson's[18] study of $[Ru(dmpe)_2]$ (dmpe = $(CH_3)_2PCH_2CH_2P(CH_3)_2$) was the first example of the cyclometallation of sp^3 C-H bonds. This complex spontaneously cyclometallates at the phosphorus metal groups and also reacts with free naphthalene to give *cis*-$[Ru(Np)(H)dmpe_2]$, (Np = 2-naphthalyl), as outlined in Reaction 4-4. This reaction was the first definite connection between inter-and intramolecular varieties of C-H bond activation.

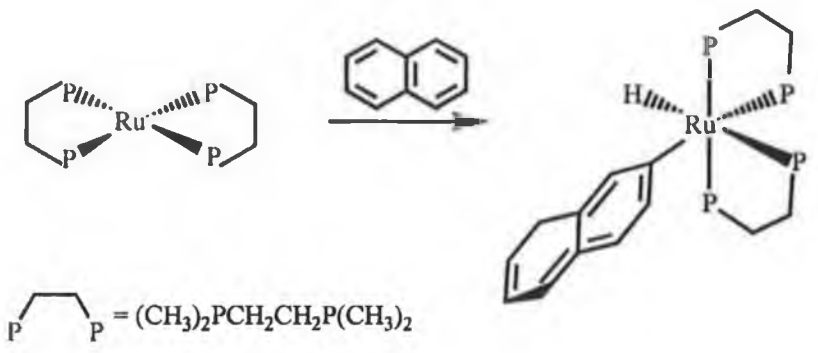

Reaction 4-4 Chatt and Davidson 1965.[18]

Discoveries in the early nineteen eighties showed that $(\eta^5\text{-}C_5R_5)Ir(CO)_2$, (R = H or CH_3) could photochemically activate C-H bonds in methane,[19] neopentane[20], cyclohexane[20] and benzene,[20] and that $[(\eta^5\text{-}C_5R_5)M(PPh_3)H_2]$, (M = Rh[21] or Ir[22]) could similarly activate C-H bonds in alkanes, thus indicating that the aim to activate the C-H bonds in alkanes *via* an intermolecular oxidative reaction is attainable under mild conditions. Since these early reports, efforts to identify the mechanism for the reaction have employed a full range of spectroscopic techniques. Investigations in low temperature gas matrices,[23] in low temperature hydrocarbon matrices,[24] in liquid noble gases,[25] and experiments in the gas phase[26] have identified the first steps of the reaction. It is thought to begin by the initial dissociation of a ligand from the electronically saturated (eighteen-electron) metal complex to form an electronically unsaturated sixteen-electron intermediate, refer to Figure 4-1. This reactive sixteen-electron intermediate rapidly

forms a complex or solvate with an alkane molecule, and in a subsequent step, the complexed alkane undergoes oxidative addition at the metal centre.

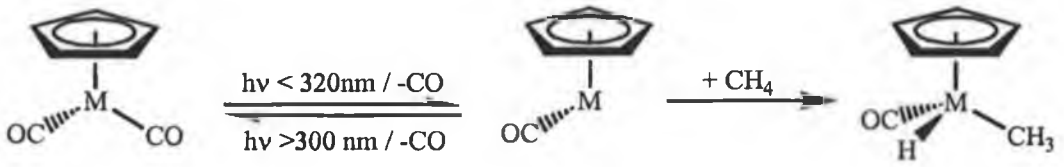

M = Rh or Ir, η^5-ring = cyclopentadienyl or pentamethylacyclopentadienyl

Figure 4-1 Intermolecular C-H bond activation observed in a methane matrix.[23]

The mechanistic details of the subsequent bond activation step are not well understood because of the difficulties in characterising short-lived alkane complex intermediates. Therefore ultra-fast spectroscopic investigations of the highly substituted $(\eta^5\text{-}C_5(CH_3)_5)M(CO)_2$ complexes have been undertaken. However, because of their low quantum yields for carbon monoxide dissociation, the reactive intermediates involved in C-H bond activation reactions formed from $(\eta^5\text{-}C_5(CH_3)_5)M(CO)_2$ have not been detected in these studies at room temperature.[27] Fortunately, the unmethylated complex, $(\eta^5\text{-}C_5H_5)Rh(CO)_2$ has higher quantum yields for carbon monoxide loss compared to the methylated $(\eta^5\text{-}C_5(CH_3)_5)Rh(CO)_2$ analogue, thereby enabling observation of the reactive intermediate directly in room temperature solutions and allowing investigation of the reaction up to 1 ns following the laser flash photolysis.[28] The reactive intermediate in a cyclohexane C-H bond activation reaction by, $(\eta^5\text{-}C_5H_5)Rh(CO)_2$ has been identified as the cyclohexane solvated species, $(\eta^5\text{-}C_5H_5)Rh(CO)(C_6H_{12})$ by sub-pico second infrared spectroscopy. It appears that partial detachment or ring slippage of the cyclopentadienyl ligand is not a contributing factor in the C-H bond activation pathway.

Photolysis of a number of arene osmium complexes have also been found to activate the C-H bonds of methane.[29] Photolysis of $(\eta^6\text{-}C_6H_3(CH_3)_3)Os(CO)H_2$ and $(\eta^6\text{-}C_6H_3(CH_3)_3)Os(CO)(CH_3)(H)$ in an argon gas matrix resulted in the reductive elimination product $(\eta^6\text{-}C_6H_3(CH_3)_3)Os(CO)$. Irradiation of $(\eta^6\text{-}C_6H_3(CH_3)_3)Os(CO)H_2$

in a methane matrix led to the production of the C-H activated product, (η^6-$C_6H_3(CH_3)_3$)Os(CO)(CH_3)(H). Furthermore, the irradiation of (η^6-$C_6H_3(CH_3)_3$)$Os(CO)_2$ in methane matrix also induces formation of the C-H activation product, (η^6-$C_6H_3(CH_3)_3$)Os(CO)(CH_3)(H). As in the case of the rhodium and iridium complexes, the initial photo-dissociation of either an carbon monoxide ligand or H_2 is postulated as the first step in the reaction mechanism, followed by insertion of the sixteen-electron intermediate into the methane molecule.

4.3 The photochemistry of 2.5-dimethylazaferrocene

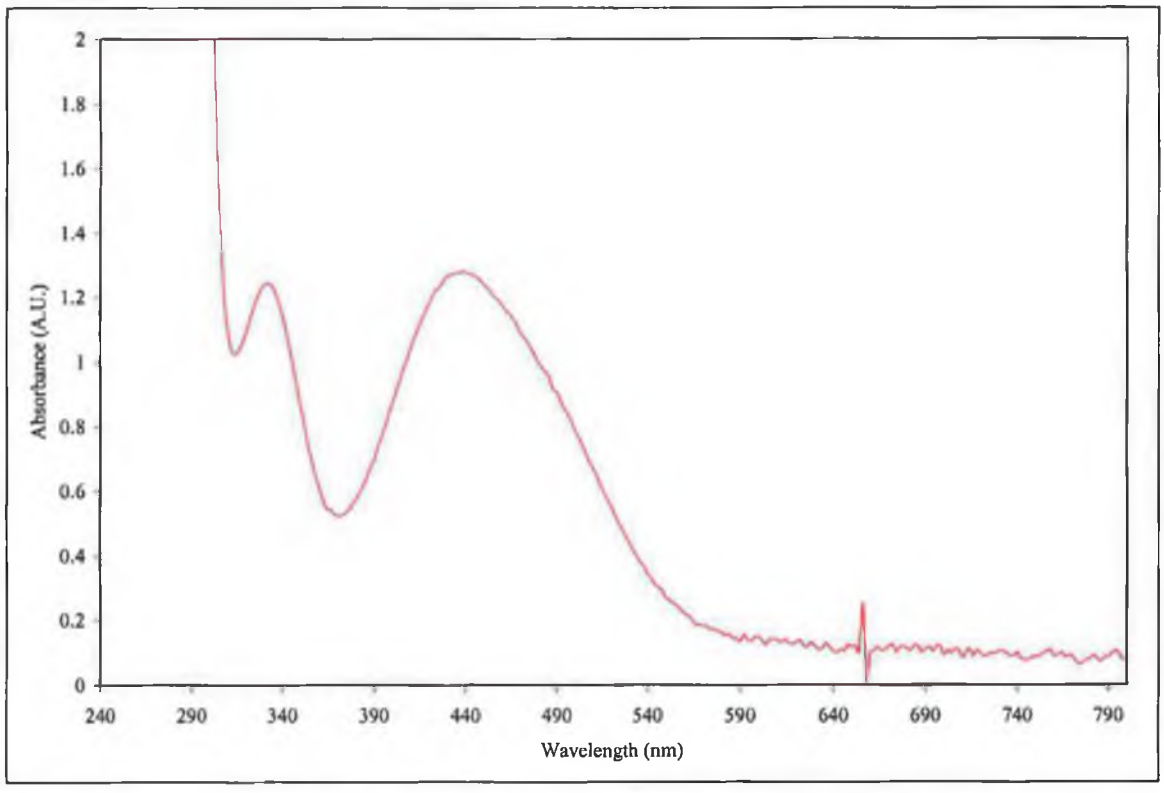

Figure 4-2 UV-vis spectrum of 2,5-dimethylazaferrocene, (η^5-C_5H_5)Fe(η^5-2,5-$(CH_3)_2C_4H_2N$) (~8.8×10^{-3} M) in cyclohexane.

The UV-vis spectrum of 2,5-dimethylazaferrocene, (η^5-C_5H_5)Fe(η^5-2,5-$(CH_3)_2C_4H_2N$) in cyclohexane as shown in Figure 4-2 displays relatively strong absorptions centred at λ = 336 nm ($\varepsilon = 1.37 \times 10^2$ L $mol^{-1}cm^{-1}$) and λ = 446 nm ($\varepsilon = 1.41 \times 10^2$ L $mol^{-1}cm^{-1}$), and it also exhibits an absorption tail right into the visible region of the spectrum (λ ~ 580 nm). The UV-vis spectrum of 2,5-dimethylazaferrocene is very similar to azaferrocene.

4.3.1 Broad band steady state photolysis of 2,5-dimethylazaferrocene monitored by UV-vis spectroscopy

All samples were degassed by three freeze-pump-thaw cycles before addition of either argon or carbon monoxide gas at one atmosphere pressure.

Photolysis of 2,5-dimethylazaferrocene, $\lambda_{exc.} > 500$ nm in degassed solvent under an argon atmosphere produced the spectral changes presented in Figure 4-3. Photolysis of the solution for one minute produced a decrease in the absorption across the entire spectrum. Since the absorption changes in the UV spectrum were found to be small following this irradiation period, subsequent irradiation times were increased. The total photolysis time was fifty-five minutes. This is substantially longer than for azaferrocene under similar conditions (i.e. three minutes). The changes in the UV spectrum were also different from those obtained with azaferrocene. Initially the absorption was reduced (first minute) and then increased across the whole spectrum until four minutes of photolysis had elapsed. Subsequent photolysis resulted in reduction in absorption. It is also evident from that the sample became turbid during photolysis. In addition, no isosbestic points were obtained during the course of the experiment. None of the components in this reaction have intense diagnostic absorptions in the infrared region thereby prohibiting the use of infrared spectroscopy as a means of identifying the photoproducts.

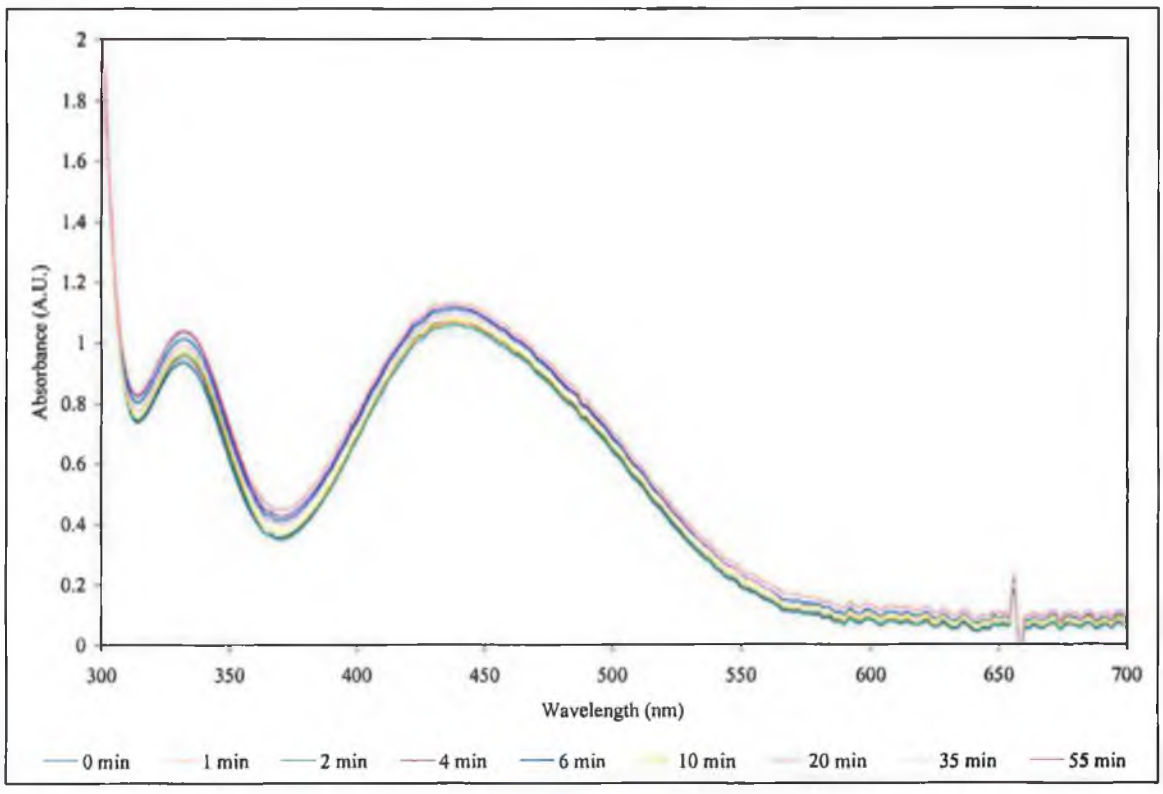

Figure 4-3 Changes observed in the UV-vis spectrum of (η^5-C_5H_5)Fe(η^5-2,5-$(CH_3)_2C_4H_2N$) (~6.6×10^{-3} M) in cyclohexane following photolysis at $\lambda_{exc.} > 500$ nm under an atmosphere of argon.

Following the photolysis experiments on azaferrocene, it was apparent that carbon monoxide was a useful trapping as the photoproducts, which result from co-ordination of carbon monoxide to the metal centre, are relatively stable. The infrared absorptions of the carbon monoxide ligand co-ordinating to the metal centre provide a convenient spectroscopic method for the detection of the photoproducts, in addition to the fact that carbonyl-stretching frequencies are quite sensitive to co-ordination modes of the remaining ligands in the photoproducts.

Broad band photolysis ($\lambda_{exc.} > 500$ nm) of 2,5-dimethylazaferrocene in cyclohexane, which had been saturated with carbon monoxide, resulted in an increase across the entire UV-vis spectrum, with no indication that the sample was becoming turbid, Figure 4-4.

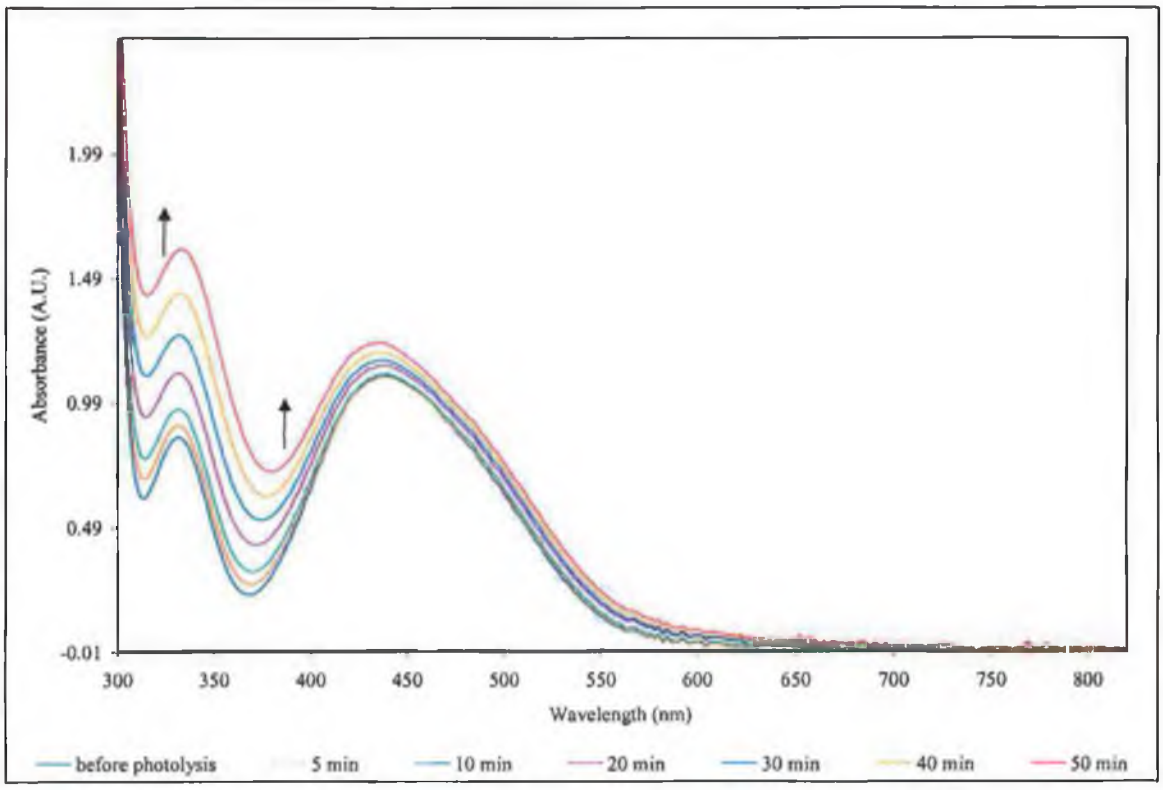

Figure 4-4 Changes observed in the UV-vis spectrum of $(\eta^5\text{-}C_5H_5)Fe(\eta^5\text{-}2,5\text{-}(CH_3)_2C_4H_2N)$ (~6×10^{-3} M) following photolysis at $\lambda_{exc.} > 500$ nm, in carbon monoxide saturated cyclohexane.

Following photolysis the solution volume was reduced under reduced pressure and an infrared spectrum of the solution was obtained. The spectrum contains nine bands in the carbonyl region at 2041, 2022, 2015, 2005, 1995, 1974, 1966, 1961, and 1793 cm^{-1}, refer to Figure 4-5. The dominant ν_{CO} bands at 2041 and 1995 cm^{-1} have been assigned to the $(\eta^5\text{-}C_5H_5)Fe(CO)_2(\eta^1\text{-}2,5\text{-}(CH_3)_2C_4H_2N)$ species, as the separation of 46 cm^{-1} is typical of a dicarbonyl complex. The wavenumber difference between the anti-symmetric and symmetric vibrational modes (46 cm^{-1}) is the same as the difference observed for $(\eta^5\text{-}C_5H_5)Fe(CO)_2(\eta^1\text{-}C_4H_4N)$ (46 cm^{-1}) and similar to the difference observed for $(\eta^5\text{-}C_5H_5)Fe(CO)_2CH_3$ (56 cm^{-1}).[30] Efforts to isolate $(\eta^5\text{-}C_5H_5)Fe(CO)_2(\eta^1\text{-}2,5\text{-}(CH_3)_2C_4H_2N)$ by an independent method failed however.

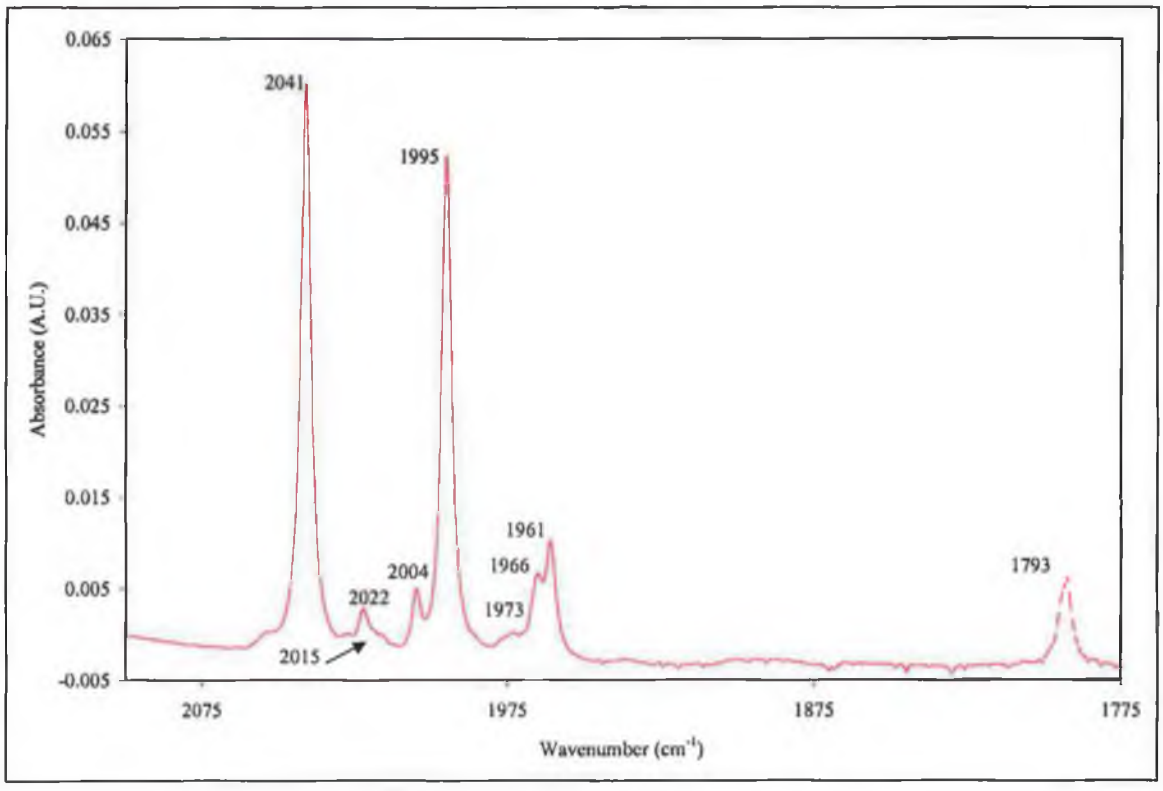

Figure 4-5 Infrared spectrum of $(\eta^5\text{-}C_5H_5)Fe(\eta^5\text{-}2,5\text{-}(CH_3)_2C_4H_2N)$ following photolysis at $\lambda_{exc.} > 500$ nm, in carbon monoxide saturated cyclohexane.

The three ν_{CO} bands at 2004, 1961 and 1793 cm^{-1} are assigned to the iron dimer, $[(\eta^5\text{-}C_5H_5)Fe(CO)_2]_2$, by comparison with an authentic sample from Aldrich Chemical Co. Based on infrared band intensities the yield of the dimer species appears to be low. The formation of the dimer species is not without precedence, it was also produced following photolysis of $(\eta^5\text{-}C_5H_5)Fe(CO)_2I$ in the presence of DMSO or pyridine.[31] The remaining two ν_{CO} bands at 2015 and 1966 cm^{-1} are relatively weak, and these are assigned to $(\eta^5\text{-}C_5H_5)Fe(CO)_2(CH_2\text{-}C_4H_2(CH_3)NH)$, while the remaining bands at 2022 and 1973 cm^{-1} are assigned to $(\eta^5\text{-}C_5H_5)Fe(CO)_2(COCH_2\text{-}C_5H_6N)$. Further discussion of the assignment of these bands to these species is forthcoming in the discussion of the photolysis results obtained with infrared spectroscopic monitoring.

4.3.2 *Broad band steady state photolysis ($\lambda_{exc.} > 500$ nm) of 2,5-dimethyl-azaferrocene monitored by infrared spectroscopy*

A solution of 2,5-dimethylazaferrocene in cyclohexane was fully degassed by the freeze-pump-thaw technique and an atmosphere of carbon monoxide added to the photolysis cell. Samples were removed by syringe from the photolysis cell and the infrared spectra recorded in an infrared solution cell.

Broad band photolysis ($\lambda_{exc.}$ > 500 nm) of 2,5-dimethylazaferrocene in carbon monoxide saturated cyclohexane solution resulted in the spectral changes presented in Figure 4-6. Nine new bands grew in the ν_{CO} region of the infrared spectrum at 2041, 2022, 2015, 2004, 1995, 1973, 1966, 1961 and 1793 cm^{-1}. The bands at 2041 and 1995 cm^{-1} are assigned to the photoproduct $(\eta^5\text{-}C_5H_5)Fe(CO)_2(\eta^1\text{-}2,5\text{-}(CH_3)_2C_4H_2N)$ as in the UV-vis monitored experiments described previously in Section 4.3.1. The bands at 2004, 1961 and 1793 cm^{-1} are those of the iron dimer $[(\eta^5\text{-}C_5H_5)Fe(CO)_2]_2$, confirmed by comparison with an authentic sample obtained from Aldrich Chemical Co. The remaining bands at 2022, 2015, 1973 and 1966 cm^{-1} would appear to be the result of secondary thermal or photochemical reactions of the η^1-substituted pyrrolyl dicarbonyl, $(\eta^5\text{-}C_5H_5)Fe(CO)_2(2,5\text{-}(CH_3)_2C_4H_2N)$. These bands have been tentatively assigned to Species 4-1, $(\eta^5\text{-}C_5H_5)Fe(CO)_2(CH_2\text{-}C_4H_2(CH_3)NH)$ and an acyl Species 4-2, $(\eta^5\text{-}C_5H_5)Fe(CO)_2(COCH_2\text{-}C_5H_6N)$, refer to Figure 4-7. These assignments were made with reference to recent literature,[13,32] which reported the ν_{CO} stretching bands for $(\eta^5\text{-}C_5H_5)Fe(CO)_2CH_3$ and $(\eta^5\text{-}C_5H_5)Fe(CO)_2(COCH_3)$ were at 2015 and 1959 cm^{-1} and 2018, 1963, 1669 (ν_{CO}-acyl) cm^{-1} in cyclohexane respectively.

Both of these complexes would be expected to display a $\nu_{N\text{-}H}$ stretch in their infrared spectra. There is a very weak band at 3482 cm^{-1}, which increases upon photolysis, which could be evidence of an $\nu_{N\text{-}H}$ stretch. However the $\nu_{N\text{-}H}$ stretch for pyrroles usually lie in the range 3450-3225 cm^{-1}, so it is difficult to be certain of this assignment.

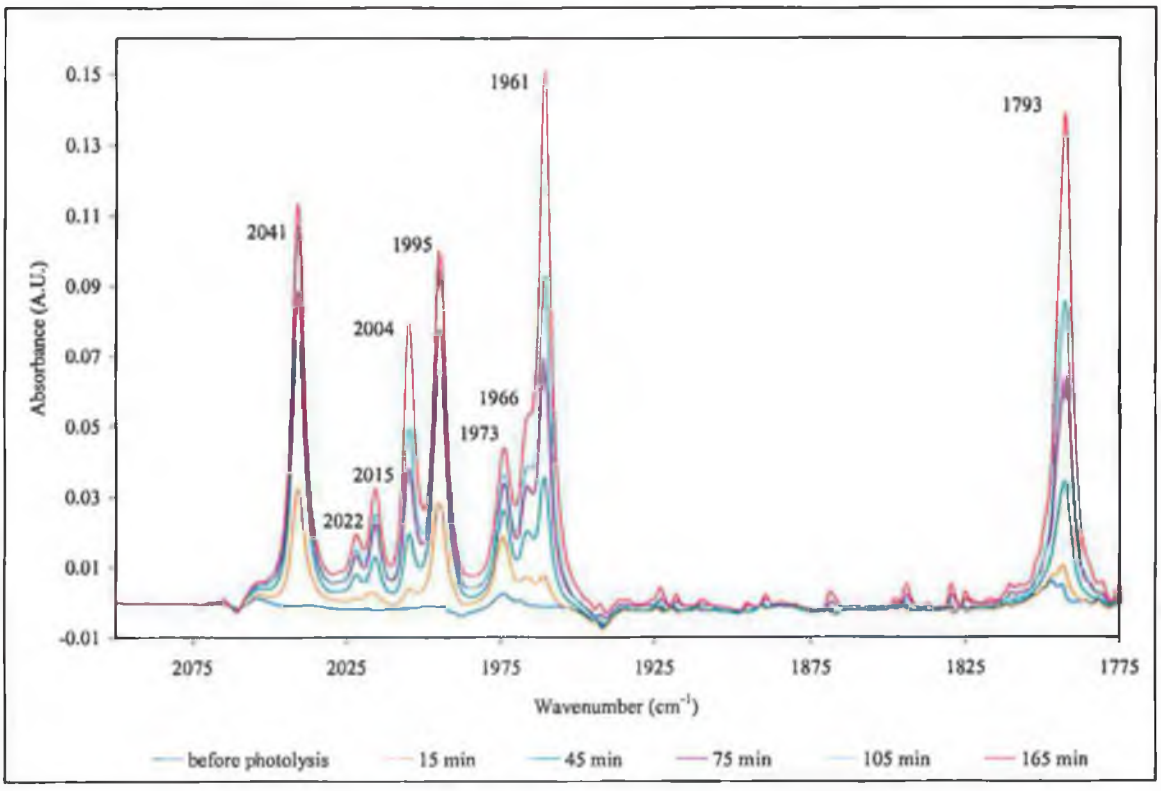

Figure 4-6 The ν_{CO} region spectral changes upon the broad band photolysis ($\lambda_{exc.}$ > 500 nm) of (η^5-C_5H_5)Fe(η^5-2,5-$(CH_3)_2C_4H_2N$) in carbon monoxide saturated solution.

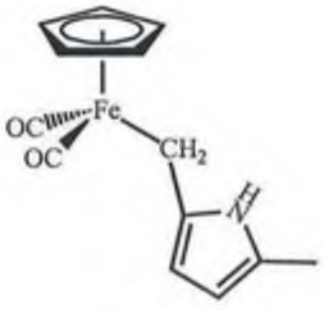

2015, 1966 cm^{-1}

Species 4-1

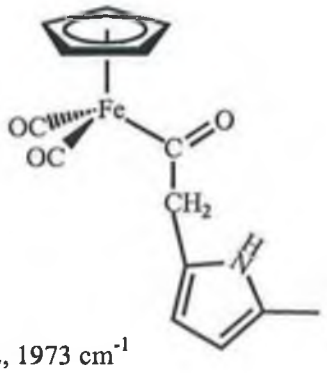

2022, 1973 cm^{-1}

Species 4-2

Figure 4-7 Proposed species assigned to the ν_{CO} bands at 2022, 2015, 1974 and 1966 cm^{-1} respectively.

The detection of an acyl ν_{CO} band in order to confirm the presence of Species 4-2 was unfortunately not achieved. This may have been because the acyl ν_{CO} mode possesses a reduced intensity compared with those of the terminal ν_{CO} modes. Also, the 1500-1600

cm^{-1} region of the spectrum where the acyl ν_{CO} mode should be located is spoiled by absorptions caused by water in the atmosphere and absorptions by the solvent (cyclohexane) used for these photolysis experiments. Attempts to remove the water absorptions by purging the infrared spectrometer before and during the experiment failed to remove these undesirable absorptions.

Photolysis of 2,5-dimethylazaferrocene with higher energy broad band irradiation ($\lambda_{exc.}$ > 410 nm), resulted in significant formation of the dimeric species, $[(\eta^5\text{-}C_5H_5)Fe(CO)_2]_2$, and significantly less formation of the dicarbonyl species, $(\eta^5\text{-}C_5H_5)Fe(CO)_2(2,5\text{-}(CH_3)_2C_4H_2N)$, based on the relative intensities of the ν_{CO} bands for each species. There was no evidence of the formation of the additional carbonyl containing species a described above following lower energy broad band photolysis ($\lambda_{exc.}$ > 500 nm).

Low-energy monochromatic pulsed photolysis ($\lambda_{exc.}$ = 532 nm) of 2,5-dimethylazaferrocene in a carbon monoxide saturated cyclohexane solution at room temperature produced very similar changes in the infrared spectra, refer to Figure 4-8, as those induced upon broad band photolysis ($\lambda_{exc.}$ > 500 nm). Following monochromatic photolysis at 532 nm, the relative intensity of most of the bands are identical, with the exception of those bands assigned to the dimeric species, $[(\eta^5\text{-}C_5H_5)Fe(CO)_2]_2$ at 2004, 1961, and 1793 cm^{-1}. The intensity of these ν_{CO} bands is much greater following broad band photolysis, therefore it appears that the formation of iron dimer is not as efficient following low energy monochromatic photolysis, as it is following low-energy broad band photolysis.

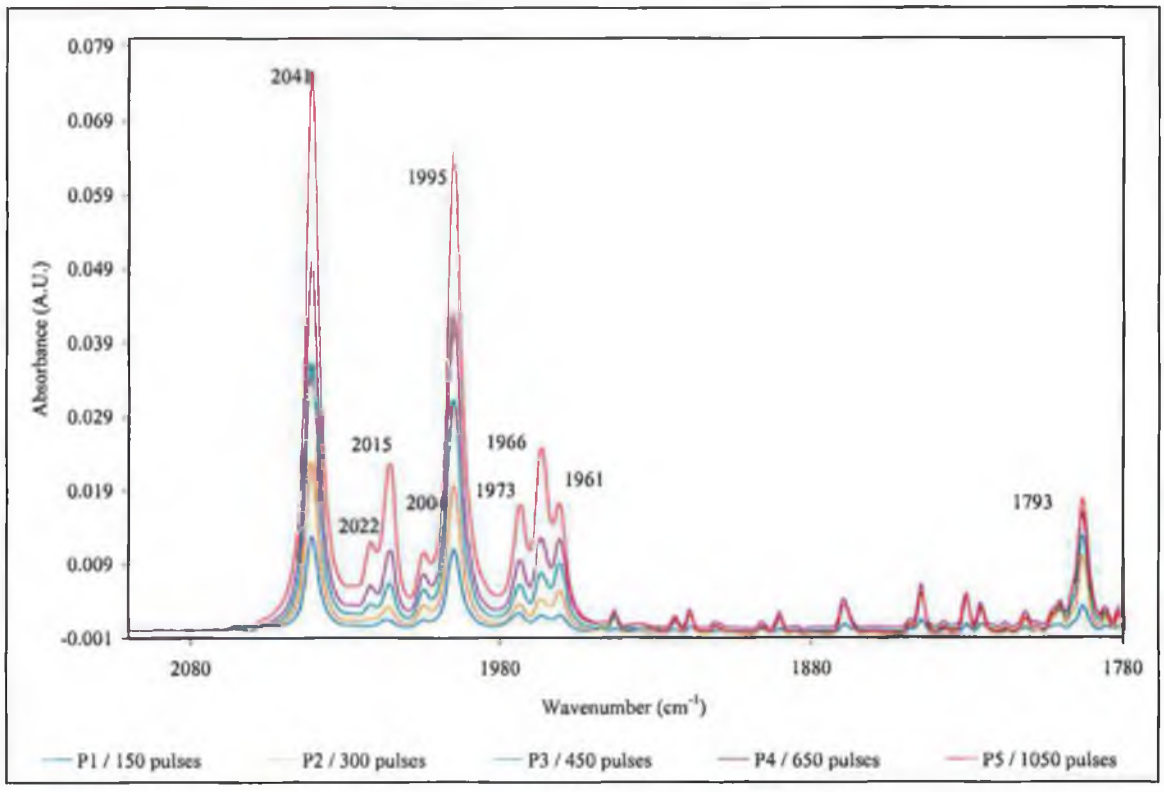

Figure 4-8 The ν_{CO} infrared spectral changes following monochromatic photolysis ($\lambda_{exc.}$ = 532 nm) of (η^5-C_5H_5)Fe(η^5-2,5-$(CH_3)_2C_4H_2N$) carbon monoxide saturated cyclohexane.

Monochromatic photolysis of 2,5-dimethylazaferrocene with higher energy photons at 355 nm in carbon monoxide saturated cyclohexane, results in the infrared spectroscopic changes presented in Figure 4-9. The two ν_{CO} stretches of the dicarbonyl, (η^5-C_5H_5)Fe$(CO)_2$(2,5-$(CH_3)_2C_4H_2N$), at 2041 and 1995 cm^{-1} dominate the spectra. Although there is some formation of the additional carbonyl containing complexes, the yield would appear to be small based on the relative intensities of the remaining ν_{CO} bands at 2022, 2015, 2004, 1973, 1966 and 1961 cm^{-1} to those of the dicarbonyl. Similar results were also obtained with azaferrocene in cyclohexane solution at ambient temperature, where additional carbonyl containing complexes were only produced upon lower energy monochromatic photolysis. Higher energy broad band photolysis (i.e. $\lambda_{exc.} > 410$ nm as opposed to $\lambda_{exc.} > 500$ nm) of 2,5-dimethylazaferrocene yields the dimer species, [(η^5-C_5H_5)Fe$(CO)_2]_2$ as the major photolysis product and to a lesser extent the dicarbonyl, (η^5-C_5H_5)Fe$(CO)_2$(2,5-$(CH_3)_2C_4H_2N$).

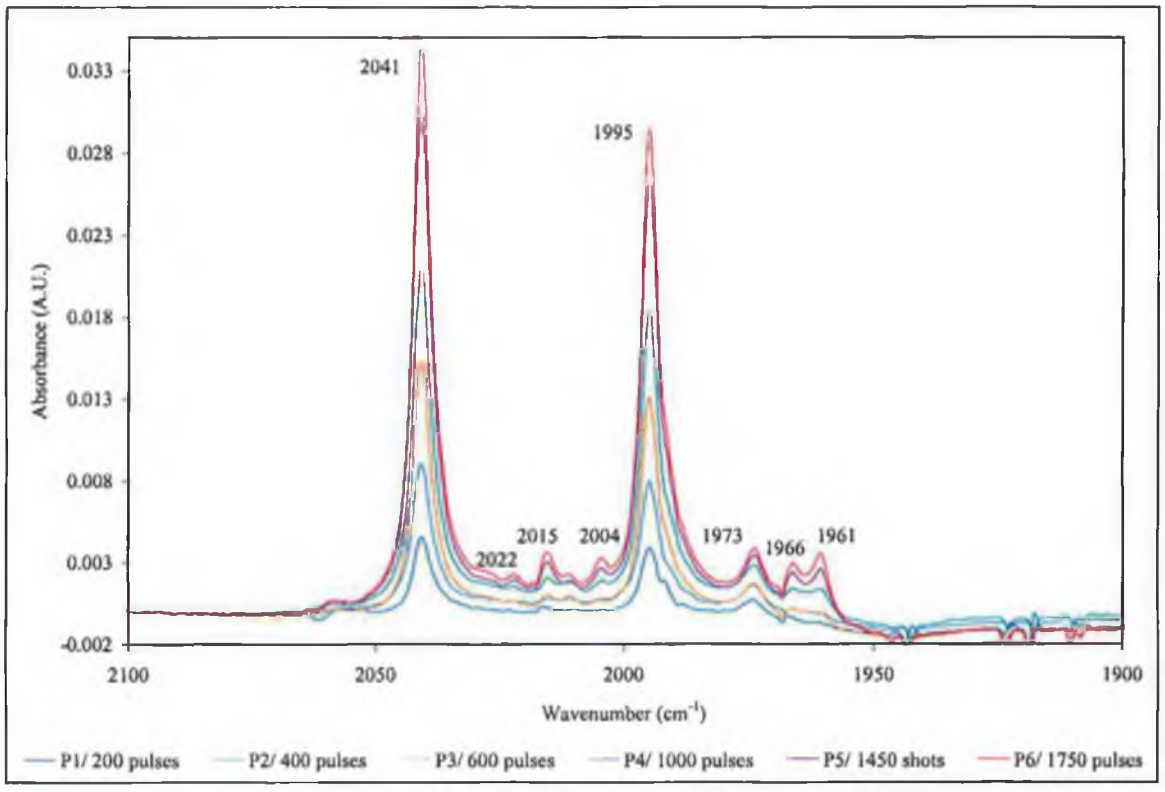

Figure 4-9 The ν_{CO} infrared spectral changes following monochromatic photolysis ($\lambda_{exc.}$ = 355 nm) of (η^5-C_5H_5)Fe(η^5-2,5-$(CH_3)_2C_4H_2N$) carbon monoxide saturated cyclohexane.

4.3.2.1 Discussion of the infrared monitored photolysis of 2,5-dimethylazaferrocene

It is clear that the 2,5-dimethylpyrrolyl ligand undergoes an hapticity change at ambient temperature upon photolysis in cyclohexane carbon monoxide saturated solution to yield (η^5-C_5H_5)Fe$(CO)_2$(η^1-2,5-$(CH_3)_2C_4H_2N$). Thus, introduction of the methyl groups α, α to the nitrogen atom did not prevent the formation of the η^1-2,5-dimethylpyrrolyl dicarbonyl complex. Nevertheless, it appears that this species is less stable than the unsubstituted η^1-pyrrolyl dicarbonyl species, (η^5-C_5H_5)Fe$(CO)_2$(η^1-C_4H_4N), and attempts to isolate the (η^5-C_5H_5)Fe$(CO)_2$(η^1-2,5-$(CH_3)_2C_4H_2N$) species failed.

The dicarbonyl species, (η^5-C_5H_5)Fe$(CO)_2$(η^1-2,5-$(CH_3)_2C_4H_2N$) and the dimer species, [(η^5-C_5H_5)Fe$(CO)_2$]$_2$ are formed following all photolysis conditions employed in this investigation of the photochemistry of 2,5-dimethylazaferrocene in carbon monoxide saturated cyclohexane solution at room temperature. Low energy irradiation ($\lambda_{exc.}$ > 500

nm or $\lambda_{exc.}$ = 532 nm) of 2,5-dimethylazaferrocene resulted in two additional carbonyl containing species being observed, Species 4-1, $(\eta^5\text{-}C_5H_5)Fe(CO)_2(CH_2\text{-}C_4H_2(CH_3)NH)$ and an acyl Species 4-2, $(\eta^5\text{-}C_5H_5)Fe(CO)_2(COCH_2\text{-}C_5H_6N)$, refer to Figure 4-7. However, formation of the dicarbonyl, $(\eta^5\text{-}C_5H_5)Fe(CO)_2(\eta^1\text{-}2,5\text{-}(CH_3)_2C_4H_2N)$, and iron dimer were the more dominant species formed following higher energy irradiation ($\lambda_{exc.}$ > 410 nm or $\lambda_{exc.}$ = 355 nm). The switch from broad band steady-state photolysis to monochromatic pulse photolysis resulted in a reduction in the formation of the dimer species, $[(\eta^5\text{-}C_5H_5)Fe(CO)_2]_2$, based on the relative intensities of the ν_{CO} bands observed in the infrared spectra following photolysis.

The mechanism for the formation of the two additional carbonyl containing species, $(\eta^5\text{-}C_5H_5)Fe(CO)_2(CH_2\text{-}C_4H_2(CH_3)NH)$ and the acyl species, $(\eta^5\text{-}C_5H_5)Fe(CO)_2(COCH_2\text{-}C_5H_6N)$, Species 4-1 and Species 4-2 respectively, observed following low energy ($\lambda_{exc.}$ > 500 nm or $\lambda_{exc.}$ = 532 nm), is at present unknown. They may be the result of a secondary thermal or photochemical process of $(\eta^5\text{-}C_5H_5)Fe(CO)_2(\eta^1\text{-}2,5\text{-}(CH_3)_2C_4H_2N)$, following its primary photochemical production. Varying certain aspects of the photolysis experiments has made it possible to gain some additional information, which may help identify which processes are responsible for the formation of $(\eta^5\text{-}C_5H_5)Fe(CO)_2(CH_2\text{-}C_4H_2(CH_3)NH)$ and the acyl species, $(\eta^5\text{-}C_5H_5)Fe(CO)_2(COCH_2\text{-}C_5H_6N)$.

The formation of $(\eta^5\text{-}C_5H_5)Fe(CO)_2(CH_2\text{-}C_4H_2(CH_3)NH)$ appears to be a secondary thermal process of the η^1-dicarbonyl species $(\eta^5\text{-}C_5H_5)Fe(CO)_2(\eta^1\text{-}2,5\text{-}(CH_3)_2C_4H_2N)$. Evidence to support this suggestion is found in experiments where, following initial photolysis of a sample of 2,5-dimethylazaferrocene in carbon monoxide saturated cyclohexane, the solution was kept in the dark for a period of time (~30 minutes). In these studies, the ν_{CO} bands of $(\eta^5\text{-}C_5H_5)Fe(CO)_2(\eta^1\text{-}2,5\text{-}(CH_3)_2C_4H_2N)$ at 2041 and 1995 cm^{-1}decay with time and new ν_{CO} bands appear at 2015 and 1966 cm^{-1}, assigned to species, $(\eta^5\text{-}C_5H_5)Fe(CO)_2(CH_2\text{-}C_4H_2(CH_3)NH)$, refer to Figure 4-10. The ν_{CO} bands of the remaining species (i.e. the iron dimer, $[(\eta^5\text{-}C_5H_5)Fe(CO)_2]_2$ and the acyl species,

$(\eta^5\text{-}C_5H_5)Fe(CO)_2(COCH_2\text{-}C_5H_6N)$) do not appear in the difference spectrum, Figure 4-10, indicating that their concentration does not change significantly with time.

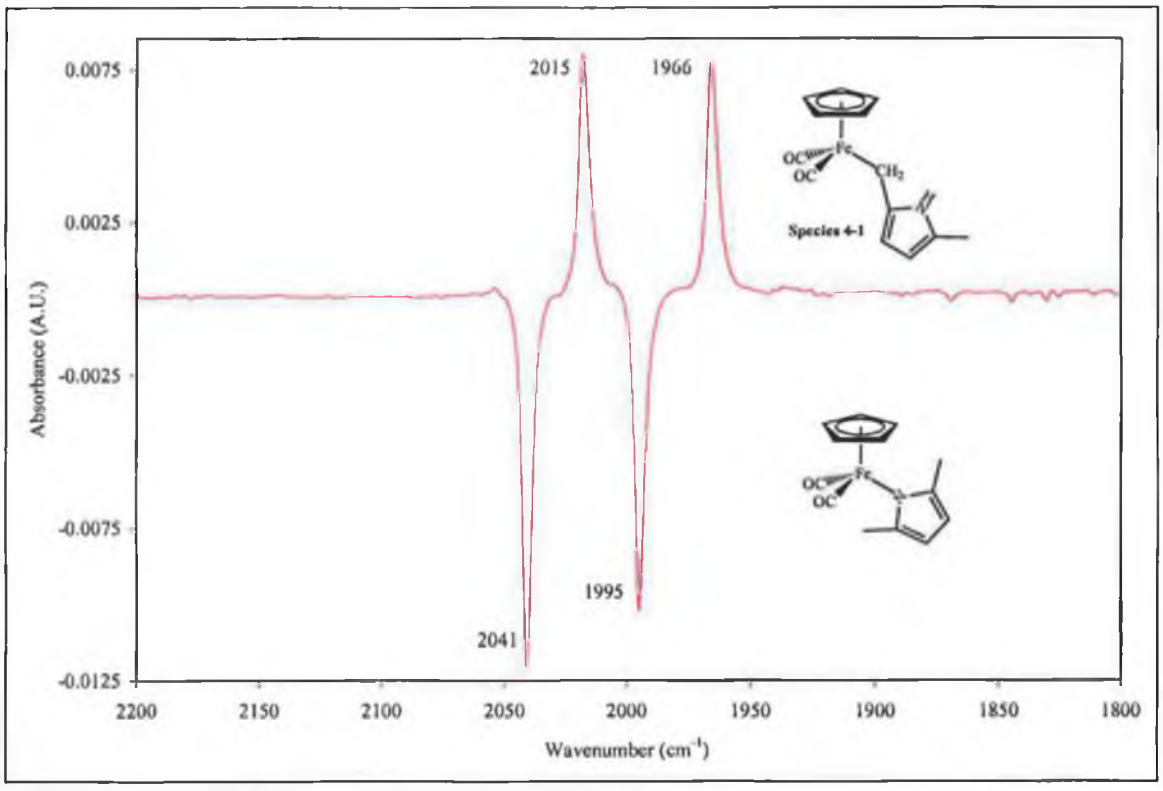

Figure 4-10 Infrared changes which occurred in the ν_{CO} region when $(\eta^5\text{-}C_5H_5)Fe(\eta^5\text{-}2,5\text{-}(CH_3)_2C_4H_2N)$ was initially photolysised ($\lambda_{exc.}$ = 532 nm) and then the solution was kept in the dark. (Difference spectrum: sample following photolysis and rest in the dark – sample following photolysis).

Identifying the mechanistic aspects of the formation of the acyl species, $(\eta^5\text{-}C_5H_5)Fe(CO)_2(COCH_2\text{-}C_5H_6N)$ is very difficult however. With the experimental data available at present, the greatest yield of the acyl species is achieved upon initial photolysis of 2,5-dimethylazaferrocene in carbon monoxide saturated cyclohexane, (refer to P1, Figure 4-11). This is based on the intensities of its ν_{CO} bands at 2022 and 1973 cm^{-1}, relative to the other carbonyl containing species. The intensity of the band at 1973 cm^{-1} assigned to the acyl species, $(\eta^5\text{-}C_5H_5)Fe(CO)_2(COCH_2\text{-}C_5H_6N)$, is greater than the intensity of the band at 1966 cm^{-1}, assigned to $(\eta^5\text{-}C_5H_5)Fe(CO)_2(CH_2\text{-}C_4H_2(CH_3)NH)$, refer to P1, Figure 4-11. While subsequent photolysis causes an increase in all of the ν_{CO} bands, the ratio of the bands at 1973 and 1966 cm^{-1} is inverted, refer to P5, Figure 4-11. A possible explanation for this could be

that further photolysis induces decarbonylation of the acyl species, to form $(\eta^5\text{-}C_5H_5)Fe(CO)_2(CH_2\text{-}C_4H_2(CH_3)NH)$. It was outlined in the literature survey preceding these results, that decarbonylation of acyl complexes of the type $(\eta^5\text{-}C_5H_5)Fe(CO)_2(COR)$ cannot be achieved thermally.[3,8]

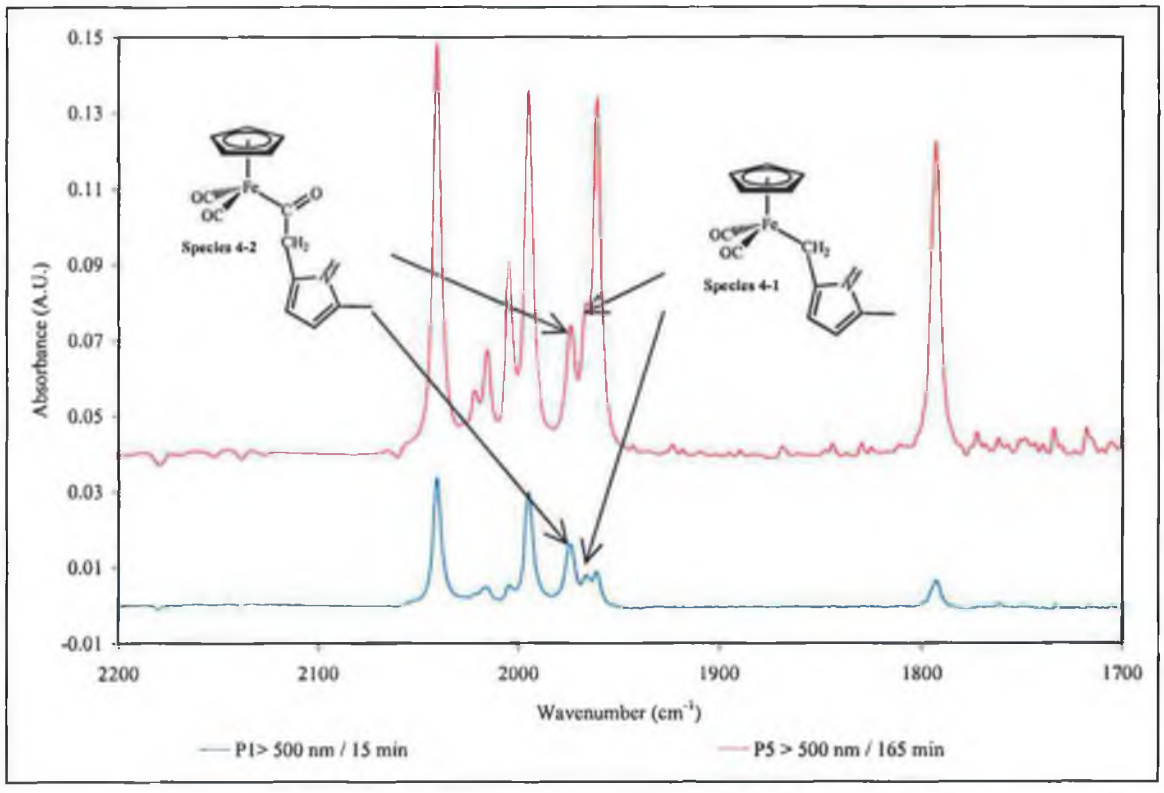

Figure 4-11 Stacked infrared spectra of $(\eta^5\text{-}C_5H_5)Fe(\eta^5\text{-}2,5\text{-}(CH_3)_2C_4H_2N)$ following photolysis P1 and P5, displaying that the ratio of the bands for Species 4-1 and 4-2 vary. P1 shows, based on ν_{CO} intensities, that formation of Species 4-2 is greater than Species 4-1, whereas further photolysis causes them both to increase, the ratio of the ν_{CO} intensities inverted, i.e. formation of Species 4-1 is greater than Species 4-2.

An explanation for the intial formation of the acyl species, $(\eta^5\text{-}C_5H_5)Fe(CO)_2(COCH_2\text{-}C_5H_6N)$ from the results at present is not possible. Nevertheless, following the review of literature reports in Section 4.1, initially it seemed more likely that the formation of the acyl species should be because of a thermal process.[2] However, the results presented in this thesis provide no evidence of such a thermal process, as the yield of the acyl species does not change upon leaving the solution in the dark following photolysis, refer to Figure 4-10.

Given these indications, it is tentatively suggested that the formation of the acyl species is a photochemical process. Rest *et al.*[4,Error! Bookmark not defined.] are the only researchers to have reported photochemical formation of acyl species from $(\eta^5\text{-}C_5H_5)Fe(CO)_2R$ type complexes, (R = alkyl). Formation of acyl complex $(\eta^5\text{-}C_5H_5)Fe(CO)(EPh_3)(COCH_3)$, (E = P, As or Sb) occurred upon photolysis of $(\eta^5\text{-}C_5H_5)Fe(CO)_2R$ at 293 K in the presence of low concentrations of the ligand, $L = EPh_3$. Therefore the formation of the acyl species in this study seems most likely a photochemical process, as the solution was maintained at 293 K and the concentration of the ligand, carbon monoxide was also low (i.e ~9 × 10^{-3} $M^{-1}s^{-1}$). In addition, according to literature reports,[3] the thermal conditions required for carbon monoxide insertion with carbon monoxide as the ligand, according to Reaction 4-1, appear to be too severe to have induced thermal carbon monoxide insertion in this instance. The photochemistry of 2,5-dimethylazaferrocene is probably best summarised as in Scheme 4-2.

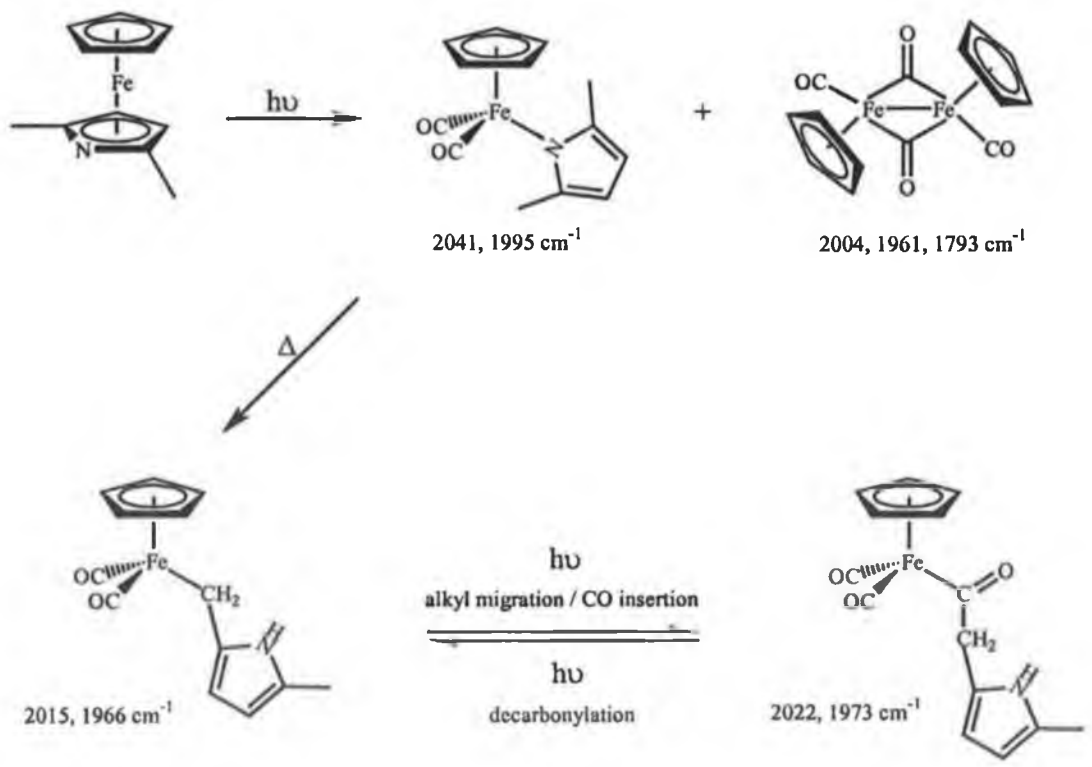

Scheme 4-2 Proposed reaction scheme following photolysis of $(\eta^5\text{-}C_5H_5)Fe(\eta^5\text{-}2,5\text{-}(CH_3)_2C_4H_2N)$ in carbon monoxide saturated cyclohexane.

4.3.3 Laser flash photolysis of 2,5-dimethylazaferrocene

In the case of azaferrocene the transient signal maximum absorption was observed at 375 nm following laser flash photolysis at $\lambda_{exc.}$ = 355 or 532 nm. This transient species was formed within the duration of the laser flash (10 ns) and there was no decay evident for this transient species even at the longest time scale available on the laser flash photolysis system, which is 10 ms. However this primary photoproduct was susceptible to further photolysis from the monitoring lamp of the laser flash system. It was proposed that the nature of this transient species was the dimeric species Figure 2-11. The introduction of two bulky substituents α, α' to the nitrogen on the pyrrolyl ligand could possibly hinder the formation of this type of dimeric species altogether, or at very least slow down the rate its formation.

Consequently, laser flash photolysis of 2,5-dimethylazaferrocene was undertaken at $\lambda_{exc.}$ = 355 and 532 nm, under both atmospheres of argon and carbon monoxide. Unlike azaferrocene, the formation of the transient species was sufficiently slow to allow it rate to be measured. A typical grow-in transient observed at 360 nm following flash photolysis of 2,5-dimethylazaferrocene is shown in Figure 4-12.

The observed rate constant ($k_{obs.}$) for the formation of this transient, is 3×10^6 s^{-1} and this remains the same within experimental error under both argon and carbon monoxide atmospheres. The lifetime of this transient species is independent of the concentration of the parent complex. This indicates that the transient species formed is not reacting with the unphotolysed parent complex. The presence of a trapping ligand (i.e. carbon monoxide) does not alter the rate of formation of the transient species, nor does it alter the lifetime of the transient species produced. This implies that the transient formed in carbon monoxide saturated solutions cannot be due to the formation of a carbonyl containing species and that reaction with carbon monoxide does not cause the decay of this species in time-scale of the UV-vis flash photolysis detection system (10 ms).

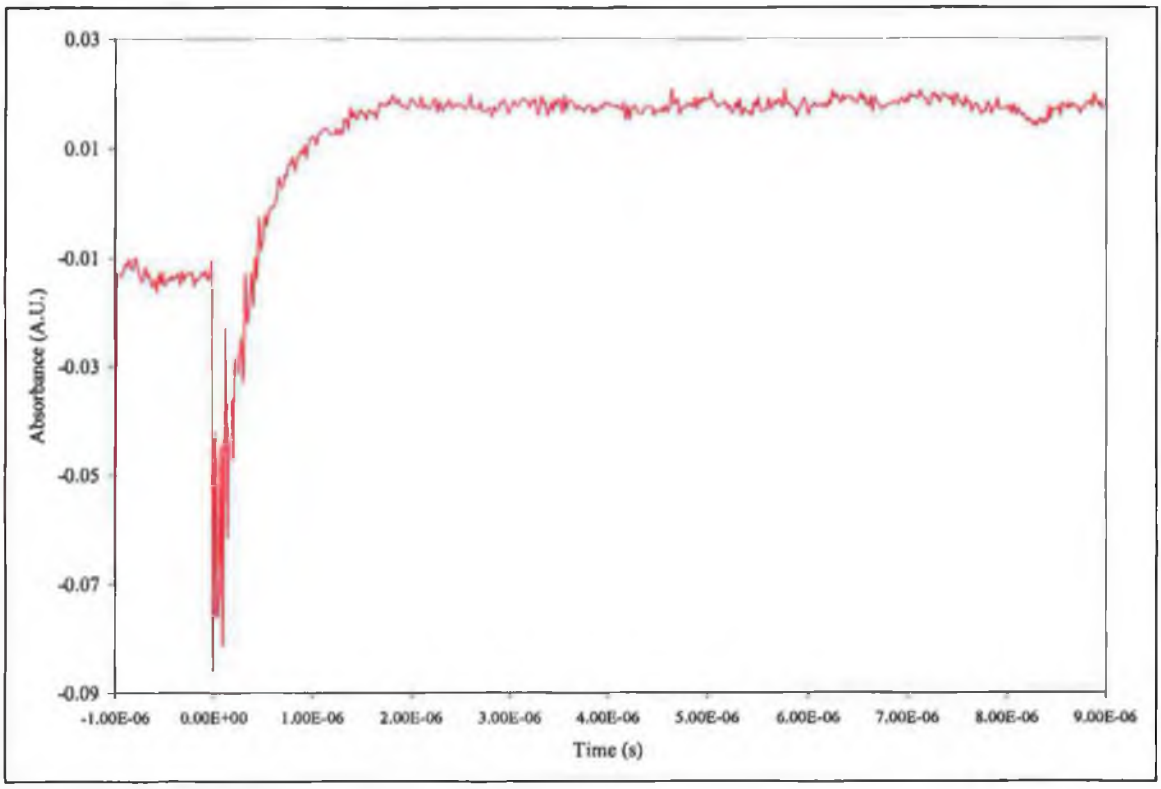

Figure 4-12 This transient is typical of those recorded following laser flash photolysis ($\lambda_{exc.}$ = 532 nm) of (η^5-C_5H_5)Fe(η^5-2,5-$(CH_3)_2C_4H_2N$), monitored at 360 nm under either an atmosphere of argon or in carbon monoxide saturated cyclohexane.

Transients recorded on a longer time-scale (10μs) reveal that there is a slight decay of this transient formed following photolysis $\lambda_{exc.}$ = 532 nm under argon, refer to Figure 4-13. However there is no decay following $\lambda_{exc.}$ = 532 nm under carbon monoxide, refer to Figure 4-14. The origin of this signal under both argon and carbon monoxide remains unknown at present. It may be that the photochemistry is complicated by the existence of spin isomers. It is conceivable that factors such as different spin (singlet-versus-triplet) may be affecting the photochemistry.

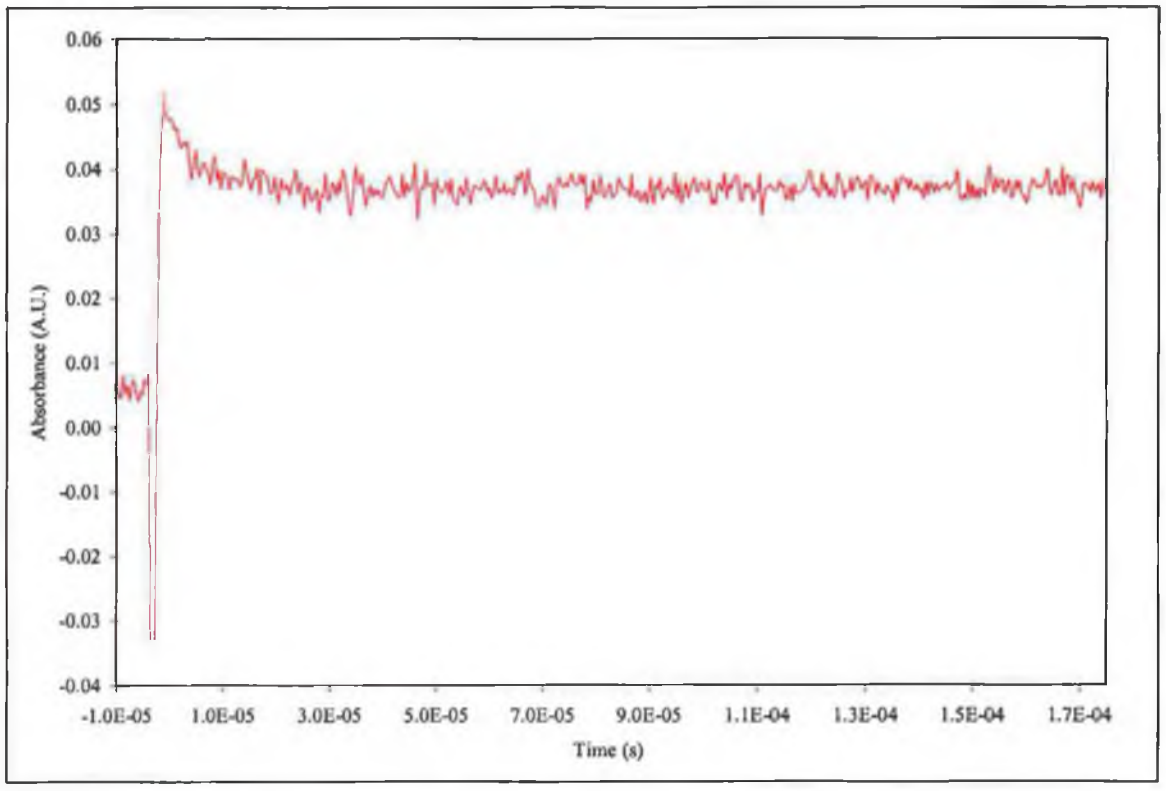

Figure 4-13 Excitation at 532 nm of (η^5-C_5H_5)Fe(η^5-2,5-$(CH_3)_2C_4H_2N$), monitored at 360 nm under Ar

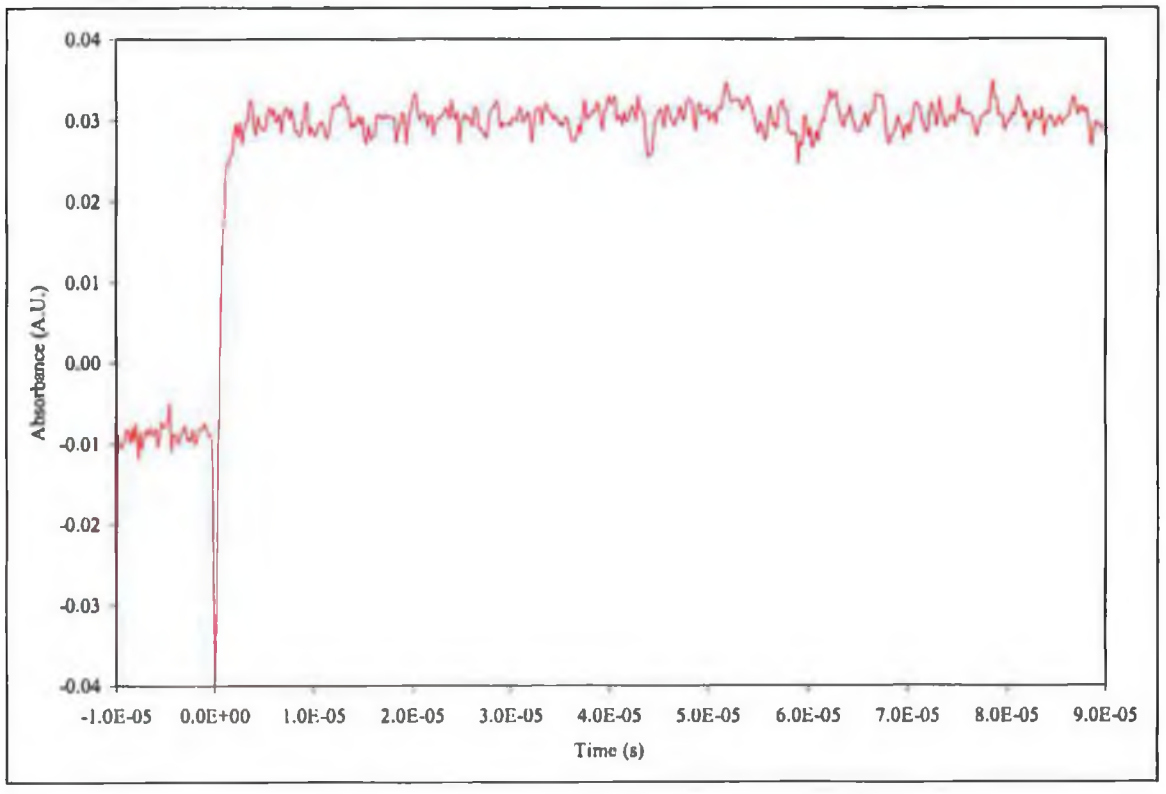

Figure 4-14 Excitation at 532 nm of (η^5-C_5H_5)Fe(η^5-2,5-$(CH_3)_2C_4H_2N$), monitored at 360 nm in carbon monoxide saturated cyclohexane.

The solution photochemistry of iron-pentacarbonyl, $Fe(CO)_5$ presented just such complications. Laser flash photolysis of $Fe(CO)_5$ in deuteriobenzene with TR-IR detection[33] revealed the formation of a solvated species $Fe(CO)_4(C_6D_6)$ which decays by first order kinetics. In carbon monoxide saturated solution, this yields almost exclusively $Fe(CO)_5$. If $Fe(CO)_5$ is added in excess to the solution, the transient species $Fe(CO)_4(C_6D_6)$ decays to form a proposed $[Fe_2(CO)_8]$ and a soluble form of $[Fe_2(CO)_9]$, which reacts further with carbon monoxide in solution to produce $Fe(CO)_5$. The fact that the decay of $Fe(CO)_4(C_6D_6)$ is independent of the concentration of carbon monoxide and $Fe(CO)_5$ suggested that a additional very reactive intermediate, I, (refer to Scheme 4-3) must be formed initially from $Fe(CO)_4(C_6D_6)$. Grevels *et al.*[33] proposed that, I is a spin isomer of $Fe(CO)_4(C_6D_6)$, intersystem crossing being the rate determining step in the decay of $Fe(CO)_4(C_6D_6)$. Other possibilities for I were postulated (i.e. naked $Fe(CO)_4$, or $Fe(CO)_3$, $Fe(CO)_3(C_6D_6)$ and a conformational isomer of $Fe(CO)_4(C_6D_6)$), but these were more difficult to rationalise with the experimental findings. The solution photochemistry of $Fe(CO)_5$ is summarised in Scheme 4-3.

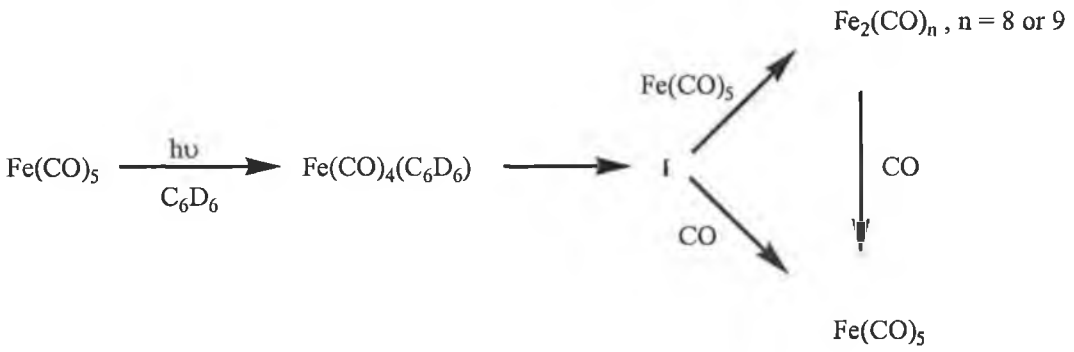

Scheme 4-3 Proposed reaction scheme following photolysis of $Fe(CO)_5$ in deuteriobenzene.[33]

Nayak, Farrell and Burkey[34] have also atrributed the unusual photochemistry of $Fe(CO)_5$ to triplet state involvement. Photolysis of $Fe(CO)_5$ in cyclohexane solution at 377 nm in the presence of PR_3 (R = C_2H_5, CH_3, C_6H_5) was preformed under conditions where the secondary photolysis of photoproducts was negligible. They observed disubstitution of $Fe(CO)_5$ by the ligands upon absorption of a single photon, which was proposed to occur from a ground state triplet intermediate $^3Fe(CO)_4$. This then reacts

with a dispersed ligand to form a triplet, $^3Fe(CO)_4L$ that subsequently loses a carbon monoxide ligand, allowing the addition of a second ligand and formation of $Fe(CO)_3L_2$, as summarised in Scheme 4-4.

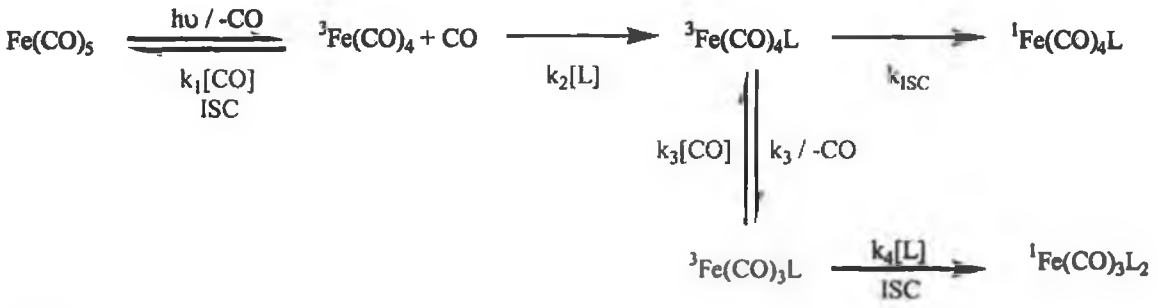

Scheme 4-4

4.3.4 Matrix isolation experiments on 2,5-dimethylazaferrocene

The photochemistry of 2,5-dimethylazaferrocene was investigated in a number of different matrixes with both broad band and monochromatic irradiation in order to observe the effect of the bulky substituents on the resulting photochemistry.

2,5-dimethylazaferrocene was isolated at high dilution in an argon matrix at 20 K. The 1600-750 cm^{-1} region of the infrared spectrum of 2,5-dimethylazaferrocene in an argon matrix at 20 K is presented in comparison with that of azaferrocene in an argon matrix at 20 K, refer to Figure 4-15. This region of the infrared spectrum of 2,5-dimethylazaferrocene contains many additional stretches compared to azaferrocene, this is to be expected given the fact that the additional methyl groups on the pyrrolyl ligand will also have C-H bending modes. There are no other significant absorptions outside the fingerprint region that are diagnostic of changes in the co-ordination mode of the 2,5-dimethylpyrrolyl ligand, as was also observed in the case of azaferrocene.

Initial photolysis was begun with a range of broad band interference filters $\lambda_{exc.} > 780$ nm to $\lambda_{exc.} > 550$ nm, however the changes induced were minimal until photolysis was begun with $\lambda_{exc.} > 495$ nm. Then a decrease in the absorption bands at 1465, 1440, 1373, 1334, 1303, 1260, 1108, 1040, 945, 835 and 818 cm^{-1} was observed, in conjunction with the growth of new bands at 1448, 1442, 1382, 1370, 1342, 1263, 1253, 1245, 1087, 1070, 1111, 959 and 947 cm^{-1}. The energy of the photolysis was progressively increased until final photolysis was with $\lambda_{exc.} > 395$ nm. This induced further growth of the initial bands, but no additional ones, refer to Figure 4-16. The UV-vis spectral changes accompanying photolysis are presented in Figure 4-17. An increase across the entire UV-vis range is observed, as was also the case for azaferrocene following broad band irradiation in an argon matrix.

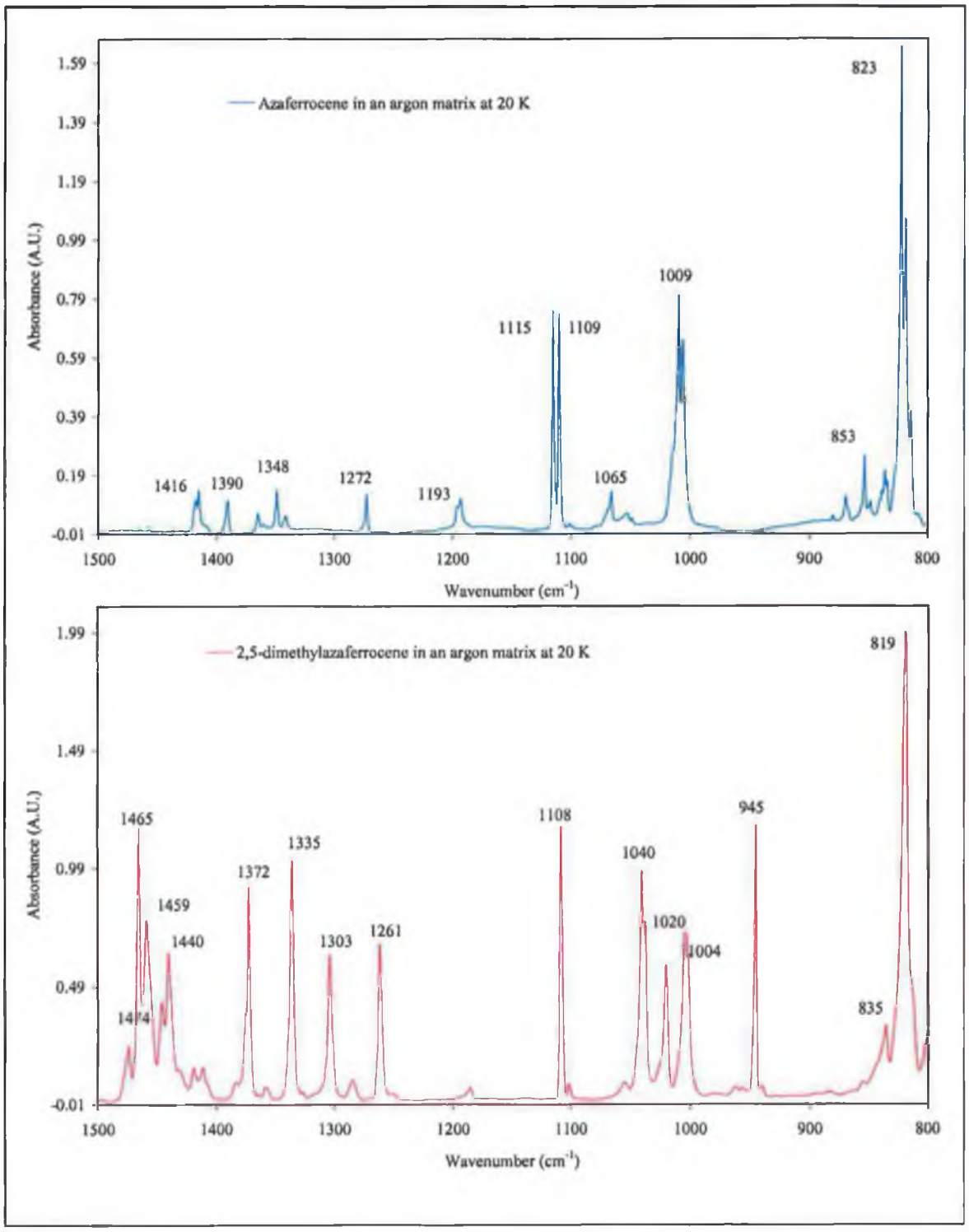

Figure 4-15 The infrared spectra of azaferrocene and 2,5-dimethylazaferrocene in argon matrixes at 20 K in the 1500-800 cm^{-1} region.

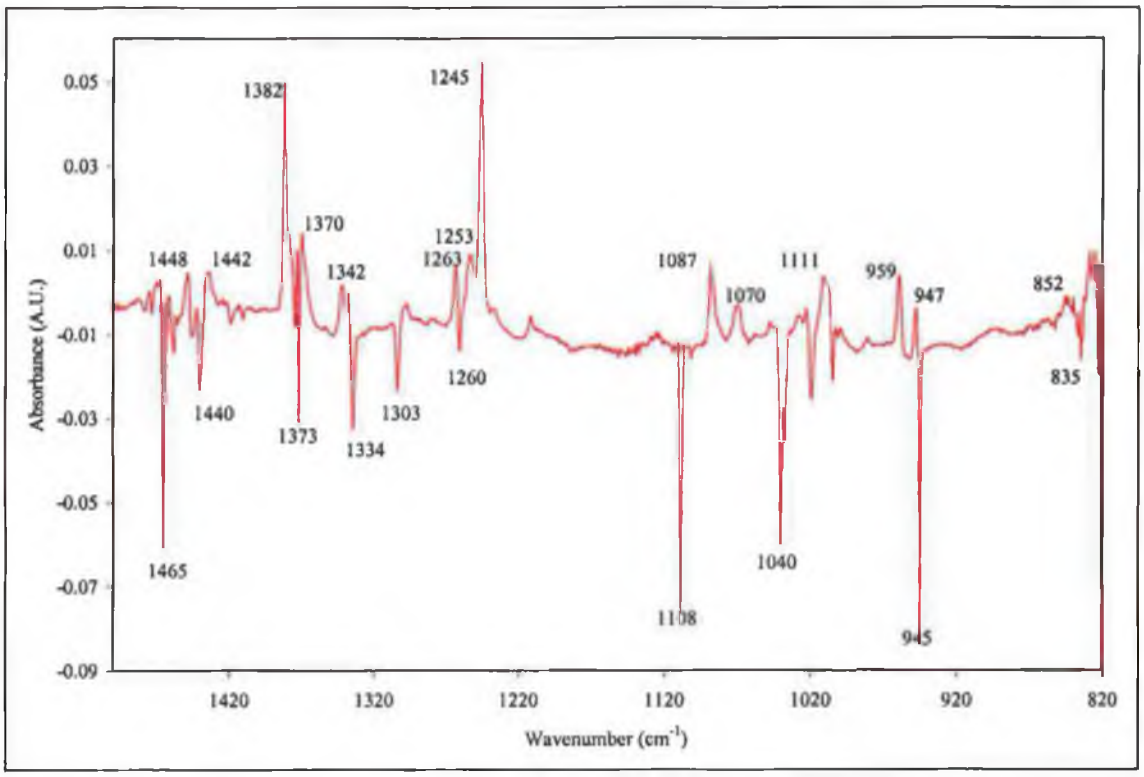

Figure 4-16 Difference spectrum (in the region 1500-820 cm^{-1}) of (η^5-C_5H_5)Fe(η^5-2,5-$(CH_3)_2C_4H_2N$) following broad band photolysis ($\lambda_{exc.}$ > 495 nm) in an argon matrix.

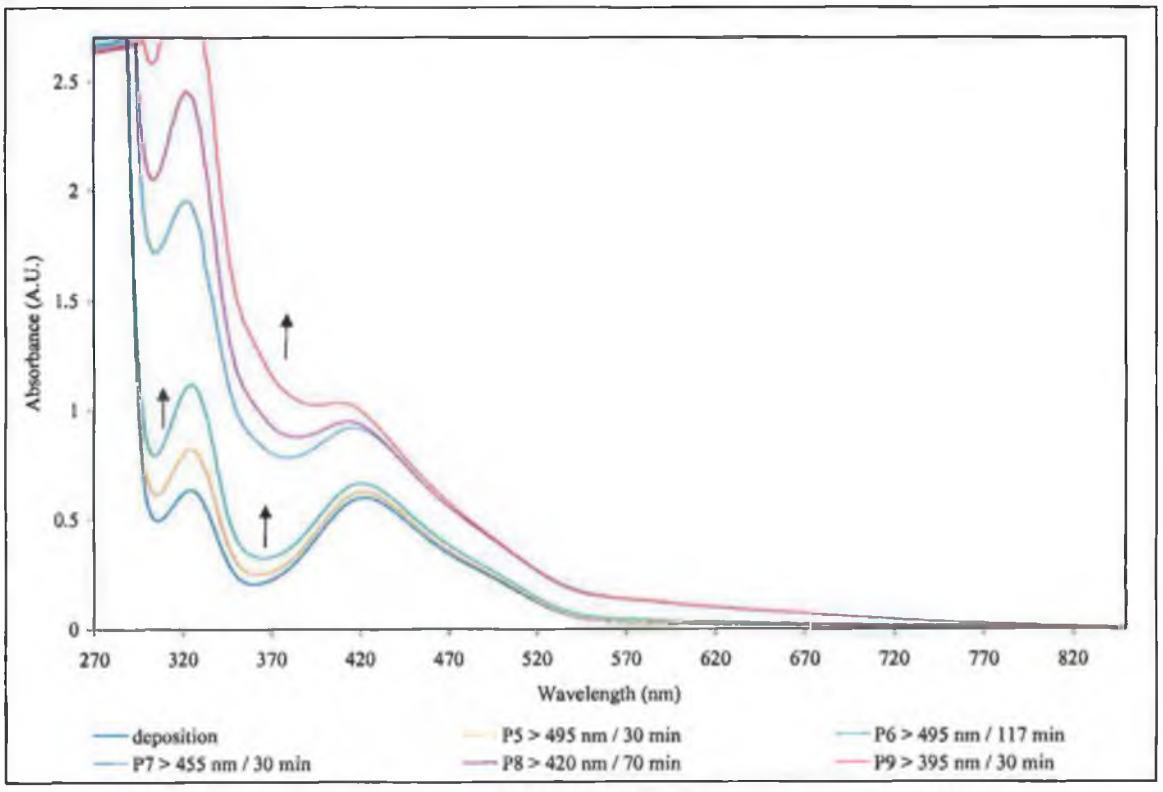

Figure 4-17 UV-vis spectral changes induced following broad band photolysis of (η^5-C_5H_5)Fe(η^5-2,5-$(CH_3)_2C_4H_2N$) in an argon matrix at 20 K.

Changes in the region 1500-800 cm^{-1} due to C-H bending frequencies of the molecule provide the only means to monitor changes in the infrared region. Although changes occur in the ν_{C-H} bending modes, the co-ordination mode of the 2,5-dimethylpyrrolyl ligand cannot be ascertained for certain because the bands in this region have not been assigned. Nevertheless, since changes in the this region are observed, it is reasonable to deduce that there is a change in the co-ordination mode of either the cyclopentadienyl ligand or the 2,5-dimethylazaferrocene ligand. Experiments on azaferrocene confirmed ring-slip of the pyrrolyl ligand, thus it is more reasonable to suppose that the co-ordination mode of the 2,5-dimethylpyrrolyl ligand is responsible for the changes observed.

As the infrared spectra of 2,5-dimethylazaferrocene and azaferrocene are quite different in the 1500-800 cm^{-1} region of the infrared spectrum, it is not possible to find any correlation between the changes observed in the case of 2,5-dimethylazaferrocene, refer to Figure 4-16 with those observed for azaferrocene, Figure 2-19.

Irradiation of 2,5-dimethylazaferrocene in a methane matrix at 12 K was with monochromatic light, initially with $\lambda_{exc.}$ = 577 nm / 48 minutes, and then by irradiation with ever increasing energy,(i.e. $\lambda_{exc.}$ = 567 nm / 60 minutes, $\lambda_{exc.}$ = 436 nm / 60 minutes, $\lambda_{exc.}$ = 405 nm / 105 minutes, $\lambda_{exc.}$ = 365 nm / 30 minutes), produced the spectral changes present in Figure 4-18. The methane matrix itself absorbs significantly in 3075-2970 cm^{-1} and 1335-1270 cm^{-1} regions of the spectrum, so these regions are prohibited from investigation. The changes induced in the methane are essentially those already observed in an argon matrix. Furthermore, as observed for azaferrocene, the use of monochromatic irradiation as opposed to broad band does not alter the photochemistry observed for 2,5-dimethylazaferrocene in the inert matrixes. As before with photolysis in an argon matrix, 2,5-dimethylazaferrocene does not have significant characteristic features outside of the 1500-800 cm^{-1} region to monitor changes in the infrared spectrum.

This experiment was primarily undertaken to investigate whether or not C-H activation was taking place upon the photolysis of 2,5-dimethylazaferrocene, however the changes

observed do not show any indication of such a process. If intermolecular C-H activation had taken place, evidence of a M-H stretch in the region 2200-2000 cm^{-1} would have been expected, however the difference spectra of the matrix following photolysis gave no indication of such a process occurring.

Failure to observed C-H activation was not unexpected however as intermolecular C-H activation is often only achieved with C-H bonds that are considered to be at least weakly activated, either because they are aryl or vinyl C-H or because they are adjacent to activating groups or atoms (e.g. aryl, carbonyl, cyano, R_3Si, R = CH_3, C_2H_5). In addition other examples of intermolecular C-H activation to date have involved second and third row transition metals, as discussed previously in the introduction of to this chapter.

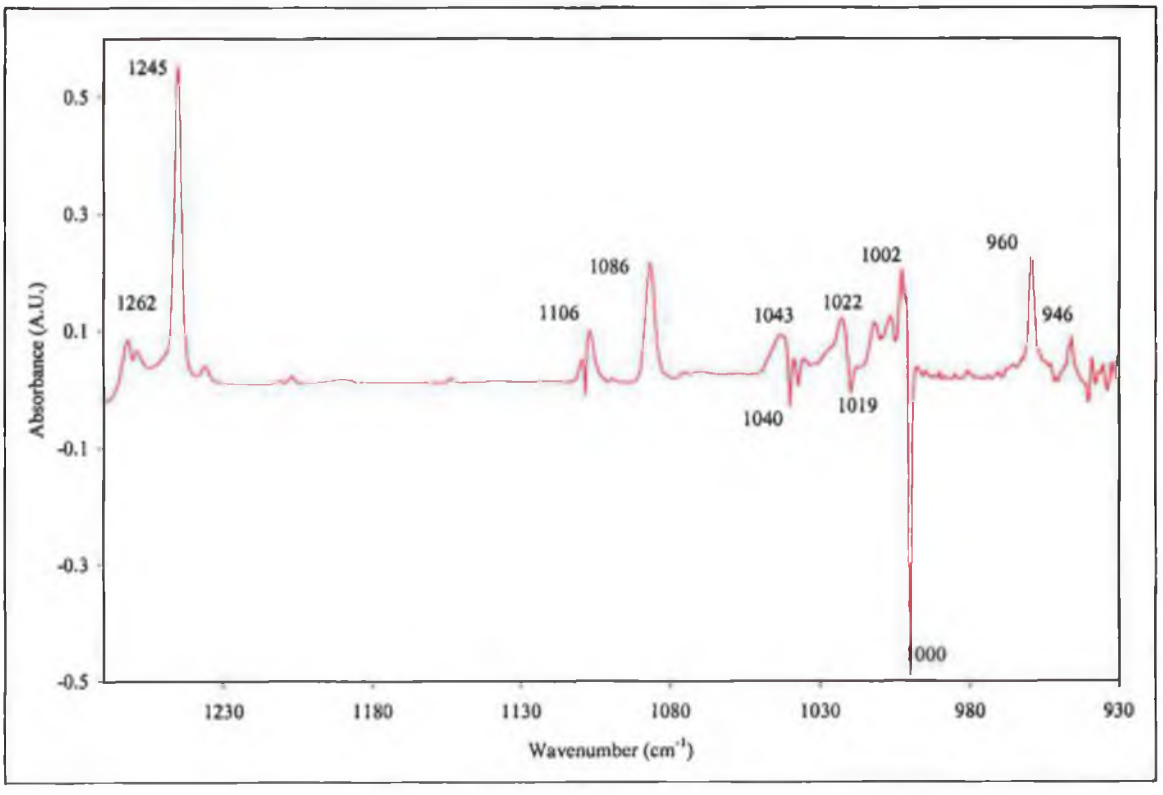

Figure 4-18 Difference spectrum of the fingerprint region (1270-900cm^{-1}) of (η^5-C_5H_5)Fe(η^5-2,5-$(CH_3)_2C_4H_2N$) following monochromatic photolysis in a methane matrix at 12 K.

The photochemistry of 2,5-dimethylazaferrocene was investigated further in carbon monoxide doped argon matrixes, with both broad band and monochromatic irradiation. 2,5-Dimethylazaferrocene was co-condensed with 2.6% carbon monoxide doped argon onto the spectroscopic cold window at 20 K. Irradiation of the sample was begun with visible light, $\lambda_{exc.} > 780$ nm, but no changes occurred in the infrared spectra. The energy of the light was progressively increased (i.e. $\lambda_{exc.} > 715$ nm, $\lambda_{exc.} > 665$ nm, $\lambda_{exc.} > 550$ nm), however no changes occurred until irradiation at $\lambda_{exc.} > 495$ nm was used. Then new bands in the ν_{CO} region of the spectrum appeared at 2044 and 1999 cm^{-1}, in addition with the decrease of the band at 2135 cm^{-1}, which is indicative of the carbon monoxide in the matrix being consumed. Further irradiation with yet higher energy light, $\lambda_{exc.} > 455$ nm, induced further growth of these ν_{CO} stretches at 2044 and 1999 cm^{-1} and the observation of a weak broad band at ~2151 cm^{-1}. Finally, when irradiation was changed to $\lambda_{exc.} > 395$ nm, an additional band, though weak, appeared at ~ 1965 cm^{-1}.

The formation of these new bands is evidence that the carbon monoxide in the matrix has begun to co-ordinate to the iron metal centre. In order for this to occur, the 2,5-dimethylpyrrolyl ligand must have undergone a change in its co-ordination mode enabling carbon monoxide to bind. The relative intensities of the three bands do not correlate to one another, which would suggest that that they are the result of three individual species.

The band at 2044 cm^{-1} is assigned to one of the carbonyl stretches expected for the dicarbonyl species, $(\eta^5\text{-}C_5H_5)Fe(CO)_2(\eta^1\text{-}2,5\text{-}(CH_3)_2C_4H_2N)$, the second ν_{CO} stretch expected for this species is suspected of being masked by the intense band at 1999 cm^{-1}. This is based on a comparison of the ν_{CO} shifts observed in going form solution spectra to matrix isolation spectra in the case of $(\eta^5\text{-}C_5H_5)Fe(CO)_2(\eta^1\text{-}C_4H_4N)$. The ν_{CO} bands for $(\eta^5\text{-}C_5H_5)Fe(CO)_2(\eta^1\text{-}C_4H_4N)$ are at 2048, 2002 cm^{-1} and 2053, 2007 cm^{-1} in cyclohexane solution and argon matrices respectively, a shift of 5 cm^{-1}. A similar shift for the ν_{CO} stretches of $(\eta^5\text{-}C_5H_5)Fe(CO)_2(\eta^1\text{-}2,5\text{-}(CH_3)_2C_4H_2N)$ would give rise to a band at 2046 and 2000 cm^{-1}, which is very close to that observed, therefore it is

probable that the lower wavenumber ν_{CO} band of the dicarbonyl, $(\eta^5\text{-}C_5H_5)Fe(CO)_2(\eta^1\text{-}2,5\text{-}(CH_3)_2C_4H_2N)$ is masked by the intense band at 1999 cm^{-1}.

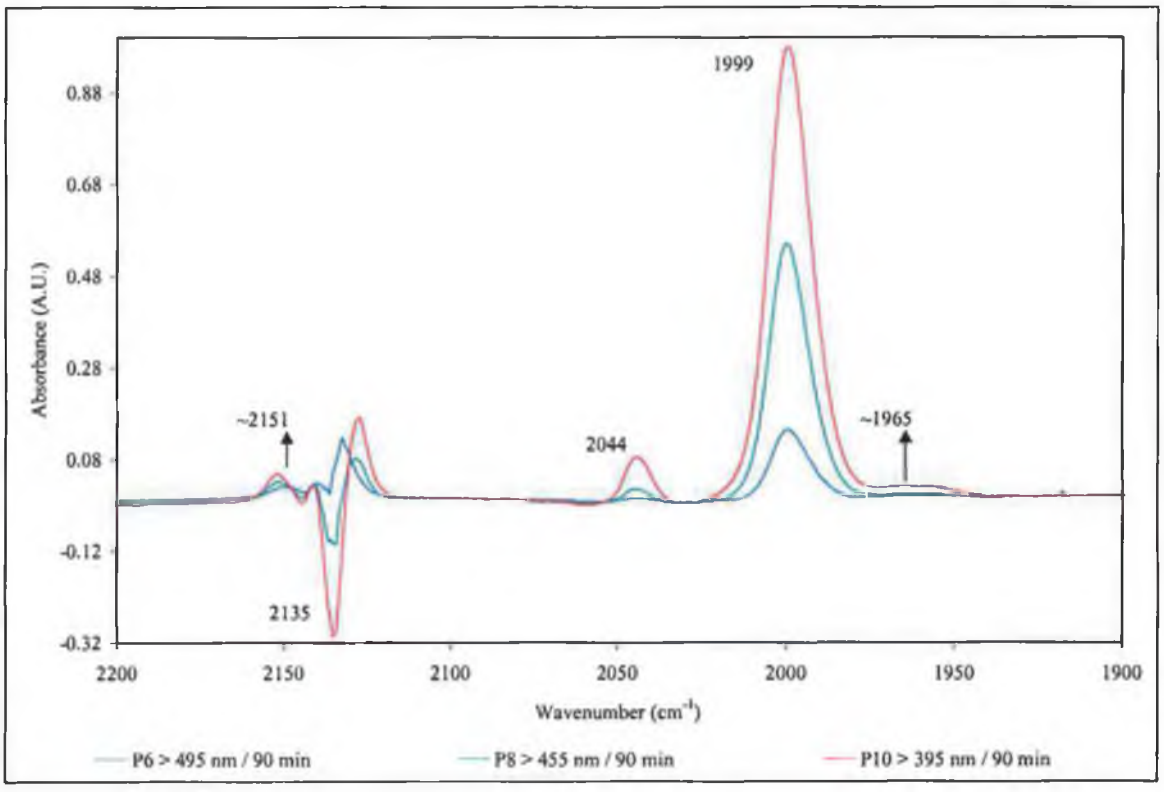

Figure 4-19 Infrared spectral changes observed following broad band irradiation of $(\eta^5\text{-}C_5H_5)Fe(\eta^5\text{-}2,5\text{-}(CH_3)_2C_4H_2N)$ in a 2.6% carbon monoxide doped argon matrix.

The strong terminal ν_{CO} band at 1999 cm^{-1} would appear to be a monocarbonyl species, which obscures the low energy band of the dicarbonyl as already outlined. The formation of an unsaturated monocarbonyl photoproduct such as $(\eta^5\text{-}C_5H_5)Fe(CO)(\eta^1\text{-}2,5\text{-}(CH_3)_2C_4H_2N)$ or a saturated monocarbonyl such as $(\eta^5\text{-}C_5H_5)Fe(CO)(\eta^3\text{-}2,5\text{-}(CH_3)_2C_4H_2N)$ does not correlate with the band position observed in this instance. If either of the aforementioned monocarbonyl photoproducts were forming the ν_{CO} band position would be expected at lower wavenumbers than those of the dicarbonyl photoproduct, $(\eta^5\text{-}C_5H_5)Fe(CO)_2(\eta^1\text{-}2,5\text{-}(CH_3)_2C_4H_2N)$. Evidence to support the expected finding of monocarbonyl photoproducts such as $(\eta^5\text{-}C_5H_5)Fe(CO)(\eta^1\text{-}2,5\text{-}(CH_3)_2C_4H_2N)$ and $(\eta^5\text{-}C_5H_5)Fe(CO)(\eta^3\text{-}2,5\text{-}(CH_3)_2C_4H_2N)$ at lower wavenumbers is present in the matrix isolation results obtained during the

photolysis of azaferrocene in carbon monoxide doped argon matrixes and $(\eta^5\text{-}C_5H_5)Fe(CO)_2(\eta^1\text{-}C_4H_4N)$ in argon matrixes. In both these cases the ν_{CO} band of the unsaturated monocarbonyl photoproduct, $(\eta^5\text{-}C_5H_5)Fe(CO)(\eta^1\text{-}C_4H_4N)$, (1974 cm^{-1}) and the η^3-cordinated monocarbonyl photoproducts, $(\eta^5\text{-}C_5H_5)Fe(CO)(\eta^3\text{-}N\text{-}C_4H_4N)$ and $(\eta^5\text{-}C_5H_5)Fe(CO)(\eta^3\text{-}C\text{-}C_4H_4N)$, (1962 and ~ 1950 cm^{-1} respectively) were at lower wavenumbers than the dicarbonyl, $(\eta^5\text{-}C_5H_5)Fe(CO)_2(\eta^1\text{-}C_4H_4N)$, (2053 and 2007 cm^{-1}).

Therefore the position of the photoproduct ν_{CO} band at 1999 cm^{-1} at what appears to be higher/equal wavenumber than the lower wavenumber band of what is believed to be the dicarbonyl photoproduct, $(\eta^5\text{-}C_5H_5)Fe(CO)_2(\eta^1\text{-}2,5\text{-}(CH_3)_2C_4H_2N)$ is inconsistent with it being the co-ordinatively unsaturated monocarbonyl photoproduct, $(\eta^5\text{-}C_5H_5)Fe(CO)(\eta^1\text{-}2,5\text{-}(CH_3)_2C_4H_2N)$. Consequently, the ν_{CO} band at 1999 cm^{-1} is tentatively assigned to the eighteen-electron hydride complex, Species 4-3 as depicted in Figure 4-20 below. Further discussion of this assignment will follow in the discussion of the matrix isolation results.

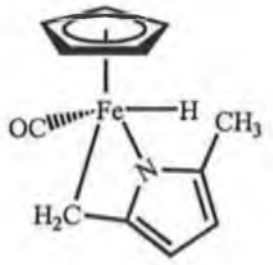

Species 4-3

Figure 4-20 Species 4-3, which is attributed to the monocarbonyl ν_{CO} band absorption at 1999 cm^{-1}.

In addition to this ν_{CO} monocarbonyl band at 1999 cm^{-1}, there is a weak broad band at 2151 cm^{-1}, which may be a metal-hydride-stretching mode, although this assignment is again made tentatively at this stage.

The remaining band at ~ 1965 cm^{-1} is tentatively assigned to η^3-azaallyl monocarbonyl photoproduct, $(\eta^5\text{-}C_5H_5)Fe(CO)(\eta^3\text{-}2,5\text{-}N\text{-}(CH_3)_2C_4H_2N)$ based on the fact that upon photolysis of azaferrocene in a carbon monoxide doped argon matrixes, the η^3-azaally

photoproduct ν_{CO} absorption band was at higher wavenumber than the η^3-ally photoproduct.

The UV-vis spectral changes, which accompanied photolysis, are presented in Figure 4-21. These show an increase across the entire spectrum upon photolysis with broad band irradiation for $\lambda_{exc.} > 495$ nm and > 455 nm. Irradiation with $\lambda_{exc.} > 395$ nm results in an additional band forming in the spectrum at approximately 600 nm, see UV-vis difference spectrum (i.e. UV-vis spectrum following $\lambda_{exc.} > 395$ nm minus the spectrum following $\lambda_{exc.} > 455$ nm) in the inset in Figure 4-21. This new band would appear to be associated with the growth of the new band in the infrared spectrum at approximately 1965 cm^{-1}. Photolysis of azaferrocene in carbon monoxide doped argon matrixes produced a similar increase in the UV-vis spectrum upon formation of the η^3-azaallyl and η^3-allyl-monocarbonyl photoproducts.

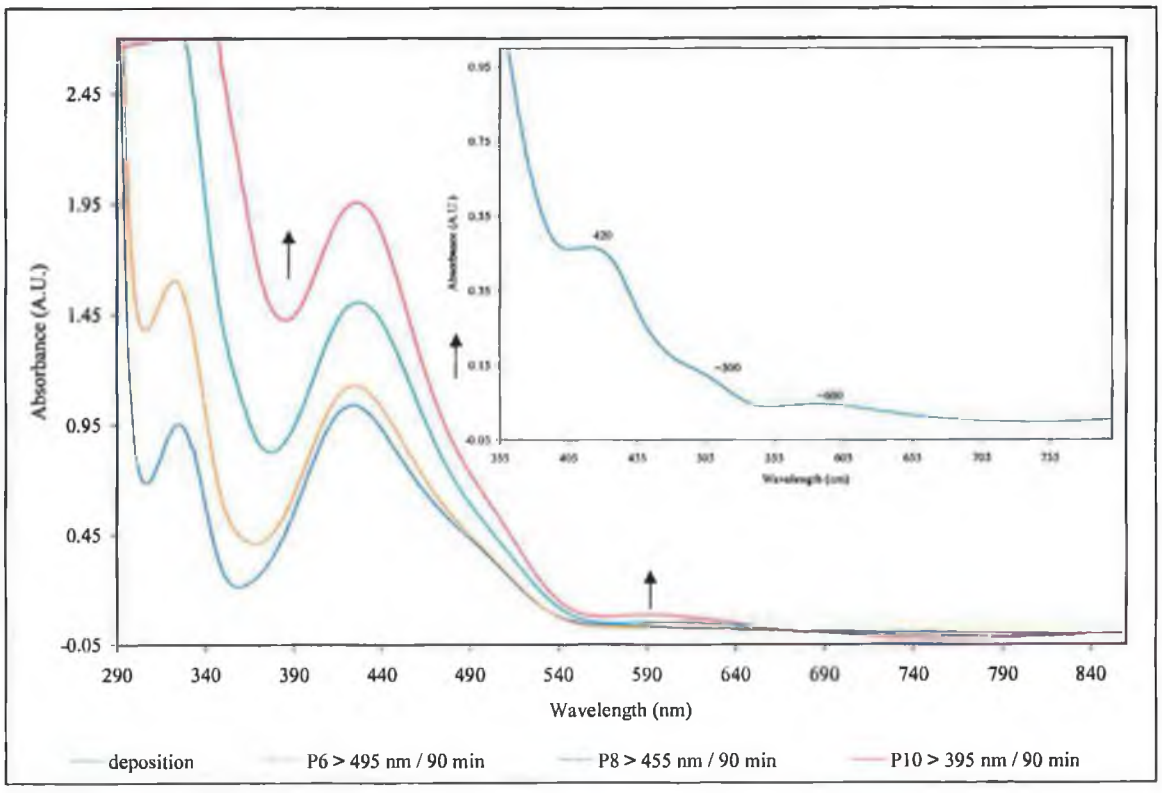

Figure 4-21 The UV-vis spectral changes observed following broad band irradiation of $(\eta^5\text{-}C_5H_5)Fe(\eta^5\text{-}2,5\text{-}(CH_3)_2C_4H_2N)$ in a 2.6% carbon monoxide doped argon matrix at 20 K. A difference spectrum (UV-vis spectrum following $\lambda_{exc.} > 395$ nm minus the spectrum following $\lambda_{exc.} > 455$ nm) is presented in the inset.

The isolation of 2,5-dimethylazaferrocene at 12 K in a 2% carbon monoxide doped argon matrix was repeated. This time monochromatic irradiation replaced broad band irradiation. Initially the matrix was irradiated at $\lambda_{exc.}$ = 577 nm (20 minutes), followed by $\lambda_{exc.}$ = 546 nm (40 minutes), which produced only slight changes in the ν_{CO} region, although it is possible to identify the growth of a band at 1999 cm^{-1} from the infrared difference spectrum recorded after photolysis. Increasing the energy to $\lambda_{exc.}$ = 436 nm, caused more substantial changes in the infrared spectrum. It becomes clearly evident that the carbon monoxide in the matrix is being consumed by the photoproduct(s), (i.e. negative absorption in the difference spectra), in addition to further increases in intensity of the band at 1999 cm^{-1}, Figure 4-22. The ν_{CO} stretch observed at 2044 cm^{-1} following broad band photolysis is also present following monochromatic photolysis and reaches its highest absorption after irradiation with $\lambda_{exc.}$ = 405 nm, refer to Figure 4-22, although the intensity of this band is small compared to the band at ν_{CO} 1999 cm^{-1}. These bands at 2044 and 1999 cm^{-1} are assigned to the dicarbonyl, $(\eta^5\text{-}C_5H_5)Fe(CO)_2(\eta^1\text{-}2,5\text{-}(CH_3)_2C_4H_2N)$ and the monocarbonyl hydride, Species 4-3 as previously observed following broadband irradiation. The weaker ν_{CO} band to lower wavenumber side of the monocarbonyl hydride at 1956 cm^{-1}, is different from that observed following broad band photolysis, where the lower wavenumber ν_{CO} band was at 1965 cm^{-1}. This ν_{CO} band at 1956 cm^{-1} can be attributed to the formation of the η^3-allyl monocarbonyl photoproduct, $(\eta^5\text{-}C_5H_5)Fe(CO)(\eta^3\text{-}2,5\text{-}C\text{-}(CH_3)_2C_4H_2N)$, as the η^3-allyl complex in the case of azaferrocene absorbed at lower energy than the η^3-azaallyl monocarbonyl complex, $(\eta^5\text{-}C_5H_5)Fe(CO)(\eta^3\text{-}2,5\text{-}N\text{-}(CH_3)_2C_4H_2N)$. The assignment of the ν_{CO} stretches is summarised in Figure 4-23.

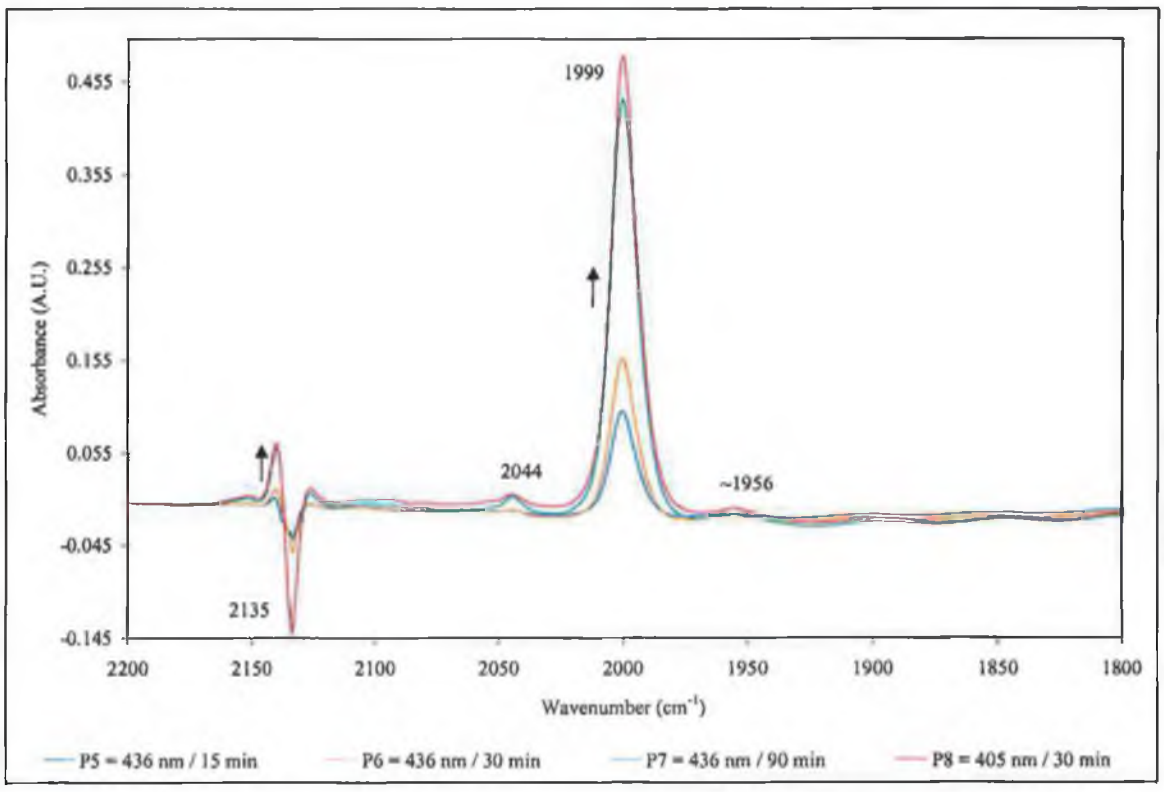

Figure 4-22 The UV-vis spectral changes of (η^5-C_5H_5)Fe(η^5-2,5-$(CH_3)_2C_4H_2N$) in a 2% carbon monoxide doped argon matrix at 12 K following monochromatic irradiation.

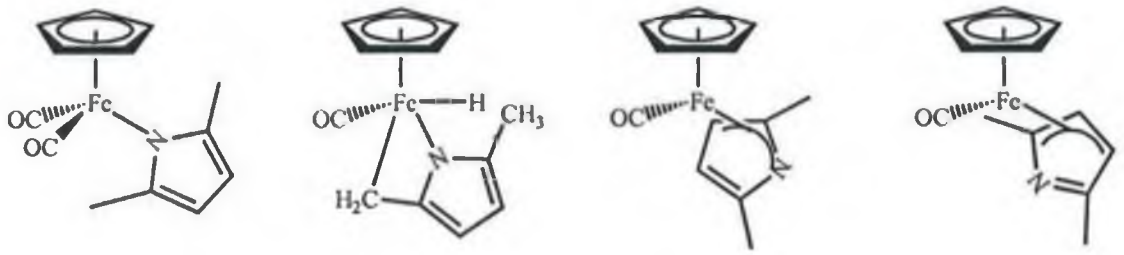

2044 cm^{-1} 1999 cm^{-1} 1965 cm^{-1} 1956 cm^{-1}

Figure 4-23 Possible structures for the photoproducts formed following photolysis of 2,5-dimethylazaferrocene in carbon monoxide doped matrixes.

4.3.4.1 Discussion of the results obtained in matrix isolation experiments

Broad band photolysis of 2,5-dimethylazaferrocene in an argon matrix at 20 K and monochromatic irradiation in a methane matrix at 12 K resulted in depletion of the infrared bands in the fingerprint region and the formation of new bands. The changes

observed in the either matrix were essentially identical, leading to the conclusion that the photoproduct(s) did not react with the matrix. The co-ordination of the pyrrolyl ligand following photolysis is not certain, but in order for changes to be observed in the fingerprint region, it seems reasonable to assume that some change in co-ordination mode has taken place.

Experiments in the reactive carbon monoxide doped argon matrices provide evidence of co-ordination of carbon monoxide to the metal centre. It appears that the 2,5-dimethylpyrrolyl ligand attains more than one type of co-ordination mode to the metal centre, as four individual species have been proposed to form following photolysis. The monocarbonyl hydride photoproduct, Species 4-3 seems to dominate the spectra of the matrix isolation photolysis experiments. This is irrespective of whether the irradiation employed is broad band or monochromatic. This assignment is based on a survey of the literature reports of ν_{CO} band positions for cyclopentadienyl-metal monocarbonyl hydride complexes, as outlined in Table 4-1.

For example when the ruthenium complex $(\eta^5\text{-}C_5H_5)Ru(CO)_2C_2H_5$[36] was photolysised in a paraffin matrix at 77 K, a monocarbonyl hydride complex, as outlined in Scheme 4-5 was observed before further photolysis induced the formation of the dicarbonyl hydride. The position of the ν_{CO} bands for the monocarbonyl hydride at 1970 cm^{-1} is higher than the lower wavenumber band of either the parent dicarbonyl $(\eta^5\text{-}C_5H_5)Ru(CO)_2C_2H_5$ or the photoproduct dicarbonyl, $(\eta^5\text{-}C_5H_5)Ru(CO)_2H$. The relative position of the ν_{CO} bands for the ruthenium monocarbonyl hydride complex is very similar to the pattern observed in this study upon photolysis of 2,5-dimethylazaferrocene in a carbon monoxide doped matrix. Although at this point in the investigation of the photochemistry of 2,5-dimethylazaferrocene, it is not possible to speculate about the mechanism, which leads to the formation of the monocarbonyl hydride complex, (Species 4-3, shown in Figure 4-20).

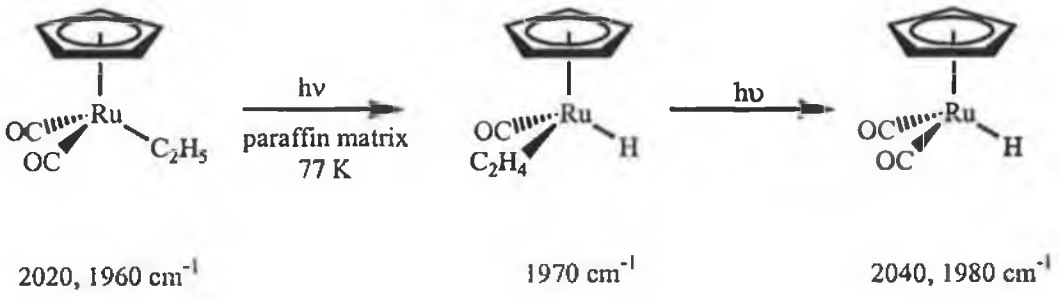

Scheme 4-5 Outline of the reaction of $(\eta^5\text{-}C_5H_5)Ru(CO)_2C_2H_5$ in a paraffin matrix at 77 K.[36]

Metal	R	ν_{CO} dicarbonyl (cm^{-1})	ν_{CO} monocarbonyl (cm^{-1})	ν_{M-H} (cm^{-1})	Medium
Os[(a)]	CH_3	2001, 1941[d]	1968	2079	hexane
Ru[(b)]	H	2020, 1960	1970	not located	Paraffin / 77 K
Rh[(c)]	CH_3	2028, 1966	2009	not located	CH_4 M / 12 K
Rh[(c)]	H	2049, 1985	2024	not located	CH_4 M / 12 K
Ir[(c)]	CH_3	2021, 1955	1991	2149	CH_4 M / 12 K
Ir[(c)]	CH_3	2021, 1954	1990	1548	CD_4 M / 12 K
Ir[(c)]	H	2040, 1977	2006	*ca.* 2184	CH_4 M / 12 K
Ir[(c)]	CH_3	2048, 1982	1997	2136	C_6F_{14}

Table 4-1 (a)For osmium, the complex formula is $(\eta^5\text{-}C_5R_5)Os(CO)_2H$, which upon photolysis in perfluorohexane solution purged with H_2, gave rise to $(\eta^5\text{-}C_5R_5)Os(CO)H_3$.[35] (b) For ruthenium, the complex formula is $(\eta^5\text{-}C_5R_5)Ru(CO)_2C_2H_5$, which upon photolysis in a paraffin matrix at gave rise to $(\eta^5\text{-}C_5R_5)Ru(CO)(H)C_2H_4$.[36] (c) For the group 10 complexes (i.e. M = Rh and Ir), the complex formula is $(\eta^5\text{-}C_5R_5)M(CO)_2$, which upon photolysis in methane matrixes at 12 K gave rise to $(\eta^5\text{-}C_5R_5)M(CO)(H)CH_3$.[23] M in the table = matrix. (d) Reference.[37]

Some of the ν_{M-H} band positions reported previously in the literature are also presented in Table 4-1 for comparison with the ν_{Fe-H} stretch tentatively assigned in this study. The metal-hydride bands are usually quite weak and broad, and as can be seen in Table 4-1 it is not always possible to detect them. One method to confirm an assignment of a metal-hydride band is by deuteration. During Rest *et al.*'s[23] investigation of the photochemistry of $(\eta^5\text{-}C_5R_5)Ir(CO)_2$complexes, where R = H or CH_3, it was evident that

intermolecular C-H activation was occurring upon photolysis of $(\eta^5\text{-}C_5(R)_5)Ir(CO)_2$ in a methane matrixes at 12 K. This lead to the formation of $(\eta^5\text{-}C_5(R)_5)Ir(CO)(H)(CH_3)$, (R = H or CH_3) complexes , which displayed $\nu_{M\text{-}H}$ stretching modes at 2184 and 2149 cm^{-1} for R = H and CH_3 respectively. Confirmation of these assignments were achieved by repeating these photolysis experiments in deuteriomethane matrixes at 12 K. These bands were no longer observed, but weak bands were detected at 1565 and 1548 cm^{-1}, for R = H and CH_3 respectively. The 2184 (CH_4)/1565 cm^{-1} (CD_4) and 2149 (CH_4)/1548 cm^{-1} (CD_4) band shifts are consistent with H/D exchange and enabled the bands at 2184 and 2149 cm^{-1} to be assigned to metal-hydride stretching modes.

The C-H activation process occurring in the case of 2,5-dimethylazaferrocene is an intramolecular process, therefore deuteration of 2,5-dimethylazaferrocene is necessary if establishment of the band at 2151 cm^{-1} as metal-hydride stretching mode is to be achieved. Attempts were made to deuterate the 2,5-pyrrolyl ligand before complexation to the iron and also to deuterate the 2,5-dimethylazaferocene complex directly. In both instances, the attempts to deuterate failed because of polymerisation of the 2,5-pyrrole and 2,5-dimethylazaferrocene, which was caused by the high temperatures and pressures required for the deuteration process. Therefore it has not been possible to use H/D exchange as a means of identifying the band at 2151 cm^{-1} as a metal-hydride.

4.4 Conclusions

2,5-dimethylazaferrocene, like azaferrocene displays an extensive photochemistry, in which haptotropic shifts of the co-ordinated η^1-2,5-dimethylpyrrolyl ligand plays a dominant role. In cyclohexane solution at room temperature, formation of the η^1-2,5-dimethylpyrrolyl complex, $(\eta^5\text{-}C_5H_5)Fe(CO)_2(\eta^1\text{-}2,5\text{-}(CH_3)_2C_4H_2N)$ is the predominant photoproduct following irradiation with high energy photons ($\lambda_{exc.}$ = 355 or > 410 nm). Lower energy photolysis ($\lambda_{exc.}$ = 532 or > 500 nm) leads to the formation of additional carbonyl containing complexes, which are believed to be due to secondary thermal and photochemical reactions of $(\eta^5\text{-}C_5H_5)Fe(CO)_2(\eta^1\text{-}2,5\text{-}(CH_3)_2C_4H_2N)$. The formation of the dicarbonyl complex shows that the lone pair on the nitrogen still acts as an efficient trap for this process, even though it is sterically hindered by the substituents α-to the nitrogen atom. This photoproduct, $(\eta^5\text{-}C_5H_5)Fe(CO)_2(\eta^1\text{-}2,5\text{-}(CH_3)_2C_4H_2N)$ is relatively unstable as attempts to isolate it failed. The presence of Species 4-1 and Species 4-2, also reveal that C-H activation must have occurred, although it is impossible to speculate at this juncture about the mechanism for formation of these additional species.

Photolysis of 2,5-dimethylazaferrocene in carbon monoxide doped argon matrixes with either broad band or monochromatic irradiation, led to the formation of a C-H activation product, Species 4-3 as the major photoproduct (based on ν_{CO} stretch intensities). In addition, the dicarbonyl, $(\eta^5\text{-}C_5H_5)Fe(CO)_2(\eta^1\text{-}2,5\text{-}(CH_3)_2C_4H_2N)$ was also identified following photolysis. Prolonged photolysis of the matrixes with broad band and monochromatic irradiation produced the η^3-monocarbonyl complexes, $(\eta^5\text{-}C_5H_5)Fe(CO)(\eta^3\text{-}2,5\text{-}N\text{-}(CH_3)_2C_4H_2N)$ and $(\eta^5\text{-}C_5H_5)Fe(CO)(\eta^3\text{-}2,5\text{-}C\text{-}(CH_3)_2C_4H_2N)$ respectively.

4.5 References

1 (a) P. M. Treichel, R. L. Shubkin, K. W. Barnett, D. Reichard, *Inorg. Chem.*, **1966**, 5, 1177.
(b) C. R. Folkes, A. J. Rest, *J. Organometall. Chem.*, **1977**, 136, 355.

2 R. B. King, M. B. Bisnette, *J. Organomet. Chem.*, **1964**, 2, 15.

3 T. H. Coffield, J. Kozikowski, R. D. Closson, *Chem. Soc., Spec. Publ.*, **1959**, 13, 126.

4 A. C. Gingell, A. J. Rest, *J. Organomet. Chem.*, **1975**, 99, C27.

5 E. Körner von Gustorf, F.-W. Grevels, *Forts. Chem. Forsch.*, **1969**, 69, 413.

6 S. R. Su, A. Wojcicki, *J. Organomet. Chem.*, **1971**, 27, 231.

7 A. Wojcicki, *Advan. Organomet. Chem.*, **1973**, 11, 87.

8 R. B. King, *J. Am. Chem. Soc.*, **1963**, 85, 1918.

9 A. Hudson, M. F. Lappert, W. B. Lednor, J. J. MacQuitty, B. K. Nicholson, *J. Chem. Soc., Dalton Trans.*, **1981**, 2159.

10 J. J. Alexander, *J. Am. Chem. Soc.*, **1975**, 97, 1729.

11 D. J. Fettes, R. Narayanaswamy, A. J. Rest, *J. Chem. Soc., Dalton Trans.*, **1981**, 2311.

12 R. H. Hooker, A. J. Rest, I. Whitwell, *J. Organomet. Chem.*, **1984**, 266, C27.

13 S. T. Belt, D. W. Ryba, P. C. Ford, *J. Am. Chem. Soc.*, **1991**, 113, 9524.

14 D. W. Ryba, R. van Eldik, P. C. Ford, *Organometallics*, **1993**, 12, 104.

15 K. L. McFarlane, B. Lee, W. Fu, R. van Eldik, P. C. Ford, *Organometallics*, **1998**, 17, 1826.

16 S. M. Massick, P. C. Ford, *Organometallics*, **1999**, 18, 4362.

17 R. H. Crabtree, *Chem. Rev.*, **1985**, 85, 245.

18 J. Chatt, J. M. Davidson, *J. Chem. Soc.*, **1965**, 843.

19 J. K. Hoyano, A. D. McMaster, W. A. G. Graham, *J. Am. Chem. Soc.*, **1983**, 105, 7190.

20 J. K. Hoyano, W. A. G. Graham, *J. Am. Chem. Soc.*, **1982**, 104, 3723.

21 (a) W. D. Jones, F. J. Feher, *Organometallics*, **1983**, 2, 562. (b) W. D. Jones, F. J. Feher, *J. Am. Chem. Soc.*, **1984**, 106, 1650.

22 (a) A. H. Janowicz, R. G. Bergman, *J. Am. Chem. Soc.*, **1982**, 104, 352.
(b) A. H. Janowicz, R. G. Bergman, *J. Am. Chem. Soc.*, **1983**, 105, 3929.

23 (a) A. J. Rest, I. Whitwell, W. A. G. Graham, J. M. Hoyano, A. D. McMaster, *J. Chem. Soc., Chem. Commun.*, **1984**, 624.
(b) A. J. Rest, I. Whitwell, W. A. G. Graham, J. M. Hoyano, A. D. McMaster, *J. Chem. Soc., Dalton Trans.*, **1987**, 1181.

24 J. Mascatti, A. J. Rest, J. *Chem. Soc.,Chem. Commun.*, **1987**, 221.

25 A. A. Bengali, B. A. Arndtsen, P. M. Burger, R. H. Schultz, B. H. Weiller, K. R. Moore, R. G. Bergman, *Pure Appl. Chem.*, **1995**, 67, 281.

26 E. P. Wasserman, C. B. Moore, R. G. Bergman, *Science*, **1992**, 255, 315.

27 (a) S. E. Bromberg, T. Q. Lian, R. G. Bergman, C. B. Harris, *J. Am. Chem. Soc.*, **1996**, 118, 2069.

(b) T. P. Dougherty, W. T. Grubbs, E. J. Heilweil, *J.. Phys. Chem.*, **1994**, 98, 9396.

28 J. B. Asbury, H. N. Ghosh, J. S. Yeston, R. G. Bergman, T. Q. Lian, *Organometallics*, **1998**, 17, 3417.

29 A. McCamley, R. N. Perutz, S. Stahl, H. Werner, *Angew. Chem., Int. Ed. Engl.*, **1989**, 28, 1690.

30 K. L. McFarlane, P. C. Ford, *Organometallics*, **1998**, 17, 1166.

31 X. Pan, C. E. Philbin, M .P. Castellani, D. R. Tyler, *Inorg. Chem.*, **1988**, 27, 671.

32 K. L. McFarlane, P. C. Ford, *Organometallics*, **1998**, 17, 1166.

33 S. P. Church, F.-W. Grevels, H. Hermann, J. M. Kelly, W. E. Klotzbücher, K. Schaffner, *J. Chem. Soc., Chem. Commun.*, **1985**, 594.

34 (a) S. K. Nayak, T. J. Burkey, *Inorg. Chem.*, **1992**, 31, 1125.

(b) S. K. Nayak, T. J. Burkey, *Inorg. Chem.*, **1994**, 33. 2236.

35 J. K. Hoyano, W. A. G. Graham, *J. Am. Chem. Soc.*, **1982**, 104, 3722.

36 R. J. Kaslauskas, M. S. Wrighton, *Organometallics*, **1982**, 1, 602.

37 J. K. Hoyano, C. J. May, W. A. G. Graham, *Inorg. Chem.*, **1982**, 21, 3095.

Chapter Five

5 Experimental

5.1 Reagents

The following solvents were of spectroscopic grade and were used without further purification: benzene, cyclohexane, heptane, hexane, pentane, toluene (Aldrich Chemicals Co.). Argon and carbon monoxide was supplied by Air products ad IIG respectively. Cyclopentadienyl-iron dicarbonyl-iodide, bis[(dicarbonyl)(η^5-cyclopentadienyl)iron], potassium metal (Aldrich Chemicals Co.) were all used without further purification. Pyrrole and diisopropylamine (Aldrich Chemicals Co.) were distilled from KOH under reduced pressure, stored over KOH under argon at low temperatures (sub 0°C). 2,5-Dimethylpyrrole (Aldrich Chemicals Co.) was distilled from KOH under reduced pressure and used immediately. Tetrahydrofuran (THF) was distilled from sodium/ benzephenone ketyl solution under nitrogen and used immediately. The carbon monoxide, methane and dinitrogen gases for matrix isolation studies were of spectroscopic grade, and supplied by Cyroservice Co.

5.2 Equipment

All synthesises were performed using conventional glassware under an inert argon atmosphere. All manipulations were carried out using solutions and solvents deoxygenated by purging with dry argon for 10-15 min. Silica gel used for chromatography was neutral silica gel pH 6.5-7.5 (B.F.Merck).

Infrared spectra were recorded on a Perkin Elmer 2000 FT-IR spectrometer, resolution 1 cm^{-1}, in sodium chloride liquid solution cells with a 0.1mm path length. The reported band maxima are considered accurate to 0.5 cm^{-1}. Typically the solvents were spectroscopic grade cyclohexane, pentane and heptane. Nuclear Magnetic Resonance spectra were measured on a Brüker model AC400 MHz spectrometer in appropriate deuterated solvent at room temperature and were calibrated according to the residual protonated solvent peak or with external TMS as a standard. UV/vis. spectra were recorded on a Hewlett Packard 8452A photodiode array spectrometer using a quartz cell of 1cm path-length. The reported band maxima in this thesis are considered accurate to ± 2 nm.

5.3 Synthesis

5.3.1 Synthesis of azaferrocene-(η^5-C_5H_5)Fe(η^5-C_4H_4N)

This compound was synthesised according to the method described by Joshi, Pauson, Qazi and Stubbs[1] with minor alterations.

25 ml of spectroscopic grade benzene was purged with argon for ~ 20 minutes after which potassium metal (0.25 g, 5.37 mmol) was suspended in it. The three-necked flask's contents were then heated until the potassium dispersed before 1 ml (15 mmol) of pyrrole was added. The mixture was brought to reflux temperature until all the potassium had reacted (10-12 hours – solution turns a light yellow colour). After cooling to room temperature cyclopentadienyliron dicarbonyl iodide (1.5 g, 5 mmol) in 25 ml of benzene (pre-purged with argon) was added and the mixture was brought to reflux temperature for an additional twelve hours. The solvent of the resulting brown mixture was removed under reduced pressure. The residue was purified by column

chromatography (SiO_2 / $CHCl_3$) to give a dark orange solid. It was further purified by vacuum sublimation at 40-50°C / rotary pump to yield a crystalline orange solid. ^1H NMR ($CDCl_3$): 5.42 ppm (s, 2H, α), 4.59ppm (s, 2H, β), 4.29 ppm (s, 5H). UV-vis-(cyclohexane): λ_{max} 336 nm & 440 nm. IR ν_{CO}: no bands. Yield: 22-24 %. Anal. Calc. C 57.79%, H 4.86%, N 7.49%. Found C 57.81%, H 4.90%, and N 7.50%.

5.3.2 Synthesis of cyclopentadienyl-iron dicarbonyl-η^1-pyrrolyl, $(\eta^5\text{-}C_5H_5)Fe(CO)_2(\eta^1\text{-}N\text{-}C_4H_4N)$

This complex was synthesised according to the method described by Zakrzewski and Giannotti[2] with minor alterations.

In a 50 ml round bottom flask, 20 ml of heptane was purged with argon for 20 minutes. Pyrrole (0.6ml, 8.7 mmol) and diisopropylamine (1.5 ml, 11.5 mmol) were then added and the solution purged with argon for another 20 minutes. Cyclopentadienyl-iron-dicarbonyl iodide (1.52 g, 5 mmol) was added. The mixture was then sonicated to ensure as much as possible of $(\eta^5\text{-}C_5H_5)Fe(CO)_2I$ dissolved in solution. The mixture was then purged with argon for a further ~ 10 minutes after which the flask is stoppered and sealed and left on the window for 2-3 days to photochemically react using visible light. The precipitaion of diisopropylamine hydrochloride, as well as a slight evolution of CO, only at the beginning of the reaction, was observed. The mixture was shaken occasionally and the black crystals of the $(\eta^5\text{-}C_5H_5)Fe(CO)_2I$ disappeared gradually to form an orange/brown solution with a copious beige precipitate.

The solution was then filtered through a hirsch funnel (diameter-2 cm) and the filtrate washed with diethyl ether. The filtrate was then pipetted into a round bottom flask and the solvent removed under vacuum. The residue was chromatographed (SiO_2 / $CHCl_3$) under gravity, the product band is the third band off the column. The band was collected

with a stream of argon over the collection flask and the solvent removed under vacuum, at room temperature. The orange/red residue was crystallised from diethyl ether / pentane to afford orange / red crystals.

M.p. 101-102°C (decomp.)(Lit.[2] m.p.101-103°C). ^{1}H NMR ($CDCl_3$): 6.34 ppm (s, 2H, α), 6.209 (s, 2H, β), 5.03 (s, 5H, Cp). ^{13}C NMR ($CDCl_3$): 86.04 ppm ($\underline{C}_5H_5$), 110.59 ppm (2C, β), 135,86 ppm (2C,α), 213.43 ppm (2 $\underline{C}O$). IR ν_{CO}: 2048cm^{-1}, 2002cm^{-1} (cyclohexane). Yield 28–33 %. Anal. Calc. C 54.37%, H 3.78%, N 5.56%. Found C 53.95%, H 3.73%, N 5.56%.

5.3.3 Synthesis of cyclopentadienyl-iron dicarbonyl-η^1-indolyl, $(\eta^5\text{-}C_5H_5)(\eta^1\text{-}N\text{-}C_8H_6N)Fe(CO)_2$

This complex was synthesised according to the method described by Pauson and Qazi[3] with minor alterations.

In a two-necked round-bottomed flask, ~ 20ml of pre-dried THF was purged gently with argon for approximately 5 minutes. Potassium metal (0.66g, 0.04 g-atom) was added to the THF under argon and the solution was slightly heated (~30° C) for 15 minutes, after which time indole (2.64 g, 45 mmol) was added to the solution. On addition of the indole, the mixture began to fizz gently, as the reaction appeared to be exothermic, the gentle heating was reduced by removing the oil bath. Formation of indolylpotassium was complete after approximately 1-1½ hours, and the solution was yellow/orange in colour. Increasing the flow of argon then evaporated off most of the solvent. After cooling, cyclopentadienyl-iron-dicarbonyl iodide (4 g, 26 mmol) in pre-purged benzene was added. The mixture was then warmed to 60° C for five hours, then cooled, filtered and concentrated. The crude mixture of cyclopentadienyl-iron-dicarbonyl indolyl was purified by column chromatography on silica with 1:1 solvent mixture of 60-80 petroleum-ether: diethyl ether. The first band eluted contained predominately iron dimer and un-reacted starting material, cyclopentadienyl-iron-dicarbonyl iodide. The second

band was eluted by gradually increasing the percentage of diethyl ether in the eluent and was a purple/pink solution. This contained the desired cyclopentadienyl-iron-dicarbonyl indolyl product.

^{1}H NMR ($CDCl_3$): 6.52, 6.85, 7.02, 7.39, 7.52 ppm (s, 6H, fused benzene ring), 5.063 ppm (s, 5H, Cp). IR ν_{CO}: 2044cm^{-1}, 1995cm^{-1} (toluene). Yield 30–35 %.

5.3.4 Synthesis of 2,5-dimethylazaferrocene, (η^5-C_5H_5)Fe(η^5-$C_4(CH_3)_2H_2N$)

This complex was synthesised according to the method described by Zakrzewski[4]

2,5-Dimethylpyrrole was distilled under reduced pressure immediately before use. A mixture of 2,5-dimethylpyrrole (5 ml, 49 mmol) and [(η^5-C_5H_5)Fe$(CO)_2]_2$ (1.42 g, 4 mmol) was brought to reflux temperature for 36 hours under an argon atmosphere. After cooling to room temperature, heptane (60 ml) was added, the resulting solid was filtered off. Analysis showed this was unreacted [(η^5-C_5H_5)Fe$(CO)_2]_2$. The filtrate was diluted with ether (40 ml) and extracted repeatedly with 5% aqueous HCl. The aqueous layer was shaken with ether (20 ml), separated and made alkaline with solid Na_2CO_3. Extraction with diethyl ether (2×30 ml), drying over $MgSO_4$ and evaporation of the solvent gave a red oil which was purified by column chromatography (SiO_2 / $CHCl_3$). This oil was washed with pentane, dried under reduced pressure and stored under argon at low temperature (sub 0°C) after which time there is some evidence of solid formation even at room temperature.

^{1}H NMR ($CDCl_3$): 4.32 ppm (s, 2H, β), 4.13 ppm (s, 5H, Cp), 2.25 ppm (s, 6H, 2 (CH_3)). IR ν_{CO}: no bands.

5.3.5 Attempted synthesis of cyclopentadienyliron dicarbonyl η^1-2,5-dimethylpyrrolyl, (η^5-C_5H_5)Fe(CO)$_2$(η^1-$C_4(CH_3)_2H_2N$)

Attempts were made to synthesise this complex by a method similar to that employed by Pauson and Qazi[3] in the synthesis of (η^5-C_5H_5)Fe(CO)$_2$(η^1-C_4H_4N), as it had been reported that the photochemical approach for the synthesis of (η^5-C_5H_5)Fe(CO)$_2$(η^1-C_4H_4N)[2] cannot be extended to alkyl derivatives.[4]

25 ml of spectroscopic grade benzene was purged with argon for ~ 20 minutes after which potassium metal (0.25 g, 5.37 mmol) was suspended in it. The three-necked flask's contents were then heated until the potassium dispersed before 1.53 ml (15 mmoles) of 2,5-dimethylpyrrole was added. The mixture was brought to reflux temperature until all the potassium had reacted (8-10 hours – solution turns light yellow colour). After cooling to room temperature cyclopentadienyliron dicarbonyl iodide (1.5 g, 5 mmol) in 25 ml of benzene (pre-purged with argon) was added and the mixture was gently heat to ~ 30° C for four to six hours. It was evident form the infrared spectra obtained of this reaction mixture that the bands of the parent complex, (η^5-C_5H_5)Fe(CO)$_2$I were diminishing in intensity and two new carbonyl bands were forming. The solvent of the resulting brown mixture was removed under reduced pressure. An infrared of the crude residue in cyclohexane reveals ν_{CO} at 2041 2004, 1961, 1995 and 1793 cm^{-1}, these are consistent with the presence of (η^5-C_5H_5)Fe(CO)$_2$(η^1-$C_4(CH_3)_2H_2N$), (ν_{CO} = 2041 and 1995 cm^{-1}) and iron dimer [(η^5-C_5H_5)Fe(CO)$_2$]$_2$, (ν_{CO} = 2004, 1961 and 1793 cm^{-1}). It was attempted to isolate (η^5-C_5H_5)Fe(CO)$_2$(η^1-$C_4(CH_3)_2H_2N$) by column chromatography (SiO_2 / CH_2Cl_2 and alumina / $CHCL_3$) under nitrogen, however all that could be identified from the different bands that were collected was the starting complex (η^5-C_5H_5)Fe(CO)$_2$I, iron dimer [(η^5-C_5H_5)Fe(CO)$_2$]$_2$ and traces of ferrocene. Attempts to isolation cyclopentadienyliron dicarbonyl η^1-2,5-dimethylpyrrolyl failed. It appears that although the substituents α, α to the nitrogen atom do not inhibit the formation of an η^1-type dicarbonyl complex, the stability of the complex is effected.

5.4 Infrared monitored steady state photolysis sample preparation

Unless otherwise stated, the samples were prepared in a specially designed cell with a degassing bulb attached to a cylindrical cell fitted with quartz windows. A side arm fitted with a rubber septum, allowed samples to be removed by syringe from the photolysis cell, and the infrared spectra were recorded in a solution cell (0.1mm). This photolysis cell was cleaned thoroughly by steeping in chromic acid for at least twelve hours prior to use. All the samples were prepared in the dark in the appropriate spectroscopic grade solvent. The samples were then degassed by three cycles of freeze-pump-thaw procedure to 10^{-3} torr, followed by a substantial liquid pump phase in order to remove any trace impurities such as water.

An atmosphere of carbon monoxide was then placed over the sample solution. The pressure of carbon monoxide that was admitted to the flash cell after the degassing process was used to determine the concentration of carbon monoxide.

5.5 Laser flash photolysis – sample preparation

Samples were prepared in a specially designed degassing bulb attached to a fluorescence cell. This cell was cleaned thoroughly by steeping in chromic acid for at least twelve hours prior to use. All the samples were prepared in the dark in the appropriate spectroscopic grade solvent such that the absorbance at $\lambda_{exc.}$ (355 nm or 532 nm) was between 0.5 and 1.5 A.U. The samples were then degassed by three cycles of freeze-pump-thaw procedure to 10^{-3} torr, followed by a substantial liquid pump phase in order to remove any trace impurities such as water.

The atmosphere of interest (argon or carbon monoxide) was then placed over the sample solution to investigate the reversibility of the process being investigated and to prevent boiling of the solvent. The pressure of carbon monoxide that was admitted to the flash

cell after the degassing process was used to determine the concentration of carbon monoxide. The solubility of carbon monoxide in cyclohexane[5] and toluene[6] was taken to be 9.0×10^{-3} M and 7.53×10^{-3} M respectively under 1 atm of carbon monoxide. Spectral changes before and after degassing the sample were recorded as well as periodic monitoring of the sample solution during the photolysis experiment.

5.5.1 Laser flash photolysis with UV-Vis detector apparatus

The excitation source is a neodymium yttrium aluminium garnet (Nd-YAG) laser, which operates at 1064 nm. Nd atoms are implanted in the host YAG crystals at approximately one per hundred. The YAG host material has the advantage of having a relatively high thermal conductivity to remove the wasted heat, thus allowing these crystals to be operated at high repetition rates of the order of many pulses per second. The frequency can be doubled, tripled, or quadrupled with non-linear optical techniques to generate a second, third or forth-harmonic frequency at 532 nm, 355 nm, or 266 nm respectively. This allows certain atomic process to be preferentially selected. The power of the laser can be amplified by applying different voltages across the amplifier flash tube. The pulse time is approximately 10 ns, the energy generated for the 266, 355 and 532 nm frequencies is typically 55 mJ, 45 mJ, and 25 mJ per pulse respectively.

The circular laser pulse is diverted *via* two Pellin Broca prisms onto the sample cuvette. When the pulse passes through the power meter situated after the first prism, but before the sample cuvette, the oscilloscope is triggered. The monitoring light source is an air-cooled 275-watt xenon arc lamp arranged at right angles to the laser beam. The monitoring beam passes through the sample and is directed to the entrance slit of an Applied Photophysics f/3 monochromator *via* a circular lens. UV-Vis filters were employed between monitoring source and sample to prevent excessive sample photo-degradation. A hamatsu 5 stage photomultipilier operating at 850V was placed at

the exit slit of the monochromator. The absorbance changes were measured by a transient digitiser (oscilloscope) *via* a variable load resistor. The digitiser, a Hewlett Packard HP 54510A oscilloscope was interfaced to a PC. All signals were recorded on floppy discs.

A typical transient signal was obtained as follows: the amount of monitoring light being transmitted through the solution before the laser flash, I_0, is recorded initially. This is the voltage corresponding to the amount of light detected by the photomultipilier tube when the source (xenon arc lamp) shutter opens, less the voltage generated by the stray light. When the monitoring source is opened while simultaneously firing the laser pulse through the sample cuvette and the amount of light transmitted through is recorded (I_t). Since I_0/I_t = absorbance, the change in intensity of the probe beam transmitted through the sample is measured as a function of time and/or wavelength.

By recording transient signals sequentially over a range of wavelengths, absorbance readings can be calculated at any time after the flash to generate a difference absorption spectrum of the transient species. Spectra are obtained as a result of point by point build-up by optically changing the wavelength of the monochromator. It is necessary that the solution is optically transparent for the monitoring light beam and hence solvents of spectroscopic transparency are required. A schematic diagram of the laser flash photolysis instrumentation is presented in Figure 5-1.

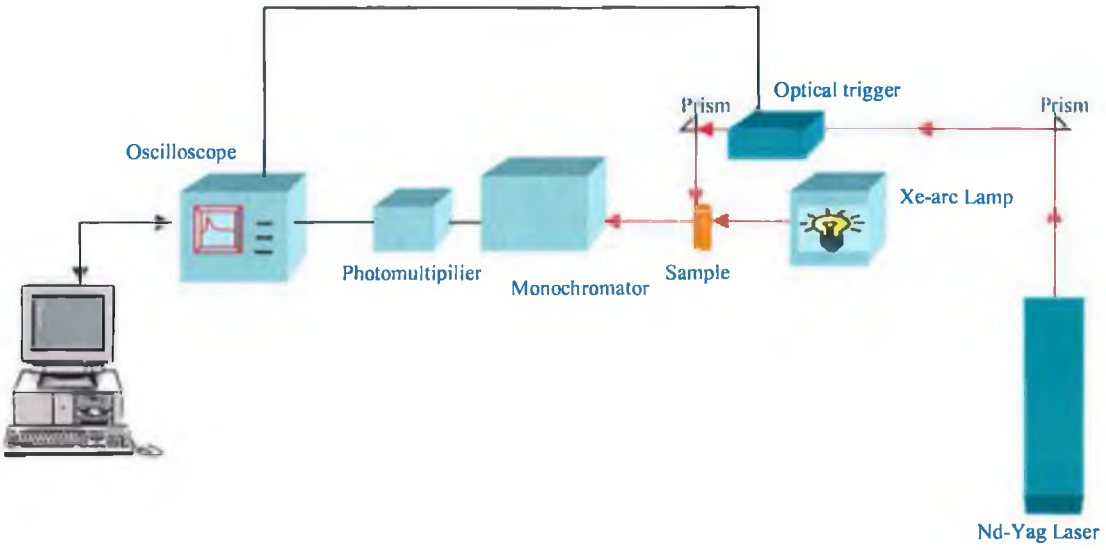

Figure 5-1 A schematic diagram of the instrumentation used in the laser flash photolysis experiments.

5.6 Matrix isolation instrumentation

The instrumentation employed for the matrix isolation experiments at York University has been described elsewhere[7]. The set-up consists of a closed cycle helium refrigerator (Air Products CS202), which cools the spectroscopic window to 12 K. The rate of deposition (0.6 Torr / min) of the matrix gas was followed with a Baratron capacitance gauge. Matrices for the experiments were deposited by slow spray on method to a cesium iodide or barium fluoride spectroscopic window cooled to 20 K, with matching outer windows on the vacuum shroud. For UV-Vis experiments all three windows were made of barium fluoride, thus giving near perfect UV-Vis transmission and allowing the IR spectrum to be monitored to 1100 cm^{-1}.

Matrixes were photolysised with a 300 W xenon arc lamp in conjunction with a water filter to remove heat (path length = 5 cm). Selective wavelength irradiation was achieved with cut-off filters, Schott interference filters (λ_{max} = 434 nm, λ_{max} = 538 nm,

full-width at half-maximum, fwhm = 10 nm). Infrared spectra were recorded on a Perkin-Elmer 580A spectrometer. UV-Vis spectra were recorded on a Perkin-Elmer Lambda 7G spectrometer.

The instrumentation employed for the matrix isolation experiments at Dublin City University is as follows. The matrixes were deposited by the slow spray-on method onto a calcium fluoride spectroscopic window cooled to 20 K. The outer windows of the vacuum shroud were chosen to match. Typically the matrix gas was deposited alone for ten minutes, before the sample was co-condensed from a right-angled tube immersed in a dewar flask containing water at the correct temperature to sublime the sample, (i.e. azaferrocene, 289-292 K; 2.5-dimethylazaferrocene, 270-273 K, and cyclopentadienyl-iron dicarbonyl-pyrrolyl, 313-316 K). This procedure produced matrixes of better quality than co-condensing sample and matrix gases from the beginning.

The rate of deposition of the matrix gas was 0.6 Torr per minute. The pressure in the gas inlet line is continuously checked by means of a separate thermotron gauge. On average the deposition time was 2-2½ hours. The spectroscopic window on which the sample and matrix gases were deposited, was cooled by a closed cycle helium refrigerator (APD Cryogenics Inc.) mounted via a double o-ring seal in a stainless steel vacuum shroud. The system was pumped to 6×10^{-5} Torr prior to cooling and achieved better than 4×10^{-7} Torr cold. The temperature is controlled by a gold/chromel thermocouple near to the spectroscopic window. The matrix gases were mixed prior to deposition in a stainless steel cylindrical chamber (fitted with a safety valve) pumped by an turbo molecular pump (Edwards) with a rotary pump for back up. The matrix spectroscopic window was cooled further to 12 K before photolysis was begun in most experiments, except in cases where the matrix appeared fragile, in these instances further cooling risked causing the matrix to crack, therefore the matrix was photolysed at 20 K.

The arrangement is such that the shroud remains stationary and the infrared spectrophotometer is mounted on a trolley with tracks on the bench to guide its movement into position. In this way the infrared spectrophotometer is placed around the vacuum shroud so that the vacuum shroud is in the pathway of the infrared beam. Matrixes were photolysed with either an Oriel 300 Watt xenon arc lamp, type XXXXX (usually used for broad band irradiation) or an Oriel 200 Watt medium pressure mercury/xenon arc lamp (usually used for monochromatic irradiation), used in conjunction with a water filter to remove heat (path length ~ 5.5 cm). Both lamps were powered with an Oriel Xe/Xe-Hg 200-500 Watt power supply model 68911. Selective wavelength irradiation was achieved with cut-off filters (broad band irradiation) and interference filters (Åndover Corporation Optical filters-monochromatic irradiation, 577, 546, 436, 405, 365, 254 nm).

Infrared spectra were recorded at (1 cm^{-1} resolution / 16 scans) on a Perkin-Elmer One spectrum FT-IR spectrophotometer.

5.7 Determination of extinction coefficients

Extinction coefficients were determined for compounds at the wavelength of excitation in the relevant solvents. The Beer-Lambert law then allows the calculation of the concentration of a sample when the absorbance of the compound is known. The Beer-Lambert law is given by:

$$A = \varepsilon c l$$

Where;

A = absorbance at the excitation wavelength (AU)

ε = molar extinction coefficient ($L\ mol^{-1}\ cm^{-1}$)

c = concentration ($mol\ L^{-1}$)

l = path-length (1 cm)

5.8 Determination of the concentration of carbon monoxide in cyclohexane and toluene

The solubility of carbon monoxide in hydrocarbon solvents was determined using the mole fraction data reported by Makrancy *et al.*[5]

The calculations for cyclohexane are as follows:

- solubility of carbon monoxide at 298 K (expressed as a mole fraction) = 9.94×10^{-4} moles^{-1}
- 1 L of cyclohexane = 779 g
- 1 mole of cyclohexane = 84 g

$\Rightarrow$ moles per litre = $1 / 84 \times 779 = 9.274$ moles L^{-1}.

$\Rightarrow$ 9.94×10^{-4} moles^{-1} = $\frac{\#[CO]}{9.274 \text{ moles } L^{-1}}$.

$\Rightarrow$ $[CO] = 9.0 \times 10^{-3}$ M at 1 atm

The calculations for toluene are:

- Solubility of carbon monoxide at 298 K (expressed as a mole fraction) = 7.98×10^{-4} moles^{-1}
- 1 L of toluene = 867 g
- 1 mole of cyclohexane = 92.07 g

$\Rightarrow$ moles per litre = $1 / 92.07 \times 867 = 9.42$ moles L^{-1}.

$\Rightarrow$ 7.98×10^{-4} moles^{-1} = $\frac{\#[CO]}{9.42 \text{ moles } L^{-1}}$

$\Rightarrow$ $[CO] = 7.53 \times 10^{-3}$ M at 1 atm.

5.9 Determination of activation parameters

The activation parameters were calculated from Arrhenius and Eyring plots.

The Arrhenius equation is: $\ln k = \ln A - E_a/RT$

Where k = rate constant

E_a = activation energy (kJ mol^{-1})

R = universal gas constant (8.314 $JK^{-1}mol^{-1}$)

T = absolute temperature (K)

A = frequency factor (the number of collisions between the reactant molecules)

A plot of the ln k, (where $k = k_{obs}/ [CO]$) *versus* 1/T gives a straight line with the slope = $-E_a/R$ and the intercept = ln A.

The Eyring equation is $\ln(k/T) = -(\Delta H^{\neq}/RT) + (\Delta S^{\neq}/R) + \ln(k/h)$

Where k = rate constant (i.e. $k = k_{obs}/ [CO]$)

$\Delta H^{\neq}$ = enthalpy change of activation (kJ mol^{-1})

$\Delta S^{\neq}$ = entropy change of activation (J $mol^{-1}K^{-1}$)

k = Boltzman's constant (1.38066×10^{-23} JK^{-1})

h = Plank's constant (6.62618×10^{-34} Js)

T = absolute temperature (K)

R = universal gas constant (8.314 $JK^{-1}mol^{-1}$)

A plot of ln k/T versus 1/T gives a straight line with slope $-\Delta H^{\neq}/RT$ and the intercept $\Delta S^{\neq}/R + \ln(k/h)$.

The activation parameters were calculated by recording the increase in the observed rate constant with increasing temperature. The temperature changes were achieved by immersing the flash photolysis cell in a temperature controlled water bath for a period of twenty minutes at the required temperature. The temperature of the water bath was increased in increments of 5 K in the temperature range 283-313 K.

5.10 References

1 K. K. Joshi, P. L. Pauson, A. R. Qazi, W. H. Stubbs, *J. Organomet. Chem.*, **1964**, 471.

2 (a) J. Zakrzewski, *J. Organomet. Chem.*, **1987**, 327, C41.

(b) C. Gianotti, J. Zakrzewski, *J. Organomet. Chem.*, **1990**, 338, 175.

3 P. L. Pauson, A. R. Qazi, *J. Organomet. Chem.*,**1967**, 7, 321.

4 J. Zakzewski, *Inorg. Chim. Acta*, **1998**, 278, 101.

5 J. Makrancy, K. Megyery-Balog, L. Rosz, D. Patyt, *Hung. J. Ind. Chem.*, **1976**, 4, 269.

6 J. C. Gjaldbek, *Acta Chem. Scad.*; **1952**, 6, 623.

7 D. M. Haddleton, A. McCamley, R. N. Perutz, *J. Am. Chem. Soc.*, **1988**, 110, 1810.

Appendix

Appendix
A

EXTINCTION COEFFICICENTS

Azaferrocene, $(\eta^5\text{-}C_5H_5)Fe(\eta^5\text{-}C_4H_4N)$ in cyclohexane at 326 nm

Concentration × 10^{-2} / M	Absorbance at 326 nm / A.U.
0.00	0.0
0.60	0.29624
1.20	0.55092
1.80	0.82673
2.40	1.12457

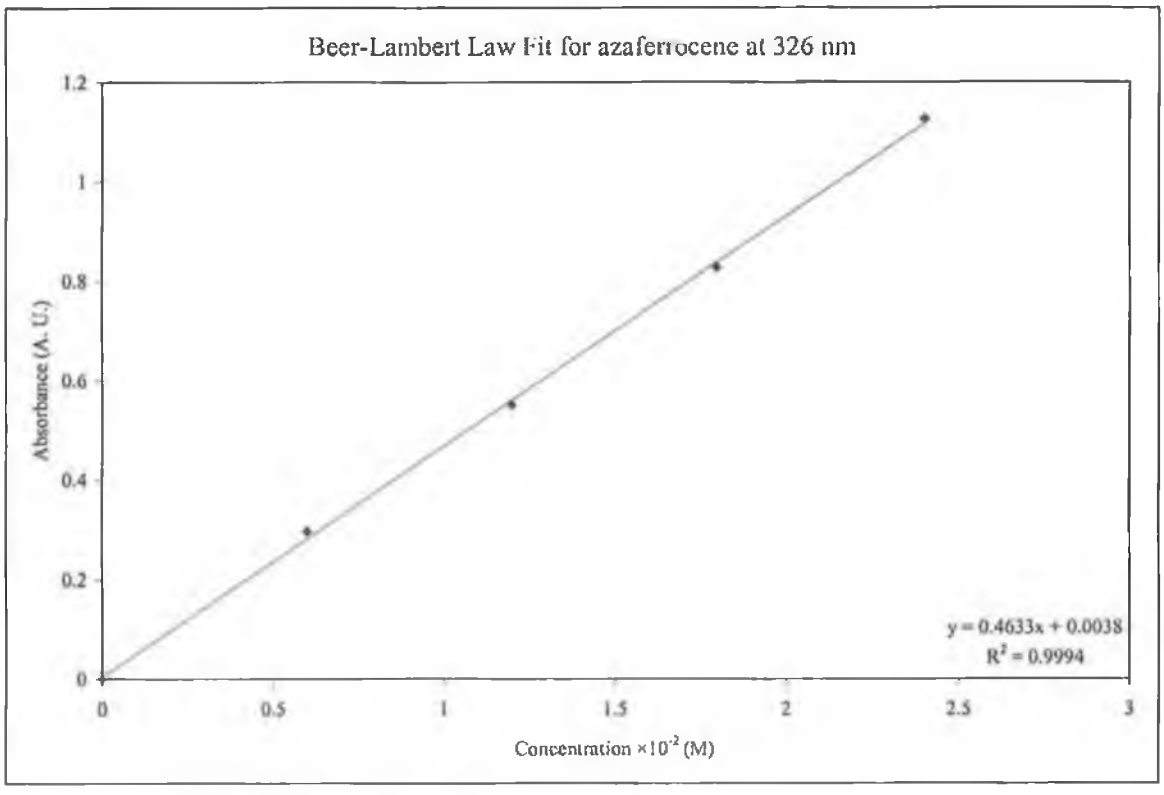

The extinction coefficient (ϵ) for azaferrocene is 46.33 L mol^{-1} cm^{-1} at 336 nm.

Azaferrocene, (η^5-C_5H_5)Fe(η^5-C_4H_4N) in cyclohexane at 424 nm

Concentration × 10^{-2} / M	Absorbance at 424 nm / A.U.
0.00	0.0
0.60	0.23796
1.20	0.45499
1.80	0.66433
2.40	0.92279

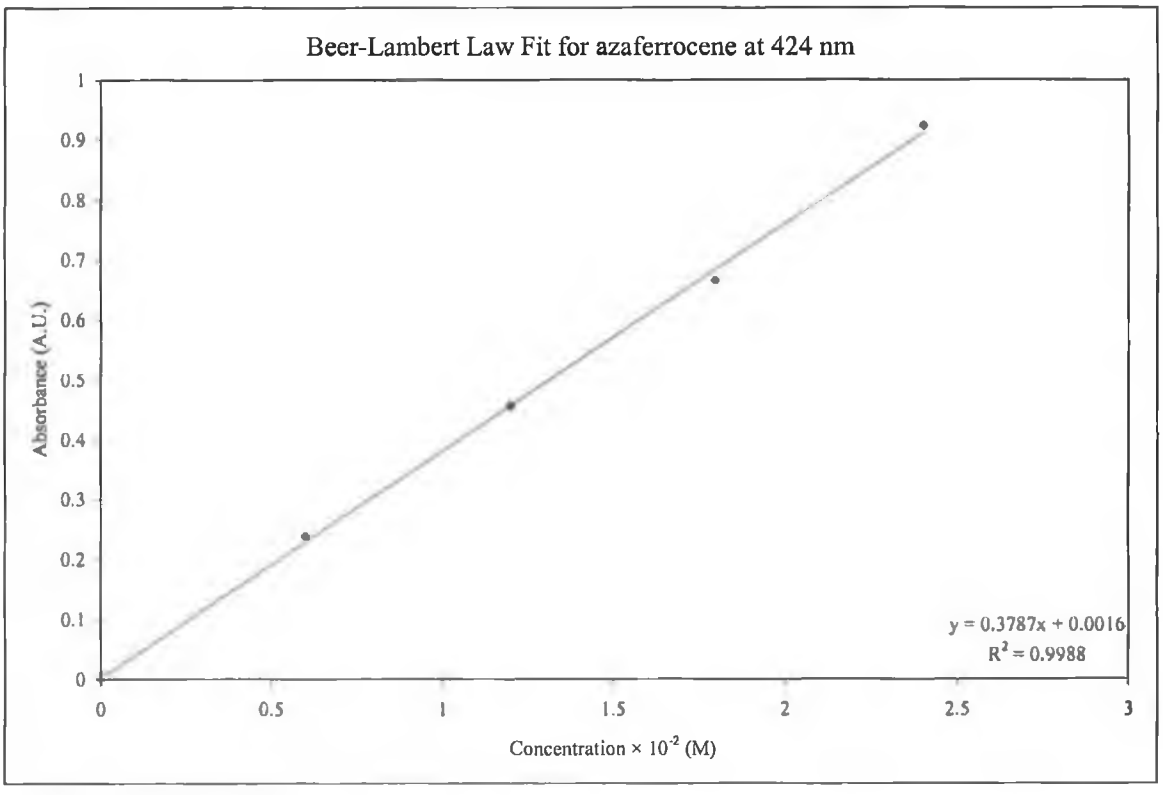

The extinction coefficient (ϵ) for azaferrocene is 37.87 L mol^{-1} cm^{-1} at 424 nm.

Cyclopentadienyl-iron dicarbonyl η^1-pyrrolyl, $(\eta^5\text{-}C_5H_5)Fe(CO)_2(\eta^1\text{-}C_4H_2N)$ in cyclohexane at 340 nm

Concentration × 10^{-4} / M	Absorbance at 340 nm / A.U.
0.00	0.0
2.35	0.34362
4.71	0.66054
7.07	1.07080
9.42	1.40052
11.78	1.71268

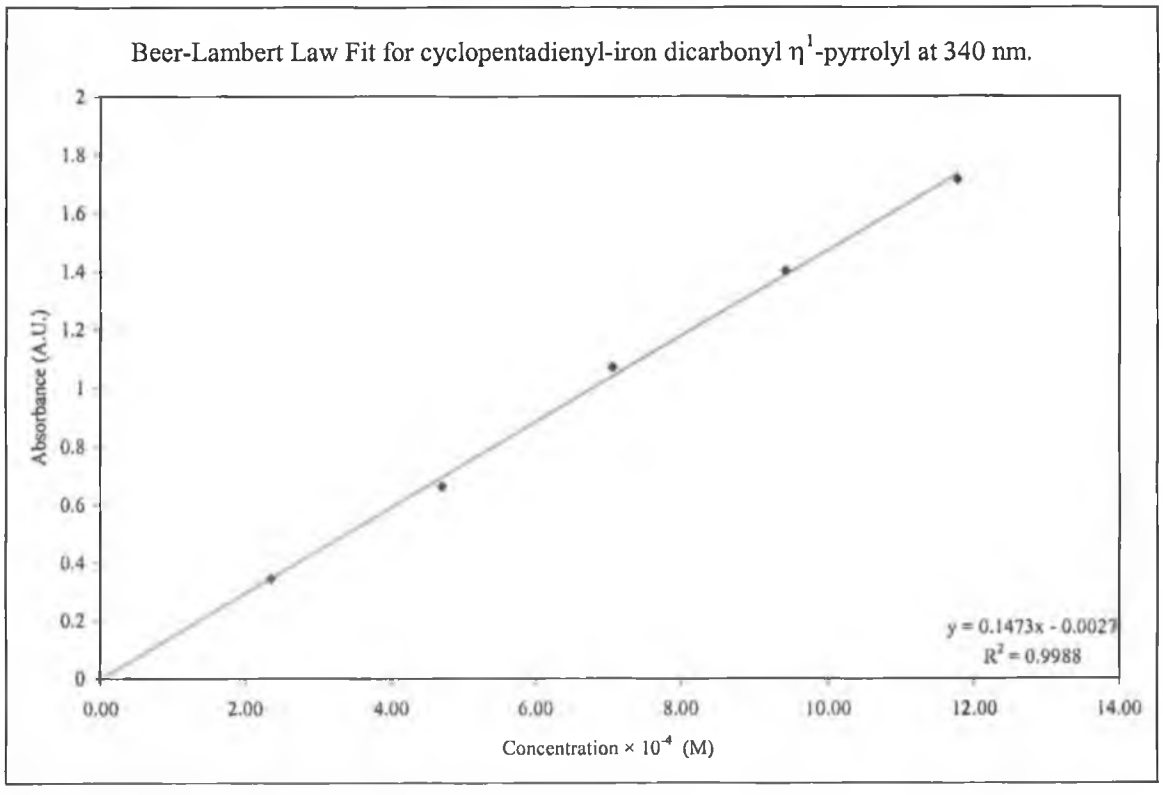

The extinction coefficient (ϵ) for cyclopentadienyl-iron dicarbonyl η^1-pyrrolyl is 1.47×10^3 L mol^{-1} cm^{-1} at 340 nm.

Cyclopentadienyl-iron dicarbonyl η^1-pyrrolyl, $(\eta^5\text{-}C_5H_5)Fe(CO)_2(\eta^1\text{-}C_4H_2N)$ in cyclohexane at 354 nm

Concentration × 10^{-4} / M	Absorbance at 354 nm / A.U.
0.00	0.0
2.35	0.30766
4.71	0.60285
7.07	0.97637
9.42	1.28270
11.78	1.56591

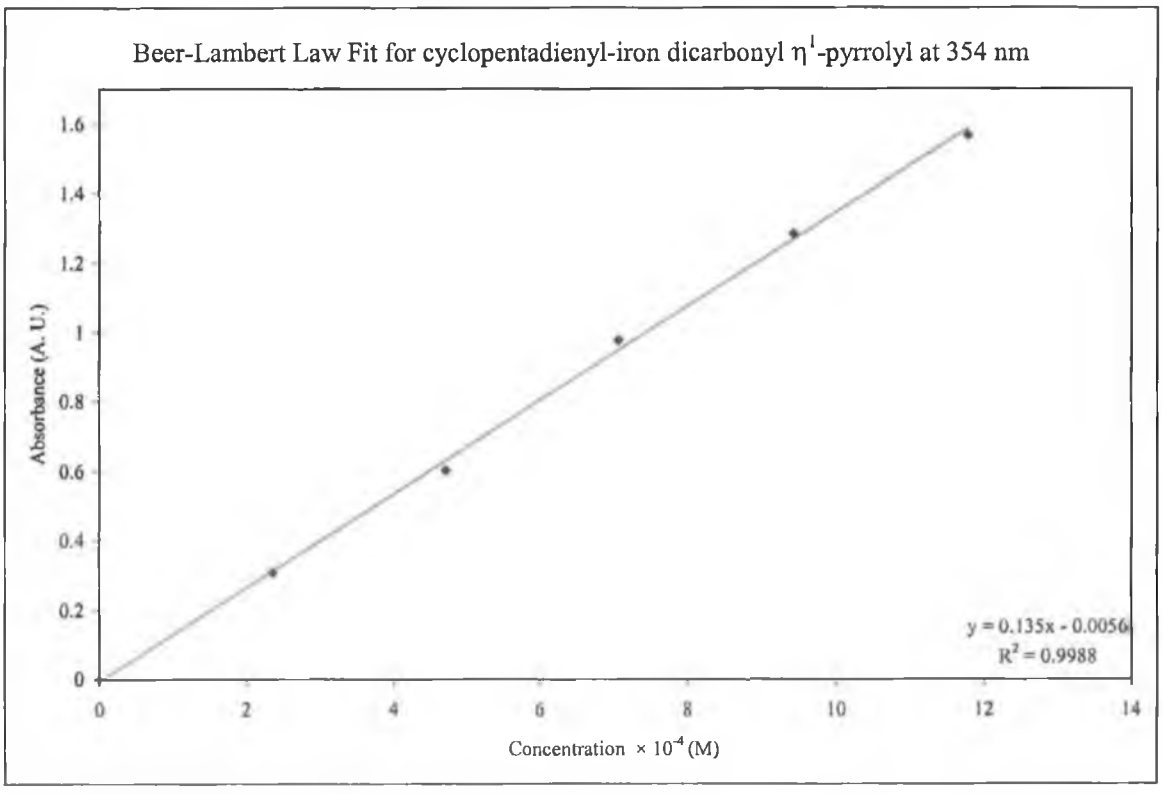

The extinction coefficient (ϵ) for cyclopentadienyl-iron dicarbonyl η^1-pyrrolyl is 1.35×10^3 L mol^{-1} cm^{-1} at 354 nm.

Cyclopentadienyl-iron dicarbonyl η^1-pyrrolyl, $(\eta^5\text{-}C_5H_5)Fe(CO)_2(\eta^1\text{-}C_4H_2N)$ in cyclohexane at 484 nm

Concentration × 10^{-4} / M	Absorbance at 484 nm / A.U.
0.00	0.0
2.35	0.07754
4.71	0.16062
7.07	0.24065
9.42	0.33091
11.78	0.43005

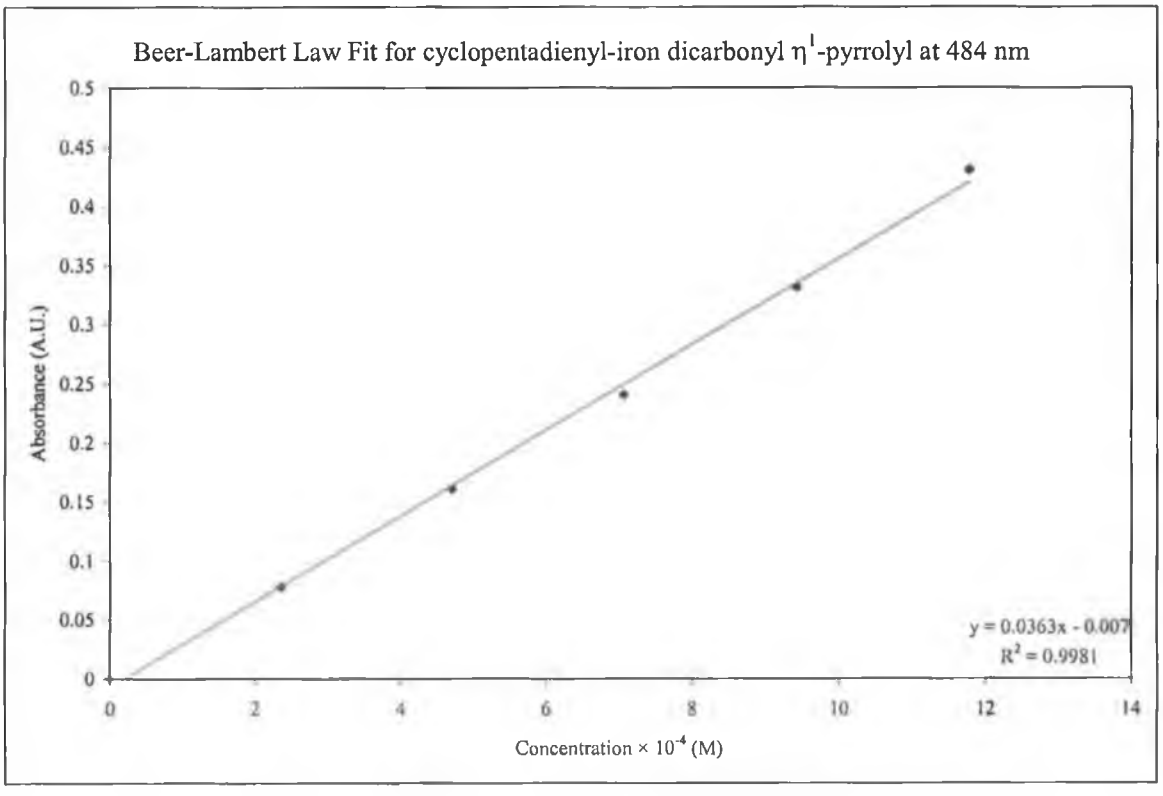

The extinction coefficient (ϵ) for cyclopentadienyl-iron dicarbonyl η^1-pyrrolyl is 3.63×10^2 L mol^{-1} cm^{-1} at 484 nm.

Cyclopentadienyl-iron dicarbonyl η^1-pyrrolyl, $(\eta^5\text{-}C_5H_5)Fe(CO)_2(\eta^1\text{-}C_4H_2N)$ in toluene at 340 nm

Concentration × 10^{-4} / M	Absorbance at 340 nm / A.U.
0.00	0.0
2.35	0.35362
4.71	0.68054
7.07	1.08079
9.42	1.41052
11.78	1.71268

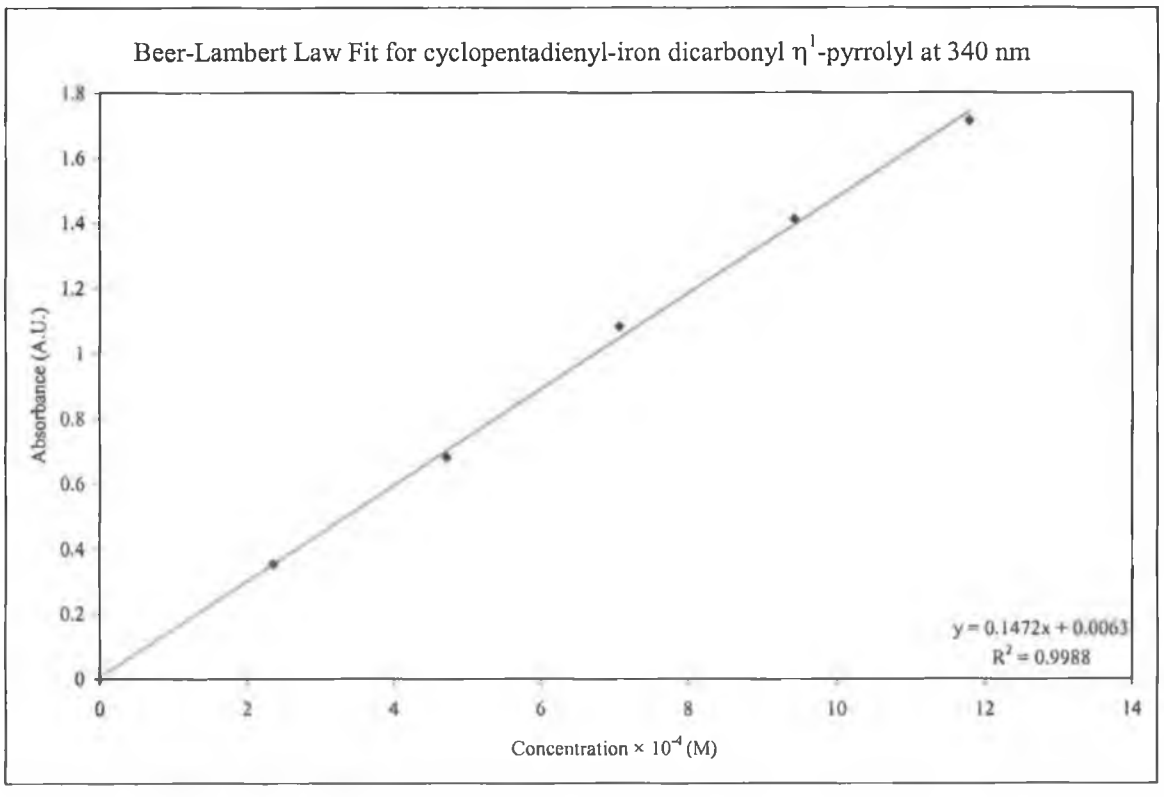

The extinction coefficient (ϵ) for cyclopentadienyl-iron dicarbonyl η^1-pyrrolyl is 1.47×10^3 L mol^{-1} cm^{-1} at 340 nm.

Cyclopentadienyl-iron dicarbonyl η^1-pyrrolyl, $(\eta^5\text{-}C_5H_5)Fe(CO)_2(\eta^1\text{-}C_4H_2N)$ in toluene at 354 nm

Concentration × 10^{-4} / M	Absorbance at 354 nm / A.U.
0.00	0.0
2.35	0.31766
4.71	0.61285
7.07	0.98637
9.42	1.29269
11.78	1.57591

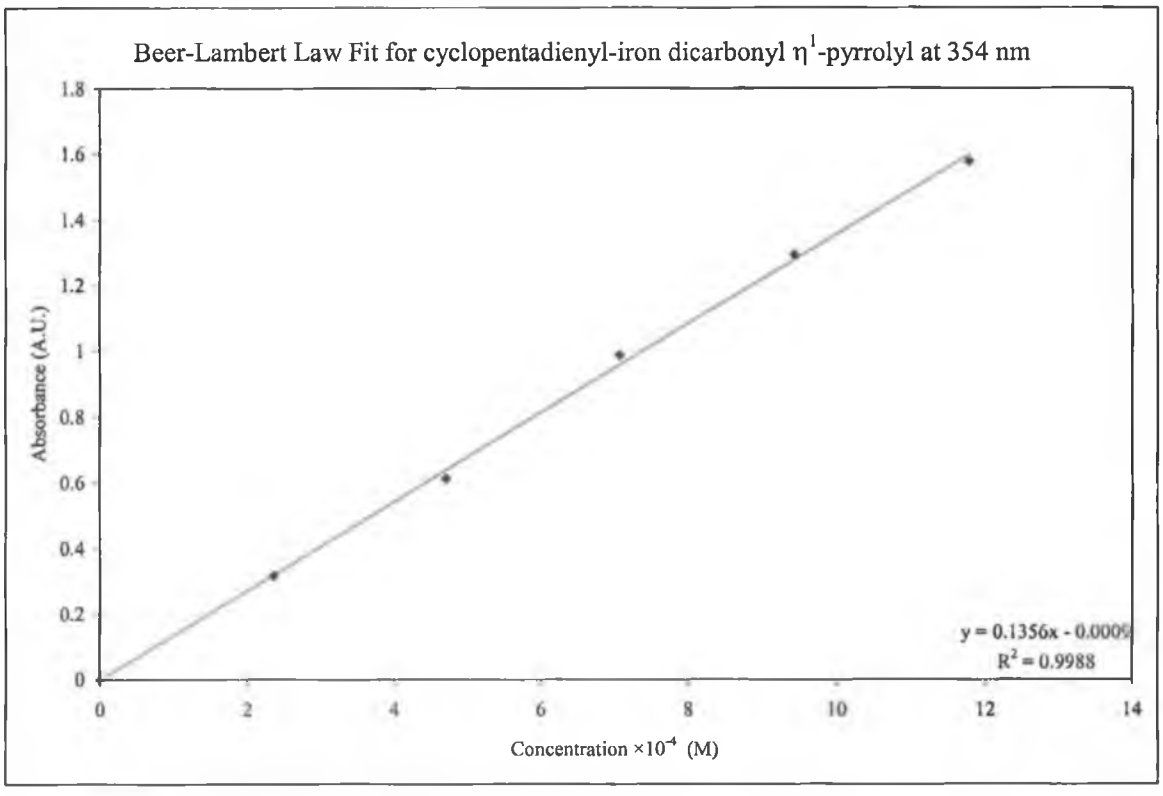

The extinction coefficient (ϵ) for cyclopentadienyl-iron dicarbonyl η^1-pyrrolyl is 1.36×10^3 L mol^{-1} cm^{-1} at 354 nm.

Cyclopentadienyl-iron dicarbonyl η^1-pyrrolyl, $(\eta^5\text{-}C_5H_5)Fe(CO)_2(\eta^1\text{-}C_4H_2N)$ in toluene at 484 nm

Concentration × 10^{-4} / M	Absorbance at 484 nm / A.U.
0.00	0.0
2.35	0.07764
4.71	0.16162
7.07	0.24165
9.42	0.34091
11.78	0.43996

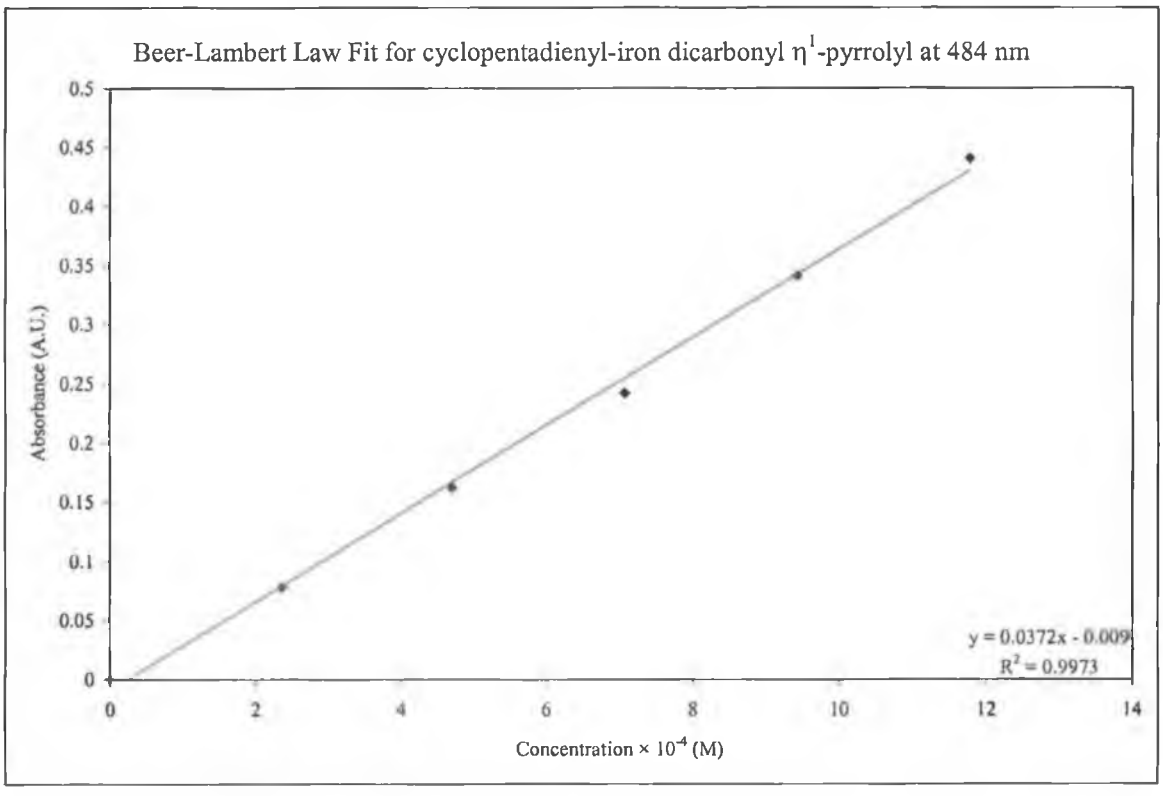

The extinction coefficient (ϵ) for cyclopentadienyl-iron dicarbonyl η^1-pyrrolyl is 3.72×10^2 L mol^{-1} cm^{-1} at 484 nm.

Cyclopentadienyl-iron dicarbonyl η^1-indolyl, $(\eta^5\text{-}C_5H_5)Fe(CO)_2(\eta^1\text{-}C_8H_6N)$ in toluene at 354 nm

Concentration × 10^{-4} / M	Absorbance at 354 nm / A.U.
0.00	0.0
2.38	0.46289
4.76	0.89206
7.14	1.26489
9.52	1.69594
11.90	2.04576

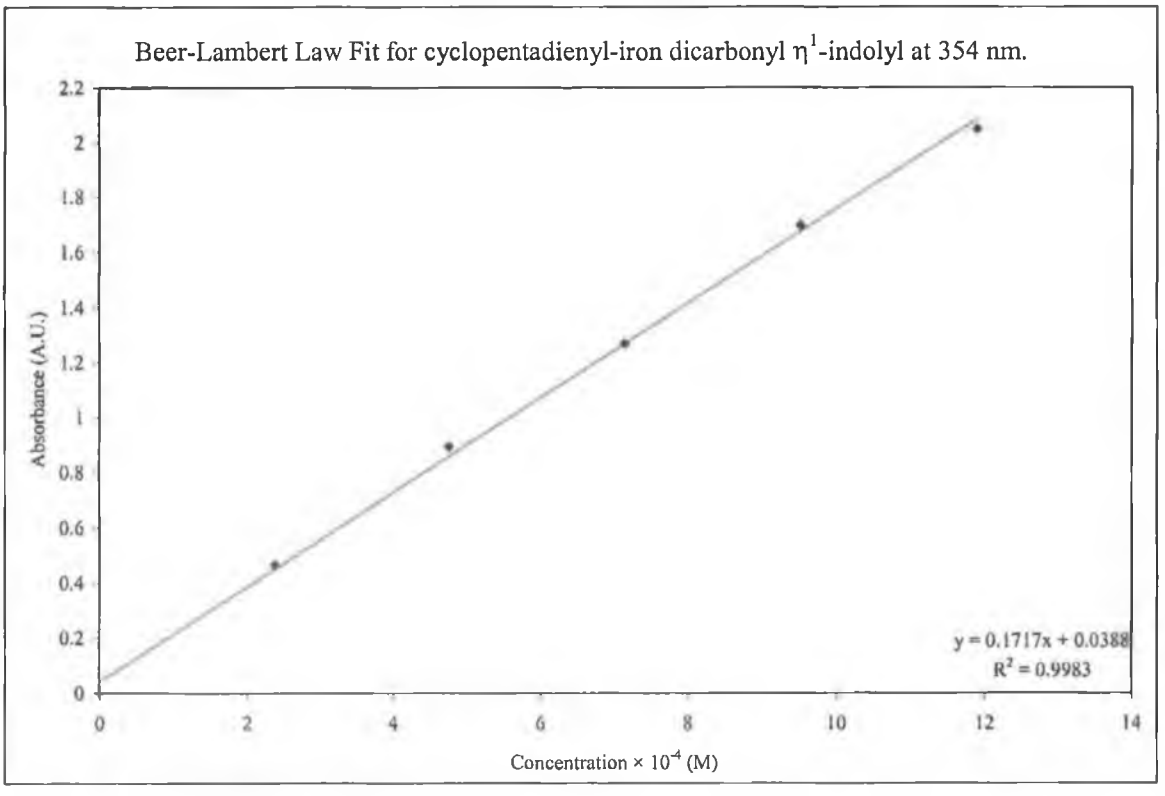

The extinction coefficient (ϵ) for cyclopentadienyl-iron dicarbonyl η^1-indolyl is 1.72×10^3 L mol^{-1} cm^{-1} at 354 nm.

Cyclopentadienyl-iron dicarbonyl η^1-indolyl, $(\eta^5\text{-}C_5H_5)Fe(CO)_2(\eta^1\text{-}C_8H_6N)$ in toluene at 358 nm

Concentration × 10^{-4} / M	Absorbance at 358 nm / A.U.
0.00	0.0
2.38	0.45172
4.76	0.86453
7.14	1.24503
9.52	1.66877
11.90	2.02078

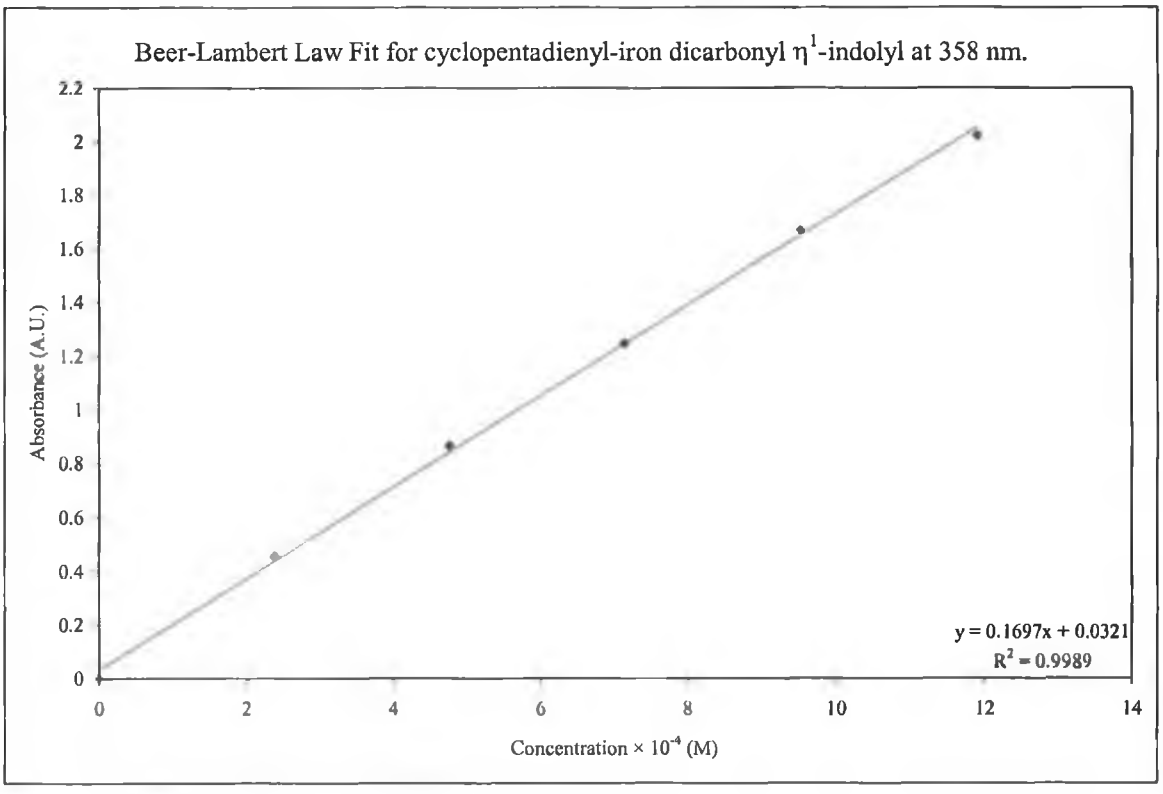

The extinction coefficient (ϵ) for cyclopentadienyl-iron dicarbonyl η^1-indolyl is 1.70×10^3 L mol^{-1} cm^{-1} at 358 nm.

Cyclopentadienyl-iron dicarbonyl η^1-indolyl, $(\eta^5\text{-}C_5H_5)Fe(CO)_2(\eta^1\text{-}C_8H_6N)$ in toluene at 518 nm

Concentration × 10^{-4} / M	Absorbance at 518 nm / A.U.
0.00	0.0
2.38	0.10294
4.76	0.23099
7.14	0.33196
9.52	0.43877
11.90	0.54682
19.03	0.86703

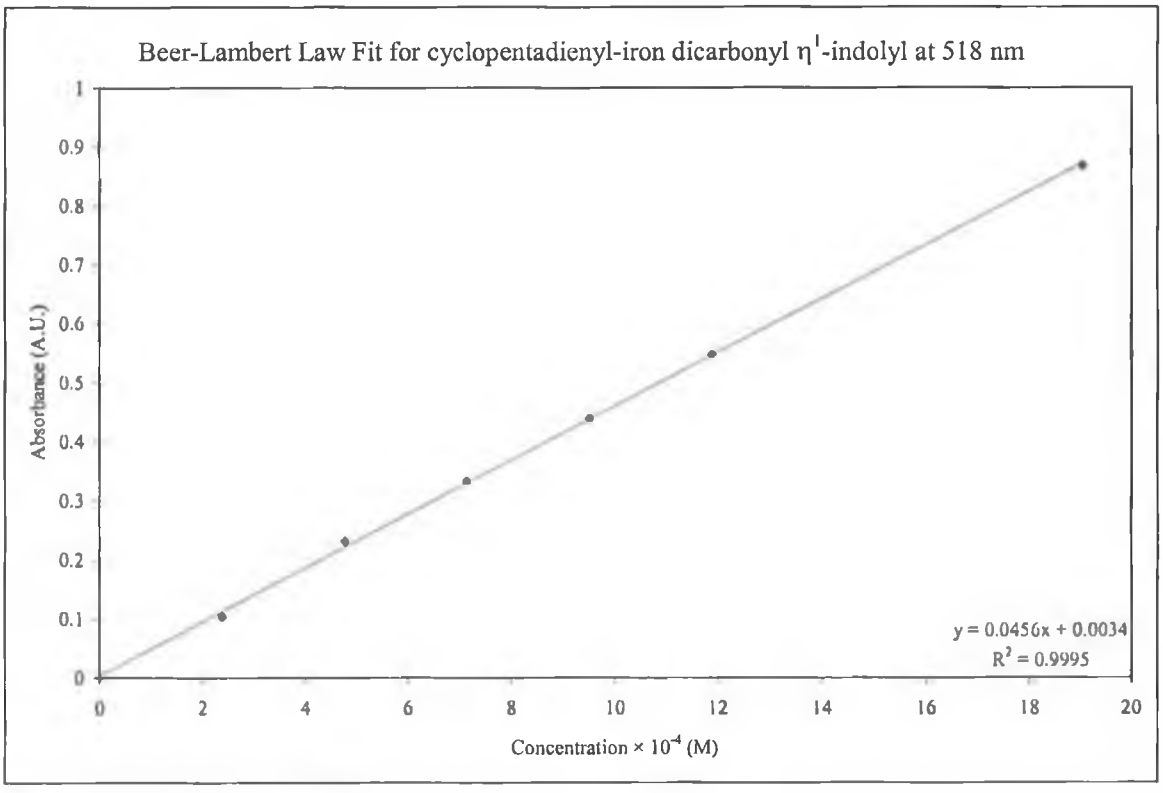

The extinction coefficient (ϵ) for cyclopentadienyl-iron dicarbonyl η^1-pyrrolyl is 4.56×10^2 L mol^{-1} cm^{-1} at 518 nm.

Cyclopentadienyl-iron dicarbonyl η^1-indolyl, $(\eta^5\text{-}C_5H_5)Fe(CO)_2(\eta^1\text{-}C_8H_6N)$ in toluene at 532 nm

Concentration × 10^{-4} / M	Absorbance at 532 nm / A.U.
0.00	0.0
2.38	0.00997
4.76	0.22661
7.14	0.32899
11.90	0.55031
19.03	0.83971

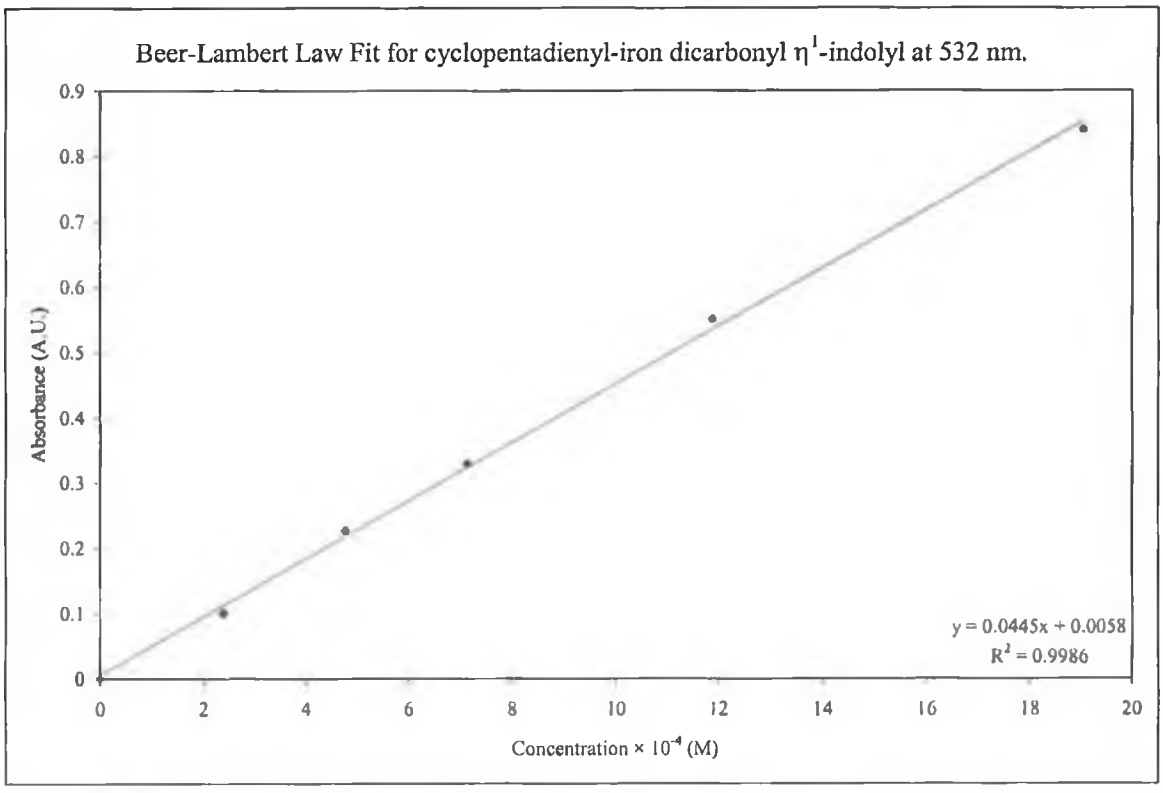

The extinction coefficient (ϵ) for cyclopentadienyl-iron dicarbonyl η^1-pyrrolyl is 4.45×10^2 L mol^{-1} cm^{-1} at 532 nm.

2,5-Dimethylazaferrocene, $(\eta^5\text{-}C_5H_5)Fe(\eta^5\text{-}2,5\text{-}(CH_3)_2C_4H_2N)$ in cyclohexane at 336 nm

Concentration × 10^{-3} / M	Absorbance at 336 nm / A.U.
0.00	0.0
1.34	0.18272
2.69	0.35460
4.03	0.54024
5.37	0.71477
6.72	0.93756

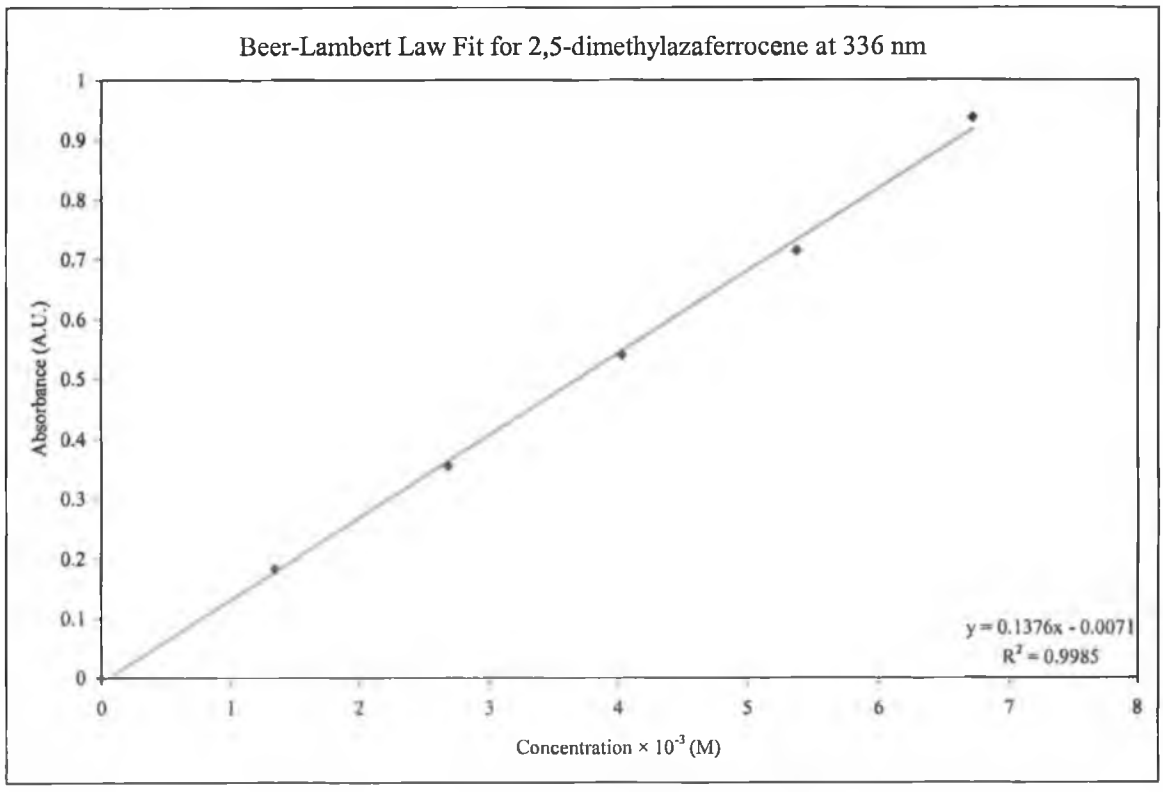

The extinction coefficient (ϵ) for 2,5-dimethylazaferrocene is 1.38×10^2 L mol^{-1} cm^{-1} at 336 nm.

2,5-Dimethylazaferrocene, (η^5-C_5H_5)Fe(η^5-2,5-$(CH_3)_2C_4H_2N$) in cyclohexane at 354 nm

Concentration × 10^{-3} / M	Absorbance at 354 nm / A.U.
0.00	0.0
1.34	0.12811
2.69	0.25079
4.03	0.37727
5.37	0.51818
6.72	0.65847

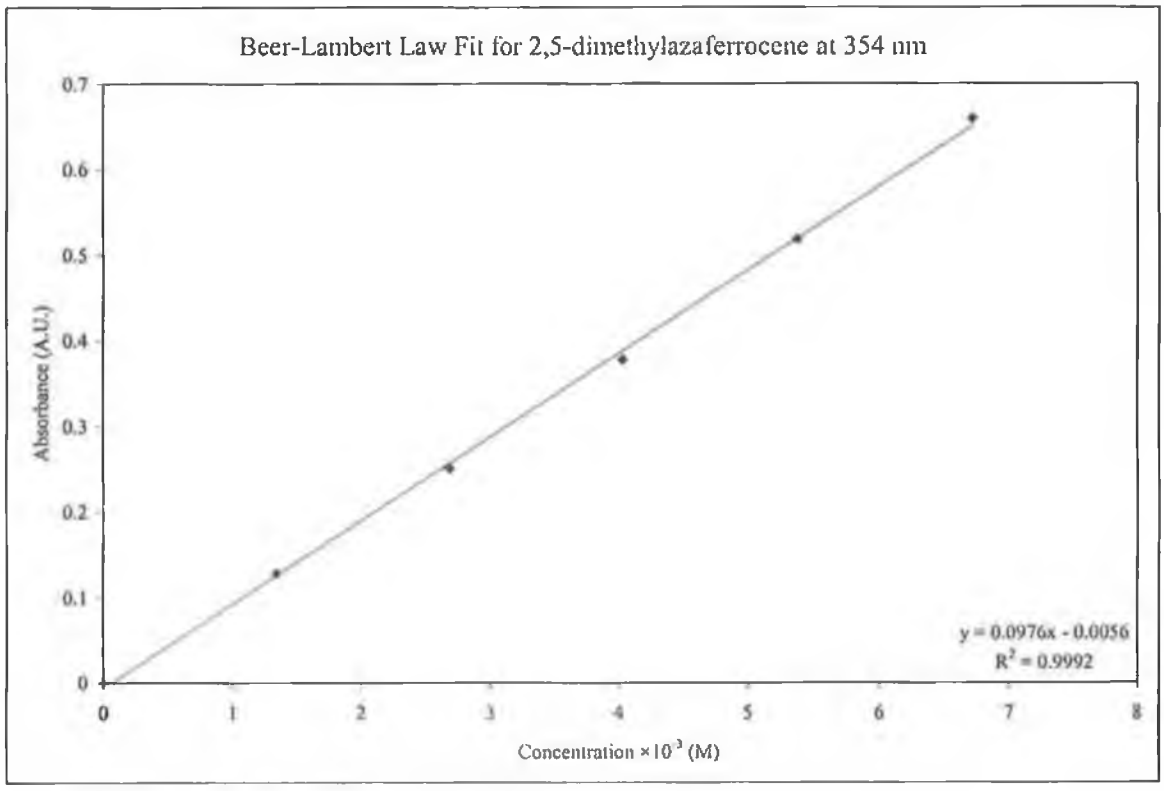

The extinction coefficient (ϵ) for 2,5-dimethylazaferrocene is 97.6 L mol^{-1} cm^{-1} at 354 nm.

2,5-Dimethylazaferrocene,(η^5-C_5H_5)Fe(η^5-2,5-$(CH_3)_2C_4H_2N$) in cyclohexane at 446 nm

Concentration × 10^{-3} / M	Absorbance at 446 nm / A.U.
0.00	0.0
1.34	0.18454
2.69	0.38277
4.03	0.58785
5.37	0.74429
6.72	0.95322

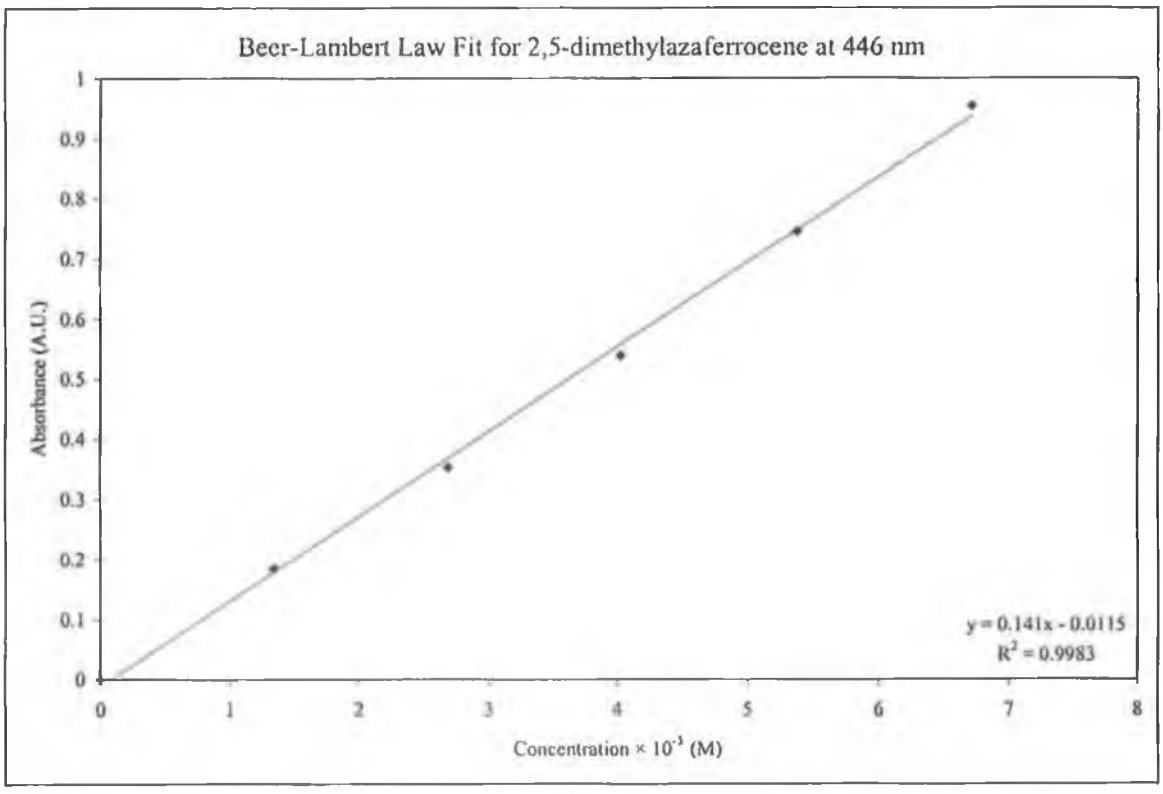

The extinction coefficient (ϵ) for 2,5-dimethylazaferrocene is 1.41 × 10^2 L mol^{-1} cm^{-1} at 446 nm.

2,5-Dimethylazaferrocene, $(\eta^5\text{-}C_5H_5)Fe(\eta^5\text{-}2,5\text{-}(CH_3)_2C_4H_2N)$ in cyclohexane at 532 nm

Concentration × 10^{-3} / M	Absorbance at 532 nm / A.U.
0.00	0.0
1.34	0.07341
2.69	0.13930
4.03	0.22663
5.37	0.29037
6.72	0.35978

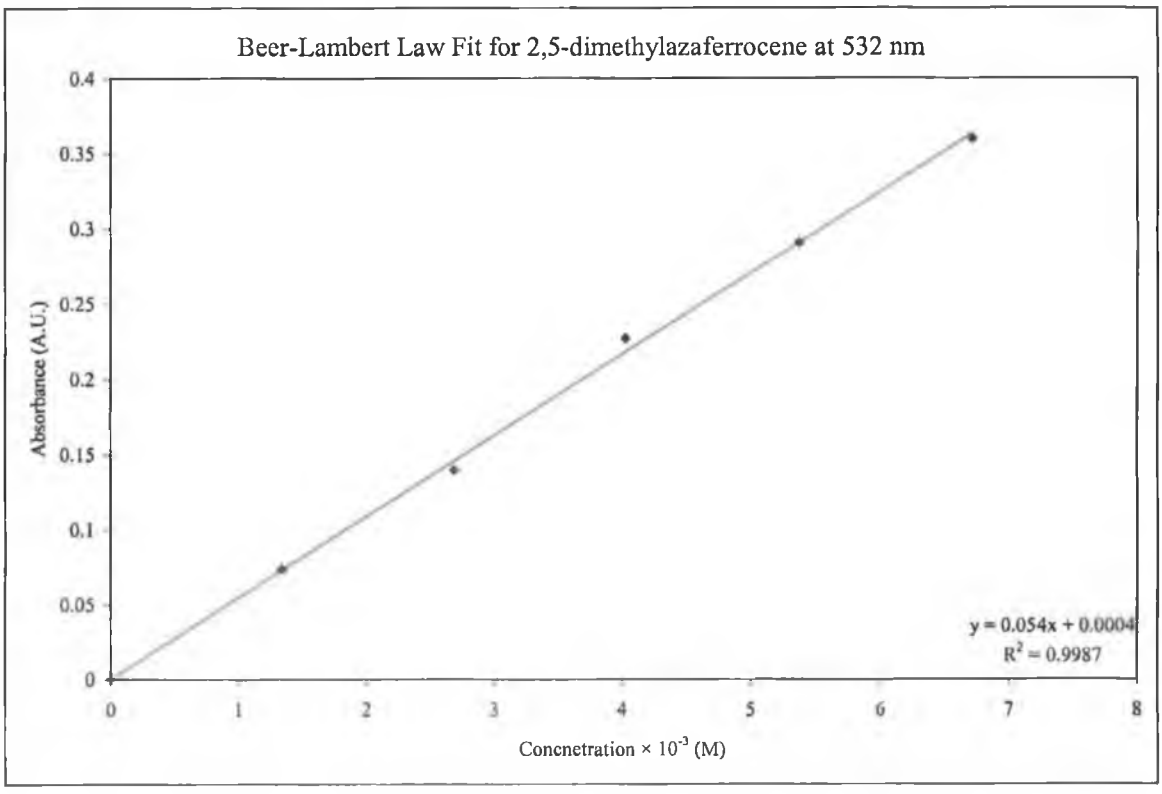

The extinction coefficient (ϵ) for 2,5-dimethylazaferrocene is 54 L mol^{-1} cm^{-1} at 532 nm.

Appendix
B

Photochemistry of $(\eta^5\text{-}C_5H_5)(\eta^5\text{-}C_4H_4N)Fe$ and $(\eta^5\text{-}C_5H_5)(\eta^1\text{-}N\text{-}C_4H_4N)Fe(CO)_2$ in Low-Temperature Matrixes and Room-Temperature Solution. Evidence for a Photoinduced Haptotropic Shift of the π-Coordinated Pyrrolyl Ligand

Davnat P. Heenan,[†] Conor Long,[†] Virginia Montiel-Palma,[‡] Robin N. Perutz,[‡] and Mary T. Pryce*,[†]

Inorganic Photochemistry Centre, Dublin City University, Dublin 9, Ireland, and Department of Chemistry, University of York, Heslington, York YO10 5DD, U.K.

Received March 27, 2000

Azaferrocene, $(\eta^5\text{-}C_5H_5)(\eta^5\text{-}C_4H_4N)Fe$, undergoes a $\eta^5 \rightarrow \eta^1$ haptotropic shift of the pyrrolyl ligand upon long-wavelength photolysis (λ_{exc} > 495 nm) both in alkane solvents at room temperature and in frozen matrixes at 12 K. Room temperature photolysis (λ_{exc} > 495 nm) in CO-saturated cyclohexane solution generated $(\eta^5\text{-}C_5H_5)(\eta^1\text{-}N\text{-}C_4H_4N)Fe(CO)_2$. Irradiation with λ_{exc} = 532 nm also produced an allyl monocarbonyl species, *exo*-$(\eta^5\text{-}C_5H_5)(\eta^3\text{-}C\text{-}C_4H_4N)Fe(CO)$, identified by IR spectroscopy. In CO-doped matrixes at 12 K both $(\eta^5\text{-}C_5H_5)(\eta^1\text{-}N\text{-}C_4H_4N)Fe(CO)$ and $(\eta^5\text{-}C_5H_5)(\eta^1\text{-}N\text{-}C_4H_4N)Fe(CO)_2$ are formed following broad-band irradiation (λ_{exc} > 495 nm) of $(\eta^5\text{-}C_5H_5)(\eta^5\text{-}C_4H_4N)Fe$, in a ratio dependent on the concentration of CO in the matrix. Initial irradiation with λ_{exc} = 538 nm followed by broad-band photolysis (λ_{exc} > 495 nm) in CO-doped matrixes formed additional monocarbonyl species, *exo*-$(\eta^5\text{-}C_5H_5)(\eta^3\text{-}C\text{-}C_4H_4N)Fe(CO)$, and a species absorbing at 1962 cm^{-1}, which is either the appropriate *endo*-isomer or aza-allyl species. Laser flash photolysis experiments of $(\eta^5\text{-}C_5H_5)(\eta^1\text{-}N\text{-}C_4H_4N)Fe(CO)_2$ in either CO-saturated cyclohexane or toluene produced $(\eta^5\text{-}C_5H_5)(\eta^1\text{-}N\text{-}C_4H_4N)Fe(CO)$, which reacted with CO with rate constants measured at 298 K of $(3.0 \pm 0.3) \times 10^8$ and $(3.3 \pm 0.3) \times 10^8$ M^{-1} s^{-1}, respectively, regenerating $(\eta^5\text{-}C_5H_5)(\eta^1\text{-}N\text{-}C_4H_4N)Fe(CO)_2$.

Introduction

The photochemical reactivity of half-sandwich compounds of the type (η^x-aromatic ligand)$M(CO)_y$ (x = 4, 5, or 6; y = 2, 3, or 4; M = V, Cr, Mn, or Co) can differ from the thermal chemistry.[1,2] For example, $(\eta^6\text{-}C_6H_6)Cr(CO)_3$ undergoes thermally induced arene exchange, while CO loss is the dominant photochemical process.[3,4] Arene exchange proceeds via a thermally induced haptotropic shift of the π-ligand,[3] but to date the only report of a photoinduced haptotropic shift for these systems comes from our investigations into the photochemistry of π-coordinated pyridine compounds.[5] This work demonstrated that these processes occur following low-energy photolysis. For instance, photolysis of $(\eta^6\text{-}C_5H_5N)Cr(CO)_3$ (λ_{exc} = 460 nm) in a CO-doped methane matrix at 10 K produced $(\eta^1\text{-}C_5H_5N)Cr(CO)_5$, while irradiation at 308 nm also produced the more familiar CO-loss product $(\eta^6\text{-}C_5H_5N)Cr(CO)_2$.

We have extended these studies to sandwich compounds related to ferrocene. Ferrocene is photoinert in dry alkane solvents, but it readily photooxidizes in haloalkanes.[6] Quantum yields for photodecomposition of ferrocene of up to unity are obtained in CCl_4/EtOH mixtures.[6] Substituted ferrocenes have been reported to photodecompose in solvents such as acetonitrile, methanol, DMSO, decalin, chloroform, or carbontetrachloride; the nature of this decomposition remains uncertain, however.[7] In all cases products are complex, and more recent work has suggested that the presence of traces of water is a prerequisite for photoactivity in some solvents.[8]

In this paper, we describe the photochemistry of azaferrocene, $(\eta^5\text{-}C_5H_5)(\eta^5\text{-}C_4H_4N)Fe$, the closest and most accessible heterocyclic analogue of ferrocene. The reason for this study is primarily to determine if the photoinduced hapticity changes observed for π-coordinated pyridine, are also observed for π-coordinated

[†] Dublin City University.
[‡] University of York.

(1) Basolo, F. *New J. Chem.* **1994**, *18*, 19.
(2) O'Connor, J. M.; Casey, C. D. *Chem. Rev.* **1987**, *87*, 307.
(3) (a) Trayler, T. G.; Stewart, K. J.; Goldberg, M. J. *J. Am. Chem. Soc.* **1984**, *106*, 4165. (b) Trayler, T. G.; Stewart, K. J.; Goldberg, M. J. *Organometallics* **1986**, *5*, 2062. (c) Trayler, T. G.; Stewart, K. J. *J. Am. Chem. Soc.* **1986**, *108*, 6977. (d) Trayler, T. G.; Goldberg, M. J. *Organometallics* **1987**, *6*, 2413. (e) Trayler, T. G.; Goldberg, M. J. *Organometallics* **1987**, *6*, 2531.
(4) (a) Strohmeier, S.; von Hobe, D. *Z. Naturforsch.* **1963**, *18B*, 770. (b) Wrighton, M. S.; Haverty, J. L. *Z. Naturforsch.* **1975**, *30B*, 254. (c) Nasielski, J.; Denishoff, O. *J. Organomet. Chem.* **1975**, *102*, 65. (d) Gilbert, A.; Kelly, J. M.; Budzwait, M.; Koerner von Gustorf, E. *Z. Naturforsch.* **1976**, *31B*, 1091. (e) Rest, A. J.; Sodeau, J. R.; Taylor, D. J. *J. Chem. Soc., Dalton Trans.* **1978**, 651.
(5) Breheny, C. J.; Draper, S. M.; Grevels, F.-W.; Klotzbücher, W. E.; Long, C.; Pryce, M. T.; Russell, G. *Organometallics* **1996**, *15*, 3679.
(6) Traverso, O.; Scandola, F. *Inorg. Chim. Acta* **1970**, *4*, 493. (b) Tarr, A. M.; Wiles, D. M. *Can. J. Chem.* **1968**, *46*, 2725. (c) von Gustorf, E. K.; Koller, H.; Jun, M.-J.; Schenck, G. O. *Chem.-Ing-Tech.* **1963**, *35*, 591.
(7) (a) Ali, L. H.; Cox, A.; Kemp, T. S. *J. Chem. Soc., Dalton Trans.* **1973**, 1468. (b) Traverso, O.; Rossi, R.; Sostero, S.; Carassiti, V. *Mol. Photochem.* **1973**, *5*, 457.
(8) Davis, J.; Vaughan, D. H.; Cardosi, M. F. *Electroanalysis* **1997**, *9*, 650.

10.1021/om0002632 CCC: $19.00
Publication on Web 00/00/0000 PAGE EST: 6.9

Table 1. Infrared Bands Observed in the CO Stretching Region for $(\eta^5\text{-}C_5H_5)Fe(CO)_2X$ Compounds and Their Photoproducts in Various Low-Temperature Matrixes and Room-Temperature Solution

complex	ν_{CO} (cm^{-1})	medium
$(\eta^5\text{-}C_5H_5)(\eta^1\text{-}C_4H_4N)Fe(CO)_2$	2053, 2007	Ar matrix
$(\eta^5\text{-}C_5H_5)(\eta^1\text{-}C_4H_4N)Fe(CO)_2$	2052, 2006	N_2 matrix
$(\eta^5\text{-}C_5H_5)(\eta^1\text{-}C_4H_4N)Fe(CO)_2$	2048, 2002	C_6H_{12}
$(\eta^5\text{-}C_5H_5)(\eta^1\text{-}C_4H_4N)Fe(CO)$	1974	Ar matrix
$(\eta^5\text{-}C_5H_5)(\eta^1\text{-}C_4H_4N)Fe(CO)$	1974	N_2 matrix
$(\eta^5\text{-}C_5H_5)Fe(CO)_2Cl$[a]	2054, 2010	CH_4 matrix
$(\eta^5\text{-}C_5H_5)Fe(CO)_2Cl$[a]	2056, 2013	N_2 matrix
$(\eta^5\text{-}C_5H_5)Fe(CO)Cl$[a]	1977	CH_4 matrix
$(\eta^5\text{-}C_5H_5)Fe(CO)Cl$[a]	1979	N_2 matrix
$(\eta^5\text{-}C_5H_5)Fe(CO)_2I$[b]	2038, 2005	C_6H_{12}
$(\eta^5\text{-}C_5H_5)(\eta^3\text{-}C_3H_5)Fe(CO)$[c]	1950	CCl_4
$(\eta^5\text{-}C_5H_5)(\eta^3\text{-}C_4H_7)Fe(CO)$[c]	1949	thin film
$(\eta^5\text{-}C_5H_5)(\eta^3\text{-}C\text{-}C_4H_4N)Fe(CO)$	ca. 1949	C_6H_{12}
$(\eta^5\text{-}C_5H_5)(\eta^3\text{-}C\text{-}C_4H_4N)Fe(CO)$	1948	CO/Ar matrix
$(\eta^5\text{-}C_5H_5)(\eta^1\text{-}N\text{-}C_4H_4N)Fe(CO)$	1962	CO/Ar matrix

[a] Reference 17. [b] Reference 10. [c] Reference 11.

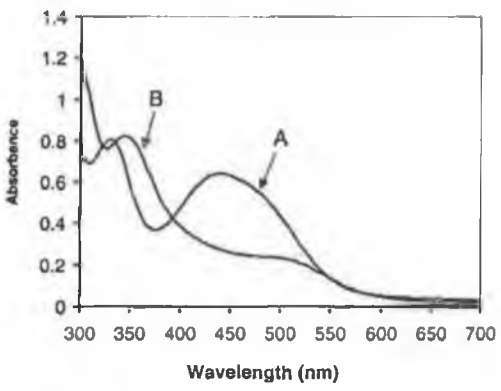

Figure 1. UV/vis spectra for $(\eta^5\text{-}C_5H_5)Fe(\eta^5\text{-}C_5H_5)$ (1.79×10^{-2} M; spectrum A) and $(\eta^5\text{-}C_5H_5)(\eta^1\text{-}N\text{-}C_4H_4N)Fe(CO)_2$ (5.91×10^{-3} M; spectrum B) in cyclohexane.

pyrroles. The presence of the nitrogen atom in the π-coordinated ligand has a number of effects. The proximate nitrogen can act as an intramolecular "trap" for ring-slip intermediates. More fundamentally, its presence reduces the symmetry of the molecule. As a consequence, the degeneracy of valence orbitals, a feature of the homocyclic analogues, is lifted. This reduces the energy of low-energy excited states, permitting access to novel photochemical processes, such as haptotropic shift reactions.

The experimental results reported here were obtained using a combination of room-temperature techniques in dry cyclohexane solution and low-temperature matrix isolation methods. Evidence is presented to demonstrate that, in common with η^6-coordinated pyridine, the η^5-pyrrolyl ligand also undergoes facile photoinduced haptotropic shifts, opening multiple coordination sites on the metal center. Moreover, experiments using monochromatic irradiation indicate that the haptotropic shifts may occur by a stepwise $\eta^5 \rightarrow \eta^3 \rightarrow \eta^1$ transformation involving the absorption of two photons. To assist with the assignment of intermediate species observed in these experiments, the photochemistry of $(\eta^5\text{-}C_5H_5)(\eta^1\text{-}N\text{-}C_4H_4N)Fe(CO)_2$ was investigated by flash photolysis techniques in solution and also by matrix isolation.

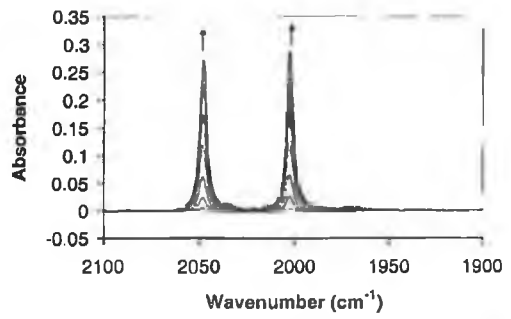

Figure 2. Spectral changes observed in the carbonyl region following photolysis (λ_{exc} > 500 nm) of $(\eta^5\text{-}C_5H_5)(\eta^5\text{-}C_4H_4N)Fe$ in CO-saturated cyclohexane at room temperature, showing formation of $(\eta^5\text{-}C_5H_5)(\eta^1\text{-}N\text{-}C_4H_4N)Fe(CO)_2$.

Results

The IR spectroscopic data for $(\eta^5\text{-}C_5H_5)(\eta^5\text{-}C_4H_4N)Fe$ and $(\eta^5\text{-}C_5H_5)(\eta^1\text{-}N\text{-}C_4H_4N)Fe(CO)_2$ and their photoproducts are given in Table 1, while the UV/vis spectra of the starting materials in cyclohexane are represented in Figure 1. Both compounds exhibit weak absorptions in the visible region. The spectrum of $(\eta^5\text{-}C_5H_5)(\eta^5\text{-}C_4H_4N)Fe$ in cyclohexane contains features centered at 326 nm (ϵ = 46 M^{-1} cm^{-1}) and 423 nm (ϵ = 38 M^{-1} cm^{-1}), while $(\eta^5\text{-}C_5H_5)(\eta^1\text{-}N\text{-}C_4H_4N)Fe(CO)_2$ has an absorption at 340 nm (ϵ = 142 M^{-1} cm^{-1}) and a weaker feature at 484 nm (ϵ = 35 M^{-1} cm^{-1}).

Steady-State Photolysis Experiments

Broad-Band Photolysis of $(\eta^5\text{-}C_5H_5)(\eta^5\text{-}C_4H_4N)Fe$ in CO-Saturated Cyclohexane Solution at Room Temperature. Visible photolysis of a CO-saturated solution of $(\eta^5\text{-}C_5H_5)(\eta^5\text{-}C_4H_4N)Fe$ in cyclohexane with broad-band radiation from a xenon-arc lamp (275 W) fitted with a filter that only transmits wavelengths greater than 500 nm produced $(\eta^5\text{-}C_5H_5)(\eta^1\text{-}N\text{-}C_4H_4N)Fe(CO)_2$ (ν_{CO} = 2048 and 2002 cm^{-1}, Table 1; reaction 1; Figure 2).[9] Experiments using a λ_{exc} > 400 nm filter

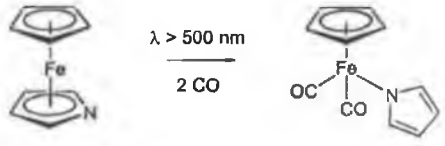

also produced the dicarbonyl species as the major product, but small amounts of $[(\eta^5\text{-}C_5H_5)Fe(CO)_2]_2$ were formed in addition (ν_{CO} = 1960 and 1793 cm^{-1}; the high-energy band at 2002 cm^{-1} is obscured by the low-energy absorption of $(\eta^5\text{-}C_5H_5)(\eta^1\text{-}N\text{-}C_4H_4N)Fe(CO)_2$). In all cases the yield of the dinuclear species appeared low (based on IR band intensities), although it was greatest in experiments where the solution was simply flushed with CO rather than rigorously degassed by freeze–pump–thaw procedures followed by admission of CO to the solution cell. It should be noted that formation of

(9) (a) We have confirmed that this reaction is photochemical by control experiments in which the solution of $(\eta^5\text{-}C_5H_5)(\eta^5\text{-}C_4H_4N)Fe$ in CO-saturated cyclohexane was kept in the dark; no $(\eta^5\text{-}C_5H_5)(\eta^1\text{-}N\text{-}C_4H_4N)Fe(CO)_2$ was formed under these conditions. (b) Martin, K. F.; Hanks, T. W. *Organometallics* **1997**, *16*, 4857.

the dinuclear species is also observed following photolysis of $(\eta^5\text{-}C_5H_5)Fe(CO)_2I$ in alkane solvents.[10]

Broad-Band Photolysis of $(\eta^5\text{-}C_5H_5)(\eta^5\text{-}C_4H_4N)$-Fe in Degassed Cyclohexane Solution at Room Temperature. Broad-band irradiation (λ_{exc} > 500 nm) of a concentrated solution of $(\eta^5\text{-}C_5H_5)(\eta^5\text{-}C_4H_4N)Fe$ in degassed cyclohexane caused the solution to become turbid and eventually produced a precipitate. After the admission of CO, the precipitate slowly disappeared and the solution clarified. Monitoring of the solution by infrared spectroscopy indicated the formation (over several hours at room temperature) of bands at 2048 and 2002 cm^{-1}, assigned to $(\eta^5\text{-}C_5H_5)(\eta^1\text{-}N\text{-}C_4H_4N)Fe(CO)_2$.

The observation of solution turbidity following irradiation in cyclohexane renders time-resolved studies on this system both difficult and prone to artifacts resulting from photoacoustic effects. As a consequence, the photochemistry of azaferrocene was not investigated by time-resolved techniques.

Monochromatic Pulsed Photolysis of $(\eta^5\text{-}C_5H_5)$-$(\eta^5\text{-}C_4H_4N)Fe$ in CO-Saturated Cyclohexane Solution at Room Temperature. Pulsed photolysis of $(\eta^5\text{-}C_5H_5)(\eta^5\text{-}C_4H_4N)Fe$ in CO-saturated cyclohexane with λ_{exc} = 355 nm produced $(\eta^5\text{-}C_5H_5)(\eta^1\text{-}N\text{-}C_4H_4N)Fe(CO)_2$ as the sole carbonyl-containing product. However, pulsed photolysis using λ_{exc} = 532 nm generated an additional species, with a single ν_{CO} band at 1949 cm^{-1} (Figure 3). We have assigned this band to $(\eta^5\text{-}C_5H_5)(\eta^3\text{-}C\text{-}C_4H_4N)$-Fe(CO) (reaction 2), as it is close to that observed for $(\eta^5\text{-}C_5H_5)(\eta^3\text{-}C_3H_5)Fe(CO)$ or $(\eta^5\text{-}C_5H_5)(\eta^3\text{-}C_4H_7)Fe(CO)$ (ν_{CO} = 1950 or 1948 cm^{-1} respectively) in CCl_4 or as a thin film.[11]

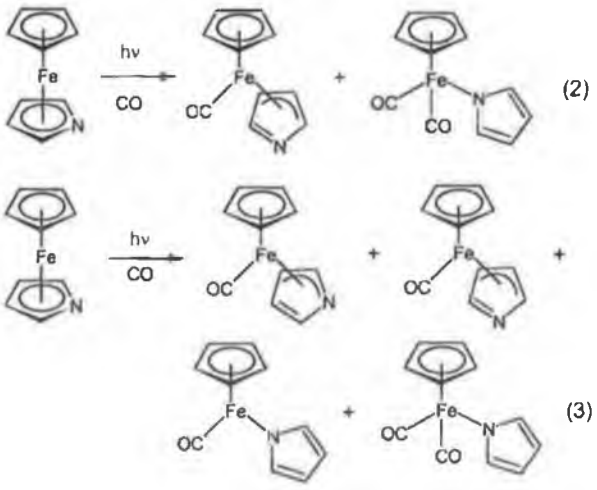

Matrix Isolation Studies

Photolysis (λ_{exc} > 495 nm) of $(\eta^5\text{-}C_5H_5)(\eta^5\text{-}C_4H_4N)$-Fe in Argon Matrixes at 12 K Containing Either 0.5% or 2% CO. Azaferrocene exhibits UV/vis bands at 325 and 424 nm in a CO-doped argon matrix. Photolysis of $(\eta^5\text{-}C_5H_5)(\eta^5\text{-}C_4H_4N)Fe$ in these matrixes with λ_{exc} > 495 nm produced two species, one with two ν_{CO} bands of approximately equal intensity (2053 and 2008 cm^{-1})

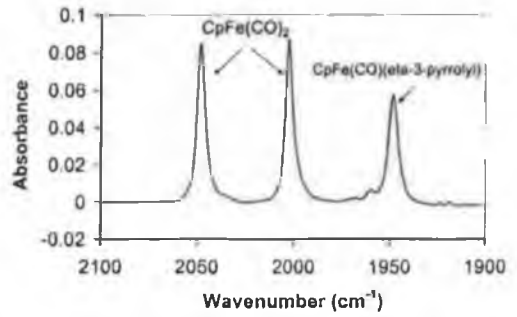

Figure 3. Infrared spectrum recorded after monochromatic irradiation (λ_{exc} = 532 nm) of $(\eta^5\text{-}C_5H_5)(\eta^5\text{-}C_4H_4N)$-Fe in CO-saturated cyclohexane at room temperature. $CpFe(CO)_2 = (\eta^5\text{-}C_5H_5)(\eta^1\text{-}N\text{-}C_4H_4N)Fe(CO)_2$; CpFe(CO)($\eta^3$-pyrrolyl) = $(\eta^5\text{-}C_5H_5)(\eta^3\text{-}C\text{-}C_4H_4N)Fe(CO)$.

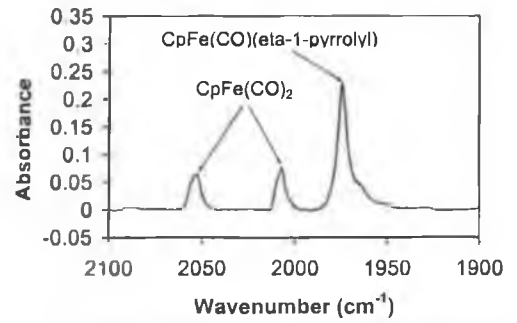

Figure 4. Infrared spectrum recorded following photolysis (λ_{exc} > 500 nm) of $(\eta^5\text{-}C_5H_5)(\eta^5\text{-}C_4H_4N)Fe$ in 0.5% CO/Ar matrix at 12 K. $CpFe(CO)_2 = (\eta^5\text{-}C_5H_5)(\eta^1\text{-}N\text{-}C_4H_4N)Fe(CO)_2$; CpFe(CO)(eta-1-pyrrolyl) = $(\eta^5\text{-}C_5H_5)(\eta^1\text{-}N\text{-}C_4H_4N)$-Fe(CO).

and the other with a single band at 1974 cm^{-1} (Figure 4).[12] The ratio of the intensity of these product bands varied with the concentration of CO in the matrix. For instance, the band at 1974 cm^{-1} band was 4 times as intense as that at 2053 and 2008 cm^{-1} for a matrix containing 0.5% CO, while it was only twice as large in a 2% CO matrix. Within individual experiments, this ratio remained constant.

The species absorbing at 2053 and 2008 cm^{-1} was assigned to $(\eta^5\text{-}C_5H_5)(\eta^1\text{-}N\text{-}C_4H_4N)Fe(CO)_2$ by comparison with the infrared spectrum of an authentic sample of $(\eta^5\text{-}C_5H_5)(\eta^1\text{-}N\text{-}C_4H_4N)Fe(CO)_2$ in the same matrix (cf. Table 1).[13] The band at 1974 cm^{-1} was assigned to the 16-electron $(\eta^5\text{-}C_5H_5)(\eta^1\text{-}N\text{-}C_4H_4N)Fe(CO)$ species (a strong absorption at 415 nm, a shoulder at 317 nm, and a weak broad feature at ca. 730–750 nm correlate with this IR band), and support for this assignment came from matrix experiments on $(\eta^5\text{-}C_5H_5)(\eta^1\text{-}N\text{-}C_4H_4N)Fe$-$(CO)_2$, which produced $(\eta^5\text{-}C_5H_5)(\eta^1\text{-}N\text{-}C_4H_4N)Fe(CO)$ and free CO on photolysis (see below). The band at 1975 cm^{-1} is asymmetric, with two further unresolved components at 1962 and 1948 cm^{-1} (see below for assignments).

(10) Pan, X.; Philbin, C. E.; Castellani, M. P.; Tyler, D. R. *Inorg. Chem.* **1988**, *27*, 671.
(11) Green, M. L. H.; Nagy, P. L. I. *J. Chem. Soc.* **1963**, 189.

(12) The 1975 cm^{-1} band also exhibited shoulders to the low-energy side at ca. 1962 and 1948 cm^{-1}, possibly indicating the formation of further carbonyl-containing species.

(13) It should be noted that the values for the ν_{CO} bands for $(\eta^5\text{-}C_5H_5)(\eta^1\text{-}N\text{-}C_4H_4N)Fe(CO)_2$ quoted in the literature are incorrect. We have confirmed our values by correlating our infrared spectral data obtained from a single sample of the compound with the results of high-resolution mass spectrometry and single-crystal X-ray diffraction techniques.

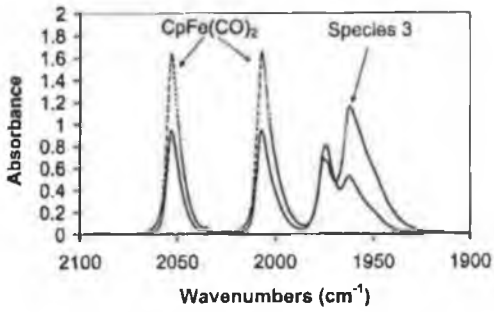

Figure 5. Infrared spectra following photolysis of (η^5-C_5H_5)(η^5-C_4H_4N)Fe in a 2% CO/Ar matrix at 12 K (a) at λ_{exc} = 538 nm for 200 min (—) and (b) subsequent photolysis at λ_{exc} > 495 nm (- - -).

Scheme 1. Broad-Band Matrix Photolysis of (η^5-C_5H_5)(η^5-*N*-C_4H_4N)Fe and (η^5-C_5H_5)(η^1-*N*-C_4H_4N)$Fe(CO)_2$

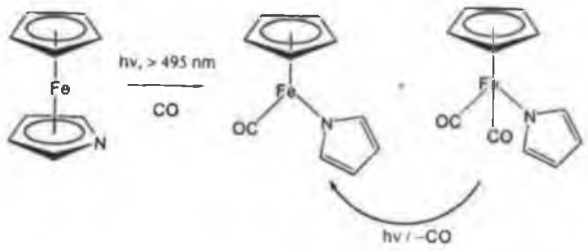

Initial Photolysis (λ_{exc} > 495 nm) of (η^5-C_5H_5)(η^5-C_4H_4N)Fe in Argon Matrixes at 12 K, Containing Either 0.5% CO or 2% CO, and Subsequent Broad-Band Photolysis (λ_{exc} > 325 nm). Initial photolysis of an argon matrix containing (η^5-C_5H_5)(η^5-C_4H_4N)Fe again produced the two carbonyl-containing species as outlined above. Changing to shorter wavelengths resulted in a change in ratio of the product bands, the intensity of the band at 1974 cm^{-1} increasing more rapidly than those at 2053 and 2008 cm^{-1}. This suggests that the dicarbonyl product is undergoing photoinduced CO loss at these excitation wavelengths (Scheme 1). This was confirmed by matrix and time-resolved experiments on (η^5-C_5H_5)(η^1-*N*-C_4H_4N)$Fe(CO)_2$ (see below).

Monochromatic Photolysis (λ_{exc} = 538 nm) of (η^5-C_5H_5)(η^5-C_4H_4N)Fe in Argon Matrixes at 12 K Containing 2% CO and Subsequent Broad-Band Photolysis with λ_{exc} > 495 nm. In contrast with the matrix experiments described above, where samples were irradiated with broad band light sources, monochromatic irradiation of (η^5-C_5H_5)(η^5-C_4H_4N)Fe in a CO-doped argon matrix with λ_{exc} = 538 nm produced four carbonyl-containing species (Figure 5a). In addition to (η^5-C_5H_5)(η^1-*N*-C_4H_4N)$Fe(CO)_2$ and (η^5-C_5H_5)(η^1-*N*-C_4H_4N)Fe(CO) previously observed, further species with ν_{CO} = 1962 and 1948 cm^{-1} were formed, the identity of which will be discussed later. Subsequent irradiation of this matrix with λ_{exc} > 495 nm resulted in a substantial increase in the intensity of the bands at 2053, 2008, 1962, and 1948 cm^{-1}, while the intensity of the band assigned to (η^5-C_5H_5)(η^1-*N*-C_4H_4N)Fe(CO) decreased slightly (Figure 5b). This experiment and related ones showed a feature at 660 nm in the UV/vis spectrum (Figure 6) which is associated with the species absorbing at 1962 and 1948 cm^{-1} in the infrared spectrum.

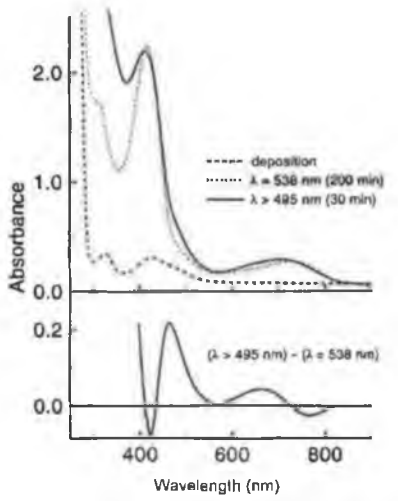

Figure 6. UV/vis spectra following photolysis of (η^5-C_5H_5)(η^5-C_4H_4N)Fe in a 2% CO/Ar matrix at 12 K. (a) following deposition (- - -), (b) at λ_{exc} = 538 nm (200 min; ···), and (c) subsequent photolysis at λ_{exc} > 495 nm (30 min; —).

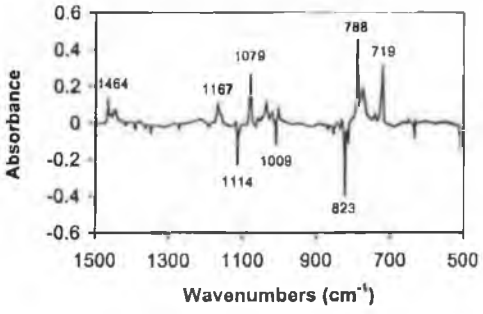

Figure 7. IR difference spectrum obtained following photolysis (λ_{exc} > 495 nm) of (η^5-C_5H_5)(η^5-C_4H_4N)Fe in an argon matrix at 12 K.

Photolysis of (η^5-C_5H_5)(η^5-C_4H_4N)Fe in an Argon or a Nitrogen Matrix at 12 K. The spectroscopic changes observed following photolysis of (η^5-C_5H_5)(η^5-C_4H_4N)Fe (λ_{exc} > 495 nm) in an argon matrix are presented in Figure 7. We have assigned these changes to the depletion of (η^5-C_5H_5)(η^5-C_4H_4N)Fe and the formation of a ring-slip product. The nature of the coordination mode of the pyrrolyl ligand is uncertain. However ab initio calculations on (η^5-C_5H_5)(η^1-*N*-C_4H_4N)-Fe were undertaken to estimate the infrared properties of this 14-electron species. The starting geometry was based on the molecular structure published for (η^5-C_5H_5)(η^1-*N*-C_4H_4N)$Fe(CO)_2$[14] but with both carbonyl ligands removed from the atom list. A full geometry optimization was undertaken at B3LYP/LANL2DZ model chemistry using the Gaussian-98 program suite.[15] The Hessian matrix, again calculated using the same model chemistry, revealed only one trivial negative frequency (−55 cm^{-1}) associated with the rotation of the (η^5-C_5H_5) ligand. The results of these calculations together with the observed band positions are presented in Table 2.[16] On the basis of these results we can assign the spectral features observed in these matrix experiments to (η^5-C_5H_5)(η^1-*N*-C_4H_4N)Fe. Photolyses in a dinitrogen matrix

(14) Powell, M. A.; Bailey, R. D.; Eagle, C. T.; Schimel, G. L.; Hanks, T. W.; Pennington, W. T. *Acta Crystallogr.* **1997**, *C53*, 1611.

Table 2. Observed (for photolysis product of azaferrocene in argon matrixes) and Calculated Band Positions for $(\eta^5\text{-}C_5H_5)(\eta^1\text{-}N\text{-}C_4H_4N)Fe$ Based on an Optimized Geometry at B3LYP/LANL2DZ Model Chemistry[a]

observed band positions (cm^{-1})	calculated band positions (cm^{-1})
719	715
772	749
781	763
788	777
831	834
1035	1009
	1012
	1023
1079	1049
	1055
1167	1142
	1154
1464	1440

[a] The calculated values have been corrected using an empirical factor of 0.98 (see ref 16).

gave rise to spectral changes, essentially identical to those observed in an argon matrix.

Photolysis of $(\eta^5\text{-}C_5H_5)(\eta^1\text{-}N\text{-}C_4H_4N)Fe(CO)_2$ in Argon and Dinitrogen Matrixes at 12 K. Photolysis (λ_{exc} > 400 nm) of $(\eta^5\text{-}C_5H_5)(\eta^1\text{-}N\text{-}C_4H_4N)Fe(CO)_2$ in an argon matrix at 12 K resulted in the depletion of the parent bands (2053 and 2007 cm^{-1}) and the formation of new bands at 2134 and 1974 cm^{-1} (the 1974 cm^{-1} band exhibited shoulders on the low-energy side).[12] These bands are assigned to free CO and $(\eta^5\text{-}C_5H_5)(\eta^1\text{-}N\text{-}C_4H_4N)Fe(CO)$, respectively. The spectral changes observed in a dinitrogen matrix were identical to those in an argon matrix. This suggests that $(\eta^5\text{-}C_5H_5)(\eta^1\text{-}N\text{-}C_4H_4N)Fe(CO)$ does not react with dinitrogen. The matrix photochemistry of $(\eta^5\text{-}C_5H_5)Fe(CO)_2Cl$ reported by Rest and co-workers[17] also identified CO loss as the dominant photochemical process, and the resulting monocarbonyl $(\eta^5\text{-}C_5H_5)Fe(CO)Cl$ species was inert to dinitrogen (exhibiting similar band positions in both methane and nitrogen matrixes, ν_{CO} = 1977 and 1979 cm^{-1}, respectively).

UV/Vis Flash Photolysis Experiments of $(\eta^5\text{-}C_5H_5)(\eta^1\text{-}N\text{-}C_4H_4N)Fe(CO)_2$ in Cyclohexane or Toluene Solution at Room Temperature. Flash photolysis of $(\eta^5\text{-}C_5H_5)(\eta^1\text{-}N\text{-}C_4H_4N)Fe(CO)_2$ produced a transient species with a λ_{max} at approximately 430 nm (λ_{exc} = 355 nm) assigned to $(\eta^5\text{-}C_5H_5)(\eta^1\text{-}N\text{-}C_4H_4N)Fe(CO)$. A typical transient signal in CO-saturated cyclohexane

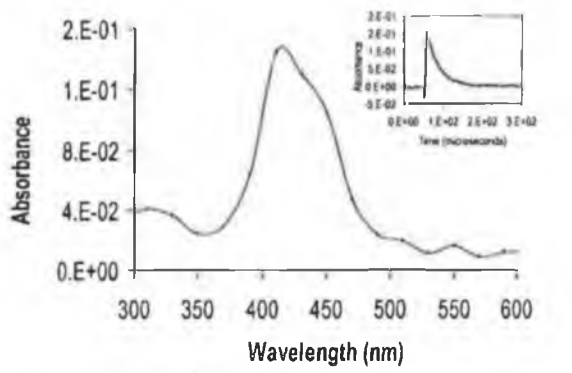

Figure 8. UV/vis difference transient absorption spectrum obtained after 2 μs following photolysis of $(\eta^5\text{-}C_5H_5)(\eta^1\text{-}N\text{-}C_4H_4N)Fe(CO)_2$ at λ_{exc} = 355 nm in cyclohexane under 1 atm of CO. The inset shows a typical transient signal observed at 420 nm.

Scheme 2. Flash Photolysis of $(\eta^5\text{-}C_5H_5)(\eta^1\text{-}N\text{-}C_4H_4N)Fe(CO)_2$ Resulting in Decarbonylation Followed by Rapid Recombination with CO

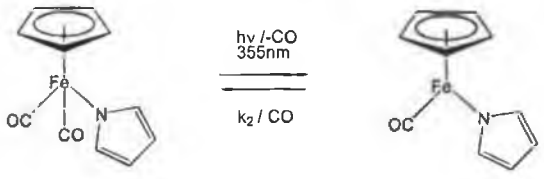

and a difference spectrum are given in Figure 8. Under these conditions, this species decays to the preirradiation baseline in less than 2 μs, indicating that the process is reversible. The steady-state UV/vis spectrum of the photolysis solution was monitored throughout the experiment and showed no significant change, confirming that the overall process is reversible.

A plot of the observed rate constant (k_{obs}) for the decay of the transient species against [CO] was linear. The slope of this plot gave the second-order rate constant (k_2) of (3.0 ± 0.3) × 10^8 M^{-1} s^{-1} at 298 K for the reaction of $(\eta^5\text{-}C_5H_5)(\eta^1\text{-}N\text{-}C_4H_4N)Fe(CO)$ with CO. Flash photolysis in CO-saturated toluene again produced a transient species with a maximum centered at 430 nm which reacted with CO with a similar rate constant of (3.3 ± 0.3) × 10^8 M^{-1} s^{-1} (see Scheme 2). These results indicate that neither the alkane nor the aromatic solvents interact to any significant extent with $(\eta^5\text{-}C_5H_5)(\eta^1\text{-}N\text{-}C_4H_4N)Fe(CO)$.

Discussion

In contrast with ferrocene, $(\eta^5\text{-}C_5H_5)(\eta^5\text{-}C_4H_4N)Fe$ is photoactive in dry hydrocarbon solvents. Broad-band photolysis of $(\eta^5\text{-}C_5H_5)(\eta^5\text{-}C_4H_4N)Fe$ at λ_{exc} > 500 nm in degassed cyclohexane at room temperature produced a precipitate together with turbidity and a deepening of the solution color. Subsequent addition of CO to the photolyzed solution yielded $(\eta^5\text{-}C_5H_5)(\eta^1\text{-}N\text{-}C_4H_4N)Fe(CO)_2$ over several hours, presumably by the slow reaction of CO with the precipitate. Attempts to isolate and characterize this precipitate failed.

Broad-band photolysis (λ_{exc} > 500 nm) of a CO-saturated cyclohexane solution ([CO] = 9.0 × 10^{-3} M)

(15) Frisch, M. J.; Trucks, G. W.; Schlegel, H. B.; Scuseria, G. E.; Robb, M. A.; Cheeseman, M. R.; Zakrzewski, V. G., Montgomery, J. A., Jr.; Stratmann, R. E.; Burant, J. C.; Dapprich, S.; Millam, J. M.; Daniels, A. D.; Kudin, K. N.; Strain, M. C.; Farkas, O.; Tomasi, J.; Barone, V.; Cossi, M.; Cammi, R.; Mennucci, B.; Pomelli, C.; Adamo, C.; Clifford, S., Ochterski, J.; Petersson, G. A.; Ayala, P. Y.; Cui, Q.; Morokuma, K.; Malick, D. K.; Abuck, A. D.; Raghavachari, K., Foresman, J. B., Cioslowski, J.; Ortiz, J. V.; Stefanov, B. B.; Liu, G.; Liashenko, A.; Piskorz, P.; Komaromi, I.; Gomperts, R.; Martin, R. L.; Fox, D. J.; Keith, T.; Al-Laham, M. A.; Peng, C. Y.; Nanayakkara, A.; Gonzalez, C.; Challacombe, M.; Gill, P. M. W.; Johnson, B.; Chen, W., Wong, M. W.; Andres, J. L.; Gonzalez, C.; Head-Gordon, M.; Replogle, E. S.; Pople, J. A. *Gaussian 98*, Revision A.3; Gaussian, Inc.: Pittsburgh, PA, 1998.

(16) The calculated band positions were corrected using a factor of 0.98, derived from calculations using the same model chemistry on half-sandwich compounds of the type $(\eta^6\text{-arene})Cr(CO)_3$, which exhibit unambiguous spectral features particularly in the ν_{CO} region.

(17) Hooker, R. H.; Mahmoud, K. A.; Rest, A. J. *J. Chem. Soc., Dalton Trans.* **1990**, 1231.

of $(\eta^5\text{-}C_5H_5)(\eta^5\text{-}C_4H_4N)Fe$ formed $(\eta^5\text{-}C_5H_5)(\eta^1\text{-}N\text{-}C_4H_4N)\text{-}Fe(CO)_2$, confirming that the η^5-coordinated pyrrolyl ligand undergoes a photoinduced haptotropic shift reaction. Another carbonyl compound, observed only following monochromatic irradiation at 532 nm, was identified as the *exo*-isomer of $(\eta^5\text{-}C_5H_5)(\eta^3\text{-}C\text{-}C_4H_4N)Fe(CO)$ (species 1). This assignment was based on a comparison of

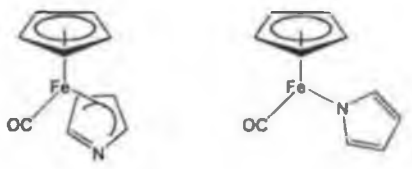

Species 1
exo-isomer

Species 2

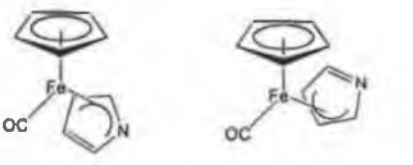

Species 3
exo-aza-allyl

Species 4
endo-isomer

its ν_{CO} band (1948 cm^{-1}) with that of $(\eta^5\text{-}C_5H_5)(\eta^3\text{-}C_3H_5)\text{-}Fe(CO)$ (1950 cm^{-1}).[11] The observation of what appears to be an intermediate η^3 species suggests that two photons are required for the overall η^5-to-η^1 transformation. Indeed, subsequent broad-band visible photolysis of the η^3-intermediate indicates that it is photosensitive, presumably yielding the η^1 species. However it is not possible to be certain of this, as the additional dicarbonyl species produced could be the result of further photolysis of the parent species still present in solution.

Matrix experiments on $(\eta^5\text{-}C_5H_5)(\eta^5\text{-}C_4H_4N)Fe$ were performed to identify the nature of ring-slip intermediates. These experiments can be divided into two groups, those in which the isolating matrix is inert and those in which the matrix material reacts with the photofragments. For this system dinitrogen, frequently used as a reactive matrix, is inert. Consequently, active matrixes used consisted of various concentrations (expressed as %) of CO in argon. Coordination of CO to the photofragments provided information on their nature by examination of the ν_{CO} absorption bands.

Long-wavelength (λ_{exc} > 495 nm) photolysis of $(\eta^5\text{-}C_5H_5)(\eta^5\text{-}C_4H_4N)Fe$ in an argon matrix resulted in depletion of the infrared bands of the parent compound, and the formation of new bands in the fingerprint region (Figure 7). Because the photoproduct(s) lack diagnostic spectroscopic features, we calculated the IR spectrum of a likely product by DFT methods. The band positions calculated for $(\eta^5\text{-}C_5H_5)(\eta^1\text{-}C_4H_4N)Fe$ provide the best match to those observed in the matrix experiment (Table 2). As mentioned above, experiments in a dinitrogen matrix produced almost identical spectral changes to those observed in argon, with no evidence for species with coordinated dinitrogen.

Experiments using CO-doped matrixes provided considerably more information on the nature of the photoproducts. In these experiments, both $(\eta^5\text{-}C_5H_5)(\eta^1\text{-}N\text{-}C_4H_4N)Fe(CO)_2$ and $(\eta^5\text{-}C_5H_5)(\eta^1\text{-}N\text{-}C_4H_4N)Fe(CO)$ (species 2) were identified following low-energy broad-band photolysis of $(\eta^5\text{-}C_5H_5)(\eta^5\text{-}C_4H_4N)Fe$ in both 0.5% and 2% CO in argon matrixes at 12 K. The former assignment was based on the known ν_{CO} band positions for $(\eta^5\text{-}C_5H_5)(\eta^1\text{-}N\text{-}C_4H_4N)Fe(CO)_2$ in the same matrix (Table 1). The latter depended on its similarity to the spectroscopic properties of $(\eta^5\text{-}C_5H_5)Fe(CO)Cl$ measured by Rest and co-workers (Table 1)[17] and the results of our investigations of the photochemistry of $(\eta^5\text{-}C_5H_5)\text{-}(\eta^1\text{-}C_4H_4N)Fe(CO)_2$ reported here. Experimental data in the literature confirm that a η^1-*N*-coordinated pyrrolyl ligand has electronic properties similar to those of the halogens, resulting in similar ν_{CO} frequencies (Table 1).[17,18]

In low-temperature matrixes the monocarbonyl and dicarbonyl species were formed concomitantly and in the same ratio throughout the photolysis with λ > 495 nm. This observation suggests that they were both formed by the reaction of CO with a single photoproduct, i.e., the 14-electron species $(\eta^5\text{-}C_5H_5)(\eta^1\text{-}N\text{-}C_4H_4N)Fe$. The observation that the ratio of mono- to dicarbonyl products was strongly dependent on the concentration of CO further supported this conclusion, the relative yield of the dicarbonyl species being greatest in matrixes containing a greater concentration of CO.

The ν_{CO} band (1974 cm^{-1}) of $(\eta^5\text{-}C_5H_5)(\eta^1\text{-}N\text{-}C_4H_4N)\text{-}Fe(CO)$ was asymmetric (Figure 4). This was true whether the monocarbonyl species was formed by photolysis of $(\eta^5\text{-}C_5H_5)(\eta^5\text{-}C_4H_4N)Fe$ in a CO-doped matrix or from $(\eta^5\text{-}C_5H_5)(\eta^1\text{-}N\text{-}C_4H_4N)Fe(CO)_2$ in an argon matrix. The shoulders on the low-energy side indicated the presence of further CO-containing species rather than a matrix effect, as only this band exhibited the asymmetry. The species absorbing at approximately 1948 cm^{-1} was assigned to $(\eta^5\text{-}C_5H_5)(\eta^3\text{-}C\text{-}C_4H_4N)Fe\text{-}(CO)$ (species 1) on the basis of the observation of a similar band in the room-temperature photolysis of $(\eta^5\text{-}C_5H_5)(\eta^5\text{-}C_4H_4N)Fe$ in CO-saturated cyclohexane (see above). The species absorbing at 1962 cm^{-1} is more difficult to assign however. This species could be either the aza-allyl isomer $(\eta^5\text{-}C_5H_5)(\eta^3\text{-}N\text{-}C_4H_4N)Fe(CO)$ or alternatively the *endo*-isomer of $(\eta^5\text{-}C_5H_5)(\eta^3\text{-}C\text{-}C_4H_4N)\text{-}Fe(CO)$ (species 3 and 4, respectively). It is generally accepted that the *endo*-isomers of allyl compounds are less stable than the *exo*-isomers and that the carbonyl stretching absorptions of the *endo*-isomers occur at lower energy than those of *exo*-isomers. Consequently, an assignment of the 1962 cm^{-1} band to species 4 is not consistent with previously published data for related systems,[19,20] and we favor the assignment of the 1962 cm^{-1} band to species 3.

The yield of the species absorbing at 1962 cm^{-1} was significantly increased by initially using monochromatic irradiation (λ_{exc} = 538 nm) followed by broad-band photolysis (λ_{exc} > 495 nm) (Figure 5). This suggests that monochromatic irradiation of $(\eta^5\text{-}C_5H_5)(\eta^5\text{-}C_4H_4N)Fe$ produced a precursor species, containing an η^3-coordinated pyrrolyl ligand, which then reacted with CO, producing the observed species. Therefore, the ultimate observation of a particular carbonyl-containing species is dependent on the initial photolysis wavelength because all precursor species are themselves photoactive.

(18) Alway, D. G.; Barnett, K. W *Inorg. Chem.* **1978**, *17*, 2826.
(19) Belmont, J. A.; Wrighton, M. S. *Organometallics* **1986**, 5, 1421.
(20) Fish, R. W.; Giering, W. P.; Marten, D.; Rosenblum, M. *J. Organomet. Chem.* **1976**, *105*, 101.

Laser flash photolysis of (η^5-C_5H_5)(η^1-*N*-C_4H_4N)Fe(CO)$_2$ produced a transient species with a λ_{max} centered at 420 nm. The primary photoproduct in solution was confirmed as the 16-electron CO-loss species. The observed rate constant for its reaction with CO varied linearly with [CO], providing estimates of the second-order rate constant of $(3.0 \pm 0.3) \times 10^8$ M^{-1} s^{-1} in cyclohexane and $(3.3 \pm 0.3) \times 10^8$ M^{-1} s^{-1} in toluene at 298 K. The magnitude of the second-order rate constants indicates that this intermediate does not interact with the solvent to any significant extent. This is in contrast with 16-electron species of the group 6 metals. For instance, the rate of displacement of solvent by CO in (η^6-C_6H_6)Cr(CO)$_2$(toluene)[21] is an order of magnitude slower than that for (η^6-C_6H_6)Cr(CO)$_2$(cyclohexane).[22]

These experiments confirmed that (η^5-C_5H_5)(η^1-*N*-C_4H_4N)Fe(CO)$_2$ undergoes photoinduced CO loss following photolysis at 355 nm, which in turn explains why the ratios of (η^5-C_5H_5)(η^1-*N*-C_4H_4N)Fe(CO) to (η^5-C_5H_5)(η^1-*N*-C_4H_4N)Fe(CO)$_2$ formed following photolysis of (η^5-C_5H_5)(η^5-C_4H_4N)Fe in CO-doped argon matrixes varied with photolysis time when $\lambda_{exc} > 325$ nm was used. With photons of these wavelengths the dicarbonyl product undergoes a photoinduced decarbonylation.

Concluding Remarks

This study demonstrates that (η^5-C_5H_5)(η^5-*N*-C_4H_4N)Fe has an extensive photochemistry which is dominated by haptotropic shifts of the coordinated pyrrolyl ligand. A photoinduced stepwise shift from η^5 through η^3 ultimately yields an η^1-coordinated species. The relative importance of the various intermediates is strongly dependent on the photolysis conditions. This reflects the photosensitive nature of many of the intermediates formed. The coordinatively unsaturated intermediates also appear to be discriminating with what they will react, a feature also observed with other iron systems. The ability of the pyrrolyl ligand to adopt a variety of coordination modes highlights its importance in elucidating the mechanistic details of photoinduced haptotropic shift reactions. Other compounds containing π-coordinated pyrrolyl ligands are currently under investigation.

Experimental Section

Materials. All operations were performed under inert gas atmospheres, and purity of all isolated products was verified by microanalysis. Spectroscopic grade cyclohexane and toluene were used as obtained (Aldrich spectroscopic grade). Gases used for the matrix experiments and for the flash photolysis experiments (Ar, N_2, and CO) were BOC research grade (99.999% purity). (η^5-C_5H_5)Fe(CO)$_2$I was supplied by Aldrich and used without further purification. The parent species, (η^5-C_5H_5)(η^5-C_4H_4N)Fe, was synthesized by the method reported by Pauson,[23] and (η^5-C_5H_5)Fe(CO)$_2$(η^1-*N*-C_4H_4N) was synthesized according to the method of Zakrzewski.[24]

Apparatus. Spectra were recorded on the following instruments: IR, Perkin-Elmer 2000 FT-IR (2 cm^{-1} resolution), UV/vis Hewlett-Packard 8452A; NMR, Bruker AC 400. The laser flash photolysis apparatus has been described previously.[5] For this work, both the 355 and the 532 nm lines of a pulsed Nd:YAG laser were used (energy approximately 35 and 80 mJ per pulse respectively; system response 20 ns). Solutions for analysis were placed in a fluorescence cuvette (d = 1 cm) attached to a degassing bulb and were degassed by three cycles of freeze–pump–thaw to 10^{-2} Torr, followed by liquid pumping to remove traces of water and carbon dioxide (this typically removed half the original volume of solvent). The absorbance of the solution at the excitation wavelength was adjusted to lie in the range 0.5–1.0. The UV/vis spectrum of the sample solution was monitored throughout the experiments to monitor changes in absorbance. The concentration of CO was determined by the pressure of CO admitted to the cell. The solubilities of CO in cyclohexane and toluene are 9.0×10^{-3} and 7.5×10^{-3} M, respectively, under 1 atm of CO at 298 K.[25,26]

The matrix isolation apparatus has been described in detail elsewhere.[27] Samples for infrared spectroscopy or for UV/vis spectra were deposited onto a CsI or BaF_2 window cooled by an Air Products CS202 closed-cycle refrigerator to 12–20 K. The outer windows of the vacuum shroud were chosen to match. Both (η^5-C_5H_5)(η^5-C_4H_4N)Fe and (η^5-C_5H_5)(η^1-*N*-C_4H_4N)Fe(CO)$_2$ were sublimed from right-angled tubes at 289–294 and 313–316 K, respectively, as the gas stream entered the vacuum shroud. The samples were deposited onto the windows at 20 K, which were then cooled to 12 K before recording the IR spectra on a Mattson Unicam Research Series FTIR spectrophotometer fitted with a TGS detector and a CsI beam splitter, which was constantly purged with dry CO_2-free air. Spectra were recorded at 1 cm^{-1} resolution with 128 scans. UV/vis spectra were recorded on a Perkin-Elmer Lambda 7G spectrophotometer. Matrixes were photolyzed through a quartz window with a 300 W Xe arc lamp and a water filter. Photolysis wavelengths were selected with cutoff or interference filters.

Acknowledgment. The authors gratefully acknowledge the support of Enterprise Ireland (D.P.H.) and CONACYT (Mexico) (V.M.P.). We also appreciate the help of Mr. V. Lafond with matrix experiments.

Supporting Information Available: A listing of the final refined geometric parameters and the results of a frequency calculation for the 14-electron (η^5-C_5H_5)(η^1-*N*-C_4H_4N)Fe species. This information is available free of charge via the Internet at http://pubs.acs.org.

OM0002632

(21) Farrell, G. Ph.D. Thesis, Dublin City University, 1992.
(22) Breheny, C. J.; Kelly, J. M.; Long, C.; O'Keeffe, S.; Pryce, M. T.; Russell, G.; Walsh, M. M. *Organometallics* **1998**, *17*, 3690.
(23) Pauson, P. L.; Qazi, A. R.; Rockett, B. *J. Organomet. Chem.* **1967**, *7*, 325.
(24) Zakrzewski, J. *J. Organomet. Chem.* **1987**, *327*, C41–C42.
(25) Boese, W. T.; Ford, P. C. *Organometallics* **1994**, *13*, 3525.
(26) Makranczy, J.; Megyery-Balog, K.; Rosz, L.; Rosz, L.; Patyt, D. *Hung. J. Ind. Chem.* **1976**, *4*, 269.
(27) Haddleton, D. M.; McCamley, A.; Perutz, R. N. *J. Am. Chem. Soc.* **1988**, *110*, 1810.